plants

Special Issue Reprint

Crop Functional Genomics and Biological Breeding

2nd Edition

Edited by
Yifeng Wang, Jie Huang, Jian Zhang and Jiezheng Ying

mdpi.com/journal/plants

MDPI

Crop Functional Genomics and Biological Breeding—2nd Edition

Crop Functional Genomics and Biological Breeding—2nd Edition

Guest Editors

Yifeng Wang
Jie Huang
Jian Zhang
Jiezheng Ying

MDPI

Basel • Beijing • Wuhan • Barcelona • Belgrade • Novi Sad • Cluj • Manchester

Guest Editors

Yifeng Wang
State Key Lab of Rice Biology and Breeding
China National Rice Research Institute
Hangzhou
China

Jie Huang
State Key Lab of Rice Biology and Breeding
China National Rice Research Institute
Hangzhou
China

Jian Zhang
State Key Lab of Rice Biology and Breeding
China National Rice Research Institute
Hangzhou
China

Jiezheng Ying
State Key Lab of Rice Biology and Breeding
China National Rice Research Institute
Hangzhou
China

Editorial Office
MDPI AG
Grosspeteranlage 5
4052 Basel, Switzerland

This is a reprint of the Special Issue, published open access by the journal *Plants* (ISSN 2223-7747), freely accessible at: https://www.mdpi.com/journal/plants/special_issues/MME1XP261H.

For citation purposes, cite each article independently as indicated on the article page online and as indicated below:

Lastname, A.A.; Lastname, B.B. Article Title. *Journal Name* **Year**, *Volume Number*, Page Range.

ISBN 978-3-7258-7685-3 (Hbk)
ISBN 978-3-7258-7686-0 (PDF)
https://doi.org/10.3390/books978-3-7258-7686-0

Contents

plants

MDPI

Editorial

Crop Functional Genomics and Biological Breeding—2nd Edition

Guangan Hu, Jie Huang, Jiezheng Ying, Jian Zhang and Yifeng Wang *

State Key Laboratory of Rice Biology and Breeding, China National Rice Research Institute, Hangzhou 311400, China; 13332564410@163.com (G.H.); huangjie@caas.cn (J.H.); yingjiezheng@caas.cn (J.Y.); zhangjian@caas.cn (J.Z.)

* Correspondence: wangyifeng@caas.cn

1. Introduction

Functional genomics serves as a critical link between genotype and phenotype, with its core mission being to elucidate gene functions and their regulatory networks at the genome-wide level. Unlike traditional reverse genetics, functional genomics leverages high-throughput sequencing, bioinformatics, and multi-omics integration to systematically reveal the genetic basis of complex agronomic traits, enabling breeders to comprehensively understand the mechanisms shaping crop yield, resistance, quality, and other traits from a genomic perspective [1]. However, technological means are ultimately tools; the fundamental goal of functional genomics is to serve breeding practices—by mining key genes and dissecting regulatory networks to provide precise operational targets for biological breeding, thereby efficiently translating foundational research outcomes into applicable breeding resources [2].

Currently, global agriculture faces multiple challenges, including continuous population growth, frequent extreme weather events, and increasing abiotic and biotic stresses, such as soil salinization, drought, pests, and diseases, alongside diminishing arable land resources. Against this backdrop, developing new crop varieties with high, stable yields and superior quality has become a crucial pathway to ensuring food security and promoting sustainable agricultural development. As a cutting-edge technology in modern agriculture, biological breeding is rapidly evolving from traditional empirical breeding to precision, molecular-design breeding. Functional genomics serves as the core driving force for biological breeding. It not only reveals the genes and their regulatory networks controlling key traits but also provides direct operational targets for modern breeding technologies such as molecular marker-assisted selection, gene-editing-based breeding, and genomic selection [3].

Building on this foundation, the Special Issue "Crop Functional Genomics and Biological Breeding—2nd Edition" in *Plants* continues to focus on recent advancements in this field. It compiles 11 research articles covering major staple crops such as rice, maize, wheat, and soybean, as well as important cash crops such as rapeseed, Zanthoxylum, and bitter gourd. Across these 11 studies, distinct commonalities emerge: research paradigms, the widespread application of multi-omics integration strategies, the close integration of gene function elucidation with breeding value exploration, and coverage spanning abiotic, biotic, and combined stresses. These fully reflect the current trend in functional genomics research towards systematization and application-oriented research. Collectively, these studies demonstrate a complete chain from gene mapping and cloning to breeding application, closely revolving around the three pillars of modern crop improvement: yield, resistance, and quality.

2. Yield-Related Gene Mining and Breeding Utilization

Regarding the genetic dissection of yield-related traits, two studies included in this Special Issue exemplify how functional genomics provides the core impetus for biological breeding. These two studies illustrate pathways for deep integration of genomic technologies with breeding practices, focusing on the regulation of agronomic traits and the evolution of polyploid genomes, respectively.

The leaf emergence rate is a key factor determining plant architecture, biomass accumulation, and final seed yield in rapeseed. However, its molecular regulatory mechanism has long remained unclear, limiting the molecular breeding of related traits. Qin et al. systematically dissected the rapid leaf emergence trait in *Brassica napus* using a functional genomics strategy that combined genetic analysis, BSA-seq, and transcriptome sequencing [4]. The study revealed that this trait is controlled by two additive–dominant major genes (2MG-EAD), a conclusion validated by genetic analysis over two consecutive years, indicating a relatively stable genetic basis. Further, BSA-seq identified three novel genomic intervals on chromosomes A02 and A04. Integrating transcriptome data enabled the refined screening of genes within these intervals, ultimately pinpointing 10 candidate genes. Notably, these candidates include not only known key regulators of development, such as *FT* and *RGL1*, but also several CLE-related genes (*CLE4*, *CLE6*, and *CLE7*), suggesting a significant role for the CLE signalling pathway in regulating leaf emergence rate. From a biological breeding perspective, this study not only provides new insights into the regulatory network of leaf development in rapeseed but, more importantly, offers actionable breeding resources-the identified candidate genes can be directly applied in molecular marker-assisted selection for developing high-yield rapeseed varieties with optimized plant architecture.

From a broader genomic perspective, a crucial mission of functional genomics is to unravel the evolutionary patterns of complex genomes, thereby laying the theoretical foundation for the use of polyploid crops in breeding. Wheat, a typical allohexaploid, exhibits significant functional differentiation among its A, B, and D over long-term evolution, an asymmetry with profound implications for unlocking breeding potential. Zhu et al. systematically identified, classified, and analyzed the evolutionary dynamics of pseudogenes in the wheat genome at the whole-genome level using a reference genome [5]. Once considered non-functional "junk" DNA, functional genomics research indicates that pseudogenes may harbour important functions in genome evolution and regulatory network remodelling, representing potential sources of heritable variation for breeding. This study revealed significant asymmetry among the three subgenomes in terms of pseudogene count, distribution, evolutionary dynamics, and selective constraints: the B subgenome contained significantly more pseudogenes, and its evolutionary patterns differed markedly from those of the A and D subgenomes. Further analysis found that pseudogene formation is closely linked to transposable elements. Still, the timing of their formation did not perfectly align with ancient genomic upheavals in the wheat lineage, suggesting the presence of more complex regulatory mechanisms. Functional enrichment analysis showed that the parental genes of pseudogenes are primarily enriched in non-core functions and tissue-specific expression. From a breeding standpoint, this research offers a new perspective on gene redundancy and divergence in polyploid genomes, providing a theoretical basis for exploiting "hidden" genetic variation in polyploid crops and long-term significance for expanding the pool of usable genetic resources for wheat breeding.

Synthesizing these two studies, the dual value of functional genomics in yield breeding becomes clear. On one hand, through modern genomic technologies like BSA-seq and transcriptomics, key agronomic traits are finely mapped and candidate genes screened, directly providing operational targets for molecular breeding—the study on rapeseed

https://doi.org/10.3390/plants15081195

leaf emergence rate exemplifies this approach, with identified candidates like *FT*, *RGL1*, and *CLE* offering resources for plant architecture improvement. On the other hand, by systematically analyzing the evolutionary history of polyploid crop genomes, potentially useful variations within complex genomes are uncovered, providing theoretical support for long-term breeding strategies—the wheat pseudogene study exemplifies this approach. Methodologically, both studies reflect significant trends in current functional genomics: the former showcases the efficiency of combining BSA-seq with transcriptome analysis for mining genes controlling agronomic traits. At the same time, the latter demonstrates a paradigm that combines large-scale genomic data with evolutionary biology analysis. Ultimately, both serve the core goal of providing actionable resources and strategies for biological breeding.

Looking ahead, the application of functional genomics in yield breeding should further deepen, including enhancing allelic variation analysis of candidate genes within breeding populations, using gene editing to create superior alleles, and deeply exploring the breeding potential arising from subgenomic asymmetry in polyploid crops. It is anticipated that, with continued advances in functional genomics research, the molecular regulatory networks governing yield-related traits will become increasingly clear, leading to more precise and efficient applications in biological breeding and thereby providing robust scientific support for achieving high-yield crop breeding goals.

3. Resistance Gene Dissection and Breeding Application

In the realm of resistance breeding, several studies in this Special Issue demonstrate the value of functional genomics in dissecting crop stress response mechanisms from multiple angles, including salt, cold, and combined stresses, as well as disease resistance.

Salt stress is a key factor limiting crop production on saline–alkali land. Shi et al. identified the NAC transcription factor *GmNAC035* in soybean, which is rapidly induced by salt and abscisic acid [6]. Overexpressing *GmNAC035* in *Arabidopsis* enhanced salt tolerance. The mechanism involved activating the SOS pathway, calcium signalling, and ABA-responsive genes while reducing oxidative damage. The study also found significant upregulation of stress-responsive genes, such as *AtRD29B* and *AtDREB2A*, in overexpressing plants, indicating that GmNAC035 enhances salt tolerance by coordinating multiple pathways. Similarly, Wang et al. identified the R2R3-MYB transcription factor *BnaMYB73* in rapeseed, whose expression was strongly induced by salt and osmotic stress [7]. Transgenic *Arabidopsis* overexpressing *BnaMYB73* exhibited higher proline accumulation, increased superoxide dismutase (SOD) and peroxidase (POD) activities under stress, along with upregulation of stress-responsive genes like *AtRD29B* and *AtDREB2A*, suggesting a conserved salt tolerance function for this transcription factor across species. Fan et al. provided a comprehensive review systematically outlining saline–alkali tolerance mechanisms from model plants to staple crops [8]. They compared the conservation and species-specificity of the SOS signalling pathway, osmotic regulation, and reactive oxygen species (ROS) scavenging in *Arabidopsis*, rice, maize, and wheat, proposing a "crop-centric" breeding strategy that offers important insights for future saline–alkali tolerant breeding.

Low-temperature stress is another major limiting factor for crop production. Zhou et al. investigated the chilling tolerance mechanism during maize germination, finding that tolerant inbred lines more strongly activated the phenylpropanoid and flavonoid biosynthesis pathways under low temperature [9]. Physiological analysis showed that tolerant lines accumulated less malondialdehyde (MDA) and exhibited higher SOD and POD activities under chilling stress. Among the identified genes, *ZmPER5*, encoding a class III peroxidase, was significantly upregulated in tolerant lines, potentially contributing to chilling tolerance by enhancing cell wall structure and ROS scavenging capacity. Other lignin-

https://doi.org/10.3390/plants15081195

and flavonoid-related genes also showed genotype-specific induction patterns consistent with chilling tolerance. In bitter gourd, a thermophilic vegetable crop sensitive to low temperature, Yang et al. identified a low-temperature-responsive NAC transcription factor, *McNAC087* [10]. Transcriptome analysis revealed significant expression differences in *McNAC087* under cold stress between tolerant and sensitive inbred lines. Subcellular localization confirmed that McNAC087 localizes to the nucleus. Overexpressing *McNAC087* in *Arabidopsis* enhanced cold tolerance by activating the ICE-CBF-COR cascade pathway and boosting antioxidant capacity, manifested by increased proline accumulation and higher antioxidant enzyme activities. It reduced MDA and ROS levels, providing a candidate gene for improving bitter gourd's cold tolerance.

In terms of disease resistance, two studies demonstrated the potential of functional genomics to identify resistance genes. Fan et al. performed a systematic analysis of the Dof transcription factor family in soybean, identifying 78 *GmDof* genes distributed across 19 chromosomes [11]. Phylogenetic analysis categorized these genes into nine subfamilies. Subcellular localization analysis indicated that most GmDof proteins are nuclear-localized. Through RNA-seq and qRT-PCR screening, *GmDof63* was found to be specifically induced upon infection by *Phytophthora sojae* and strongly induced by salicylic acid (SA) and ethylene (ETH) treatments. Soybean plants overexpressing *GmDof63* showed enhanced resistance to Phytophthora root rot, accompanied by significant upregulation of several pathogenesis-related (PR) genes. Furthermore, the promoters of these PR genes contained numerous AAAG or TTTC motifs, suggesting that GmDof63 may directly or indirectly regulate their expression, thereby participating in the soybean defence response against *P. sojae*. In rice, Sanglou et al. characterized the spotted leaf mutant HM113, which exhibits spontaneous lesion formation and enhanced resistance to bacterial blight [12]. Through map-based cloning and CRISPR/Cas9 gene editing, the study confirmed that a single nucleotide substitution (A847T) in a gene encoding a cysteine-rich receptor-like kinase (CRK), resulting in a serine-to-cysteine change, was responsible for the phenotype. Introducing a frameshift mutation upstream of the A847T site using CRISPR/Cas9 eliminated the spotted leaf phenotype and abolished bacterial blight resistance, indicating that this gene acts as a gain-of-function resistance gene. This study provides a new exploitable allele for breeding rice disease resistance.

Under field conditions, crops often face multiple stresses simultaneously. Cao et al. explored the synergistic responses of rice seedlings to brown planthopper (BPH) infestation and high-temperature stress [13]. Interestingly, high-temperature pretreatment enhanced rice resistance to BPH, while BPH infestation did not affect rice tolerance to high temperature. Transcriptome analysis indicated that differentially expressed genes induced by high temperature were enriched in metabolic processes and the phenylpropanoid biosynthesis pathway, potentially linked to the formation of cross-tolerance. Using weighted gene co-expression network analysis (WGCNA), the study further identified two modules, magenta and black, associated with biological processes such as protein folding and transmembrane transport, and screened candidate genes potentially regulating responses to both stresses. This research emphasizes the importance of investigating combined stresses and provides new genetic resources for developing multi-resistant rice varieties.

Looking across these resistance studies, the core value of functional genomics in stress-resistance breeding is clearly evident. From single stress to combined stress, and from staple to specialty crops, these studies demonstrate the powerful efficacy of multi-omics integration strategies in dissecting crop. mechanisms. Through genome-wide identification, phylogenetic analysis, expression profiling, and transgenic functional validation, researchers have not only revealed the molecular regulatory networks underlying responses to salt stress, cold stress, pathogen infection, and combined high-temperature insect stress

in crops, but also identified key gene resources with potential for breeding applications. Particularly noteworthy is the study on combined stress, reflecting the deepening of functional genomics research from single stressors towards multifactorial interactions, which more closely aligns with actual field production demands. These research outcomes provide important targets for molecular marker-assisted selection and gene-editing-based breeding and lay a solid foundation for developing new crop varieties with multiple resistance and broad adaptability.

4. Genetic Regulation and Improvement of Quality Traits

Quality improvement constitutes one of the three pillars of modern breeding, directly impacting the commercial value and market competitiveness of agricultural products. One study featured in this Special Issue focuses on the speciality crop Zanthoxylum and employs a multi-omics joint analysis strategy to uncover key genes involved in coumarin biosynthesis, providing new insights for the genetic improvement of quality traits.

Coumarin compounds are crucial sources of the characteristic numbing and aromatic flavours in Zanthoxylum pericarp; their content and composition directly affect flavour quality and commercial value. Chen et al. studied two Zanthoxylum varieties, Z. bungeanum (red prickly ash) and Z. armatum (green prickly ash, known as Tengjiao), systematically analyzing mature pericarps using widely targeted metabolomics and transcriptome sequencing [14]. The study detected 583 metabolites, with flavonoids, phenolic acids, and alkaloids as the main components. Twenty-four coumarin compounds were identified, with most showing significantly higher content in Z. armatum compared to Z. bungeanum. By jointly analyzing metabolomic and transcriptomic data, the study further identified 56 candidate genes highly correlated with the accumulation of scopoletin and scopolin. Functional validation experiments demonstrated that transient overexpression of *CCoAOMT*, *COMT*, and *F6H* genes in *Nicotiana benthamiana* significantly increased scopoletin and scopolin content, confirming the crucial roles of these genes in coumarin biosynthesis.

This study fully demonstrates the efficiency of integrating metabolomic and transcriptomic strategies in quality trait research. Compared to traditional single-omics analysis, multi-omics joint analysis captures both metabolite accumulation and gene expression changes simultaneously, allowing rapid identification of key regulatory genes through correlation analysis and significantly shortening the timeline from trait dissection to gene identification. This research paradigm applies not only to Zanthoxylum but also provides a methodological framework for quality improvement in other speciality crops, such as tea plants, medicinal herbs, and speciality fruits and vegetables.

From a broader perspective, research on the genetic regulation of quality traits is progressively moving from traditional analyses of single traits to a new stage characterized by multi-omics integration and the systematic dissection of metabolic pathways. In staple crops like rice, maize, and wheat, regulatory networks for quality-related traits such as starch synthesis, protein accumulation, and lipid metabolism are being progressively elucidated, providing important targets for molecular design breeding [15,16]. However, for speciality crops such as Zanthoxylum, tea, and medicinal herbs, genetic research on quality traits lags, with significant gaps in understanding the mechanisms of synthesis for flavour compounds and active ingredients. The study on Zanthoxylum included in this Special Issue represents an active exploration in this context, and its multi-omics integration paradigm can serve as a methodological reference for quality improvement in other speciality crops.

It is worth noting that quality improvement in speciality crops is of significant practical importance. With consumption upgrading and diversifying market demands, consumer

https://doi.org/10.3390/plants15081195

focus on agricultural products has shifted from solely yield to comprehensive qualities, including flavour, nutrition, and functionality. The research on coumarins in Zanthoxylum not only helps elucidate the synthesis mechanism of the numbing flavour compounds but also provides gene resources for targeted improvement of Zanthoxylum flavour quality, underscoring the unique value of functional genomics research in meeting diversified market demands. In the future, efforts should be intensified to advance the genetic dissection of quality traits in speciality crops, and to promote the integrated application of metabolic engineering and gene editing technologies for quality improvement, thereby providing scientific support to meet diverse market needs.

5. Conclusions and Perspectives

The Special Issue "Crop Functional Genomics and Biological Breeding—2nd Edition" compiles 11 cutting-edge research articles that systematically showcase the central role of functional genomics in crop improvement. These studies closely align with the three pillars of modern crop breeding—yield, resistance, and quality—and cover staple crops such as rice, maize, wheat, and soybean, as well as speciality crops such as rapeseed, Zanthoxylum, and bitter gourd. Collectively, they illustrate a complete chain from gene discovery to breeding application.

Looking across these 11 studies, several important trends in current crop functional genomics research are evident. Firstly, multi-omics integration has become a powerful paradigm for dissecting complex traits—the combined application of genomics, transcriptomics, metabolomics, BSA-seq, WGCNA, and other techniques greatly enhances the efficiency and precision of gene discovery. Secondly, research perspectives are expanding from single stresses to combined stresses; the study on the synergistic response of rice to high temperature and brown planthopper provides a model for addressing multifactorial interactions in the field. Thirdly, the distance from gene discovery to breeding application is shortening; several candidate genes featured in this Special Issue already have potential for use in molecular marker-assisted selection or gene-editing-based breeding, reflecting the tangible driving force of functional genomics for biological breeding.

Looking ahead, research in crop functional genomics should continue to focus on several directions. First, enhance allelic variation analysis of candidate genes within breeding populations and use gene-editing technologies to create superior alleles, accelerating the translation from gene discovery to variety improvement. Second, deepen research on responses to combined stresses. In the context of climate change, multiple stresses, such as high temperatures, drought, salinity, pests, and diseases, often occur simultaneously or sequentially. Dissecting the mechanisms underlying crop synergistic responses to multifactorial interactions is crucial for developing widely adaptable varieties. Third, expand functional genomics research on speciality crops. Explorations of crops such as Zanthoxylum and bitter gourd indicate that speciality crops harbour abundant genetic resources for quality and resistance, warranting further exploration to meet diversified market demands. Fourth, promote the deep integration of multi-omics data with intelligent breeding technologies. Leveraging artificial intelligence and machine learning algorithms to construct genotype-phenotype prediction models can facilitate the leap from gene discovery to variety selection.

We believe these research outcomes not only deepen our understanding of the mechanisms underlying crop yield, resistance, and quality formation but also provide directly applicable gene resources and technical solutions for biological breeding. The deep integration of functional genomics and biological breeding will provide robust scientific support for addressing global climate change, ensuring food security, and promoting the sustainable development of green agriculture.

https://doi.org/10.3390/plants15081195

Author Contributions: All the authors participated in the editing of this Research Topic. G.H. wrote the draft, and all the other authors provided suggestive comments on the editorial. All authors have read and agreed to the published version of the manuscript.

Funding: This project was funded by the National Natural Science Foundation of China (32372070) and the Agricultural Science and Technology Innovation Program (ASTIP).

Data Availability Statement: No new data were created or analyzed in this study. Data sharing is not applicable to this article.

Conflicts of Interest: The authors declare no conflicts of interest.

References

1. Huang, X.H.; Wei, X.H.; Sang, T.; Zhao, Q.A.; Feng, Q.; Zhao, Y.; Li, C.Y.; Zhu, C.R.; Lu, T.T.; Zhang, Z.W.; et al. Genome-wide association studies of 14 agronomic traits in rice landraces. *Nat. Genet.* **2010**, *42*, 961–976. [CrossRef] [PubMed]
2. Varshney, R.K.; Pandey, M.K.; Bohra, A.; Singh, V.K.; Thudi, M.; Saxena, R.K. Toward the sequence-based breeding in legumes in the post-genome sequencing era. *Theor. Appl. Genet.* **2019**, *132*, 797–816. [CrossRef] [PubMed]
3. Hickey, L.T.; Hafeez, A.N.; Robinson, H.; Jackson, S.A.; Leal-Bertioli, S.C.M.; Tester, M.; Gao, C.X.; Godwin, I.D.; Hayes, B.J.; Wulff, B.B.H. Breeding crops to feed 10 billion. *Nat. Biotechnol.* **2019**, *37*, 744–754. [CrossRef] [PubMed]
4. Qin, M.F.; Liu, X.; Song, J.; Zhao, F.X.; Shi, Y.J.; Xu, Y.; Guo, Z.T.; Zhang, T.Y.; Wu, J.P.; Wang, J.X.; et al. Genetic Analyses, BSA-Seq, and Transcriptome Analyses Reveal Candidate Genes Controlling Leaf Plastochron in Rapeseed (*Brassica napus* L.). *Plants* **2025**, *14*, 1719. [CrossRef] [PubMed]
5. Zhu, H.F.; Tang, H.; Li, Y.; Yang, N.; Wang, Q.; Yang, F.; Wan, H.S.; Yang, W.Y.; Li, J.; Liu, Z.H. A Genome-Wide Pseudogene Map Reveals the Asymmetric Evolution of the A, B, and D Subgenomes in Common Wheat. *Plants* **2026**, *15*, 818. [CrossRef] [PubMed]
6. Shi, W.T.; Ye, S.X.; Xin, Y.T.; Jin, H.M.; Hu, M.L.; Zheng, Y.P.; Zhan, Y.H.; Liu, H.B.; Gan, Y.; Zheng, Z.F.; et al. NAC Transcription Factor *GmNAC035* Exerts a Positive Regulatory Role in Enhancing Salt Stress Tolerance in Plants. *Plants* **2025**, *14*, 1391. [CrossRef] [PubMed]
7. Wang, L.M.; Zhang, Y.Z.; Zhou, X.Y.; Xu, X.; Zhang, H.X.; Sun, N.; Li, D.; Liu, Y.F. BnaMYB73, a *Brassica napus* L. R2R3-MYB Transcription Factor, Enhances Plant Salt and Osmotic Stress Tolerance. *Plants* **2026**, *15*, 694. [CrossRef] [PubMed]
8. Fan, D.L.; Ruan, J.; Xu, Q.N.; Ying, J.Z.; Wang, Y.F.; Tong, X.H.; Li, Z.Y.; Cheng, Y.; Xue, D.W.; Zhang, J.; et al. From Model Plants to Staple Crops: Molecular Mechanisms of Plant Saline-Alkali Tolerance. *Plants* **2026**, *15*, 532. [CrossRef] [PubMed]
9. Zhou, S.N.; Yu, X.L.; Tan, J.; Sun, H.X.; Yang, W.; Jiang, L.Y.; Zang, Z.Y.; Ci, J.B.; Ren, X.J. Transcriptomics Reveals Cold Tolerance Maise Lines Involved in the Phenylpropanoid and Flavonoid Pathways. *Plants* **2026**, *15*, 161. [CrossRef] [PubMed]
10. Yang, X.T.; Wang, K.; Guan, F.; Shi, B.; Xie, Y.Y.; Du, C.; Tang, T.; Yang, Z.; Ma, S.J.; Wan, X.J. The Bitter Gourd Transcription Factor *McNAC087* Confers Cold Resistance in Transgenic Arabidopsis. *Plants* **2025**, *14*, 3440. [CrossRef] [PubMed]
11. Fan, S.J.; Chen, H.Y.; Huo, Y.H.; Song, Y.; Wang, P.W.; Zhang, Z.; Jiang, L.Y. Genome-Wide Analysis of the *Dof* Gene Family in Soybean and Functional Identification of *GmDof63* in Response to *Phytophthora sojae* Infection. *Plants* **2025**, *14*, 3621. [CrossRef] [PubMed]
12. Sanglou, R.K.; Kampire, M.G.; Xu, X.; Wu, J.L.; Gong, J.Y.; Zhang, X.B. Functional Characterization of Rice Spotted-Leaf Mutant *HM113* Reveals an Amino Acid Substitution in a Cysteine-Rich Receptor-like Kinase. *Plants* **2025**, *14*, 3429. [CrossRef] [PubMed]
13. Cao, D.Y.; Ping, Y.C.; Lin, Y.R.; Hu, J.Y.; Wang, Z.M.; Yuan, W.; Li, T.T.; Liu, L.X.; Zhang, B.; Xiong, S.J.; et al. Synergistic Response Mechanisms in Rice Seedlings Exposed to Brown Planthopper Infestation and High-Temperature Stress. *Plants* **2025**, *14*, 1644. [CrossRef] [PubMed]
14. Chen, S.Q.; Shen, L.W.; Zeng, Y.J.; Feng, S.J.; Luo, H.; Wang, G. Integrated Metabolomic and Transcriptomic Analyses Reveal the Coumarin Biosynthesis Pathway and Key Regulatory Genes in the Pericarp of *Zanthoxylum*. *Plants* **2026**, *15*, 769. [CrossRef] [PubMed]
15. Canher, B.; Lanssens, F.; Zhang, A.; Bisht, A.; Mazumdar, S.; Heyman, J.; Wolf, S.; Melnyk, C.W.; De Veylder, L. The regeneration factors ERF114 and ERF115 regulate auxin-mediated lateral root development in response to mechanical cues. *Mol. Plant* **2022**, *15*, 1543–1557. [CrossRef] [PubMed]
16. Kim, D.B.; Na, C.; Hwang, I.; Lee, D.W. Understanding protein translocation across chloroplast membranes: Translocons and motor proteins. *J. Integr. Plant Biol.* **2023**, *65*, 408–416. [CrossRef] [PubMed]

plants

MDPI

Review

From Model Plants to Staple Crops: Molecular Mechanisms of Plant Saline–Alkali Tolerance

Delong Fan [1,2,†], Jing Ruan [1,2,†], Qinan Xu [1,2,†], Jiezheng Ying [2], Yifeng Wang [2], Xiaohong Tong [2], Zhiyong Li [2], Yu Cheng [2], Dawei Xue [1,*], Jian Zhang [2,3,*] and Jie Huang [2,*]

[1] College of Life and Environmental Sciences, Hangzhou Normal University, Hangzhou 311121, China; fdllytc@163.com (D.F.); jingr627@163.com (J.R.); xuqinan0119@163.com (Q.X.)
[2] State Key Laboratory of Rice Biology and Breeding, China National Rice Research Institute, Hangzhou 311400, China; yingjiezheng@caas.cn (J.Y.); wangyifeng@caas.cn (Y.W.); tongxiaohong@caas.cn (X.T.); lizhiyong@caas.cn (Z.L.); chengyu@caas.cn (Y.C.)
[3] National Nanfan Research Institute (Sanya), Chinese Academy of Agricultural Sciences, Sanya 572024, China
* Correspondence: dwxue@hznu.edu.cn (D.X.); zhangjian@caas.cn (J.Z.); huangjie@caas.cn (J.H.)
† These authors contributed equally to this work.

Abstract

Soil salinization, as a key constraint to global agricultural sustainable development, has threatened over one billion hectares of farmland, posing severe challenges to staple crop production. Therefore, this review summarizes important advances in the molecular mechanisms of salt–alkali tolerance from the model plant *Arabidopsis thaliana* to staple crops (rice, maize, and wheat) and compares the commonalities and differences in physiological structure and molecular regulatory networks among these species. Studies have shown that plants respond to saline–alkali stress mainly through conserved mechanisms, including salt overly sensitive (SOS) signaling pathway-mediated ion homeostasis, accumulation of osmoprotectants, reactive oxygen species (ROS) scavenging, and coordination of multiple hormone signals. However, different species have evolved unique adaptive strategies: Arabidopsis has revealed core regulatory pathways, but its simple root system limits direct application in crops; rice employs root barriers and a stem node "ion filter" to precisely regulate Na^+ transport; maize utilizes the C4 photosynthetic pathway along with efficient osmotic adjustment and tissue compartmentalization to enhance tolerance; and wheat achieves ion detoxification through *TaHKT* allele variation and vacuolar sequestration. Looking forward, future breeding for salt–alkali tolerance should adopt a "crop-centric" approach, focusing on the mining and molecular design of superior alleles, combined with gene editing and multi-trait integration, to provide a theoretical basis and strategic support for developing high-yield and stable crop varieties adapted to saline–alkali lands.

Keywords: saline–alkali stress; model plant; staple crops; SOS signaling pathway; molecular breeding

1. Introduction

Soil salinization is one of the most severe abiotic stresses facing global agricultural production and ecological security [1]. It is primarily manifested in three stress types: salt stress (mainly caused by neutral salts, which inhibit plant growth through high osmotic pressure and ion toxicity), alkali stress (primarily induced by alkaline salts, which damage root systems via high pH and trigger nutrient deficiencies), and the more complex and severe saline–alkali stress (involving both neutral and alkaline salts, characterized by

multiple synergistic hazards including high osmotic pressure, ion toxicity, strong alkalinity, and soil compaction). It is estimated that over one billion hectares of land worldwide are affected by salinization, and this number continues to grow, posing a significant threat to global food security and sustainable agricultural development [2]. Against this backdrop, gaining a deeper understanding of the molecular mechanisms of plant saline–alkali tolerance and utilizing modern molecular breeding techniques to develop new crop varieties adapted to saline–alkaline environments have become major strategic demands in the fields of agriculture and life sciences.

During long-term evolution, plants have developed a series of complex and sophisticated mechanisms to cope with saline–alkali stress [3]. These mechanisms encompass multiple levels, including the regulation of ion homeostasis (such as SOS signaling pathway-mediated Na^+ efflux and vacuolar sequestration), osmotic balance adjustment (e.g., the accumulation of compatible solutes like proline and glycine betaine), the activation of ROS scavenging systems, and the integration and reprogramming of plant hormone signaling networks (such as ABA and ethylene). A profound understanding of these fundamental physiological and molecular processes forms the theoretical foundation for conducting saline–alkali tolerance breeding.

Research on model plants, represented by *Arabidopsis thaliana* (*A. thaliana*), has made irreplaceable contributions to our understanding of the "core toolkit" for plant saline–alkali tolerance [4]. Its clear genetic background, mature transgenic systems, and rich mutant libraries have enabled scientists to systematically elucidate the core roles of key components in stress response at the molecular level, such as the SOS pathway, NHX transporters, HKT regulators, and key transcription factors like DREB/CBF and NAC [5–10]. However, as a dicotyledonous short-cycle herbaceous plant, *A. thaliana* has a simple root system architecture, lacks a long-distance ion transport and filtration system, and exhibits significant differences in physiological responses compared to monocotyledonous staple crops such as rice (*Oryza sativa* L.), maize (*Zea mays* L.), and wheat (*Triticum aestivum* L.) [11]. Consequently, directly applying research findings from model plants to crop improvement faces numerous challenges, creating an urgent need to dissect the mechanisms and validate gene functions within the specific genetic contexts of the crops themselves [12].

As the three major staple crops globally, rice, maize, and wheat have evolved unique adaptation strategies to cope with saline–alkali stress. For instance, rice relies on its well-developed root barrier and the "ion filter" function of its stem nodes to finely regulate the allocation of Na^+ to the shoots, particularly the panicles [13]. Maize benefits from its highly efficient C4 photosynthetic pathway, which maintains relatively stable carbon assimilation efficiency under stress, coupled with strong osmotic adjustment and tissue-level ion compartmentalization capabilities [14]. Wheat, through complex allelic variations in *TaHKT* genes and efficient vacuolar sequestration mechanisms, achieves ion redistribution and detoxification [15]. The existence of these species-specific mechanisms implies that future breeding strategies must shift from a "model-oriented" to a "crop-centric" approach, deeply mining and utilizing the superior alleles present in crop germplasm resources [16].

This review aims to systematically summarize recent research advances in the molecular mechanisms of saline–alkali tolerance, spanning from the model plant *A. thaliana* to the staple crops rice, maize, and wheat. The article will focus on comparing the commonalities and specificities among different species in areas such as ion homeostasis, osmotic regulation, antioxidant defense, and signal transduction networks. It will also summarize the unique physiological and structural adaptations they have evolved. Finally, this paper will provide perspectives on future research directions and breeding strategies, with the goal of offering a solid theoretical foundation and feasible technical pathways for advancing

https://doi.org/10.3390/plants15040532

the genetic improvement of saline–alkali tolerant crops and the effective utilization of saline–alkali soil resources.

2. The Molecular Mechanisms of Saline–Alkali Stress Tolerance in *A. thaliana*

As a model organism in plant biology research, *A. thaliana* has become the preferred material for studying plant saline–alkali tolerance mechanisms, owing to its advantages such as a small genome (approximately 135 Mb), short life cycle (6–8 weeks), high genetic transformation efficiency (can exceed 80%), and extensive T-DNA insertion mutant libraries [17,18]. During long-term evolution, *A. thaliana* has developed a comprehensive regulatory network for saline–alkali tolerance, spanning from signal perception to systemic responses.

Among these, the SOS pathway is the most thoroughly studied core signaling pathway [19]. This pathway is initiated by the increase in cytosolic Ca^{2+} signals triggered by salt stress. The calcium sensor protein SOS3 and its homolog SCaBP8 perceive the elevated Ca^{2+} and interact with the serine/threonine protein kinase SOS2, relieving its autoinhibition and thereby activating SOS2 [20,21]. The activated SOS2 subsequently phosphorylates and activates the plasma membrane-localized Na^+/H^+ antiporter SOS1, which utilizes the proton gradient established by the plasma membrane H^+-ATPase to actively pump Na^+ out of the cell, directly reducing the cytosolic Na^+ concentration [22]. In addition to this plasma membrane efflux mechanism, sequestering excess Na^+ into the vacuole represents another crucial detoxification strategy. This process is primarily carried out by vacuolar membrane Na^+/H^+ antiporters, such as *AtNHX1* and *AtNHX2*, which utilize the inward H^+ gradient generated by the vacuolar membrane H^+-ATPase and H^+-PPase to pump cytosolic Na^+ into the vacuole [6]. It is noteworthy that the SOS2 kinase can also phosphorylate and activate NHX transporters, indicating that the plasma membrane efflux and vacuolar sequestration processes are coordinately regulated through signaling pathways (Figure 1) [23]. Regarding the restriction of Na^+ uptake, the high-affinity potassium transporter AtHKT1;1 in *A. thaliana* plays a unique role. It is primarily expressed in the pericycle and xylem parenchyma cells, where it facilitates the recirculation of Na^+ from the xylem to the phloem by loading Na^+ from the xylem sap into the surrounding parenchyma cells. This process effectively reduces Na^+ transport to the aerial leaves, thereby protecting the photosynthetic organs [7,24].

Beyond ionic toxicity, osmotic stress and oxidative stress are also major components of salt damage. In terms of osmotic adjustment, plants reduce cellular osmotic potential by synthesizing and accumulating compatible solutes. In *A. thaliana*, proline accumulation serves as a classic example; salt stress strongly induces the expression of *P5CS1*, a key gene in its biosynthesis, while repressing the degradation gene *ProDH*. This process is precisely regulated by various transcription factors (Figure 1) [25]. Biosynthetic pathways for solutes like glycine betaine and trehalose have also been confirmed to contribute to osmotic protection [26]. In coping with oxidative stress, *A. thaliana* possesses a complex ROS scavenging network. The enzymatic system includes superoxide dismutase (SOD), ascorbate peroxidase (APX), and catalase (CAT), among others. The high salt sensitivity of the cytosolic *APX1* mutant underscores its critical role. The non-enzymatic system relies on antioxidants such as ascorbic acid (ASA) and glutathione (GSH) [27,28].

Plant hormones are core signaling molecules regulating the salt stress response, forming a complex integrative network. Abscisic acid (ABA), the primary stress hormone, rapidly accumulates under salt stress and transmits signals via the PYR/PYL/RCAR receptor-PP2C-SnRK2 core signaling module. Activated SnRK2s kinases phosphorylate downstream transcription factors like AREB/ABF, thereby activating a multitude of stress-

responsive genes and regulating stomatal closure to reduce water loss [29,30]. The ethylene signaling pathway is closely linked to salt tolerance, as its key transcription factor EIN3 can directly activate the expression of SOS1 and SOS2, establishing a direct bridge between hormone signaling and ion homeostasis regulation (Figure 1) [31]. Furthermore, hormone signals such as brassinosteroids (BR), jasmonic acid (JA), and salicylic acid (SA) engage in extensive crosstalk with stress signaling pathways through their core components, finely balancing plant growth and defense responses [32].

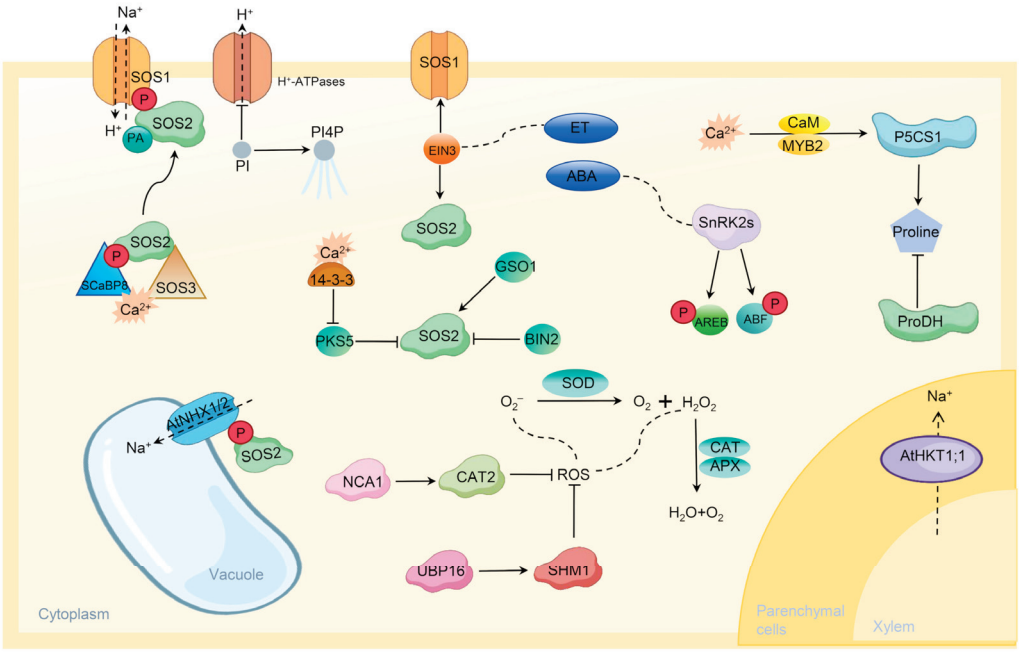

Figure 1. Research advances in *A. thaliana* tolerance to saline–alkali stress. Under saline–alkali stress, cytosolic Ca^{2+} levels rapidly increase and are perceived by calcium-binding proteins SOS3 and SCaBP8. These sensor proteins activate the protein kinase SOS2, which in turn phosphorylates and activates the plasma membrane Na^+/H^+ antiporter SOS1. SOS1 utilizes the proton gradient established by the plasma membrane H^+-ATPase to actively pump Na^+ out of the cell, directly reducing cytosolic Na^+ concentration. This core SOS pathway is also regulated by phospholipid signaling molecules (PI, PI4P, and PA). The vacuolar membrane Na^+/H^+ antiporters AtNHX1 and AtNHX2 pump Na^+ from the cytoplasm into the vacuole. The high-affinity potassium transporter AtHKT1;1 facilitates the recirculation of Na^+ from the xylem to the phloem by loading Na^+ from the xylem sap into surrounding parenchyma cells. Saline–alkali stress strongly induces the expression of *P5CS1*, a key gene in proline synthesis while suppressing the expression of the degradation gene *ProDH*, thereby enhancing *A. thaliana*'s tolerance to salt and osmotic stress. The massive accumulation of reactive oxygen species (ROS) activates its antioxidant system, which includes increasing the activity of antioxidant enzymes (such as CAT2) and synthesizing antioxidant compounds, to scavenge ROS and protect cells from oxidative damage. The ubiquitin-specific protease UBP16 stabilizes serine hydroxymethyltransferase SHM1 through deubiquitination, thereby indirectly regulating ROS levels. Abscisic acid (ABA) levels rise rapidly under salt stress. Activated SnRK2s kinases phosphorylate downstream transcription factors such as AREB/ABF, which subsequently activate the expression of numerous stress-responsive genes and regulate stomatal closure to reduce water loss. The ethylene signaling pathway is closely linked to saline–alkali tolerance. Its key transcription factor EIN3 can directly activate the expression of *SOS1* and *SOS2*, establishing a direct bridge between hormone signaling and ion homeostasis regulation.

In response to alkaline stress, plants have evolved specific adaptation mechanisms distinct from those for salt stress. The high-pH environment caused by alkaline stress poses a severe challenge to cellular pH homeostasis. Plants activate specific signaling pathways to counter this stress. The calcium sensor SCaBP3 dissociates from the plasma membrane

H^+-ATPase AHA2 under alkaline stress, relieving the inhibition of its proton pump activity and promoting H^+ efflux to lower the apoplastic pH (Figure 1). The DnaJ-like molecular chaperone J3 indirectly enhances H^+-ATPase function by inhibiting PKS5 kinase activity, working cooperatively to maintain pH homeostasis [33]. Additionally, the sorghum AT1 gene influences H_2O_2 efflux by modulating the phosphorylation status of the aquaporin PIP2;1, and loss of its function can enhance plant alkaline tolerance [34].

3. The Molecular Mechanisms of Saline–Alkali Stress Tolerance in Rice

Saline–alkali stress severely constrains the growth and development of rice, with its primary damage mechanisms including ionic toxicity, osmotic stress, and oxidative damage. To cope with this adversity, rice has evolved multi-layered physiological response mechanisms, specifically manifested in processes such as ion homeostasis regulation, osmotic balance maintenance, and ROS scavenging [35]. Regarding ion homeostasis, maintaining intracellular Na^+/K^+ balance is crucial for rice's saline–alkali tolerance. Since Na^+ and K^+ share transport systems, rice employs strategies such as limiting Na^+ uptake, enhancing efflux, and vacuolar sequestration to alleviate Na^+ toxicity under saline–alkali stress [36]. For instance, the plasma membrane Na^+/H^+ antiporter OsSOS1 mediates Na^+ efflux from cells, while vacuolar membrane Na^+/H^+ antiporters like OsNHX1 sequester excess Na^+ into the vacuole, thereby maintaining a low cytosolic Na^+/K^+ ratio [37,38]. Furthermore, members of the high-affinity K^+ transporter family, such as OsHKT1;1 and SKC1, effectively reduce Na^+ accumulation in leaves [39]. Chloride channel proteins OsCLC1 and OsCLC2 enhance plant salt tolerance and normal development by mediating Cl^- transport into the vacuoles [40]. HCO_3^- transporters encoded by SLC4 family genes help maintain cytosolic pH homeostasis by extruding HCO_3^- (Figure 2) [40].

In terms of osmotic adjustment, saline–alkali stress increases osmotic potential, inducing rice to accumulate soluble osmolytes such as sucrose, proline, glycine betaine, and polyamines to lower cellular osmotic potential and stabilize protein structures and membrane systems [26]. Upregulated expression of proline biosynthesis-related genes *OsP5CS1*, *OsP5CS2*, and *OsP5CR* promotes proline accumulation, enhancing rice tolerance to saline–alkali and osmotic stress [41]. Trehalose synthesis genes *OsTPS1*, *OsTPS2*, and *OsTPS4* improve resistance to high salt, high pH, and drought stress by increasing trehalose content (Figure 2) [42]. The synthesis of some secondary metabolites, like diterpenoids and phenylpropanoids, has also been shown to participate in the saline–alkali stress response [43]. Concurrently, increased activities of antioxidant enzymes such as SOD, CAT, and POD in the roots help mitigate damage induced by high-pH alkaline stress [44]. Concerning the ROS scavenging mechanism, ion imbalance and osmotic disturbance caused by saline–alkali stress lead to ROS accumulation, which disrupts cellular metabolism and damages biological macromolecules. Rice mitigates ROS toxicity through enzymatic and non-enzymatic antioxidant systems: the enzymatic system includes respiratory burst oxidase homologs (RBOHs), SOD, and APX; the non-enzymatic system relies on antioxidants like ascorbic acid, secondary metabolites, and carotenoids [28]. Additionally, rice enhances its saline–alkali tolerance by maintaining nutrient balance, regulating intracellular pH homeostasis, and ensuring normal nitrogen metabolism.

https://doi.org/10.3390/plants15040532

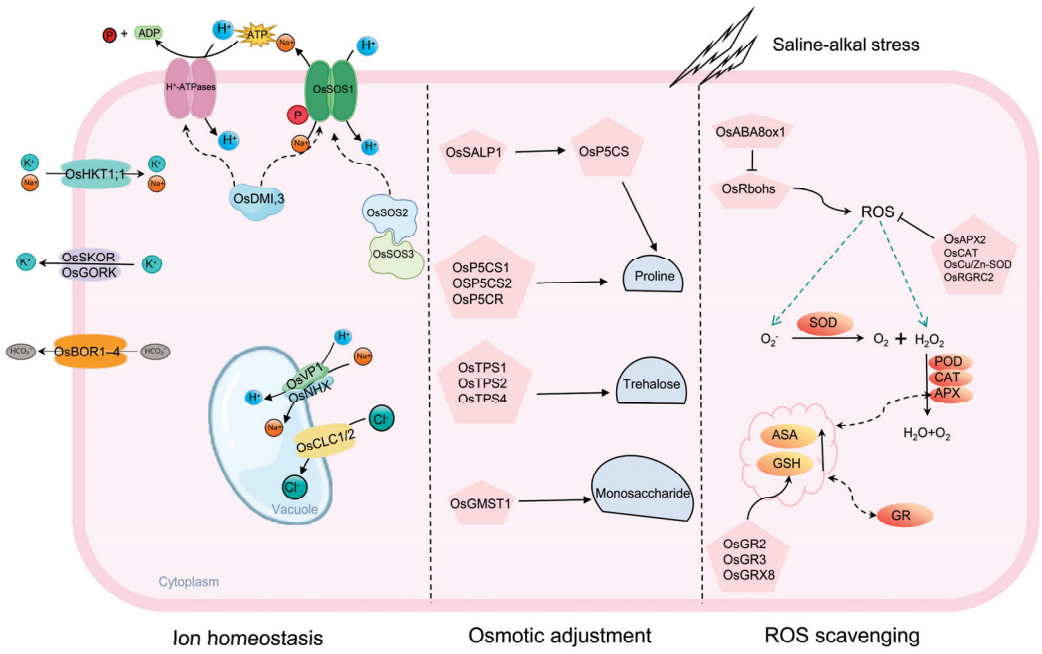

Figure 2. Research advances in rice tolerance to saline–alkali stress. In rice, the exclusion of Na^+ from shoots is regulated by the Na^+/H^+ antiporter OsSOS1. OsDMI3 enhances salt tolerance during root growth by modulating OsSOS1 and H^+-ATPase under salt stress. The transporter OsHKT1;1 contributes to reduced Na^+ accumulation in leaves, while the shaker-like potassium channels OsSKOR and OsGORK regulate K^+ homeostasis. The vacuolar Na^+/H^+ antiporter OsNHX sequesters excess cytosolic Na^+ into the vacuole, thereby enhancing tolerance to saline–alkali stress. OsVP1 also facilitates Na^+/H^+ exchange and improves rice salt resistance by pumping H^+ from the cytoplasm into the vacuole. The chloride channel proteins OsCLC1 and OsCLC2 mediate Cl^- transport into the vacuole, bolstering plant salt tolerance and normal development. The HCO_3^- transporter encoded by the *SLC4* family gene helps maintain cytosolic pH homeostasis by extruding HCO_3^-. The upregulated expression of proline biosynthesis genes *OsP5CS1*, *OsP5CS2*, and *OsP5CR* promotes proline accumulation, enhancing rice tolerance to both saline–alkali and osmotic stress. Similarly, trehalose synthesis genes *OsTPS1*, *OsTPS2*, and *OsTPS4* increase trehalose content, thereby improving resistance to high salt, high pH, and drought stress. Under saline–alkali stress, *OsABA8ox1* reduces ROS accumulation and scavenges ROS produced by *OsRbohs*, conferring tolerance in rice plants. Superoxide dismutase (SOD), the first enzyme in the antioxidant system, converts accumulated O_2^- into O_2 and H_2O_2. Subsequently, POD, CAT, and APX decompose H_2O_2 into H_2O and O_2.

At the molecular level, saline–alkali stress activates various signaling molecules, including phospholipids, hormones, and Ca^{2+}, which subsequently initiate downstream response networks to maintain ion homeostasis and osmotic balance, thereby alleviating growth inhibition. For example, the Ca^{2+}/calmodulin-dependent protein kinase gene *OsDMI3* coordinates Na^+ and H^+ transmembrane transport by regulating *OsSOS1* and the plasma membrane H^+-ATPase genes *OsHA3*/*OsHA8*, promoting root growth under saline–alkali stress (Figure 2) [45]. Overexpression of *OsCam1-1* induces ABA accumulation, thereby improving salt tolerance; conversely, inhibiting the key ABA catabolism gene *OsABA8ox1* helps scavenge plasma membrane peroxides and enhances salt tolerance (Figure 2) [46,47]. To date, over 40 transcription factors involved in the saline–alkali stress response have been identified, spanning families such as AP2/ERF, bZIP/HD-Zip, MYB/MYC, WRKY, and NAC. These factors play a central regulatory role in stress signal transduction by recognizing and binding to cis-acting elements in downstream target genes [44,48].

4. The Molecular Mechanisms of Saline–Alkali Stress Tolerance in Maize

The saline–alkali tolerance of maize is a complex quantitative trait controlled by multiple genes, and elucidating its molecular mechanisms is crucial for breeding new maize varieties with enhanced tolerance. In recent years, the integrated application of multi-omics technologies—such as genomics, transcriptomics, proteomics, and metabolomics—has greatly advanced this field, leading to a series of important discoveries in ion homeostasis regulation, osmotic balance, oxidative stress response, and nutrient uptake [49].

The SOS signaling pathway in maize has now been fully elucidated: under salt stress conditions, elevated cytosolic Ca^{2+} levels are perceived by the ZmSOS3 protein. ZmSOS3 then binds to and activates ZmSOS2. The activated ZmSOS3-ZmSOS2 complex subsequently phosphorylates ZmSOS1, thereby activating its Na^+ transport activity to promote Na^+ efflux (Figure 3) [50]. Furthermore, this pathway is finely modulated by negative regulators like ZmSK3/ZmSK4 and positive regulators like ZmSCaBP8 [51]. In addition to root efflux, xylem Na^+ unloading is a key process limiting Na^+ transport to the shoots. Genes such as ZmHKT1;1, ZmHKT1;2, and ZmHAK4, expressed in the stele parenchyma cells, are responsible for transferring Na^+ from the xylem to surrounding cells (Figure 3) [52–54]. Moreover, the root endodermal Casparian strip acts as an apoplastic barrier, playing a vital role in restricting Na^+ influx. The *ZmSTL1/ZmESBL* gene encodes a DIR family protein that positively regulates Casparian strip development [55]. Its upregulated expression under salt stress enhances the barrier function of the Casparian strip, effectively preventing Na^+ from entering the stele via the apoplastic pathway. Loss of function of this gene leads to a sharp increase in shoot Na^+ content, indicating that the developmental plasticity of the Casparian strip is an important mechanism for maize adaptation to salt stress. Beyond Na^+, the homeostatic balance of K^+ and Cl^- is equally critical. *ZmHKT2* has been identified as a QTL negatively regulating K^+ content in shoots; loss of its function conversely enhances salt tolerance [56]. Regarding Cl^- regulation, ZmRR1 upregulates the expression of the vacuolar membrane Cl^- transporter ZmMATE29 by suppressing the cytokinin signaling pathway, promoting Cl^- sequestration into root cortical vacuoles and thereby enhancing salt tolerance (Figure 3) [57]. A non-synonymous polymorphism, SNP307-T, impairs this pathway, resulting in reduced salt tolerance.

In response to alkaline stress, *ZmNSA1* encodes an EF-hand calcium-binding protein that affects root proton efflux and Na^+ extrusion by negatively regulating the expression of plasma membrane H^+-ATPases [58]. Additionally, the Gγ protein SbAT1 (and its maize ortholog) has been shown to negatively regulate alkaline stress tolerance by influencing the phosphorylation of the aquaporin PIP2 and H_2O_2 efflux; its knockout significantly improves maize survival rate (Figure 3) [59]. Meanwhile, other mechanisms collectively constitute the saline–alkali tolerance network in maize. Metabolomic analyses have identified several marker metabolites associated with osmotic stress resistance and revealed that functional variations in genes such as *ZmCS3*, *ZmUGT*, and *ZmCYP709B2* correlate with salt tolerance [60]. Overexpression of the glycine betaine synthesis-related gene *ZmGB1* and the raffinose synthesis gene *ZmGolS1* both enhance salt tolerance [61,62]. At the signal transduction level, *ZmMPK3* can phosphorylate and stabilize the transcription factor ZmGRF1, forming a signaling module that regulates saline–alkali tolerance [63].

https://doi.org/10.3390/plants15040532

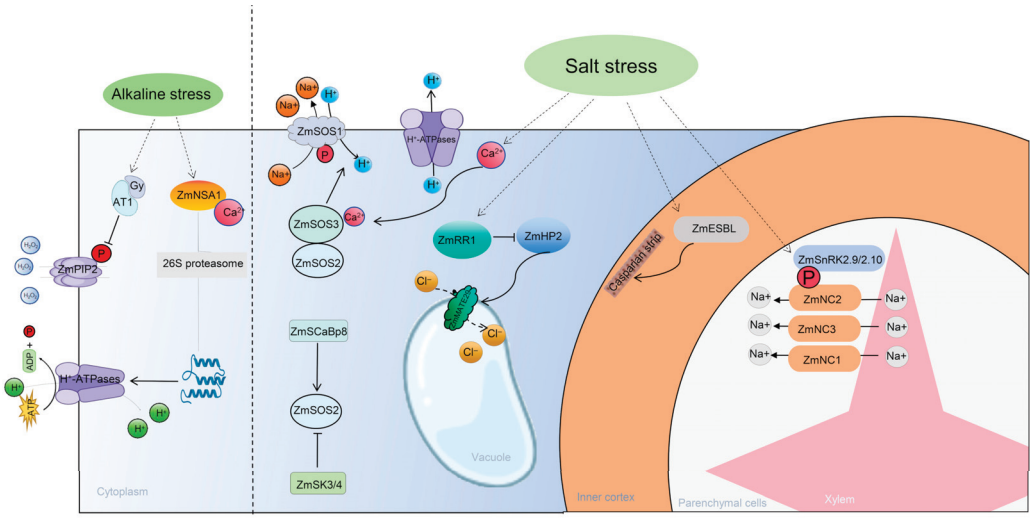

Figure 3. Research advances in maize tolerance to saline–alkali stress. Salt stress triggers an increase in cytosolic Ca^{2+} concentration, which activates the SOS signaling pathway and consequently enhances ZmSOS1-mediated root Na^+ efflux. Salt stress promotes the degradation of ZmRR1, alleviating its inhibitory effect on *ZmHP2*. The enhanced cytokinin signaling pathway mediated by *ZmHP2* upregulates the transcription of *ZmMATE29*, facilitating Cl^- sequestration into the vacuoles of root cortical cells. This process reduces Cl^- accumulation in the shoots and improves salt tolerance in maize. Salt stress leads to increased transcription of *ZmESBL*, which promotes the development of the Casparian strip and strengthens its barrier function. This enhanced barrier prevents excessive Na^+ from entering the root stele via the apoplastic pathway while promoting Na^+ exclusion from the shoots, thereby improving maize salt tolerance. Na^+-selective transporters (ZmNC1, ZmNC2, ZmNC3, and ZmHAK11) unload Na^+ from the xylem into surrounding parenchyma cells, thereby enhancing shoot Na^+ exclusion and salt tolerance in maize. Under alkaline stress, AT1 pairs with the G-protein β subunit, reducing the phosphorylation of the plasma membrane aquaporin PIP2 and decreasing its H_2O_2 efflux activity. This leads to elevated intracellular ROS levels, resulting in a severely alkaline-sensitive phenotype. Concurrently, Ca^{2+} binds to ZmNSA1 and induces its degradation via the 26S proteasome pathway. The degradation of ZmNSA1 subsequently increases the transcription levels of MHAs (plasma membrane H^+-ATPases), promoting H^+ efflux.

5. The Molecular Mechanisms of Saline–Alkali Stress Tolerance in Wheat

As one of the world's most important cereal crops, the stable production of wheat is crucial for ensuring global food security. However, saline–alkali stress severely restricts its cultivation area and production potential. To address this challenge, wheat has evolved a series of complex physiological and molecular adaptation mechanisms during its long-term evolution. Its saline–alkali tolerance is a complex quantitative trait controlled by multiple genes, involving the synergistic action of multiple layers, including the accumulation of osmotic adjustment compounds, regulation of ion homeostasis, scavenging of reactive oxygen species (ROS), and hormonal signaling networks. In terms of osmotic adjustment, wheat initiates the primary stress response by activating the calcium signaling system, which includes proteins such as CaM, CML, CDPK, CBL, and CIPK. Studies have shown that overexpression of *TaCAM2-D* significantly enhances dual tolerance to both drought and saline–alkali stress, whereas silencing *TaCDPK27* leads to impaired root development and increased salt sensitivity in wheat seedlings [64]. Concurrently, wheat maintains cell turgor by accumulating osmolytes like proline. The expression of *TaP5CS*, a key gene in proline biosynthesis, is significantly upregulated under saline–alkali stress. This process is finely regulated by various transcription factors, including TaMYB, TaPIMP1, and TaPTF1, forming a complex osmotic protection network (Figure 4) [65–67]. Saline–alkali tolerance-

related genes *TaSC* and *TaSRG* play key roles in osmotic adjustment by regulating the rate of proline biosynthesis.

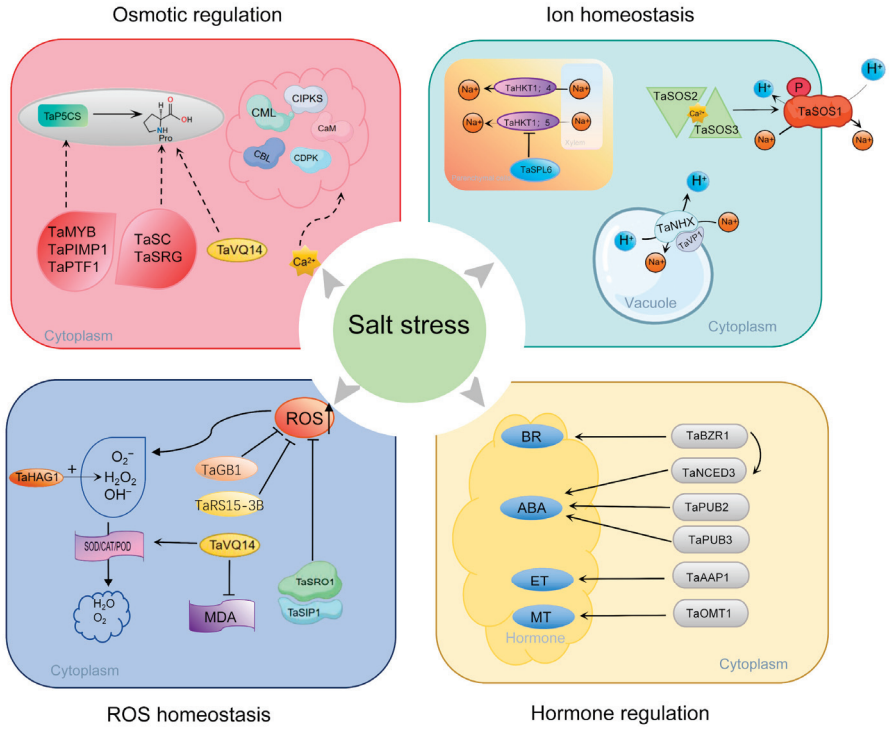

Figure 4. Research advances in wheat tolerance to saline–alkali stress. Under saline–alkali stress, the rapid increase in salt concentration around wheat roots induces osmotic stress, leading to the activation of hyperosmosensors. This triggers calcium ion signaling and initiates a series of responses involving *CDPKs*, *CBLs*, and *CIPKs*. The upregulated expression of proline biosynthesis-related genes such as *TaMYB*, *TaPIMP1*, *TaPTF1*, and *TaSC* promotes proline accumulation, enhancing wheat tolerance to saline–alkali and osmotic stress. Ca^{2+} binds to SOS3 and SOS2, activating SOS1 through phosphorylation. The activated SOS1 facilitates the efflux of Na^+ into the xylem apoplast or soil. The NHX (Na^+/H^+ antiporter) family plays a critical role in sequestering Na^+ into vacuoles. Furthermore, under saline–alkali stress, the key agronomic trait-related factor TaSRO1 in wheat enhances ROS scavenging capacity. Antioxidant enzymes such as SOD, CAT, and POD are utilized to eliminate excess reactive oxygen species and mitigate oxidative stress. Hormones, including ABA, ET, BR, and MT, also play regulatory roles in the response to saline–alkali stress.

In maintaining ion homeostasis, wheat employs multiple coordinated pathways to regulate Na^+ transport and compartmentalization. The high-affinity potassium transporters TaHKT1;5 and TaHKT1;4 transfer Na^+ from the xylem to surrounding parenchyma cells, effectively reducing Na^+ transport to the shoots [15,68]. This process is finely regulated by the transcription factor TaSPL6. The allelic variant *TaSPL6-DIn*, which contains an insertion mutation, loses its inhibitory effect on TaHKT1;5, thereby enhancing plant saline–alkali tolerance (Figure 4) [69,70]. The classic SOS signaling pathway plays a central role in plasma membrane Na^+ efflux. *TaSOS1* has been confirmed to possess Na^+/H^+ exchange activity in yeast and transgenic tobacco, and it improves saline–alkali tolerance [71]. Furthermore, the vacuolar membrane Na^+/H^+ antiporter family TaNHX, in coordination with the proton pump TaVP1, sequesters excess Na^+ into the vacuole, effectively alleviating cytosolic Na^+ toxicity [72]. Research indicates that coexpression of *TaNHX1* and *TaVP1* significantly enhances saline–alkali tolerance in transgenic plants.

Regarding ROS balance, wheat relies on both enzymatic and non-enzymatic antioxidant systems to maintain redox homeostasis. Key antioxidant enzymes include SOD, CAT, and POD. *TaVQ14* effectively reduces oxidative damage by increasing the activities of

CAT and SOD, raising proline content, and simultaneously decreasing malondialdehyde (MDA) levels (Figure 4) [73]. Genes such as *TaGB1* and *TaRS15-3B* also enhance saline–alkali tolerance by boosting the functionality of the antioxidant system. It is noteworthy that ROS plays a dual role in plant stress responses: excessive accumulation causes oxidative damage, whereas moderate accumulation acts as a signaling molecule to activate defense mechanisms [74,75]. The histone acetyltransferase TaHAG1 positively regulates saline–alkali tolerance by modulating the transcription of genes related to H_2O_2 production [76]. Meanwhile, the TaSRO1-TaSIP1 protein interaction module ensures the stress response is not overactivated through precise negative regulation of ROS signaling; the balance of this module is crucial for plant survival (Figure 4) [77].

Plant hormones act as central hubs in integrating saline–alkali stress signals and regulating the global response. ABA, a key stress hormone, has its signal transduction mediated by E3 ubiquitin ligases such as TaPUB2 and TaPUB3 [78]. In the ethylene biosynthesis pathway, *TaAAP1* enhances ethylene levels, improving saline–alkali tolerance during wheat germination and the seedling stage [79]. The core transcription factor TaBZR1 in the brassinosteroid signaling pathway directly activates *TaNCED3*, a key gene in ABA synthesis, as well as ROS-scavenging genes *TaGPX2* and *TaGPX3*, thereby mediating the crosstalk of hormone signals and synergistic enhancement of antioxidant defense [80]. Additionally, the melatonin synthesis gene *TaOMT1* enhances the antioxidant system by elevating endogenous melatonin levels, playing a significant role in re-establishing redox homeostasis (Figure 4) [81]. These findings provide a new theoretical basis for in-depth analysis of the molecular mechanisms of saline–alkali tolerance in wheat and lay an important foundation for the molecular breeding of saline–alkali-tolerant wheat varieties.

6. Comparative Analysis of Molecular Mechanisms in Plant Response to Saline–Alkali Stress

Saline–alkali stress is one of the major abiotic stressors facing global agricultural production [19]. Understanding plant tolerance mechanisms is crucial for breeding stress-resistant crop varieties. Research using *A. thaliana* as a model plant has provided a fundamental theoretical framework and candidate gene resources for plant biology [5]. However, applying findings from this model plant to staple crop breeding requires careful consideration of significant differences in physiological structure, photosynthetic pathways, and ecological adaptation [82].

Ion homeostasis maintenance is a fundamental survival mechanism for all plants. This process is typically achieved through SOS pathway-mediated intracellular Na^+ efflux and vacuolar membrane NHX-type Na^+/H^+ antiporter-mediated vacuolar sequestration (Table 1) [83]. *A. thaliana* has a relatively simple root system architecture, and its saline–alkali tolerance primarily relies on cellular-level regulation, with overall root salt exclusion capacity being relatively weak [84]. In contrast, cereal crops have evolved more complex regulatory strategies involving root and vascular systems. As a salt-sensitive crop, rice's saline–alkali tolerance largely depends on root salt exclusion capacity and selective Na^+ transport in stem nodes [85]. Tolerant rice varieties effectively limit initial Na^+ uptake through outer root cells, and their stem nodes function as efficient "ion filters." Transporters like OsHKT1;5 reload Na^+ from the xylem sap into surrounding parenchyma cells, sequestering it in lower leaf sheaths and older leaves, thereby minimizing Na^+ transport to photosynthetically active new leaves and reproductive organs (Table 1) [86,87]. Maize and wheat, also belonging to the Poaceae family, employ a different strategies: both exhibit moderate root salt exclusion capacity but emphasize tissue-level ion compartmentalization, effectively isolating absorbed Na^+ in older leaves as an adaptive strategy of sacrificing older leaves to protect new ones [88]. Additionally, maize maintains a high K^+/Na^+ ratio

through an efficient K^+ uptake system, forming an important physiological basis for its tolerance, while tolerant wheat varieties retain Na^+ in roots and basal stem nodes via genes such as TaHKT1;5 (Table 1) [15,36,68].

Differences in photosynthetic pathways represent another key factor in the divergence of saline–alkali tolerance strategies. *A. thaliana*, rice, and wheat are all C3 plants; under saline–alkali stress, stomatal closure leads to CO_2 deficiency, significantly inhibiting photosynthesis (Table 1) [89]. As a C4 plant, maize can efficiently fix low-concentration CO_2 in mesophyll cells via phosphoenolpyruvate carboxylase (PEPC), forming C4 acids (e.g., malate). These acids are then transported to bundle sheath cells for decarboxylation, releasing concentrated CO_2 to create a localized high-CO_2 microenvironment around Rubisco. This mechanism directly ensures the efficient operation of the Calvin cycle even under partially closed stomatal conditions, thereby maintaining relatively stable photosynthetic efficiency [90,91]. Meanwhile, due to the CO_2-concentrating mechanism, maize's reliance on stomatal conductance is reduced. This means that maize requires fewer open stomata to acquire the same amount of CO_2, significantly minimizing water loss through transpiration [92]. In saline–alkaline environments, this characteristic allows maize to utilize limited water resources more efficiently, maintain cellular turgor pressure and basic metabolic activities, and delay dehydration damage. Therefore, the C4 photosynthetic pathway not only directly safeguards energy synthesis by "maintaining CO_2 supply," but also optimizes the balance between "carbon acquisition and water loss." Overall, this enhances the plant's physiological resilience and survival capacity under stress conditions.

At the molecular regulatory level, homology and specificity coexist. Key transcription factor families identified in *A. thaliana*—such as DREB/CBF, NAC, MYB, and WRKY—are involved in the saline–alkali stress response in all three crops. For example, overexpression of *OsDREB* or *OsNAC1* significantly enhances rice tolerance [93,94]. However, the regulatory networks in crops are more complex and are linked to specific agronomic traits and developmental stages. Saline–alkali tolerance in crops like wheat and barley is closely associated with chromosomal loci such as Kna1 and Nax, which often encode HKT-type transporters, highlighting the central role of natural structural gene variation (Table 1) [95]. Breeding selection pressures have also shaped unique allelic variation pools, leading to diversification and specialization in the molecular basis of tolerance [39].

In summary, *A. thaliana*, rice, maize, and wheat share a conserved cellular and molecular "toolkit," including mechanisms for ion homeostasis, osmotic adjustment, and antioxidant defense. The primary differences lie in higher-level physiological and structural adaptations: rice relies on a sophisticated filtration system built by its roots and stem nodes; maize benefits from the high efficiency of the C4 photosynthetic pathway and strong osmotic adjustment capacity; and both maize and wheat excel at tissue-level ion compartmentalization.

Table 1. Comparative analysis of saline–alkali tolerance mechanisms among *A. thaliana*, rice, maize, and wheat.

Mechanism Category	*A. thaliana*	Rice	Maize	Wheat	References
Classification	Dicotyledon, Brassicaceae.	Monocotyledon, Poaceae.	Monocotyledon, Poaceae.	Monocotyledon, Poaceae.	[96]
Root Salt Exclusion	Regulation by ion channels and transporters on the cell membrane.	Synergistic action of cortical and endodermal cells to reduce Na^+ upward transport.	Developed root structure that effectively reduces partial Na^+ uptake.	Root exudates and root architecture contribute to salt exclusion.	[22,85,88]

Table 1. *Cont.*

Mechanism Category	*A. thaliana*	Rice	Maize	Wheat	References
Na^+ Selective Transport	The SOS pathway exports Na^+ from the cell or sequesters it into the vacuole; *AtHKT1;1* mediates xylem Na^+ unloading.	High expression of *OsHKT1;5* retrieves Na^+ from the xylem back into the perivascular cells, reducing shootward transport.	*ZmHKT1* and its homologous genes mediate xylem Na^+ unloading.	*TaHKT1;5*, *TaHKT2;1*, and their homologs regulate Na^+ transport and distribution.	[7,39,52,70]
Vacuolar Sequestration	Sequesters Na^+ into the vacuole via NHX-type Na^+/H^+ antiporters.	The OsNHX family, particularly *OsNHX1*, *OsNHX4*, and *OsNHX5*.	The *ZmNHX* family exhibits strong sequestration capacity in leaves, especially within bundle sheath cells.	The *TaNHX* family: tolerant varieties can sequester more Na^+ in the vacuoles of mesophyll cells.	[83]
Tissue-Level Compartmentalization	Not significant.	A key mechanism; stem nodes act as crucial "filters".	A key mechanism; capable of accumulating Na^+ in older leaves, protecting new leaves.	A key mechanism; employs a similar "sacrifice old leaves" strategy.	[36,57,72,88]
Major Compatible Solutes	Proline, glycine betaine, soluble sugars.	Proline, glycine betaine, soluble sugars.	Proline	Proline, glycine betaine, soluble sugars.	[26]
Photosynthetic Type	C3 plant, sensitive to CO_2 deficiency caused by stomatal closure.	C3 plant; stomatal conductance declines rapidly under salt stress, leading to significant photosynthesis inhibition.	C4 plant; maintains relatively high intercellular CO_2 concentration and stable photosynthesis even when stomata are partially closed.	C3 plant; sensitive to stomatal limitations, but carbon assimilation stability varies among cultivars.	[14,89]
Core Signaling	ABA is the core signal, regulating a large number of stress-responsive genes.	The ABA signaling pathway is crucial, regulating stomatal closure and tolerance gene expression.	ABA signaling is core, but its interaction with hormones like JA and BR may be crop-specific.	ABA signaling is core, and its balance with hormones like cytokinin influences the senescence process.	[29,46,78]
Key Transcription Factors	*DREB/CBF*, *NAC*, *MYB*, *WRKY*, etc.	*OsDREB*, *OsNAC*, *OsbZIP*, etc.	*ZmDREB*, *ZmbZIP*, *ZmNAC*, etc.	*TaDREB*, *TaNAC*, *TaWRKY*, etc.	[31,44,48,63,94]

7. Perspectives

With the ongoing intensification of global climate change and cropland salinization–alkalinization, research on plant saline–alkali tolerance is progressively transitioning from fundamental mechanism exploration to a critical phase of targeted crop improvement [19]. However, current research still faces challenges, including the translational bottleneck from model systems to crop application and deeper issues such as the coordinated regulation of multiple genes and the integration of species-specific adaptation mechanisms [82]. Future studies should place greater emphasis on shifting from "gene characterization" to

"system design," constructing crop-specific saline–alkali tolerance regulatory networks by integrating multi-omics data and systems biology approaches [32]. This entails not only an in-depth investigation into the functional divergence and regulatory logic of core gene families like *SOS*, *NHX*, and *HKT* across different crop genetic backgrounds but also consideration of their complexities at the levels of tissue-specific expression, allelic variation, and post-transcriptional modifications. This will lay a solid theoretical foundation for achieving genuine "molecular design breeding" [16].

Concurrently with the deepening of mechanistic research, the precise regulation of crop-specific stress-tolerant structures will become a vital direction for future breeding. Staple food crops have developed unique saline–alkali tolerance structures through long-term evolution and artificial selection, such as the "ion filter" in rice stem nodes, the Casparian strip barrier in maize roots, and the ion retention zones in wheat basal internodes. These structures serve as crucial vehicles for crops to cope with saline–alkali stress at the whole-plant level. Utilizing gene-editing technologies to precisely regulate genes governing the development and function of these structures—for instance, enhancing the expression efficiency of *OsHKT1;5* in rice stem nodes or optimizing the *ZmSTL1*-mediated lignification degree of the Casparian strip in maize—can achieve a leap from cellular tolerance to whole-plant structural adaptation. Furthermore, as saline–alkali tolerance is a typical complex quantitative trait, its improvement urgently requires the integration and pyramiding of multi-layered tolerance mechanisms. Future breeding strategies should no longer be confined to stacking single genes or pathways but should focus on the synergistic optimization of multiple systems, including ion homeostasis, osmotic adjustment, antioxidant defense, hormone signaling networks, and photosynthetic carbon metabolism. For example, through multi-gene stacking strategies, cellular-level osmotic adjustment capacity (e.g., efficient proline synthesis) can be organically integrated with whole-plant structural adaptations (e.g., maintenance of the C4 photosynthetic system and organ-level ion compartmentalization) to develop new germplasm with broad-spectrum and durable stress resilience. This necessitates closer collaboration between breeders and molecular biologists to establish cross-scale trait integration and evaluation systems.

Moreover, fully exploiting and utilizing the natural variation harbored within crop germplasm resources is another key to breaking through the bottlenecks in saline–alkali tolerance breeding [95]. With decreasing costs of genome sequencing and advances in functional genomics technologies, resequencing core germplasm resources combined with GWAS and mutant library screening enables the efficient identification of superior alleles key to regulating ion transport, sequestration efficiency, and stress signal transduction [97]. Employing gene editing-assisted rapid domestication strategies to introduce these natural variants or artificially optimized versions into elite cultivar backgrounds will significantly accelerate the development and selection of saline–alkali tolerant varieties [98].

In recent years, gene-editing technologies such as CRISPR/Cas9 have provided revolutionary tools for precisely improving salt–alkaline tolerance within the genetic background of staple crops. Compared to traditional breeding methods, CRISPR/Cas9 technology can shorten the breeding cycle, thereby significantly reducing costs. At the same time, CRISPR/Cas9 is more accurate than conventional breeding, as it only induces mutations in target genes without altering others. For instance, using CRISPR-Cas9 to target and knock out the negative regulator *OsRR22* in rice significantly enhances the plant's salt tolerance [99,100] and editing the drought- and salt-tolerant gene *OsDST* improves salt–alkaline tolerance in the indica rice cultivar MTU1010 [101]. In wheat, leveraging the polyploid nature of the crop, CRISPR-Cas9-mediated simultaneous editing of TaSPL6 in the A, B, and D subgenomes can alleviate its inhibition of TaHKT1;5, thereby enhancing Na^+ retention without affecting yield-related traits [70]. In maize, precise editing of the promoter

regions of *ZmSK3/ZmSK4* or *ZmHKT2* can release their suppression of the SOS pathway or optimize ion transport efficiency [51]. Moreover, with the maturation of base editing and prime editing technologies, it has become possible to achieve precise substitution of specific amino acid sites without generating DNA double-strand breaks. For example, targeted evolution of the transmembrane domains of *OsHKT1;5* or *ZmHKT1;1* can optimize their Na^+/K^+ transport selectivity [56]. In the future, combining genome-wide CRISPR screening with machine learning predictions holds promise for discovering more conserved or species-specific regulatory nodes for salt–alkaline tolerance, enabling an upgrade from single-gene editing to precise multi-gene regulatory networks. This approach will facilitate the development of new high-yield and stable cereal varieties adapted to marginal soils.

On the basis of systematically deciphering the molecular mechanisms of plant intrinsic saline–alkaline tolerance, harnessing beneficial rhizospheric and endophytic microorganisms to enhance plant salt resistance has emerged as a promising ecological strategy to improve crop productivity in saline–alkaline environments through microbiome research. Existing studies indicate that core microbial groups in the rhizosphere community, such as Pseudomonas, show significantly higher abundance under salt stress. Functional profiling reveals a significant enrichment of pathways related to energy metabolism, ABC transporters, amino acid biosynthesis, and ion regulation. These functional traits are directly linked to microbial adaptation to salt stress and their plant growth-promoting effects, including phosphorus solubilization, nitrogen fixation, and the synthesis of ACC deaminase and IAA. Notably, Pseudomonas aeruginosa isolated from the rhizosphere of Spartina alterniflora has demonstrated efficient phosphorus solubilization, nitrogen fixation, and high salt tolerance [102]. Utilizing beneficial rhizospheric and endophytic microorganisms as bio-inoculants to regulate the rhizosphere microenvironment, enhance nutrient uptake and stress tolerance in plants, and thereby construct a synergistic "plant-microbe" system represents a sustainable and efficient bioremediation pathway for increasing crop yield in saline–alkaline soils.

However, transitioning from laboratory breakthroughs to large-scale field applications presents multiple practical challenges for these technologies. First, the target trait is regulated by multiple factors, involving a complex quantitative genetic basis and often exhibiting genetic trade-offs with agronomic traits such as yield and quality. Second, field salinity stress is characterized by high spatiotemporal heterogeneity and is frequently intertwined with other stressors such as drought and nutrient deficiencies, necessitating crops with comprehensive stress resilience. Third, strong genotype-by-environment interactions mean that gene effects validated in controlled settings may exhibit unstable expression or diminished efficacy in the complex field environment. Additionally, regulatory policies and public acceptance of genetically modified crops constitute significant constraints for commercialization. To address these challenges, future sustainable solutions should focus on multidimensional synergistic innovations: at the strategic level, promoting a "crop-centric" systematic design breeding approach to synergistically optimize complete stress response pathways—from ion homeostasis to photosynthetic efficiency—through genomic selection and multi-gene stacking technologies; at the technical level, employing multi-candidate gene combination analyses to identify robust gene combinations that perform consistently across diverse stress scenarios; at the resource level, enhancing the exploration and utilization of hidden genetic variation in wild relatives and local landraces. Only through the integrated cycle of in-depth molecular mechanism elucidation, breakthroughs in intelligent breeding technologies, and field adaptability validation can we develop a new generation of crop varieties truly suited to saline–alkaline ecosystems and capable of achieving sustainable production.

https://doi.org/10.3390/plants15040532

In summary, future research on plant saline–alkali tolerance must steadfastly adhere to a "crop-centric" path, deeply integrating cutting-edge basic biology with the practical needs of breeding. Through interdisciplinary convergence and technology integration, we can gradually achieve precise design, systematic optimization, and smart breeding of saline–alkali tolerance traits. Only in this way can a solid bridge be built between the sustainable utilization of saline–alkali land resources and global food security, providing core technological support for constructing a climate-resilient modern agricultural system.

Author Contributions: Conceptualization, J.H., J.Z. and D.X.; writing—original draft preparation, D.F., J.R. and Q.X.; writing—review and editing, D.F., J.R., Q.X., J.Y., Y.W., X.T., Z.L., Y.C., D.X, J.Z. and J.H.; funding acquisition, J.H. and J.Z. All authors have read and agreed to the published version of the manuscript.

Funding: This project was funded by the National Key R&D Program of China (Grant No. 2024YFF1000600), the Nanfan special project of CAAS (YBXM2435), the Biological Breeding National Science and Technology Major Project (Grant No. 2023ZD040662), and the Zhejiang Provincial Natural Science Foundation (Grant No. LQN25C130011).

Data Availability Statement: No new data were created or analyzed in this study.

Conflicts of Interest: The authors declare no conflicts of interest.

References

1. Ashraf, M.; Munns, R. Evolution of approaches to increase the salt tolerance of crops. *Crit. Rev. Plant Sci.* **2022**, *41*, 128–160. [CrossRef]
2. Ismail, A.M.; Horie, T. Genomics, physiology, and molecular breeding approaches for improving salt tolerance. *Annu. Rev. Plant Biol.* **2017**, *68*, 405–434. [CrossRef]
3. Van Zelm, E.; Zhang, Y.; Testerink, C. Salt tolerance mechanisms of plants. *Annu. Rev. Plant Biol.* **2020**, *71*, 403–433. [CrossRef]
4. Weigel, D.; Glazebrook, J. *Arabidopsis: A Laboratory Manual*; Cold Spring Harbor Laboratory Press: Woodbury, NY, USA, 2002; p. 354.
5. Zhu, J.-K. Salt and drought stress signal transduction in plants. *Annu. Rev. Plant Biol.* **2002**, *53*, 247–273. [CrossRef]
6. Apse, M.P.; Aharon, G.S.; Snedden, W.A.; Blumwald, E. Salt tolerance conferred by overexpression of a vacuolar Na^+/H^+ antiport in Arabidopsis. *Science* **1999**, *285*, 1256–1258. [CrossRef]
7. Mäser, P.; Eckelman, B.; Vaidyanathan, R.; Horie, T.; Fairbairn, D.J.; Kubo, M.; Yamagami, M.; Yamaguchi, K.; Nishimura, M.; Uozumi, N. Altered shoot/root Na^+ distribution and bifurcating salt sensitivity in Arabidopsis by genetic disruption of the Na^+ transporter *AtHKT1*. *FEBS Lett.* **2002**, *531*, 157–161. [CrossRef] [PubMed]
8. Rus, A.; Baxter, I.; Muthukumar, B.; Gustin, J.; Lahner, B.; Yakubova, E.; Salt, D.E. Natural variants of *AtHKT1* enhance Na^+ accumulation in two wild populations of Arabidopsis. *PLoS Genet.* **2006**, *2*, e210. [CrossRef] [PubMed]
9. Yamaguchi-Shinozaki, K.; Shinozaki, K. Transcriptional regulatory networks in cellular responses and tolerance to dehydration and cold stresses. *Annu. Rev. Plant Biol.* **2006**, *57*, 781–803. [CrossRef] [PubMed]
10. Nakashima, K.; Takasaki, H.; Mizoi, J.; Shinozaki, K.; Yamaguchi-Shinozaki, K. NAC transcription factors in plant abiotic stress responses. *Biochim. Biophys. Acta Gene Regul. Mech.* **2012**, *1819*, 97–103. [CrossRef]
11. Kitomi, Y.; Itoh, J.-I.; Uga, Y. Genetic mechanisms involved in the formation of root system architecture. In *Rice Genomics, Genetics and Breeding*; Springer: Berlin/Heidelberg, Germany, 2018; pp. 241–274.
12. Zhang, H.; Zhu, J.; Gong, Z.; Zhu, J.-K. Abiotic stress responses in plants. *Nat. Rev. Genet.* **2022**, *23*, 104–119. [CrossRef]
13. Krishnamurthy, P.; Ranathunge, K.; Franke, R.; Prakash, H.; Schreiber, L.; Mathew, M. The role of root apoplastic transport barriers in salt tolerance of rice (*Oryza sativa* L.). *Planta* **2009**, *230*, 119–134. [CrossRef]
14. Stefanov, M.A.; Rashkov, G.D.; Yotsova, E.K.; Borisova, P.B.; Dobrikova, A.G.; Apostolova, E.L. Effects of Salt Stress on the Photosynthesis of Maize and Sorghum. *Ecol. Balkan.* **2020**, *12*, 147–154. Available online: http://web.uni-plovdiv.bg/mollov/EB/2020_SE3/147-154_eb.20SE313.pdf (accessed on 1 February 2026).
15. Byrt, C.S.; Xu, B.; Krishnan, M.; Lightfoot, D.J.; Athman, A.; Jacobs, A.K.; Watson-Haigh, N.S.; Plett, D.; Munns, R.; Tester, M. The Na^+ transporter, TaHKT 1; 5-D, limits shoot Na^+ accumulation in bread wheat. *Plant J.* **2014**, *80*, 516–526. [CrossRef] [PubMed]
16. Bailey-Serres, J.; Parker, J.E.; Ainsworth, E.A.; Oldroyd, G.E.; Schroeder, J.I. Genetic strategies for improving crop yields. *Nature* **2019**, *575*, 109–118. [CrossRef] [PubMed]
17. Meyerowitz, E.M. Prehistory and history of Arabidopsis research. *Plant Physiol.* **2001**, *125*, 15–19. [CrossRef]

18. Koornneef, M.; Meinke, D. The development of Arabidopsis as a model plant. *Plant J.* **2010**, *61*, 909–921. [CrossRef]
19. Zhu, J.-K. Abiotic stress signaling and responses in plants. *Cell* **2016**, *167*, 313–324. [CrossRef]
20. Quan, R.; Lin, H.; Mendoza, I.; Zhang, Y.; Cao, W.; Yang, Y.; Shang, M.; Chen, S.; Pardo, J.M.; Guo, Y. SCABP8/CBL10, a putative calcium sensor, interacts with the protein kinase SOS2 to protect Arabidopsis shoots from salt stress. *Plant Cell* **2007**, *19*, 1415–1431. [CrossRef]
21. Halfter, U.; Ishitani, M.; Zhu, J.-K. The Arabidopsis SOS2 protein kinase physically interacts with and is activated by the calcium-binding protein SOS3. *Proc. Natl. Acad. Sci. USA* **2000**, *97*, 3735–3740. [CrossRef]
22. Qiu, Q.-S.; Guo, Y.; Dietrich, M.A.; Schumaker, K.S.; Zhu, J.-K. Regulation of SOS1, a plasma membrane Na^+/H^+ exchanger in *Arabidopsis thaliana*, by SOS2 and SOS3. *Proc. Natl. Acad. Sci. USA* **2002**, *99*, 8436–8441. [CrossRef] [PubMed]
23. Qiu, Q.-S.; Guo, Y.; Quintero, F.J.; Pardo, J.M.; Schumaker, K.S.; Zhu, J.-K. Regulation of vacuolar Na^+/H^+ exchange in *Arabidopsis thaliana* by the salt-overly-sensitive (SOS) pathway. *J. Biol. Chem.* **2004**, *279*, 207–215. [CrossRef]
24. Sunarpi, X.; Horie, T.; Motoda, J.; Kubo, M.; Yang, H.; Yoda, K.; Horie, R.; Chan, W.Y.; Leung, H.Y.; Hattori, K. Enhanced salt tolerance mediated by *AtHKT1* transporter-induced Na^+ unloading from xylem vessels to xylem parenchyma cells. *Plant J.* **2005**, *44*, 928–938. [CrossRef] [PubMed]
25. Szabados, L.; Savouré, A. Proline: A multifunctional amino acid. *Trends Plant Sci.* **2010**, *15*, 89–97. [CrossRef]
26. Chen, T.H.; Murata, N. Glycinebetaine protects plants against abiotic stress: Mechanisms and biotechnological applications. *Plant Cell Environ.* **2011**, *34*, 1–20. [CrossRef]
27. Pnueli, L.; Liang, H.; Rozenberg, M.; Mittler, R. Growth suppression, altered stomatal responses, and augmented induction of heat shock proteins in cytosolic ascorbate peroxidase (Apx1)-deficient Arabidopsis plants. *Plant J.* **2003**, *34*, 187–203. [CrossRef]
28. Mittler, R.; Vanderauwera, S.; Gollery, M.; Van Breusegem, F. Reactive oxygen gene network of plants. *Trends Plant Sci.* **2004**, *9*, 490–498. [CrossRef]
29. Cutler, S.R.; Rodriguez, P.L.; Finkelstein, R.R.; Abrams, S.R. Abscisic acid: Emergence of a core signaling network. *Annu. Rev. Plant Biol.* **2010**, *61*, 651–679. [CrossRef] [PubMed]
30. Park, S.-Y.; Fung, P.; Nishimura, N.; Jensen, D.R.; Fujii, H.; Zhao, Y.; Lumba, S.; Santiago, J.; Rodrigues, A.; Chow, T.-F.F. Abscisic acid inhibits type 2C protein phosphatases via the PYR/PYL family of START proteins. *Science* **2009**, *324*, 1068–1071. [CrossRef]
31. Peng, J.; Li, Z.; Wen, X.; Li, W.; Shi, H.; Yang, L.; Zhu, H.; Guo, H. Salt-induced stabilization of EIN3/EIL1 confers salinity tolerance by deterring ROS accumulation in Arabidopsis. *PLoS Genet.* **2014**, *10*, e1004664. [CrossRef] [PubMed]
32. Yang, Y.; Guo, Y. Elucidating the molecular mechanisms mediating plant salt-stress responses. *New Phytol.* **2018**, *217*, 523–539. [CrossRef]
33. Yang, Y.; Wu, Y.; Ma, L.; Yang, Z.; Dong, Q.; Li, Q.; Ni, X.; Kudla, J.; Song, C.; Guo, Y. The Ca^{2+} sensor SCaBP3/CBL7 modulates plasma membrane H^+-ATPase activity and promotes alkali tolerance in Arabidopsis. *Plant Cell* **2019**, *31*, 1367–1384. [CrossRef]
34. Zhang, H.; Yu, F.; Xie, P.; Sun, S.; Qiao, X.; Tang, S.; Chen, C.; Yang, S.; Mei, C.; Yang, D.; et al. A Gγ protein regulates alkaline sensitivity in crops. *Science* **2023**, *379*, 6638. [CrossRef]
35. Singhal, R.K.; Sodani, R.; Chauhan, J.; Sharma, M.K.; Yashu, B.R. Physiological adaptation and tolerance mechanism of rice (*Oryza sativa* L.) in multiple abiotic stresses. *Int. J. Pure App. Biosci.* **2017**, *5*, 459–466.
36. Assaha, D.V.; Ueda, A.; Saneoka, H.; Al-Yahyai, R.; Yaish, M.W. The role of Na^+ and K^+ transporters in salt stress adaptation in glycophytes. *Front. Physiol.* **2017**, *8*, 509. [CrossRef]
37. Martínez-Atienza, J.; Jiang, X.; Garciadeblas, B.; Mendoza, I.; Zhu, J.-K.; Pardo, J.M.; Quintero, F.J. Conservation of the salt overly sensitive pathway in rice. *Plant Physiol.* **2007**, *143*, 1001–1012. [CrossRef]
38. Fukuda, A.; Nakamura, A.; Tagiri, A.; Tanaka, H.; Miyao, A.; Hirochika, H.; Tanaka, Y. Function, intracellular localization, and the importance in salt tolerance of a vacuolar Na^+/H^+ antiporter from rice. *Plant Cell Physiol.* **2004**, *45*, 146–159. [CrossRef] [PubMed]
39. Ren, Z.; Gao, J.; Li, L.; Cai, X.; Huang, W.; Chao, D.; Zhu, M.; Wang, Z.; Luan, S.; Lin, H. A rice quantitative trait locus for salt tolerance encodes a sodium transporter. *Nat. Genet.* **2005**, *37*, 1141–1146. [CrossRef] [PubMed]
40. Diédhiou, C.; Golldack, D. Salt-dependent regulation of chloride channel transcripts in rice. *Plant Sci.* **2006**, *170*, 793–800. [CrossRef]
41. Kavi Kishor, P.B.; Hima Kumari, P.; Sunita, M.; Sreenivasulu, N. Role of proline in cell wall synthesis and plant development and its implications in plant ontogeny. *Front. Plant Sci.* **2015**, *6*, 544. [CrossRef]
42. Hassan, M.U.; Nawaz, M.; Shah, A.N.; Raza, A.; Barbanti, L.; Skalicky, M.; Hashem, M.; Brestic, M.; Pandey, S.; Alamri, S. Trehalose: A key player in plant growth regulation and tolerance to abiotic stresses. *J. Plant Growth Regul.* **2023**, *42*, 4935–4957. [CrossRef]
43. Isah, T. Stress and defense responses in plant secondary metabolites production. *Biol. Res.* **2019**, *52*, 39. [CrossRef] [PubMed]
44. Fang, S.; Hou, X.; Liang, X. Response mechanisms of plants under saline-alkali stress. *Front. Plant Sci.* **2021**, *12*, 667458. [CrossRef]
45. Wang, Q.; Shen, T.; Ni, L.; Chen, C.; Jiang, J.; Cui, Z.; Wang, S.; Xu, F.; Yan, R.; Jiang, M. Phosphorylation of *OsRbohB* by the protein kinase *OsDMI3* promotes H_2O_2 production to potentiate ABA responses in rice. *Mol. Plant* **2023**, *16*, 882–902. [CrossRef]

46. Saeng-ngam, S.; Takpirom, W.; Buaboocha, T.; Chadchawan, S. The role of the OsCam1-1 salt stress sensor in ABA accumulation and salt tolerance in rice. *J. Plant Biol.* **2012**, *55*, 198–208. [CrossRef]
47. Liu, X.; Xie, X.; Zheng, C.; Wei, L.; Li, X.; Jin, Y.; Zhang, G.; Jiang, C.-J.; Liang, Z. RNAi-mediated suppression of the abscisic acid catabolism gene OsABA8ox1 increases abscisic acid content and tolerance to saline–alkaline stress in rice (*Oryza sativa* L.). *Crop. J.* **2022**, *10*, 354–367. [CrossRef]
48. Jin, J.F.; Wang, Z.Q.; He, Q.Y.; Wang, J.Y.; Li, P.F.; Xu, J.M.; Zheng, S.J.; Fan, W.; Yang, J.L. Genome-wide identification and expression analysis of the NAC transcription factor family in tomato (*Solanum lycopersicum*) during aluminum stress. *BMC Genom.* **2020**, *21*, 288. [CrossRef] [PubMed]
49. Farooqi, M.Q.U.; Nawaz, G.; Wani, S.H.; Choudhary, J.R.; Rana, M.; Sah, R.P.; Afzal, M.; Zahra, Z.; Ganie, S.A.; Razzaq, A. Recent developments in multi-omics and breeding strategies for abiotic stress tolerance in maize (*Zea mays* L.). *Front. Plant Sci.* **2022**, *13*, 965878. [CrossRef]
50. Zhou, X.; Li, J.; Wang, Y.; Liang, X.; Zhang, M.; Lu, M.; Guo, Y.; Qin, F.; Jiang, C. The classical SOS pathway confers natural variation of salt tolerance in maize. *New Phytol.* **2022**, *236*, 479–494. [CrossRef]
51. Li, J.; Zhou, X.; Wang, Y.; Song, S.; Ma, L.; He, Q.; Lu, M.; Zhang, K.; Yang, Y.; Zhao, Q. Inhibition of the maize salt overly sensitive pathway by *ZmSK3* and *ZmSK4*. *J. Genet. Genom.* **2023**, *50*, 960–970. [CrossRef]
52. Zhang, M.; Liang, X.; Wang, L.; Cao, Y.; Song, W.; Shi, J.; Lai, J.; Jiang, C. A HAK family Na^+ transporter confers natural variation of salt tolerance in maize. *Nat. Plants* **2019**, *5*, 1297–1308. [CrossRef]
53. Zhang, M.; Li, Y.; Liang, X.; Lu, M.; Lai, J.; Song, W.; Jiang, C. A teosinte-derived allele of an *HKT1* family sodium transporter improves salt tolerance in maize. *Plant Biotechnol. J.* **2023**, *21*, 97–108. [CrossRef]
54. Zhang, M.; Cao, Y.; Wang, Z.; Wang, Z.Q.; Shi, J.; Liang, X.; Song, W.; Chen, Q.; Lai, J.; Jiang, C. A retrotransposon in an *HKT1* family sodium transporter causes variation of leaf Na^+ exclusion and salt tolerance in maize. *New Phytol.* **2018**, *217*, 1161–1176. [CrossRef] [PubMed]
55. Wang, Y.; Cao, Y.; Liang, X.; Zhuang, J.; Wang, X.; Qin, F.; Jiang, C. A dirigent family protein confers variation of Casparian strip thickness and salt tolerance in maize. *Nat. Commun.* **2022**, *13*, 2222. [CrossRef] [PubMed]
56. Cao, Y.; Liang, X.; Yin, P.; Zhang, M.; Jiang, C. A domestication-associated reduction in K^+-preferring *HKT* transporter activity underlies maize shoot K^+ accumulation and salt tolerance. *New Phytol.* **2019**, *222*, 301–317. [CrossRef]
57. Yin, P.; Liang, X.; Zhao, H.; Xu, Z.; Chen, L.; Yang, X.; Qin, F.; Zhang, J.; Jiang, C. Cytokinin signaling promotes salt tolerance by modulating shoot chloride exclusion in maize. *Mol. Plant* **2023**, *16*, 1031–1047. [CrossRef] [PubMed]
58. Cao, Y.; Zhang, M.; Liang, X.; Li, F.; Shi, Y.; Yang, X.; Jiang, C. Natural variation of an EF-hand Ca^{2+}-binding-protein coding gene confers saline-alkaline tolerance in maize. *Nat. Commun.* **2020**, *11*, 186. [CrossRef]
59. Wang, P.; Ma, J.F. Knockout of a gene encoding a Gγ protein boosts alkaline tolerance in cereal crops. *aBIOTECH* **2023**, *4*, 180–183. [CrossRef]
60. Liang, X.; Liu, S.; Wang, T.; Li, F.; Cheng, J.; Lai, J.; Qin, F.; Li, Z.; Wang, X.; Jiang, C. Metabolomics-driven gene mining and genetic improvement of tolerance to salt-induced osmotic stress in maize. *New Phytol.* **2021**, *230*, 2355–2370. [CrossRef]
61. Liu, S.; Yang, J.; Yin, C.; Mao, S.; Cheng, Q.; Yan, J.; Jiang, C.; Wang, X.; Liang, X.; Zhao, H. Identification of salt-responsive genetic variants using cross-condition multi-omics association analysis in maize. *Plant Commun.* **2025**, *6*, 101219. [CrossRef]
62. Liang, X.; Yin, P.; Li, F.; Cao, Y.; Jiang, C. *ZmGolS1* underlies natural variation of raffinose content and salt tolerance in maize. *J. Genet. Genom.* **2025**, *52*, 346–355. [CrossRef]
63. Yin, P.; Wang, H.; Ye, Z.; Li, Y.; Liang, X.; Jiang, C. The *ZmMPK3-ZmGRF1* module promotes maize growth by enhancing cell proliferation under salt stress. *Sci. Bull.* **2025**, *71*, 269–272. [CrossRef] [PubMed]
64. Yue, J.-Y.; Jiao, J.-L.; Wang, W.-W.; Wang, H.-Z. The calcium-dependent protein kinase TaCDPK27 positively regulates salt tolerance in wheat. *Int. J. Mol. Sci.* **2022**, *23*, 7341. [CrossRef]
65. Aycan, M.; Baslam, M.; Mitsui, T.; Yildiz, M. The *TaGSK1*, *TaSRG*, *TaPTF1*, and *TaP5CS* gene transcripts confirm salinity tolerance by increasing proline production in wheat (*Triticum aestivum* L.). *Plants* **2022**, *11*, 3401. [CrossRef]
66. Rahaie, M.; Xue, G.-P.; Naghavi, M.R.; Alizadeh, H.; Schenk, P.M. A MYB gene from wheat (*Triticum aestivum* L.) is up-regulated during salt and drought stresses and differentially regulated between salt-tolerant and sensitive genotypes. *Plant Cell Rep.* **2010**, *29*, 835–844. [CrossRef]
67. Zhang, Z.; Liu, X.; Wang, X.; Zhou, M.; Zhou, X.; Ye, X.; Wei, X. An R2R3 MYB transcription factor in wheat, *TaPIMP* 1, mediates host resistance to Bipolaris sorokiniana and drought stresses through regulation of defense-and stress-related genes. *New Phytol.* **2012**, *196*, 1155–1170. [CrossRef]
68. Tounsi, S.; Ben Amar, S.; Masmoudi, K.; Sentenac, H.; Brini, F.; Véry, A.-A. Characterization of two *HKT1*; 4 transporters from Triticum monococcum to elucidate the determinants of the wheat salt tolerance Nax1 QTL. *Plant Cell Physiol.* **2016**, *57*, 2047–2057. [CrossRef]
69. Coskun, D. SPOTLIGHT: *TaSPL6-D*, a transcriptional repressor of *TaHKT1; 5-D* in bread wheat (*Triticum aestivum* L.) and a novel target for improving salt tolerance in crops. *J. Plant Physiol.* **2024**, *303*, 154351. [CrossRef]

70. Wang, M.; Cheng, J.; Wu, J.; Chen, J.; Liu, D.; Wang, C.; Ma, S.; Guo, W.; Li, G.; Di, D. Variation in *TaSPL6-D* confers salinity tolerance in bread wheat by activating *TaHKT1; 5-D* while preserving yield-related traits. *Nat. Genet.* **2024**, *56*, 1257–1269. [CrossRef] [PubMed]
71. Xu, H.; Jiang, X.; Zhan, K.; Cheng, X.; Chen, X.; Pardo, J.M.; Cui, D. Functional characterization of a wheat plasma membrane Na^+/H^+ antiporter in yeast. *Arch. Biochem. Biophys.* **2008**, *473*, 8–15. [CrossRef] [PubMed]
72. Brini, F.; Hanin, M.; Mezghani, I.; Berkowitz, G.A.; Masmoudi, K. Overexpression of wheat Na^+/H^+ antiporter *TNHX1* and H^+-pyrophosphatase *TVP1* improve salt-and drought-stress tolerance in *Arabidopsis thaliana* plants. *J. Exp. Bot.* **2007**, *58*, 301–308. [CrossRef]
73. Cheng, X.; Yao, H.; Cheng, Z.; Tian, B.; Gao, C.; Gao, W.; Yan, S.; Cao, J.; Pan, X.; Lu, J. The wheat gene *TaVQ14* confers salt and drought tolerance in transgenic *Arabidopsis thaliana* plants. *Front. Plant Sci.* **2022**, *13*, 870586. [CrossRef]
74. Xiong, X.-X.; Liu, Y.; Zhang, L.-L.; Li, X.-J.; Zhao, Y.; Zheng, Y.; Yang, Q.-H.; Yang, Y.; Min, D.-H.; Zhang, X.-H. G-Protein β-subunit gene *TaGB1-B* enhances drought and salt resistance in wheat. *Int. J. Mol. Sci.* **2023**, *24*, 7337. [CrossRef] [PubMed]
75. Guo, J.; Yang, Y.; Wang, T.; Wang, Y.; Zhang, X.; Min, D.; Zhang, X. Analysis of Raffinose Synthase Gene Family in Bread Wheat and Identification of Drought Resistance and Salt Tolerance Function of *TaRS15-3B*. *Int. J. Mol. Sci.* **2023**, *24*, 11185. [CrossRef]
76. Zheng, M.; Lin, J.; Liu, X.; Chu, W.; Li, J.; Gao, Y.; An, K.; Song, W.; Xin, M.; Yao, Y. Histone acetyltransferase *TaHAG1* acts as a crucial regulator to strengthen salt tolerance of hexaploid wheat. *Plant Physiol.* **2021**, *186*, 1951–1969. [CrossRef]
77. Wang, M.; Wang, M.; Zhao, M.; Wang, M.; Liu, S.; Tian, Y.; Moon, B.; Liang, C.; Li, C.; Shi, W. *TaSRO1* plays a dual role in suppressing *TaSIP1* to fine tune mitochondrial retrograde signalling and enhance salinity stress tolerance. *New Phytol.* **2022**, *236*, 495–511. [CrossRef] [PubMed]
78. Kim, M.S.; Kim, J.H.; Amoah, J.N.; Seo, Y.W. Wheat (*Triticum aestivum* L.) Plant U-box E3 ligases *TaPUB2* and *TaPUB3* enhance ABA response and salt stress resistance in Arabidopsis. *FEBS Lett.* **2022**, *596*, 3037–3050. [CrossRef] [PubMed]
79. Wang, K.; Zhai, M.; Cui, D.; Han, R.; Wang, X.; Xu, W.; Qi, G.; Zeng, X.; Zhuang, Y.; Liu, C. Genome-wide analysis of the amino acid permeases gene family in wheat and *TaAAP1* enhanced salt tolerance by accumulating ethylene. *Int. J. Mol. Sci.* **2023**, *24*, 13800. [CrossRef]
80. Yang, R.; Yang, Z.; Xing, M.; Jing, Y.; Zhang, Y.; Zhang, K.; Zhou, Y.; Zhao, H.; Qiao, W.; Sun, J. *TaBZR1* enhances wheat salt tolerance via promoting ABA biosynthesis and ROS scavenging. *J. Genet. Genom.* **2023**, *50*, 861–871. [CrossRef]
81. Shamloo-Dashtpagerdi, R.; Aliakbari, M.; Lindlöf, A.; Tahmasebi, S. A systems biology study unveils the association between a melatonin biosynthesis gene, O-methyl transferase 1 (OMT1), and wheat (*Triticum aestivum* L.) combined drought and salinity stress tolerance. *Planta* **2022**, *255*, 99. [CrossRef]
82. Mickelbart, M.V.; Hasegawa, P.M.; Bailey-Serres, J. Genetic mechanisms of abiotic stress tolerance that translate to crop yield stability. *Nat. Rev. Genet.* **2015**, *16*, 237–251. [CrossRef]
83. Apse, M.P.; Blumwald, E. Na^+ transport in plants. *FEBS Lett.* **2007**, *581*, 2247–2254. [CrossRef]
84. Julkowska, M.M.; Testerink, C. Tuning plant signaling and growth to survive salt. *Trends Plant Sci.* **2015**, *20*, 586–594. [CrossRef] [PubMed]
85. Gao, J.P.; Chao, D.Y.; Lin, H.X. Understanding abiotic stress tolerance mechanisms: Recent studies on stress response in rice. *J. Integr. Plant Biol.* **2007**, *49*, 742–750. [CrossRef]
86. Kobayashi, N.I.; Yamaji, N.; Yamamoto, H.; Okubo, K.; Ueno, H.; Costa, A.; Tanoi, K.; Matsumura, H.; Fujii-Kashino, M.; Horiuchi, T. *OsHKT1*; 5 mediates Na^+ exclusion in the vasculature to protect leaf blades and reproductive tissues from salt toxicity in rice. *Plant J.* **2017**, *91*, 657–670. [CrossRef] [PubMed]
87. Suzuki, K.; Yamaji, N.; Costa, A.; Okuma, E.; Kobayashi, N.I.; Kashiwagi, T.; Katsuhara, M.; Wang, C.; Tanoi, K.; Murata, Y. *OsHKT1; 4*-mediated Na^+ transport in stems contributes to Na^+ exclusion from leaf blades of rice at the reproductive growth stage upon salt stress. *BMC Plant Biol.* **2016**, *16*, 22. [CrossRef]
88. Munns, R.; Tester, M. Mechanisms of salinity tolerance. *Annu. Rev. Plant Biol.* **2008**, *59*, 651–681. [CrossRef] [PubMed]
89. Chaves, M.M.; Flexas, J.; Pinheiro, C. Photosynthesis under drought and salt stress: Regulation mechanisms from whole plant to cell. *Ann. Bot.* **2009**, *103*, 551–560. [CrossRef]
90. Wang, L.; Czedik-Eysenberg, A.; Mertz, R.A.; Si, Y.; Tohge, T.; Nunes-Nesi, A.; Arrivault, S.; Dedow, L.K.; Bryant, D.W.; Zhou, W.; et al. Comparative analyses of C4 and C3 photosynthesis in developing leaves of maize and rice. *Nat. Biotechnol.* **2014**, *32*, 1158–1165. [CrossRef]
91. Majeran, W.; van Wijk, K.J. Cell-type-specific differentiation of chloroplasts in C4 plants. *Trends Plant Sci.* **2009**, *14*, 100–109. [CrossRef]
92. Ghannoum, O. C4 photosynthesis and water stress. *Ann. Bot.* **2009**, *103*, 635–644. [CrossRef]
93. Ito, Y.; Katsura, K.; Maruyama, K.; Taji, T.; Kobayashi, M.; Seki, M.; Shinozaki, K.; Yamaguchi-Shinozaki, K. Functional analysis of rice *DREB1/CBF*-type transcription factors involved in cold-responsive gene expression in transgenic rice. *Plant Cell Physiol.* **2006**, *47*, 141–153. [CrossRef]

94. Hu, H.; Dai, M.; Yao, J.; Xiao, B.; Li, X.; Zhang, Q.; Xiong, L. Overexpressing a *NAM*, *ATAF*, and *CUC (NAC)* transcription factor enhances drought resistance and salt tolerance in rice. *Proc. Natl. Acad. Sci. USA* **2006**, *103*, 12987–12992. [CrossRef] [PubMed]
95. Munns, R.; James, R.A.; Xu, B.; Athman, A.; Conn, S.J.; Jordans, C.; Byrt, C.S.; Hare, R.A.; Tyerman, S.D.; Tester, M. Wheat grain yield on saline soils is improved by an ancestral Na^+ transporter gene. *Nat. Biotechnol.* **2012**, *30*, 360–364. [CrossRef] [PubMed]
96. Thorne, R.F. An updated phylogenetic classification of the flowering plants. *Aliso* **1992**, *13*, 365–389. [CrossRef]
97. Al-Tamimi, N.; Brien, C.; Oakey, H.; Berger, B.; Saade, S.; Ho, Y.S.; Schmöckel, S.M.; Tester, M.; Negrão, S. Salinity tolerance loci revealed in rice using high-throughput non-invasive phenotyping. *Nat. Commun.* **2016**, *7*, 13342. [CrossRef]
98. Li, T.; Yang, X.; Yu, Y.; Si, X.; Zhai, X.; Zhang, H.; Dong, W.; Gao, C.; Xu, C. Domestication of wild tomato is accelerated by genome editing. *Nat. Biotechnol.* **2018**, *36*, 1160–1163. [CrossRef] [PubMed]
99. Zhang, A.; Liu, Y.; Wang, F.; Li, T.; Chen, Z.; Kong, D.; Bi, J.; Zhang, F.; Luo, X.; Wang, J.; et al. Enhanced rice salinity tolerance via CRISPR/Cas9-targeted mutagenesis of the *OsRR22* gene. *Mol. Breed.* **2019**, *39*, 47. [CrossRef]
100. Han, X.; Chen, Z.; Li, P.; Xu, H.; Liu, K.; Zha, W.; Li, S.; Chen, J.; Yang, G.; Huang, J.; et al. Development of novel rice germplasm for salt-tolerance at seedling stage using CRISPR-Cas9. *Sustainability* **2022**, *14*, 2621. [CrossRef]
101. Santosh Kumar, V.V.; Verma, R.K.; Yadav, S.K.; Yadav, P.; Watts, A.; Rao, M.V.; Chinnusamy, V. CRISPR-Cas9 mediated genome editing of drought and salt tolerance (*OsDST*) gene in indica mega rice cultivar MTU1010. *Physiol. Mol. Biol. Plants* **2020**, *26*, 1099–1110. [CrossRef]
102. Li, X.; Gao, X.; Yu, S.; Du, F.; Liu, J.; Kan, X.; Liu, X.; Yao, D. Rhizosphere microbiota diversity and salt stress-alleviating functional genes in coastal wild salt-tolerant plants. *Microbiol. Res.* **2026**, *303*, 128397. [CrossRef]

plants

MDPI

Article

NAC Transcription Factor *GmNAC035* Exerts a Positive Regulatory Role in Enhancing Salt Stress Tolerance in Plants

Wanting Shi †, Sixin Ye †, Yiting Xin †, Hongmiao Jin, Meiling Hu, Yueping Zheng, Yihua Zhan, Hongbo Liu, Yi Gan, Zhifu Zheng * and Tian Pan *

The Key Laboratory for Quality Improvement of Agricultural Products of Zhejiang Province, College of Advanced Agricultural Sciences, Zhejiang A&F University, Hangzhou 311300, China; 2022101012015@stu.zafu.edu.cn (W.S.); 2022601022033@stu.zafu.edu.cn (S.Y.); xyt2023601022035@stu.zafu.edu.cn (Y.X.); jhm@stu.zafu.edu.cn (H.J.); hml@stu.zafu.edu.cn (M.H.); zhengyp@zafu.edu.cn (Y.Z.); yhzhan@zafu.edu.cn (Y.Z.); hbliu@zafu.edu.cn (H.L.); zjuganyi@163.com (Y.G.)
* Correspondence: zzheng@zafu.edu.cn (Z.Z.); tianpan@zafu.edu.cn (T.P.)
† These authors contributed equally to this work.

Abstract: Soybean, a globally significant and versatile crop, serves as a vital source of both oil and protein. However, environmental factors such as soil salinization pose substantial challenges to its cultivation, adversely affecting both yield and quality. Enhancing the salt tolerance of soybeans can mitigate yield losses and promote the development of the soybean industry. Members of the plant-specific transcription factor family NAC play crucial roles in plant adaptation to abiotic stress conditions. In this study, we screened the soybean *GmNAC* family genes potentially involved in the salt stress response and identified 18 *GmNAC* genes that may function during the early stages of salt stress. Among these, the *GmNAC035* gene exhibited a rapid increase in expression within one hour of salt treatment, with its expression being induced by abscisic acid (ABA) and methyl jasmonate (MeJA), suggesting its significant role in the soybean salt stress response. We further elucidated the role of *GmNAC035* in soybean salt tolerance. GmNAC035, a nuclear-localized transcriptional activator, enhances salt tolerance when overexpressed in Arabidopsis, reducing oxidative damage and boosting the expression of stress-responsive genes. It achieves this by regulating key stress response pathways, including the SOS pathway, calcium signaling, and ABA signaling. These findings highlight the potential of *GmNAC035* as a genetic engineering target to improve crop salt tolerance.

Keywords: soybean; NAC; transcription factor; salt tolerance; stress-related genes

1. Introduction

Globally, soybean (*Glycine max* L.) ranks among the most significant crops. It plays a crucial role as an essential provider of oil and protein, which are used for human food and animal feed. Its economic and nutritional significance makes it a focal point of agricultural research, particularly in the context of enhancing yield and stress tolerance [1]. However, soybean production faces numerous challenges, among which abiotic stresses pose a significant threat to crop productivity. Salinity is one of the most prevalent environmental stresses. The intensification of soil salinization and the degradation of irrigated land directly affect dryland agriculture on 2.6 billion hectares worldwide. Projections suggest that by 2050, the primary and secondary salinization of agricultural soils will directly affect half of the world's arable land, leading to substantial crop losses worldwide [2–4]. Therefore, understanding the molecular mechanisms of soybean's response to salt stress is crucial for formulating strategies to improve its salt tolerance.

Salt stress has a negative impact on soybeans across various aspects, such as physiological, biochemical, and molecular procedures. High salinity disrupts ionic homeostasis, leading to the accumulation of ions such as sodium (Na^+) and chloride (Cl^-), which impair cellular functions and damage plant tissues. Additionally, salt stress induces oxidative stress, which then results in the overproduction of reactive oxygen species (ROS) that cause cellular damage. These physiological disruptions ultimately lead to reduced photosynthesis, stunted growth and development, and decreased yield [5–7]. Given the increasing salinization of arable land due to irrigation practices and climate change, there is an urgent need to identify and characterize genes that confer salt tolerance in soybeans in order to improve the salt tolerance and total yield of soybeans through breeding initiatives [8]. Among the various gene families involved in plant stress responses, the NAC (NAM, ATAF, and CUC) family has emerged as a key regulator of abiotic stress tolerance [9]. NAC proteins are marked by a well-conserved N-terminal domain that binds to DNA and a changeable C-terminal domain for transcriptional activation [10]. They participate in a diverse array of biological activities, such as growth and development, senescence and reactions to stress [10]. Notably, NAC transcription factors have been well established as key regulators in mediating plant adaptive responses to various abiotic stresses, including drought, high salinity, and cold conditions, underscoring their significant potential as prime targets for stress-tolerance genetic engineering in crops [11].

The NAC family ranks among the largest plant-specific transcription factor families. In different plant species, more than 100 members of this family have been identified [10,11]. In recent years, significant progress has been made in elucidating the roles of NAC transcription factors in stress responses. Studies in Arabidopsis have shown that *NAC* genes such as *ANAC019*, *ANAC055*, and *ANAC072* are induced by salt stress and participate in the regulation of stress-responsive genes [12]. Similarly, in rice (*Oryza sativa* L.), the *NAC* genes *OsNAC2*, *OsNAC5*, and *OsNAC6* have been demonstrated to confer tolerance to multiple abiotic stresses, including salinity and drought [13–16]. These results emphasize the consistent function of NAC transcription factors in stress responses among different plant species. In soybeans, the NAC family has also been a subject of extensive research, with several members identified as potential regulators of stress responses. For example, studies have shown that *GmNAC06*, *GmNAC11*, *GmNAC085*, and *GmNAC109* can be induced by salt stress. Moreover, when these genes are overexpressed in transgenic plants, they can enhance the plants' salt tolerance [17–20]. Additionally, *GmNAC3*, *GmNAC8*, *GmNAC12*, and *GmNAC19* have been implicated in the regulation of drought tolerance [21–24], further underscoring the multifaceted roles of NAC transcription factors in soybean stress responses. Despite these advancements, the functional characterization of *NAC* genes in soybeans remains incomplete, and the molecular mechanisms by which they contribute to salt tolerance are not yet fully understood.

This study focused on screening the *GmNAC* family genes in soybeans that are potentially associated with the salt stress response. We found that the expression of the *GmNAC035* gene witnessed a sharp rise within an hour after salt treatment. This notable increase strongly suggests that *GmNAC035* is likely to be a key player in how soybeans respond to salt stress. Building on this discovery, we carried out further research to clarify the specific role of *GmNAC035* in enhancing plants' tolerance to salt. GmNAC035 is a nuclear-localized transcriptional activator. When overexpressed in Arabidopsis, it can enhance the plant's salt tolerance, reduce oxidative damage, and promote the expression of stress-responsive genes. *GmNAC035* holds the potential to bolster a plant's resilience to salt stress through the modulation of pivotal stress-response pathways. These pathways encompass the salt overly sensitive (SOS) signaling cascade, the calcium-mediated signaling network, and the abscisic acid (ABA) signaling pathway. The discoveries from this research

point out that *GmNAC035* holds promise as an option for genetic engineering. It has the ability to boost the salt tolerance of crops and offer precious candidate gene resources for the development of salt-tolerant soybean varieties.

2. Results

2.1. Expression Patterns of Predicted GmNAC Genes in Roots Under Salt Stress Conditions

A total of 152 *GmNAC* TFs were identified in earlier studies through a complete genome-wide survey [25]. More recently, studies have identified 180 *GmNAC* genes in the soybean genome Wm82.a2.v1, revealing 32 new *GmNAC* genes [26,27]. Given the increasingly sophisticated development of whole-genome sequencing technology, we conducted a re-identification of the *GmNAC* family genes in the most recent Wm82.a4.v1 version of the soybean genome. The NAC domain was used as the prototype sequence to search against all the deduced protein sequences from the soybean genome. A total of 173 *GmNAC* genes were identified (Table S1). Compared with the previous version, five new *GmNAC* genes were discovered. To maintain consistency in scientific nomenclature, we adopted a naming system that assigns numbers after the *GmNAC* prefix based on chromosome order and locus position, consistent with previous studies [25]. The newly identified *GmNAC* genes were numbered sequentially from *GmNAC184* onward (Table S2), maintaining alignment with the naming conventions of the previously described 180 *GmNAC* genes.

Given the pivotal role of the *NAC* genes in plant development and stress responses, we further investigated its members involved in salt stress responses to identify potential candidate genes for enhancing soybean salt tolerance. Utilizing published RNA-seq databases (Table S3), we analyzed the expression patterns of the *GmNAC* gene family at 1, 2, 4, and 24 h post salt treatment. The results revealed that 101 genes were upregulated following salt treatment, underscoring the broad involvement of *GmNAC* genes in the soybean salt stress response (Figure S1). In this study, we notably focused on genes that were largely induced within 1 h of salt treatment, as these genes are likely to play a critical role in the early stages of stress response, facilitating rapid salt signal perception and transduction. Our analysis identified 48 *GmNAC* genes that were significantly upregulated at 1 h post-treatment, including *GmNAC085* and *GmNAC109*, which have been previously reported, thereby validating the reliability of our findings (Figure 1A). To further elucidate the potential developmental functions of these *GmNAC* genes, we analyzed the expression profiles of the 48 upregulated genes across various developmental stages and tissues using transcriptomic data from the Phytozome database (Table S4). Given that roots serve as the primary organs for sensing soil stress and are essential for anchoring, nutrient and water absorption, storage, and transport, we examined the expression of these genes in particular in root tissues. The results indicated that 18 of the 48 *GmNAC* genes exhibited high expression levels in soybean roots (Figure 1B).

To further confirm the expression patterns of these 18 *GmNAC* genes under salt treatment, we employed qRT-PCR with gene-specific primers to analyze the expression levels of 18 *GmNAC* genes predicted to be associated with salt stress at 0.5, 1, and 2 h post-treatment (Figure 2). The results indicated that the expression levels of all 18 genes increased to varying degrees following salt treatment. We observed that the expression level of most *GmNAC* genes increased with prolonged treatment time. Interestingly, the expression levels of *GmNAC021*, *GmNAC035*, *GmNAC036*, and *GmNAC088* rapidly increased at 1 h post-salt treatment but decreased at 2 h, suggesting that these genes may play significant roles in the early stages of salt stress response. In this study, we selected *GmNAC035* as the focus for our subsequent research since *GmNAC035* responds to salt relatively more strongly and rapidly.

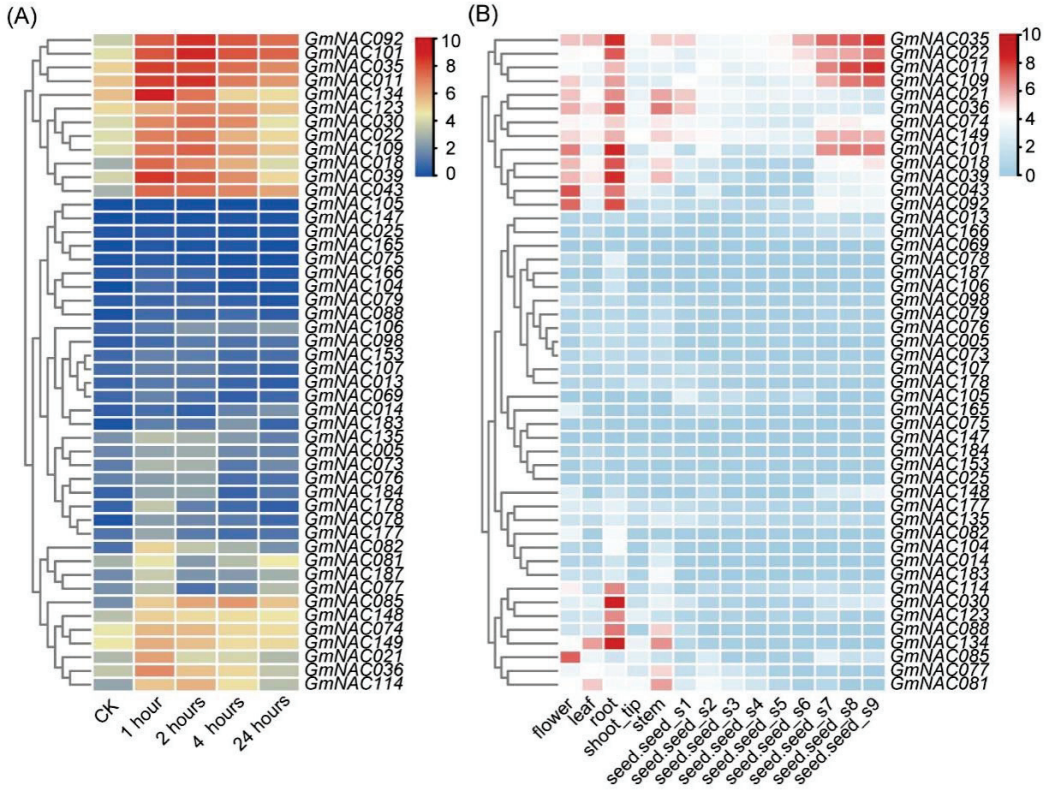

Figure 1. Expression profiles of *GmNAC* genes under NaCl stress and in different tissues. (**A**) Expression profiles of *GmNAC* genes with at least a 2-fold up-regulation in expression after 1 h of treatment with 100 mM NaCl in soybean roots. (**B**) Expression profiles of *GmNAC* genes in different tissues. The RPKM normalized values of the genes were log2-transformed and visualized as a heatmap. The gene IDs are shown in Table S1.

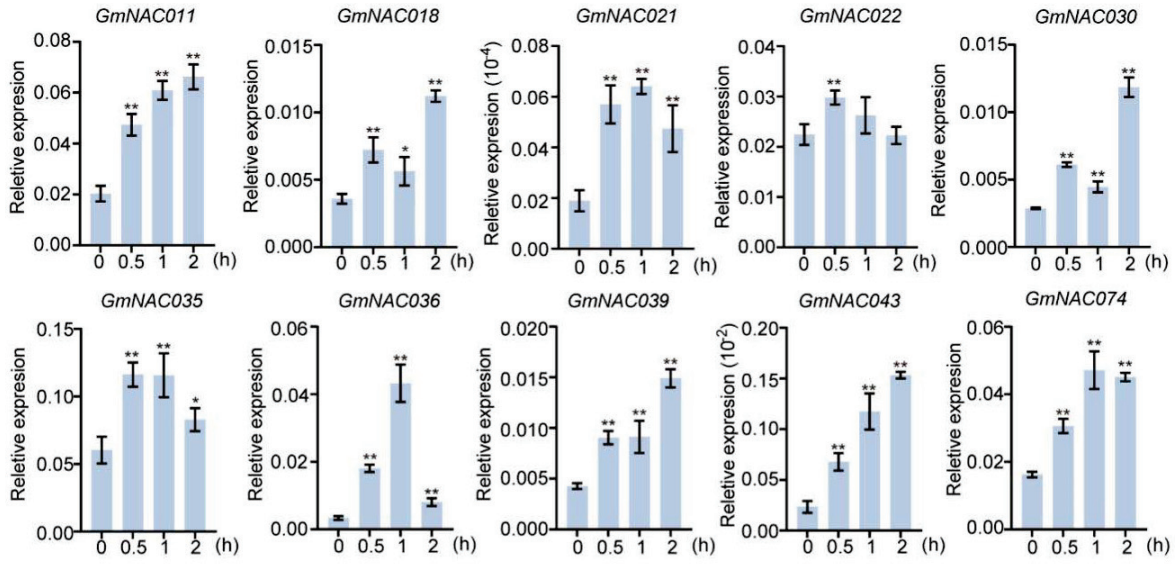

Figure 2. *Cont*.

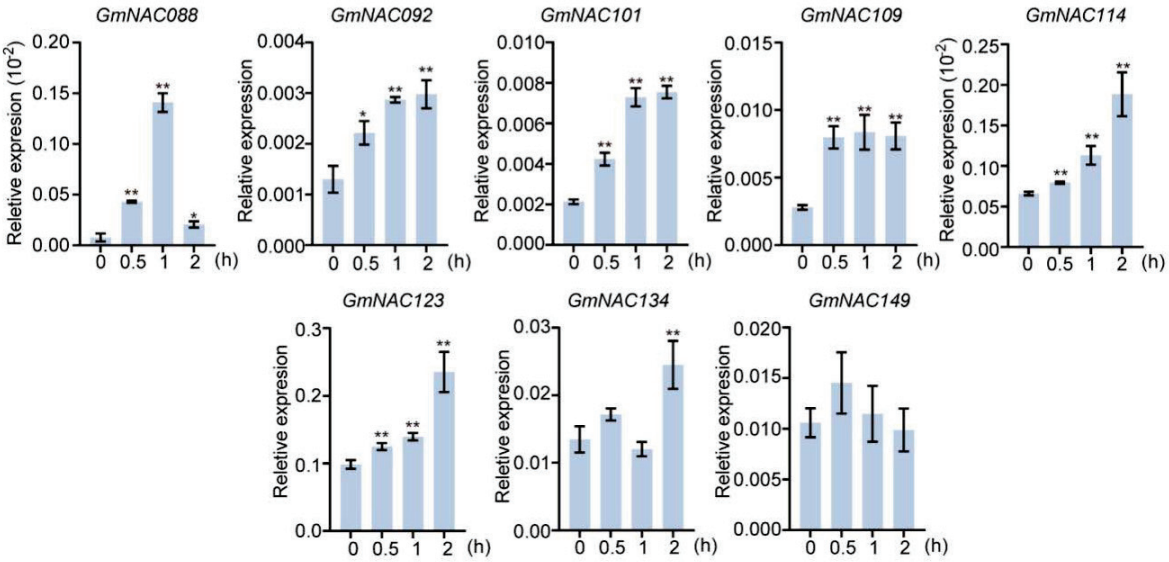

Figure 2. Transcriptional levels of 18 *GmNAC* genes in "Tianlong No. 1" soybean under treatment with 150 mM NaCl. Representative data from two biological replicates are shown. Each sample was analyzed in three technical replicates. The data represent the mean ± SD, * $p < 0.05$, ** $p < 0.01$ (Student's *t*-test).

2.2. The Expression of GmNAC035 Is Induced by Hormonal Signals, and It Encodes a Nuclear-Localized Protein with Self-Transactivation Activity

To investigate the function of the *GmNAC035* gene, we initially examined its spatio-temporal expression patterns by collecting samples from various soybean tissue parts. The findings indicated that *GmNAC035* displayed a constitutive expression pattern, with the highest expression level observed in leaves and roots (Figure 3A). By analyzing the expression patterns of *GmNAC* family genes after NaCl treatment, we discovered that *GmNAC035* could respond rapidly to salt stress. Prior research has demonstrated that plant hormones play a vital role in mitigating the detrimental phenotypes induced by abiotic stress in plants and enhancing plant growth adaptation [28]. To determine whether *GmNAC035* responds to hormone signals, we treated soybean leaves with various hormones and assessed the expression levels of *GmNAC035* at different time points post-treatment. Following abscisic acid (ABA) treatment, the expression level of *GmNAC035* increased continuously and significantly, reaching over 20-fold that of the control at 48 h (Figure 3B). The expression level of *GmNAC035* peaked 24 h after methyl jasmonate (MeJA) treatment and was approximately eight-fold that of the control (Figure 3C). The prompt response of *GmNAC035* to hormone treatment strongly implied that it may have a specific function in the hormone signal transduction pathway during the salt stress response.

Previous reports have indicated that *NAC* family genes belong to a class of nuclear-localized transcription factors with transcriptional activation activity [29]. To confirm whether GmNAC035 participates in the transcriptional activation process, we inserted the full-length *GmNAC035* gene into the pGBKT7 vector and introduced it into the yeast strain AH109. The negative control, positive control, and BD-*GmNAC035* transformants all exhibited favorable growth on synthetic defined (SD)/-Trp medium. Nevertheless, only the yeast cells of the positive control and BD-*GmNAC035* were able to survive on SD/-Trp/-His/-Leu medium (Figure 3D). To further analyze the subcellular localization of GmNAC035, we constructed a *GmNAC035-GFP* fusion vector. Subsequently, the empty *GFP* vector and the *GmNAC035-GFP* fusion vector were transiently transformed into tobacco leaf epidermal cells. Using laser confocal microscopy, we observed that the fluorescence signal of the empty GFP vector was distributed across the cytoplasm, nucleus, and cell membrane.

Conversely, the fluorescence signal of the GmNAC035-GFP fusion protein colocalized with the nuclear marker protein and was exclusively located in the nucleus (Figure 3E). These findings suggest that GmNAC035 is a transcription factor that is localized in the nucleus and participates in transcriptional activation.

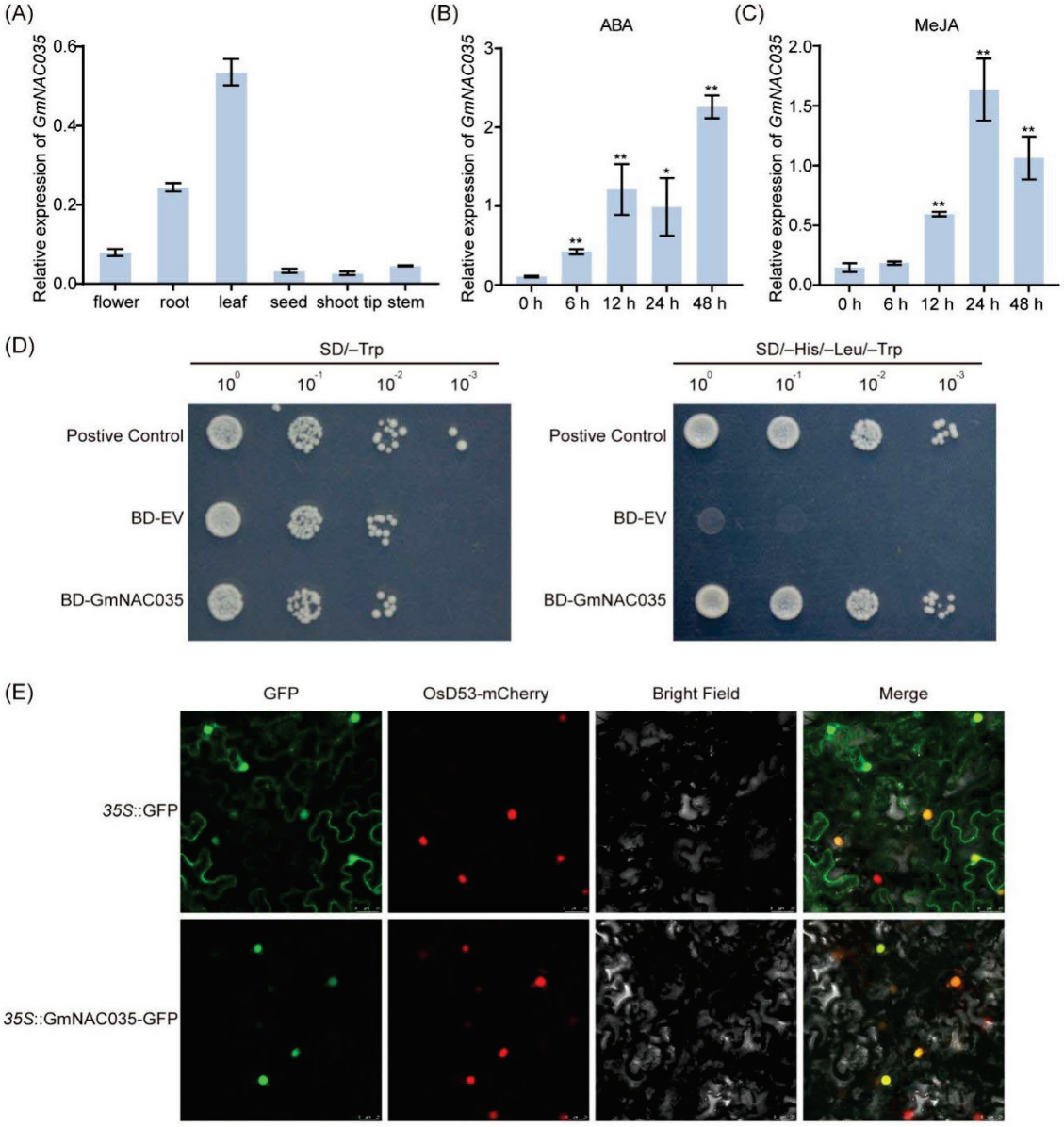

Figure 3. Expression pattern of the *GmNAC035* gene in "Tianlong No. 1" soybean and analysis of the transcriptional activity and subcellular localization of the GmNAC035 protein. (**A**) Transcriptional levels of the *GmNAC035* gene in different tissues. (**B**,**C**) Transcriptional levels of the *GmNAC035* gene under stress of 150 μM ABA and 100 mM MeJA, respectively. Representative data from two biological replicates are shown. Each sample was analyzed in three technical replicates. The data represent the mean ± SD, * $p < 0.05$, ** $p < 0.01$ (Student's *t*-test). (**D**) Determination of the transcriptional self-activation activity of the GmNAC035 protein in yeast. Yeasts transformed with BD-GmNAC035, negative control (BD-EV), and positive control (BD-GmNAN181) plasmids were grown on SD/-Trp medium and SD/-His/-Leu/-Trp medium. (**E**) Analysis of the subcellular localization of the GmNAC035 protein. *35S::GFP* was used as the control. Scale bar = 25 μm.

2.3. The Overexpression of GmNAC035 Improves Salt Stresses Tolerance of Arabidopsis

To further validate the role of *GmNAC035* in responding to salt stress, we generated transgenic *Arabidopsis thaliana* lines overexpressing *GmNAC035*. After obtaining homozy-

gous and stable Arabidopsis overexpression lines, we conducted an expression analysis on three of these lines using RT-qPCR. The results indicated that the expression level of *GmNAC035* was significantly elevated (Figure 4B). Simultaneously, we exposed wild-type Arabidopsis and the *GmNAC035*-overexpressing lines to different concentrations of NaCl (0 mM, 75 mM, 100 mM, and 125 mM) on 1/2 MS for 6 days. The results demonstrated that there was no significant disparity between the two types of lines under normal conditions (Figure 4A). However, when exposed to 100 mM and 125 mM salt concentrations, the fresh weight of the *GmNAC035*-overexpressing lines was significantly higher than that of the wild type (Figure 4C). Although there was no significant difference in root length between the overexpressing Arabidopsis lines and the wild type (Figure S2), the number of lateral roots in the overexpressing lines was obviously greater than that in the wild type (Figure 4D). Additionally, we determined the survival rates of different Arabidopsis lines when exposed to a 100 mM salt concentration. The results revealed that the survival rate of the overexpressing lines was notably greater than that of the wild type (Figure 4E). These results provided evidence that *GmNAC035* positively regulates salt resistance in Arabidopsis.

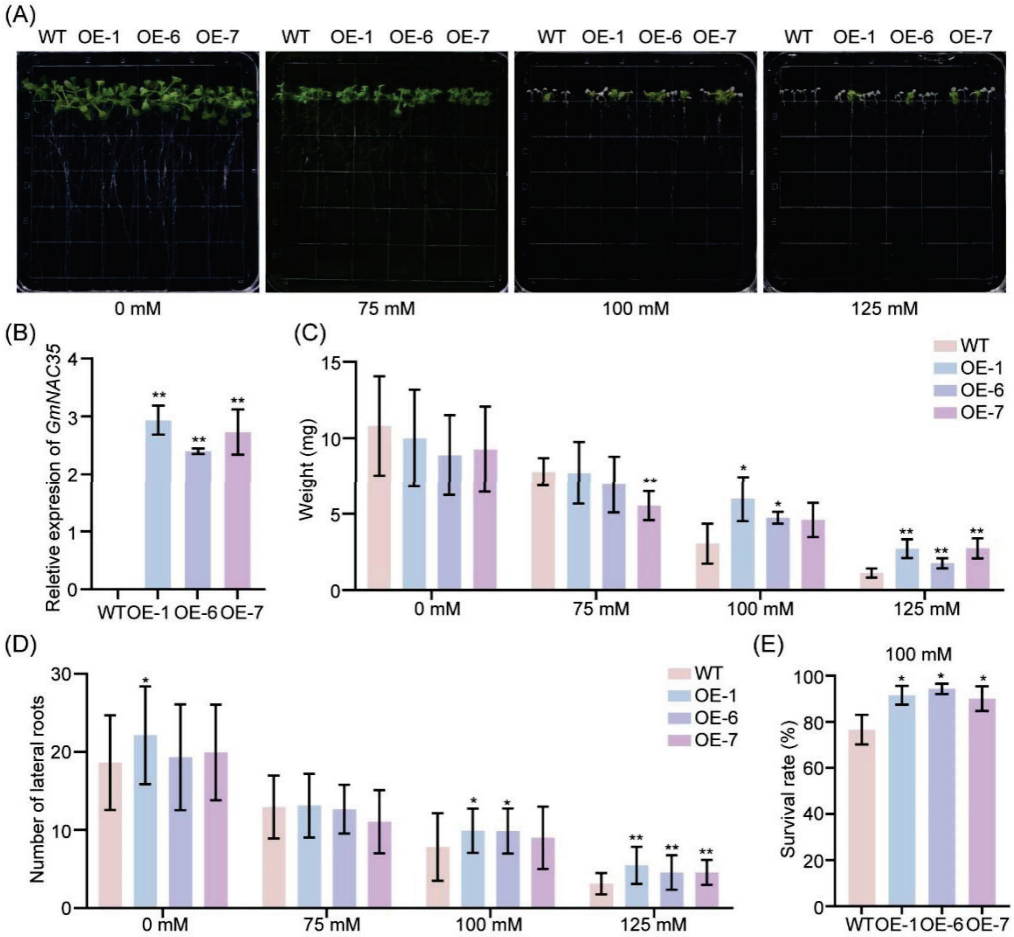

Figure 4. Overexpression of *GmNAC035* increases salt tolerance in Arabidopsis. (**A**) Phenotypic observation of wild-type and *GmNAC035* overexpression Arabidopsis lines under salt stress at different concentrations. (**B**) Transcriptional levels of the *GmNAC035* gene in wild-type Arabidopsis and transgenic lines. RT-qPCR analysis was performed using the $2^{-\Delta CT}$ method. (**C**,**D**) Statistical analysis of the fresh weight (**C**) and the number of lateral roots (**D**) of wild-type Arabidopsis and overexpression lines under salt stress at different concentrations. (**E**) Statistical analysis of the survival rate of overexpression lines under 100 mM salt stress. The data represent the mean ± SD. $n > 65$. * $p < 0.05$, ** $p < 0.01$ (Student's *t*-test).

2.4. GmNAC035 Contributed to the Elimination of ROS

An increasing body of evidence indicates that salt stress triggers the rapid generation and accumulation of ROS, which impose toxic impacts on plants by inducing oxidative stress [30]. Hydrogen peroxide (H_2O_2) and superoxide anions (O_2^-) are the main components of ROS in plants. 3,3′-Diaminobenzidine (DAB) and nitroblue tetrazolium (NBT) can be used to detect H_2O_2 and O_2^-, respectively. DAB reacts with H_2O_2 to form a brown precipitate, while NBT reacts with O_2^- to produce a blue formazan precipitate. To ascertain whether *GmNAC035* participates in the ROS accumulation process, we stained Arabidopsis plants treated with 0 mM and 100 mM NaCl using DAB and NBT, respectively. The results demonstrated that in the absence of salt stress, there were negligible differences in ROS accumulation among different Arabidopsis lines. However, when subjected to 100 mM NaCl, compared with the control, the ROS accumulation level in the *GmNAC035*-overexpressing Arabidopsis lines was relatively lower (Figure 5A,B), which was consistent with the phenotype after salt stress. Malondialdehyde (MDA), which results from peroxidation reactions, acts as an indicator for gauging the extent of plasma membrane impairment and the intensity of stress-induced responses. To evaluate whether *GmNAC035* is involved in the oxidative damage process, we measured the MDA concentration (Table S5). In normal growth circumstances, there was no significant disparity in MDA content between the control plants and the *GmNAC035*-overexpressing lines. However, after exposure to 100 mM NaCl, the content of MDA in the *GmNAC035*-overexpressing lines was prominently lower than that in the wild type (Figure 5C). This finding suggested that the *GmNAC035*-overexpressing lines endured less oxidative damage under salt stress. In order to maintain the redox homeostasis of ROS and resist the harmful effects caused by ROS and biotic/abiotic stresses, plants have developed scavenging mechanisms [31]. These mechanisms make use of enzymatic components and non-enzymatic antioxidants, such as superoxide dismutase (SOD) and peroxidase (POD) [32]. Subsequently, we measured the activities of SOD and POD in different Arabidopsis lines under salt stress (Table S5). We found that without exposure to salt, the SOD activity in the *GmNAC035*-overexpressing Arabidopsis lines was significantly higher than that in the wild type. Upon exposure to 100 mM NaCl, the SOD activity in the overexpressing lines was markedly lower than that in the wild type (Figure 5D). In contrast, the POD activity in the overexpressing lines was consistently significantly higher than that in the wild type (Figure 5E). These results imply that POD in the *GmNAC035*-overexpressing lines plays a more crucial role in alleviating oxidative damage.

2.5. Overexpression of GmNAC035 Increases Expression of Genes Related to Abiotic Stress Resistance

Throughout the evolutionary process, plants have evolved diverse adaptive strategies to contend with high-salt stress [6]. To elucidate the potential molecular mechanism underpinning the enhanced salt tolerance of plants overexpressing the *GmNAC035* gene, we investigated the transcriptional abundance of abiotic stress-related genes under salt stress conditions (Table S6). The salt overly sensitive (SOS) pathway assumes a pivotal and indispensable role in endowing plants with the capacity to endure salt stress. This pathway encompasses three key proteins, namely SOS1, SOS2, and SOS3 [30]. The cytoplasmic calcium signal induced by salt stress is sensed by SOS3, a calcium-binding protein with an EF-hand structure. Subsequently, SOS3 interacts with and activates the serine/threonine protein kinase SOS2. The activated SOS2 phosphorylates SOS1, thereby promoting its activity. SOS1, a plasma membrane-localized Na^+/H^+ antiporter located downstream in the SOS pathway, enhances plant salt tolerance by facilitating the efflux of excess intracellular Na^+ and regulating the long-distance transport of Na^+ in plants [6,33,34]. In plants, the activity

of SOS1 is strictly regulated: it is activated under high-salt conditions and inactivated through various regulatory mechanisms under low-salt conditions to achieve intracellular sodium homeostasis. Our results indicated that, despite the absence of a significant difference in the expression level of *AtSOS1* in the *GmNAC035*-overexpressing Arabidopsis lines compared to the control under salt stress conditions, the expression levels of *AtSOS3* and *AtSOS2* were significantly higher than those in the control (Figure 6A–C). This is advantageous for promoting the activity of AtSOS1 and consequently enhancing the efflux of excess sodium ions in the *GmNAC035*-overexpressing lines. Moreover, NHX1 plays a crucial role in maintaining Na^+/K^+ homeostasis within the vacuole under salt stress conditions, and overexpression of *NHX1* exerts a positive influence on plant salt tolerance [6,35]. We also found that the expression level of *AtNHX1* in the *GmNAC035*-overexpressing Arabidopsis lines was almost twice as high as that in the control (Figure 6D).

Under salt stress conditions, plant cells are capable of sensing high concentrations of sodium ions and initiating calcium influx, resulting in a rapid and transient elevation in the cytoplasmic calcium concentration. This directly modulates the transcription levels of genes involved in the salt stress response. This process needs to be interpreted by different calcium sensors, including calmodulin (CaM), calcium-dependent protein kinases (CDPKs), calmodulin-like proteins (CMLs), and calcineurin B-like protein/calcineurin B-like protein-interacting protein kinase (CBL/CIPK) [36]. Our findings demonstrated that the expression levels of two calcium sensors, *AtCDPK6* [37] and *AtCBL1* [38], which positively govern plant salt tolerance, were significantly higher in the *GmNAC035*-overexpressing lines than in the control after salt stress treatment (Figure 6E,F).

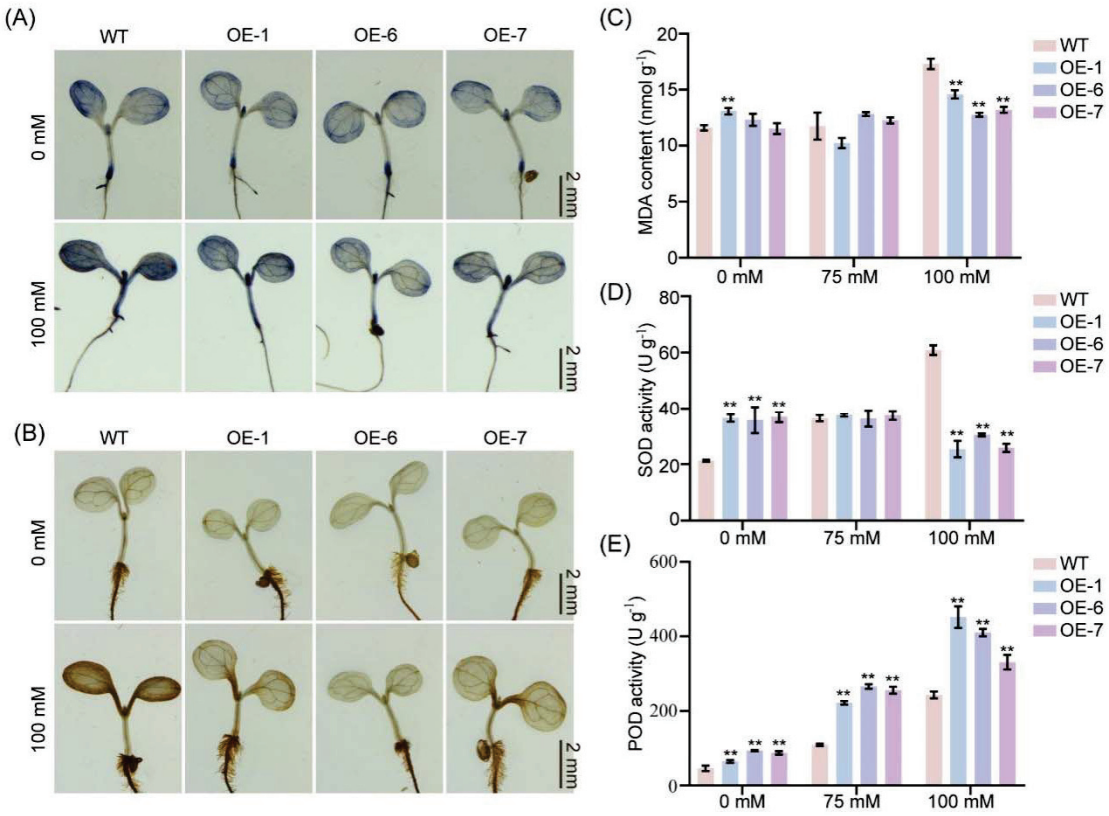

Figure 5. Visualization of ROS and determination of antioxidant enzyme activities. (**A**,**B**) Staining observations of NBT (**A**) and DAB (**B**) in wild-type and *GmNAC035*-overexpressing Arabidopsis lines under 0 mM and 100 mM salt stress. Scale bar = 2 mm. (**C**–**E**) MDA content (**C**), SOD activity (**D**), and POD activity (**E**) in wild-type and *GmNAC035*-overexpressing Arabidopsis lines under 0 mM, 75 mM, and 100 mM salt stress. The data represent the mean ± SD. ** $p < 0.01$ (Student's *t*-test).

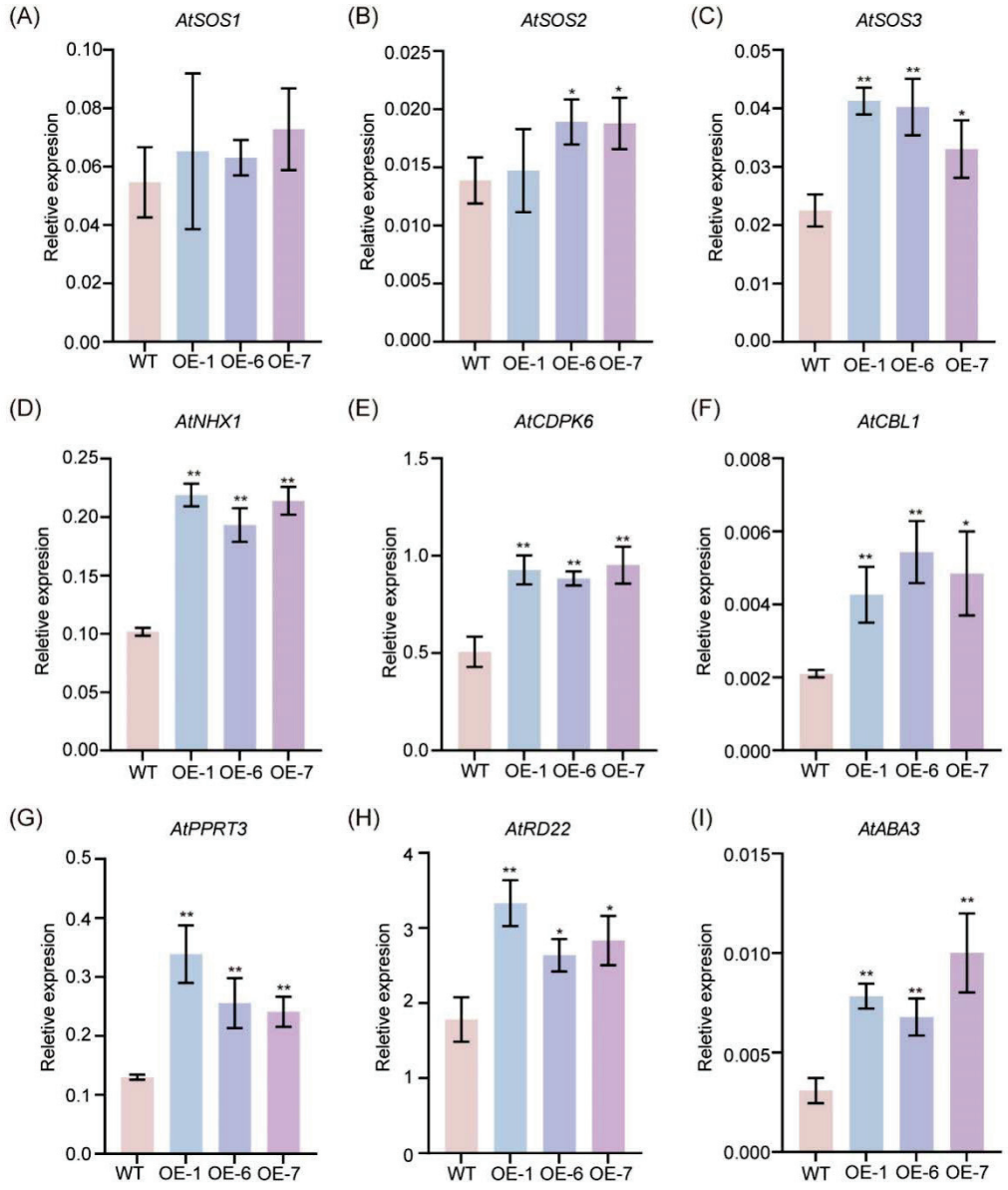

Figure 6. Transcriptional levels of salt tolerance-related genes in wild type and *GmNAC035*-overexpressing Arabidopsis lines, including *AtSOS1/2/3* (**A**–**C**), *AtNHX1* (**D**), *AtCDPK6* (**E**), *AtCBL1* (**F**), *AtPPRT3* (**G**), *AtRD22* (**H**), and *AtABA3* (**I**). Leaves were collected from Arabidopsis seedlings treated with 100 mM NaCl for 6 days. RT-qPCR analysis was performed using the $2^{-\Delta CT}$ method. Representative data from two biological replicates are shown. Each sample was analyzed in three technical replicates. The data represent the mean ± SD. * $p < 0.05$, ** $p < 0.01$ (Student's *t*-test).

ABA is the principal phytohormone accountable for salt and osmotic stress signaling in plant cells [6,33]. The findings of our research suggested that the expression levels of *AtABA3* [39], which is associated with ABA biosynthesis; *AtRD22* [40,41], an ABA-mediated osmotic stress response factor; and *AtPPRT3* [42], which positively governs ABA signaling, were also significantly higher in the *GmNAC035*-overexpressing lines than in the control after salt stress treatment (Figure 6G–I). These results suggest that *GmNAC035* may positively regulate plant tolerance to salt stress by modulating the expression levels of key genes related to salt tolerance regulation and genes in the ABA signaling pathway.

3. Discussion

Soybean (*Glycine max*), as a typical salt-sensitive crop, is susceptible to the negative effects of salt stress at all stages of growth and development [43]. Salt stress not only

significantly reduces soybean yield but also adversely affects its quality. Therefore, breeding salt-tolerant soybean varieties has become an important goal in current soybean breeding. A new approach to improving the efficiency of selecting salt-tolerant varieties is provided by the application of molecular breeding technology. Among plant-specific transcription factor families, NAC proteins, which are one of the largest, are commonly found in different terrestrial plants [44]. Research indicates that the NAC transcription factor family exerts a vital regulatory influence on various aspects of plants, including their growth process, development stages, and how they respond to stress [11]. In this study, we conducted a genome-wide analysis based on the latest version of the soybean genome (Wm82.a4.v1) and identified a total of 173 *GmNAC* genes, including five newly discovered gene members. To screen for potential salt-tolerant *GmNAC* genes, we systematically analyzed RNA-Seq databases under salt stress conditions and found that 101 *GmNAC* genes were upregulated under salt stress, with 48 genes being significantly induced within one hour of salt treatment. Considering that roots are the primary organs for sensing soil stress and the first line of defense against stress, we combined tissue-specific expression databases to screen out 18 *GmNAC* genes mainly expressed in roots. It was confirmed through RT-qPCR validation that salt stress truly and significantly induced the expression levels of these genes. Notably, *GmNAC021*, *GmNAC035*, *GmNAC036*, and *GmNAC088* showed a transient but significant increase in expression within one hour after salt treatment, suggesting their potential involvement in the early signaling cascade of salt stress response.

Based on these findings, we selected *GmNAC035* for further investigation. *GmNAC035* has the highest expression levels in leaves and roots. The expression of this gene responds to both ABA and MeJA treatments, indicating its potential involvement in the ABA and JA signaling pathways, both of which play important roles in plant stress responses [45]. Yeast transcription activation experiments confirmed that GmNAC035 possesses typical transcription activation functions. Subcellular localization studies using GFP fusion proteins revealed that GmNAC035 is specifically localized in the nucleus, consistent with the characteristics of NAC family proteins as nuclear-localized transcription factors [44]. To elucidate the salt tolerance function of *GmNAC035*, we constructed transgenic Arabidopsis lines overexpressing *GmNAC035*. Under salt stress conditions, the transgenic plants exhibited significantly enhanced salt tolerance, manifested as increased biomass and improved survival rates. Meanwhile, we also noticed that the *GmNAC035*-overexpressing transgenic Arabidopsis lines had significantly more lateral roots than the wild type, but there was no significant difference in root length. Since the development of lateral roots plays a vital role in plants' adaptation to the environment and their ability to cope with abiotic stresses, this change in root system architecture is likely to affect the plant's tolerance to high salt and drought [20].

Salt stress has the potential to elevate the production of ROS and change the redox state within cells. This alteration can cause DNA damage, and in the end, give rise to oxidative stress, which exerts a negative impact on plant growth [46]. We subsequently investigated the physiological mechanisms by which *GmNAC035* confers salt tolerance to plants. Findings revealed a reduced accumulation of reactive ROS and MDA content in the *GmNAC035*-overexpressing transgenic Arabidopsis lines after salt stress, indicating that overexpression of *GmNAC035* effectively alleviates oxidative damage caused by salt stress. SOD catalyzes the dismutation of O_2^- to H_2O_2, which is then decomposed by POD and CAT enzymes into H_2O and O_2 [47]. In our study, prior to salt treatment, *GmNAC035*-overexpressing lines displayed markedly higher SOD and POD activities compared to wild-type plants, demonstrating that *GmNAC035* overexpression enhances the antioxidant system. However, under salt stress conditions, while POD activity remained significantly elevated in the overexpression lines, SOD activity failed to increase further, implying

a more pivotal role for POD in combating oxidative damage in these transgenic plants. Given that the antioxidant machinery in higher plants involves both enzymatic and non-enzymatic components [31], it is reasonable to speculate that non-enzymatic antioxidants may also contribute substantially to the observed mitigation of oxidative stress in these overexpression lines.

It is well known that, when exposed to saline environments, plants initiate intricate salt tolerance mechanisms that encompass multiple genetic pathways. The *GmNAC* transcription factors likely confer enhanced stress resistance through their regulatory influence on downstream stress-responsive gene networks. In this study, further research revealed that the expression of several key salt stress response genes (*AtSOS2*, *AtSOS3* and *AtNHX1*) was significantly upregulated in transgenic plants. Research has shown that the SOS pathway, which consists of SOS1, SOS2, and SOS3, is essential for sustaining ion homeostasis when plants are exposed to salt stress [48]. NHXs are putative Na^+/H^+ exchangers that are responsible for transporting Na^+ from the cytoplasm into the vacuole. During salt stress, the SOS3–SOS2 complex exerts a positive regulatory effect on NHX activity [49]. The upregulation of *AtSOS2* and *AtSOS3* suggests that *GmNAC035* may enhance salt tolerance by activating the SOS and NHX pathway, promoting sodium ion efflux and maintaining intracellular ion balance. CDPKs and CBLs, as important calcium signal sensors, play key roles in stress signal transduction [50]. In our study, the expression levels of *AtCDPK6* and *AtCBL1* were significantly increased in transgenic plants, highlighting the important role of calcium signaling in *GmNAC035*-mediated salt tolerance. Notably, under salt stress conditions, the expression of ABA biosynthesis and signaling-related genes (*AtABA3*, *AtRD22*, and *AtPPRT3*) was significantly upregulated in transgenic plants, further confirming *GmNAC035*'s involvement in ABA-mediated stress responses. As a pivotal hormone regulating plant responses to abiotic stress, the upregulation of genes associated with ABA suggests that *GmNAC035* may enhance plant adaptability to osmotic stress by modulating the ABA signaling pathway.

This study systematically elucidated the multiple regulatory roles of *GmNAC035* in plant salt tolerance, providing new insights into the molecular mechanisms of NAC transcription factors in plant stress responses and offering valuable candidate gene resources for soybean salt-tolerant breeding. Future research should be predominantly concentrated on conducting genetic transformation of *GmNAC035* in soybeans to evaluate its potential impact on soybean yield and quality.

4. Materials and Methods

4.1. Identification of NAC Genes in the Soybean Genome and Analysis of Tissue-Specific Expression

The Phytozome database (https://phytozome-next.jgi.doe.gov/, accessed on 14 September 2023) was used to download all protein sequences of soybean (version: Glycine max Wm82.a4.v1) [51]. The HMM model file (PF02365) for the NAM domain was retrieved from the Pfam database (http://pfam.xfam.org/, accessed on 14 September 2023) [52]. Using the HMMsearch tool (version 3.0) with default parameters [53], sequences containing the NAM domain were screened from the complete protein sequences of soybean and Arabidopsis. Newly identified GmNAC family genes were named in accordance with previous studies (Table S2) [25,26].

Based on the RNA-Seq database [54], the expression levels of genes belonging to the *GmNAC* family in the roots of soybean under salt stress conditions were analyzed, and heatmaps depicting *GmNAC* gene expression under salt stress were generated using TBtools-II (version 2.142) software. Expression data of GmNAC genes upregulated under salt stress across various tissues were extracted from the soybean tissue expression database

(Glycine max Wm82.a4) using Blast (https://phytozome-next.jgi.doe.gov/, accessed on 23 September 2023). Subsequently, tissue-specific expression heatmaps of GmNAC genes were constructed using TBtools.

4.2. Plant Materials, Growth Conditions, and Stress Treatments

The soybean cultivar Tianlong No. 1 [55] was used as the wild type. Soybean seeds were germinated for 6 days on vermiculite and then transferred to 1/2 Hoagland nutrient solution (Macklin, Shanghai, China) for growth in the plant growth chamber under a 16 h (28 °C) light/8 h (22 °C) dark photoperiod. The relative humidity was maintained at 60%. Quantities of 200 mM NaCl, 150 μM ABA, and 100 mM MeJA, which were prepared using 1/2 Hoagland nutrient solution, were applied to treat the plants when the first trifoliate leaves were fully expanded [22,56,57]. Samples were collected at 0 h, 6 h, 12 h, 24 h, and 48 h after treatment for subsequent RNA extraction.

4.3. RNA Extraction and RT-qPCR Analysis

Total RNA was extracted from soybean and Arabidopsis using the Steady Pure Universal RNA Extraction Kit (Accurate Biotechnology, Hunan, China). According to the manufacturer's protocol, TB Green Premix Ex Taq^{TM} II (Takara, Tokyo, Japan) was used for RT-qPCR analysis of the cDNA, which was detected via the fully automatic medical PCR analysis system (Gentier 96R, TIANLONG, Shaanxi, China). The specific primers used in this experiment are listed in Table S7. The transcriptional levels of the target genes were analyzed with GmCons4 and AtActin2 serving as internal reference genes [58]. The RT-qPCR data were analyzed using the $2^{-\Delta CT}$ method. The data presented here are representative of two biological replicates. Each sample underwent analysis with three technical replicates, and Excel 2016 was employed to assess statistical significance.

4.4. Subcellular Localization of GmNAC035

The full-length CDS sequence of *GmNAC035* was amplified from Tianlong No. 1 using the KOD FX (TOYOBO, Osaka, Japan), following the manufacturer's instructions. The pCAMBIA1305-GFP plasmid with the 35S promoter and the NOS Terminator was digested with QuickCut Spe I (Takara, Tokyo, Japan), and then the digested plasmid and the GmNAC035 gene fragment excluding the stop codon were ligated using the In-Fusion snap assembly master mix (Takara, Tokyo, Japan) [59,60]. The positive recombinant plasmid, pCAMBIA1305-GmNAC035-GFP (Figure S3), was transformed into Escherichia coli DH5α strain (YEASON, Shanghai, China) according to the manufacturer's instructions. Subsequently, the positive plasmid was introduced into the *Agrobacterium tumefaciens* GV3101 strain [61] and transiently expressed in tobacco leaves, as described previously [62]. Leaves were collected 48 h after transformation. OsD53-mCherry was used as a nuclear marker and came from Nanjing Agricultural University [63]. The empty vector served as a negative control. Observations were made using a laser scanning confocal microscope (LSM980, Carl Zeiss, Oberkochen, Germany). Regarding GFP signals, the excitation wavelength was configured at 488 nm, while the emission wavelength spanned from 505 to 530 nm. When it came to mCherry signals, an excitation wavelength of 587 nm was employed, and the emission wavelengths were measured within the 600–630 nm interval.

4.5. Transcriptional Self-Activation Activity Analysis

The pGBKT7 plasmid (Clontech, CA, USA) was digested by QuickCut *Eco*R I (Takara, Tokyo, Japan), and then the full-length CDS sequence of the *GmNAC035* gene was recombined with the linearized pGBKT7 plasmid using the In-Fusion snap assembly master mix (Takara, Tokyo, Japan). Following the manufacturer's instructions, the positive recombinant plasmid, pGBKT7-GmNAC035, was transformed into the yeast strain AH109

(YEASON, Shanghai, China). The pGBKT7-GmNAC181 plasmid was used as a positive control [64], and the empty pGBKT7 vector served as a negative control. The growth of positive colonies on SD/-Trp medium confirmed the presence of the transgene, while the growth on SD/-His/-Leu/-Trp medium indicated transcriptional activation activity. The information regarding the pGBKT7 vector is available at Clontech (https://www.takarabio.com/documents/Vector%20Documents/pGBKT7%20Vector%20Information.pdf, accessed on 10 January 2024).

4.6. Plant Transformation and Screening of Transgenic Plants

To obtain Arabidopsis thaliana plants overexpressing GmNAC035, we used the pCAMBIA 1300 plant expression vector containing the constitutive promoter pUBQ10 [65]. The pCAMBIA1300-GmNAC035 plasmid (Figure S3) was introduced into the Agrobacterium tumefaciens GV3101 strain [61]. The floral dip method was performed as described previously to transform the wild-type (WT) Arabidopsis Col 0 plants. [66]. Seeds harvested from transformed plants were screened for hygromycin resistance (40 mg/L). The expression levels of GmNAC035 in T_3 generation lines were detected using RT-qPCR, with specific primers listed in Table S7. Homozygous T_3 plants were used for further analysis.

4.7. Salt Tolerance Analysis of GmNAC035 Overexpression Lines

Seeds of three GmNAC035 overexpression transgenic lines and WT Arabidopsis were sterilized and incubated at 4 °C for 3 days, followed by cultivation on 1/2 MS medium for 4 days. The medium was prepared by mixing 2.22 g/L of PhytoTech M519 Murashige & Skoog Basal Medium with Vitamins (PhytoTech, Lenexa, KS, USA), 5 g/L of Gelzan™ CM (Sigma, Saint Louis, MO, USA), and 10 g/L of sucrose (Sigma, Saint Louis, MO, USA). After the mixture was prepared, the pH value was adjusted to 5.7–5.8 using 1 M KOH. The seedlings were then transferred to 1/2 MS medium mixed with different concentrations of NaCl (0 mM, 75 mM, 100 mM, and 125 mM) for salt stress treatment for 6 days. Seedlings were photographed, and their fresh weight, lateral root number, and survival rate under 100 mM NaCl stress were measured. MDA content and the activities of SOD and POD were determined using 100 mg of leaf tissue. The assays were performed using the Malondialdehyde (MDA) Content Assay Kit (Beijing Solarbio Science & Technology, Beijing, China), Peroxidase (POD) Activity Assay Kit (Beijing Solarbio Science & Technology, Beijing, China), and Superoxide Dismutase (SOD) Activity Assay Kit (Beijing Solarbio Science & Technology, Beijing, China), following the manufacturer's protocol. Under salt stress, plants produce hydrogen peroxide (H_2O_2) and superoxide (O_2^-), which mediate various physiological and biochemical processes. H_2O_2 and O_2^- were detected using 3, 3′-diaminobenzidine (DAB) (Shanghai yuanye Bio-Technology, Shanghai, China) and nitroblue tetrazolium (NBT) (Shanghai yuanye Bio-Technology, Shanghai, China), respectively. Leaves were immersed in 5 mg/mL DAB (aqueous solution, pH 3.8) and 0.5 mg/mL NBT (aqueous solution, pH 7.5) in the dark for 20 h. Afterward, the leaves were transferred to 95% ethanol and boiled in a water bath for 15 min. After cooling, the leaves were soaked in 95% ethanol at room temperature until completely decolorized [67].

5. Conclusions

In this study, 173 *GmNAC* genes were re-identified in the latest soybean genome database (Wm82.a4.v1), with 101 being salt-induced and 48 hypothesized as being crucial for the early salt stress response. Additionally, 18 *GmNAC* genes highly expressed in roots and rapidly responsive to salt stress were verified. Notably, the expression of *GmNAC035* was rapidly upregulated within one hour after salt treatment. GmNAC035 functions as

a nuclear-localized transcriptional activator. Our exploration of the regulatory function of *GmNAC035* in salt tolerance has shown that it plays a positive role in modulating plants' ability to withstand salt stress by mitigating oxidative damage and fine-tuning the expression of genes associated with the salt stress response, including the SOS pathway, calcium signaling, and ABA signaling. Our findings suggested that *GmNAC035* plays a regulatory role in plant salt tolerance, thereby offering novel genetic resources for enhancing soybean salt tolerance.

Supplementary Materials: The following supporting information can be downloaded at: https://www.mdpi.com/article/10.3390/plants14091391/s1. Figure S1: Expression profiles of *GmNAC* transcription factors in soybean in response to salt stress; Figure S2: Statistical analysis of root lengths of wild-type Arabidopsis and overexpression lines under salt stress at different concentrations; Figure S3: Schematic diagram of the vector used in this study; Table S1: Inventory of soybean *GmNAC* family; Table S2: ID and name of *GmNAC* family in different versions; Table S3: The expression of *GmNAC* family in salt-treated soybean root; Table S4: The expression of *GmNAC* genes in various organizations; Table S5: MDA content and determination of antioxidant enzyme activities; Table S6: The expression of salt tolerance-related genes; Table S7: Primers used for vector construction and RT-qPCR.

Author Contributions: Conceptualization, T.P. and Z.Z.; validation and formal analysis, W.S., S.Y., H.J., M.H. and Y.Z. (Yueping Zheng); data curation, Y.X., H.J., Y.Z. (Yihua Zhan), H.L. and Y.G.; writing—original draft preparation, W.S.; writing—review and editing, T.P.; funding acquisition, T.P. All authors have read and agreed to the published version of the manuscript.

Funding: This research was supported by the Biological Breeding-National Science and Technology Major Project (2023ZD0403201), the Zhejiang Provincial Natural Science Foundation of China (LQ24C130001), and the Program for Research and Development of Zhejiang A&F University (2022LFR109).

Data Availability Statement: The original contributions presented in the study are included in the article/Supplementary Materials.

Conflicts of Interest: The authors declare no conflicts of interest.

References

1. Staniak, M.; Szpunar-Krok, E.; Kocira, A. Responses of soybean to selected abiotic stresses-photoperiod, temperature and water. *Agriculture* **2023**, *13*, 146. [CrossRef]
2. Li, L.; Huang, Z.; Zhang, Y.; Mu, Y.; Li, Y.; Nie, L. Regulation of 2-acetyl-1-pyrroline (2-AP) biosynthesis and grain quality in fragrant rice under salt stress. *Field Crop Res.* **2025**, *322*, 109747. [CrossRef]
3. Shahid, I.; Batool, S.; Hassan, M.; Ismail, H.; Mehnaz, S.; Deeba, F.; Anwar, M.; Zulfiqar, F.; Iqbal, R.; Ali, H.M. A decade of progress in rhizoengineering to exploit plant microbiome for salt stress amelioration. *Plant Stress* **2024**, *11*, 100325. [CrossRef]
4. Singh, V.; Singh, J.; Singh, A. Salinity tolerance in soybeans: Physiological, molecular, and genetic perspectives. In *Soybean Improvement: Physiological, Molecular and Genetic Perspectives*; Springer: Berlin/Heidelberg, Germany, 2022; pp. 99–108.
5. Munns, R.; Tester, M. Mechanisms of salinity tolerance. *Annu. Rev. Plant Biol.* **2008**, *59*, 651–681. [CrossRef] [PubMed]
6. Van Zelm, E.; Zhang, Y.; Testerink, C. Salt tolerance mechanisms of plants. *Annu. Rev. Plant Biol.* **2020**, *71*, 403–433. [CrossRef]
7. Liang, X.; Li, J.; Yang, Y.; Jiang, C.; Guo, Y. Designing salt stress-resilient crops: Current progress and future challenges. *J. Integr. Plant Biol.* **2024**, *66*, 303–329. [CrossRef]
8. Leung, H.S.; Chan, L.Y.; Law, C.H.; Li, M.W.; Lam, H.M. Twenty years of mining salt tolerance genes in soybean. *Mol. Breed.* **2023**, *43*, 45. [CrossRef]
9. Baillo, E.H.; Kimotho, R.N.; Zhang, Z.; Xu, P. Transcription factors associated with abiotic and biotic stress tolerance and their potential for crops improvement. *Genes* **2019**, *10*, 771. [CrossRef] [PubMed]
10. Han, K.; Zhao, Y.; Sun, Y.; Li, Y. NACs, generalist in plant life. *Plant Biotechnol. J.* **2023**, *21*, 2433–2457. [CrossRef]
11. Shao, H.; Wang, H.; Tang, X. NAC transcription factors in plant multiple abiotic stress responses: Progress and prospects. *Front. Plant Sci.* **2015**, *6*, 902. [CrossRef]

12. Tran, L.S.P.; Nakashima, K.; Sakuma, Y.; Simpson, S.D.; Fujita, Y.; Maruyama, K.; Fujita, M.; Seki, M.; Shinozaki, K.; Yamaguchi-Shinozaki, K. Isolation and functional analysis of Arabidopsis stress-inducible NAC transcription factors that bind to a drought-responsive *cis*-element in the early responsive to dehydration stress 1 promoter. *Plant Cell* **2004**, *16*, 2481–2498. [CrossRef]
13. Li, Y.; Han, S.; Sun, X.; Khan, N.U.; Zhong, Q.; Zhang, Z.; Zhang, H.; Ming, F.; Li, Z.; Li, J. Variations in *OsSPL10* confer drought tolerance by directly regulating *OsNAC2* expression and ROS production in rice. *J. Integr. Plant Biol.* **2023**, *65*, 918–933. [CrossRef] [PubMed]
14. Mao, C.; Ding, J.; Zhang, B.; Xi, D.; Ming, F. *OsNAC2* positively affects salt-induced cell death and binds to the *OsAP37* and *OsCOX11* promoters. *Plant J.* **2018**, *94*, 454–468. [CrossRef] [PubMed]
15. Takasaki, H.; Maruyama, K.; Kidokoro, S.; Ito, Y.; Fujita, Y.; Shinozaki, K.; Yamaguchi-Shinozaki, K.; Nakashima, K. The abiotic stress-responsive NAC-type transcription factor *OsNAC5* regulates stress-inducible genes and stress tolerance in rice. *Mol. Genet. Genomics* **2010**, *284*, 173–183. [CrossRef] [PubMed]
16. Nakashima, K.; Tran, L.S.P.; Van Nguyen, D.; Fujita, M.; Maruyama, K.; Todaka, D.; Ito, Y.; Hayashi, N.; Shinozaki, K.; Yamaguchi-Shinozaki, K. Functional analysis of a NAC-type transcription factor *OsNAC6* involved in abiotic and biotic stress-responsive gene expression in rice. *Plant J.* **2007**, *51*, 617–630. [CrossRef]
17. Li, M.; Chen, R.; Jiang, Q.; Sun, X.; Zhang, H.; Hu, Z. *GmNAC06*, a NAC domain transcription factor enhances salt stress tolerance in soybean. *Plant Mol. Biol.* **2021**, *105*, 333–345. [CrossRef]
18. Hao, Y.J.; Wei, W.; Song, Q.X.; Chen, H.W.; Zhang, Y.Q.; Wang, F.; Zou, H.F.; Lei, G.; Tian, A.G.; Zhang, W.K. Soybean NAC transcription factors promote abiotic stress tolerance and lateral root formation in transgenic plants. *Plant J.* **2011**, *68*, 302–313. [CrossRef]
19. Hoang, X.L.T.; Chuong, N.N.; Hoa, T.T.K.; Doan, H.; Van, P.H.P.; Trang, L.D.M.; Huyen, P.N.T.; Le, D.T.; Tran, L.-S.P.; Thao, N.P. The drought-mediated soybean *GmNAC085* functions as a positive regulator of plant response to salinity. *Int. J. Mol. Sci.* **2021**, *22*, 8986. [CrossRef]
20. Yang, X.; Kim, M.Y.; Ha, J.; Lee, S.H. Overexpression of the soybean NAC gene *GmNAC109* increases lateral root formation and abiotic stress tolerance in transgenic Arabidopsis plants. *Front. Plant Sci.* **2019**, *10*, 1036. [CrossRef]
21. Chen, Z.; Yang, X.; Tang, M.; Wang, Y.; Zhang, Q.; Li, H.; Zhou, Y.; Sun, F.; Cui, X. Molecular Characterization and Drought Resistance of *GmNAC3* Transcription Factor in *Glycine max* (L.) Merr. *Int. J. Mol. Sci.* **2022**, *23*, 12378. [CrossRef]
22. Yang, C.; Huang, Y.; Lv, W.; Zhang, Y.; Bhat, J.A.; Kong, J.; Xing, H.; Zhao, J.; Zhao, T. *GmNAC8* acts as a positive regulator in soybean drought stress. *Plant Sci.* **2020**, *293*, 110442. [CrossRef] [PubMed]
23. Yang, C.; Huang, Y.; Lv, P.; Antwi-Boasiako, A.; Begum, N.; Zhao, T.; Zhao, J. NAC transcription factor *GmNAC12* improved drought stress tolerance in soybean. *Int. J. Mol. Sci.* **2022**, *23*, 12029. [CrossRef] [PubMed]
24. Cui, X.; Tang, M.; Li, L.; Chang, J.; Yang, X.; Chang, H.; Zhou, J.; Liu, M.; Wang, Y.; Zhou, Y. Expression patterns and molecular mechanisms regulating drought tolerance of soybean [*Glycine max* (L.) Merr.] conferred by transcription factor gene *GmNAC19*. *Int. J. Mol. Sci.* **2024**, *25*, 2396. [CrossRef]
25. Le, D.T.; Nishiyama, R.; Watanabe, Y.; Mochida, K.; Yamaguchi-Shinozaki, K.; Shinozaki, K.; Tran, L.S.P. Genome-wide survey and expression analysis of the plant-specific NAC transcription factor family in soybean during development and dehydration stress. *DNA Res.* **2011**, *18*, 263–276. [CrossRef] [PubMed]
26. Melo, B.P.; Fraga, O.T.; Silva, J.C.F.; Ferreira, D.O.; Brustolini, O.J.; Carpinetti, P.A.; Machado, J.P.B.; Reis, P.A.; Fontes, E.P. Revisiting the soybean GmNAC superfamily. *Front. Plant Sci.* **2018**, *9*, 1864. [CrossRef]
27. Amin, N.; Du, Y.; Lu, L.; Khalifa, M.A.; Ahmad, N.; Ahmad, S.; Wang, P. *GmNAC3* acts as a key regulator in soybean against drought stress. *Curr. Plant Biol.* **2024**, *38*, 100346. [CrossRef]
28. Yu, Z.; Duan, X.; Luo, L.; Dai, S.; Ding, Z.; Xia, G. How plant hormones mediate salt stress responses. *Trends Plant Sci.* **2020**, *25*, 1117–1130. [CrossRef]
29. Olsen, A.N.; Ernst, H.A.; Leggio, L.L.; Skriver, K. NAC transcription factors: Structurally distinct, functionally diverse. *Trends Plant Sci.* **2005**, *10*, 79–87. [CrossRef]
30. Yang, Y.; Guo, Y. Elucidating the molecular mechanisms mediating plant salt-stress responses. *New Phytol.* **2018**, *217*, 523–539. [CrossRef]
31. Van Breusegem, F.; Van Montagu, M.; Inzé, D. Engineering stress tolerance in maize. *Outlook Agric.* **1998**, *27*, 115–124. [CrossRef]
32. Bowler, C.; Montagu, M.v.; Inze, D. Superoxide dismutase and stress tolerance. *Annu. Rev. Plant Physiol. Plant Mol. Biol.* **1992**, *43*, 83–116. [CrossRef]
33. Zhao, C.; Zhang, H.; Song, C.; Zhu, J.K.; Shabala, S. Mechanisms of plant responses and adaptation to soil salinity. *Innovation* **2020**, *1*, 100017. [CrossRef]
34. Lu, K.K.; Song, R.F.; Guo, J.X.; Zhang, Y.; Zuo, J.X.; Chen, H.H.; Liao, C.Y.; Hu, X.Y.; Ren, F.; Lu, Y.T. CycC1; 1–WRKY75 complex-mediated transcriptional regulation of SOS1 controls salt stress tolerance in Arabidopsis. *Plant Cell* **2023**, *35*, 2570–2591. [CrossRef] [PubMed]

35. Apse, M.P.; Aharon, G.S.; Snedden, W.A.; Blumwald, E. Salt tolerance conferred by overexpression of a vacuolar Na^+/H^+ antiport in *Arabidopsis*. *Science* **1999**, *285*, 1256–1258. [CrossRef]
36. Ren, H.; Zhang, Y.; Zhong, M.; Hussian, J.; Tang, Y.; Liu, S.; Qi, G. Calcium signaling-mediated transcriptional reprogramming during abiotic stress response in plants. *Theor. Appl. Genet.* **2023**, *136*, 210. [CrossRef] [PubMed]
37. Xu, J.; Tian, Y.S.; Peng, R.H.; Xiong, A.S.; Zhu, B.; Jin, X.F.; Gao, F.; Fu, X.Y.; Hou, X.L.; Yao, Q.H. AtCPK6, a functionally redundant and positive regulator involved in salt/drought stress tolerance in Arabidopsis. *Planta* **2010**, *231*, 1251–1260. [CrossRef]
38. Shi, S.; Chen, W.; Sun, W. Comparative proteomic analysis of the *Arabidopsis cbl1* mutant in response to salt stress. *Proteomics* **2011**, *11*, 4712–4725. [CrossRef]
39. Barrero, J.M.; Rodríguez, P.L.; Quesada, V.; Piqueras, P.; Ponce, M.R.; Micol, J.L. Both abscisic acid (ABA)-dependent and ABA-independent pathways govern the induction of *NCED3*, *AAO3* and *ABA1* in response to salt stress. *Plant Cell Environ.* **2006**, *29*, 2000–2008. [CrossRef]
40. Yu, S.; Lan, X.; Zhou, J.; Gao, K.; Zhong, C.; Xie, J. Dioscorea composita *WRKY3* positively regulates salt-stress tolerance in transgenic *Arabidopsis thaliana*. *J. Plant Physiol.* **2022**, *269*, 153592. [CrossRef]
41. Chong, X.; Liu, Y.; Li, P.; Wang, Y.; Zhou, T.; Chen, H.; Wang, H. Heterologous expression of chrysanthemum TCP transcription factor *CmTCP13* enhances salinity tolerance in *Arabidopsis*. *Plants* **2024**, *13*, 2118. [CrossRef]
42. Liu, Y.; Peng, L.; Gao, X.; Liu, Y.; Liu, Z.; Li, X.; Yang, Y.; Wang, J. *AtPPRT3*, a novel E3 ubiquitin ligase, plays a positive role in ABA signaling. *Plant Cell Rep.* **2020**, *39*, 1467–1478. [CrossRef]
43. Phang, T.H.; Shao, G.; Lam, H.M. Salt tolerance in soybean. *J. Integr. Plant Biol.* **2008**, *50*, 1196–1212. [CrossRef]
44. Puranik, S.; Sahu, P.P.; Srivastava, P.S.; Prasad, M. NAC proteins: Regulation and role in stress tolerance. *Trends Plant Sci.* **2012**, *17*, 369–381. [CrossRef] [PubMed]
45. Yang, T.; Lv, R.; Li, J.; Lin, H.; Xi, D. Phytochrome A and B negatively regulate salt stress tolerance of *Nicotiana tobacum* via ABA–jasmonic acid synergistic cross-talk. *Plant Cell Physiol.* **2018**, *59*, 2381–2393. [CrossRef] [PubMed]
46. Suzuki, N.; Koussevitzky, S.; Mittler, R.; Miller, G. ROS and redox signalling in the response of plants to abiotic stress. *Plant Cell Environ.* **2012**, *35*, 259–270. [CrossRef] [PubMed]
47. Yan, L.; Lu, M.; Riaz, M.; Tong, K.; Yu, H.; Gao, G.; Niu, Y. Exogenous proline enhances salt acclimation in soybean seedlings: Modifying physicochemical properties and controlling proline metabolism through the ornithine-glutamate dual pathway. *Ecotoxicol. Environ. Saf.* **2025**, *294*, 118012. [CrossRef]
48. Ji, H.; Pardo, J.M.; Batelli, G.; Van Oosten, M.J.; Bressan, R.A.; Li, X. The salt overly sensitive (SOS) pathway: Established and emerging roles. *Mol. Plant* **2013**, *6*, 275–286. [CrossRef]
49. Yang, Y.; Guo, Y. Unraveling salt stress signaling in plants. *J. Integr. Plant Biol.* **2018**, *60*, 796–804. [CrossRef]
50. Kudla, J.; Becker, D.; Grill, E.; Hedrich, R.; Hippler, M.; Kummer, U.; Parniske, M.; Romeis, T.; Schumacher, K. Advances and current challenges in calcium signaling. *New Phytol.* **2018**, *218*, 414–431. [CrossRef]
51. Goodstein, D.M.; Shu, S.; Howson, R.; Neupane, R.; Hayes, R.D.; Fazo, J.; Mitros, T.; Dirks, W.; Hellsten, U.; Putnam, N. Phytozome: A comparative platform for green plant genomics. *Nucleic Acids Res.* **2012**, *40*, D1178–D1186. [CrossRef]
52. Mistry, J.; Chuguransky, S.; Williams, L.; Qureshi, M.; Salazar, G.A.; Sonnhammer, E.L.; Tosatto, S.C.; Paladin, L.; Raj, S.; Richardson, L.J. Pfam: The protein families database in 2021. *Nucleic Acids Res.* **2021**, *49*, D412–D419. [CrossRef] [PubMed]
53. Potter, S.C.; Luciani, A.; Eddy, S.R.; Park, Y.; Lopez, R.; Finn, R.D. HMMER web server: 2018 update. *Nucleic Acids Res.* **2018**, *46*, W200–W204. [CrossRef] [PubMed]
54. Belamkar, V.; Weeks, N.T.; Bharti, A.K.; Farmer, A.D.; Graham, M.A.; Cannon, S.B. Comprehensive characterization and RNA-Seq profiling of the HD-Zip transcription factor family in soybean (*Glycine max*) during dehydration and salt stress. *BMC Genomics* **2014**, *15*, 950. [CrossRef]
55. Zhao, Z.; Wang, R.; Zhao, X.; Xiong, W.; Tao, G.; Wu, S. Introduction, popularization and application of a new spring soybean variety "Tianlong No. 1" with high yield and good quality. *Soybean Sci. Technol.* **2014**, *2*, 49–52.
56. Xu, C.; Shan, J.; Liu, T.; Wang, Q.; Ji, Y.; Zhang, Y.; Wang, M.; Xia, N.; Zhao, L. CONSTANS-LIKE 1a positively regulates salt and drought tolerance in soybean. *Plant Physiol.* **2023**, *191*, 2427–2446. [CrossRef]
57. Dong, L.; Hou, Z.; Li, H.; Li, Z.; Fang, C.; Kong, L.; Li, Y.; Du, H.; Li, T.; Wang, L. Agronomical selection on loss-of-function of *GIGANTEA* simultaneously facilitates soybean salt tolerance and early maturity. *J. Integr. Plant Biol.* **2022**, *64*, 1866–1882. [CrossRef]
58. Wei, Z.; Pan, T.; Zhao, Y.; Su, B.; Ren, Y.; Qiu, L. Rab5a and its GEFs are involved in post-Golgi trafficking of storage proteins in developing soybean cotyledon. *J. Exp. Bot.* **2020**, *71*, 808–822. [CrossRef] [PubMed]
59. Zhou, C.; Lin, Q.; Ren, Y.; Lan, J.; Miao, R.; Feng, M.; Wang, X.; Liu, X.; Zhang, S.; Pan, T. A CYP78As-small grain4-coat protein complex II pathway promotes grain size in rice. *Plant Cell* **2023**, *35*, 4325–4346. [CrossRef]
60. Wang, F.; Cheng, Z.; Wang, J.; Zhang, F.; Zhang, B.; Luo, S.; Lei, C.; Pan, T.; Wang, Y.; Zhu, Y. Rice STOMATAL CYTOKINESIS DEFECTIVE2 regulates cell expansion by affecting vesicular trafficking in rice. *Plant Physiol.* **2022**, *189*, 567–584. [CrossRef]

61. Höfgen, R.; Willmitzer, L. Storage of competent cells for Agrobacterium transformation. *Nucleic Acids Res.* **1988**, *16*, 9877. [CrossRef]
62. Pan, T.; Wang, Y.; Jing, R.; Wang, Y.; Wei, Z.; Zhang, B.; Lei, C.; Qi, Y.; Wang, F.; Bao, X. Post-Golgi trafficking of rice storage proteins requires the small GTPase Rab7 activation complex MON1-CCZ1. *Plant Physiol.* **2021**, *187*, 2174–2191. [CrossRef] [PubMed]
63. Zhou, F.; Lin, Q.; Zhu, L.; Ren, Y.; Zhou, K.; Shabek, N.; Wu, F.; Mao, H.; Dong, W.; Gan, L. D14-SCF^{D3}-dependent degradation of D53 regulates strigolactone signalling. *Nature* **2013**, *504*, 406–410. [CrossRef] [PubMed]
64. Wang, X.; Chen, K.; Zhou, M.; Gao, Y.; Huang, H.; Liu, C.; Fan, Y.; Fan, Z.; Wang, Y.; Li, X. *GmNAC181* promotes symbiotic nodulation and salt tolerance of nodulation by directly regulating *GmNINa* expression in soybean. *New Phytol.* **2022**, *236*, 656–670. [CrossRef] [PubMed]
65. Jin, H.; Gao, S.; Xia, Y.; Hu, M.; Zheng, Y.; Ye, S.; Zhan, Y.; Yan, M.; Liu, H.; Gan, Y. *GmGIF5* promotes cell expansion by negatively regulating cell wall modification. *Int. J. Mol. Sci.* **2025**, *26*, 492. [CrossRef]
66. Clough, S.J.; Bent, A.F. Floral dip: A simplified method for Agrobacterium-mediated transformation of *Arabidopsis thaliana*. *Plant J.* **1998**, *16*, 735–743. [CrossRef]
67. Li, W.; Zeng, Y.; Yin, F.; Wei, R.; Mao, X. Genome-wide identification and comprehensive analysis of the NAC transcription factor family in sunflower during salt and drought stress. *Sci. Rep.* **2021**, *11*, 19865. [CrossRef]

plants

MDPI

Article

Synergistic Response Mechanisms in Rice Seedlings Exposed to Brown Planthopper Infestation and High-Temperature Stress

Danyun Cao [1], Yuchen Ping [1], Yiru Lin [1], Jinyan Hu [1], Zimeng Wang [1], Wei Yuan [1], Tongtong Li [1], Linxin Liu [1], Bo Zhang [2], Shijiao Xiong [3], Cong Dang [1,4,*] and Dawei Xue [1,4,*]

[1] College of Life and Environmental Sciences, Hangzhou Normal University, Hangzhou 311121, China; cdddyun@163.com (D.C.); pingyc01@gmail.com (Y.P.); 13958806614@163.com (Y.L.); h574023292@outlook.com (J.H.); 15256196768@163.com (Z.W.); 13714031710@163.com (W.Y.); 2023111010042@stu.hznu.edu.cn (T.L.); lancerllx@163.com (L.L.)
[2] National Key Laboratory of Rice Biology and Breeding, Institute of Insect Sciences, Zhejiang University, Hangzhou 310058, China; zhangbo2021@zju.edu.cn
[3] Xianghu Laboratory, Hangzhou 311231, China; xiongshijiao@zju.edu.cn
[4] Zhejiang Provincial Key Laboratory for Genetic Improvement and Quality Control of Medicinal Plants, Hangzhou Normal University, Hangzhou 311121, China
* Correspondence: dangcong@hznu.edu.cn (C.D.); dwxue@hznu.edu.cn (D.X.)

Abstract: Recently, rice yield has been severely affected by both brown planthopper (BPH, *Nilaparvata lugens*) infestation and high-temperature stress. Numerous previous studies have identified genes conferring resistance to BPH and high-temperature tolerance in rice, respectively. However, it remains unclear how rice synergistically responds to these two stress factors. In the present study, we found that pre-treatment with high temperature can enhance rice seeding resistance to BPH, while BPH feeding did not alter the high-temperature tolerance of rice. This result can be elucidated by the subsequent transcriptome analysis. Differentially expressed genes (DEGs) following high-temperature treatment were enriched in metabolic processes and phenylpropanoid biosynthesis pathways, thereby enhancing rice resistance to BPH. Further weighted gene co-expression network analysis (WGCNA) indicated that genes in the magenta and black modules were predominantly associated with the protein folding and transmembrane transport biological processes. And several candidate genes, including *Loc_Os01g02170* and *Loc_Os01g59870*, were identified that may play crucial roles in simultaneously regulating rice resistance to BPH and high-temperature stress. This research will provide new gene resources for cultivating rice with compound traits and provide ideas for the mechanism analysis of rice response to multiple stresses.

Keywords: synergistic response; transcriptome; brown planthopper; high temperature; stress; rice

1. Introduction

Rice (*Oryza sativa*) is one of the most important food crops in the world, which feeds at least half the world population [1]. In natural paddies, rice will face a plethora of biotic and abiotic stresses at the same time, including biotic stresses such as pathogens, insects, pests and weeds, and abiotic stresses such as salt, drought, heavy metals, heat and cold, which seriously affect plant growth and crop yield, leading to large-scale yield reduction [2–5]. In order to cope with various stresses, plants have evolved a series of complicated molecular and physiological mechanisms [6]. Therefore, it is very significant

for agricultural practice to understand how rice responds to multiple kinds of stresses and cultivate stress-resistant varieties.

Brown planthopper (BPH, *Nilaparvata lugens*) is a disastrous pest in rice cultivation. In recent decades, more than 70 BPH-resistance/QTLs genes have been detected in rice [7,8]. These BPH-resistant genes may enhance rice resistance to BPH by either influencing plant defense pathways such as salicylic acid (SA) and jasmonic acid (JA) or altering the volatile components and physical morphological structure of rice, thereby inducing certain levels of antibiosis or antixenosis against BPH [9]. For example, *OsBPH1/9* activates salicylic acid and jasmonic acid signaling pathways in rice and confers both antixenosis and antibiosis to brown planthopper [10]. *OsBph14* confers antibiosis resistance by inhibiting BPH feeding and reducing BPH growth rate and longevity [11,12]. Besides the above genes, a number of other pathway genes which were identified by the reverse genetics approach also participated in the pathway of rice resistance to BPH. *OsAOC* and *OsMYC2*, which are involved in the JA pathway, are significantly upregulated under BPH attack. BPH adult females laid more eggs on *osaoc* mutants than on WT plants, and the *osmyc2* mutants are susceptible to planthoppers in the field [13]. *OsEBF2* may reduce the content of ethylene in rice by inhibiting the expression of ethylene response factor genes and then positively regulates the rice resistance to BPH [14]. However, few of these BPH-resistant genes are associated with high-temperature stress in rice.

To mitigate the adverse effects of high-temperature stress, plants employ a diverse array of regulatory mechanisms. Heat shock factors (HSFs) and heat shock proteins (HSPs) play dominant roles in high-temperature stress. HSPs are regulated by HSFs and are induced in response to high-temperature stress. Some heat-responsive signal molecules (e.g., Ca^{2+}, NO, hormones) also act upstream of high-temperature stress [15,16]. Cyclic nucleotide-gated ion channels (CNGCs) genes *OsCNGC14* and *OsCNGC16* affect Ca^{2+} influx to the cytosol in response to heat treatments [17]. Rice *Theromotolerance 2* (*OsTT2*), encoding a G gamma subunit, confers thermotolerance in rice during both vegetative and reproductive growth. A natural allele with loss of *OsTT2* function was associated with greater retention of wax at high temperatures and increased thermotolerance [18].

In recent years, some multiple stress response genes have been found and studied in rice. Transcription factors always involve multiple stresses. The expression of *OsWRKY45* was induced by infestation of the BPH, cold stress and drought stress. *OsWRKY45* negatively regulated the resistance of BPH, while silencing *OsWRKY45* enhanced the H_2O_2 and ethylene levels induced by BPH and improved the resistance of rice to BPH [19]. The expression level of *OsWRKY76* could be activated by both rice blast and low-temperature stress. Overexpression of *OsWRKY76* inhibited the basic resistance to rice blast, while increasing the cold tolerance. After inoculation with rice blast, the overexpressed plants of *OsWRKY76* withered [20]. Expression of *OsNAC6* was induced by *Magnaporthe oryzae.* The tolerance of overexpressing *OsNAC6* to rice blast was slightly improved [21]. Overexpressed *OsNAC6* under the control of root-specific promoters or constitutive promoters showed drought tolerance, while *osnac6* mutants showed drought sensitivity. This gene enhanced drought tolerance by mediating the adaptation of root structure, including the increase in root number and root diameter [22]. Rice calcium-dependent protein kinase *OsCPK10* was upregulated in rice leaves after rice blast infection; meanwhile, the expression of this gene was also induced by drought stress. *OsCPK10* could reduce the level of lipid peroxidation, protect the integrity of the cell membrane and enhance the detoxification ability of rice plants to H_2O_2 by regulating the accumulation of catalase protein. This gene could mediate the resistance to rice blast by reducing the accumulation of H_2O_2 during the growth of necrotizing fungi. This also improved drought tolerance of rice under the constitutive accumulation of *OsCPK10* [23].

In the actual situation of rice fields, multiple stress factors exist at the same time. However, in most previous studies, there was only one single stress factor targeted. Recently, due to climate warming, rice varieties evolution, insecticide resistance and other reasons, high temperature and BPH infestation have become the major stress factors affecting rice yield, and it still remains unclear how rice responds to these two stress factors. In this study, the response of rice seedlings to high temperature and feeding by BPH was analyzed by transcriptome sequencing technology, which provided new gene resources for cultivating rice with compound traits and provided ideas for the mechanism analysis of rice response to multiple stresses.

2. Materials and Methods

2.1. Plants and BPH Population

The rice plants used in this study were variety ZH11 (Zhonghua No. 11), which is always used as wild type in BPH-resistant and heat-stress gene functions. All rice plants were cultivated under 26 ± 1 °C (day and night), 80–90% relative humidity and a light/dark period of 14 h/10 h. The rice seedlings were sown in hydroponics boxes (12.5 cm in depth, 8.5 in width and 11.5 cm in height).

The *Nilaparvata lugens* population was fed on susceptible rice variety TN1 (Taichung Native 1) in a climate-controlled plant incubator at 26 ± 1 °C, 14 h/10 h light/dark cycle and 80% relative humidity.

2.2. Performance Observation of Rice Seedings Under Heat and BPH Stress

Fourteen-day individual rice seeding plants were infested with 15 3rd instar BPH nymphs. Five treatments were conducted in this experiment. Treatment 1: rice seedings were cultured at 25 °C for 12 days (25 °C: 12 d). Treatment 2: rice seedings were cultured at 38 °C for 12 days (38 °C: 12 d). Treatment 3: rice seedings were infested by BPH nymphs at 25 °C for 12 days (25 °C, BPH: 12 d). Treatment 4: rice seedings were infested by BPH nymphs at 25 °C for 1 day and then cultured at 38 °C for 11 days (25 °C, BPH: 1 d + 38 °C: 11 d). Treatment 5: rice seedings were cultured at 38 °C for 1 day and then infested by BPH nymphs at 25 °C for 11 days (38 °C: 1 d + 25 °C, BPH: 11 d). During these treatments, the survival condition of rice plants was recorded. Each treatment contained 8 replicates.

2.3. Chlorophyll Extraction

After these treatments finished, total chlorophylls were extracted using 45% ethanol, 45% acetone and 10% H_2O at 4 °C for 12 h. The contents of chlorophyll were calculated using Arnon's formula with absorbance of the supernatant measured at 663 nm and 645 nm using an ultraviolet spectrophotometer (Shimadzu, Kyoto, Japan).

2.4. Sample Collection, RNA Isolation and Transcriptome Sequencing

The whole rice seeding plants were sampled immediately after 8 h of high-temperature and BPH treatment, and each treatment contained 3 replicates. Total RNA was isolated using the Eastep® Super Total RNA Extraction Kit (Shanghai Promega Biological Products, Ltd., Shanghai, China). The mRNA with polyA structure in total RNA was enriched by Oligo (dT) magnetic beads, and the RNA was interrupted to a fragment with a length of about 300 bp by ion interruption. After the library was constructed, PCR amplification was used to enrich the library fragments, and then the library was selected according to the fragment size, and the library size was 450 bp. Finally, these libraries were sequenced by the second next-generation sequencing (NGS) based on the Illumina sequencing platform.

The raw data for each sample were counted separately, including sample name, Q30, percentage of fuzzy bases, Q20 (%) and Q30 (%). The 3′ end joint is removed by Cutadapt,

and the removed part has at least 10 bp overlap (AGATCGGAAG) with the known joint, allowing 20% base mismatch; reads with average mass fraction lower than Q20 were removed. The fragments per kilobase of transcript per million mapped reads (FPKM) values were screened by difference multiple $|\log_2 \text{FoldChange}| > 1$. For the downstream analysis, in the case of differentially expressed genes (DEGs) expression, a cutoff at *p*-value of 0.05 was used for the up- and downregulated genes.

For each DEG, Gene Ontology (GO) and Kyoto Encyclopedia of Genes and Genomes (KEGG) enrichment analyses were conducted. Additionally, the proportion of DEGs enriched in a specific pathway was compared to the proportion of DEGs across all pathways. A DEG was considered significantly enriched when the *p*-value from the test was less than 0.05.

2.5. Quantitative Real-Time RT–PCR (qRT–PCR) Analysis

Total RNA was isolated by Eastep® Super Total RNA Extraction Kit (Shanghai Promega Biological Products, Ltd., Shanghai, China). The 1000 ng total RNA of each sample was reverse-transcribed by Hifair® III 1st Strand cDNA Synthesis SuperMix for qPCR (gDNA digester plus) kit (Yeasen Biotechnology Co. Ltd., Shanghai, China). Three independent biological samples were collected and analyzed. RT-qPCR was performed on the BIOER Line Gene 9600 Plus using Hieff® qPCR SYBR® Green Master Mix (No Rox) (Yeasen Biotechnology Co. Ltd., Shanghai, China). Primers used for target gene detection by RT-qPCR are listed in the Supporting Information, Table S1. Rice *ubiquitin* gene was used as internal reference, and $2^{-\triangle\triangle Ct}$ method was used to calculate the relative transcript levels of related genes [24].

2.6. Weighted Gene Co-Expression Network Analysis

The weighted gene co-expression network analysis (WGCNA) was constructed using the R software package WGCNA v1.72 [25]. The parameters were set as follows: -network type = unsigned, -soft power = 9, -module identification method = dynamic tree cut, -minimum module size = 30, -the threshold to merge modules with high similarity = 0.5. Ultimately, the target genes were clustered into 10 characteristic modules. Principal component analysis was performed on the genes in each module, with the first principal component defined as the module membership (MM), which characterizes the overall expression profile of the genes within the module. By treating tissue types as phenotypic traits, the correlation and statistical significance (*p* value) of each module's MM with the trait indicators were calculated to identify key modules significantly associated with specific traits. In module analysis, gene significance (GS) was defined as the absolute value of the correlation between gene expression and the target trait. The novel regulatory gene interaction network was visualized using Cytoscape v3.9.1.

2.7. Statistical Analysis

The significance of variation in all treatments was evaluated by one-way ANOVA followed by Tukey's HSD test. Statistical analysis was performed in Prism v. 8.0 software.

3. Results

3.1. Performance of Rice Seedings That Suffered Both Heat and BPH Stress

Rice seeding cultured at 25 °C was regarded as the control treatment (Figure 1A). During the seeding stage of rice plants under the dual stress of high temperature (38 °C) and infestation by brown planthoppers, it can be observed that after being infested by BPH nymphs for one day, and then suffering from high-temperature stress, the performance is similar with the treatment of heat stress without BPH infestation (Figure 1B,D,F). However,

when rice plants are treated with high temperature for one day, and then exposed to BPH stress, they exhibited better growth when subjected to subsequent BPH infestation (Figure 1C,E), and the chlorophyll contents in these two treatments are consistent with the rice performances (Figure 1F). It is noteworthy that all BPHs died after being exposed to the sustained high-temperature condition for just 1 day; hence, the treatment in which rice seedings were exposed to both heat and BPH stress simultaneously for 12 days was excluded from this experiment. In summary, prior exposure to high temperature can enhance the BPH resistance of rice plants, while prior exposure to BPH could not change the heat resistance. The genes and mechanisms regulating these phenotypic adjustments need further in-depth investigation.

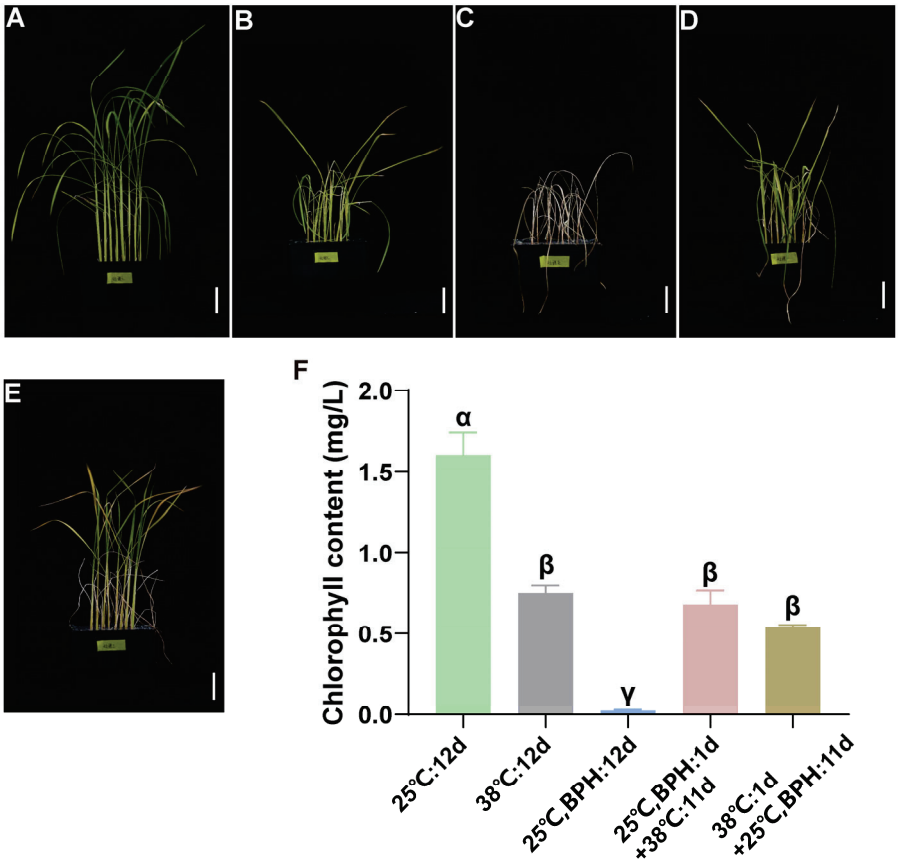

Figure 1. The performance of rice seedings that suffered both heat and BPH stress. (**A**–**E**) Different plant performances of rice seedings under five treatments; (**F**) chlorophyll content in rice seedings under five treatments. Mean ± SE, n = 8, different letters indicate significant differences between different treatments using Tukey's HSD test ($p < 0.05$).

3.2. Transcriptome Analysis of Rice Seedings That Suffered Both Heat and BPH Stress

To investigate the gene expression profiles of rice seedings that suffered both heat and BPH stress, we conducted transcriptomic analysis of plants subjected to four distinct experimental treatments: BPH-infested group (ZH11_B), high-temperature-stressed group (ZH11_H), both BPH-infested and high-temperature-stressed group (ZH11_B_H) and the untreated control group (ZH11). The results demonstrated that, compared to the control group, BPH infestation induced 1110 upregulated genes and 1493 downregulated genes, while high-temperature stress led to the upregulation of 1535 genes and downregulation of 1002 genes. When rice seeding suffered both BPH infestation and high-temperature stress, the number of upregulated and downregulated genes both exceeded 2000 (Figure 2A,B). The principal component analysis (PCA) revealed two distinct gene expression patterns

corresponding to BPH infestation and high-temperature stress, respectively (Figure 2C), which indicated the transcriptomic data were solid.

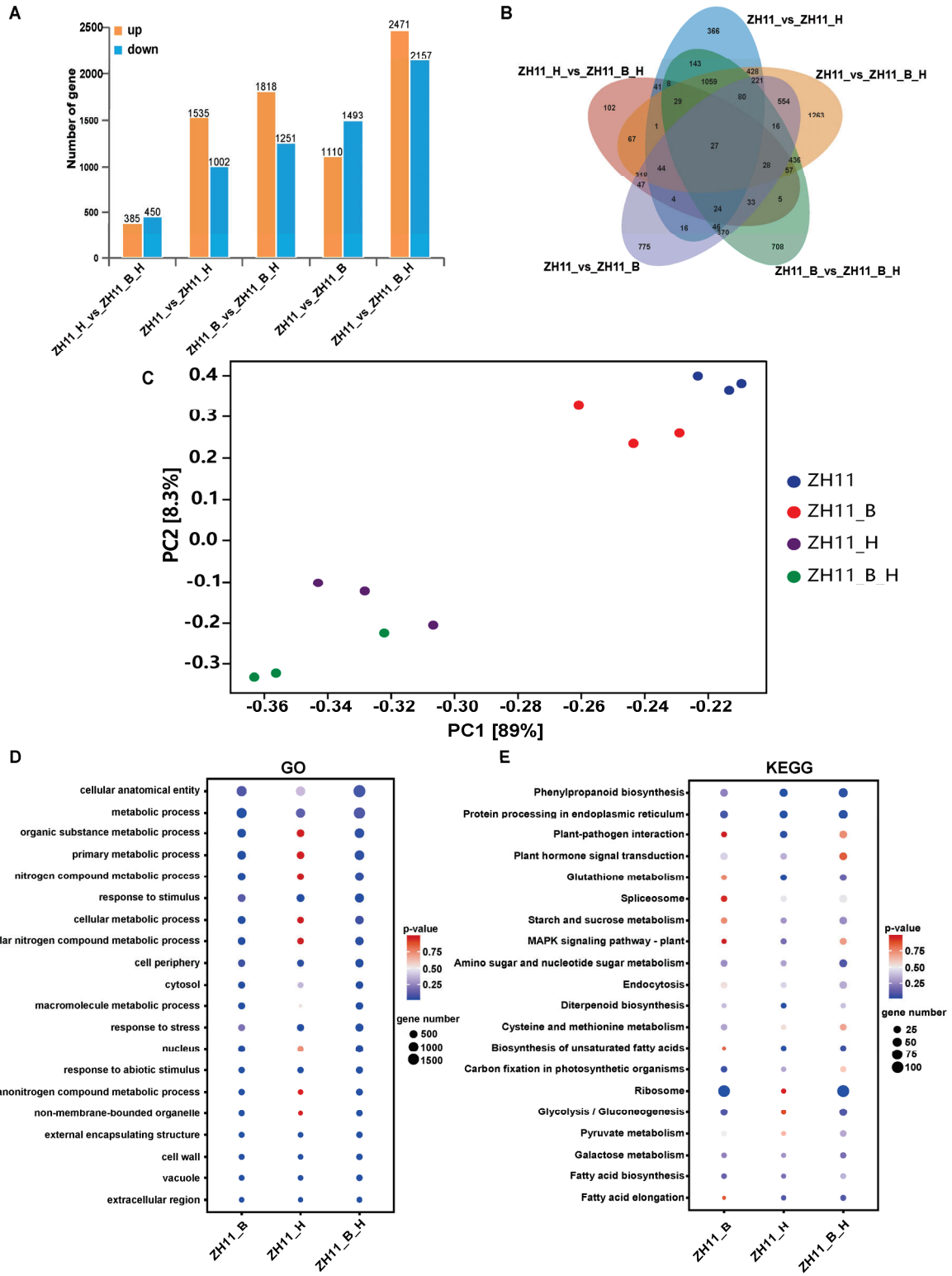

Figure 2. Transcriptome analysis of rice seedings that suffered both heat and BPH stress. (**A**) Histogram of differentially expressed genes (DEGs) from the transcriptome analysis; (**B**) Venn diagram of DEGs from the transcriptome analysis; (**C**) principal component analysis (PCA) of all the gene expression patterns; (**D**) top 20 terms of the DEGs GO enrichment analysis; (**E**) top 20 terms of the DEGs KEGG enrichment analysis.

Functional enrichment analysis of these DEGs revealed distinct biological patterns. GO enrichment analysis (Figure 2D) demonstrated that DEGs response to BPH infestation were primarily enriched in the pathways including cellular anatomical entity, metabolic process, macromolecule metabolic process, and so on. In contrast, DEGs induced by high-temperature stress were predominantly associated with metabolic process, response to stimulus, cell periphery and response to stress. When the two stress treatments were combined, DEGs showed enrichment patterns similar to BPH infestation, including cellular anatomical entity, metabolic process and macromolecule metabolic process. KEGG pathway analysis indicated that DEGs from both BPH-infestation and high-temperature-stress treatments were significantly enriched in protein processing in phenylpropanoid biosynthesis, ribosome and endoplasmic reticulum pathways (Figure 2E). To validate the accuracy of the transcriptomic data, some DEGs were selected to be verified by quantitative real-time PCR (qPCR) analysis (Figure S1), and most tested genes showed highly consistent expression patterns between qPCR results and RNA-seq data.

3.3. Analysis of the ROS Metabolic Regulation, SA and JA Pathways in Rice Seedings That Suffered Both Heat and BPH Stress

The enrichment analysis revealed a substantial number of DEGs in the reactive oxygen species (ROS), salicylic acid (SA) and jasmonic acid (JA) pathways under both stress conditions; thus, the DEGs in these three pathways were annotated and compared. In the ROS pathway (Figure 3A), genes such as the transcription factors *OsWRKY10*, *OsbHLH57* and stress-activated protein kinases *OsSAPK1*, *OsSAPK2* and *OsSAPK9* were significantly upregulated by BPH infestation, while their expression remained unaffected when they suffered high-temperature stress. In addition, high-temperature treatment induced significant upregulation of metallothionein *OsMT2b*, ARGONAUTE protein *OsAGO2*, transcription factors *OsbZIP20*, *OsbZIP71* and salicylic acid glucosyltransferase *OsSGT1*. These genes are also induced by the two-stress combination. Moreover, natural resistance-associated macrophage protein *OsNRAMP1* and ethylene-responsive transcription factor *OsERF48* are also significantly upregulated under both heat and BPH stress, whereas genes such as abscisic acid-stress-ripening-inducible 1 protein *OsASR5*, glutamine synthetase *OsGS1* and WINDHOSE protein *OsWIH2* are significantly downregulated by the two-stress combination.

In the SA pathway (Figure 3B), genes including DnaJ protein *OsDjA6*, protein tyrosine phosphatase *OsPTP1*, acyl-CoA-binding protein *OsACBP5*, WRKY transcription factor *OsWRKY67* and *OsWRKY33* are upregulated under combined BPH and high-temperature stress. Similarly, in the JA pathway (Figure 3C), genes such as WRKY transcription factor *OsWRKY28*, early responsive leucine-rich repeat receptor-like kinase *OsLRR-RLK1* and JA-amino acid synthetase *OsJar1* are upregulated under the combined stress conditions. In contrast, the expression levels of ROP GTPase *OsRAC3*, TCP family transcription factor *OsTCP21*, dehydration-responsive element-binding protein *OsDREB6* and protein tyrosine phosphatase *OsPTP2* are significantly downregulated under the combined stress treatment. These expression changes may be associated with the enhanced insect resistance observed in rice under high-temperature conditions.

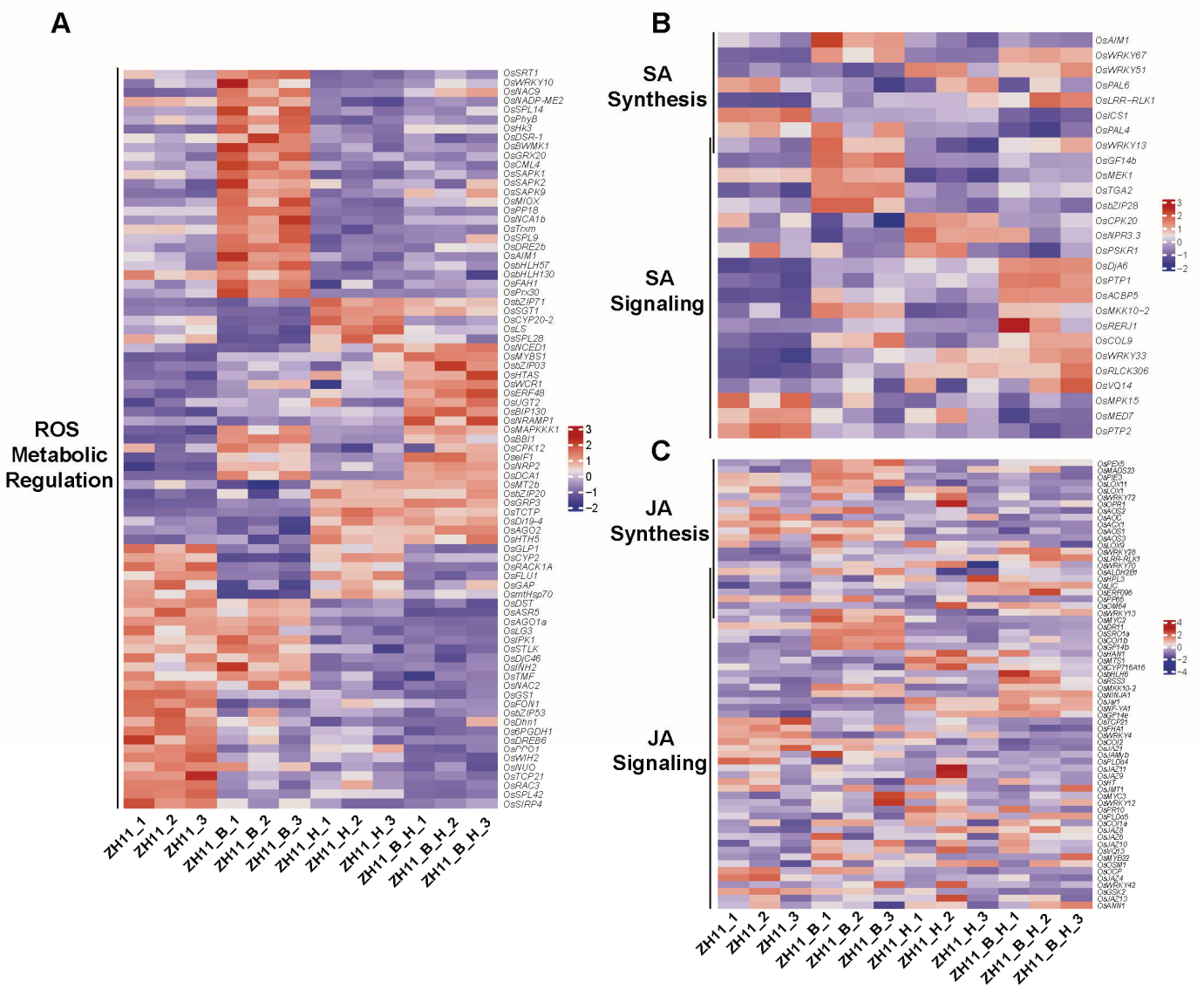

Figure 3. Gene expression in ROS metabolic regulation (**A**), salicylic acid (**B**) and jasmonic acid (**C**) pathways.

3.4. Weighted Gene Co-Expression Network Analysis for the DEGs from Transcriptome

To further identify the genes associated with resistance to BPH infestation and high-temperature stress, a WGCNA was performed based on all DEGs from transcriptome. According to the different gene expression patterns, 10 distinct color-coded modules were clustered. Among these modules, three modules, including lightyellow, magenta and black, showed significant correlations with both BPH infestation and high-temperature stress (Figure 4A). Within these color modules, both the magenta (cor = 0.69, $p < 0.001$) and black (cor = 0.2, $p = 0.017$) modules demonstrated significant correlations between module membership (MM) and gene significance (GS), while the lightyellow module exhibited a moderate correlation (cor = 0.29, $p = 0.082$) (Figure 4B–D). These results indicate that the magenta and black modules represent transcriptional signatures associated with rice responses to combined BPH infestation and high-temperature stress.

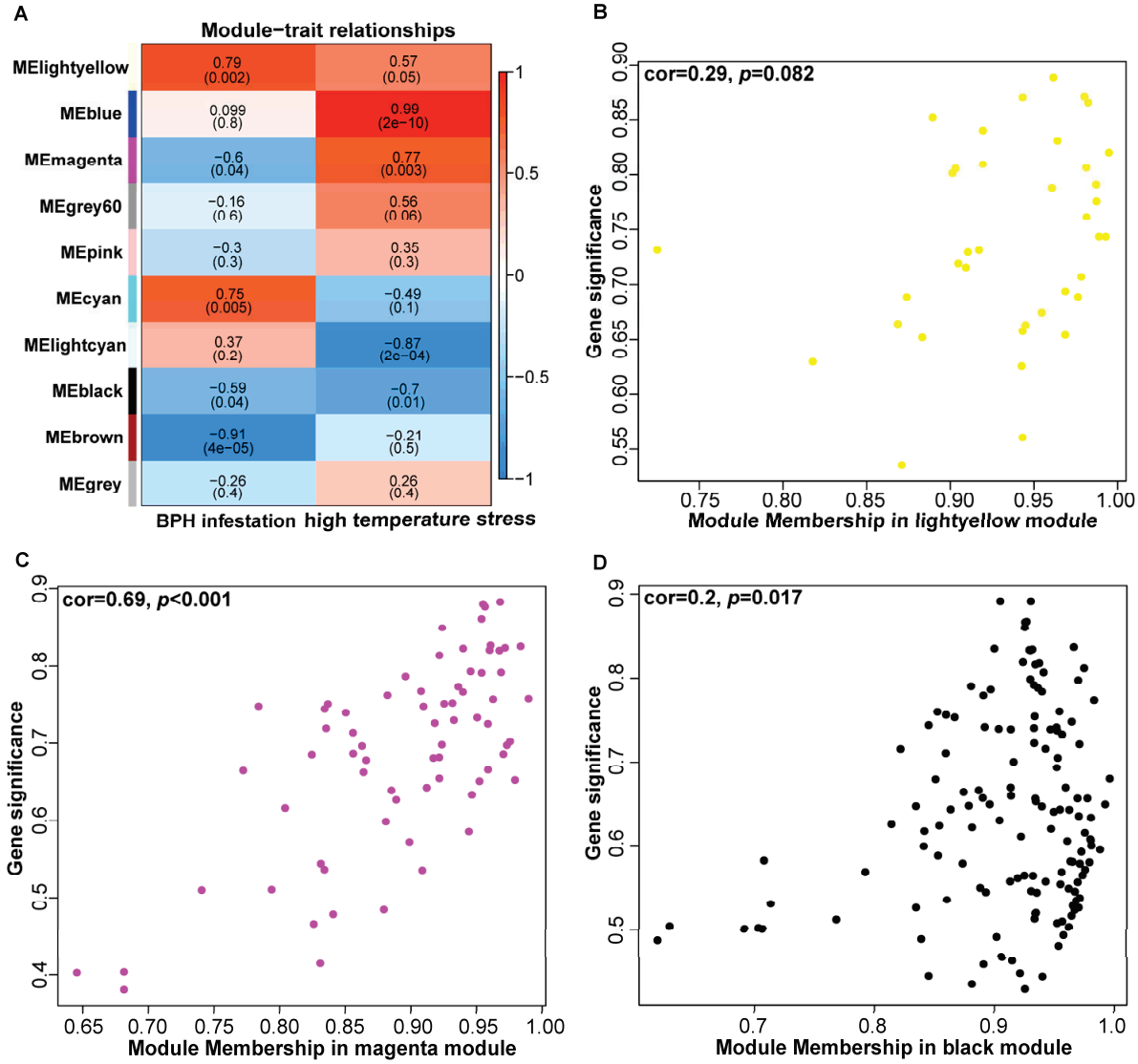

Figure 4. Weighted gene co-expression network analysis (WGCNA) for the DEGs. (**A**) Correlation heatmap between the modules and two phenotypic traits (BPH infestation and high-temperature stress); (**B**) correlation scatterplot between module membership and gene significance within the lightyellow module (cor = 0.29, $p = 0.082$); (**C**) correlation scatterplot between module membership and gene significance within the magenta module (cor = 0.69, $p < 0.001$); (**D**) correlation scatterplot between module membership and gene significance within the black module (cor = 0.2, $p = 0.017$).

Then, genes in the magenta and black modules were further analyzed. GO enrichment analysis demonstrated that genes within the magenta module were predominantly associated with the protein folding and transmembrane transport biological processes (Figure 5A). Meanwhile, the black module genes were significantly enriched in biological processes including cell wall organization, lipid transport and response to chemicals (Figure 5B). Network analysis of the 65 members in the magenta module was performed using Cytoscape (Figure 6A). By screening for high-weight members, we identified *Loc_Os01g02170*, *Loc_Os03g11690* and *Loc_Os12g42380* as core genes within this module. Similarly, in the black module, *Loc_Os01g59870*, *Loc_Os05g39050* and *Loc_Os06g45990* were identified as core genes (Figure 6B). These genes are likely to play crucial roles in rice responses to both BPH infestation and high-temperature stress, which need further functional characterization in future studies.

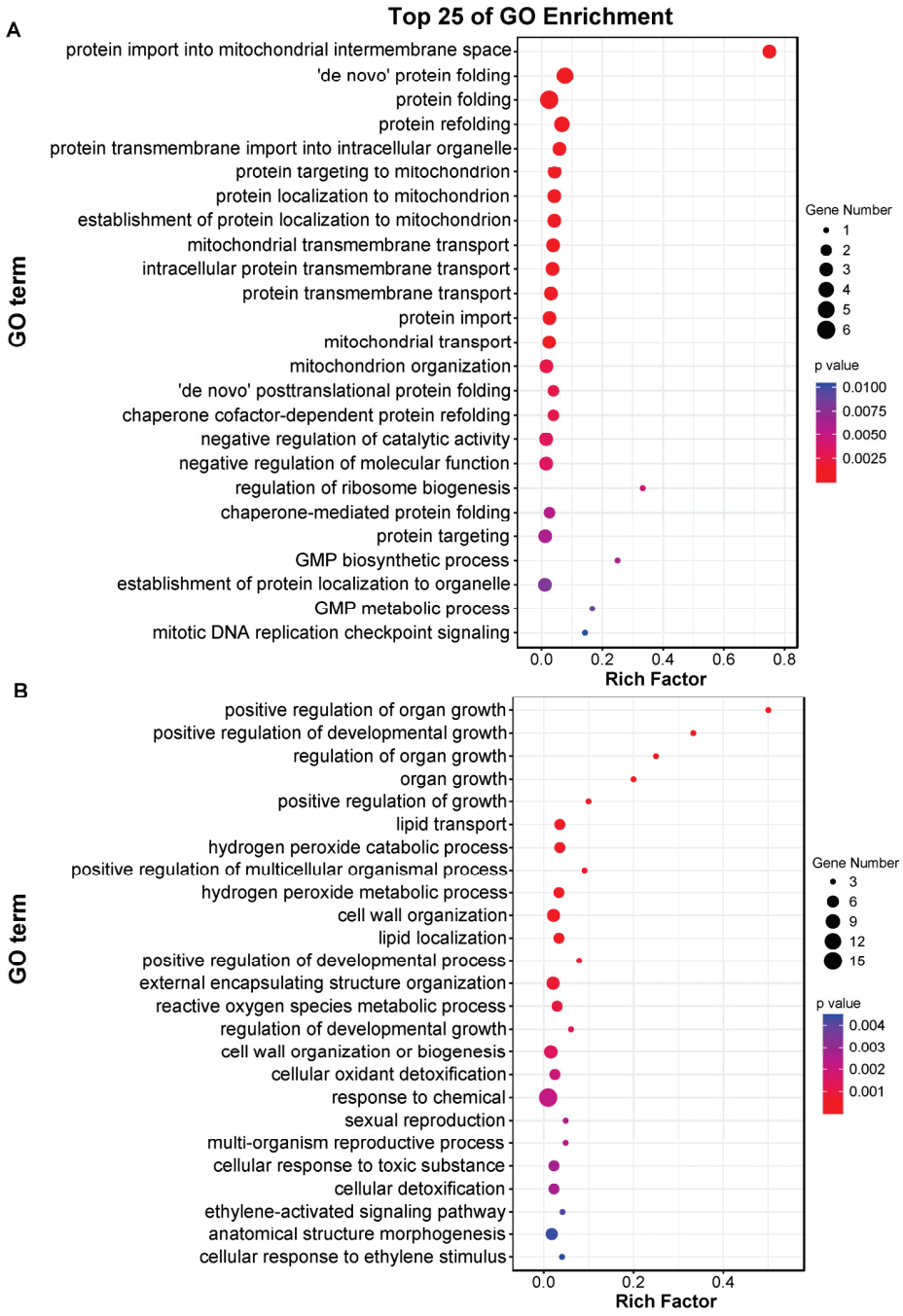

Figure 5. GO enrichment of the DEGs in the magenta (**A**) and black (**B**) modules.

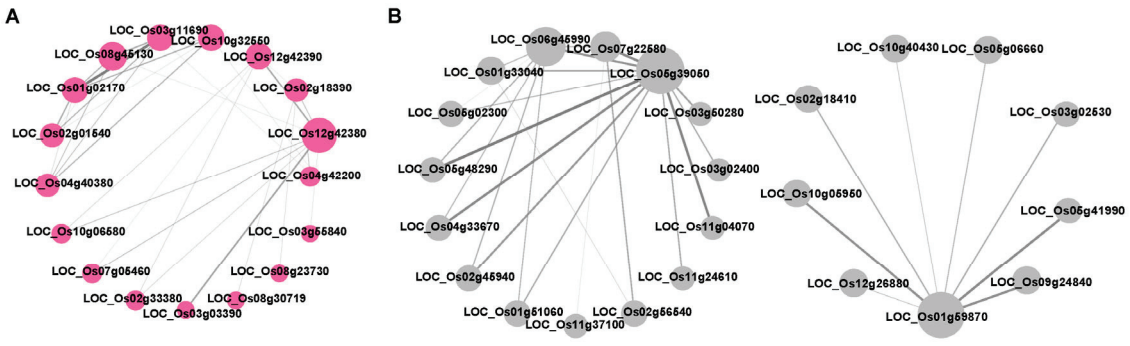

Figure 6. Gene functional network analysis in magenta (**A**) and black (**B**) modules.

4. Discussion

Currently, in rice-growing regions, particularly in southern China, rice yield is severely affected by both high temperatures and brown planthopper (BPH). Numerous previous studies have identified genes conferring resistance to BPH and high-temperature tolerance in rice, respectively. However, there has been little research integrating these two types of stress factors, one biotic (BPH) and the other abiotic (high temperature). In the present study, we found that pre-treatment with high temperature can enhance rice resistance to BPH, but BPH feeding did not alter the high-temperature tolerance of rice (Figure 1). This result can be elucidated by the subsequent transcriptome sequencing data.

Differentially expressed genes (DEGs) following high-temperature treatment were enriched in metabolic processes and phenylpropanoid biosynthesis pathways (Figure 2D,E), which included metallothionein *OsMT2b*, ARGONAUTE protein *OsAGO2*, salicylic acid (SA) glucosyltransferase *OsSGT1*, transcription factors *OsbZIP20* and *OsbZIP71*, and other metabolism-related genes (Figure 3A). These genes have been reported to be involved in defense regulation in rice. For instance, *OsAGO2* can activate early defense immunity, such as the recombination of defense-related gene expression and the accumulation of reactive oxygen species, which may also be associated with BPH resistance [26]. *OsSGT1* encodes a salicylic acid glucosyltransferase, a key enzyme for SA metabolism, catalyzing the conversion of free SA to SA O-β-glucoside, and plays an important role in plant resistance regulation [27]. Phenylpropanoid is an important precursor for SA synthesis. High-temperature stress also led to a decrease in the transcription levels of SA synthesis pathway genes *OsPAL4* and *OsICS1* (Figure 3B), which are key genes for SA synthesis and may thus affect rice resistance to BPH. It has been reported that in *OsPAL4*-knockout rice, two flavonoid phytoalexins, sakuranetin and naringenin, are almost completely absent, and the levels of SA and jasmonic acid (JA) in the roots are also reduced, which may also lead to a decrease in rice resistance to BPH [28]. Meanwhile, calcium-dependent protein kinase *OsCPK20* was significantly induced by high temperature, and its high expression can also enhance rice's immune capacity [29]. In the ribosome pathway, ribosome-inactivating protein *OsRIP1* was upregulated by BPH infestation, and the recombinant *OsRIP1* was toxic to brown planthoppers, suggesting that this ribosome pathway gene plays an important role in rice resistance to BPH [30]. Thus, high-temperature pre-treatment induced the expression of these BPH-resistance-related genes, thereby enhancing rice resistance to BPH. However, further validations of key metabolites and the accumulation of JA and SA are still required.

Through transcriptome screening, we have also identified several genes that respond simultaneously to BPH feeding and high-temperature stress. In-depth exploration and functional analysis of these genes could lead to the development of new rice varieties that are resistant to both high temperatures and BPH. These genes include natural resistance-associated macrophage protein *OsNRAMP1* and ethylene-responsive transcription factor *OsERF48*, WRKY transcription factor *OsWRKY28*, early responsive leucine-rich repeat receptor-like kinase *OsLRR-RLK1* and JA-amino acid synthetase *OsJar1*, which have been reported to respond to various stresses. *OsNRAMP1* is involved in rice's response to low-temperature stress [31]. *OsERF48* regulates the expression of calmodulin gene *OsCML16*, thereby enhancing rice's drought tolerance. Overexpression of this gene can also affect physiological indicators such as superoxide dismutase, catalase and malondialdehyde, thereby enhancing redox homeostasis and membrane stability [32,33]. *OsWRKY28* positively regulates rice's resistance to sheath blight, while negatively regulating resistance to blast and bacterial blight. In the mutant *oswrky28*, the contents of SA and JA are higher than in the wild type [34]. *OsLRR-RLK1* positively regulates resistance to the rice stem borer and may be involved in the perception of herbivore-associated molecular patterns [35].

OsJAR1 is crucial for the accumulation of JA-IIe in crops when they are fed upon by pests. It catalyzes the synthesis of JA-Ile, the active form of JA that triggers the JA signaling pathway, also playing an important role in rice under high-temperature stress [36].

After the weighted gene co-expression network analysis (WGCNA), we identified several candidate genes that may play crucial roles in simultaneously regulating rice resistance to BPH and high-temperature stress. These genes include *Loc_Os01g02170*, *Loc_Os03g11690*, *Loc_Os12g42380*, *Loc_Os05g39050*, *Loc_Os06g45990* and *Loc_Os01g59870*. Notably, *Loc_Os01g59870* encodes lipid transfer protein *LTPL65*, which has been reported to be induced by BPH feeding [37]. Additionally, *LTP* family genes have been implicated in plant responses to high-temperature stress [38]. This suggests that *LTPL65* may have an important function in simultaneously responding to BPH feeding and high-temperature stress, warranting further in-depth investigation in the future.

However, when high-temperature and BPH stresses occur simultaneously, the entire process becomes highly complex. High temperature can affect not only plant growth but also the feeding behavior of herbivorous insects. It has been reported that high temperature can reprogram the JA signaling-mediated plant-induced defense. For instance, potato tuber moth *Phthorimaea operculella* grew heavier on leaves co-stressed by high temperature and insect herbivory than on leaves pre-stressed by herbivory alone [39]. And in warmer years, the damage caused by pests on temperature-sensitive plants is more severe [40]. However, in the present study, high-temperature pre-treatment enhanced rice resistance to BPH. Based on our analyses, high-temperature pre-treatment may have upregulated the expression of defense-related genes in rice. Therefore, when analyzing the interaction between rice responses to high-temperature and BPH-feeding stresses, the specific functions of each gene need to be investigated in depth. Moreover, there may be a certain balance between rice regulation of resistance to high temperature and BPH, in which phytohormones may play an important coordinating role in this balance mechanism.

Although we have identified some candidate genes that respond to both BPH infestation and high-temperature stress, their functional validation is still lacking. In the future, we will use gene editing techniques to create rice mutants of these genes, study their functions and regulatory networks, and conduct relevant phenotypic validation in the field. It should be noted that this experiment used sustained high temperature to identify some candidate genes. However, in the actual field situation, high temperature is not always sustained. In the future, we will also simulate the actual field environment, which includes periodic high temperatures, to further investigate the functions of these candidate genes. And the other rice growth stages, especially the reproductive growth period, will also be taken into consideration in the future.

5. Conclusions

In summary, under the escalating pressures of global climate change and intensive agricultural practices, rice cultivation is anticipated to confront increasingly complex biotic and abiotic stresses in field environments. To address these challenges, it is imperative to systematically investigate the functional roles of stress-responsive genes and their regulatory networks through advanced genomics, transcriptomics and metabolomics approaches. In this study, pre-treatment with high temperature can enhance rice seeding resistance to BPH, and it can be elucidated by the DEGs following high-temperature treatment, which were enriched in metabolic processes and phenylpropanoid biosynthesis pathways. Further WGCNA indicated that genes in the magenta and black modules were predominantly associated with the protein folding and transmembrane transport biological processes. And several candidate genes, including *Loc_Os01g02170* and *Loc_Os01g59870*, were identified that may play crucial roles in simultaneously regulating rice resistance to BPH and high-

temperature stress. This research will enable the precise engineering of novel crop cultivars with multiplex traits, combining enhanced multiple stress resilience and yield potential.

Supplementary Materials: The following supporting information can be downloaded at https://www.mdpi.com/article/10.3390/plants14111644/s1, Figure S1: the verification of some DEGs by quantitative real-time PCR, Table S1: primers used in the quantitative real-time PCR experiment.

Author Contributions: Conceptualization, C.D., D.X. and D.C.; methodology, D.C., C.D., Z.W. and W.Y.; visualization, D.C., C.D., Y.P., B.Z. and S.X.; resources, Y.L., J.H. and L.L.; writing—original draft, D.C. and C.D.; writing—review and editing, D.C., C.D., T.L. and D.X.; supervision and funding acquisition, C.D., J.H. and D.X. All authors have read and agreed to the published version of the manuscript.

Funding: This work was supported and funded by Natural Science Foundation of Zhejiang province in China (LQ24C140003), National Natural Science Foundation of China (32402356), Interdisciplinary Research Project of Hangzhou Normal University (2025JCXK01), Natural Science Foundation of Zhejiang province in China (LMS25C130005) and the National Undergraduate Training Programs for Innovation and Entrepreneurship of China.

Data Availability Statement: All data supporting this study are included in the article.

Conflicts of Interest: The authors declare no conflicts of interest.

References

1. Gutaker, R.M.; Groen, S.C.; Bellis, E.S.; Choi, J.Y.; Pires, I.S.; Bocinsky, R.K.; Slayton, E.R.; Wilkins, O.; Castillo, C.C.; Negrao, S.; et al. Genomic history and ecology of the geographic spread of rice. *Nat. Plants* **2020**, *6*, 492–502. [CrossRef] [PubMed]
2. Zhou, Y.B.; Liu, C.; Tang, D.Y.; Yan, L.; Wang, D.; Yang, Y.Z.; Gui, J.S.; Zhao, X.Y.; Li, L.G.; Tang, X.D.; et al. The receptor-like cytoplasmic kinase STRK1 phosphorylates and activates CatC, thereby regulating H_2O_2 homeostasis and improving salt tolerance in rice. *Plant Cell* **2018**, *30*, 1100–1118. [CrossRef] [PubMed]
3. Reddy, I.; Kim, B.K.; Yoon, I.S.; Kim, K.H.; Kwon, T.R. Salt tolerance in rice: Focus on mechanisms and approaches. *Rice Sci.* **2017**, *24*, 123–144. [CrossRef]
4. Singh, A.; Jones, S.; Ganapathysubramanian, B.; Sarkar, S.; Mueller, D.; Sandhu, K.; Nagasubramanian, K. Challenges and opportunities in machine-augmented plant stress phenotyping. *Trends Plant Sci.* **2021**, *26*, 53–69. [CrossRef]
5. Xu, G.; Li, C.T.; Gui, W.; Xu, M.Q.; Lu, J.; Qian, M.S.; Zhang, Y.Y.; Yang, G.Q. Colonization of *Piriformospora indica* enhances rice resistance against the brown planthopper *Nilaparvata lugens*. *Pest Manag. Sci.* **2024**, *80*, 4386–4398. [CrossRef]
6. Zhang, Q.; Teng, R.; Yuan, Z.; Sheng, S.; Xiao, Y.; Deng, H.; Tang, W.; Wang, F. Integrative transcriptomic analysis deciphering the role of rice bHLH transcription factor Os04g0301500 in mediating responses to biotic and abiotic stresses. *Front. Plant Sci.* **2023**, *14*, 1266242. [CrossRef]
7. Shi, S.J.; Wang, H.Y.; Zha, W.J.; Wu, Y.; Liu, K.; Xu, D.Z.; He, G.C.; Zhou, L.; You, A.Q. Recent advances in the genetic and biochemical mechanisms of rice resistance to brown planthoppers (*Nilaparvata lugens* Stal). *Int. J. Mol. Sci.* **2023**, *24*, 16959. [CrossRef]
8. Yan, L.H.; Luo, T.P.; Huang, D.H.; Wei, M.Y.; Ma, Z.F.; Liu, C.; Qin, Y.Y.; Zhou, X.L.; Lu, Y.P.; Li, R.B.; et al. Recent advances in molecular mechanism and breeding utilization of brown planthopper resistance genes in rice: An integrated review. *Int. J. Mol. Sci.* **2023**, *24*, 12061. [CrossRef]
9. Guo, J.; Chen, R.; Du, B.; Zhu, L.; He, G. Progress in exploitation and utilization of brown planthopper resistance gene in rice. *Sci. Sin. Vitae* **2022**, *52*, 1326–1334. [CrossRef]
10. Zhao, Y.; Huang, J.; Wang, Z.Z.; Jing, S.L.; Wang, Y.; Ouyang, Y.D.; Cai, B.D.; Xin, X.F.; Liu, X.; Zhang, C.X.; et al. Allelic diversity in an NLR gene *BPH9* enables rice to combat planthopper variation. *Proc. Natl. Acad. Sci. USA* **2016**, *113*, 12850–12855. [CrossRef]
11. Cheng, X.Y.; Zhu, L.L.; He, G.C. Towards understanding of molecular interactions between rice and the brown planthopper. *Mol. Plant* **2013**, *6*, 621–634. [CrossRef] [PubMed]
12. Du, B.; Zhang, W.L.; Liu, B.F.; Hu, J.; Wei, Z.; Shi, Z.Y.; He, R.F.; Zhu, L.L.; Chen, R.Z.; Han, B.; et al. Identification and characterization of *Bph14*, a gene conferring resistance to brown planthopper in rice. *Proc. Natl. Acad. Sci. USA* **2009**, *106*, 22163–22168. [CrossRef] [PubMed]
13. Xu, J.; Wang, X.J.; Zu, H.Y.; Zeng, X.; Baldwin, I.T.; Lou, Y.G.; Li, R. Molecular dissection of rice phytohormone signaling involved in resistance to a piercing-sucking herbivore. *New Phytol.* **2021**, *230*, 1639–1652. [CrossRef] [PubMed]

14. Ma, F.L.; Li, Z.X.; Wang, S.Y.; Li, K.J.; Tang, F.; Jia, J.X.; Zhao, Q.J.; Jing, P.H.; Yang, W.Q.; Hua, C.M.; et al. The F-box protein OsEBF2 confers the resistance to the brown planthopper (*Nilparvata lugens* Stal). *Plant Sci.* **2023**, *327*, 474–487. [CrossRef]
15. Kan, Y.; Mu, X.R.; Gao, J.; Lin, H.X.; Lin, Y.S. The molecular basis of heat stress responses in plants. *Mol. Plant* **2023**, *16*, 1612–1634. [CrossRef]
16. Yang, Y.X.; Zhang, C.; Zhu, D.; He, H.Y.; Wei, Z.R.; Yuan, Q.L.; Li, X.X.; Gao, X.; Zhang, B.; Gao, H.S.; et al. Identifying candidate genes and patterns of heat-stress response in rice using a genome-wide association study and transcriptome analyses. *Crop J.* **2022**, *10*, 1633–1643. [CrossRef]
17. Cui, Y.M.; Lu, S.; Li, Z.; Cheng, J.W.; Hu, P.; Zhu, T.Q.; Wang, X.; Jin, M.; Wang, X.X.; Li, L.Q.; et al. CYCLIC NUCLEOTIDE-GATED ION CHANNELs 14 and 16 promote tolerance to heat and chilling in rice. *Plant Physiol.* **2020**, *183*, 1794–1808. [CrossRef]
18. Kan, Y.; Mu, X.R.; Zhang, H.; Gao, J.; Shan, J.X.; Ye, W.W.; Lin, H.X. *TT2* controls rice thermotolerance through SCT1-dependent alteration of wax biosynthesis. *Nat. Plants* **2022**, *8*, 53–67. [CrossRef]
19. Huangfu, J.Y.; Li, J.C.; Li, R.; Ye, M.; Kuai, P.; Zhang, T.F.; Lou, Y.G. The transcription factor OsWRKY45 negatively modulates the resistance of rice to the brown planthopper *Nilaparvata lugens*. *Int. J. Mol. Sci.* **2016**, *17*, 697. [CrossRef]
20. Yokotani, N.; Sato, Y.; Tanabe, S.; Chujo, T.; Shimizu, T.; Okada, K.; Yamane, H.; Shimono, M.; Sugano, S.; Takatsuji, H.; et al. WRKY76 is a rice transcriptional repressor playing opposite roles in blast disease resistance and cold stress tolerance. *J. Exp. Bot.* **2013**, *64*, 5085–5097. [CrossRef]
21. Nakashima, K.; Tran, L.S.P.; Van Nguyen, D.; Fujita, M.; Maruyama, K.; Todaka, D.; Ito, Y.; Hayashi, N.; Shinozaki, K.; Yamaguchi-Shinozaki, K. Functional analysis of a NAC-type transcription factor OsNAC6 involved in abiotic and biotic stress-responsive gene expression in rice. *Plant J.* **2007**, *51*, 617–630. [CrossRef] [PubMed]
22. Lee, D.K.; Chung, P.J.; Jeong, J.S.; Jang, G.; Bang, S.W.; Jung, H.; Kim, Y.S.; Ha, S.H.; Choi, Y.D.; Kim, J.K. The rice OsNAC6 transcription factor orchestrates multiple molecular mechanisms involving root structural adaptions and nicotianamine biosynthesis for drought tolerance. *Plant Biotechnol. J.* **2017**, *15*, 754–764. [CrossRef] [PubMed]
23. Bundó, M.; Coca, M. Calcium-dependent protein kinase OsCPK10 mediates both drought tolerance and blast disease resistance in rice plants. *J. Exp. Bot.* **2017**, *68*, 2963–2975. [CrossRef]
24. Bustin, S.A.; Benes, V.; Garson, J.A.; Hellemans, J.; Huggett, J.; Kubista, M.; Mueller, R.; Nolan, T.; Pfaffl, M.W.; Shipley, G.L.; et al. The MIQE guidelines: Minimum information for publication of quantitative real-time PCR experiments. *Clin. Chem.* **2009**, *55*, 611–622. [CrossRef]
25. Langfelder, P.; Horvath, S. WGCNA: An R package for weighted correlation network analysis. *BMC Bioinf.* **2008**, *9*, 559. [CrossRef]
26. Wang, Z.Y.; Chen, D.Y.; Sun, F.; Guo, W.; Wang, W.; Li, X.J.; Lan, Y.; Du, L.L.; Li, S.; Fan, Y.J.; et al. *ARGONAUTE 2* increases rice susceptibility to rice black-streaked dwarf virus infection by epigenetically regulating *HEXOKINASE 1* expression. *Mol. Plant Pathol.* **2021**, *22*, 1029–1040. [CrossRef]
27. Li, D.Y.; Zhou, J.; Zheng, C.; Zheng, E.S.; Liang, W.F.; Tan, X.J.; Xu, R.M.; Yan, C.Q.; Yang, Y.; Yi, K.K.; et al. OsTGAL1 suppresses the resistance of rice to bacterial blight disease by regulating the expression of salicylic acid glucosyltransferase OsSGT1. *Plant Cell Environ.* **2022**, *45*, 1584–1602. [CrossRef]
28. Duan, L.; Liu, H.B.; Li, X.H.; Xiao, J.H.; Wang, S.P. Multiple phytohormones and phytoalexins are involved in disease resistance to *Magnaporthe oryzae* invaded from roots in rice. *Physiol. Plant.* **2014**, *152*, 486–500. [CrossRef] [PubMed]
29. Fu, L.W.; Yu, X.C.; An, C.C. *OsCPK20* positively regulates *Arabidopsis* resistance against *Pseudomonas syringae* pv. tomato and rice resistance against *Magnaporthe grisea*. *Acta Physiol. Plant.* **2014**, *36*, 273–282.
30. De Zaeytijd, J.; Chen, P.Y.; Scheys, F.; Subramanyam, K.; Dubiel, M.; De Schutter, K.; Smagghe, G.; Van Damme, E.J.M. Involvement of OsRIP1, a ribosome-inactivating protein from rice, in plant defense against *Nilaparvata lugens*. *Phytochemistry* **2020**, *170*, 112190. [CrossRef]
31. Zhang, X.; Xu, H.; Tang, J.; Yang, J.; Guo, Z.; Xiao, Y.; Ge, Y.; Liu, T.; Hu, Q.; Ao, H.; et al. Cadmium absorption and translocation in rice plants are influenced by lower air temperatures during grain filling stage. *Sci. Total Environ.* **2024**, *954*, 176742. [CrossRef]
32. Jung, H.; Chung, P.J.; Park, S.H.; Redillas, M.; Kim, Y.S.; Suh, J.W.; Kim, J.K. Overexpression of *OsERF48* causes regulation of *OsCML16*, a calmodulin-like protein gene that enhances root growth and drought tolerance. *Plant Biotechnol. J.* **2017**, *15*, 1295–1308. [CrossRef]
33. Wang, Y.X.; Huang, L.Y.; Du, F.P.; Wang, J.; Zhao, X.Q.; Li, Z.K.; Wang, W.S.; Xu, J.L.; Fu, B.Y. Comparative transcriptome and metabolome profiling reveal molecular mechanisms underlying *OsDRAP1*-mediated salt tolerance in rice. *Sci. Rep.* **2021**, *11*, 5166. [CrossRef] [PubMed]
34. Zhu, X.Y.; Zhao, Y.D.; Shi, C.M.; Xu, G.J.; Wang, N.N.; Zuo, S.M.; Ning, Y.S.; Kang, H.X.; Liu, W.D.; Wang, R.Y.; et al. Antagonistic control of rice immunity against distinct pathogens by the two transcription modules via salicylic acid and jasmonic acid pathways. *Dev. Cell* **2024**, *59*, 1609–1622. [CrossRef]
35. Hu, L.F.; Ye, M.; Kuai, P.; Ye, M.F.; Erb, M.; Lou, Y.G. OsLRR-RLK1, an early responsive leucine-rich repeat receptor-like kinase, initiates rice defense responses against a chewing herbivore. *New Phytol.* **2018**, *219*, 1097–1111. [CrossRef] [PubMed]

36. Fukumoto, K.; Alamgir, K.M.; Yamashita, Y.; Mori, I.C.; Matsuura, H.; Galis, I. Response of rice to insect elicitors and the role of OsJAR1 in wound and herbivory-induced JA-Ile accumulation. *J. Integr. Plant Biol.* **2013**, *55*, 775–784. [CrossRef]
37. Wang, F.; Ning, D.; Chen, Y.; Dang, C.; Han, N.; Liu, Y.; Ye, G. Comparing gene expression profiles between Bt and non-Bt rice in response to brown planthopper infestation. *Front. Plant Sci.* **2015**, *6*, 1181. [CrossRef] [PubMed]
38. Gangadhar, B.H.; Sajeesh, K.; Venkatesh, J.; Baskar, V.; Abhinandan, K.; Yu, J.W.; Prasad, R.; Mishra, R.K. Enhanced tolerance of transgenic potato plants over-expressing non-specific lipid transfer protein-1 (StnsLTP1) against multiple abiotic stresses. *Front. Plant Sci.* **2016**, *7*, 1228. [CrossRef]
39. Zhong, J.; Zhang, J.; Zhang, Y.; Ge, Y.; He, W.; Liang, C.; Gao, Y.; Zhu, Z.; Machado, R.A.R.; Zhou, W. Heat stress reprograms herbivory-induced defense responses in potato plants. *BMC Plant Biol.* **2024**, *24*, 677. [CrossRef]
40. Meineke, E.K.; Davis, C.C.; Davies, T.J. Phenological sensitivity to temperature mediates herbivory. *Glob. Change Biol.* **2021**, *27*, 2315–2327. [CrossRef]

plants

MDPI

Article

Genetic Analyses, BSA-Seq, and Transcriptome Analyses Reveal Candidate Genes Controlling Leaf Plastochron in Rapeseed (*Brassica napus* L.)

Mengfan Qin [1,2,†], Xiang Liu [1,†], Jia Song [1], Feixue Zhao [1], Yiji Shi [1], Yu Xu [1], Zhiting Guo [1], Tianye Zhang [1], Jiapeng Wu [1], Jinxiong Wang [3], Wu Li [2], Keqi Li [1], Shimeng Li [3,*], Zhen Huang [1] and Aixia Xu [1,*]

[1] College of Agronomy, Northwest A&F University, Yangling 712100, China; qinmf@nwafu.edu.cn (M.Q.); liux@nwafu.edu.cn (X.L.); s13563403318@163.com (J.S.); 17873555895@163.com (F.Z.); shiyj0718@nwafu.edu.cn (Y.S.); xuyu_xy@nwafu.edu.cn (Y.X.); 18003852705@163.com (Z.G.); giornozhang@nwafu.edu.cn (T.Z.); jiapengwuu@outlook.com (J.W.); likeqi1218@sina.com (K.L.); huang_zhen.8@163.com (Z.H.)

[2] Crop Research Institute, Guangdong Academy of Agricultural Science, Guangzhou 510640, China; liwu@gdaas.cn

[3] Institute of Agricultural Sciences, Xizang Academy of Agriculture and Animal Husbandry Sciences, Lhasa 850000, China; wjxwang9619@163.com

* Correspondence: li_shimeng90@163.com (S.L.); xuaixia2013@163.com (A.X.)

† These authors contributed equally to this work.

Abstract: The leaf plastochron serves as an indicator of the rate of leaf appearance, biomass accumulation, and branch number, while also impacting plant architecture and seed yield. However, research on the leaf plastochron of crops remains limited. In this study, 2116C exhibited a rapid leaf plastochron compared to ZH18 during both rosette and bud periods. There were significant positive correlations among the leaf plastochron and primary branch number of the F_2 populations (r ranging from 0.395 to 0.635, $p < 0.01$). Genetic analyses over two years demonstrated that two equally dominant genes might govern the leaf plastochron. Through bulk segregant analysis sequencing (BSA-seq), three novel genomic intervals were identified on chromosomes A02 (9.04–9.48 Mb and 13.52–13.66 Mb) and A04 (19.84–20.14 Mb) of ZS11 and Darmor-*bzh* reference genomes. By gene functional annotations, single-nucleotide variation (SNV) analyses, transcriptome data from parents, genetic progeny, and natural accessions, we identified ten candidate genes within the intervals, including *FLOWERING LOCUS T*, *RGL1*, *MYB-like*, *CYP96A8*, *BLH3*, *NIT2*, *ASK6*, and three *CLAVATA3/ESR (CLE)-related* genes. These findings lay the molecular foundation for further exploration into the leaf plastochron and the implications in plastochron-related breeding in rapeseed.

Keywords: *Brassica napus* L.; leaf plastochron; genetic analysis; BSA-seq; gene expression; candidate gene

1. Introduction

The leaf plastochron, defined as the temporal interval between the initiation of two successive leaf primordia at the shoot apical meristem (SAM), is a critical parameter in plant developmental studies [1,2]. The shorter the leaf plastochron indicates, the faster the rate of leaf initiation and leaf appearance. The final number of leaves depends upon the rate and pattern of leaf initiation during the growth phase [3,4]. During leaf axillary meristem development, axillary buds are regulated by diverse signals together to form into branches, e.g., polar transport of auxin, abscisic acid from buds, cytokinins from root

tips, strigolactone, sugar signaling, and red light [5–8]. Consequently, the higher final leaf count corresponds to the more axillary meristems, potentially leading to enhanced branch formation. It is known that leaves and branches serve as key organs for photosynthesis and the architecture of rapeseed [8,9]. Thus, the leaf plastochron holds significance for improving biomass, plant architecture, and photosynthesis in crops.

Despite the importance of leaf plastochron pattern in the plant architecture, little is known about the genetic regulation and molecular mechanisms of the leaf plastochron. Leaf initiation originates from shoot apical meristems (SAMs), whose organization and function were maintained by the conserved WUSCHEL-CLAVATA3 (WUS-CLV3) feedback loop [10]. In rice (*Oryza sativa* L.), mutations in *PLASTOCHRON1* (*PLA1*) and *PLA2* accelerate leaf initiation without altering phyllotaxy [1,2,11]. *PLA1* regulates the leaf plastochron by modulating meristem developmental timing, and *PLA2* may mediate non-cell-autonomous signals from immature leaves to suppress new leaf initiation in the shoot apical meristem. Both of them act as the downstream of the GA signal transduction pathway [12], and PLA1 also regulates leaf inclination through the brassinolide pathway [13]. In maize (*Zea mays*), *ZmPLA1* maintains the dividing of cells in a proliferative and undifferentiated state for a longer time, thereby stimulating the duration of leaf elongation, which could increase organ growth, seedling vigor, biomass, and seed yield [14]. In addition, the leaf plastochron will also vary according to the light and cumulative temperature, which influences the duration of nutrient growth, developmental rate, total leaf number, biomass, and seed yield of plants [15–17]. Although the mechanisms underlying leaf plastochron regulation remain to be elucidated in dicot crops such as rapeseed, the identified regulatory links to SAMs and hormone signaling provide a directional framework for future exploration.

Rapeseed (*Brassica napus* L., AACC, 2n = 38) is a globally significant oil crop with extensive cultivation areas and is one of the four largest oil crops in the world. It not only provides edible oil for humans and protein-rich feed for animals, but also provides a series of novel vegetables, such as sprouts, leaves, and shoots [18–20]. The rapid-plastochron varieties could grow fast with more leaves, branches, and shoots, which have certain application value for vegetable, edible oil, green manure, and oil-vegetable-dual-purpose rapeseed. Therefore, it is meaningful to explore and identify rapid plastochron germplasm and genetic resources to facilitate the utilization and improvement of leaf plastochron-related traits. In this study, two rapeseed inbred lines with various plant plastochrons were used for progeny population construction. We performed major genes plus polygenes inheritance analyses for plastochron-related traits across two years among F_2 populations and constructed bulk pools using extreme F_2 individuals for Bulked Segregant Analysis (BSA) sequencing to identify candidate genomic intervals. Candidate genes were then predicted by gene sequence variation and expression information within the intervals. These results will help to expand our knowledge of the genetic mechanism of leaf plastochron and provide a theoretical basis for plastochron-related breeding and molecular biology in rapeseed.

2. Results

2.1. Investigation of Plastochron for the Parents

To investigate the leaf plastochron pattern in rapeseed, the rates of leaf appearance of ZH18 (slow-plastochron line) and 2116C (rapid-plastochron line) were continuously counted before the wintering period. During the pre-winter growth process, there were two peaks of leaf plastochron in both lines, and the leaf appearance rate showed the characteristics of 'slow-rapid' alternation. ZH18 had the fastest leaf plastochron in the 3rd–4th and 7th–8th leaves, while 2116C had the fastest in the 5th–8th and the 10th–13th leaves. The final number of fully expanded leaves of ZH18 and 2116C were 8 leaves and

14 leaves, while their visible leaves were 13 leaves and 20 leaves, respectively (Figure 1). The average leaf appearance rate was 3.2 days/leaf in ZH18 and 5.1 days/leaf in 2116C. 2116C consistently had significantly higher leaf numbers and leaf plastochron than ZH18 at the rosette stage (Figure 1), which indicated that there was likely to be a certain mutation consistently affecting the leaf appearance and plastochron all the time.

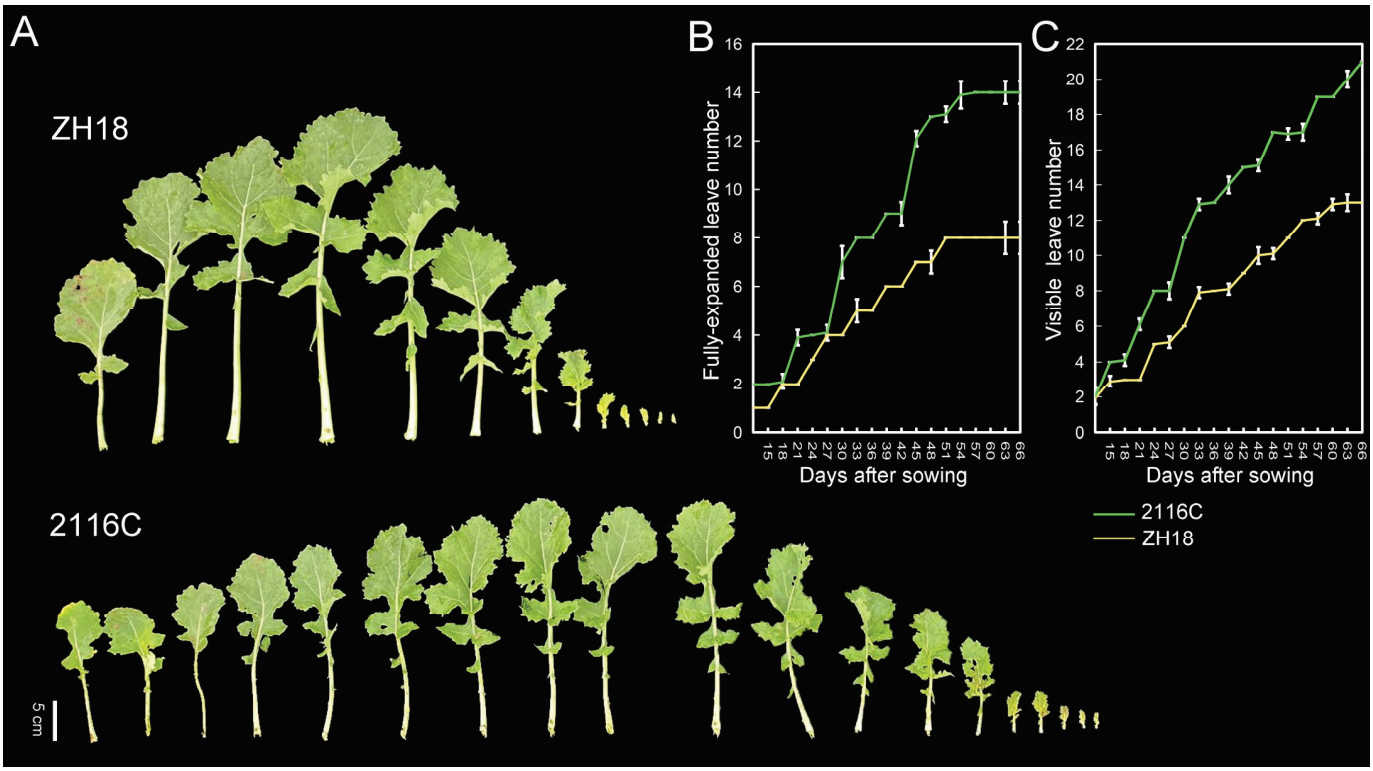

Figure 1. Leaf appearance rate at the rosette stage of ZH18 and 2116C. (**A**) Final leaf number of ZH18 and 2116C on the 69th day after sowing; (**B**) fully expanded leaves; and (**C**) visible leaves during the rosette stage. The x-axis is the number of days after sowing, and the y-axis is the leaf number. The green and yellow lines indicate 2116C and ZH18, respectively.

2.2. Phenotype Investigation for the Parents and Genetic Population

To conveniently study the genetic characteristics of the leaf plastochron, we subsequently used the leaf number at the same number of days after sowing to represent the leaf plastochron of the individual. From the phenotypic survey results of the 2021–2022 and 2022–2023 cropping seasons (Table S1), the mean values of expanded leaf number at the rosette stage were 5.3 and 7.5 in ZH18, 12.2 and 13.6 in 2116C, 9.6 and 10.1 in F_1 plants, and 8.1 and 9.1 in F_2 population, respectively. During the bud stage, the mean values of the number of leaves were 7.6 and 10.6 in ZH18, 23.1 and 18.4 for 2116C, 14.9 and 15.5 in the F_1 plants, and 17 and 14.9 in the F_2 population, respectively. The number of leaves in F_1 was intermediate between the two parents, and the leaf number of the F_2 population showed a unimodal distribution (Figure 2). Therefore, the leaf plastochron at the rosette-bud stages of rapeseed has a quantitative trait genetic character. The correlation analysis showed that there were highly significant correlations among leaf plastochron at the rosette stage and the bud stage ($p < 0.01$) with the primary branch number ($p < 0.01$) (Table S2). These results indicated that there might be an intrinsic positive correlation between the leaf plastochron and the primary branch number.

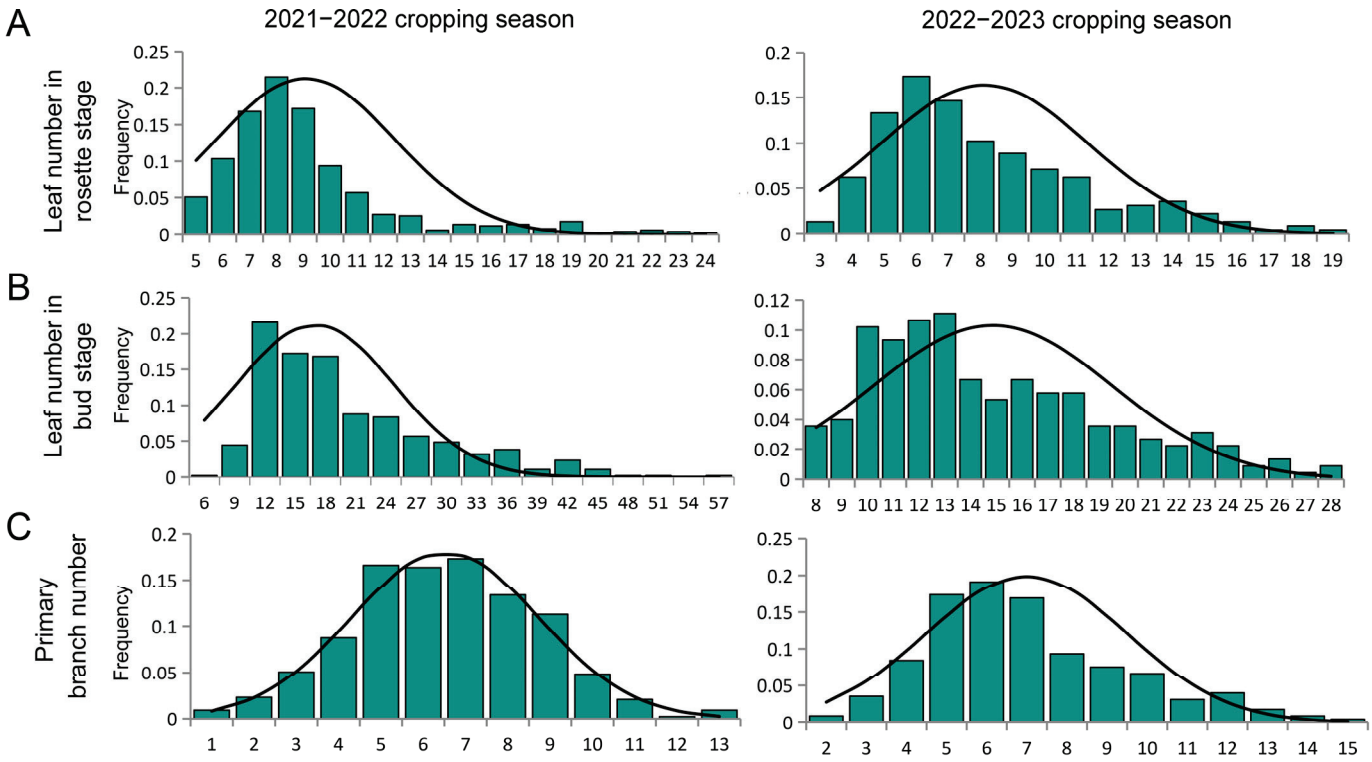

Figure 2. Statistical analyses of leaf plastochron-related traits among the F_2 populations. Frequency distribution of (**A**) leaf number in the rosette stage, (**B**) leaf number in the bud stage, and (**C**) primary branch number across 2021–2022 and 2022–2023 cropping seasons.

2.3. Genetic Analysis of Leaf Plastochron in Rapeseed

To predict the mixed major genes plus polygenes inheritance of leaf plastochron in rapeseed, we utilized the leaf number of ZH18, 2116C, F_1, and F_2 in the 2021–2022 and 2022–2023 cropping seasons for genetic model prediction. Based on the principle of minimum Akaike's information criterion (AIC) value, the alternative models for leaf plastochron at the rosette stage were one major gene with equal additive-dominance (1MG-EAD) and two major genes with equal additive-dominance (2MG-EAD), and those for leaf plastochron at the bud stage were 2MG-EAD and two major genes plus polygenes with completely dominance and additive-dominance (MX2-CD-AD) across the two cropping seasons (Table 1). Similarly, the most appropriate genetic models for primary branch numbers were 2MG-EA and 2MG-EAD. In the fitness test, the models with more counts of significant *p*-values ($p < 0.05$) were selected as the optimal genetic models (Table S3). Taken together, the 2MG-EAD genetic model was the most appropriate model for leaf plastochron after the fitness test.

Using the 2MG-EAD model, we predicted the genetic parameters for leaf-related traits. The additive effects of major genes were consistently negative, with heritability exceeding 86.4% (Table S4). It was evident that leaf plastochron was mainly controlled by two equally dominant effect genes with high heritability and negative additive-dominant effects. These results could provide cues for the exploration of leaf plastochron in rapeseed.

Table 1. Candidate genetic models for leaf plastochron-related traits.

Trait	Model of (2021–2022)	AIC Value	Log Max Likelihood Value	Model (2022–2023)	AIC Value	Log Max Likelihood Value
Leaf number in the rosette stage	1MG-EAD	2516.879	−1253.44	2MG-EAD	1210.203	−601.102
	1MG-AD	2518.637	−1253.319	1MG-AD	1212.56	−600.28
	2MG-EAD	2525.118	−1258.559	MX2-CD-AD	1217.865	−605.933
	2MG-EA	2534.13	−1263.065	2MG-A	1218.415	−604.208
	MX2-ADI-ADI	2546.923	−1261.461	1MG-EAD	1218.642	−604.321
Leaf number in the bud stage	2MG-EAD	2936.697	−1464.349	MX2-CD-AD	1352.254	−673.127
	2MG-EA	2942.665	−1467.333	MX2-EAD-AD	1352.505	−674.253
	1MG-AD	2946.55	−1467.275	2MG-EAD	1353.224	−672.612
	MX2-ADI-AD	2969.929	−1475.965	MX2-AD-AD	1354.104	−672.052
	MX2-ADI-ADI	2975.617	−1475.808	1MG-AD	1357.429	−672.715
Primary branch number	2MG-EA	1959.893	−975.9467	2MG-EAD	1089.852	−540.926
	2MG-EAD	1962.112	−977.0562	1MG-EAD	1091.632	−540.816
	1MG-EAD	1964.117	−977.0583	1MG-AD	1093.476	−540.738
	1MG-NCD	1964.168	−977.0842	1MG-NCD	1098.71	−544.355
	1MG-AD	1966.149	−977.0747	2MG-A	1099.805	−544.902

MG: major genes; MX: major genes plus polygenes; A: additive; AD: additive-dominant; ADI: additive-dominance-epistasis; CD: completely dominance; NCD: negatively CD; EA: equal additive; EAD: equal additive-dominance.

2.4. Primary QTL Identification Based on BSA Analyses

To gain further access to the genome intervals controlling leaf plastochron, BSA sequencing for the parents and F_2 population was approached. During the 2021–2022 cropping season, the two parents, along with two bulked pools B1 (slow plastochron bulk pool with 30 plants from 600 F_2 individuals) and B2 (rapid-plastochron bulk pool with 30 plants from 600 F_2 individuals) were selected for whole-genome resequencing (Figure 3). The number of leaves at the rosette stage and the bud stage was counted (Figure 2A,B). The reference genome alignment and read coverage statistics for resequencing of four samples were stated, and sequencing coverage at least 1X was >89.9% for the parents and F_2 bulked pools (Table S5).

For the ZS11 v0 genome assembly, alignment of the reads from ZH18 and 2116C to the reference genome revealed a total of 2,264,093 and 2,069,863 SNPs, respectively. There were 3,366,717 and 3,416,689 SNPs determined from the B1 and B2 bulked pools, and 51,833 SNPs were shared among P1, P2, B1, and B2 (Figure 3C). In addition, 610,689, 583,140, 901,648, and 610,689 small InDels were detected from ZH18, 2116C, B1, and B2, respectively (Figure S1 and Table S5). Twenty genomic regions with a total length of 0.89 Mb were identified based on SNPs with a confidence interval of 95 on chromosomes A02, A03, and A04 (Figure 3E and Table S6). Twenty-eight regions on chromosomes A02 and A04 with a confidence interval of only 90 were obtained from 1,073,929 small InDels (Figure S2 and Table S6).

For the Darmor-*bzh* V10 genome assembly, a total of 765,950 SNPs and 207,694 InDels were shared among P1, P2, B1, and B2 (Figures 3D and S1). A total of 28 genomic regions associated with SNPs were identified with a confidence interval of 95 on chromosomes A02 and A04 (Figure 3F and Table S7), while 17 regions for InDels with a confidence interval of only 90 were on chromosomes A02, A03, and A04 (Figure S3 and Table S7). Overall, the QTL outcomes of SNPs were preferred due to genetic density and the higher confidence interval, and 107 and 113 genes were located in the intervals from ZS11 and Darmor-*bzh*, respectively (Table 2).

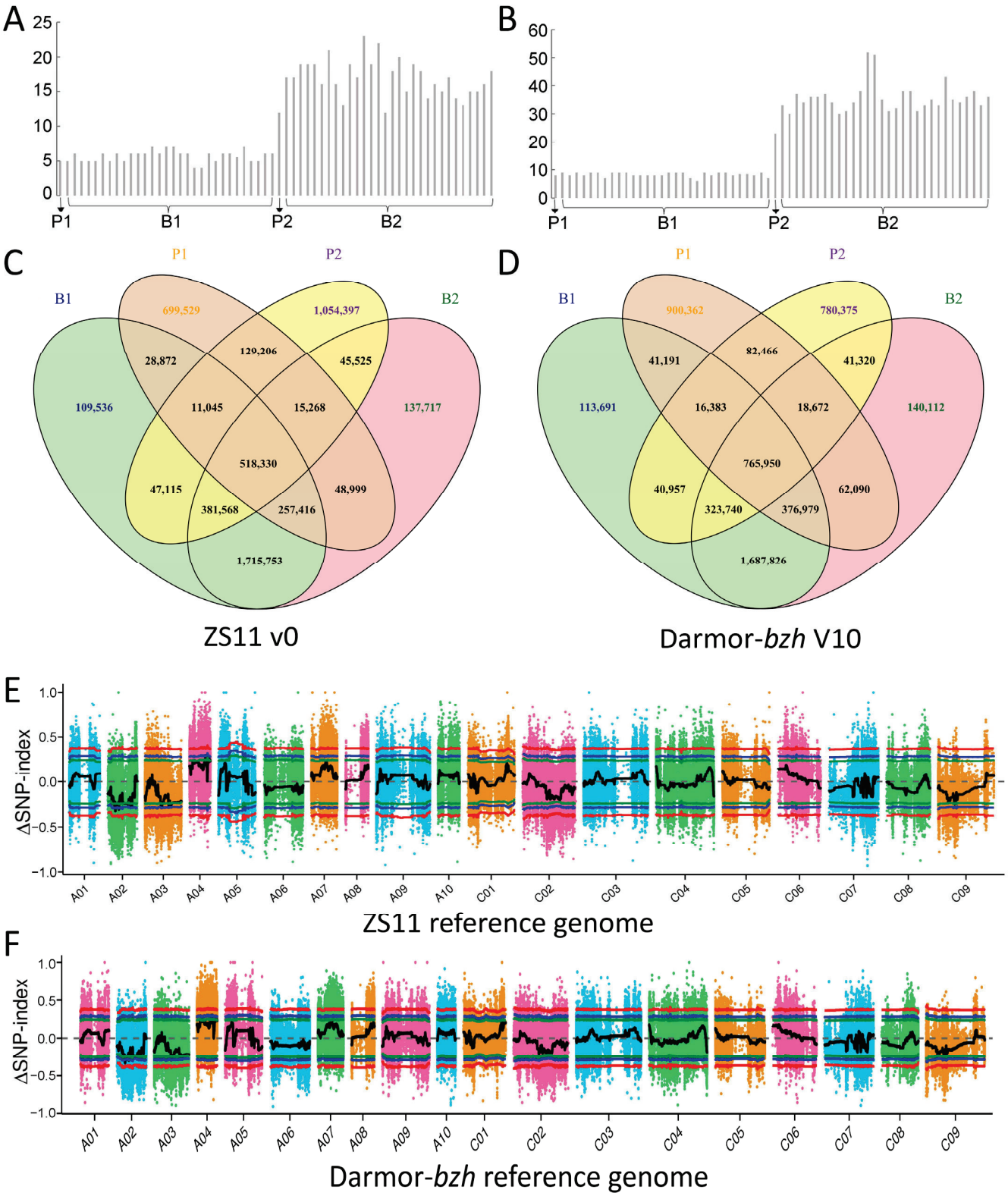

Figure 3. Leaf plastochron QTL identification based on BSA-seq. Leaf number in (**A**) the rosette stage and (**B**) the bud stage; Venn diagrams of SNPs identified in the samples aligned to (**C**) ZS11 v0 and (**D**) Darmor-bzh reference genome; and ΔSNP-index based on (**E**) the ZS11 v0 and (**F**) the Darmor-*bzh* V10 reference genome. The red, blue, and green lines represent confidence thresholds of 0.99, 0.95, and 0.90, respectively. Different colors are used to distinguish the axes representing the different chromosomes.

Table 2. Candidate genomic intervals for leaf plastochron-related traits.

QTL Label	Chr	Start	End	Interval Length (Mb)	No. of Gene	Reference Genome
qPLA.A02-1	A02	9,045,489	9,478,410	0.43	53	ZS11 v0
qPLA.A02-2	A02	13,517,525	13,661,121	0.14	19	ZS11 v0
qPLA.A04	A04	19,839,469	20,142,478	0.30	35	ZS11 v0
qPLA.A02-1	A02	9,066,916	9,477,102	0.41	46	Darmor-*bzh* V10
qPLA.A02-2	A02	13,609,227	13,728,641	0.12	14	Darmor-*bzh* V10
qPLA.A04	A04	17,128,404	17,432,209	0.30	53	Darmor-*bzh* V10

The intervals between ZS11 and Darmor-*bzh* showed high genome collinearity, and 90 genes of ZS11 have more than 30% protein identity with that of Darmor-*bzh* (Figure S4 and Table S8), suggesting that the QTL intervals were conserved in rapeseed. Taken together, the candidate intervals controlling plant plastochron might be located in A02:9.04−9.48 Mb (labeled as qPLA.A02-1), A02:13.52−13.66 Mb (labeled as qPLA.A02-2), and A04:19.84−20.14 Mb (labeled as qPLA.A04) of the ZS11 genome.

2.5. Gene Annotations and Sequence Variants Analyses in Candidate Genes

Within the three QTL intervals, a total of 90 genome genes were identified in the ZS11 genome (Table 2). Among these genes, 15 genes might be the causal genes that annotated as *FLOWERING LOCUS T* (*BnaA02G0156900ZS*), DELLA protein (*BnaA02G0158200ZS* and *BnaA02G0160500ZS*), Senescence-associated protein (*BnaA02G0160200ZS*), *ACCELERATED CELL DEATH 6* (*BnaA02G0160300ZS*), *MYB-like* (*BnaA02G0160600ZS*), bifunctional nuclease 1 (*BnaA02G0214800ZS*), *CYP96A8* (*BnaA02G0215600ZS*), *BLH3* (*BnaA02G0215300ZS*), *Nitrilase 2* (*BnaA04G0200300ZS*), GSK3-like protein kinase (*BnaA04G0200700ZS*), G-protein coupled receptor (*BnaA04G0201800ZS*), and CLAVATA3/ESR (CLE)-related protein (*BnaA04G0201700ZS*, *BnaA04G0201900ZS*, and *BnaA04G0202000ZS*). According to SNP and InDel annotations, there were 604 and 247 variants identified among 12 of the 15 genes, including 312 in upstream, 325 in downstream, 142 in intron, 1 in 5′ UTR, 1 in 3′ UTR, 29 leading to synonymous coding, and 41 leading to non-synonymous coding (Figure 4A and Table S9). *BnaA04G0201700ZS* and *BnaA04G0201800ZS* only showed 143 and 70 variants in upstream, downstream, and synonymous coding.

Variation information of 2311 rapeseed accessions extracted 5143 SNPs and 990 small InDels from the 15 genes mentioned above, and 203 SNPs and 150 InDels from BSA sequencing were not detected in the database (Figure 4C,D), which were unique to the variations between the parents in this study. Among the parental-specific variants, they were distributed over 12 genes (Table S10), resulting in four altered protein sequences of them (*BnaA02G0215300ZS*, *BnaA02G0160600ZS*, *BnaA04G0200700ZS*, and *BnaA04G0201900ZS*). Among the 498 common variants, 27 variants were distributed in nine genes (*BnaA02G0156900ZS*, *BnaA02G0158200ZS*, *BnaA02G0160500ZS*, *BnaA02G0160600ZS*, *BnaA02G0215600ZS*, *BnaA04G0200300ZS*, *BnaA04G0200700ZS*, *BnaA04G0201900ZS*, and *BnaA04G0202000ZS*) and caused alterations of the encoded proteins (Table S10). The allele frequency of these variants ranged between 0.01 and 0.85 (Figure 4E), and those with low allele frequency variants were more likely to be the candidate loci.

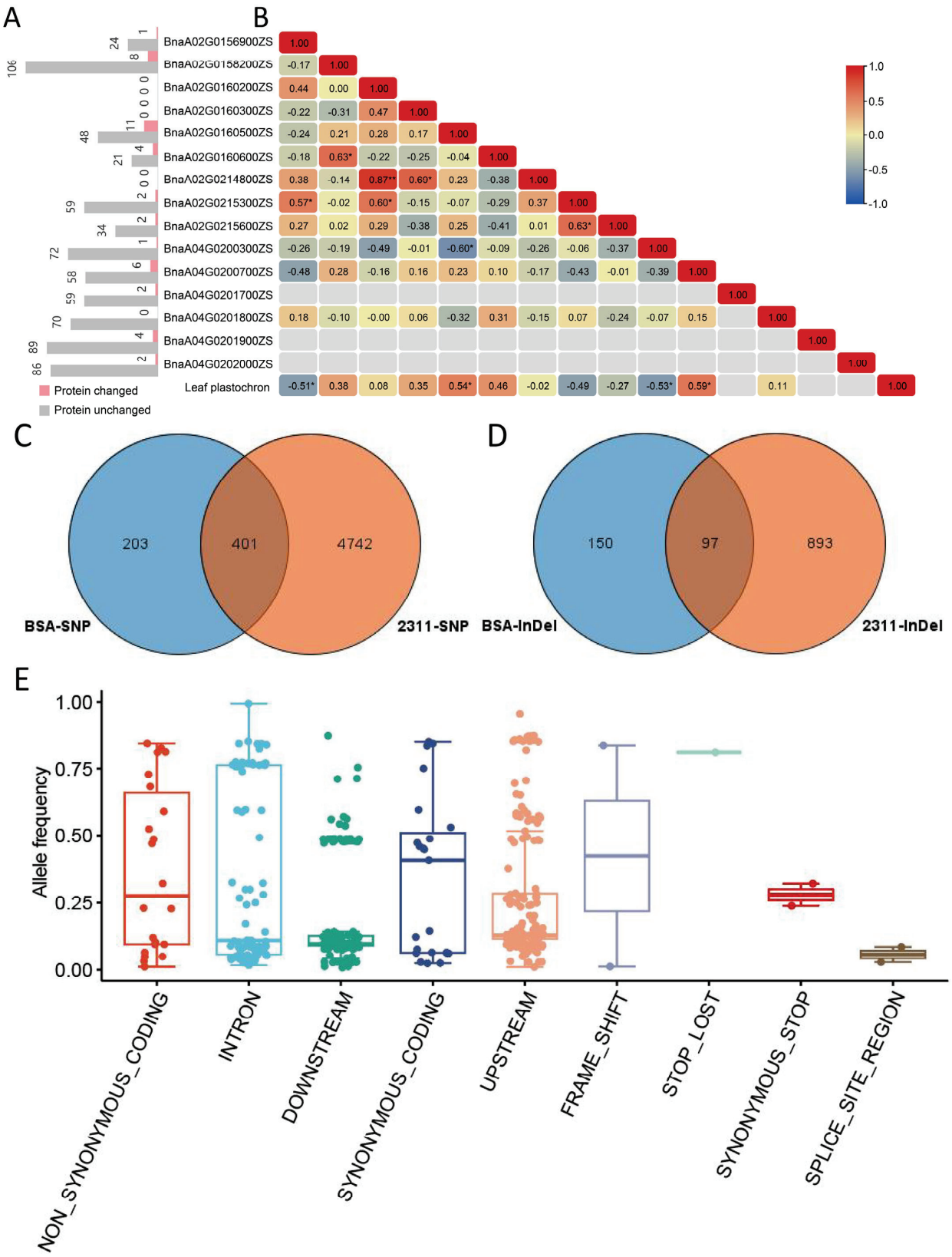

Figure 4. SNP/InDel variation and gene expression analyses of candidate genes. (**A**) Number of SNP/InDel in candidate genes leading to protein sequence change; (**B**) heatmap of correlation between candidate gene expression and leaf plastochron; The asterisk * represents a significance $p < 0.05$ and ** represents a significance $p < 0.01$. (**C**) SNP and (**D**) InDel Venn plots from BSA versus that from the 2311 accessions in BnIR database; and (**E**) allele frequency distribution of the common variants among the 2311 accessions.

2.6. Gene Expression Analyses in Candidate Genes

Given that the results of the phenotypic analyses suggest that plant plastochron might be controlled by continuous regulation, the candidate genes should be consistently expressed, whether at the stem tip or in leaf-associated tissues. For genes with protein sequence alterations, the expression of candidate genes may not correlate with leaf plastochron. For genes with unaltered protein sequences, the expression should correlate with leaf plastochron, and there were SNPs/InDel in their upstream, downstream, or UTR regions.

The principal components analysis (PCA) based on FPKM of the 15 candidate genes showed that the 12 RNA-seq samples were effectively divided into slow-plastochron and rapid-plastochron groups (Figure S5). For the gene expression among the parents and $F_{2:3}$ families, only four genes (*BnaA02G0158200ZS*, *BnaA04G0201700ZS*, *BnaA04G0201900ZS*, and *BnaA04G0202000ZS*) did not show detected expression abundances, and the other genes showed different expression trends (Figure S6). The expressions of *BnaA02G0160500ZS* and *BnaA04G0200700ZS* displayed significantly positive correlations to leaf plastochron ($p < 0.05$, $r = 0.54$ and 0.59, respectively), while *BnaA02G0156900ZS* and *BnaA04G0200300ZS* showed negative correlations to leaf plastochron ($p < 0.05$, $r = -0.51$ and -0.53, respectively) (Figure 4B). In the public gene expression data, three genes (*BnaA04G0201700ZS*, *BnaA04G0201900ZS*, and *BnaA04G0202000ZS*) did not express, and three genes (*BnaA02G0158200ZS*, *BnaA02G0160600ZS*, and *BnaA04G0201800ZS*) showed low expression in all of these tissues (Table S11). *BnaA02G0156900ZS* was not expressed in cotyledons and roots but was highly expressed in different-period leaves (Table S11). In addition, we observed that there were three tandem repeats of *CLE* genes within the qPLA.A04 interval, and although they were not detected to be expressed in this study, since *WUS-CLV* was an essential feedback regulatory loop for maintaining the stability of the shoot apical meristem, we considered them as potential candidate genes as well.

Taken together, we regarded *BnaA02G0156900ZS* (*FT*), *BnaA02G0160500ZS* (*RGL1*), and *BnaA02G0160600ZS* (*MYB-like*) as potential candidate genes for qPLA.A02-1, *BnaA02G0215600ZS* (*CYP96A8*) and *BnaA02G0215300ZS* (*BLH3*) for qPLA.A02-2, and *BnaA04G0200300ZS* (*NIT2*), *BnaA04G0200700ZS* (*ASK6*), *BnaA04G0201700ZS* (*CLE4*), *BnaA04G0201900ZS* (*CLE6*), and *BnaA04G0202000ZS* (*CLE7*) for qPLA.A04 (Table 3).

Table 3. Candidate gene information for controlling leaf plastochron in the genomic intervals.

Gene ID	Genomic Position	Best Hit to *A. thaliana*	Function Description
BnaA02G0156900ZS	A02:9104462−9107270	*AT1G65480*	Protein FLOWERING LOCUS T
BnaA02G0160500ZS	A02:9357771−9367517	*AT1G66350*	DELLA protein RGL1
BnaA02G0160600ZS	A02:9375716−9377422	*AT1G56650*	MYB-like, a putative MYB domain-containing transcription factor
BnaA02G0215300ZS	A02:13571765−13573401	*AT1G75410*	BLH3, BEL1-like homeodomain protein 3
BnaA02G0215600ZS	A02:13592588−13594117	*AT1G47620*	CYP96A8, a member of CYP96A
BnaA04G0200300ZS	A04:19944280−19946261	*AT3G44300*	NIT2, nitrilase 2
BnaA04G0200700ZS	A04:19964345−19967629	*AT2G30980*	ASK6, a shaggy-related protein kinase
BnaA04G0201700ZS	A04:20020034−20020282	*AT2G31081*	CLAVATA3/ESR (CLE)-related protein 4
BnaA04G0201900ZS	A04:20029992−20030249	*AT2G31082*	CLAVATA3/ESR (CLE)-related protein 7
BnaA04G0202000ZS	A04:20059635−20059880	*AT2G31085*	CLAVATA3/ESR (CLE)-related protein 6

3. Discussion

Leaves are essential photosynthetic organs, and the leaf plastochron can affect the number of leaves, number of branches, biomass, and yield directly or indirectly, which is an important indicator of plant biology. In rice and wheat, the shorter the leaf plastochron, the less time tillers can be produced, which is important for yield and uniformity in

grains [21]. In this study, significant positive correlations were found among the leaf plastochron, primary branch number, biomass, and seed yields (Table S2). Branches originated from axillary buds, and the leaves in the main stem, along with environmental factors, affected the number of branches and plant morphology [8,22], and multiple studies have reported positive correlations between branch number and biomass/seed yield [23–25]. These results are consistent with previous studies on the relationship between branch number and yield [26–28], i.e., the more branches, the higher the individuals' biomass and seed yield. A branch number QTL was previously mapped via GWAS to a 22.0 Mb position on chromosome A03 [23], near which a QTL was also identified on the ZS11 v0 genome in this study (Table S7). Some allelic SNPs within the candidate genes exhibited significant effects on branch number (Figure 5), suggesting a potential intrinsic linkage among leaf plastochron, branch development, and biomass/seed yield. However, additional approaches are required to validate whether the observed associations represent causal relationships, genetic linkage, or coincidental occurrences.

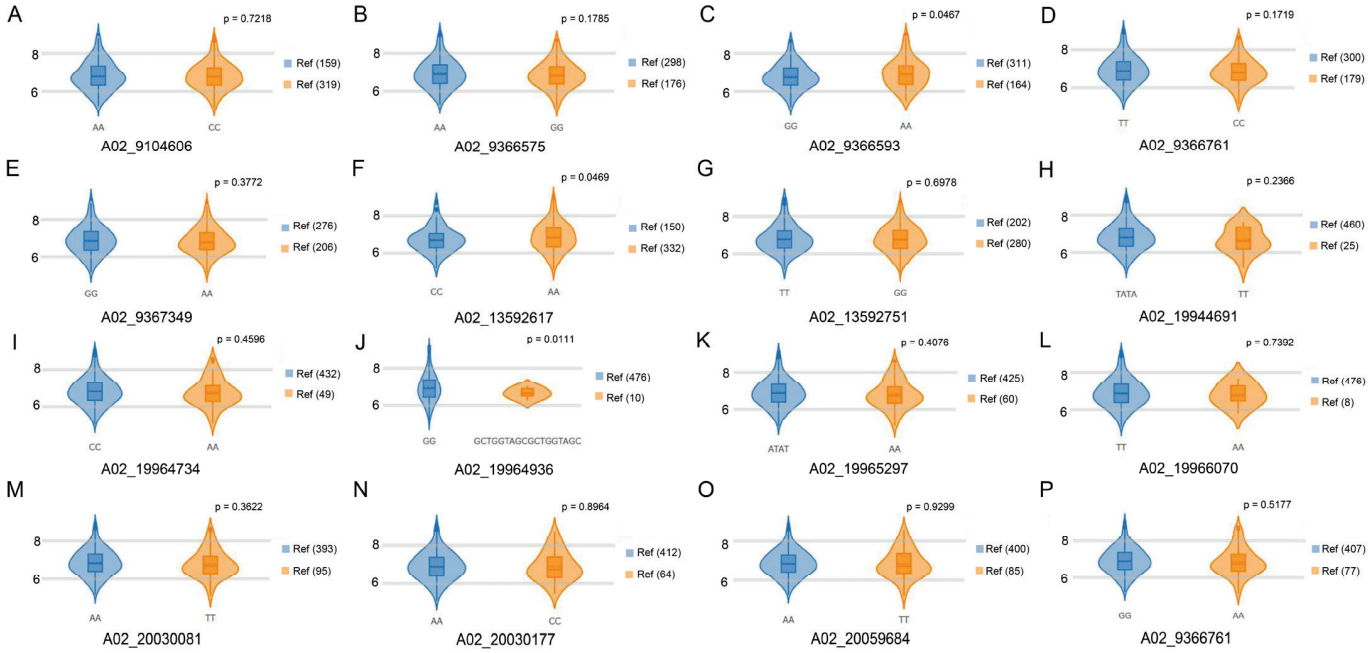

Figure 5. The relationships of branch numbers for 16 SNVs shared with natural accessions. (**A**–**P**) Violin diagrams of branch numbers of different genotypes. The individual numbers of the genotype are listed in the braces. The *p*-value was calculated by *t*-test.

To date, there are no genetic studies reported on leaf plastochron in rapeseed, and three novel QTL intervals were identified in this study. Notably, among the 10 leaf plastochron related candidate genes investigated in this study (including *FLOWERING LOCUS T*, *RGL1*, *MYB-like*, *CYP96A8*, *NIT2*, *ASK6*, and *CLE4/6/7*), 16 single-nucleotide variations (SNVs) were identified in natural populations. Of these, 3 allelic SNVs exhibited significant associations with branch number (Figure 5), while 13 SNVs showed correlations with flowering time (Figure S7), with allele frequencies ranging from 0.01 to 0.72. These results suggest that these candidate genes may participate in the regulation of both branch number and flowering time, extending their functional roles beyond leaf plastochron modulation. Consequently, superior haplotypes or genetic engineering targeting these leaf plastochron-related genes could be strategically employed in breeding programs to optimize plant architecture, early flowering, and yield-related traits, even breeding novel vegetables.

Three candidate genes, *BnaA02G0156900ZS* (*FT*), *BnaA02G0160500ZS* (*RGL1*), and *BnaA02G0160600ZS* (MYB-like), were identified in the qPLA.A02-1 interval.

BnaA02G0156900ZS encoded an FT mobile signaling protein, whose mRNA was expressed in the leaves and responded to long-day conditions, but the protein was required by the shoot apical meristem [29,30]. The *ft-10* mutant had 36 leaves, while wild-type plants developed 15 rosette leaves at flowering [31]. There was one SNP that caused the protein change Ile49Leu located in the phosphatidyl ethanolamine-binding protein (PEBP) domain, which might be the functional site of *BnaA02G0156900ZS*. *BnaA02G0160500ZS* (*RGL1*), encoding a DELLA protein, negatively regulated GA responses and restrained the cell proliferation and expansion that drove plant growth [32,33]. There was no significant difference in gene expression between slow-plastochron lines and rapid-plastochron lines, but one InDel led to a frameshift, one SNP stop loss, and nine SNP non-synonymous coding (Table S9). Compared with the wild type, leaf senescence occurred earlier in the mutant *rgl1-1*, whose *DELLA* repression was removed, and overexpression of *RGL1* resulted in significantly increased leaf longevity in age-triggered senescence [34,35]. *BnaA02G0160600ZS* encoded a putative MYB domain containing a transcription factor that participated in several developmental processes. *R2R3-Myb* genes controlled a very early step of axillary meristem initiation, which impacted the axillary meristem formation [36], and overexpression of *Cymbidium CcMYB24* increased the number of leaves in *Arabidopsis* [37], suggesting that *MYB* members also functioned in the establishment of leaf primordia and branches.

In the qPLA.A02-1 interval, *BnaA02G0215300ZS* encoded a BEL1-like homeodomain protein, which was found ubiquitously in plants and played important roles in regulating the meristem. In *Arabidopsis thaliana*, three BELL-family proteins, ATH1, PNY, and PNF, were combined to keep the initiation and maintenance of the SAM [38]. BLH proteins interact with *KNOX* genes to regulate early internode patterning events, while PNY-STM heterodimers are critical for SAM function [38,39]. *BnaA02G0215600ZS*, a cytochrome P450 family member, had two SNP missense variants between the parents that caused protein changes Phe10Leu and Leu55Arg. *PLA1*, encoding cytochrome P450 CYP78A11, acts as a developmental timekeeper for leaf initiation in rice, orchestrating leaf number, tiller number, primary branch development, leaf inclination, leaf elongation, and leaf maturation through GA and brassinosteroid signaling pathways [1,2,11–13,40]. Deleting the P450 family member *MAX1* led to more branches via the strigolactone synthesis pathway, and overexpression of *BnaMAX1* could restore the multi-branch phenotype [27,41].

BnaA04G0200300ZS was homologous with *AtNIT2*, and mutants of *AtNIT2* reduced sensitivity to 3-Indoleacetonitrile (IAN), increased sensitivity to IAA, showing more rosette leaves in short days in *Arabidopsis* [42,43]. The gene *BnaA04G0200700ZS* encoded the apoptosis signal-regulating kinase (ASK) protein, also known as *BRZ-INSENSITIVE-LONG HYPOCOTYL 1* (*BIL1*), *BRASSINAZOLE-RESISTANT 1* (*BZR1*), and *BRASSINOSTEROID INSENSITIVE 2* (*BIN2*). Phosphorylation of BRI1 EMS SUPPRESSOR 1 (BES1) and BZR1 by BIN2 facilitated their interaction with 14-3-3 proteins, leading to their translocation from the nucleus to the cytoplasm, thereby impeding their nuclear activities as transcription factors in *Arabidopsis* [44,45]. BIL1/AtSK23 also phosphorylated *MONOPTEROS/AUXIN RESPONSE FACTOR 5* at threonine 163 and serine 647, which could integrate *PHLOEM INTERCALATED WITH XYLEM* and cytokinin signaling in secondary growth [46]. CLE peptides played a role in controlling the growth and maturation of different tissues in *Arabidopsis*, including the apical and vascular meristems. Notably, CLV3 and CLE40 were recognized as CLE peptides that modulated the WUS-CLV feedback loop within SAM [47]. However, three members of CLE peptides were identified in qPLA.A04 without expression in the shoot tips, implying that they may not participate in leaf plastochron controlling.

4. Materials and Methods

4.1. Plant Plantation and Phenotype Collection

The winter rapeseed inbred lines ZH18 (slow-plastochron line) and 2116C (rapid-plastochron line) were provided by the rapeseed germplasm resource lab of Northwest A&F University, from which F_1 and F_2 populations were constructed. ZH18, 2116C, F_1, and F_2 were planted in the Caoxinzhuang experimental base (34°30′ N, 108°09′ E) of Northwest A&F University in Yangling during the 2021–2022 and 2022–2023 cropping seasons (experimental design was displayed in Figure S8). The F_2 populations contained 600 and 225 individuals in the two cropping seasons, respectively. The plants during the 2021–2022 season were used for the analyses of the leaf plastochron pattern and inheritance, and those during the 2022–2023 cropping season were utilized for studying the inheritance aspects of leaf plastochron. Row length, row spacing, and plant spacing were set to 2 m, 35 cm, and 10 cm, respectively. Drill sowing was used, and thinning out of seedlings was performed before the two-leaf stage. Other field management was kept in alignment with local agronomic protocols.

Leaf plastochron variation patterns in the two parental lines were investigated every 3 days starting from 15 days after sowing, with one row examined during each observation. The numbers of fully expanded leaves and visible leaves were recorded, with five representative plants assessed per survey and two replicates. The F_2 plants were investigated one by one, and border row plants were excluded from evaluations to avoid marginal effects. The leaf numbers were investigated in the rosette stage and the bud stage, representing the leaf plastochron of the plants. The effective primary branch numbers were in the final flowering period. Biomass and seed yields were obtained from 40 F_2 plants exhibiting extreme leaf plastochron phenotypes, including 20 individuals each from fast-plastochron and slow-plastochron plants. The mature aboveground biomass was placed into net bags, and both the sun-dried plant weight and seed weight were measured.

The extreme 10 $F_{2:3}$ families were selected from the F_2 population during the 2021–2022 cropping season, and 30 individuals for each family were planted in the chamber with condition settings (24 °C day/16 °C night temperatures and 14 h/10 h light/dark cycle). Given the trait segregation in $F_{2:3}$ families, plant individuals with higher leaf numbers were selected from fast-plastochron families, and low-leaf-number lines were chosen from slow-plastochron families. The stem apexes of five plants were selected from each $F_{2:3}$ family. A total of 12 samples, including two parental lines, were used for RNA sequencing.

4.2. Segregation Analysis for Leaf Plastochron-Related Traits

During the 2021–2022 and 2022–2023 cropping seasons, ZH18, 2116C, F_1, and F_2 populations were used for segregation analysis by using G4F2 (P_1, P_2, F_1, and F_2) of the SEA v2.0.1 R package [48]. According to the AIC minimum criterion, 4 models with the minimum AIC values were selected as candidate models from the 24 models [48]. Then, the fitness test was conducted for each candidate model separately, and the module with the minimum *p*-value ($p < 0.05$) was taken into consideration as the best model [48].

4.3. DNA Isolation and BSA-Sequencing

The two parents (ZH18 and 2116C) and two extremely bulked pools (B1 and B2) from the 600 F_2 individuals were used for BSA-seq. The F_2 bulked pools were constructed by the top 30 slow-/rapid-plastochron individuals, respectively. Genomic DNA was isolated from the fresh leaves using the cetyl trimethyl ammonium bromide (CTAB) protocol [49]. DNA was randomly broken into 350 bp fragments by ultrasonic waves, and the DNA fragments were used for sequencing library construction and Illumina HiSeq sequencing. Whole-genome re-sequencing in 20X and 30X coverage was performed on the parents and

the bulked pools, respectively. Whole-genome sequences were generated using paired-end sequencing on the Illumina Hiseq platform. BSA (bulked segregant analysis) sequencing library preparation and sequencing were conducted at Biomarker Technologies Corporation (Beijing, China).

Raw reads were filtered by fastp v0.21.0 [50], then clean reads were obtained for subsequent analysis. The reads were mapped to the reference genome ZS11 v0 and Darmor-*bzh* V10 using Burrows-Wheeler-Alignment software (BWA) v2.2 [51,52]. Duplicate reads were sorted and removed with SAMtools v1.9 [53]. SNP and small InDel variant detections were performed by the HaplotypeCaller algorithm of GATK v3.8 [54], and the variants were annotated using SnpEff v3.6c software with the default parameters [55].

4.4. SNP-Index Calculation and QTL Detection

Before association analysis, variants were filtered with the criteria: filter out variants with (I) multiple genotypes, (II) with coverage less than 4X in the bulked pools, (III) that were homozygous and consistent between the two bulked pools or between the two parents, and (IV) that were inconsistent between the pool and parent with the same trait. Calculating the SNP-index is an association analysis method to find the significant differences in genotype frequency between the pools, and the ΔSNP(InDel)-index was obtained [56]. To determine and obtain the association threshold, the DISTANCE/SNPNUM method was used, and the regions higher than the threshold were considered trait-related candidate regions [57].

4.5. RNA Isolation and RNA-Seq Analyses

The stem apexes of ZH18, 2116C, and extremely $F_{2:3}$ families were sampled for RNA isolation. The RNA isolation protocol followed the manufacturer's instructions for the RNAprep kit, and the first strand of cDNA synthesis was performed using the FastKing Premix Kit (Tiangen, Beijing, China). The cDNA library preparations and sequencing experiments were conducted by the sequencing cooperation of Grandomics company (Wuhan, China), and the libraries were sequenced on an MGI platform. The fastp v0.21.0 was employed to obtain clean data from raw data [50], and the clean reads were mapped to the reference genome ZS11 v0 using Hisat 2.0 with default parameters [51]. Novel transcripts were identified by the Stringtie v2.1.7. Gene expression levels were determined using the fragments per kilobase of exon per million fragments mapped (FPKM).

4.6. Gene Prediction in the Mapping Interval

All genes within the targeted mapping intervals were identified from the *Brassica napus* ZS11 v0 genome [51]. Gene annotations were performed by BLAST in Nr (NCBI non-redundant protein sequences, https://ftp.ncbi.nlm.nih.gov/blast/db/, accessed on 20 April 2024.), Pfam (Protein family, http://pfam-legacy.xfam.org/https://ftp.ncbi.nlm.nih.gov/blast/db/, accessed on 27 January 2025.), KOG/COG (Clusters of Orthologous Groups of proteins, https://www.ncbi.nlm.nih.gov/research/cog/, accessed on 28 January 2024.), Swiss-Prot (https://www.expasy.org/resources/UniProtKB-swiss-prot, accessed on 20 January 2024.), KO (KEGG Ortholog database, https://www.genome.jp/kegg/ko.html, accessed on 20 January 2024.), and GO (Gene Ontology, https://geneontology.org/, accessed on 20 January 2024.) databases.

4.7. Candidate Gene Expression and Variants in the Public Database

The TPM value of target genes in the public transcriptome was extracted from the BnIR database [58], including cotyledon, vegetative rosette, leaves, root, seed, silique, and stem peel. The SNP and InDel information of 2311 rapeseed accessions were obtained from

the BnIR database as well [58]. The single-nucleotide variations (SNVs), flowering time, and branch number of natural accessions were from the public data [59,60].

4.8. Data Analyses and Visualization

The phenotypic data were analyzed and visualized by Excel 2016 and R 4.0.2 (https://www.r-project.org/, accessed on 20 January 2024.). Significant differences were evaluated using the *t*-test method, and the p-value < 0.05 was considered to be significant. Data were means ± SD (standard deviation) of the biological samples. The visualizations of the BSA results were performed using BMKCloud v2024 (www.biocloud.net, accessed on 28 January 2024.).

5. Conclusions

In the present study, morphology, genetics, genomics, and transcriptomics were integrated to analyze the genetic mechanisms of leaf plastochron in rapeseed. Leaf expansion of the rapid-plastochron line 2116C was consistently faster than that of the slow-plastochron line ZH18, and the leaf plastochron showed a significant positive correlation with primary branch number. Genetic analyses demonstrated that leaf plastochron was mainly controlled by two equally dominant effect genes (2MG-EAD) via segregation analysis, and three novel associated intervals were detected in chromosome A02 (9.04–9.48 Mb and 13.52–13.66 Mb) and A04 (19.84–20.14 Mb) by BSA sequencing. A total of 10 candidate genes were identified in the intervals, including *FT* (*BnaA02G0156900ZS*), *RGL1* (*BnaA02G0160500ZS*), *MYB-like* (*BnaA02G0160600ZS*), *CYP96A8* (*BnaA02G0215600ZS*), *BLH3* (*BnaA02G0215300ZS*), *NIT2* (*BnaA04G0200300ZS*), *ASK6* (*BnaA04G0200700ZS*), and *CLEs* (*BnaA04G0201700ZS*, *BnaA04G0201900ZS*, and *BnaA04G0202000ZS*). These results could provide a foundation for exploring the leaf plastochron of 2116C and plastochron-related breeding in rapeseed.

Supplementary Materials: The following supporting information can be downloaded at: https://www.mdpi.com/article/10.3390/plants14111719/s1, Figure S1 Venn diagrams of InDels indentifed in the samples; Figure S2 ΔInDel-index calculated based on the ZS11 v0 reference genome; Figure S3 ΔInDel-index calculated based on the Darmor-bzh V10 reference genome; Figure S4 Genome collinearity analyses between the intervals of ZS11 and Darmor-bzh; Figure S5 Principal components analysis (PCA) for the 12 RNA-seq samples based on the candidate gene expression; Figure S6 Boxplots of candidate gene expression and leaf number in the RNA-seq samples; Figure S7 The relationships between flowering time and 24 SNVs shared with natural accessions; Figure S8 Experimental design; Table S1 Statistics of leaf plastochron-related traits in the four-generation population; Table S2 Pearson correlation coefficients among leaf plastochron, primary branch number, biomass, and seed yield; Table S3: Fitness tests of candidate models for ZH18 × 2116 C hybrid combinations; Table S4 Estimates of genetic parameters of leaf plastochron-related traits; Table S5 Statistics of the sequencing data for the four samples; Table S6 Statistical table of candidate genomic intervals on the ZS11 genome; Table S7: Statistics of candidate genomic intervals on the Darmor-bzh genome; Table S8: Results of protein sequence alignment between Darmor-bzh and ZS11; Table S9: Annotation of SNP and InDel in the candidate genes; Table S10: Statistics of variants detected between BSA sequencing and 2311 accessions; Table S11: Candidate gene expression patterns in different tissues of ZS11.

Author Contributions: Conceptualization, Z.H. and A.X.; Data curation, X.L. and J.S.; Formal analysis, M.Q., X.L., J.S. and W.L.; Funding acquisition, M.Q. and S.L.; Investigation, X.L., J.S., F.Z., Y.S., Y.X., Z.G., T.Z., J.W. (Jiapeng Wu), J.W. (Jinxiong Wang) and K.L.; Resources, A.X.; Supervision, M.Q., W.L., S.L., Z.H. and A.X.; Validation, X.L.; Visualization, M.Q.; Writing—original draft, M.Q. and J.S.; Writing—review and editing, Z.H. and A.X. All authors have read and agreed to the published version of the manuscript.

Funding: This research was supported by the National Natural Science Foundation of China (32401932), the China Postdoctoral Science Foundation (2024M750587), the Open Fund of Guangdong Provincial Key Laboratory of Crop Genetic Improvement (202504), and the Lhasa Key Science and Technology Planning Project (LSKJ202430).

Data Availability Statement: The raw sequencing data generated in this study are available in SRA (https://www.ncbi.nlm.nih.gov/sra, accessed on 24 January 2025.) of NCBI with the accession numbers PRJNA1055329 and PRJNA1207201.

Conflicts of Interest: The authors declare no conflicts of interest.

References

1. Kawakatsu, T.; Itoh, J.-I.; Miyoshi, K.; Kurata, N.; Alvarez, N.; Veit, B.; Nagato, Y. PLASTOCHRON2 Regulates Leaf Initiation and Maturation in Rice. *Plant Cell* **2006**, *18*, 612–625. [CrossRef] [PubMed]
2. Miyoshi, K.; Ahn, B.-O.; Kawakatsu, T.; Ito, Y.; Itoh, J.-I.; Nagato, Y.; Kurata, N. PLASTOCHRON1, a timekeeper of leaf initiation in rice, encodes cytochrome P450. *Proc. Natl. Acad. Sci. USA* **2004**, *101*, 875–880. [CrossRef]
3. Padilla, J.M.; Otegui, M.E. Co-ordination between Leaf Initiation and Leaf Appearance in Field-grown Maize (*Zea mays*): Genotypic Differences in Response of Rates to Temperature. *Ann. Bot.* **2005**, *96*, 997–1007. [CrossRef]
4. Strable, J.; Nelissen, H. The dynamics of maize leaf development: Patterned to grow while growing a pattern. *Curr. Opin. Plant Biol.* **2021**, *63*, 102038. [CrossRef] [PubMed]
5. Prusinkiewicz, P.; Crawfordb, S.; Smitha, R.S.; Ljungc, K.; Bennett, T.; Ongaro, V.; Leyser, O. Control of bud activation by an auxin transport switch. *Proc. Natl. Acad. Sci. USA* **2009**, *106*, 17431–17436. [CrossRef]
6. Li, Z.; Ding, Y.; Xie, L.; Jian, H.; Gao, Y.; Yin, J.; Li, J.; Liu, L. Regulation by sugar and hormone signaling of the growth of *Brassica napus* L. axillary buds at the transcriptome level. *Plant Growth Regul.* **2020**, *90*, 571–584. [CrossRef]
7. Chen, Z.; Chen, Y.; Shi, L.; Wang, L.; Li, W. Interaction of Phytohormones and External Environmental Factors in the Regulation of the Bud Dormancy in Woody Plants. *Int. J. Mol. Sci.* **2023**, *24*, 17200. [CrossRef] [PubMed]
8. Zhu, Y.; Wagner, D. Plant Inflorescence Architecture: The Formation, Activity, and Fate of Axillary Meristems. *Cold Spring Harb. Perspect. Biol.* **2020**, *12*, a034652. [CrossRef]
9. Wang, C.; Yang, J.; Chen, W.; Zhao, X.; Wang, Z. Contribution of the leaf and silique photosynthesis to the seeds yield and quality of oilseed rape (*Brassica napus* L.) in reproductive stage. *Sci. Rep.* **2023**, *13*, 4721. [CrossRef]
10. Somssich, M.; Je, B.I.; Simon, R.; Jackson, D. CLAVATA-WUSCHEL signaling in the shoot meristem. *Development* **2016**, *143*, 3238–3248. [CrossRef]
11. Ahn, B.; Miyoshi, K.; Itoh, J.-I.; Nagato, Y.; Kurata, N. A Recessive Heterochronic Mutation, plastochron1, Shortens the Plastochron and Elongates the Vegetative Phase in Rice. *Plant Cell* **2002**, *105*, 654–659. [CrossRef]
12. Mimura, M.; Nagato, Y.; Itoh, J. Rice PLASTOCHRON genes regulate leaf maturation downstream of the gibberellin signal transduction pathway. *Planta* **2012**, *235*, 1081–1089. [CrossRef]
13. Xiong, Y.; Xie, J.; Zhang, X.; Li, Y.; Tian, W.; Ni, J.; Zhu, Z.; Wang, Y.; Wen, X.; Sang, X. PLASTOCHRON1 regulates leaf inclination through Brassinolide pathway in *Oryza sativa*. *Crop Sci.* **2021**, *61*, 1280–1288. [CrossRef]
14. Sun, X.; Cahill, J.; Van Hautegem, T.; Feys, K.; Whipple, C.; Novak, O.; Delbare, S.; Versteele, C.; Demuynck, K.; De Block, J.; et al. Altered expression of maize PLASTOCHRON1 enhances biomass and seed yield by extending cell division duration. *Nat. Commun.* **2017**, *8*, 14752. [CrossRef]
15. Dhami, N.; Cazzonelli, C.I. Short photoperiod attenuates CO_2 fertilization effect on shoot biomass in *Arabidopsis thaliana*. *Physiol. Mol. Biol. Plants* **2021**, *27*, 825–834. [CrossRef]
16. Duan, T.; Chapman, S.C.; Holland, E.; Rebetzke, G.J.; Guo, Y.; Zheng, B. Dynamic quantification of canopy structure to characterize early plant vigour in wheat genotypes. *J. Exp. Bot.* **2016**, *67*, 4523–4534. [CrossRef] [PubMed]
17. Zhang, Z.; Christensen, M.; Nan, Z.; Whish, J.P.M.; Bell, L.W.; Wang, J.; Wang, Z.; Sim, R. Plant development and solar radiation interception of four annual forage plants in response to sowing date in a semi-arid environment. *Ind. Crops Prod.* **2019**, *131*, 41–53. [CrossRef]
18. Banaś, K.; Piwowar, A.; Harasym, J. The potential of rapeseed (canola) oil nutritional benefits wide spreading via oleogelation. *Food Biosci.* **2023**, *56*, 103162. [CrossRef]
19. Liu, G.; Yan, L.; Wang, S.; Yuan, H.; Zhu, Y.; Xie, C.; Wang, P.; Yang, R. A novel type of sprout food development: Effects of germination on phytic acid, glucosinolates, and lipid profiles in rapeseed. *Food Biosci.* **2023**, *55*, 102893. [CrossRef]
20. Huang, H.; Shi, Y.; Liu, T.; Zhou, Y. Oilseed-Vegetable-Dual-Purpose Rape Key Technology Research and Its Application Prospect Analysis. *Agric. Sci.* **2014**, *5*, 1291–1295. [CrossRef]
21. McMASTER, G.S. Phytomers, phyllochrons, phenology and temperate cereal development. *J. Agric. Sci.* **2005**, *143*, 137–150. [CrossRef]

22. Wang, B.; Smith, S.M.; Li, J. Genetic Regulation of Shoot Architecture. *Annu. Rev. Plant Biol.* **2018**, *69*, 437–468. [CrossRef]
23. Luo, X.; Ma, C.; Yue, Y.; Hu, K.; Li, Y.; Duan, Z.; Wu, M.; Tu, J.; Shen, J.; Yi, B.; et al. Unravelling the complex trait of harvest index in rapeseed (*Brassica napus* L.) with association mapping. *BMC Genomics* **2015**, *16*, 379. [CrossRef]
24. Lu, K.; Xiao, Z.; Jian, H.; Peng, L.; Qu, C.; Fu, M.; He, B.; Tie, L.; Liang, Y.; Xu, X.; et al. A combination of genome-wide association and transcriptome analysis reveals candidate genes controlling harvest index-related traits in Brassica napus. *Sci. Rep.* **2016**, *6*, 36452. [CrossRef]
25. Hu, J.; Chen, B.; Zhao, J.; Zhang, F.; Xie, T.; Xu, K.; Gao, G.; Yan, G.; Li, H.; Li, L.; et al. Genomic selection and genetic architecture of agronomic traits during modern rapeseed breeding. *Nat. Genet.* **2022**, *54*, 694–704. [CrossRef] [PubMed]
26. Qin, M.; Song, J.; Guo, N.; Zhang, M.; Zhu, Y.; Huang, Z.; Xu, A. Genome-Wide Association Analyses Reveal Candidate Genes Controlling Harvest Index and Related Agronomic Traits in *Brassica napus* L. *Agronomy* **2022**, *12*, 814. *Agronomy* **2022**, *12*, 814. [CrossRef]
27. Zheng, M.; Zhang, L.; Tang, M.; Liu, J.; Liu, H.; Yang, H.; Fan, S.; Terzaghi, W.; Wang, H.; Hua, W. Knockout of two BnaMAX1 homologs by CRISPR/Cas9 targeted mutagenesis improves plant architecture and increases yield in rapeseed (*Brassica napus* L.). *Plant Biotechnol. J.* **2020**, *18*, 644–654. [CrossRef]
28. Zhang, C.; Gong, R.; Zhong, H.; Dai, C.; Zhang, R.; Dong, J.; Li, Y.; Liu, S.; Hu, J. Integrated multi-locus genome-wide association studies and transcriptome analysis for seed yield and yield-related traits in *Brassica napus*. *Front. Plant Sci.* **2023**, *14*, 1153000. [CrossRef]
29. Jaeger, K.E.; Wigge, P.A. FT protein acts as a long-range signal in *Arabidopsis*. *Curr. Biol.* **2007**, *17*, 1050–1054. [CrossRef] [PubMed]
30. Jackson, S.D.; Hong, Y. Systemic movement of FT mRNA and a possible role in floral induction. *Front. Plant Sci.* **2012**, *3*, 127. [CrossRef]
31. Mao, Y.; Sun, J.; Cao, P.; Zhang, R.; Fu, Q.; Chen, S.; Chen, F.; Jiang, J. Functional analysis of alternative splicing of the FLOWERING LOCUS T orthologous gene in Chrysanthemum morifolium. *Hortic. Res.* **2016**, *3*, 16058. [CrossRef]
32. Nelissen, H.; Rymen, B.; Jikumaru, Y.; Demuynck, K.; Van Lijsebettens, M.; Kamiya, Y.; Inzé, D.; Beemster, G.T.S. A Local Maximum in Gibberellin Levels Regulates Maize Leaf Growth by Spatial Control of Cell Division. *Curr. Biol.* **2012**, *22*, 1183–1187. [CrossRef]
33. Wen, C.K.; Chang, C. Arabidopsis RGL1 encodes a negative regulator of gibberellin responses. *Plant Cell* **2002**, *14*, 87–100. [CrossRef]
34. Chen, L.; Xiang, S.; Chen, Y.; Li, D.; Yu, D. Arabidopsis WRKY45 Interacts with the DELLA Protein RGL1 to Positively Regulate Age-Triggered Leaf Senescence. *Mol. Plant* **2017**, *10*, 1174–1189. [CrossRef] [PubMed]
35. Chen, M.; Maodzeka, A.; Zhou, L.; Ali, E.; Wang, Z.; Jiang, L. Removal of DELLA repression promotes leaf senescence in Arabidopsis. *Plant Sci.* **2014**, *219–220*, 26–34. [CrossRef]
36. Muller, D.; Schmitz, G.; Theres, K. Blind homologous R2R3 Myb genes control the pattern of lateral meristem initiation in *Arabidopsis*. *Plant Cell* **2006**, *18*, 586–597. [CrossRef] [PubMed]
37. Li, G.; Cheng, L.; Li, Z.; Zhao, Y.; Wang, Y. Over-expression of CcMYB24, encoding a R2R3-MYB transcription factor from a high-leaf-number mutant of Cymbidium, increases the number of leaves in Arabidopsis. *PeerJ* **2023**, *11*, e15490. [CrossRef] [PubMed]
38. Rutjens, B.; Bao, D.; van Eck-Stouten, E.; Brand, M.; Smeekens, S.; Proveniers, M. Shoot apical meristem function in Arabidopsis requires the combined activities of three BEL1-like homeodomain proteins. *Plant J.* **2009**, *58*, 641–654. [CrossRef]
39. Smith, H.M.; Hake, S. The interaction of two homeobox genes, BREVIPEDICELLUS and PENNYWISE, regulates internode patterning in the Arabidopsis inflorescence. *Plant Cell* **2003**, *15*, 1717–1727. [CrossRef]
40. Wang, L.; Ming, L.; Liao, K.; Xia, C.; Sun, S.; Chang, Y.; Wang, H.; Fu, D.; Xu, C.; Wang, Z.; et al. Bract suppression regulated by the miR156/529-SPLs-NL1-PLA1 module is required for the transition from vegetative to reproductive branching in rice. *Mol. Plant* **2021**, *14*, 1168–1184. [CrossRef]
41. Booker, J.; Sieberer, T.; Wright, W.; Williamson, L.; Willett, B.; Stirnberg, P.; Turnbull, C.; Srinivasan, M.; Goddard, P.; Leyser, O. MAX1 encodes a cytochrome P450 family member that acts downstream of MAX3/4 to produce a carotenoid-derived branch-inhibiting hormone. *Dev. Cell* **2005**, *8*, 443–449. [CrossRef] [PubMed]
42. Normanly, J.; Grisafi, P.; Fink, G.R.; Bartel, B. Arabidopsis mutants resistant to the auxin effects of indole-3-acetonitrile are defective in the nitrilase encoded by the NIT1 gene. *Plant Cell* **1997**, *9*, 1781–1790. [CrossRef] [PubMed]
43. Yang, S.; Zhang, T.; Wang, Z.; Zhao, X.; Li, R.; Li, J. Nitrilases NIT1/2/3 Positively Regulate Flowering by Inhibiting MAF4 Expression in Arabidopsis. *Front. Plant Sci.* **2022**, *13*, 889460. [CrossRef] [PubMed]
44. Han, S.; Cho, H.; Noh, J.; Qi, J.; Jung, H.-J.; Nam, H.; Lee, S.; Hwang, D.; Greb, T.; Hwang, I. BIL1-mediated MP phosphorylation integrates PXY and cytokinin signalling in secondary growth. *Nat. Plants* **2018**, *4*, 605–614. [CrossRef]
45. Yin, Y.; Wang, Z.Y.; Mora-Garcia, S.; Li, J.; Yoshida, S.; Asami, T.; Chory, J. BES1 accumulates in the nucleus in response to brassinosteroids to regulate gene expression and promote stem elongation. *Cell* **2002**, *109*, 181–191. [CrossRef]

46. Gampala, S.S.; Kim, T.W.; He, J.X.; Tang, W.; Deng, Z.; Bai, M.Y.; Guan, S.; Lalonde, S.; Sun, Y.; Gendron, J.M.; et al. An essential role for 14-3-3 proteins in brassinosteroid signal transduction in Arabidopsis. *Dev. Cell* **2007**, *13*, 177–189. [CrossRef]
47. Leibfried, A.; To, J.P.C.; Busch, W.; Stehling, S.; Kehle, A.; Demar, M.; Kieber, J.J.; Lohmann, J.U. WUSCHEL controls meristem function by direct regulation of cytokinin-inducible response regulators. *Nature* **2005**, *438*, 1172–1175. [CrossRef]
48. Wang, J.-T.; Zhang, Y.-W.; Du, Y.-W.; Ren, W.-L.; Li, H.-F.; Sun, W.-X.; Ge, C.; Zhang, Y.-M. SEA v2.0: An R software package for mixed major genes plus polygenes inheritance analysis of quantitative traits. *Acta Agron. Sin.* **2022**, *48*, 1416–1424. [CrossRef]
49. Doyle, J.J. Isolation of plant DNA from fresh tissue. *Focus* **1990**, *12*, 13–15.
50. Chen, S.; Zhou, Y.; Chen, Y.; Gu, J. fastp: An ultra-fast all-in-one FASTQ preprocessor. *Bioinformatics* **2018**, *34*, i884–i890. [CrossRef]
51. Song, J.M.; Guan, Z.; Hu, J.; Guo, C.; Yang, Z.; Wang, S.; Liu, D.; Wang, B.; Lu, S.; Zhou, R.; et al. Eight high-quality genomes reveal pan-genome architecture and ecotype differentiation of *Brassica napus*. *Nat. Plants* **2020**, *6*, 34–45. [CrossRef] [PubMed]
52. Rousseau-Gueutin, M.; Belser, C.; Da Silva, C.; Richard, G.; Istace, B.; Cruaud, C.; Falentin, C.; Boideau, F.; Boutte, J.; Delourme, R.; et al. Long-read assembly of the *Brassica napus* reference genome Darmor-bzh. *Gigascience* **2020**, *9*, giaa137. [CrossRef]
53. Li, H.; Handsaker, B.; Wysoker, A.; Fennell, T.; Ruan, J.; Homer, N.; Marth, G.; Abecasis, G.; Durbin, R.; Subgroup, G.P.D.P. The Sequence Alignment/Map format and SAMtools. *Bioinformatics* **2009**, *25*, 2078–2079. [CrossRef] [PubMed]
54. McKenna, A.; Hanna, M.; Banks, E.; Sivachenko, A.; Cibulskis, K.; Kernytsky, A.; Garimella, K.; Altshuler, D.; Gabriel, S.; Daly, M.; et al. The Genome Analysis Toolkit: A MapReduce framework for analyzing next-generation DNA sequencing data. *Genome Res.* **2010**, *20*, 1297–1303. [CrossRef] [PubMed]
55. Cingolani, P.; Platts, A.; Wang, L.L.; Coon, M.; Nguyen, T.; Wang, L.; Land, S.J.; Lu, X.; Ruden, D.M. A program for annotating and predicting the effects of single nucleotide polymorphisms, SnpEff. *Fly* **2014**, *6*, 80–92. [CrossRef]
56. Takagi, H.; Abe, A.; Yoshida, K.; Kosugi, S.; Natsume, S.; Mitsuoka, C.; Uemura, A.; Utsushi, H.; Tamiru, M.; Takuno, S.; et al. QTL-seq: Rapid mapping of quantitative trait loci in rice by whole genome resequencing of DNA from two bulked populations. *Plant J.* **2013**, *74*, 174–183. [CrossRef]
57. Abe, A.; Kosugi, S.; Yoshida, K.; Natsume, S.; Takagi, H.; Kanzaki, H.; Matsumura, H.; Yoshida, K.; Mitsuoka, C.; Tamiru, M.; et al. Genome sequencing reveals agronomically important loci in rice using MutMap. *Nat. Biotechnol.* **2012**, *30*, 174–178. [CrossRef] [PubMed]
58. Yang, Z.; Wang, S.; Wei, L.; Huang, Y.; Liu, D.; Jia, Y.; Luo, C.; Lin, Y.; Liang, C.; Hu, Y.; et al. BnIR: A multi-omics database with various tools for *Brassica napus* research and breeding. *Mol. Plant* **2023**, *16*, 775–789. [CrossRef]
59. Li, F.; Chen, B.; Xu, K.; Gao, G.; Yan, G.; Qiao, J.; Li, J.; Li, H.; Li, L.; Xiao, X.; et al. A genome-wide association study of plant height and primary branch number in rapeseed (*Brassica napus*). *Plant Sci.* **2016**, *242*, 169–177. [CrossRef]
60. Zhang, G.; Peng, Y.; Zhou, J.; Tan, Z.; Jin, C.; Fang, S.; Zhong, S.; Jin, C.; Wang, R.; Wen, X.; et al. Genome-Wide Association Studies of Salt-Alkali Tolerance at Seedling and Mature Stages in *Brassica napus*. *Front. Plant Sci.* **2022**, *13*, 857149. [CrossRef]

plants

MDPI

Article

Functional Characterization of Rice Spotted-Leaf Mutant *HM113* Reveals an Amino Acid Substitution in a Cysteine-Rich Receptor-like Kinase

Ringki Kuinamei Sanglou, Marie Gorette Kampire, Xia Xu, Jian-Li Wu, Junyi Gong * and Xiaobo Zhang *

State Key Laboratory of Rice Biology and Breeding, China National Rice Research Institute, Hangzhou 311400, China; ringki007@gmail.com (R.K.S.); kamgorette@gmail.com (M.G.K.); mailxuxia@163.com (X.X.); beishangd@163.com (J.-L.W.)

* Correspondence: junyigong8107@163.com (J.G.); zhangxiaobo@caas.cn (X.Z.)

Abstract

The spotted-leaf mutant, characterized by spontaneous lesion formation resembling pathogen-induced hypersensitive cell death, serves as an ideal model for studying the molecular mechanisms behind rice (*Oryza sativa*) disease resistance and programmed cell death, as these plants display hypersensitive responses that mimic those triggered by pathogen infection. In this study, we generated a knockout line using CRISPR/Cas9 technology in homologous mutant *HM113*-induced calli. *LOC_Os07g30510* encodes a cysteine-rich receptor kinase with a DUF26 domain, consisting of 688 amino acids. *HM113* was localized to the cytosol and expressed in most rice tissues at various growth stages. A single nucleotide substitution from A to T was observed at the 847th base of *LOC_Os07g30510*, causing an amino acid change from serine to cysteine. Our results demonstrated that the A847T mutation was responsible for the spotted-leaf phenotype in the *HM113* mutant through gene editing technology, as new frameshift mutations were introduced upstream of the A847T site in the *HM113* gene. The mutation phenotype of *HM113* was eliminated and resistance to bacterial blight was also lost, indicating that it is a gain-of-function gene.

Keywords: rice; spotted leaf; bacterial blight; defense response; resistance; reactive oxygen species

1. Introduction

Rice, also known as *Oryza sativa* L., is the most widely cultivated and ancient agricultural crop globally, consumed by rural and urban people, and the primary food source for nearly half of the global population [1]. Bacterial blight (BB) is a severe disease that affects rice crops, significantly impacting global rice production and resulting in substantial losses and damage. The estimated yield losses due to this disease range from 20% to 80%, posing a significant threat to rice production [2–4]. Spotted-leaf mutants are a crucial class that exhibit spontaneous cell death, resulting in necrotic lesions or spots on leaves, regardless of whether the stress is biotic or abiotic [5]. These mutants are also known as lesion-mimic mutants (LMMs) and display spontaneous lesions in the absence of pathogen attack, environmental stress, or mechanical damage. Many LMMs exhibit constitutive activation of defense pathways, resulting in enhanced resistance to specific pathogens [6,7].

In rice, several LMMs have shown increased resistance to the blast fungus *Magnaporthe oryzae*. Several lesion-mimic mutants in rice, such as *oscul3a* and *LIL1*, have shown ROS accumulation, increased expression of disease-related genes, and significant resistance to *Magnaporthe oryzae* and *Xanthomonas oryzae* pv. *oryzae* (*Xoo*). These include the upregulation of pathogenesis-related (PR) genes, accumulation of reactive oxygen species (ROS), and higher expression of salicylic acid (SA)- and jasmonic acid (JA)-dependent signaling genes [8,9]. Likewise, disease resistance to bacterial blight caused by *Xanthomonas oryzae* pv. *oryzae* (*Xoo*) is higher in LMMs than in wild-type cultivars such as IR64, due to constitutive expression of defense-related genes and an increase in basal immune responses [6]. The symptoms are similar to those caused by pathogens or an infection-induced hypersensitive response (HR), hence the term "spotted-leaf mutants" [10]. Plants have developed a host defense mechanism against these pathogens; one of the most common is the hypersensitive response (HR), a crucial innate immune response that involves the rapid induction of localized cell death during an incompatible interaction between a plant and a pathogen [11]. The hypersensitive response is characterized by a burst of reactive oxygen species (ROS), the expression of pathogenesis-related (PR) genes, the accumulation of phytoalexins or antimicrobial compounds, and alterations in the cell wall, all of which contribute to the suppression of pathogen development [12]. Programmed cell death (PCD) is followed by disease-like spots, which trigger the plant's defensive response, enhance the expression of defensive genes, and promote plant tolerance to diseases such as rice blast and bacterial blight. Similarly, lesion mimics mutants provide natural resources for understanding the processes of plant-programmed cell death and defensive responses [13].

In recent years, many rice LLM genes have been discovered and isolated. Over 80 spotted-leaf mutants have been identified, with most being recessive and some regulated by dominant or semi-dominant genes. *Spl 40* [14], *HM47* [15], and *HM143* [16] are one gene controlled by a single recessive nuclear gene. *Spl26*, the spotted-leaf trait, is governed by a dominant nuclear gene on the short arm of chromosome 7 [17]. The gene *Spl24* is known to be semi-dominant [18].

They also encode various proteins with diverse roles and functional categories related to rice defense responses and HR cell death signaling mechanisms. These proteins, encoded by spotted-leaf genes in rice, include membrane-associated proteins [19], splicing factor 3 subunit 3 [20], U-box domain-containing proteins [21], and splicing factor 3b subunit 3 (SF3B3), a protein found in *Spl5* that might be involved in the early splicing of RNAs, which regulates defense mechanisms and cell death [20]. Additionally, *Spl7* encodes a heat stress transcription factor protein that confers resistance to environmental stress [22]. It was found that *Spl11*, one of the most extensively studied rice LMMs, encodes a U-box/Armadillo repeat protein with E3 ubiquitin ligase activity and resistance to various diseases. Ubiquitination may play a role in managing plant programmed cell death (PCD) and pathogen defense [23]. These findings suggest that several proteins work together to prevent HR cells from dying and to enhance disease resistance.

Many genes that produce receptor-like protein kinases (RLKs) were also cloned. The plasma membrane-localized receptor-like kinases (RLKs) play a key role in sensing and transducing external stimuli to activate downstream signaling pathways [24]. The rice gene *Xa21*, a unique disease-resistance gene, encodes receptors similar to kinases with leucine-rich repeats in the extracellular, transmembrane, and serine-threonine protein kinase domains, contributing to understanding disease resistance. This gene is also resistant to multiple races of *Xanthomonas oryzae* pv. *oryzae* (*Xoo*) [25]. The Rice *Spl36* gene regulates the defense response of rice and encodes a protein kinase with receptor-like properties. The loss-of-function mutant *Spl36* exhibits an enhanced resistance to the rice bacterial blight

strain *HM73* [26]. The *Lmm24,* which regulates cell death and defense responses, encodes a receptor-like cytoplasmic kinase [5]. Another resistance gene, Pto, and the Arabidopsis receptor-like kinase 902 (AtRLK902) carry a protein kinase domain. Pto confers resistance to *Pseudomonas syringae* pv tomato (Pst) [27], and AtRLK902 resists infection by the bacterial pathogen Pseudomonas syringae [28].

We previously identified a new dominant homozygous lethal spotted-leaf mutant, *HM113*, derived from ethyl methane sulfonate (EMS) mutagenesis of IR64. The mutant *HM113* was fine-mapped to the long arm of chromosome 7. Three weeks after sowing, the mutant *HM113* developed brown lesions on its leaves, showed programmed cell death, and exhibited increased resistance to multiple bacterial blight pathogen races [29]. Here, we demonstrated that the mutation caused the spotted-leaf phenotype in *HM113* and that *LOC_Os07g30510* is the target gene of the dominant mutant, confirmed through gene editing technology. Specifically, editing the upstream mutation site of the *HM113* gene resulted in frameshift mutations; the mutation phenotype disappeared, along with resistance to bacterial blight. This indicates that it is a gain-of-function gene.

2. Results

2.1. HM113 Was Cloned, and It Encodes a Cysteine-Rich Receptor Kinase That Has a DUF26 Domain

The novel single dominant nuclear gene *SPLHM113* was mapped to the long arm of chromosome 7 by [29]. The previous study obtained 698 F2 individual plants from *HM113*/Moroberekan and *HM113*/CPSLO17 F2 populations for fine mapping. The gene *SPLHM113* was located between RM21605 and RM418, with a physical distance of about 308 kb (Figure 1A). Additionally, the mapped region contained 39 potential open reading frames (ORFs), as shown in the Rice genome annotation project database (http://rice.plantbiology.msu.edu/ (accessed on 23 June 2024)), seen in (Figure 1B). Among these, *LOC_Os07g30510,* highlighted in red in (Figure 1B), was identified as a candidate gene. To identify potential SNPs or indels linked to the dominant mutant phenotype, we used NGS technology. The reference genome was the indica rice MH63, and we resequenced the genomes of *HM113* and three other IR64 background lines. This analysis produced four VCF files. Using Excel's "vlookup" function, we compared the SNPs within the 308 kb candidate region. A SNP may be the mutation we are searching for if it is unique to the *HM113* mutant. The same method was applied to compare indel VCF files; however, no *HM113*-specific indels were detected. From this analysis, we identified 19 SNPs specific to *HM113*; of these, 7 SNPs were located in exonic regions, and 5 of these were nonsynonymous, resulting in amino acid substitutions (supplemental data Table S2). For confirmation, we used Sanger sequencing after designing primers to amplify each of the seven exonic SNP-containing regions by PCR. This confirmed that only a single nonsynonymous SNP was consistently associated with the mutant phenotype. As shown in (Figure 1C), the mutation was confirmed in the first exon of *LOC_Os07g30510* through PCR amplification and sequencing. The nucleotide mutation changed from A to T at position 847, resulting in an amino acid change from serine to cysteine (Figure 1D). The gene consists of 7 exons and 6 introns, with a total length of 4054 nucleotides. It is predicted that *LOC_Os07g30510* encodes a cysteine-rich receptor kinase containing a domain of unknown function 26. As a result, *LOC_Os07g30510* was identified as a candidate gene responsible for the mutant phenotype.

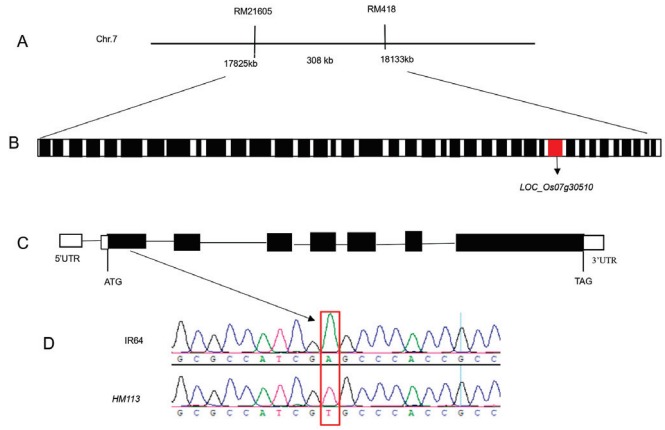

Figure 1. Map-based cloning of *HM113*. (**A**) The gene *HM113* is positioned on chromosome 7, specifically between the markers RM21605 and RM418. (**B**) In the 308 kb area, 39 ORFs were identified. The red box indicates *LOC_Os07g30510*, while the other black boxes represent different open reading frames (ORFs). (**C**) *LOC_Os07g30510* gene structure: white boxes are 5′UTR and 3′UTR, black boxes are exons, and lines are introns. (**D**) A to T point mutation sequence analysis in WT IR64 and *HM113* in the 1st exon.

2.2. HM113 Is Widespread Expressed and HM113 Localizes to the Cytosol

The quantitative reverse transcription-polymerase chain reaction (qRT-PCR) was used to measure the relative expression of *HM113* at different developmental stages of IR64. Total RNA was extracted from various tissues of the wild-type IR64 at different stages and then converted into complementary DNA (cDNA). Our results showed that HM113 was widely expressed across all examined tissues, with the highest expression levels observed in the sheath during the tillering stage (Figure 2A). These findings indicate that HM113 is a broadly expressed gene.

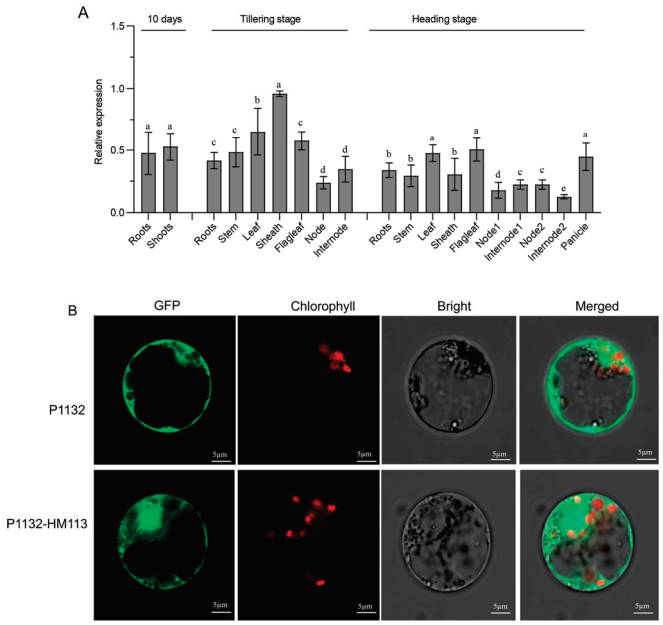

Figure 2. Relative Expression Analysis of *HM113* in Wild-Type IR64 and Subcellular Localization of HM113 in Rice Protoplasts. (**A**) The quantitative relative expression level of the *HM113* gene was determined in various tissues of wild-type IR64 rice at both the 10-day, tillering stage and the heading stage. Different letters indicate significant differences at $p < 0.05$ by Duncan's multiple test. (**B**) The top picture (P1132) represents the GFP signal in rice protoplasts alone. Bars = 5 μm. The bottom image (P1132-HM113) represents the HM113 fusion protein in rice protoplasts. Bars = 5 μm.

To determine the subcellular localization of HM113, we performed rice protoplast transformation using polyethylene glycol (PEG) as a mediator. The coding sequence of HM113 was fused with green fluorescent protein (GFP) at its N-terminal. When transiently expressed in rice protoplasts, the GFP signal was confined to the cytosol (Figure 2B). Our data clearly showed that HM113 is a protein localized in the cytosol.

2.3. The Phenotype Characterization of Knockout Lines in HM113

We used CRISPR/Cas9 to verify the function of the target gene in the *HM113* mutant background. The background was checked to ensure that the seeds are not heterozygous. The genotype was confirmed by PCR detection at the specific mutation site of *HM113*, at position 847, involving an A-to-T mutation. A total of 15 independent lines were generated through Cas-9-mediated editing. Three independent knockout lines (Cr-1, Cr-6, and Cr-9) with growth characteristics similar to those of IR64 were selected for further study. Further sequencing of these lines revealed that Cr-6 had a 1 bp insertion, while Cr-1 and Cr-9 had a 2 bp deletion at the target site, leading to a frameshift mutation (Figure 3A).

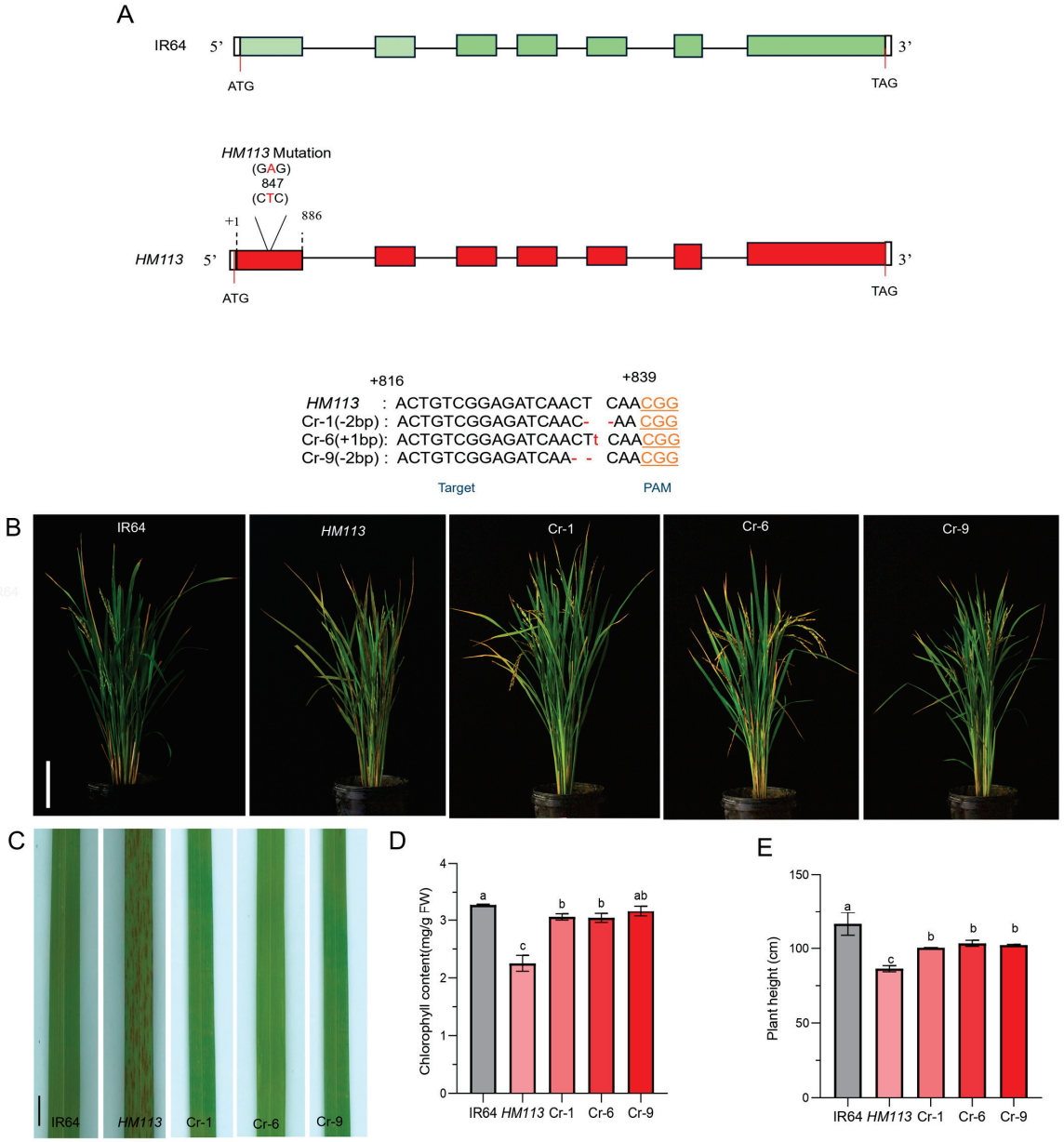

Figure 3. *Cont.*

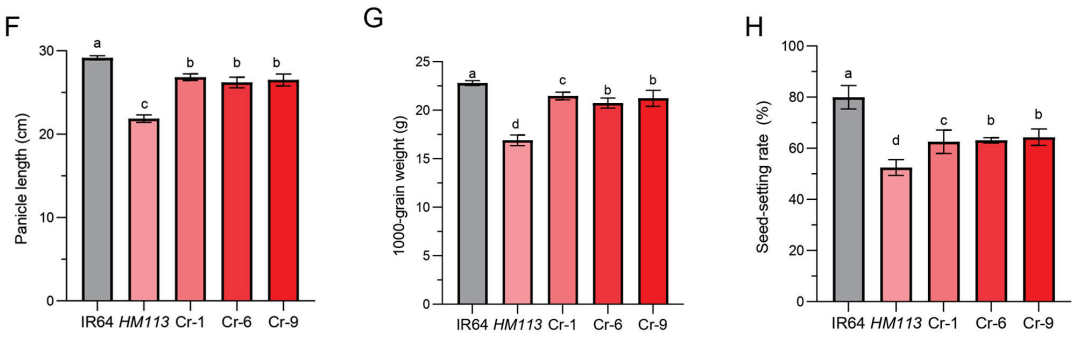

Figure 3. Phenotypic identification and functional validation of the *HM113* knockout strain. (**A**) CRISPR/Cas9-mediated mutation at the target site of knockout lines (Cr-1, Cr-6, and Cr-9), small red letters indicate the corresponding base insertions, dot lines indicate deletions; (**B**) Plant phenotypes of wild-type IR64, mutant *HM113*, and knockout lines Cr-1, Cr-6, and Cr-9 at the filling stage. Bar = 15 cm. (**C**) Leaf Phenotype of wild-type IR64, mutant *HM113*, and knockout lines Cr-1, Cr-6, and Cr-9 at the filling stage. Bar = 2 cm. (**D**) Chlorophyll content. (**E**) Plant height (**F**) Panicle length (**G**) 1000-grain weight (**H**) and Seed setting rate of wild-type IR64, mutant *HM113*, and knockout lines Cr-1, Cr-6, and Cr-9. Values are means ± SD, (n = 3). Different letters indicate significant differences according to One-way ANOVA and Duncan's test ($p < 0.05$).

Through these phenotype observations, we found that when the gain-of-function gene *HM113* homozygous mutant was knocked out using the CRISPR/Cas9 method, the plants did not exhibit a spotted-leaf phenotype and displayed a similar phenotype to the wild type (Figure 3B,C). The total chlorophyll content of Cr-1, Cr-6, and Cr-9 was the same as that of the wild type, and their chlorophyll levels were significantly higher than in the mutant *HM113* (Figure 3D). Although the other agronomic traits of the knockout lines did not fully return to wild-type levels, they demonstrated significant improvement compared to the mutant *HM113* (Figure 3E–H). Taken together, these results indicate the efficiency of CRISPR/Cas9 and confirm that *LOC_Os07g30510* is our target locus, responsible for the lesion mimic phenotype in *HM113*.

2.4. Reactive Oxygen Species Accumulation in the Knockout Lines

It has been shown that, at the physiological level, ROS play a crucial signaling role in plant growth and development. However, excessive ROS can cause oxidative damage to proteins, lipids, and nucleic acids, leading to lesion formation and cell death [30]. To verify our findings, we measured physiological and biochemical indicators in the wild-type IR64, the mutant *HM113*, and the three knockout lines Cr-1, Cr-6, and Cr-9. We evaluated whether they exhibited similar plant phenotypes to those of the wild-type or the mutant.

The hydrogen peroxide content (H_2O_2) in the wild-type IR64 and the knockout transgenic lines Cr-1, Cr-6, and Cr-9 was significantly lower compared to the mutant *HM113* (Figure 4A). This indicated increased oxidative stress. The malondialdehyde (MDA), which measures membrane lipid peroxidation, was highest in the mutant *HM113* compared to the MDA concentrations in IR64, Cr-1, Cr-6, and Cr-9, which remained stable and exhibited lower concentration than the mutant *HM113*, suggesting less membrane damage (Figure 4B).

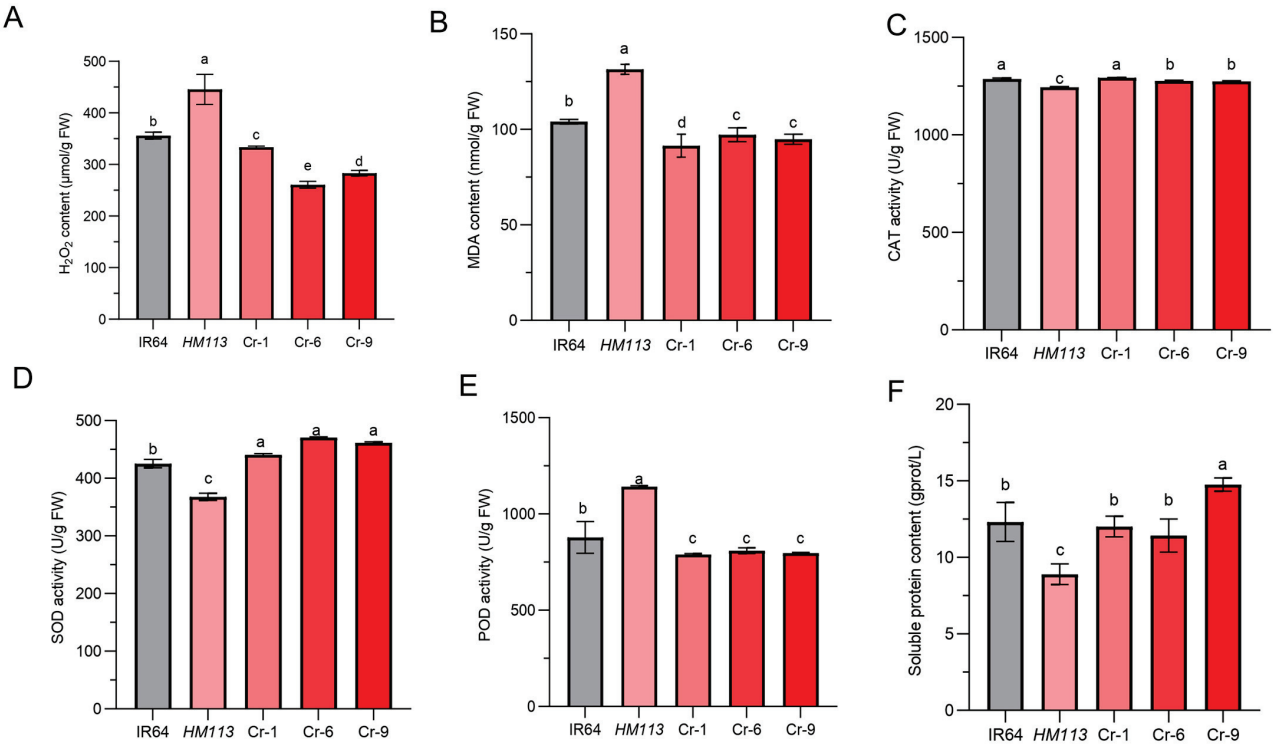

Figure 4. Physiological performance of transgenic lines, mutants, and wild types at the tillering stage. (**A**). H_2O_2 content (**B**). MDA content (**C**). CAT activity (**D**). SOD activity (**E**). POD activity (**F**). Soluble protein content. Data are means ± SD (n = 3). Different letters indicate significant differences according to Duncan's multiple test ($p < 0.05$).

Furthermore, we examined the reactive oxygen species scavenging enzymes, including catalase (CAT), superoxide dismutase (SOD), and peroxidase (POD), along with their respective content levels. While the activities of catalase (CAT) (Figure 4C) were significantly lower in *HM113*, the three knockout lines recovered similarly to the wild-type, indicating a limited capacity for ROS detoxification. The activity of Superoxide dismutase (SOD) was the lowest in the mutant *HM113* compared to the wild type IR64 and the knockout lines Cr-1, Cr-6, and Cr-9 (Figure 4D). At the same time, the Peroxidase (POD) level was higher in the mutant *HM113* compared to the wild type IR64 and the knockout lines Cr-1, Cr-6, and Cr-9 (Figure 4E), indicating that the gain-of-function by *HM113* is causing the disorder in the ROS scavenging system. Furthermore, the soluble protein content in the knockout lines Cr-1, Cr-6, and Cr-9 also returned to wild-type levels (Figure 4F). In conclusion, the results indicate that knocking out the mutant alleles can restore the normal functions of the reactive oxygen species scavenging system to normal levels in the knockout lines, thereby preventing the accumulation of reactive oxygen species and preventing oxidative damage to cells. This also suggests that the dominant mutation in the *LOC_Os07g30510* gene can increase ROS accumulation in cells, triggering cell damage and death, which leads to lesion formation in *HM113*.

2.5. Knockout Line Exhibits Resistance Comparable to Wild Type

Previous studies indicated that *HM113* exhibits disease resistance to multiple races, while *PX0347* demonstrates the highest level of resistance [29]. To determine that the enhanced resistance resulted from the mutation of *HM113*, the knockout lines, the mutant, and the wild types were inoculated with the bacterial blight strain *PX0347*. We found that the knockout lines Cr-1, Cr-6, and Cr-9 were all infected with the same pathogen as the wild-type. They showed significantly higher lesion length and disease index compared to the mutant *HM113*,

indicating their resistance to the pathogen (Figure 5A–C). These results showed that knocking out the gene of the function mutant can reduce the resistance of plants to bacterial blight, and the mutant allele is responsible for the increased resistance to *HM113*.

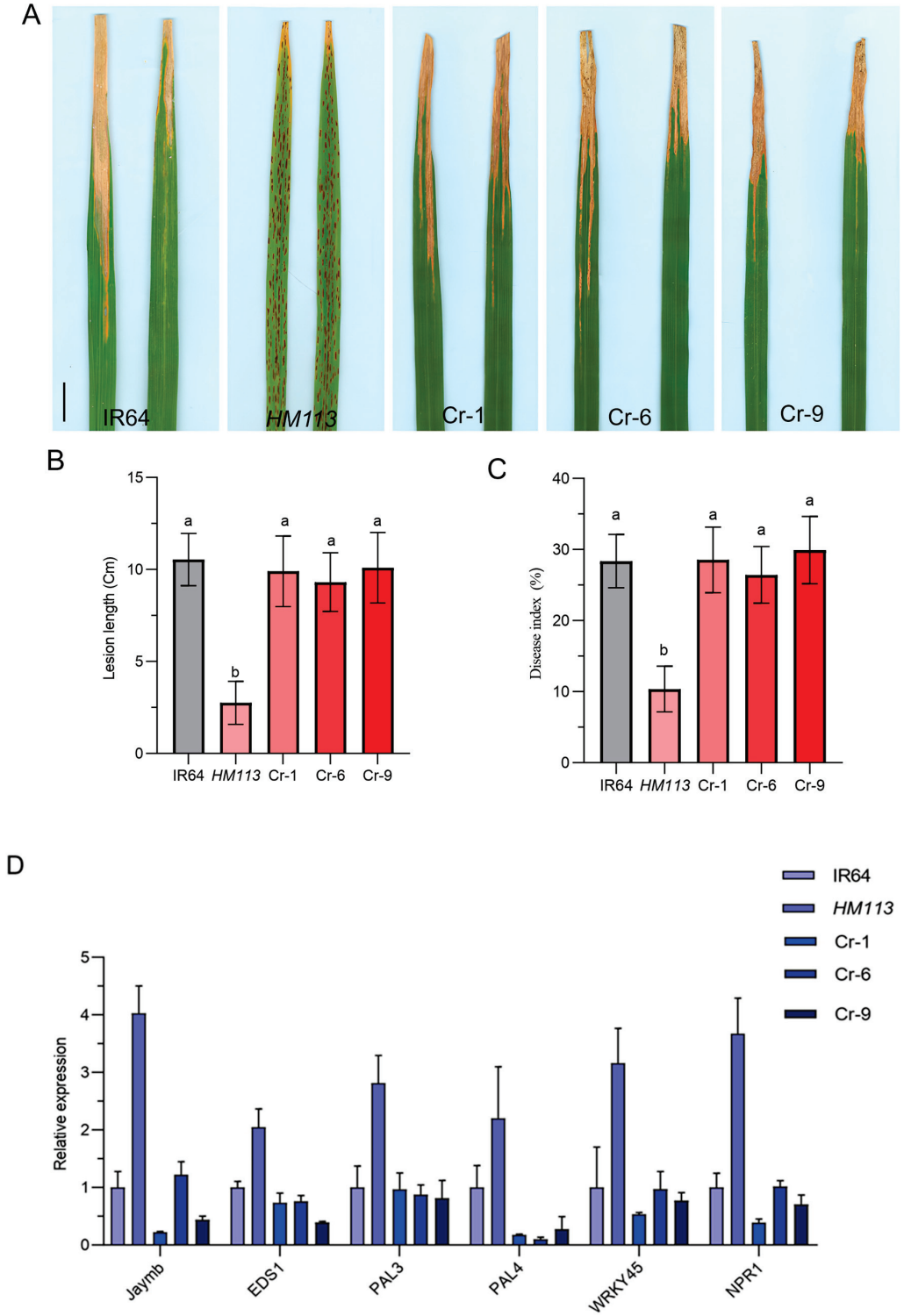

Figure 5. Disease evaluation and relative expression of defense response genes. (**A**) Responses of Wild-type IR64, mutant *HM113*, and knockout lines to bacterial blight race *PXO37* during the tillering stage. Bar = 5 cm; (**B**). Lesion Length; (**C**). Disease Index; Different letters indicate significant differences at $p < 0.05$ by Duncan's multiple test. (**D**). Analysis of defense response gene expression levels in wild-type, mutant, and knockout lines, at the tillering stage. Data are means ± SD (n = 3).

To further assess the enhanced disease resistance associated with the *HM113* mutation, gene expression levels of defense response genes [29] in the IR64 wild-type, *HM113* mutant, and knockout lines were measured by qRT-PCR. According to the results of qRT-PCR, we found that the expression level of the defense response genes in the knockout lines was significantly lower compared to the mutant *HM113*, indicating that after knocking out the mutant allele, the defense response cannot be activated as effectively as in the mutant, which led to a decrease in the disease resistance of the knockout lines to the bacterial blight pathogen (Figure 5D). These findings demonstrated that the gain-of-function mutation initiates the rice defense response and that *HM113* enhances rice resistance to *Xoo*. A dominant mutation in the mutant *HM113* can promote ROS accumulation, cell death, and an immune system response.

3. Discussion

The spotted-leaf mutants spontaneously develop necrotic lesions in plants, which impact production and provide a unique opportunity to study programmed cell death in plant defense mechanisms. Previously, we isolated a spotted-leaf mutant from the EMS-induced mutant library of indica rice IR64 and found that the gene *LOC_Os07g30510* may control the *HM113* spotted-leaf phenotype. Brown lesions were observed on the leaves three weeks after sowing in natural conditions, spreading to the sheaths during the heading stage. The mutant also exhibited enhanced disease resistance to several races of *Xoo* strains [29]. In the present study, to understand the function of *HM113* in rice, we generated a knockout line using CRISPR/Cas9 technology in the homologous mutant *HM113*-induced calli.

Despite its poor agronomic traits, the rice spotted-leaf mutant can achieve high yields by enhancing photosynthetic efficiency, disease resistance, and response to environmental stress [30]. In this study, as seen in some of the lesion mimic mutants, *LMMs* like *Lmm28* [31], *Spl24* [18], *Spl36* [26], and *Spl26* [32] exhibited reduced agronomic characteristics, including plant height, panicle length, and grain yield, in rice due to disruptions in ROS regulation and programmed cell death, resulting in lower agronomic traits in the plants.

Similarly, the mutation significantly decreased all the agronomic characteristics studied in the mutant *HM113* compared to the wild-type IR64, impacting yield and its components. However, we found that knocking out the *HM113* mutant gene in transgenic knockout lines increased the agronomic traits, and the chlorophyll content returned to levels similar to the wild type, which was comparable to other rice lesion mimic mutants, *Spl26* [17] and *Spl42* [33]. This finding suggests that the *HM113* mutation can directly influence lesion formation and indirectly affect agronomic performance, indicating that a dominant mutation can lead to reduced yield.

The development of lesions is due to the excessive buildup of H_2O_2, which is the primary factor responsible for it [5]. The degree of membrane cellular damage can be indirectly reflected by the accumulation of MDA, which is one of the most critical products of membrane lipid peroxidation [34]. Similarly, *HM113* had elevated levels of MDA and H_20_2, suggesting that the accumulation of cell death may have contributed to the development of necrotic lesions. The oxidation-reduction reaction within plant cells generates reactive oxygen species (ROS). A novel lesion mimic mutant *LIL1*, which also displayed spontaneous light-induced lesions independent of pathogen attack. These lesions were associated with reactive oxygen species ROS accumulation and programmed cell death (PCD), and with upregulated expression of defense-related genes, particularly PR1, PR10, POX22.3, and POC1 [9]. However, gene mutations disrupt the plant's internal environment in many spotted mutants, affecting the balance of ROS production [35–37]. The mutation in *HM113*, A847T (*LOC_Os07g30510*), disrupted the balance of reactive oxygen species

(ROS). Here, we observed a significant decrease in CAT and SOD levels, while the POD level was upregulated, leading to ROS accumulation. This caused the accumulation of H_20_2, which acts as a signaling molecule that activates programmed cell death (PCD) pathways in plants [5]. We further measured multiple metacaspase genes. The metacaspase gene encodes a cysteine-dependent protease that regulates cell death in plants. Our results indicated that the mutant *HM113* expressed a high level of these metacaspase genes (*OsMC2*–*OsMC7*) (Supplemental Data Figure S2), which are essential regulators of PCD in plants [38]. This observation revealed the biological connection between the mutation of *LOC_Os07g30510*, ROS, and PCD. Additionally, this further demonstrates how the mutation in *LOC_Os07g30510* leads to excessive ROS accumulation, resulting in increased metacaspase expression and the development of PCD, cell death, and this elucidates the conclusion that *LOC_Os07g30510* controls ROS signaling and PCD.

In this study, the initially observed spotted-leaf phenotype disappeared when we knocked out the gain-of-function gene *HM113*. These results suggest that a dominant mutation in *HM113* can induce cell death, resulting in the spotted-leaf phenotype. ROS signals play a crucial role in plant development; however, excessive amounts in rice *LMMs* lead to cell death and lesion formation [17]. For instance, some dominant genes, such as *Spl26*, exhibit increased ROS levels, enhanced disease resistance, and upregulated defense-related genes [17]. Similarly, *spl11* demonstrates an elevated defense response, and its mutation results in lesion formation. The protein U-box/ARM, encoded by this gene, regulates cell death [23]. Another gain-of-function gene, *Spl7*, enhances disease resistance and affects agronomic traits such as plant height and grain yield [22]. The *LIL1* mutant also displayed increased resistance to rice blast fungus (*Magnaporthe grisea*) [9]. Previous studies have shown that H_2O_2 is produced in response to various environmental and developmental stimuli, which are essential for regulating programmed cell death in plants [39]. In our studies, the mutant *HM113* exhibited higher levels of H_2O_2, resulting in severe cell death, which suggests that the toxic accumulation of H_2O_2 contributes to cell death in plants. However, after knocking out the mutated gene, the H_2O_2 levels returned to normal, and reactive oxygen species functioned similarly to those in the wild type. These findings imply that the H_2O_2 buildup in mutant *HM113*, or the mutation itself, may be caused by the mutant gene. The knockout line also exhibited the same level of MDA content as the wild type, which is induced by reactive oxygen species and membrane lipid peroxidation. Overall, *HM113* indicates that the dominant mutation in the *HM113* gene disrupts the intracellular reactive oxygen species scavenging system, leading to excessive H_2O_2 accumulation and ultimately triggering programmed cell death, resulting in spotted-leaf phenotypes [40]. Nevertheless, further research is needed to elucidate the specific molecular pathways through which the *HM113* mutation affects the reactive oxygen species scavenging system.

Studies have shown that the formation of lesions in spotted-leaf mutants often increases disease resistance [5,18,21,40]. Generally, excessive ROS buildup causes lesion formation, activating defense response genes and increasing resistance to disease pathogens [6,30]. In this study, the mutant allele *HM113* induced lesion formation, upregulated the expression of numerous defense response genes, and enhanced plant resistance to bacterial blight pathogens. Salicylic acid (SA) and jasmonic acid (JA) are crucial regulators of plant defense mechanisms, triggering conserved pathogen defense pathways in rice [41]. Lesions are also associated with a high level of H_20_2 accumulation. For example, *Spl40* and *OsSPL24* activation of the SA and JA signaling pathways is likely responsible for increased disease resistance [14,18], and the spotted-leaf mutant lm-Zh also showed enhanced resistance to these pathogens, with defense-related genes *OsPR1a*, *OsPR1b*, *OsPR10*, *OsPAL1*, *OsAOS2*, and *WRKY45* upregulated in lm-Zh leaves [34]. Here, the SA and JA metabolic

pathways were activated in the *HM113* mutant, as evidenced by the upregulated expression of genes essential to the JA and SA signaling pathways (Supplemental Data Figure S1). However, the knockout lines showed reduced resistance to *PXO347*, marked by lower gene expression in typical defense responses. The expression levels of these defense response genes returned to wild-type levels, with some even lower than the wild type, indicating a similar response to the pathogen. These results suggested that the mutated gene *HM113* positively regulates the immune response in rice, and the mutation impairs plant growth and development, activates a defense response, and enhances disease resistance. Still, the plant disease resistance mechanism is exceptionally complex.

A single nucleotide mutation, from A to T, was identified at position 847 in the first exon of the gene *LOC_Os07g30510*, which was initially cloned from rice cultivar 93-11 [9]. Although both genes are dominant, we were unable to observe the overexpression phenotype of *HM113* in the wild type, unlike Zhou et al., who achieved the phenotype by overexpressing *LIL1* in a wild-type background. Instead, we obtained the desired result only by knocking out the mutant allele using CRISPR/Cas9. *HM113* and *LIL1* are both lesion-mimic mutants that can help us understand the hypersensitive response (HR), such as cell death, which is controlled in rice; however, their genetic composition and mechanism may vary. *HM113* exhibited a single base substitution (A847T) and displayed a dominant gain-of-function phenotype, whereas *LIL1* has a (Val429 to Ile) mutation in the kinase domain, acting as a semi-dominant allele. When we knocked out the *HM113* gene using CRISPR/Cas9, the phenotype of the knockout lines was similar to that of the wild-type, resulting in the elimination of the mutant phenotype. In contrast, the overexpression of *LIL1* induced a *LIL1*-like lesion phenotype in Nipponbare and also displayed increased expression of defense-related genes, as well as enhanced resistance to the rice blast fungus and enhanced ROS accumulation. Both of these mutants, however, exhibited disease resistance and HR-like cell death. While the mutant *LIL1* exhibited a disruption of CRK activity, *HM113* showed a gain-of-function signaling, indicating that different mutation pathways can lead to similar immune responses.

The subcellular localization of HM113 was found in the cytosol, although a transmembrane domain (301-323aa) was expected, suggesting that HM113 may be involved in signal transduction or metabolic pathways. However, this needs further investigation, as GFP-based localization and transient overexpression can sometimes mislead in identifying protein targets [42,43]. Other strategies include co-localization with organelle markers, biochemical fractionation, the development of a transmembrane domain-deleted HM113 mutant, and the establishment of stable expression in rice. Immunolocalization or immunogold electron microscopy with a specific antibody can also help determine HM113 localization more accurately [44]. The protein kinase has become a crucial component in plants' signal transduction pathways in response to numerous environmental signals. The predicted cysteine-rich repeat kinase (CRK), encoded by *LOC_Os07g30510*, belongs to a sub-family that is distinguished by one or more extracellular DUF26 domains with a C-X8-C-X2-C motif. The stress-antifungal domain is the name given to the DUF26 domain [9]. CRKs feature an RLK domain, an extracellular domain for receiving signals, a single-pass transmembrane domain, and a conserved intracellular serine/threonine protein kinase domain responsible for signal transduction [45,46]. These dominant lesions mimic mutant genes, known for their gain-of-function characteristics, which are involved in essential processes such as initiating spontaneous cell death and enhancing plant immunity. By improving our understanding of plant defense mechanisms, stress signaling, and programmed cell death, these genes can promote the development of disease-resistant varieties. However, further investigation is necessary to elucidate the molecular pathways and their potential effects on sustainable rice cultivation. Ultimately, our findings indicated that the mutation in *HM113* causes the spotted-leaf phenotype and that *LOC_Os07g30510*

is the target gene of the *HM113* dominant mutant, as confirmed by the use of gene editing technology. After altering the upstream mutation site of the *HM113* gene, which caused a frameshift, the mutation phenotype of *HM113* was eliminated, and resistance to bacterial blight was subsequently lost: this indicates that it functions as a gain-of-function gene.

4. Materials and Methods

4.1. Plant Material and Growth Conditions

This study utilized the WT IR64 and *HM113* mutants from an EMS-induced mutant bank of IR64. The wild-type IR64 and mutant *HM113* were cultivated in the paddy field during the summer. In contrast, using standard water and fertilizer management, transgenic rice knockout lines were grown in a greenhouse at the China National Rice Research Institute (CNRRI) in Fuyang, Hangzhou, China.

4.2. Agronomic Traits Evaluation

After attaining full maturity, the main agronomic characteristics, including plant height, panicle length, 1000-grain weight, and seed-setting rate, were determined from three randomly selected plants of IR64, *HM113*, and the T1 knockout lines. The analysis used the mean of three replicates.

4.3. CRISPR/CAS9 Vector Construction

The knockout construct using CRISPR/CAS9 was created using a previously published method by [47], and the mutant calli were modified via Agrobacterium tumefaciens-mediated transformation. The procedure provided by [48] was used for all Agrobacterium tumefaciens transformations.

4.4. Physiological Parameters Measurement

During the tillering stage, the total chlorophyll of the knockout lines *HM113* and IR64 was extracted from the top two leaves of the plants. Likewise, the activities of ROS scavenging enzymes, such as catalase (CAT), superoxide dismutase (SOD), and peroxidase (POD), as well as enzymatic activities like H_2O_2, MDA, and soluble proteins, were evaluated using the corresponding test kit from the (Nanjing Jiancheng Bioengineering Institute, Nanjing, China) following the manufacturer's instructions. The mean value of three biological replicates was analyzed using Student's *t*-test, one-way ANOVA, and Duncan's test.

4.5. Disease Evaluation

At the maximum tillering stage, five fully expanded leaves from *HM113*, IR64, and the knockout lines were selected and inoculated with PX037 bacterial strains using the leaf clipping method described by [49]. The *Xanthomonas oryzae pv. oryzae* strain was grown on WF-P medium (20.0 g sucrose, 5.0 g peptone, 0.5 g calcium nitrate, 0.82 g sodium phosphate, 0.2 g ferrous sulfate, 17.0 g agar in 1 L distilled water). The strain was collected and diluted with sterile water for inoculation, after which the OD600 value was adjusted to 1.0. The length of the disease lesion was measured 14 days after inoculation using a transparent plastic ruler. The disease index (%) was calculated following the leaf-clip inoculation method described by [49], as (lesion length ÷ leaf length) × 100, where lesion length is the distance from the cut site to the visible end of the lesion, and leaf length is the total length of the inoculated leaf. The mean value of five independent leaves was used for analysis, and statistical significance was determined using Student's *t*-test.

4.6. Subcellular Localization

For Subcellular localization, the plasmid P1132 was used to create a GFP vector, which was then examined in rice protoplasts of HM113. The whole coding sequence (CDS) of

HM113 was amplified using a specific primer design. After the PCR was amplified, we purified the PCR product using a Gel extraction and clean-up kit. The PCR product was then merged with the PAN580 vector. The GFP signal was detected by viewing using a Zeiss LSM700 confocal microscope (Carl Zeiss, Oberkochen, Germany) 48 h after transformation.

4.7. RNA Extraction and Gene Expression Analysis

To assess the expression level, the total RNA was isolated from various tissues, including roots, shoots, stem, leaf, sheath, flag leaf, node, internode, node 1, internode 1, and panicle of wild-type IR64 using the NucleoZOL reagent (MACHEREY-NAGEL, Düren, Germany), according to the manufacturer's instructions at various developmental stages. The RNA samples were treated with the PrimeScript™ RT Master Mix (TaKaRa, Dalian, China), and 1 μg was used to synthesize first-strand cDNA for reverse transcription-PCR. Quantitative real-time PCR (qRT-PCR) was performed using PowerUp ™ SYBR ™ Green Master Mix (Thermo Fisher Scientific, Waltham, MA, USA) and a Thermal Cycler Dice Real Time System II (TaKaRa, Dalian, China) according to the manufacturer's instructions. As an internal control, rice ubiquitin (*LOC_Os03g13170*) was used. Three replicates were performed for each test and were analyzed using the $2^{-\Delta\Delta Ct}$ method.

4.8. Map-Based Cloning

The mutation was previously mapped to chromosome 7 by [29]. Using SSR markers and fine-mapping with segregating F_2 populations, the causal locus was confined to a ~308 kb interval on the long arm of chromosome 7, flanked by markers RM21605 and RM418 [29]. For further fine mapping, F_2 individual plants of the mutant type were obtained from the crosses *HM113*/Moroberekan, *HM113*/Nekken, and *HM113*/CPSLO17. The Gramene website (http://www.gramene.org/ accessed on 23 June 2024) was used to obtain simple sequence repeat (SSR) markers. After comparing the sequences between the japonica cultivar Nipponbare and the indica cultivar 9311 in the public database on the website (https://ensembl.gramene.org/index.html accessed on 23 June 2024), insertion/deletion (InDel) markers were designed using Primer3 input. Sangon Biotech Co., Ltd. (Shanghai, China) synthesized the primers. The detection and PCR reaction were carried out as previously described by [15]. The Supplementary Table S1 lists the primer sequences used for fine mapping.

5. Conclusions

Our study demonstrated that the mutant *HM113* was a gain-of-function gene that encoded a cysteine-rich receptor-like kinase (CRK) which disrupted reactive oxygen species (ROS) and led to excessive H_2O_2 accumulation, lesion formation, and programmed cell death. The CRISPR/Cas9 knockout of the mutant allele restored wild-type traits, confirming the gain-of-function nature. These results identify *LOC_Os07g30510* as a key regulator of ROS signalling and defense in rice, providing the basis for developing disease-resistant varieties with improved yield stability.

Supplementary Materials: The following supporting information can be downloaded at: https://www.mdpi.com/article/10.3390/plants14223429/s1, Figure S1: Defense-related gene expression levels in HM113 and IR64 involved in the JA and SA pathways; Figure S2: Analysis of cell death and ROS-associated parameters of IR64 and HM113 at the tillering stage; Figure S3: CRISPR/Cas9 sequence data and its target sequence (ACTGTCGGAGATCAACTCAACGG); Table S1: The primers used in the study are listed. Table S2: Comparison of SNPs and indels within the 308 kb candidate region on chromosome 7 for identifying *HM113*-specific mutations based on resequencing data.

Author Contributions: Data curation, R.K.S.; Formal analysis, R.K.S. and M.G.K.; Investigation, R.K.S. and M.G.K.; Methodology, R.K.S. and X.X.; Supervision, X.Z. and J.G.; Validation, X.Z. and J.G.;

Visualization, J.-L.W.; Writing—original draft, R.K.S. and J.-L.W. All authors have read and agreed to the published version of the manuscript.

Funding: This work was supported by the Zhejiang Provincial Natural Science Foundation of China under Grant No. LD25C130001.

Data Availability Statement: Data is contained within the article or Supplementary Materials.

Acknowledgments: We thank all the colleagues whose contributions have been cited in this article. We also acknowledge the China Scholarship Council for providing a fully covered PhD scholarship to Ringki Kuinamei Sanglou for conducting research at the China National Rice Research Institute.

Conflicts of Interest: The authors declare no conflicts of interest.

References

1. Khan, M.A.; Naeem, M.; Iqbal, M. Breeding Approaches for Bacterial Leaf Blight Resistance in Rice (*Oryza sativa* L.), Current Status and Future Directions. *Eur. J. Plant Pathol.* **2014**, *139*, 27–37. [CrossRef]
2. Fiyaz, R.A.; Dustakar, S.; Chaithanya, K.; Mounika, K.; Chiranjeevi, M.C.; Laha, G.S.; Viraktamath, B.C.; Rao, L.V.S.; Sundaram, R.M. Genetic Improvement of Rice for Bacterial Blight Resistance: Present Status and Future Prospects. *Rice Sci.* **2022**, *29*, 118–132. [CrossRef]
3. Korinsak, S.; Darwell, C.T.; Wanchana, S.; Praphaisal, L.; Korinsak, S.; Thunnom, B.; Patarapuwadol, S.; Toojinda, T. Identification of Bacterial Blight Resistance Loci in Rice (*Oryza sativa* L.) against Diverse *Xoo* Thai Strains by Genome-Wide Association Study. *Plants* **2021**, *10*, 518. [CrossRef] [PubMed]
4. Liu, W.; Liu, J.; Triplett, L.; Leach, J.E.; Wang, G.L. Novel Insights into Rice Innate Immunity against Bacterial and Fungal Pathogens. *Annu. Rev. Phytopathol.* **2014**, *52*, 213–241. [CrossRef] [PubMed]
5. Zhang, Y.; Liu, Q.; Zhang, Y.; Chen, Y.; Yu, N.; Cao, Y.; Zhan, X.; Cheng, S.; Cao, L. LMM24 Encodes Receptor-Like Cytoplasmic Kinase 109, Which Regulates Cell Death and Defense Responses in Rice. *Int. J. Mol. Sci.* **2019**, *20*, 3243. [CrossRef] [PubMed]
6. Wu, C.; Bordeos, A.; Madamba, M.R.S.; Baraoidan, M.; Ramos, M.; Wang, G.L.; Leung, H. Rice Lesion-Mimic Mutants with Enhanced Resistance to Diseases. *Mol. Genet. Genom.* **2008**, *279*, 605–619. [CrossRef]
7. Wu, J.; Yang, R.; Yang, Z.; Yao, S.; Zhao, S.; Wang, Y.; Li, P.; Song, X.; Jin, L.; Zhao, J. Lesion mimic mutants: Unveiling cell death and defense mechanisms in plants. *Int. J. Mol. Sci.* **2020**, *21*, 3121. [CrossRef]
8. Liu, Q.N.; Ning, Y.S.; Zhang, Y.X.; Yu, N.; Zhao, C.D.; Zhan, X.D.; Wu, W.X.; Chen, D.B.; Wei, X.J.; Wang, G.L.; et al. OsCUL3a Negatively Regulates Cell Death and Immunity by Degrading OsNPR1 in Rice. *Plant Cell* **2017**, *29*, 345–359. [CrossRef]
9. Zhou, Q.; Zhang, Z.; Liu, T.; Gao, B.; Xiong, X. Identification and Map-Based Cloning of the Light-Induced Lesion Mimic Mutant 1 (LIL1) Gene in Rice. *Front. Plant Sci.* **2017**, *8*, 2122. [CrossRef]
10. Ma, J.; Yang, S.; Wang, D.; Tang, K.; Feng, X.X.; Feng, X.Z. Genetic Mapping of a Light-Dependent Lesion Mimic Mutant Reveals the Function of Coproporphyrinogen III Oxidase Homolog in Soybean. *Front. Plant Sci.* **2020**, *11*, 557. [CrossRef]
11. Fekih, R.; Tamiru, M.; Kanzaki, H.; Abe, A.; Yoshida, K.; Kanzaki, E.; Saitoh, H.; Takagi, H.; Natsume, S.; Undan, J.R.; et al. The Rice (*Oryza sativa* L.) Lesion Mimic Resembling, Which Encodes an AAA-Type ATPase, Is Implicated in Defense Response. *Mol. Genet. Genom.* **2015**, *290*, 611–622. [CrossRef]
12. Du, D.; Liu, M.; Xing, Y.; Chen, X.; Zhang, Y.; Zhu, M.; Lu, X.; Zhang, Q.; Ling, Y.; Sang, X.; et al. Semi-Dominant Mutation in the Cysteine-Rich Receptor-Like Kinase Gene, ALS1, Conducts Constitutive Defence Response in Rice. *Plants* **2019**, *21*, 25–34. [CrossRef] [PubMed]
13. Yin, Z.; Chen, J.; Zeng, L.; Goh, M.; Leung, H.; Khush, G.S.; Wang, G.L. Characterizing Rice Lesion Mimic Mutants and Identifying a Mutant with Broad-Spectrum Resistance to Rice Blast and Bacterial Blight. *Mol. Plant Microbe Interact.* **2000**, *13*, 868–876. [CrossRef] [PubMed]
14. Sathe, A.P.; Su, X.; Chen, Z.; Chen, T.; Wei, X.; Tang, S.; Zhang, X.B.; Wu, J.L. Identification and Characterization of a Spotted-Leaf Mutant spl40 with Enhanced Bacterial Blight Resistance in Rice. *Rice* **2019**, *12*, 68. [CrossRef] [PubMed]
15. Feng, B.H.; Yang, Y.; Shi, Y.F.; Shen, H.C.; Wang, H.M.; Huang, Q.N.; Xu, X.; Lü, X.G.; Wu, J.L. Characterization and Genetic Analysis of a Novel Rice Spotted-Leaf Mutant HM47 with Broad-Spectrum Resistance to *Xanthomonas oryzae* pv. *oryzae*. *J. Integr. Plant Biol.* **2013**, *55*, 473–483. [CrossRef]
16. Shen, H.C.; Shi, Y.F.; Feng, B.H.; Wang, H.M.; Xu, X.; Huang, Q.; Lü, X.G.; Wu, J.L. Identification and Genetic Analysis of a Novel Rice Spotted-Leaf Mutant with Broad-Spectrum Resistance to *Xanthomonas oryzae* pv. *oryzae*. *J. Integr. Agric.* **2014**, *13*, 713–721. [CrossRef]
17. Shang, H.; Li, P.; Zhang, X.; Xu, X.; Gong, J.; Yang, S.; He, Y.; Wu, J.L. The Gain-of-Function Mutation, OsSpl26, Positively Regulates Plant Immunity in Rice. *Int. J. Mol. Sci.* **2022**, *23*, 14168. [CrossRef]

18. Chen, Z.; Chen, T.; Sathe, A.P.; He, Y.; Zhang, X.B.; Wu, J.L. Identification of a Novel Semi-Dominant Spotted-Leaf Mutant with Enhanced Resistance to *Xanthomonas oryzae* pv. oryzae in Rice. *Int. J. Mol. Sci.* **2018**, *19*, 3766. [CrossRef]
19. Lorrain, S.; Lin, B.; Auriac, M.C.; Kroj, T.; Saindrenan, P.; Nicole, M.; Balagué, C.; Roby, D. VASCULAR ASSOCIATED DEATH1, a Novel GRAM Domain–Containing Protein, Is a Regulator of Cell Death and Defense Responses in Vascular Tissues. *Plant Cell* **2004**, *16*, 2217–2232. [CrossRef]
20. Chen, X.; Hao, L.; Pan, J.; Zheng, X.; Jiang, G.; Jin, Y.; Gu, Z.; Qian, Q.; Zhai, W.; Ma, B. *SPL5*, a Cell Death and Defense-Related Gene, Encodes a Putative Splicing Factor 3b Subunit 3 (SF3b3) in Rice. *Mol. Breed.* **2012**, *30*, 939–949. [CrossRef]
21. Ma, J.; Wang, Y.; Ma, X.; Meng, L.; Jing, R.; Wang, F.; Wang, S.; Cheng, Z.; Zhang, X.; Jiang, L.; et al. Disruption of Gene SPL35, Encoding a Novel CUE Domain-Containing Protein, Leads to Cell Death and Enhanced Disease Response in Rice. *Plant Biotechnol. J.* **2019**, *17*, 1679–1693. [CrossRef]
22. Yamanouchi, U.; Yano, M.; Lin, H.; Ashikari, M.; Yamada, K. A Rice Spotted Leaf Gene, Spl7, Encodes a Heat Stress Transcription Factor Protein. *Proc. Natl. Acad. Sci. USA* **2002**, *99*, 7530–7535. [CrossRef] [PubMed]
23. Zeng, L.R.; Qu, S.; Bordeos, A.; Yang, C.; Baraoidan, M.; Yan, H.; Xie, Q.; Nahm, B.H.; Leung, H.; Wang, G.L. Spotted Leaf11, a Negative Regulator of Plant Cell Death and Defense, Encodes a U-Box/Armadillo Repeat Protein Endowed with E3 Ubiquitin Ligase Activity. *Plant Cell* **2004**, *16*, 2795–2808. [CrossRef] [PubMed]
24. Quezada, E.H.; García, G.X.; Arthikala, M.K.; Melappa, G.; Lara, M.; Nanjareddy, K. Cysteine-Rich Receptor-Like Kinase Gene Family Identification in the Phaseolus Genome and Comparative Analysis of Their Expression Profiles Specific to Mycorrhizal and Rhizobial Symbiosis. *Genes* **2019**, *10*, 59. [CrossRef] [PubMed]
25. Andaya, C.B.; Ronald, P.C. A Catalytically Impaired Mutant of the Rice Xa21 Receptor Kinase Confers Partial Resistance to *Xanthomonas oryzae* pv. *oryzae*. *Physiol. Mol. Plant Pathol.* **2003**, *62*, 203–208. [CrossRef]
26. Rao, Y.; Jiao, R.; Wang, S.; Wu, X.; Ye, H.; Pan, C.; Li, S.; Xu, D.; Zhou, W.; Dai, G.; et al. SPL36 Encodes a Receptor-Like Protein Kinase That Regulates Programmed Cell Death and Defense Responses in Rice. *Rice* **2021**, *14*, 34. [CrossRef]
27. Hong, S.W.; Jon, J.H.; Kwak, J.M.; Nam, H.G. Identification of a Receptor-Like Protein Kinase Gene Rapidly Induced by Abscisic Acid, Dehydration, High Salt, and Cold Treatment in Arabidopsis thaliana. *Plant Physiol.* **1997**, *113*, 1203–1212. [CrossRef]
28. Zhao, Y.; Wu, G.; Shi, H.; Tang, D. Receptor-Like Kinase 902 Associates with and Phosphorylates Brassinosteroid-Signaling Kinase 1 to Regulate Plant Immunity. *Mol. Plant* **2019**, *12*, 59–70. [CrossRef]
29. Guo, D.; Shi, Y.F.; Wang, H.M.; Zhang, X.B.; Song, L.X.; Xu, X.; He, Y.; Guo, L.; Wu, J.L. Characterization and Gene Fine Mapping of a Rice Dominant *Spotted-Leaf* Mutant. *Acta Agron. Sin.* **2016**, *42*, 966–975. [CrossRef]
30. Kang, S.G.; Lee, K.E.; Singh, M.; Kumar, P.; Matin, M.N. Rice Lesion Mimic Mutants (*Lmm*): The Current Understanding of Genetic Mutations in the Failure of ROS Scavenging during Lesion Formation. *Plants* **2021**, *10*, 1598. [CrossRef]
31. Qi, P.; Tian, M.; Yang, S.; Shui, Y.; Li, P.; Yin, W.; Li, Q.; Bai, D.; Huang, Q.; Li, Y.; et al. Phenotypic Characterization and Gene Mapping of the Lesion Mimic Mutant *lmm28* in Rice. *Agronomy* **2024**, *14*, 3048. [CrossRef]
32. Chen, T.; Chen, Z.; Sathe, A.P.; Zhang, Z.; Li, L.; Shang, H.; Tang, S.; Zhang, X.; Wu, J. Characterization of a Novel Gain-of-Function *Spotted-Leaf* Mutant with Enhanced Disease Resistance in Rice. *Rice Sci.* **2019**, *26*, 372–383. [CrossRef]
33. Li, P.; Shang, H.; Xu, X.; Gong, J.; Wu, J.L.; Zhang, X. A Novel Single Base Mutation in *OsSPL42* Leads to the Formation of Leaf Lesions in Rice. *Int. J. Mol. Sci.* **2024**, *25*, 11871. [CrossRef] [PubMed]
34. Sun, L.; Wang, Y.; Liu, L.L.; Wang, C.; Gan, T.; Zhang, Z.; Wang, Y.; Wang, D.; Niu, M.; Long, W.; et al. Isolation and Characterization of a *Spotted Leaf 32* Mutant with Early Leaf Senescence and Enhanced Defense Response in Rice. *Sci. Rep.* **2017**, *7*, 41846. [CrossRef]
35. Asada, K. Production and Scavenging of Reactive Oxygen Species in Chloroplasts and Their Functions. *Plant Physiol.* **2006**, *141*, 391–396. [CrossRef]
36. Kawano, T. Roles of the Reactive Oxygen Species-Generating Peroxidase Reactions in Plant Defense and Growth Induction. *Plant Cell Rep.* **2003**, *21*, 829–837. [CrossRef]
37. Whitaker, C.; Beckett, R.P.; Minibayeva, F.V.; Kranner, I. Production of Reactive Oxygen Species in Excised, Desiccated and Cryopreserved Explants of *Trichilia dregeana* Sond. *S. Afr. J. Bot.* **2010**, *76*, 112–118. [CrossRef]
38. Bansal, R.; Rana, N.; Singh, A.; Dhiman, P.; Mandlik, R.; Sonah, H.; Deshmukh, R.; Sharma, T.R. Evolutionary Understanding of Metacaspase Genes in Cultivated and Wild *Oryza* Species and Its Role in Disease Resistance Mechanism in Rice. *Genes* **2020**, *11*, 1412. [CrossRef]
39. Apel, K.; Hirt, H. Reactive Oxygen Species: Metabolism, Oxidative Stress, and Signal Transduction. *Annu. Rev. Plant Biol.* **2004**, *55*, 373–399. [CrossRef]
40. Matin, M.N.; Pandeya, D.; Baek, K.-H.; Lee, D.-S.; Lee, J.-H.; Kang, H.-D.; Kang, S.-G. Phenotypic and Genotypic Analysis of Rice Lesion Mimic Mutants. *Plant Pathol. J.* **2010**, *26*, 159–168. [CrossRef]
41. Sharma, A.; Gupta, R.; Mehta, P. Regulation of Plant Defense Mechanisms by Salicylic Acid and Jasmonic Acid in Rice. *Plant Sci. J.* **2023**, *15*, 123–130.
42. Snapp, E.L. Design and use of fluorescent fusion proteins in cell biology. *Curr. Protoc. Cell Biol.* **2005**, *27*, 21.4.1–21.4.13. [CrossRef]

43. Bhat, R.A.; Lahaye, T.; Panstruga, R. The visible touch: In planta visualization of protein–protein interactions by fluorophore-based methods. *Plant Methods* **2006**, *2*, 12. [CrossRef] [PubMed]
44. Von Heijne, G. Membrane-protein topology. *Nat. Rev. Mol. Cell Biol.* **2006**, *7*, 909–918. [CrossRef] [PubMed]
45. Chen, Z. A Superfamily of Proteins with Novel Cysteine-Rich Repeats. *Plant Physiol.* **2001**, *126*, 473–476. [CrossRef] [PubMed]
46. Chern, M.; Xu, Q.; Bart, R.S.; Bai, W.; Ruan, D.; Sze-To, W.H.; Canlas, P.E.; Jain, R.; Chen, X.; Ronald, P.C. A Genetic Screen Identifies a Requirement for Cysteine-Rich Receptor-Like Kinases in Rice NH1 (*OsNPR1*)-Mediated Immunity. *PLoS Genet.* **2016**, *12*, e1006049. [CrossRef]
47. Ma, X.; Zhang, Q.; Zhu, Q.; Liu, W.; Chen, Y.; Qiu, R.; Wang, B.; Yang, Z.; Li, H.; Lin, Y.; et al. A Robust CRISPR/Cas9 System for Convenient, High-Efficiency Multiplex Genome Editing in Monocot and Dicot Plants. *Mol. Plant* **2015**, *8*, 1274–1284. [CrossRef]
48. Toki, S.; Hara, N.; Ono, K.; Onodera, H.; Tagiri, A.; Oka, S.; Tanaka, H. Early Infection of Scutellum Tissue with *Agrobacterium* Allows High-Speed Transformation of Rice. *Plant J.* **2006**, *47*, 969–976. [CrossRef]
49. Kauffman, H.E. An Improved Technique for Evaluating Resistance of Rice Varieties to *Xanthomonas oryzae*. *Plant Dis. Rep.* **1973**, *57*, 537–541.

plants

MDPI

Article

The Bitter Gourd Transcription Factor *McNAC087* Confers Cold Resistance in Transgenic Arabidopsis

Xuetong Yang [1,2,3], Kai Wang [1,2,3], Feng Guan [1,2,3], Bo Shi [1,2,3], Yuanyuan Xie [1,2,3], Chang Du [4], Tong Tang [5], Zheng Yang [6], Shijie Ma [7] and Xinjian Wan [1,2,3,*]

1 Institute of Vegetables and Flowers, Jiangxi Academy of Agricultural Sciences, Nanchang 330200, China; yangxuetong@jxaas.cn (X.Y.); wangkai@jxaas.cn (K.W.); guanfeng_0813@163.com (F.G.); shibo_jiangxi@163.com (B.S.); m18073933758@163.com (Y.X.)
2 Jiangxi Key Laboratory of Horticultural Crops (Fruit, Vegetable & Tea) Breeding, Jiangxi Academy of Agricultural Sciences, Nanchang 330200, China
3 Jiangxi Engineering Research Center of Vegetable Molecular Breeding, Jiangxi Academy of Agricultural Sciences, Nanchang 330200, China
4 Guangdong Provincial Key Laboratory of Biotechnology for Plant Development, School of Life Science, South China Normal University, Guangzhou 510631, China; duchang@m.scnu.edu.cn
5 Department of Computer Science and Information Technologies, Elviña Campus, University of A Coruña, 15001 A Coruña, Spain; tongtang@scu.edu.cn
6 Zhengzhou Research Base, State Key Laboratory of Cotton Bio-Breeding and Integrated Utilization, School of Agricultural Sciences, Zhengzhou University, Zhengzhou 450001, China; yangz@zzu.edu.cn
7 Crop Research Institute, Anhui Academy of Agricultural Sciences, Hefei 230031, China; mashijie@nwafu.edu.cn
* Correspondence: xinjian71@163.com

Abstract

Low-temperature stress severely restricts the growth, development, and yield of bitter gourd (*Momordica charantia* L.), a warm-loving crop with inherent low cold tolerance. *NAC* transcription factors (TFs) serve as crucial regulators in plant responses to abiotic stresses like cold, while their roles in coping with cold stress in bitter gourd remain unclear. This study identified cold-responsive genes in bitter gourd and characterized the candidate *NAC* TF *McNAC087* through transcriptome analysis. Transcriptome sequencing of cold-tolerant (R) and cold-sensitive (S) bitter gourd inbred lines under 5 °C stress (0 h, 6 h, 12 h, 24 h) revealed 1157 co-expressed differentially expressed genes (DEGs), enriched via Kyoto Encyclopedia of Genes and Genomes (KEGG) analysis in cold tolerance-related pathways (signal transduction, carbohydrate/amino acid metabolism). RT-qPCR showed higher *McNAC087* expression in R than S under cold stress, and subcellular localization confirmed it as a nucleus-localized protein. *McNAC087* overexpression in Arabidopsis enhanced cold tolerance after sequential stress (−14 °C for 1.5 h, 4 °C for 16 h, and 22 °C recovery for 2 days), with less damage compared to wildtype (WT). Physiologically, overexpressing lines had higher proline, elevated superoxide dismutase/peroxidase/catalase (SOD/POD/CAT) activities, lower malondialdehyde/hydrogen peroxide/superoxide anion (MDA/H_2O_2/O_2^-) accumulation under cold stress, and upregulated *ICE-CBF-COR* pathway marker genes (*CBF1*, *DREB2A*, *RD29A*, *COR47*). In conclusion, *McNAC087* enhances Arabidopsis cold tolerance by regulating physiology and activating cold-responsive genes, providing insights for bitter gourd cold tolerance mechanisms and crop breeding.

Keywords: bitter gourd; *McNAC087*; overexpression; cold stress; physiological regulation

1. Introduction

Temperature is a crucial factor in accurately assessing the geographical distribution of plants, functioning as the pre-eminent limiting factor [1]. Low temperatures pose a significant challenge, hindering plant growth, delaying development, and compromising yield potential. When exposed to low-temperature stress, plants experience alterations in their molecular regulatory networks, enzyme activities, various osmoregulatory substances, and cell structures [2]. At the stage of seed germination, low temperature inhibits enzyme activity in the seed, hinders water absorption, reduces the germination rate and prolongs the germination time [3]. At the seedling stage, low temperature leads to slow-growing, abnormal leaf development, and the inhibition of photosynthesis. At the flowering and fruiting stages, low temperature affects flower bud differentiation, pollen viability, pollination and fertilization, resulting in flower and fruit drop, poor fruit development, and a significant decline in yield and quality. Under conditions of low-temperature stress, younger tissues and organs sustain more severe damage. Moreover, the sensitivity of plants to low temperatures is heightened during the reproductive stage in comparison to the vegetative stage [4].

The transcriptional regulation of genes represents one of the most critical mechanisms that underlies plant resistance to harmful environments [5]. The transcription factor family exerts an essential role in coping with cold stress by modulating the levels of cold-related genes through either activation or repression processes in plants. The *CBF* transcription factor (*CBF*) family has been intensively discussed as a master regulator governing the response to cold stress in the plant kingdom. The *ICE-CBF-COR* signaling pathway is the most extensively investigated molecular regulatory mechanism governing plant responses to low-temperature conditions [6]. When subjected to low temperatures that do not cause freezing, plants can swiftly induce and upregulate the expression of *CBF* genes within 15 min, which is subsequently followed by the triggering of downstream cold-responsive (*COR*) genes. At present, CBF homologous genes have been characterized in a range of crops, encompassing rice, tomato, maize, wheat, and barley. Most of these genes are induced by low temperatures and regulate plant tolerance to low temperatures [1,7]. In addition, improved cold tolerance can be achieved through *CBF*-independent pathway, for example, the *SD6* (encoding a *bHLH* transcription factor)-*ICE2* molecular module senses ambient temperature to regulate seed dormancy, under normal temperature, the *SD6* gene is highly expressed, and *ICE2* gene expression is significantly inhibited to promote seed germination. At low temperature, the expression of the *SD6* gene was significantly inhibited, and the expression of the *ICE2* gene was upregulated so that the seeds remained dormant [8]. *NAC* TF serve as pivotal plant-specific regulators in plant development, stress responses, and metabolic pathways, exerting multifaceted functions across diverse biological processes throughout the entire plant life cycle [9,10]. *NACs* modulate cell differentiation, organogenesis, and developmental phase transitions via the regulation of specific target gene expression [11]. *NACs* participate in mediating plant tolerance to cold stress [3]. For instance, *SlNAC3*, which belongs to the NAC transcription factor family in tomato, plays a role in promoting the early adaptive response under 4 °C low-temperature stress [12]. *OsNAC5* exerts a positive regulatory effect on cold tolerance by maintaining the balance between ABA and ROS signaling [13]. By engaging in the *CBF–COR* pathway, *GmNAC20* contributes to the regulation of cold tolerance in soybean [14]. *MaICE1* targets the *MaNAC1* gene in banana, and the *MaNAC1* protein engages in interactions with *MaCBF1* to regulate the ability of banana fruit to tolerate cold stress [15].

Bitter gourd has distributed large-scale cultivation around the world except for cold regions. Owing to their unique bitter taste characteristics and diverse application values, bitter gourd plays an irreplaceable role in numerous fields, including food processing,

pharmaceutical research and development, and agricultural production. Bitter gourd is a warm-loving crop with heat tolerance, yet its cold tolerance is extremely limited. As a crucial environmental limiting factor, low-temperature stress severely hinders the growth process, physiological metabolism, and morphogenesis of bitter gourd especially in the early spring and late autumn. In-depth analysis of the key genes involved in low-temperature tolerance and the molecular regulatory mechanism of bitter gourd can lay a solid theoretical foundation, provide a technical path for genetic improvement, and significantly accelerate the breeding process of new varieties of bitter gourd with low-temperature tolerance to obtain excellent varieties that can adapt to complex environments. However, there is no available information on how *NAC* transcription factors regulate plant resistance to low temperature.

The focus of this study was to determine the key genes that respond to low-temperature stress in bitter gourd. According to the transcriptome data analysis of cold-tolerant and cold-sensitive materials subjected to low-temperature stress for 0 h, 6 h, 12 h and 24 h, gene expression measurements and gene overexpression verification revealed that the expression of the transcription factor *McNAC087* in bitter gourd was closely related to how plants respond to low-temperature stress, which offers a theoretical basis for the genetic improvement of bitter gourd.

2. Results

2.1. Morphological Responses of Momordica charantia L. Under Low-Temperature Stress

Under low-temperature stress, bitter gourd seedling growth was significantly inhibited. Cold-tolerant inbred line (R) and cold-sensitive inbred line (S) seedlings underwent 5 °C exposure for 0, 6, 12, and 24 h, and different low-temperature response reactions were observed as the low-temperature treatment time increased. The most significant differences in seedling morphology were observed at 24 h of low-temperature treatment, with S seedlings exhibiting typical damage characteristics, including leaf wilting, drooping, curling, and dehydration. However, R is not sensitive to low-temperature treatment, and there were no obvious changes in leaf morphology (Figure 1).

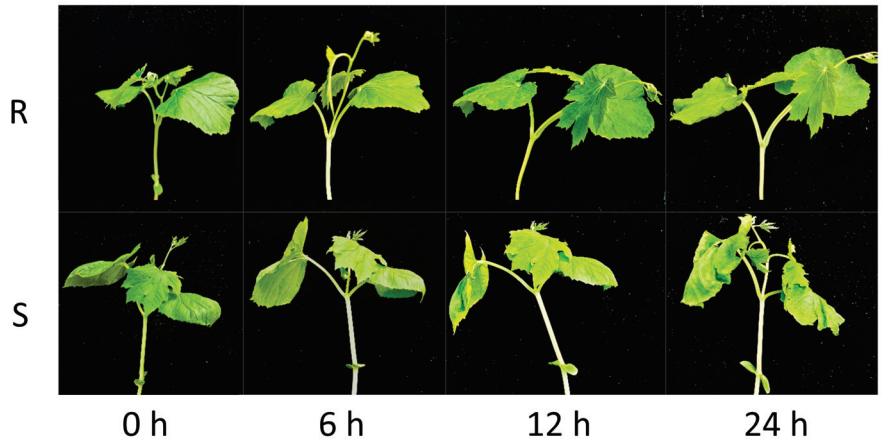

Figure 1. Phenotypic observations of cold-tolerant (R) and cold-sensitive (S) bitter gourd under cold exposure treatment for 0, 6, 12, and 24 h. Seedlings at the four-leaf and one-heart stage were treated with 5 °C low temperature.

2.2. RNA Sequencing

To identify and characterize the transcriptome of the bitter gourd seedlings under cold stress, we sequenced the R and S leaves treated at 5 °C for 0, 6, 12, and 24 h. Each treatment and each stage were repeated in triplicate, resulting in the construction of 24 cDNA libraries. The total number of raw reads ranged from 37,975,582 to 48,058,064, and the percentage

of clean reads was greater than 99.51%. The percentage of clean reads with a Q30-based percentage (Phred value > 30) was greater than 96.71%, with a GC content of 46.37–54.02% (Table 1). The results indicated that the quality of the transcriptome sequencing data was highly reliable and that in-depth analysis could be conducted.

Table 1. Basic statistics of transcriptome sequencing data for bitter gourd seedling samples. Seedlings at the four-leaf and one-heart stage were treated with 5 °C low temperature. Leaf samples were collected from the cold-tolerant line (R) and cold-sensitive line (S) at 4 time points: 0 h (before cold stress, control), 6 h, 12 h, and 24 h post treatment, with 3 biological replicates per time point. Sample naming: R-derived samples = RM (0 h), RL1 (6 h), RL2 (12 h), RL3 (24 h); S-derived samples = SM (0 h), SL1 (6 h), SL2 (12 h), SL3 (24 h); "-1/-2/-3" indicate biological replicates. All base quantities are in bp.

Sample	Total Raw Reads	Total Clean Reads (%)	Total Clean Bases	Clean Reads Q30 (%)	GC Content (%)
RM-1	40,018,692	39,893,848 (99.69%)	5,892,853,624	5,735,816,993 (97.34%)	2,721,951,784 (46.19%)
RM-2	42,835,104	42,663,970 (99.60%)	6,294,026,844	6,122,549,196 (97.28%)	2,904,925,895 (46.15%)
RM-3	39,476,622	39,366,156 (99.72%)	5,810,570,919	5,671,334,032 (97.60%)	2,686,534,839 (46.24%)
RL1-1	40,893,740	40,743,182 (99.63%)	6,022,858,080	5,824,480,038 (96.71%)	2,745,037,914 (45.58%)
RL1-2	48,058,064	47,896,750 (99.66%)	7,073,938,218	6,849,945,058 (96.83%)	3,226,081,644 (45.61%)
RL1-3	39,433,994	39,265,546 (99.57%)	5,830,950,164	5,654,256,539 (96.97%)	2,681,993,642 (46.00%)
RL2-1	37,975,582	37,825,924 (99.61%)	5,597,834,381	5,444,217,924 (97.26%)	2,546,110,109 (45.48%)
RL2-2	43,237,410	43,027,214 (99.51%)	6,367,927,150	6,162,603,972 (96.78%)	2,882,536,185 (45.27%)
RL2-3	42,298,414	42,158,916 (99.67%)	6,270,987,686	6,109,302,688 (97.42%)	2,862,340,959 (45.64%)
RL3-1	41,215,956	41,046,658 (99.59%)	6,039,075,711	5,864,527,892 (97.11%)	2,803,041,196 (46.42%)
RL3-2	36,423,022	36,315,076 (99.70%)	5,346,884,016	5,211,124,486 (97.46%)	2,483,918,080 (46.46%)
RL3-3	45,698,842	45,556,060 (99.69%)	6,708,210,242	6,539,270,593 (97.48%)	3,116,849,459 (46.46%)
SM-1	41,163,672	41,035,338 (99.69%)	6,066,036,632	5,911,629,664 (97.45%)	2,810,644,738 (46.33%)
SM-2	40,644,408	40,503,714 (99.65%)	5,989,237,980	5,836,799,898 (97.45%)	2,777,363,713 (46.37%)
SM-3	38,901,736	38,791,550 (99.72%)	5,733,378,673	5,595,459,985 (97.59%)	2,656,090,816 (46.33%)
SL1-1	44,059,370	43,907,724 (99.66%)	6,508,407,863	6,302,246,629 (96.83%)	2,931,273,138 (45.04%)
SL1-2	43,099,768	42,949,204 (99.65%)	6,353,584,714	6,184,131,820 (97.33%)	2,907,200,197 (45.76%)
SL1-3	39,855,366	39,681,250 (99.56%)	5,881,590,044	5,693,476,583 (96.80%)	2,666,575,152 (45.34%)
SL2-1	42,366,614	42,212,362 (99.64%)	6,236,239,419	6,076,107,478 (97.43%)	2,846,297,902 (45.64%)
SL2-2	44,085,818	43,874,656 (99.52%)	6,486,341,791	6,278,963,701 (96.80%)	2,938,327,609 (45.30%)
SL2-3	43,235,248	43,092,714 (99.67%)	6,380,155,079	6,217,591,803 (97.45%)	2,915,883,323 (45.70%)
SL3-1	45,315,638	45,165,830 (99.67%)	6,686,262,990	6,520,401,992 (97.52%)	3,074,245,023 (45.98%)
SL3-2	38,973,144	38,818,152 (99.60%)	5,753,672,630	5,581,677,280 (97.01%)	2,647,618,786 (46.02%)
SL3-3	40,610,978	40,486,400 (99.69%)	5,970,974,264	5,823,732,363 (97.53%)	2,746,837,661 (46.00%)

2.3. Sample Analysis

The Pearson correlation coefficient (r) was utilized to represent the correlation between gene expression levels among samples. The closer r is to 1, the more similar the expression patterns are between samples. As shown in Figure 2a, the three replicate samples strongly correlated, with r values close to 1. The results of principal component analysis (PCA) revealed that the variance explained by the two principal components was 53.5% and 22%. The distribution of sample scores on these two principal components was clearly separated, indicating that there were distinguishable differences between sample populations according to PCA (Figure 2b). The violin plot compares the differences in the distributions of the different groups and shows the distributions of the R and S samples with different stress durations (Figure 2c).

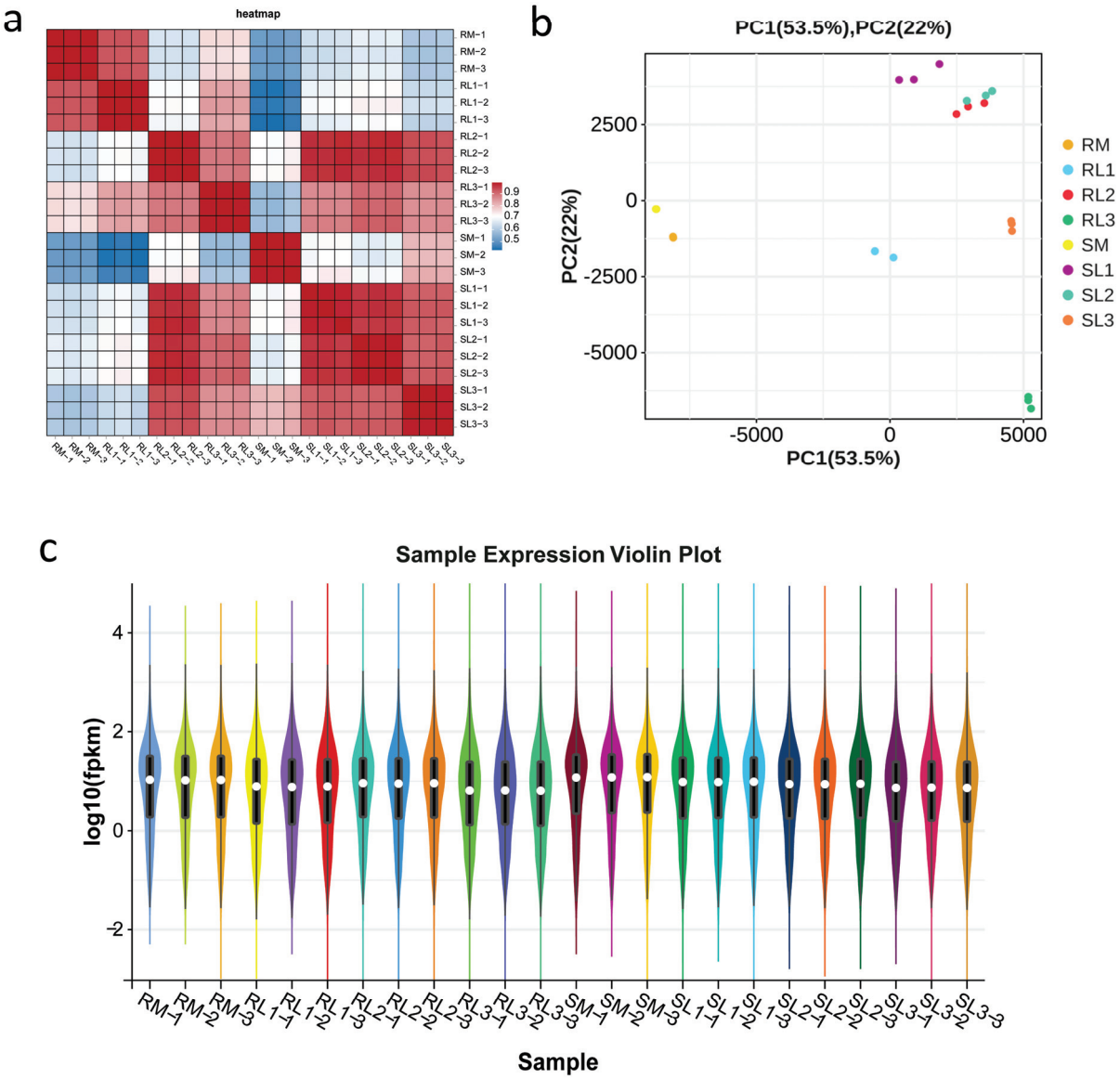

Figure 2. Transcriptome analysis of bitter gourd cultivars under cold stress. (**a**) Pearson's correlation coefficient of bitter gourd under cold stress. (**b**) PCA of the transcriptome data of bitter gourd under cold stress. (**c**) Violin plot of bitter gourd expression.

2.4. Statistical Analysis of the Differentially Expressed Gene (DEG)

DEGs were identified according to the screening criteria FDR < 0.05 and |log2 (fold change)| > 2, and the statistics of the number of DEGs under different cultivars (R and S) and low-temperature treatment times are shown in Figure 3a. There were 4037 (1246 upregulated, 2791 downregulated), 6580 (2824 upregulated, 3756 downregulated), 7689 (2376 upregulated, 5313 downregulated), 5019 (1455 upregulated, 3564 downregulated), 7134 (2143 upregulated, 4991 downregulated), and 9584 (2643 upregulated, 6941 downregulated) DEGs in RM-vs-RL1, RM-vs-RL2, RM-vs-RL3, SM-vs-SL1, SM-vs-SL2, and SM-vs-SL3, respectively, as well as 104, 1108, 745, 141, 280, and 1266 specific genes, respectively. The results indicated that there were more downregulated genes in each comparison group under cold stress. Comparative analysis of six sets of DEGs among the two bitter gourd cultivars yielded 1157 co-expressed genes (Figure 3b).

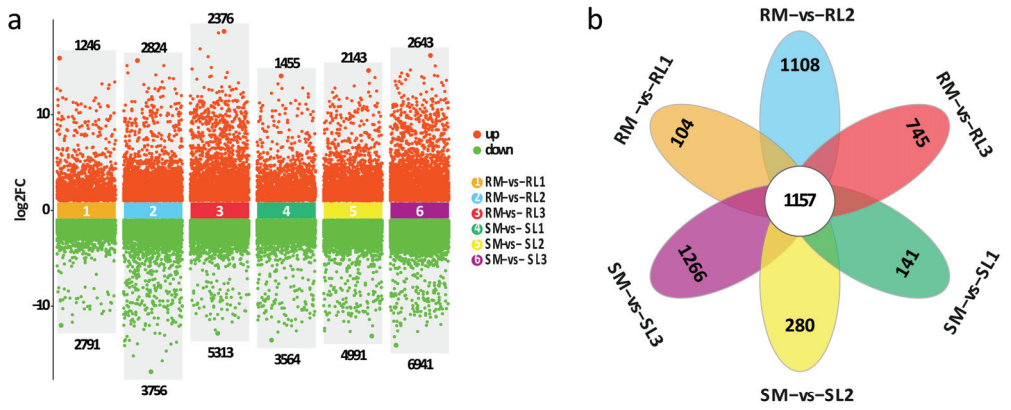

Figure 3. Identification of DEGs among two bitter gourd cultivars under cold stress. (**a**) Volcano plots of DEGs among different comparison groups. (**b**) Venn diagram of DEGs among different comparison groups.

2.5. GO/KEGG Annotation of Cold Stress Genes and Identification of Candidate Gene McNAC087

Gene Ontology (GO) term analysis of the DEGs identified in the six comparison groups revealed their ability to improve the resistance of bitter gourd to low temperatures. The results revealed that 20 significantly enriched terms were annotated and that the DEGs were functionally categorized into cellular component and molecular function terms, but no enriched DEGs were associated with biological process terms. DEGs in the CC category were enriched in nucleotide-excision repair complex (GO:0000109), DNA repair complex (GO:1990391), nuclear ubiquitin ligase complex (GO:0000152), anaphase-promoting complex (GO:0005680), cullin-RING ubiquitin ligase complex (GO:0031461), ubiquitin ligase complex (GO:0000151), transferase complex (GO:1990234), and external encapsulating structure (GO:0030312) terms. The molecular function category included 12 terms, with GO:0016740 (transferase activity), GO:0140096 (catalytic activity), GO:0140110 (protein transcription regulator activity), ubiquitin-like protein transferase activity (GO:0019787), DNA-binding transcription factor activity (GO:0003700), and ubiquitin-protein transferase activity (GO:0004842) being the top 6 terms (Figure 4a).

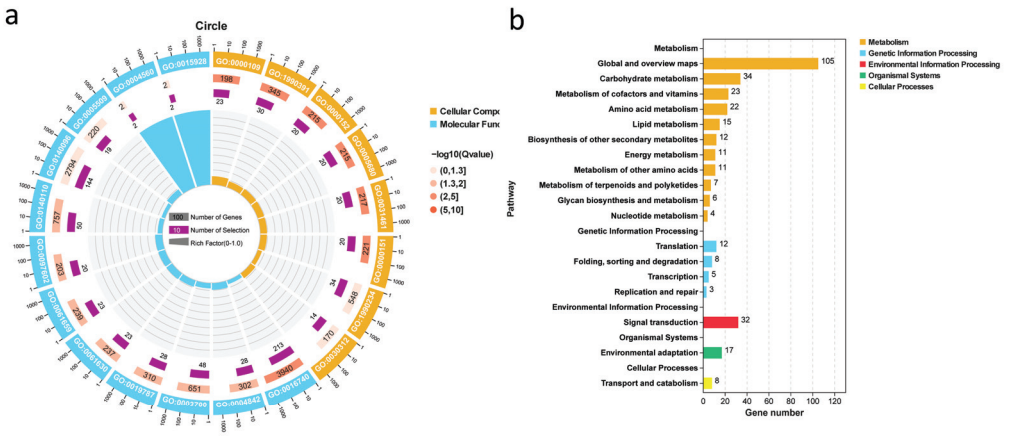

Figure 4. Functional enrichment of DEGs. (**a**) Enriched GO terms in 1157 co-expressed genes. (**b**) Enriched KEGG pathways associated with the 1157 co-expressed genes. The GO term annotations are presented in Table S1.

The main biochemical metabolic pathways and signal transduction pathways associated with the DEGs were identified by significantly enriched metabolic pathways, so we also performed KEGG pathway analysis on the DEGs related to the cold stress response. The top 20 KEGG pathways were divided into five main categories: metabolism, genetic

information processing, environmental information processing, organismal systems and cellular processes. Among these pathways, carbohydrate metabolism, signal transduction, amino acid metabolism, and lipid metabolism were closely related to the cold tolerance of bitter gourd (Figure 4b). To date, many *NAC* TFs have been demonstrated to be involved in plant stress responses through direct or indirect regulation of downstream stress-related genes, interactions with other proteins, metabolic regulation, and signal transduction of some hormones [3]. *NAC* TFs play diverse regulatory roles in plant stress responses, and they may regulate the pathways involved in the cold tolerance of bitter gourd. Therefore, we chose *McNAC087* in our co-expressed gene set for functional verification, and experiments were conducted to explore the correlation between *McNAC087* and differential pathways in a follow-up study.

2.6. Confirmation of DEGs by RT-qPCR

Nine genes related to cold and environmental stress tolerance were selected, including *NAC087*, *MAPKKK20*, *PMAT1*, *PAL*, *WRKY50*, *CBP60D*, *ABCG10*, *FAD4*, and *RIPK*, from the set of 1157 DEGs. The expression levels of *NAC087*, *PMAT1*, and *RIPK* in R were consistently greater than those in across all cold stress treatment time points (0 h, 6 h, 12 h, and 24 h). The expression levels of *MAPKKK20*, *PAL*, and *WRKY50* were greater in R than in S, especially at 6 h and 24 h of cold stress. In contrast, the expression levels of *ABCG10*, *FAD4*, and *RIPK* peaked in SM after 24 h of cold treatment (Figure 5). The results also confirmed that the general trends of the RNA-seq and RT-qPCR results were consistent.

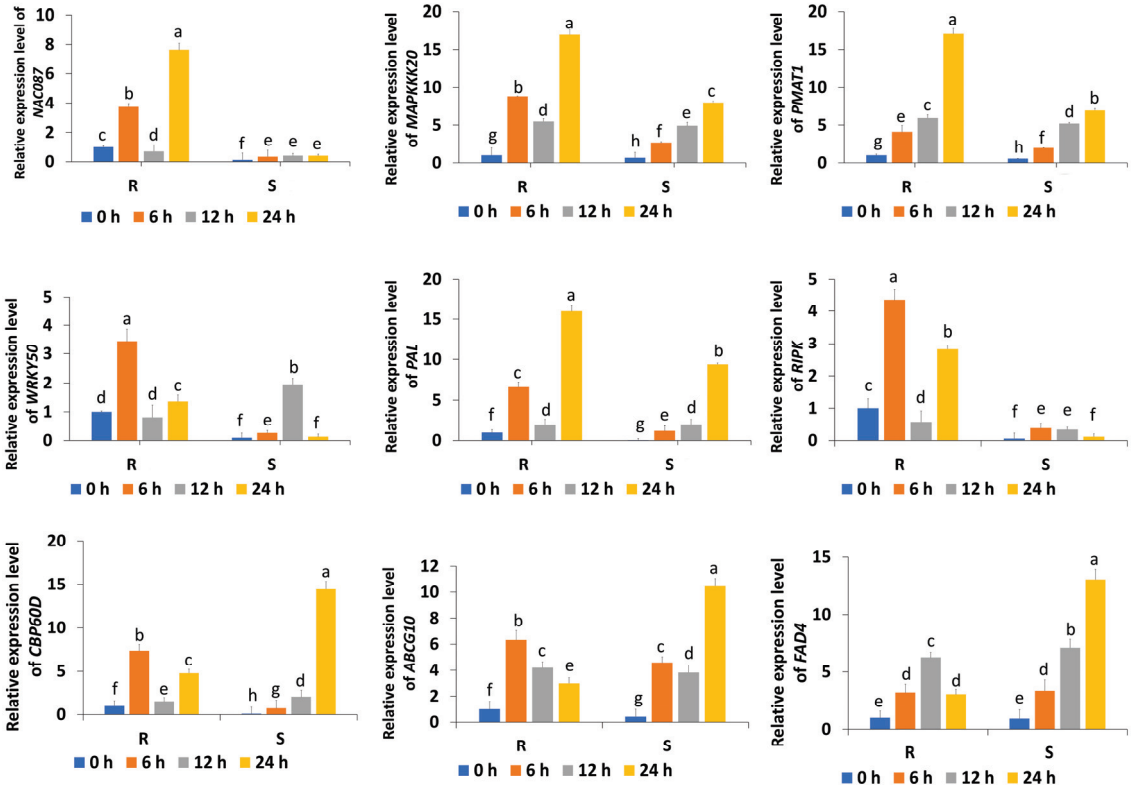

Figure 5. Relative expression levels of genes expressed in response to cold stress, as determined by RT-qPCR. All data are expressed as the means ± standard deviations from three independent experimental replicates. Statistical significance was assessed via analysis of variance (ANOVA), with Duncan's multiple range test performed subsequently; distinct letters above the bars denote notable differences at $p < 0.05$. R represents the cold-tolerant bitter gourd, and S represents the cold-sensitive bitter gourd. The blue, orange, gray, and yellow bars indicate the relative expression levels at 0 h, 6 h, 12 h, and 24 h of cold stress treatment, respectively.

2.7. The Overexpression of McNAC087 Enhances the Cold Resistance of Transgenic Arabidopsis

To investigate the role of McNAC087 in response to low-temperature stress, we constructed the recombinant plasmid pCAMBIA1300-*McNAC087* and transformed it into Arabidopsis using the floral dip technique. The low-temperature stress treatment process involved first exposing four-week-old Col-0 and *McNAC087* overexpressing (OE) lines to −14 °C for 1.5 h, then transferring them to 4 °C for 16 h, and finally placing them at 22 °C for a 2-day recovery period. When grown under ambient conditions, wild-type and transgenic plants showed no apparent differences in morphology; however, the *McNAC087*-overexpressing plants presented a superior growth phenotype, with lower degrees of wilting and yellowing than did the control plants under cold stress treatment (Figure 6a). Moreover, among Arabidopsis plants exhibiting wilting and yellowing symptoms, McNAC087-overexpressing lines exhibited a survival rate varying between 90% and 92%, whereas that of wild-type plants was merely 23% (Figure 6c). Hence, the findings suggested that overexpressing the McNAC087 gene boosted the cold tolerance of the plants.

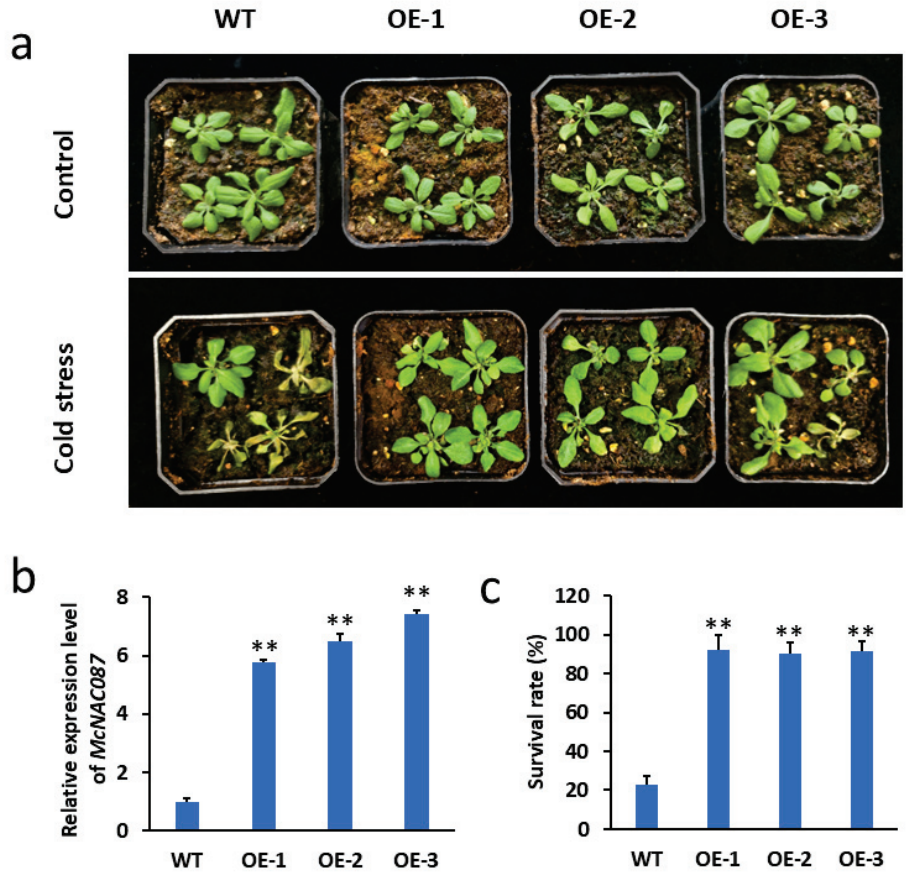

Figure 6. Functional identification of *McNAC087* in transgenic *Arabidopsis thaliana*. (**a**) Phenotypic characteristics of the *McNAC087* transgenic lines and the WT plants under cold stress treatment (−14 °C for 1.5 h, then transferred to 4 °C for 16 h, and finally placed at 22 °C for a 2-day recovery period). Control plants (WT) were kept at 22 °C during the entire experimental period, with no low-temperature treatment applied. (**b**) Relative expression level of *McNAC087* in transgenic *Arabidopsis thaliana*. (**c**) The survival rate of the *McNAC087* transgenic lines and the WT plants under cold stress treatment (−14 °C for 1.5 h, then transferred to 4 °C for 16 h, and finally placed at 22 °C for a 2-day recovery period). Control plants (WT) were kept at 22 °C during the entire experimental period, with no low-temperature treatment applied. Each data reflects the average of three separate experimental repetitions, with error bars denoting the standard errors. Student's *t* test was employed to evaluate the statistical significance of differences between groups, where ** $p < 0.01$ denotes a highly significant difference.

2.8. Overexpression of the McNAC087 Gene Alters Physiological Traits Under Low-Temperature Stress

To gain a deeper understanding of how the *McNAC087* gene influences plant physiological traits under low-temperature stress (4 °C for 24 h), we measured the MDA content, proline content, and activities of SOD, POD, and CAT in Col-0 plants and *McNAC087*-overexpressing lines. The findings revealed that under normal growth conditions, there were no significant differences in proline content, MDA content, or SOD, POD, or CAT activity between the OE lines and Col-0 plants. However, under low-temperature stress, the OE lines presented significantly greater proline contents and antioxidant enzyme activities (POD, SOD, and CAT) than the Col-0 plants did, whereas MDA accumulation showed the opposite trend (Figure 7c–g). Additionally, detection of H_2O_2 and O_2^- accumulation via 3,3′-Diaminobenzidine (DAB) and nitroblue tetrazolium (NBT) staining revealed that the OE lines produced less H_2O_2 and O_2^- than did the Col-0 plants under low-temperature stress (Figure 7a,b). These findings indicate that *McNAC087* enhances cold stress tolerance by modulating these physiological characteristics.

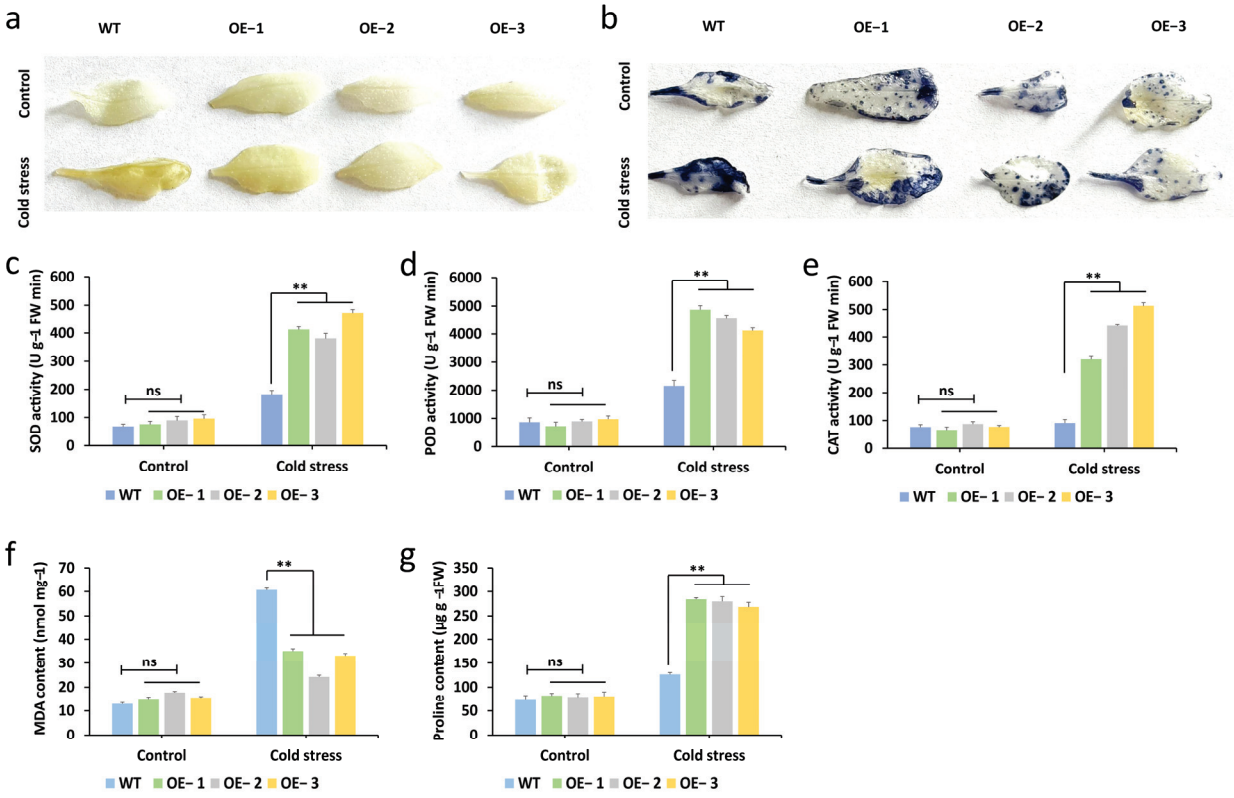

Figure 7. Physiological changes in the *McNAC087* transgenic lines under normal and cold stress conditions. (**a**) DAB staining was used to detect H_2O_2. (**b**) NBT staining was used to detect O^{2-}. (**c**–**e**) The enzymatic activities of SOD, POD, and CAT in the transgenic lines and WT plants under normal growth conditions and cold stress. (**f**,**g**). The contents of MDA and proline in the transgenic lines and WT plants under normal and cold stress. Each data point represents the mean of three independent experimental replicates, with error bars indicating standard errors. The statistical significance of the intergroup differences was assessed using Student's *t* test, where ** $p < 0.01$ denotes a highly significant difference, ns indicates non-significant difference.

2.9. Analysis of the Expression Patterns of Cold-Responsive Genes in Arabidopsis

To explore the potential molecular mechanism by which *McNAC087* regulates cold stress responses, we selected nine stress-responsive marker genes (*CBF1*, *CBF2*, *CBF3*, *RCI2A*, *DREB2A*, *RD29A*, *COR47*, *COR15a*, and *KIN1*) and analyzed their expression levels

in Col-0 plants and OE lines under cold stress (4 °C for 24 h). Under normal conditions, the expression levels of *CBF1*, *CBF2*, *RCI2A*, *DREB2A*, *RD29A*, and *COR47* were greater in the overexpression lines than in the Col-0 plants. In contrast, the expression levels of *CBF3*, *COR15a*, and *KIN1* were only weakly correlated with those of *McNAC087*. Moreover, upon cold stress treatment, the expression of all the tested genes in *McNAC087*-overexpressing plants significantly increased. When compared with Col-0 plants, the transcript levels of the *CBF1*, *CBF3*, *DREB2A*, *RD29A*, *COR47*, and *COR15a* genes increased significantly. In summary, these results suggested that the overexpression of the *McNAC087* gene, which improved cold tolerance, may be associated with the expression of these stress-responsive marker genes (Figure 8).

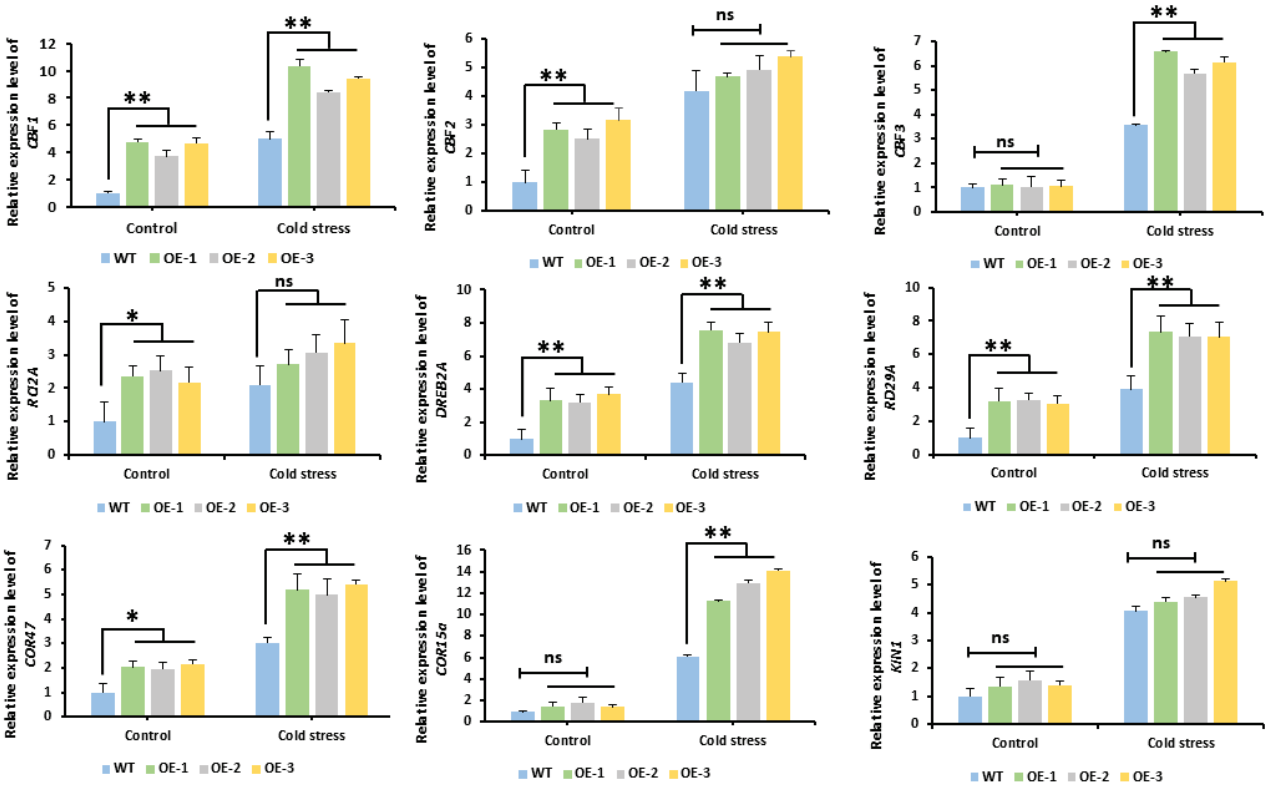

Figure 8. Expression profiling of stress-responsive genes in *Arabidopsis thaliana* exposed to cold stress in wild-type plants and transgenic lines. Each data point signifies the mean of three independent experimental repetitions, with error bars showing standard errors. The statistical significance of differences among groups was determined via Student's *t* test, where * $p < 0.05$ indicates a statistically significant difference, ** $p < 0.01$ denotes a highly significant difference, and ns indicates non-significant difference.

2.10. Subcellular Localization of McNAC087

To explore the properties of McNAC087, we utilized a transient expression experiment in Arabidopsis protoplasts to characterize where the *McNAC087* protein localizes at the subcellular level. Confocal microscopy revealed that the 35S:GFP fusion protein exhibited diffuse green fluorescence throughout the cell (Figure 9a–e). In contrast, the pYBA1132:McNAC087-GFP fusion protein displayed intense nuclear fluorescence in transformed cells, indicating that McNAC087 localized to the nucleus (Figure 9f–j).

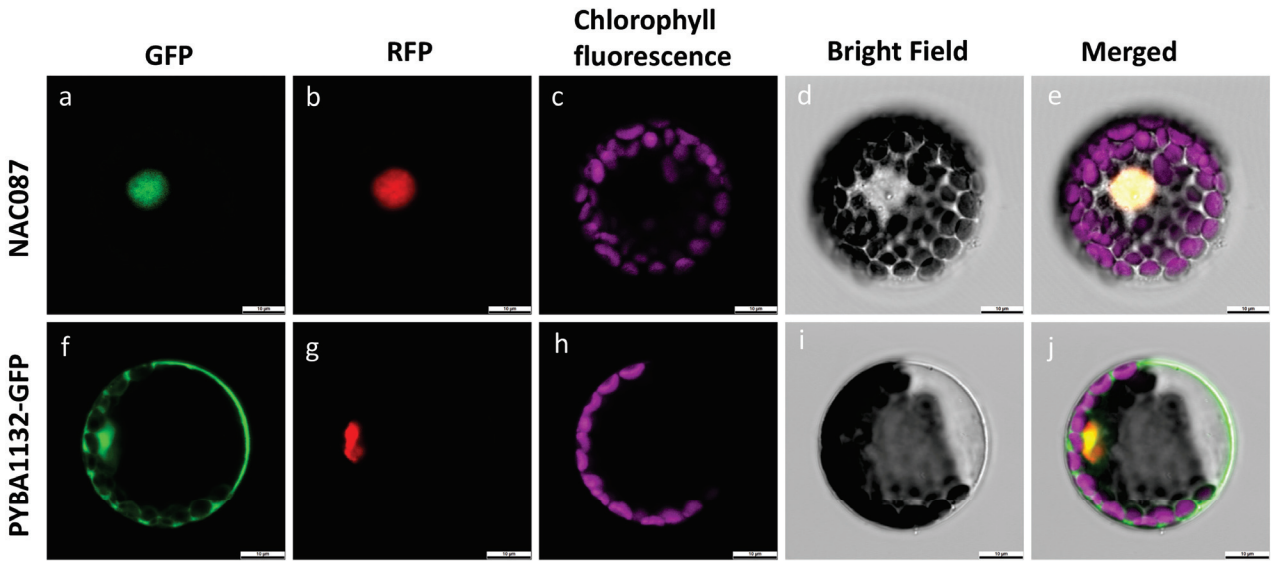

Figure 9. Subcellular localization of McNAC087 (**a**) GFP fluorescence of NAC087; (**b**) RFP fluorescence (nuclear marker) of NAC087; (**c**) Chlorophyll fluorescence of NAC087-expressing cells; (**d**) Bright field image of NAC087-expressing cells; (**e**) Merged image of NAC087, RFP, chlorophyll fluorescence, and bright field. (**f**) GFP fluorescence of pYBA1132-GFP; (**g**) RFP fluorescence (nuclear marker) of pYBA1132-GFP; (**h**) Chlorophyll fluorescence of pYBA1132-GFP-expressing cells; (**i**) Bright field image of pYBA1132-GFP-expressing cells; (**j**) Merged image of pYBA1132-GFP, RFP, chlorophyll fluorescence, and bright field. Scale bars are 10 μm.

3. Discussion

Low temperature is a critical abiotic constraint restricting plant germination, growth, and geographic distribution in modern agricultural production. This phenomenon is particularly pronounced for tropical vegetables cultivated in nontropical regions or other areas prone to cold stress [16]. One of the most fundamental and effective approaches to address this issue lies in breeding cold-tolerant bitter gourd varieties with intrinsic cold resistance. To gain deeper insights into how bitter gourd responds to cold-induced stress, it is crucial to detect cold-induced tolerance-associated genes and dissect their regulatory mechanisms. The *NAC* (*NAM*, *ATAF1/2* and *CUC2*) transcription factor family is the fourth largest TF family in plants and is widely present in various species. NAC proteins participate in nearly all stages of plant growth and development, including cell division, secondary wall formation, shoot apical meristem establishment, floral organ development, fruit ripening, and leaf senescence [3,17]. As plant-specific transcription factors, NAC proteins play pivotal roles in plant responses to abiotic stresses. *CaNAC064* acts as a positive regulator of cold tolerance in pepper plants [18]. The overexpression of *AmNAC24* improved cold and osmotic stress tolerance in *Arabidopsis thaliana*, potentially through the maintenance of ROS homeostasis [19]. *ONAC095* has contrasting regulatory effects on cold and drought stress tolerance in rice; it functions as a negative regulator of drought responses but acts as a positive regulator of cold responses [20]. *PeNAC-19* significantly responds to cold stress in tobacco and Arabidopsis, and it can increase cold stress tolerance in yeast [21]. However, to date, not only are functional studies on members of the *NAC* family in bitter gourd scarce, but research examining the biological roles of these family members in the response of bitter gourd to abiotic stresses also remains insufficient. For this study, we performed transcriptome sequencing analyses on the leaves of R and S plants at different time points under cold stress. Through the analysis of core gene sets across six groups of differentially expressed genes—specifically RM-vs-RL1, RM-vs-RL2, RM-vs-RL3, SM-vs-SL1, SM-vs-SL2, and SM-vs-SL3—1157 core genes with potential roles in low-temperature

responses were identified. Further functional characterization of these genes revealed that they are involved mainly in carbohydrate metabolism, signal transduction, amino acid metabolism, and lipid metabolism, among other processes. Studies have shown that *NAC* transcription factors can participate in hormone signal transduction to respond to plant stress [3]. We focused on one *NAC* TF, *NAC087*, which indicated that the expression level of *McNAC087* in R was consistently greater than that in SM at 0 h, 6 h, 12 h, and 24 h under cold stress treatment according to RT-qPCR. On the basis of these results, we propose that *NAC087* may be involved in the response to cold stress.

Low temperature represents a major abiotic factor that constrains germination, growth, and distribution [22]. When subjected to cold stress, plants typically undergo various physiological and biochemical alterations while regulating expression of genes to facilitate cold acclimation [23,24]. To safeguard cells against reactive oxygen species (ROS)-induced damage, plants have developed a dedicated antioxidant protection system, which includes antioxidant enzymes and antioxidants, during long-term evolution. In plants, CAT, POD, and SOD are the main antioxidant enzymes. These compounds are able to reduce ROS accumulation and further prevent the peroxidation of membrane lipids, prevent damage to cell structures, and increase plant cold resistance [25]. In addition, when plants are exposed to low-temperature stress, elevated proline levels increase the water retention capacity of cells or tissues, and proline functions as a protectant for enzymes and cellular structures and serves as a carbohydrate source [26]. Moreover, the buildup of H_2O_2, O_2^-, and MDA can impair the integrity of the plasma membrane and oxidize biological macromolecules in plants [27]. After *JfDREB1A* was introduced into *A. thaliana*, the survival rate of transgenic Arabidopsis plants increased, primarily by preserving cell membrane stability, reducing electrical conductivity, and increasing the activities of antioxidant enzymes such as SOD, POD, and CAT [28]. Moreover, *MbMYBC1* overexpression in Arabidopsis increased the activity levels of CAT, POD and SOD, along with the content of proline, under low-temperature and drought stresses [29]. *VvWRKY28*-overexpressing Arabidopsis lines presented changes in many physiological and biochemical indicators to adapt to cold and high salt stress, including increased activities of SOD, POD, and CAT; increased contents of chlorophyll and proline; and decreased contents of MDA [30]. In the present study, heterologous overexpression of the McNAC087 gene in Arabidopsis enhanced cold tolerance. This increase was likely linked to changes in the following physiological parameters of the *McNAC087* transgenic lines under cold stress: reduced MDA content; decreased H_2O_2 and O_2^- levels, increased proline content, and increased POD, SOD, and CAT activities.

Together, the three aforementioned key components, the *ICE*, *CBF*, and *COR* genes, constitute a crucial signaling pathway known as the *ICE-CBF-COR* cascade. This is a cold-responsive pathway that mitigates cold stress in plants [31]. To further investigate the possible molecular mechanism of the *McNAC087* response to cold stress, the transcription levels of genes related to the *ICE-CBF-COR* cascade (*CBF1*, *CBF2*, *CBF3*, *RCI2A*, *DREB2A*, *RD29A*, *COR47*, *COR15A* and *KIN1*) were detected via RT-qPCR. Under cold stress, all of these genes were induced under cold stress in both wild-type and transgenic *McNAC087* Arabidopsis. The gene expression of *CBF1*, *DREB2A*, *RD29A* and *COR47* was upregulated in the *McNAC087* overexpression lines compared with the wild type, both under normal and cold conditions. Therefore, *McNAC087* may regulate *Arabidopsis thaliana* tolerance to cold stress by modulating the *ICE-CBF-COR* pathway.

McNAC087 is activated under cold stress and regulates the expression of downstream target genes, including *DREB2A*, *COR47*, *COR15a*, *CBF1*, and *CBF3*. These regulated genes also promote the expression of COR genes. The latter then promote proline accumulation, enhance ROS scavenging capacity, and inhibit the accumulation of MDA. Through these combined effects, plants achieve higher cold tolerance (Figure 10).

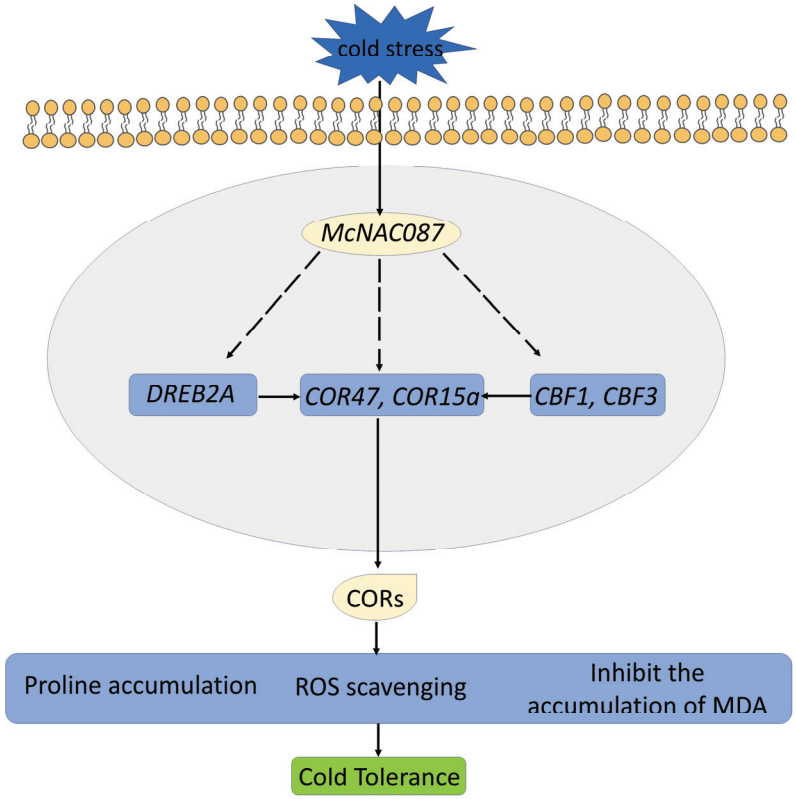

Figure 10. A proposed model illustrating the mechanism of *McNAC087* mediating cold tolerance in plants.

However, the investigation into the cold-responsive characteristics of the bitter gourd *McNAC087* gene in this study was conducted on the basis of overexpressing plants in Arabidopsis. To further clarify the key mechanism of *McNAC087* in the response of bitter gourd to low temperatures, *McNAC087*-overexpressing transgenic bitter gourd materials will be created in the future. Field identification will be carried out to evaluate the growth performance of *McNAC087* transgenic bitter gourd under natural low-temperature conditions. Moreover, various technical approaches, such as transcriptome sequencing, proteome sequencing, and yeast one-hybrid assays, will be employed to analyze in detail the molecular mechanism by which *McNAC087* regulates cold tolerance in bitter gourd. In addition, plans have been made to introduce the *McNAC087* gene identified from bitter gourd into other thermophilic vegetable crops, aiming to explore its potential for improving the cold tolerance of different crops, assess its application value in agricultural production, and contribute to the breeding of cold-tolerant vegetable varieties.

4. Materials and Methods

4.1. Plant Materials, Growing Conditions, and Cold Stress Treatment

The experimental materials used were bitter gourd inbred lines "0208" (cold stress tolerant, abbreviated as "R") and "2206" (cold stress sensitive, abbreviated as "S"), provided by the Jiangxi Academy of Agricultural Sciences, China. After soaking in water for 24 h, the seeds were germinated in a 32 °C incubator for 48 h (with 80% relative humidity to prevent seed dehydration), the germinated seeds were sown in seedling trays filled with nutrient soil. The core component of the nutrient soil was commercially available Pindstrup seedling-specific peat (Denmark) (Model: 505+, particle size: 0–6 mm, pH value: 6), which was purchased from a formal horticultural substrate supplier. Subsequently, it was mixed and formulated with other modified substrates at the following volume ratio:

60% Pindstrup peat + 25% perlite + 15% vermiculite. One seed was sown per cell of the tray, and then covered with a 1–2 cm thick layer of nutrient soil. Subsequently, the seedling trays were placed in a growth chamber for cultivation, with the cultivation conditions of 30 °C/28 °C (day/night), 14 h/10 h photoperiod, and 10,000 lx light intensity. When the seedlings reached the four-leaf and one-heart stage, they were subjected to low-temperature treatment (5 °C). The selection of 5 °C as the cold stress temperature was based on previous studies on bitter gourd cold tolerance [16], this temperature is defined as a typical "chilling stress" for bitter gourd seedlings, which can induce obvious cold-responsive phenotypes (e.g., leaf wilting, electrolyte leakage) without causing irreversible cell death. This setting ensures that we can accurately capture the dynamic changes in physiological and molecular responses during the initial phase of cold response, which aligns with the core objective of this experiment: identifying cold-responsive genes by comparing the transcriptome differences between R and S. Leaf samples were collected from R and S at four time points—0 h (before cold stress, control), 6 h, 12 h, and 24 h post-treatment—with three biological replicates per time point. All samples were immediately frozen in liquid nitrogen and stored at −80 °C. For clarity, the samples from R at the above time points were designated as RM (0 h), RL1 (6 h), RL2 (12 h), and RL3 (24 h), respectively; corresponding samples from S were named SM (0 h), SL1 (6 h), SL2 (12 h), and SL3 (24 h), respectively.

Arabidopsis seeds were disinfected three times with 70% alcohol, each time for one minute. Finally, the disinfected Arabidopsis seeds were placed on sterile filter paper. After drying, the seeds were sown in a half MS solid medium (containing 1.5% sucrose) and placed at 4 °C for three days for stratification. Then, they were cultured in a 22 °C incubator (16 h day/8 h night). After Arabidopsis grew two leaves, uniformly sized healthy seedlings were selected and transferred to nutrient soil with substrate/vermiculite/perlite (3:1:1).

4.2. RNA Isolation and Transcriptome Sequencing

The total RNA of 24 samples, including RM, RL1, RL2, RL3, SM, SL1, SL2 and SL3 (three biological replicates per material), was extracted using the Plant RNA Kit (Omega Bio-Tek, Norcross, GA, USA) according to the manufacturer's instructions. To determine the purity of the nucleic acid, a Nanodrop 2000 (Thermo Fisher Scientific, Waltham, MA, USA) was used to determine the OD value. The RNA integrity was determined via an Agilent 2100 (Agilent Technologies, Santa Clara, CA, USA). Finally, the samples were processed by Guangzhou Kidio Biotechnology Co., Ltd. (Guangzhou, China) and sequenced on an Illumina NovaSeq X Plus (Illumina, Inc., San Diego, CA, USA).

4.3. Identification of Differentially Expressed Genes and Bioinformatic Analysis

To obtain high-quality clean reads, the sequencing data generated by sequencing machines were further filtered via fastp [32]. Reads with adapter contaminants, more than 10% of nucleotides of undetermined identity, and a low-quality (Q value ≤ 20) base percentage over 50% were removed from subsequent analysis. The short read alignment tool Bowtie2 [33] was employed to conduct the alignment with Ribosome RNA (rRNA). The clean reads were subsequently mapped to the reference genome [34]. To quantify the expression abundance and variations, the fragments per kilobase of transcript per million mapped reads (FPKM) value was computed using RNA-Seq by Expectation Maximization (RSEM) [35]. DESeq2 [36] was subsequently employed to conduct differential expression analysis of the RNAs. The thresholds for screening DEGs were set as FDR < 0.05 and $|\log2$ (fold change)$| > 2$. To explore the biological functions of the target genes, we used GO (http://www.geneontology.org/ (accessed on 5 April 2025)) to comprehensively describe the properties of genes and their products, as well as KEGG (http://www.genome.jp/kegg/

(accessed on 10 April 2025)), to identify significantly enriched metabolic pathways and signal transduction pathways among the DEGs [37,38].

4.4. Arabidopsis Transformation and Cold Stress Tolerance Evaluation

The complete coding sequence of *McNAC087* was amplified from R cDNA using gene-specific primers (Supplementary Table S2) and inserted into the overexpression vector pCAMBIA1302, resulting in the 35S:McNAC087-GFP construct. The recombinant plasmid was subsequently introduced into *Agrobacterium tumefaciens* GV3101 through freeze–thaw technique, and transgenic Arabidopsis plants were generated via the floral dip method. Transgenic plants were selected on 1/2 MS media supplemented with 50 μg/mL hygromycin. Homozygous T3 lines were used for RT-qPCR and phenotype analysis.

To assess cold tolerance, 4-week-old soil-grown transgenic and wild-type (WT) plants were subjected to cold stress at −14 °C for 1.5 h and then transferred to a 4 °C environment for 16 h, followed by a 2-day recovery period at 22 °C to obtain the phenotypes and survival rates. The sequential stress regime (−14 °C → 4 °C → 22 °C) was designed to simulate the "freeze–thaw cycle" that bitter gourd may encounter in natural field conditions (e.g., sudden night frost in early spring followed by gradual temperature rise the next day): the short-term −14 °C treatment (1.5 h) mimics acute freezing stress (to induce cell ice damage), the subsequent 4 °C incubation (16 h) simulates the prolonged low-temperature period after freezing, and the 22 °C recovery step is used to evaluate the plant's ability to repair freeze damage—this directly matches the objective of verifying whether *McNAC087* overexpression enhances "freezing tolerance" (a key aspect of cold stress). Additionally, in the physiological parameter determination (Section 4.6), we set a 4 °C for 24 h treatment as a "chronic chilling stress control"—this comparison helps distinguish whether *McNAC087* specifically improves freezing tolerance or broadly enhances chilling tolerance, thereby clarifying the functional specificity of the gene. Control plants (WT) were kept at 22 °C during the entire experimental period, with no low-temperature treatment applied. Three independent transgenic lines (OE-1, OE-2, OE-3) and WT plants were included in each experiment. Each line was tested using no fewer than 40 plants, and the experiment was conducted with independent replication at least three times.

4.5. RNA Extraction and Quantitative Real-Time PCR Analysis

In order to obtain genes involved in low-temperature resistance, hub DEGs were identified across six comparative groups: RM-vs-RL1, RM-vs-RL2, RM-vs-RL3, SM-vs-SL1, SM-vs-SL2, and SM-vs-SL3. Total RNA samples were isolated using TIANGEN RNA Extraction Kit (Beijing, China) then converted into cDNA via reverse transcription according to Transcriptor First-Strand cDNA Synthesis Kit (Roche, Mannheim, Germany). Totally, eleven genes were selected for RT-qPCR to verify the accuracy of the transcriptome data, and nine stress-responsive marker genes (*CBF1*, *CBF2*, *CBF3*, *RCI2A*, *DREB2A*, *RD29A*, *COR47*, *COR15a*, and *KIN1*) were used to analyze their expression levels in Col-0 plants and OE lines. The primers were designed via Primer 5.0 software (Supplementary Table S2). RT-qPCR was performed on a QuantStudio 7 Flex Real-Time PCR System (Applied Biosystems, Waltham, MA, USA). We assessed the relative gene expression levels according to the $2^{-\Delta\Delta CT}$ method [39].

4.6. Determination of Physiological Parameters

Seeds of WT and *McNAC087*-overexpressing Arabidopsis were grown in soil, and cold stress (4 °C for 24 h) was applied to the plants at 4 weeks. 3,3′-Diaminobenzidine (DAB) and nitroblue tetrazolium (NBT) staining were employed to assess H_2O_2 and O_2^- levels. Immerse intact leaves in DAB (pH adjusted to 3.8 with 1 M HCl, freshly prepared before use) and NBT (prepared with 50 mM sodium phosphate buffer, pH 7.8) solution,

vacuum infiltrate for 15 min (0.08 MPa) to ensure solution penetration, respectively. After incubating the leaves at 25 °C in the dark for 8 h, destain them with boiling 95% ethanol until chlorophyll is removed. Finally, observe the staining status of the leaves. SOD, POD, and CAT activities, as well as MDA and proline levels, were assayed using spectrophotometric methods. Fresh leaf tissues (0.5 g each) were collected from 4-week-old rosette leaves in transgenic Arabidopsis. The tissues were ground into a homogenate in a pre-cooled mortar with extraction buffer provided in the corresponding kit (tissue:buffer = 1:9, w/v) under ice-bath conditions. The homogenate was placed in a centrifuge tube, centrifuged at 8000× g for 10 min at 4 °C, and the supernatant was subsequently collected to serve as the crude enzyme solution. (for SOD, POD and CAT activity determination) or metabolite extract (for MDA and proline content determination). Repeated freezing and thawing were avoided throughout the process to prevent enzyme activity loss or metabolite degradation. SOD, POD, CAT, MDA and proline were measured using Detection Kit (BC0175, BC0095, BC0205, BC0025 and BC0295; Solarbio, Beijing, China) according to the manufacturer's instruction.

4.7. Subcellular Localization Analysis of McNAC087

The coding sequence CDS of McNAC087 without the stop codon was PCR-amplified and fused to the N-terminus of green fluorescent protein (GFP) in the pYBA1132 vector. The resulting McNAC087:GFP construct was then delivered into Arabidopsis mesophyll protoplasts via polyethylene glycol (PEG)-mediated transfection. Following incubation in the dark for 24 h, the localization results were visualized using a laser scanning confocal microscope (IX83-FV1200, Olympus, Tokyo, Japan).

5. Conclusions

In the present study, a total of 1157 co-expressed genes were identified through comparative analysis of DEG sets between two bitter gourd cultivars via RNA sequencing. KEGG analysis indicated that the signal transduction pathway has a close correlation with cold tolerance in bitter gourd, and *NAC* transcription factors may regulate this pathway. The relative expression levels of *McNAC087* in R were consistently greater than those in SM at all cold stress treatment time points, suggesting that *McNAC087* is poised to play a pivotal role in boosting cold tolerance. Subcellular localization analyses revealed that McNAC087 is nuclear-localized. Overexpressing *McNAC087* in Arabidopsis was found to increase cold resistance in transgenic seedlings, as demonstrated by higher proline accumulation, enhanced activities of antioxidant enzymes, elevated antioxidant enzyme activities, and positive regulation of cold-induced gene expression. Collectively, these findings provide valuable insights into the mechanisms underlying cold regulation in bitter gourd.

Supplementary Materials: The following supporting information can be downloaded at: https://www.mdpi.com/article/10.3390/plants14223440/s1, Table S1: GO term annotations; Table S2: List of primers and their uses.

Author Contributions: Conceptualization, X.W., C.D. and T.T.; investigation, K.W. and X.Y.; writing—original draft preparation, X.Y.; writing—review and editing, K.W., Z.Y. and S.M.; visualization, F.G., B.S. and Y.X.; supervision, X.W. All authors have read and agreed to the published version of the manuscript.

Funding: This research was funded by the Basic Research Project of Jiangxi Academy of Agricultural Sciences (JXSNKYJCRC202436), the Jiangxi Provincial Project for Cultivating Young Scientific and Technological Talents in the Early Career Stage (20244BCE52267), the China Agriculture Research System of MOF and MARA (CARS-23).

Data Availability Statement: The raw sequencing data generated in this study are available in SRA of NCBI with the accession number PRJNA1331498.

Conflicts of Interest: The authors declare no conflicts of interest. The funders had no role in the design of the study; in the collection, analyses, or interpretation of data; in the writing of the manuscript; or in the decision to publish the results.

Abbreviations

The following abbreviations are used in this manuscript:

TF	Transcription factor
COR	Cold-responsive
rRNA	Ribosomal RNA
FPKM	Fragment per kilobase of transcript per million mapped reads
RSEM	RNA-seq by expectation maximization
DEGs	Differentially expressed genes
GO	Gene ontology
WT	Wild-type
DAB	3,3′-diaminobenzidine
NBT	Nitroblue tetrazolium
MDA	Malondialdehyde
POD	Peroxidase
SOD	Superoxide dismutase
CAT	Catalase
GFP	Green fluorescent protein
PEG	Polyethylene glycol
PCA	Principal Component Analysis
ROS	Reactive oxygen species

References

1. Shi, Y.; Ding, Y.; Yang, S. Molecular regulation of CBF signaling in cold acclimation. *Trends Plant Sci.* **2018**, *23*, 623–637. [CrossRef]
2. Ritonga, F.N.; Chen, S. Physiological and molecular mechanism involved in cold stress tolerance in plants. *Plants* **2020**, *9*, 560. [CrossRef]
3. Diao, P.; Chen, C.; Zhang, Y.; Meng, Q.; Lv, W.; Ma, N. The role of NAC transcription factor in plant cold response. *Plant Signal. Behav.* **2020**, *15*, 1785668. [CrossRef] [PubMed]
4. Wong, C.E.; Li, Y.; Labbe, A.; Guevara, D.; Nuin, P.; Whitty, B.; Diaz, C.; Golding, G.B.; Gray, G.R.; Weretilnyk, E.A.; et al. Transcriptional profiling implicates novel interactions between abiotic stress and hormonal responses in *Thellungiella*, a close relative of Arabidopsis. *Plant Physiol.* **2006**, *140*, 1437–1450. [CrossRef]
5. Chinnusamy, V.; Zhu, J.; Zhu, J.K. Cold stress regulation of gene expression in plants. *Trends Plant Sci.* **2007**, *12*, 444–451. [CrossRef] [PubMed]
6. Wang, D.Z.; Jin, Y.N.; Ding, X.H.; Wang, W.J.; Zhai, S.S.; Bai, L.P.; Guo, Z.F. Gene regulation and signal transduction in the ICE-CBF-COR signaling pathway during cold stress in plants. *Biochemistry* **2017**, *82*, 1103–1117. [CrossRef]
7. Yu, H.; Kong, X.; Huang, H.; Wu, W.; Park, J.; Yun, D.J.; Lee, B.H.; Shi, H.; Zhu, J.K. *STCH4/REIL2* confers cold stress tolerance in Arabidopsis by promoting rRNA processing and CBF protein translation. *Cell Rep.* **2020**, *30*, 229–242.e225. [CrossRef] [PubMed]
8. Xu, F.; Tang, J.; Wang, S.; Cheng, X.; Wang, H.; Ou, S.; Gao, S.; Li, B.; Qian, Y.; Gao, C.; et al. Antagonistic control of seed dormancy in rice by two bHLH transcription factors. *Nat. Genet.* **2022**, *54*, 1972–1982. [CrossRef]
9. Olsen, A.N.; Ernst, H.A.; Leggio, L.L.; Skriver, K. NAC transcription factors: Structurally distinct, functionally diverse. *Trends Plant Sci.* **2005**, *10*, 79–87. [CrossRef]
10. Han, K.; Zhao, Y.; Sun, Y.; Li, Y. NACs, generalist in plant life. *Plant Biotechnol. J.* **2023**, *21*, 2433–2457. [CrossRef]
11. Xiong, H.; He, H.; Chang, Y.; Miao, B.; Liu, Z.; Wang, Q.; Dong, F.; Xiong, L. Multiple roles of NAC transcription factors in plant development and stress responses. *J. Integr. Plant Biol.* **2025**, *67*, 510–538. [CrossRef]
12. Wang, T.; Ma, X.; Chen, Y.; Wang, C.; Xia, Z.; Liu, Z.; Gao, L.; Zhang, W. *SlNAC3* suppresses cold tolerance in tomatoes by enhancing ethylene biosynthesis. *Plant Cell Environ.* **2024**, *47*, 3132–3146. [CrossRef]

13. Li, R.; Song, Y.; Wang, X.; Zheng, C.; Liu, B.; Zhang, H.; Ke, J.; Wu, X.; Wu, L.; Yang, R.; et al. *OsNAC5* orchestrates *OsABI5* to fine-tune cold tolerance in rice. *J. Integr. Plant Biol.* **2024**, *66*, 660–682. [CrossRef]
14. Hao, Y.J.; Wei, W.; Song, Q.X.; Chen, H.W.; Zhang, Y.Q.; Wang, F.; Zou, H.F.; Lei, G.; Tian, A.G.; Zhang, W.K.; et al. Soybean NAC transcription factors promote abiotic stress tolerance and lateral root formation in transgenic plants. *Plant J.* **2011**, *68*, 302–313. [CrossRef]
15. Shan, W.; Kuang, J.F.; Lu, W.J.; Chen, J.Y. Banana fruit NAC transcription factor *MaNAC1* is a direct target of *MaICE1* and involved in cold stress through interacting with *MaCBF1*. *Plant Cell Environ.* **2014**, *37*, 2116–2127. [CrossRef] [PubMed]
16. Niu, Y.; Liu, Z.; He, H.; Han, X.; Qi, Z.; Yang, Y. Gene expression and metabolic changes of *Momordica charantia* L. seedlings in response to low temperature stress. *PLoS ONE* **2020**, *15*, e0233130. [CrossRef] [PubMed]
17. Shao, H.; Wang, H.; Tang, X. NAC transcription factors in plant multiple abiotic stress responses: Progress and prospects. *Front. Plant Sci.* **2015**, *6*, 902. [CrossRef]
18. Hou, X.M.; Zhang, H.F.; Liu, S.Y.; Wang, X.K.; Zhang, Y.M.; Meng, Y.C.; Luo, D.; Chen, R.G. The NAC transcription factor *CaNAC064* is a regulator of cold stress tolerance in peppers. *Plant Sci.* **2020**, *291*, 110346. [CrossRef] [PubMed]
19. Dorjee, T.; Cui, Y.; Zhang, Y.; Liu, Q.; Li, X.; Sumbur, B.; Yan, H.; Bing, J.; Geng, Y.; Zhou, Y.; et al. Characterization of NAC gene family in *Ammopiptanthus mongolicus* and functional analysis of *AmNAC24*, an osmotic and cold-stress-induced NAC gene. *Biomolecules* **2024**, *14*, 182. [CrossRef]
20. Huang, L.; Hong, Y.; Zhang, H.; Li, D.; Song, F. Rice NAC transcription factor ONAC095 plays opposite roles in drought and cold stress tolerance. *BMC Plant Biol.* **2016**, *16*, 203. [CrossRef]
21. Xu, Y.; Li, P.; Ma, F.; Huang, D.; Xing, W.; Wu, B.; Sun, P.; Xu, B.; Song, S. Characterization of the NAC transcription factor in Passion Fruit (*Passiflora edulis*) and functional identification of *PeNAC-19* in cold stress. *Plants* **2023**, *12*, 1393. [CrossRef] [PubMed]
22. Peng, M.; Chang, Y.; Chu, G.; Wang, M. Low-temperature tolerance and transcriptome analyses during seed germination of *Anabasis aphylla*. *J. Plant Interact.* **2019**, *14*, 254–264. [CrossRef]
23. Barrero-Gil, J.; Huertas, R.; Rambla, J.L.; Granell, A.; Salinas, J. Tomato plants increase their tolerance to low temperature in a chilling acclimation process entailing comprehensive transcriptional and metabolic adjustments. *Plant Cell Environ.* **2016**, *39*, 2303–2318. [CrossRef]
24. Li, S.; Yang, Y.; Zhang, Q.; Liu, N.; Xu, Q.; Hu, L. Differential physiological and metabolic response to low temperature in two zoysiagrass genotypes native to high and low latitude. *PLoS ONE* **2018**, *13*, e0198885. [CrossRef]
25. Liu, A.; Hu, Z.; Bi, A.; Fan, J.; Gitau, M.M.; Amombo, E.; Chen, L.; Fu, J. Photosynthesis, antioxidant system and gene expression of bermudagrass in response to low temperature and salt stress. *Ecotoxicology* **2016**, *25*, 1445–1457. [CrossRef]
26. Khedr, A.H.; Abbas, M.A.; Wahid, A.A.; Quick, W.P.; Abogadallah, G.M. Proline induces the expression of salt-stress-responsive proteins and may improve the adaptation of *Pancratium maritimum* L. to salt-stress. *J. Exp. Bot.* **2003**, *54*, 2553–2562. [CrossRef]
27. Li, J.; Li, Y.; Yin, Z.; Jiang, J.; Zhang, M.; Guo, X.; Ye, Z.; Zhao, Y.; Xiong, H.; Zhang, Z.; et al. *OsASR5* enhances drought tolerance through a stomatal closure pathway associated with ABA and H_2O_2 signaling in rice. *Plant Biotechnol. J.* **2017**, *15*, 183–196. [CrossRef] [PubMed]
28. Han, L.; Ma, K.; Zhao, Y.; Mei, C.; Mamat, A.; Wang, J.; Qin, L.; He, T. The cold-stress responsive gene *DREB1A* involved in low-temperature tolerance in Xinjiang wild walnut. *PeerJ* **2022**, *10*, e14021. [CrossRef]
29. Liu, W.; Wang, T.; Wang, Y.; Liang, X.; Han, J.; Han, D. *MbMYBC1*, a *M. baccata* MYB transcription factor, contribute to cold and drought stress tolerance in transgenic Arabidopsis. *Front. Plant Sci.* **2023**, *14*, 1141446. [CrossRef] [PubMed]
30. Liu, W.; Liang, X.; Cai, W.; Wang, H.; Liu, X.; Cheng, L.; Song, P.; Luo, G.; Han, D. Isolation and functional analysis of *VvWRKY28*, a Vitis vinifera WRKY transcription factor gene, with functions in tolerance to cold and salt stress in transgenic *Arabidopsis thaliana*. *Int. J. Mol. Sci.* **2022**, *23*, 3418. [CrossRef]
31. Hwarari, D.; Guan, Y.; Ahmad, B.; Movahedi, A.; Min, T.; Hao, Z.; Lu, Y.; Chen, J.; Yang, L. ICE-CBF-COR signaling cascade and its regulation in plants responding to cold stress. *Int. J. Mol. Sci.* **2022**, *23*, 1549. [CrossRef] [PubMed]
32. Chen, S.; Zhou, Y.; Chen, Y.; Gu, J. fastp: An ultra-fast all-in-one FASTQ preprocessor. *Bioinformatics* **2018**, *34*, i884–i890. [CrossRef] [PubMed]
33. Langmead, B.; Salzberg, S.L. Fast gapped-read alignment with Bowtie 2. *Nat. Methods* **2012**, *9*, 357–359. [CrossRef]
34. Kim, D.; Langmead, B.; Salzberg, S.L. HISAT: A fast spliced aligner with low memory requirements. *Nat. Methods* **2015**, *12*, 357–360. [CrossRef]
35. Li, B.; Dewey, C.N. RSEM: Accurate transcript quantification from RNA-Seq data with or without a reference genome. *BMC Bioinform.* **2011**, *12*, 323. [CrossRef]
36. Love, M.I.; Huber, W.; Anders, S. Moderated estimation of fold change and dispersion for RNA-seq data with DESeq2. *Genome Biol.* **2014**, *15*, 550. [CrossRef]
37. Kanehisa, M.; Goto, S. KEGG: Kyoto encyclopedia of genes and genomes. *Nucleic Acids Res.* **2000**, *28*, 27–30. [CrossRef]

38. Kanehisa, M. Toward understanding the origin and evolution of cellular organisms. *Protein Sci.* **2019**, *28*, 1947–1951. [CrossRef] [PubMed]
39. Livak, K.J.; Schmittgen, T.D. Analysis of relative gene expression data using real-time quantitative PCR and the $2(^{-\Delta\Delta C(T)})$ Method. *Methods* **2001**, *25*, 402–408. [CrossRef]

plants

MDPI

Article

Genome-Wide Analysis of the *Dof* Gene Family in Soybean and Functional Identification of *GmDof63* in Response to *Phytophthora sojae* Infection

Sujie Fan, Haiyuan Chen, Yuhan Huo, Yang Song, Piwu Wang, Zhuo Zhang * and Liangyu Jiang *

Plant Biotechnology Center, College of Agronomy, Jilin Agriculture University, Changchun 130118, China; fansujie@jlau.edu.cn (S.F.); ch42@foxmail.com (H.C.); huoyuhan666@163.com (Y.H.); song-yang@jlau.edu.cn (Y.S.); peiwuw@163.com (P.W.)

* Correspondence: zhangzhuo20122025@163.com (Z.Z.); liangyuj@jlau.edu.cn (L.J.)

Abstract

Phytophthora root and stem infection by *Phytophthora sojae* is a global and devastating disease of soybeans. Selecting disease-resistant varieties is the most economical and effective measure for controlling this disease. Delving into the disease resistance and defense molecular mechanisms can lay a theoretical foundation for solving this problem. Here, we screened the soybean genome and identified 78 *GmDof* genes distributed on nineteen chromosomes. Subcellular localization analysis revealed that the majority of GmDof proteins were located in the cell nucleus. Phylogenetic analysis categorized these genes into nine subfamilies. Gene structure analysis showed that all *GmDofs* contained 0 to 2 introns, and most of them did not have introns. Motif and conserved domain analysis showed that all GmDofs contained a common motif (motif-1) and a typical conserved C_2-C_2 domain. The prediction of *cis*-acting elements in promoter regions revealed numerous *cis*-regulatory elements responsible for stress responses, plant growth and development, plant hormone responses, and light responses. RNA-seq and quantitative real-time PCR results showed that *GmDof63* (Glyma.16G145000) was specifically expressed at high levels after *P. sojae* infection. *GmDof63* was strongly induced by SA and ETH treatments. The soybean seedlings overexpressing *GmDof63* displayed enhanced resistance to *P. sojae* infection compared with the wild-type soybean seedlings. Further experiments indicated that the expression levels of pathogenesis-related protein genes *PR1a*, *PR4*, *PR5a*, and *PR10* were significantly up-regulated in *GmDof63*-overexpressing transgenic soybean seedlings. Taken together, these findings reveal the mechanism by which *GmDof63* directly or indirectly regulates the expression of *PR* genes to modulate the soybean response to *P. sojae* infection.

Keywords: soybean; *Phytophthora sojae*; Dof transcription factors; genome-wide characterization; GmDof63

1. Introduction

Soybean [*Glycine max* (L.) Merr.] is an important food and economic crop worldwide, and the significance and urgency of soybean research have become increasingly prominent [1,2]. Phytophthora root and stem rot of soybean is a devastating disease caused by *Phytophthora sojae*, leading to stunting, death or premature senescence of seedlings [3]. It can result in crop failure in the severely affected fields, causing billions of dollars of economic losses to the global soybean production each year [3,4]. Although several *P. sojae* strains and quantitative trait loci (QTLs) related to *P. sojae* resistance in soybean have been

identified, the mechanisms underpinning the functions and regulation of resistance genes remain to be studied [5–7].

The DNA binding with one finger (Dof) family is a plant-specific class of transcription factors [8–10]. Members of the Dof family have been identified in many species, such as *Arabidopsis thaliana* [11], *Oryza sativa* [11], *G. max* [12], *Zea mays* [13], *Solanum tuberosum* [14], *Prunus persica* [15], and *Capsicum annuum* [16]. Dof transcription factors (TFs) typically consist of 200–400 amino acid residues and contain oligomerization sites [17]. The highly conserved domain consists of 50–52 residues at the N-terminus, containing a C_2-C_2 zinc finger domain $CX_2CX_{21}CX_2C$ [18,19]. Dof TFs recognize and bind to the AAAG-rich sequences or the CTTTT sequence of their target genes [20].

Dof TFs play a crucial role in various biological processes, including plant growth and development, signal transduction, and abiotic stress responses [21–23]. In Arabidopsis, the overexpression of *OBP4* (a Dof TF) promotes cell proliferation in the differentiation zone and induces the formation of callus [24]. In blueberry plants, *VcDof2* and *VcDof45* are considered to play significant roles in the flowering and fruit development processes, and *VcDof1*, *VcDof11* and *VcDof15* exhibit positive responses and upregulated expression under abiotic stress conditions [25]. The amount of oil contained in the seeds of cotton growing on specific land is related to *GhDof1*. When *GhDof1* is highly expressed, the oil content in cotton seeds will increase, while the protein content will decrease [26]. The cycling Dof factor 2 (CDF2) causes Arabidopsis to become insensitive to photoperiod and to delay flowering by reducing the level of *CONSTANS* [27]. In apple plants, MdCDOF3 and MdDOF3.6 activate the cytokinin oxidase *MdCKX7* in response to sorbitol signals, thereby accelerating the leaf senescence process [28]. The wheat endosperm-specific TF TaDOF6 promotes grain development by regulating the expression of *TaSWEET13h* and facilitating the transport of sugars and gibberellins [29]. SlDof22 can bind to the promoter of *SlSOS1* to down-regulate the expression of this gene, which compromises the salt stress tolerance [30]. In *Camellia sinensis*, *CsDOF51* and *CsDOF12* exhibit significant expression changes under drought stress and high-temperature stress, respectively, and *CsDOF44* shows significant changes under both conditions [31].

To date, the precise roles of Dof or Dof-like proteins in regulating biotic stress responses remain poorly understood. In tobacco, *Sar8.2b* can be activated by the Dof TF, which is related to systemic acquired resistance [32]. The atypical Dof TF OsDes1 can specifically recognize the promoter region of the defense-related gene *OsPR1b*, thereby activating the expression of *OsPR1b* to enhance the resistance to *Xanthomonas oryzae* pv. *oryzae* [33]. However, few studies report the *Dof* genes responsive to *P. sojae* infection in soybean. On another note, salicylic acid (SA), Methyl jasmonic acid (MeJA), ethylene (ETH), and abscisic acid (ABA) are all small molecule hormones, and they can coordinate the defense responses of plants through a complex signaling network, thereby regulating plant immunity [34–37]. Dof TFs have been shown to mediate responses to various hormone signals. *SsDOF1-7* in sugarcane have been shown to contain several *cis*-elements involved in SA, MeJA, and ABA responses [38]. In Arabidopsis, a DOF transcription factor gene, *OBP3*, is mainly responsive to SA, and DOF5.8 positively regulates the target gene *ANAC069* under abiotic stress conditions [39]. *FtDof* gene was mainly up-regulated under MeJA treatment but down-regulated under SA, ABA, gibberellic acid (GA), and indole-3-acetic acid (IAA) treatment in Tartary buckwheat [40]. The *VvDOF3* gene was rapidly induced by exogenous SA, MeJA, and powdery mildew infection [41]. These findings suggest that Dof TFs may play a key role by regulating the levels of plant hormone signals in response to environmental stress.

In this work, we sought to uncover the functional roles of the *Dof* gene family members in soybean defense against *P. sojae* infection. In order to do this, we identified 78 *Dof* family genes in soybean and analyzed their physicochemical properties, chromosomal

localization, evolutionary relationships, gene structures, conserved motifs, intraspecies and interspecies collinearity, and promoter elements. We employed RNA sequencing and the quantitative RT-PCR method to screen out the key *Dof* gene in soybean response to *P. sojae* infection. Subsequently, *GmDof63* (Glyma.16G145000) was chosen for further analysis. Notably, *GmDof63* was significantly upregulated under SA and ETH treatments. The soybean seedlings overexpressing *GmDof63* displayed enhanced resistance to *P. sojae* infection compared with the wild-type (WT) soybean seedlings. These findings lay a good framework for further research into the involvement of the soybean *Dof* gene in defense against *P. sojae* infection.

2. Results

2.1. Identification and Characterization of the Dof Genes in Soybean

In this study, a total of 78 *Dof* genes were identified in the soybean genome and renamed as *GmDof1* to *GmDof78* based on the location order of soybean chromosomes from top to bottom. The GmDofs showed the amino acid sequence lengths ranging from 171 aa (GmDof18) to 503 aa (GmDof35), the molecular weights ranging from 19.65 kDa (GmDof18) to 54.73 kDa (GmDof35), and the theoretical pI ranging from 4.69 to 10.23, with 26 members having the pI less than 7 and 52 members having the pI greater than 7. Except for GmDof37, GmDof47, and GmDof60, the other members were unstable proteins. All the GmDofs were identified as hydrophilic proteins. Subcellular localization prediction indicated that except for GmDof47, located in the cytoplasm, and GmDof19 and GmDof60, located in the chloroplast, the other GmDofs were located in the cell nucleus (Table S1).

2.2. Chromosome Localization of GmDofs

According to the soybean genome database, 78 soybean *Dof* genes were unevenly distributed among 20 chromosomes, with the exception of chromosome 14 (Figure 1). The number of *GmDofs* in each chromosome differed considerably. Chromosome 13 had the largest number (11) of *GmDofs*, followed by chromosome 15 (8) and chromosome 7 (6). Chromosomes 4, 6, and 19 had five *GmDofs*; chromosomes 2, 5, 8, 17, and 18 had four *GmDofs*; chromosomes 1 and 11 had three *GmDofs*; and chromosomes 3, 9, 10, 12, 16, and 20 had two *GmDofs*.

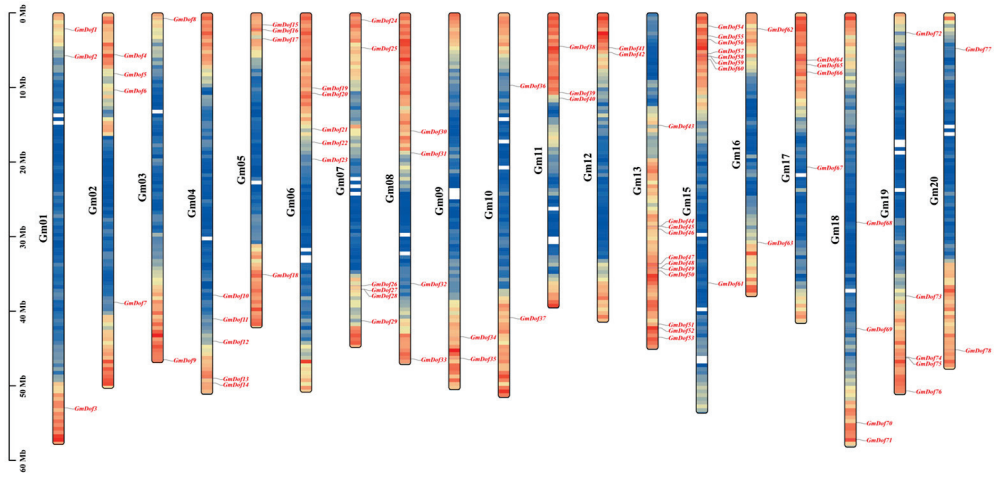

Figure 1. Genomic localization of soybean Dof members on chromosomes. Gene spacing are set at 200 kilobases, which is used to calculate the gene density on each chromosome. The color will gradually change from blue (low gene density) to red (high gene density) to represent this difference.

2.3. Phylogenetic Relationships of GmDofs

To ensure the reliability of the analysis, we employed the Maximum likelihood (ML) method to perform multiple sequence alignment of GmDofs and 36 Arabidopsis Dof members and constructed a phylogenetic tree of all Dof proteins (Figure 2). The phylogenetic clustering of GmDofs was associated with the uneven distribution of their conserved domains. The GmDofs were clustered into nine subfamilies (A, B1, B2, C1, C2.1, C2.2, C3, D1, and D2), which showed significant differences in the number of GmDofs. Overall, the evolutionary tree structure of GmDofs is mainly related to the evolutionary relationships between species, and the genes of species with evolutionary relationships tend to cluster on the same branch of the evolutionary tree.

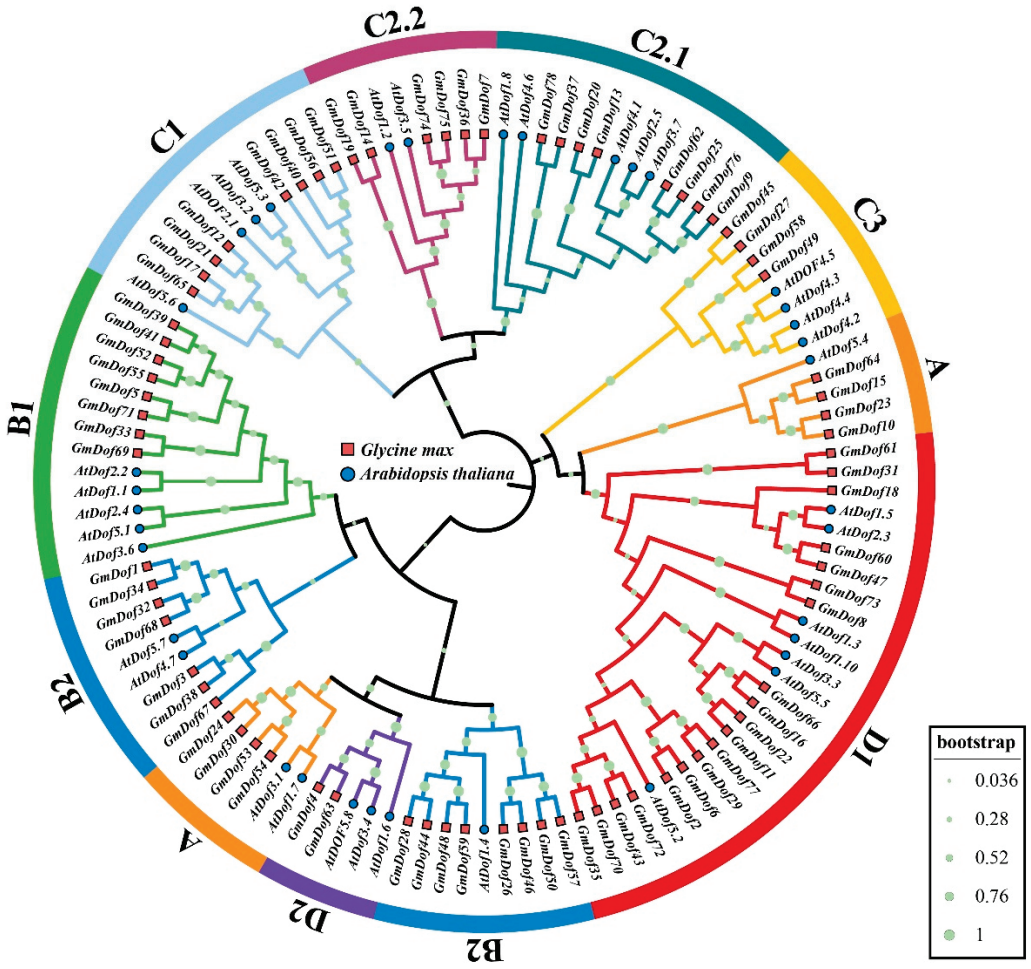

Figure 2. Phylogenetic tree of the Dof proteins in soybean and Arabidopsis.

2.4. Gene Structures and Motif Distribution of GmDofs

To examine the structural diversity of GmDofs, we investigated the number of exon-introns and the distribution of conserved domains of GmDofs. This analysis provided evidence for unveiling the evolution of structural diversity in the soybean Dof family. Almost all *GmDofs* contained very few or no introns (Figure 3). The genes in the A, B2, and D2 subfamilies did not contain introns. The *GmDofs* classified in the same subfamily showed similar gene structures. To elucidate the evolution of GmDofs, MEME analysis identified 20 conserved motifs. Notably, N-terminal regions contained a highly conserved motif-1, and GmDofs within the same subfamily displayed similar motif composition (Figure 3). Most A subfamily members contained motif-1 and motif-14. B1 subfamily members contained motif-1, motif-10, and motif-13. Most B2 subfamily members contained motif-1, motif-17, and motif-20. Most C1 subfamily members contained motif-1 and motif-9.

Most C2.1 subfamily members contained motif-1 and motif-18. C2.2 subfamily members contained motif-1 and motif-6. Most C3 subfamily members contained motif-1 and motif-10. Most D1 subfamily members contained motif-1, motif-2, motif-3, motif-4, motif-5, motif-6, motif-7, motif-8, motif-11, motif-12, motif-16, motif-18, and motif-19. D2 subfamily members only contained motif-1. All GmDofs contained the typical conserved Dof domain, categorized under the zinc finger superfamily, indicating evolutionary conservation of functional domains among GmDofs.

Figure 3. Visualization of motifs, domains, and gene structures of soybean Dof members.

2.5. Collinearity of GmDofs

To further elucidate the potential functions of the *GmDofs*, we analyzed the duplication events giving rise to *GmDofs*. The distribution of *GmDofs* varied among different chromosomes, indicating substantial differences in their chromosomal evolution. The soybean genome carries 110 *GmDof* gene pairs involved in duplication events, which are located on different chromosomes, with the greatest number of *GmDof* homologous gene pairs on chromosome 13 (Figure 4). The findings indicate that gene segmental duplication events may have been the main driving force behind the evolution of *GmDofs*. Furthermore, we calculated the synonymous (Ks) and non-synonymous (Ka) substitution rates (Ka/Ks) of 110 segmentally duplicated pairs (Table S2). The Ka/Ks ratios for segmentally duplicated gene pairs ranged from 0.07 to 0.64, with an average of 0.29, indicating that the *GmDofs* have undergone strong negative purifying selection pressure. Furthermore, the frequency distribution of the Ka/Ks ratios showed that more than 78% of duplicated gene pairs had ratios ranging from 0.1 and 0.3. These results demonstrate the conserved evolution of soybean *Dof* genes.

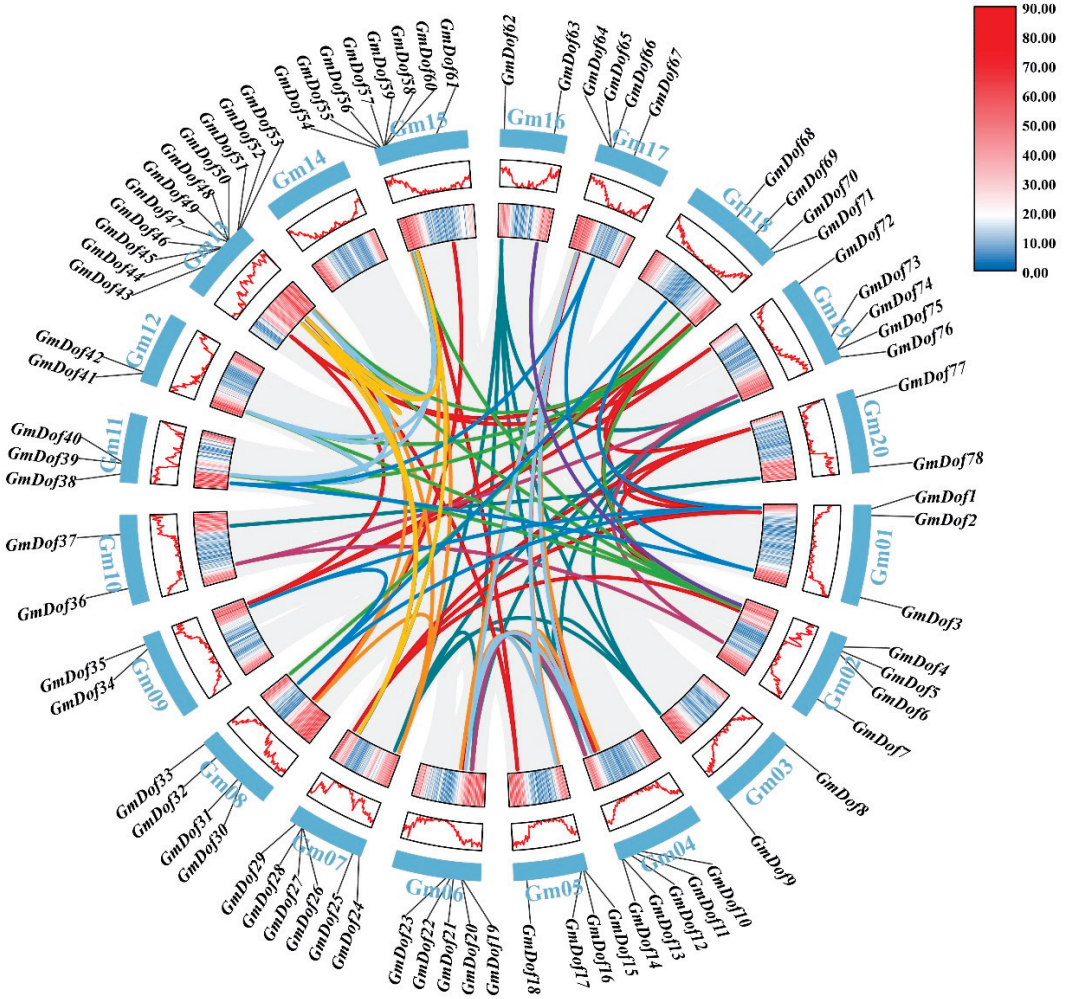

Figure 4. Synteny analysis of interchromosomal relationships of soybean *Dof* members. This curved structure represents chromosomes, and the different colored lines indicate segmental gene pairs.

2.6. Interspecies Collinearity of GmDofs

To further investigate the gene duplications in the *Dof* genes, we analyzed the collinearity of *GmDofs* with the *Dof* genes in other species, including *A. thaliana*, *O. sativa*, *Nicotiana tabacum*, and *S. tuberosum* (Figure 5). The results showed that the collinear gene pairs in rice, a monocot model plant, were significantly fewer than those in dicot genomes. In addition, more genetic overlap was found between soybean and *S. tuberosum* than between soybean and other plants, signifying a closer evolutionary relationship of soybean to *S. tuberosum*.

2.7. Predicted Cis-Acting Elements in the Promoters of GmDofs

In this study, PlantCARE was used to analyze the *cis*-acting elements in the sequence upstream (2 kb) from the start codon of each *GmDof*. The results showed that the responsive elements were widely present in the *Dof* family genes of soybean (Figure 6A). All *cis*-acting elements were classified into four categories according to their functions: stress response, plant growth and development, plant hormone response, and light response (Figure 6B,C). Stress response-related element analysis showed that MYC, a drought-responsive element, was the most numerous (29.35%), and STRE (a stress-responsive element) was the second most numerous element (16.57%). The promoters of 92.30% of *GmDofs* contained the MYC element, and those of 78.21% of *GmDofs* contained the STRE element, suggesting that *GmDofs* played a role in regulating drought and stress responses. Plant growth and development-related element analysis showed that the AAGAA motif, an auxin-responsive

element, was the most numerous (52.76%). The promoters of 87.18% of *GmDofs* contained the AAGAA motif, suggesting that most *GmDofs* played a role in regulating auxin responses. The analysis of plant hormone response-related elements showed that ABRE was the most numerous element (33.12%), which was the ABA-responsive element. The promoters of 83.33% of *GmDofs* contained the ABRE element, suggesting that *GmDofs* played an important role in regulating ABA response. Among the light-responsive elements, the box 4 element was the most numerous (43.69%). The promoters of 97.44% of *GmDofs* contained the box 4 element, suggesting that *GmDofs* played an important role in light response.

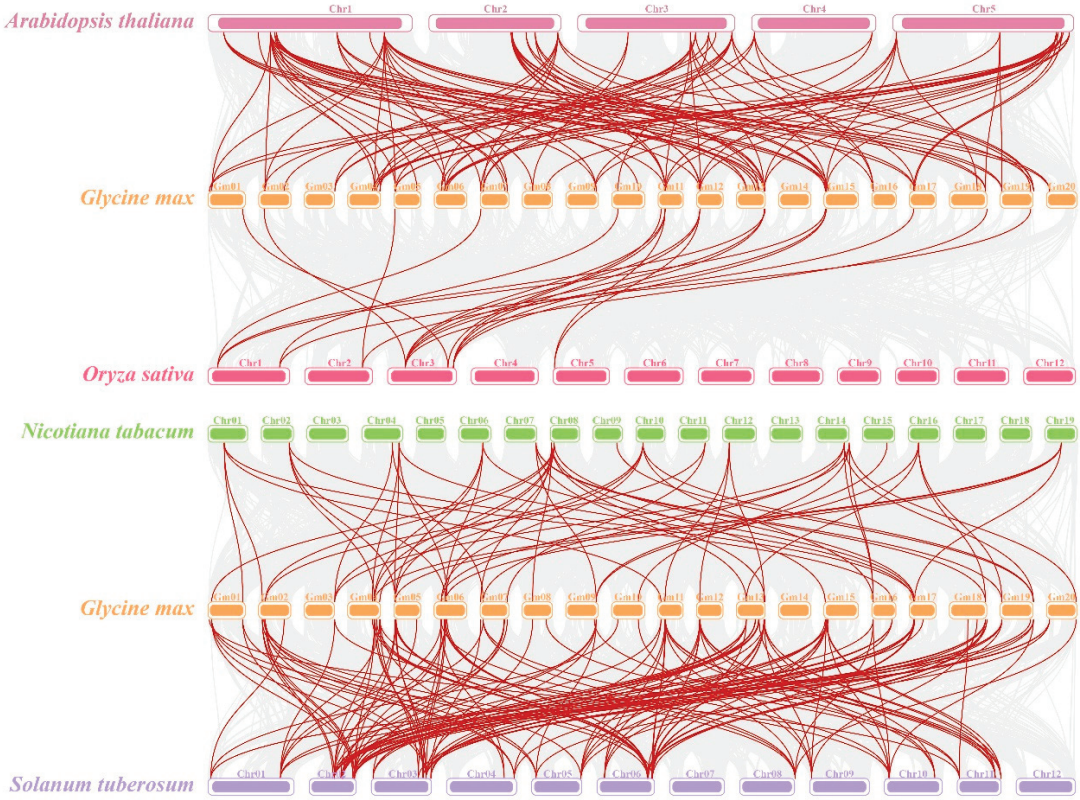

Figure 5. Synteny analysis of *Dof* genes. Each horizontal line represents a chromosome, and the red lines indicate the *Dof* homologous gene pairs.

2.8. Screening of Dof Genes in Soybean After P. sojae Infection

Hypocotyls of JN4507 and JN28 seedlings were inoculated with *P. sojae* isolate PSR01. At 48 h post-inoculation of *P. sojae*, it was observed that the JN28 soybean seedlings remained firm, with only slight browning of the stems, while the JN4507 soybean seedlings exhibited extended lesions, with the entire plant wilting and emitting a foul odor (Figure 7A). The seedling incubation assay demonstrated that JN28 showed a strong immune response against *P. sojae* isolate PSR01, whereas JN4507 was completely susceptible.

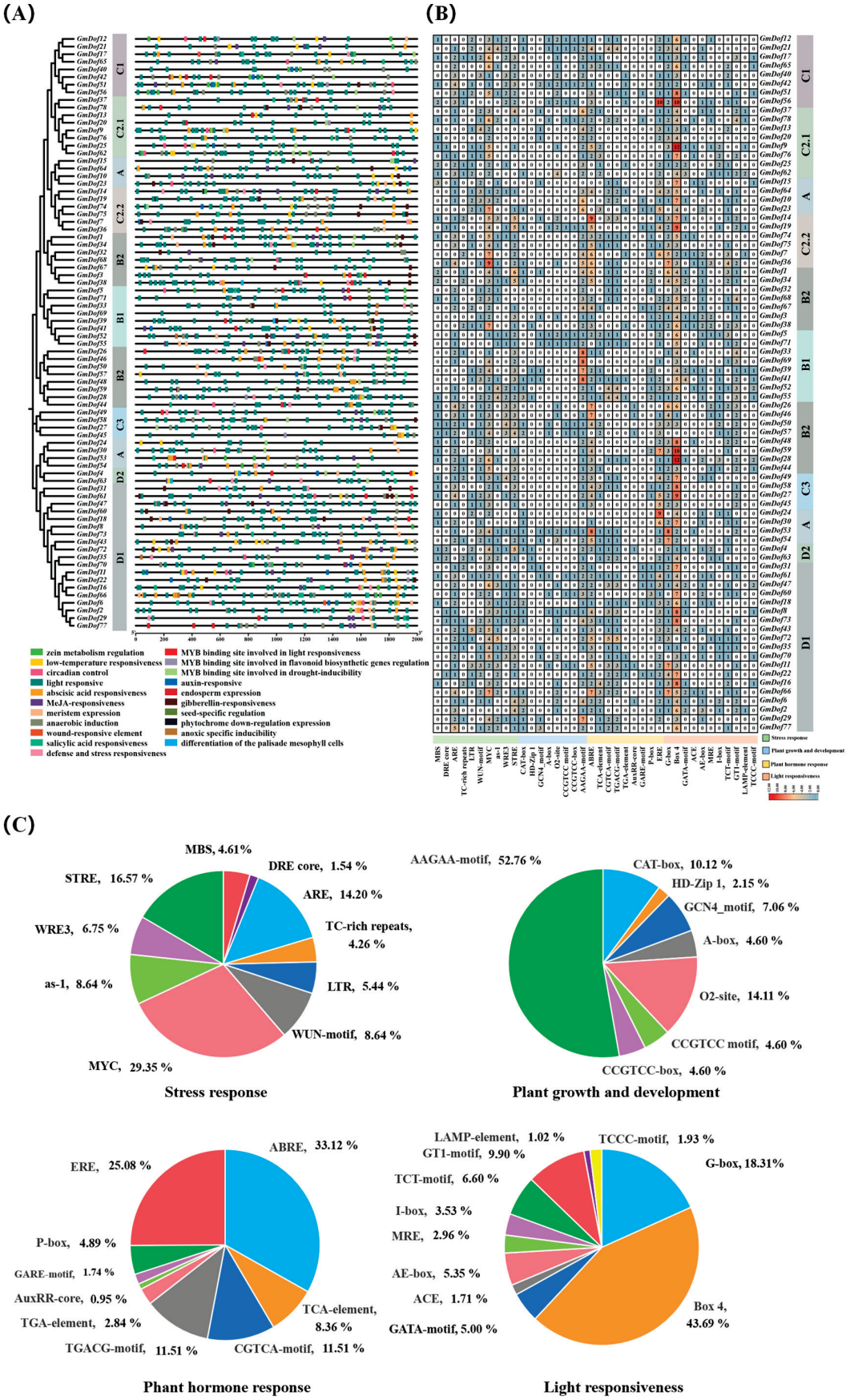

Figure 6. *Cis*-acting elements in the promoters of soybean *Dof* members. (**A**) Variations in different types of *cis*-acting elements. (**B**) Number of *cis*-acting elements. (**C**) Pie charts show the proportion of different *cis*-acting elements in each category.

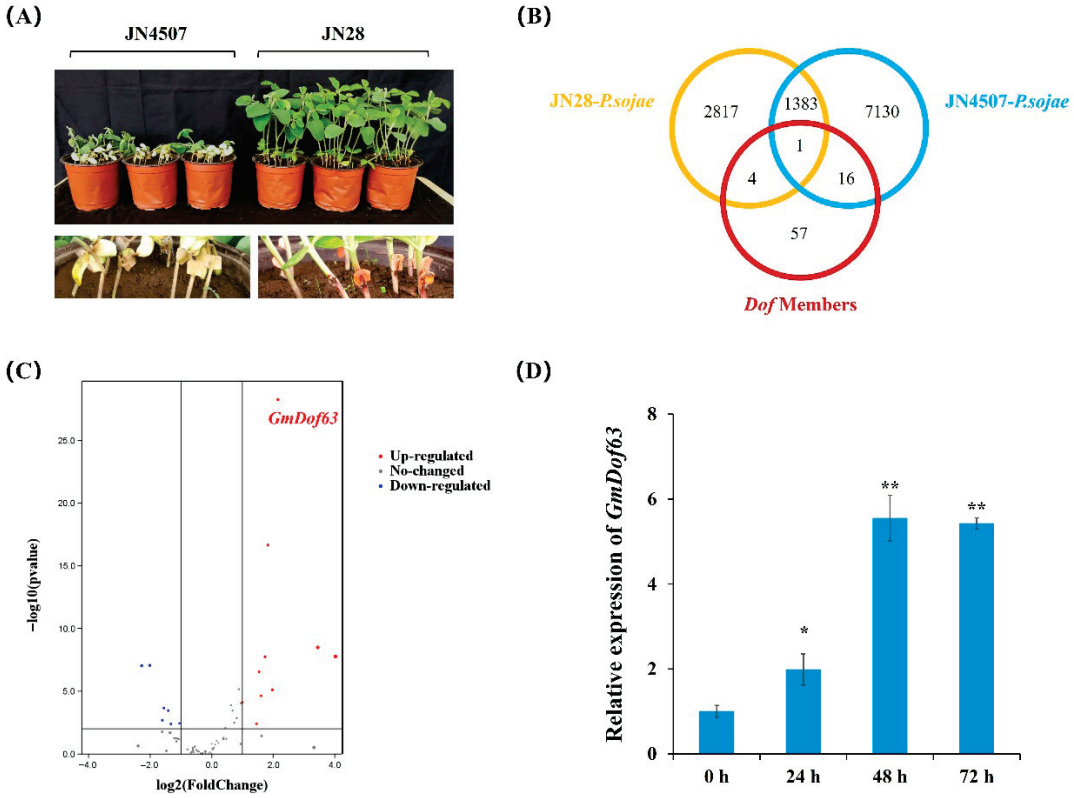

Figure 7. Screening of *Dof* genes in soybean after *P. sojae* infection. (**A**) The phenotypic characteristics of the resistant variety and the susceptible variety after *P. sojae* infection. (**B**) Overlapping between JN28-*P. sojae*, JN4507-*P. sojae* and *Dof* genes. (**C**) Volcano plot of soybean Dof members. (**D**) Expression levels of *GmDof63* in JN28 seedlings during *P. sojae* infection. Three biological replicates were used for each sample, and Student's *t*-test (* $p < 0.05$, ** $p < 0.01$) was conducted to determine statistical significance. Error bars represent ±SD.

To determine whether Dof members control *P. sojae* infection, we profiled the expression of *GmDofs* in soybean seedlings during *P. sojae* infection by RNA sequencing. We collected three replicates of *P. sojae*-treated JN28 and JN4507 samples at 48 h post-inoculation to capture the transcriptional changes during *P. sojae* infection. The control samples were inoculated with an agar block without *P. sojae*. The differentially expressed genes were identified by a pairwise comparison of the transcriptome datasets (JN28-*P.* sojae vs. JN4507-P. *sojae*) (Figure 7B). We further identified the significantly upregulated expression of *GmDof63* (Glyma.13G329000) through the volcano plot (Figure 7C). Quantitative RT-PCR results indicated that the expression of *GmDof63* was upregulated in the highly resistant soybean variety JN28 after *P. sojae* infection ($p < 0.01$), and the accumulation of *GmDof63* peaked at 48 h post-inoculation (Figure 7D). These results indicated that *GmDof63* was a potentially crucial gene in soybean during *P. sojae* infection.

2.9. Sequence Characteristics and Expression Pattern of GmDof63

To study *GmDof63* expression, we first cloned the complete sequence of *GmDof63* from JN28 using the RT-PCR technique, which contained a 711 bp open reading frame that encodes a 236-amino acid protein with the zinc finger domain $CX_2CX_{21}CX_2C$ (Figure 8A). We further explored the expression pattern of *GmDof63* in soybean under different stresses. As shown in Figure 8B, the expression of *GmDof63* was significantly upregulated at 6 h and reached a peak at 24 h after SA treatment, and the expression of *GmDof63* was significantly upregulated at 24 h and reached a peak at 24 h after ETH treatment, but the expression

level of the *GmDof63* did not show any significant change after treatment with MeJA and ABA. The results suggested that *GmDof63* participates in multiple signaling pathways.

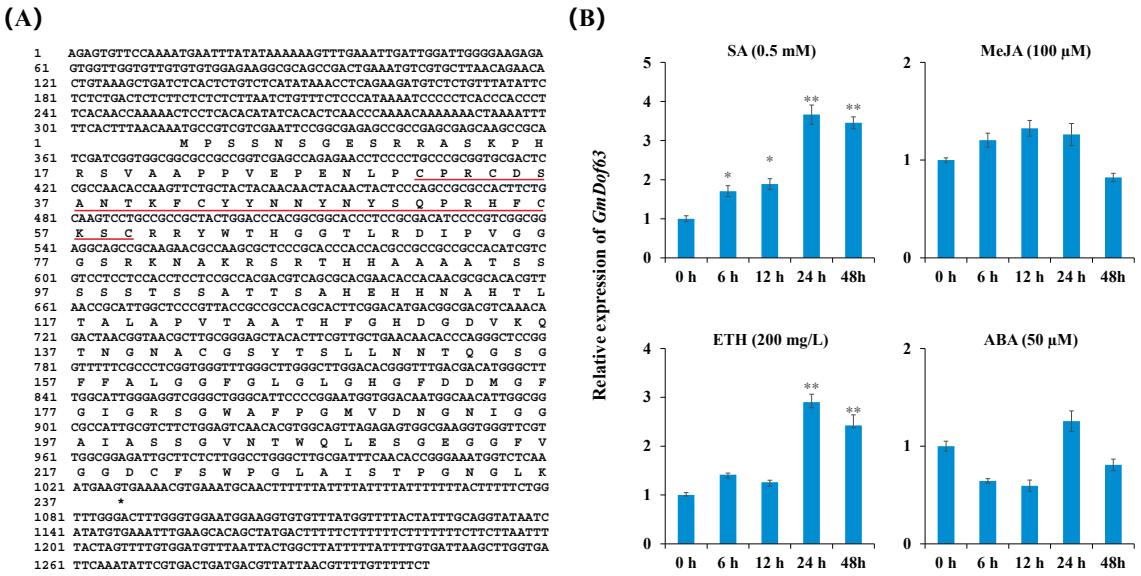

Figure 8. Sequence characteristics and expression pattern of *GmDof63*. (**A**) The *GmDof63* gene sequence and the GmDof63 protein sequence. The zinc finger domain $CX_2CX_{21}CX_2C$ are underlined in red. (**B**) Expression pattern of *GmDof63* in soybean under different stresses. The various treatments were the 0.5 mM SA treatment, 100 μM MeJA treatment, 200 mg/L ETH treatment and 50 μM ABA treatment. Three biological replicates were used for each sample, and Student's *t*-test (* $p < 0.05$, ** $p < 0.01$) was performed to determine statistical significance. Error bars represent ±SD.

2.10. Subcellular Localization of GmDof63

To investigate the subcellular localization of GmDof63, 35S::GFP vector or 35S:: GmDof63-GFP vector (Figure 9A) was transformed into Arabidopsis mesophyll protoplasts. H2B-mCherry was chosen as the nuclear marker protein, which can encode histone H2B fused with the red fluorescent protein mCherry. As can be seen from Figure 9B, the transformed cells carrying 35S::GFP showed a strong green fluorescence signal throughout the entire cell, whereas the transformed cells carrying 35S::GmDof63-GFP showed a strong green fluorescence signal only in the nucleus, and this finding was consistent with the location of the nuclear marker protein H2B-mCherry. These results suggested that GmDof63 is a nucleus-localized transcription factor.

2.11. GmDof63 Enhances Resistance of Transgenic Soybean Seedlings to P. sojae

We next focused on the function of *GmDof63*. To confirm the functions of *GmDof63* in soybean response to *P. sojae*, we constructed a *GmDof63*-overexpressing vector 35S::*GmDof63* with BAR as the selective marker (Figure 10A). We then used an efficient *Agrobacterium*-mediated transformation system described by Paz et al. (2004) [42] and Li et al. (2017) [43] to generate *GmDof63*-overexpressing transgenic soybean seedlings. In the T0 and T2 generations, the transgenic soybean seedlings were verified by the BAR LibertyLink strip (Envirologix, Portland, OR, USA) (Figure S1). Three lines of positive transgenic soybean seedlings were inoculated with *P. sojae* zoospores in a hydroponic assay. The zoospore suspension was prepared according to the method described by Shrestha et al. (2016) [44] and Yang et al. (2021) [45]. Under standard culture conditions, no significant differences in leaf phenotype were observed between transgenic and WT plants. However, the WT soybean roots exhibited extended lesions, browning, and wilting, while the *GmDof63*-overexpressing soybean roots remained firm with only slight browning (Figure 10B). Quantitative RT-PCR

results showed that the expression of *GmDof63* in *GmDof63*-overexpressing soybean roots was higher than that of WT soybean roots at 48 h post-inoculation (Figure 10C). The relative accumulation of *P. sojae* was significantly lower in *GmDof63*-overexpressing soybean roots than in WT soybean roots at 48 h post-inoculation (Figure 10D). The above results indicated that the *GmDof63*-overexpressing transgenic soybean seedlings displayed enhanced resistance to *P. sojae* infection compared with the WT soybean seedlings.

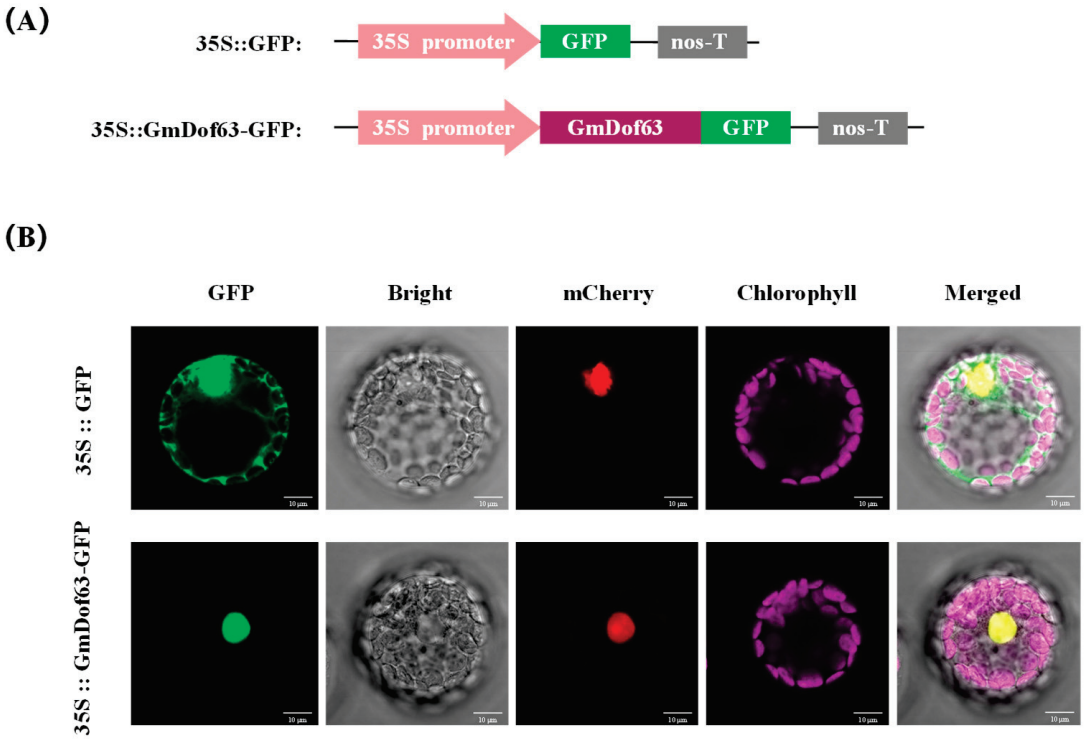

Figure 9. Subcellular location of GmDof63 in the Arabidopsis mesophyll protoplasts. (**A**) Construction of 35S::GFP vector and 35S::GmDof63-GFP vector. (**B**) 35S::GFP vector or 35S::GmDof63-GFP vector was transiently expressed in the Arabidopsis mesophyll protoplasts, respectively. The green fluorescence signal indicates the 35S::GmDof63-GFP or 35S::GFP protein, and the red fluorescence signal indicates the nuclear marker protein H2B-mCherry, and the fluorescence signals were observed under a confocal microscope. Scale bars = 10 μm.

Pathogenesis-related (*PR*) genes are some of the most important genes in the defense response of plants against pathogens [46–49]. To test whether GmDof63 can regulate the expression of *PR* genes, we performed quantitative RT-PCR analysis in roots of *GmDof63*-overexpressing and WT soybean at 48 h post-inoculation. The expression of *PR1a*, *PR4*, *PR5a*, or *PR10* in *GmDof63*-overexpressing soybean roots was higher than that of WT soybean roots (Figure 10E). Previous research has revealed that Dof proteins often recognize the AAAG or TTTC motif in their target promoters [50–52], so we analyzed the AAAG or TTTC motif in the promoter sequence of the *PR* genes. The result showed that a large number of AAAG or TTTC motifs were present in the promoter sequence of *PR1a*, *PR4*, *PR5a*, and *PR10* (Figure S2), indicating that *GmDof63* may directly or indirectly regulate the expression of *PR* genes to modulate the soybean response to *P. sojae* infection.

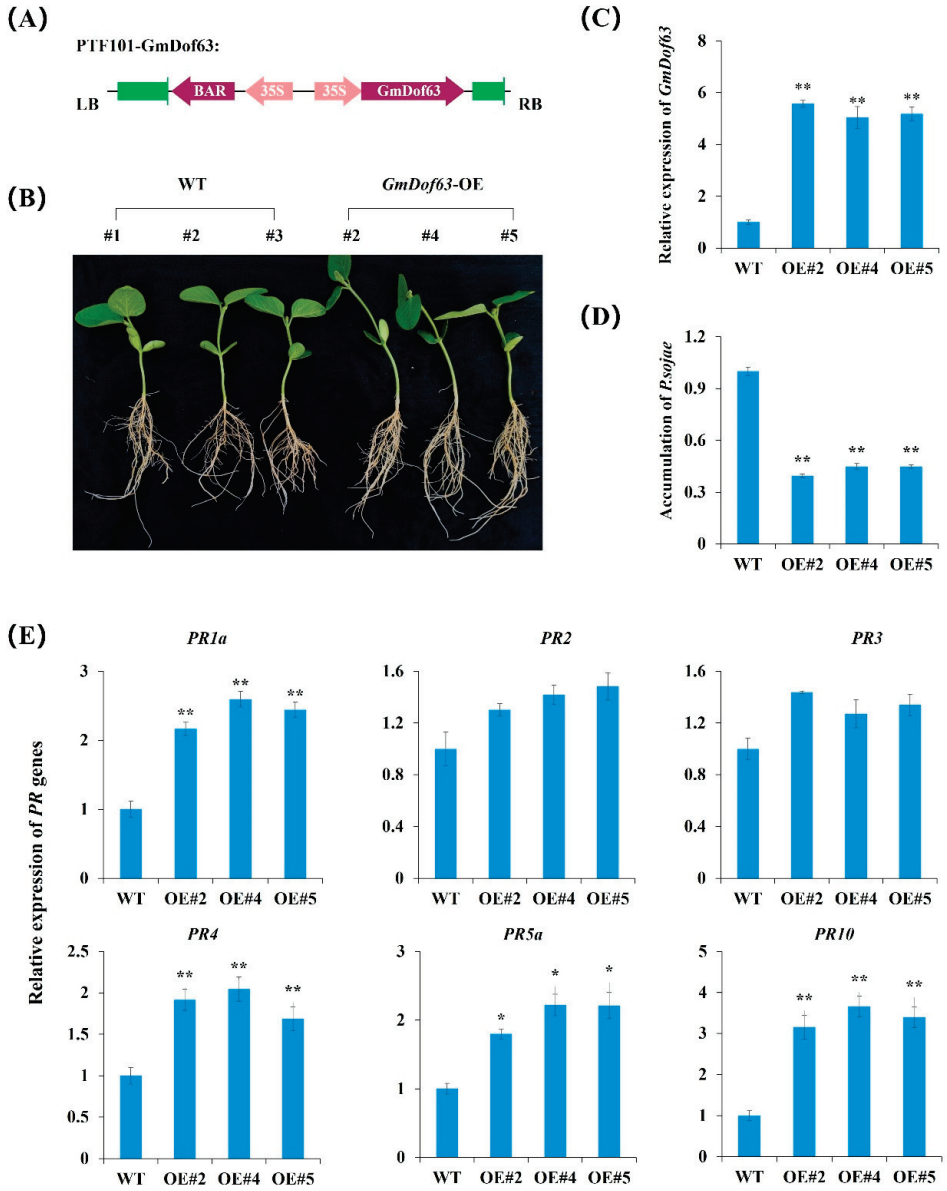

Figure 10. *GmDof63* enhances soybean resistance to *P. sojae*. (**A**) Construction of *GmDof63*-overexpressing vector 35S::*GmDof63*. (**B**) Phenotypes of WT and *GmDof63*-overexpressing transgenic soybean seedlings treated with *P. sojae* for 48 h in the soybean root hydroponic assay. (**C**) Relative expression levels of *GmDof63* in WT and *GmDof63*-overexpressing transgenic soybean seedlings at 48 h post-inoculation. (**D**) Accumulation of *P. sojae* in WT and *GmDof63*-overexpressing transgenic soybean seedlings at 48 h post-inoculation. The relative accumulation of *P. sojae* in roots was measured based on the relative expression of *P. sojae* housekeeping gene *PsACT* (XM_009530461.1) to soybean housekeeping gene *GmActin* (Glyma.18G290800.1) ($\Delta Ct = Ct_{HK\ of\ P.\ sojae} - Ct_{HK\ of\ soybean}$). (**E**) Relative expression levels of *PR1a* (AF136636), *PR2* (M37753), *PR3* (AF202731), *PR4* (BT090788), *PR5a* (M21297), *PR10* (FJ960440) in *GmDof63*-overexpressing transgenic soybean seedlings were compared with those in WT. WT, wild type. Three biological replicates were used for each sample, and Student's *t*-test (* $p < 0.05$, ** $p < 0.01$) was performed to determine statistical significance. Error bars represent ±SD.

3. Discussion

The Dof family is a type of plant-specific TFs belonging to the single zinc finger protein superfamily. With the development of bioinformatics, since the first *Dof* gene was cloned from maize, the *Dof* gene family has been deeply identified and analyzed in plants such as Arabidopsis, rice, maize, potato and sweet pepper [23,53]. However, the research on

Dof genes in soybean is still limited, and there are few reports on the roles of *Dof* genes in response to *P. sojae* infection.

In this study, we identified 78 members of the Dof family in soybean and analyzed their physicochemical properties, chromosomal localization, evolutionary relationships, gene structures, intraspecies and interspecies collinearity, and promoter elements. Subcellular localization is an important characteristic of proteins, and protein function is closely related to protein localization [54,55]. For example, proteins in the cell nucleus mainly participate in gene transcription and DNA repair [56]. In this study, the subcellular localization prediction showed that 75, 1, and 2 GmDofs were located in the cell nucleus, cytoplasm, and chloroplast, respectively.

Motif, conserved domain, and gene structure prediction indicated that all GmDofs contained a common motif (motif-1), suggesting that this motif may play a key role. The diversity of motifs among different Dof members may be related to their complex functions. Different gene families have their own conserved domains. All GmDofs had a complete C_2-C_2 single-finger zinc structure, which was consistent with the research results of Wu et al. (2019) [57] and Luo et al. (2022) [58]. Gene structure analysis showed that all *GmDofs* had 0 to 2 introns, and most of them did not have introns. This feature indicated that the gene structure of *GmDofs* was conserved.

The evolution and expansion of gene families are closely related to gene duplication. The occurrence of gene duplication may be due to fragment duplication, tandem duplication or whole-genome duplication [59,60]. Some duplicated genes may retain similar functions and show partial or complete divergence from each other [61]. Many TF families in plants have undergone gene duplication events [62]. In this study, we discovered that *GmDofs* were unevenly distributed on chromosomes other than chromosome 14. Homology analysis showed that the soybean genome contained 110 pairs of *Dof* homologous genes, all of which originated from fragment duplication, indicating that fragment replication may have played a dominant role in the evolution and expansion of the *GmDof* family. In addition, the Ka/Ks values of 110 pairs of *Dof* homologous genes were all less than 1, indicating that the *Dof* genes have undergone purifying selection during long-term evolution. Interspecies collinearity showed that the number of co-linear *Dof* gene pairs of soybean with monocotyledonous model plants such as rice was significantly lower than that with dicotyledonous plants such as *A. thaliana*, *O. sativa*, *N. tabacum* and *S. tuberosum*, and the gene overlap with *S. tuberosum* was the most, indicating a closer evolutionary relationship with *S. tuberosum*.

Dof TFs play a significant role in regulating plant growth and development, stress responses, and plant hormone signal transduction [63–67]. Studies have shown that *cis*-acting elements are involved in the responses to various environmental stresses [68–71]. The MYC and STRE elements play an important role in stress responses. The AAGAA-motif element is involved in plant responses to environmental stresses. ABRE played an important role in regulating ABA response. The Box 4 element acts as a photosensitive element, participating in the plant response to light conditions. We can further understand the functions of *GmDofs* by analyzing the *cis*-acting elements of the promoters of *GmDofs*. The most common *cis*-acting elements predicted in the promoter region of *GmDofs* contained MYC, STRE, AAGAA-motif, ABRE, and Box 4 elements. Therefore, *GmDofs* play a crucial role in plant growth and development, stress responses, and plant hormone signal transduction.

Phytophthora root and stem rot, a devastating disease caused by *P. sojae*, has caused serious losses to soybean production worldwide. Studies have confirmed that there are extensive genetic variations (including those conferring disease resistance) in major crops, providing an opportunity to utilize these variations to enhance the soybean response to *P. sojae*. For example, miR393 and miR166 have been found to play a crucial role in respond-

ing to *P. sojae* infection [72]. Overexpression of the bHLH transcription factor *GmPIB1* can enhance resistance to *P. sojae* [73]. The zinc finger protein-type TF GmZFP03 boosts the resistance to *P. sojae* by targeting the promoters of two *SOD1* genes and activating their expression [74]. GmCAT1 can slightly cause cell death in Arabidopsis and promote the development of *P. sojae*, and the interaction between PsAvh113-GmDPB-GmCAT1 may be a potential defense mechanism that is conducive to the infection of *P. sojae* [75]. However, the natural variations in *Dof* genes have not been examined in soybeans responding to *P. sojae* infection. Here, we identified one *Dof* gene, *GmDof63*, in soybean via RNA sequencing, which exhibited an upregulated expression in the resistant materials. The function of *GmDof63* was verified through genetic transformation. The *GmDof63*-overexpressing transgenic soybean seedlings demonstrate enhanced resistance to *P. sojae*. Quantitative RT-PCR results showed that the expression level of *GmDof63* significantly increased in *GmDof63*-overexpressing transgenic soybean after *P. sojae* infection, and the relative accumulation of *P. sojae* was significantly lower in *GmDof63*-overexpressing transgenic soybean than in WT soybean, further indicating that this gene played a role in the response to *P. sojae* infection.

Much research has shown that Dof TFs play a key role in mediating plant hormone pathways [38–41,76]. We discovered the similar research result that the transcription level of *GmDof63* in soybean seedlings was significantly induced after spraying SA and ETH. Previous studies have shown that transcription factors can specifically bind to the promoters of *PR* genes to regulate their expression, thereby responding to pathogen infection [77,78]. In this study, the expression levels of *PR1a*, *PR4*, *PR5a* and *PR10* were significantly upregulated in *GmDof63*-overexpressing transgenic soybean seedlings, and a large number of AAAG or TTTC motifs were present in the promoter sequence of *PR1a*, *PR4*, *PR5a*, and *PR10*, so we speculated that *GmDof63* may directly or indirectly regulate the expression of these *PR* genes. Furthermore, previous research has also revealed that *PRs* usually function as effector genes for systemic acquired resistance (SAR), and this resistance is mediated by SA [79,80]. So, we speculate that the high expression levels of *PR* genes indicate the activation of the SA signaling pathway. Taken together, these findings suggested that *GmDof63* may serve as a key regulatory center for the SA and ETH signaling pathways, integrating these pathways to cope with *P. sojae* infection.

In the follow-up work, the phenotypes of *GmDof63*-overexpressing transgenic soybean and the expression levels of *GmDof63* and *PRs* will be evaluated at multiple time points after *P. sojae* infection, which could offer a more detailed understanding of the temporal dynamics of the defense response. Now, the functional verification of *GmDofs* in response to *P. sojae* infection can not only reveal the molecular mechanism underpinning the soybean response to pathogen infection but also provide direct molecular markers and candidate genes for the breeding of new varieties with specific disease resistance traits, demonstrating promising application prospects.

4. Materials and Methods

4.1. Identification of Dof Members in Soybean Genome

The soybean Wm82.a4.v1 genome was downloaded from the Soybase database (https://www.soybase.org/ (accessed on 12 April 2023)) for the identification of *Dof* genes. The nucleotide and protein sequences of Dof family members of *A. thaliana* were downloaded from TAIR (https://www.arabidopsis.org/ (accessed on 12 April 2023)), and the nucleotide and protein sequences of Dof family members of *O. sativa* were downloaded from the Rice Genome Annotation Project (http://rice.uga.edu/ (accessed on 12 April 2023)). The Hidden Markov Model file corresponding to the Dof domain (PF02701) was downloaded from the Pfam database (http://pfam.xfam.org/ (accessed on 13 April 2023)). Dof

members were searched from the soybean database via HMMER 3.0 (http://hmmer.org/ (accessed on 15 April 2023)). The BLASTp v2.12.0 tool was used to compare these sequences against the acquired Dof protein sequences of *O. sativa* and *A. thaliana*, and the genes with E-values $\leq 1 \times 10^{-5}$ were retained. These collected putative Dof members were confirmed by the Pfam (http://pfam.sanger.ac.uk/ (accessed on 15 April 2023)) and InterPro (https://www.ebi.ac.uk/interpro/ (accessed on 15 April 2023)) databases. The longest CDS transcript in the same gene was selected as the representative sequence.

4.2. Physicochemical Characterization of Soybean Dof Members

The physicochemical properties of the predicted proteins of soybean *Dof* genes were calculated via the ProtParam tool (https://web.expasy.org/protparam/ (accessed on 26 April 2023)), including amino acid sequence length, theoretical isoelectric point (pI), molecular weight, instability index, aliphatic index, and grand average of hydropathicity. The subcellular localization of the soybean Dof members was predicted by Wolf Psort online (https://wolfpsort.hgc.jp/ (accessed on 18 May 2023)), and the top predicted position was selected as the result.

4.3. Chromosomal Location Analysis of Soybean Dof Members

Gene Location Visualize from GTF/GFF module in Tbtools v2.310 software was used to map all non-redundant soybean *Dof* genes on the 20 soybean chromosomes on the basis of the information in the soybean database.

4.4. Phylogenetic Analysis of Soybean Dof Members

The amino acid sequences of Dof members from soybean and Arabidopsis were selected for phylogenetic analysis. ClustalW and ClustalX with default parameters were used for multiple sequence alignment. The phylogenetic tree was constructed by the Maximum likelihood (ML) method in MEGA12 software, with the Bootstrap value set at 1000. Subsequently, iTOL (https://itol.embl.de/ (accessed on 23 April 2023)) was used for visualization and beautification of the phylogenetic tree.

4.5. Gene Structure and Motif Analysis of Soybean Dof Members

The structure of soybean *Dof* genes, including cDNA sequences and the corresponding genomic DNA sequences, was extracted from the soybean genome annotation file. Finally, TBtools v2.310 was used for visualization analysis. Online MEME (http://www.OMIcsclass.com/article/67 (accessed on 19 May 2023)) was employed to analyze the motif structure of soybean Dof members, with the maximum number, minimum width, and maximum width of motifs set at 20, 6, and 50, respectively.

4.6. Analysis of Collinearity and KaKs of Soybean Dof Members

The genome sequences and annotation files of Arabidopsis (TAIR10.55) and rice (v7.0) were downloaded from the Phytozome v13 website (https://phytozome-next.jgi.doe.gov/ (accessed on 23 May 2023)). The genome sequences and annotation files of tobacco (Niben261) were downloaded from the Sol Genomics Network database (https://solgenomics.net/ (accessed on 23 May 2023)). The genome sequences and annotation files of potato (SolTub_3.0) were downloaded from the Ensemble Plants database (https://plants.ensembl.org/index.html (accessed on 23 May 2023)). The MCScanX program was used to analyze the collinearity of *Dof* members in soybean with those in Arabidopsis, rice, tobacco, and potato. The syntenic relationships within *Dof* members of soybean were visualized using the TBtools software. The non-synonymous/synonymous substitution rate (Ka/Ks) is an important indicator for measuring the selection pressure on gene evolution. TBtools software was used to visualize and analyze the Ka/Ks results (Ka/Ks < 1 indi-

cates purifying selection, Ka/Ks = 1 indicates neutral evolution, and Ka/Ks > 1 indicates positive selection).

4.7. Prediction of Cis-Acting Elements of Soybean Dof Members

The 2000 bp sequence upstream of each soybean *Dof* member was downloaded from the Phytozome v13 website. The sequences were analyzed via the CARE search tool in the PlantCARE database (http://bioinformatics.psb.ugent.be/webtools/plantcare/html (accessed on 26 May 2023)). The *cis*-acting elements were visualized and summarized by the Basic Biosequence View and HeatMap modules in TBtools.

4.8. Plant Materials and Pathogen Strain

Jinong 4507 (JN4507) is a soybean variety susceptible to *P. sojae* infection. The high-yield variety Jinong 28 (JN28), developed by the Plant Biotechnology Center of the Jilin Agricultural University, is resistant to *P. sojae* infection. The special variety Dongnong 50 (DN50), developed by the College of Agriculture of the Northeast Agricultural University, is susceptible to *P. sojae* infection. In this study, JN28 was used for gene isolation, and DN50 was used for soybean transformation. Soybean seedlings were grown in a greenhouse with vermiculite as the growth medium. The seedlings were cultivated under a photoperiod of 16L/8D, 25 °C, and the relative humidity of 70%.

P. sojae race 1 (PSR01), a dominant race in Jilin Province, was kindly provided by Professor Shuzhen Zhang from Northeast Agricultural University. PSR01 was cultured on V8 juice agar in a polystyrene dish and activated by incubation at 22–25 °C.

4.9. Resistance Identification, RNA Extraction, and Transcriptome Sequencing

To examine the phenotypes of JN4507 and JN28 in response to *P. sojae* infection, we used a sterile scalpel to inoculate the agar plugs covered by mycelia (2 cm × 2 cm) on wounded hypocotyls of 14-day-old soybean seedlings. The inoculum was prepared from 7-day-old fungal cultures grown on V8 juice agar. We extracted total RNA from the inoculation point of soybean seedlings with Trizol reagent (Sangon Biotech, Shanghai, China). RNA quality was determined by the Qubit2.0 RNA test kit (Thermo-Life, Waltham, MA, USA). A high-quality RNA sample (OD260/280 of 1.8 to 2.2, OD260/230 $\geq$ 2.0, RIN $\geq$ 6.5, 28S:18S $\geq$ 1.0, >10 μg) was used to construct the sequencing library. The transcriptome sequencing work was carried out by Sangon Biotech.

4.10. Quantitative RT-PCR

One Step RT-PCR Kit (Code No. PCR-311, TOYOBO, Tokyo, Japan) was used for standard expression determination, and the specific primers for the target genes and housekeeping genes were designed with Primer 5 software. The reaction procedure was described as follows: 95 °C for 30 s; followed by 40 cycles of 95 °C for 5 s, 60 °C for 15 s, and 72 °C for 45 s. The relative expression levels were calculated by the $2^{-\Delta\Delta CT}$ method. *GmActin* (Glyma.18G290800.1) was used as the internal control.

4.11. Primer Sequences Used in the Present Study

The specific primers used for all assays are listed in Table S3.

5. Conclusions

A total of 78 soybean *Dof* genes were identified and phylogenetically divided into 9 subfamilies. Gene structure analysis showed that all *GmDofs* contained 0 to 2 introns, and most of them did not have introns. Motif and conserved domain analysis showed that all GmDofs contained a common motif (motif-1) and a typical conserved C_2-C_2 domain. Investigations into CREs indicated the presence of various stress-responsive, plant growth

and development, hormone-responsive, and light-responsive regulatory elements in the promoter region of *GmDofs*. Subsequently, RNA-seq and qRT-PCR results showed that *GmDof63* was specifically expressed at high levels after *P. sojae* infection. *GmDof63* was strongly induced by SA and ETH treatments. *GmDof63* enhanced resistance to *P. sojae* infection in *GmDof63*-overexpressing transgenic soybean seedlings. Furthermore, the expression levels of *PR* genes *PR1a*, *PR4*, *PR5a*, and *PR10* were significantly up-regulated in *GmDof63*-overexpressing transgenic soybean seedlings. Our study provides a basis for further research on the functions of soybean *Dof* family members in biotic stress tolerance.

Supplementary Materials: The following supporting information can be downloaded at: https://www.mdpi.com/article/10.3390/plants14233621/s1, Table S1: Detailed information of all identified soybean Dof members; Table S2: Segmental duplication of *GmDofs* among *Glycine max* chromosomes; Table S3: Oligonucleotide primers used in this study; Table S4: Source data underlying the graphs presented in the main figures. Figure S1: Detection of the T0 and T2 transgenic plants with PAT/Bar LibertyLink strips. Figure S2: The AAAG or TTTC motif in the promoter sequence of *PR1a*, *PR4*, *PR5a*, and *PR10*.

Author Contributions: Conceptualization, S.F.; Data curation, H.C.; Formal analysis, H.C.; Funding acquisition, Z.Z. and S.F.; Investigation, Y.H.; Methodology, H.C.; Project administration, S.F.; Resources, Y.H.; Software, H.C.; Supervision, P.W.; Validation, Z.Z.; Visualization, Y.S.; Writing—original draft, S.F.; Writing—review and editing, L.J. All authors have read and agreed to the published version of the manuscript.

Funding: This research was funded by Key Agricultural Technology Research and Development Program of Jilin Province (20240303011NC), Science and Technology Research Program of the Jilin Provincial Department of Education (JJKH20240437KJ) and Science and Technology Development Plan Project of Jilin Province (20220101340JC).

Data Availability Statement: Data are contained within the article and Supplementary Materials.

Acknowledgments: We would like to thank Shuzhen Zhang and her team (Soybean Research Institute, Key Laboratory of Soybean Biology of Chinese Education Ministry, Northeast Agricultural University, Harbin, China) for providing the *Phytophthora sojae* race 1 strain used in this study.

Conflicts of Interest: The authors declare no conflicts of interest.

References

1. Schmitthenner, A.F. Problems and progress in control of *Phytophthora* root rot of soybean. *Plant Dis.* **1985**, *69*, 362–368. [CrossRef]
2. Anderson, T.R.; Buzzell, R.I. Diversity and frequency of races of *Phytophthora megasperma* f. sp. *glycinea* in soybean fields in Essex County, Ontario, 1980–1989. *Plant Dis.* **1992**, *76*, 587–589. [CrossRef]
3. Tyler, B.M. *Phytophthora sojae*: Root rot pathogen of soybean and model oomycete. *Mol. Plant Pathol.* **2007**, *8*, 1–8. [CrossRef]
4. Chang, K.F.; Hwang, S.F.; Ahmed, H.U.; Zhou, Q.; Strelkov, S.E.; Conner, R.L.; McLaren, D.L.; Henriquez, M.A.; Harding, M.W.; Turnbull, G.D. First report of *Phytophthora sojae* causing root rot in soybean [*Glycine max* (L.) Merr.] in Alberta, Canada. *Crop Prot.* **2017**, *91*, 49–56. [CrossRef]
5. Demirbas, A.; Rector, B.G.; Lohnes, D.G.; Fioritto, R.J.; Graef, G.L.; Cregan, P.B.; Shoemarker, R.C.; Specht, J.E. Simple sequence repeat markers linked to the soybean *Rps* genes for Phytophthora resistance. *Crop Sci.* **2001**, *41*, 1220–1227. [CrossRef]
6. Burnham, K.D.; Dorrance, A.E.; Francis, D.M. *Rps8*, a new locus in soybean for resistance to *Phytophthora sojae*. *Crop Sci.* **2003**, *43*, 101–110. [CrossRef]
7. Ping, J.; Fitzgerald, J.C.; Zhang, C.; Lin, F.; Bai, Y.; Wang, D.; Aggarwal, R.; Rehman, M.; Crasta, O.; Ma, J. Identification and molecular mapping of *Rps11*, a novel gene conferring resistance to *Phytophthora sojae* in soybean. *Theor. Appl. Genet.* **2016**, *129*, 445–451. [CrossRef]
8. Zou, X.; Sun, H. DOF transcription factors: Specific regulators of plant biological processes. *Front. Plant Sci.* **2023**, *14*, 1044918. [CrossRef]
9. Liu, J.; Jin, Y.; Wu, Y.S.; Liu, Y.; Wang, W.b.; Ren, S.S.; Diao, S.F.; Chen, Y.L. Advances on the structural characteristics and function of *Dof* gene in plant. *Biotechnol. Bull.* **2020**, *36*, 180–219. [CrossRef]

10. Wang, T.; Yue, J.J.; Wang, X.J.; Xu, L.; Li, L.B.; Gu, X.P. Genome-wide identification and characterization of the *Dof* gene family in moso bamboo (*Phyllostachys heterocycla* var. *Pubescens*). *Genes Genom.* **2016**, *38*, 733–745. [CrossRef]
11. Lijavetzky, D.; Carbonero, P.; Vicente-Carbajosa, J. Genome-wide comparative phylogenetic analysis of the rice and Arabidopsis *Dof* gene families. *BMC Evol. Biol.* **2003**, *3*, 17. [CrossRef]
12. Gou, C.; Zhang, G.; Deng, Z.; Lin, C.; Li, H.; Liu, H.; Fang, X. Genome-wide analysis of the DNA-binding with one finger gene family reveals soybean expression pattern and functional analysis. *Int. J. Mol. Sci.* **2025**, *26*, 6192. [CrossRef]
13. Yanagisawa, S.; Izui, K. Molecular cloning of two DNA-binding proteins of maize that are structurally different but interact with the same sequence motif. *J. Biol. Chem.* **1993**, *268*, 16028–16036. [CrossRef] [PubMed]
14. Venkatesh, J.; Park, S.W. Genome-wide analysis and expression profiling of DNA-binding with one zinc finger (Dof) transcription factor family in potato. *Plant Physiol. Biochem.* **2015**, *94*, 73–85. [CrossRef]
15. Chen, M.; Liu, X.; Huan, L.; Sun, M.; Liu, L.; Chen, X.; Gao, D.; Li, L. Genome-wide analysis of *Dof* family genes and their expression during bud dormancy in peach (*Prunus persica*). *Sci. Hortic.* **2017**, *214*, 18–26. [CrossRef]
16. Wu, Z.; Cheng, J.; Cui, J.; Xu, X.; Liang, G.; Luo, X.; Chen, X.; Tang, X.; Hu, K.; Qin, C. Genome-wide identification and expression profile of *Dof* transcription factor gene family in pepper (*Capsicum annuum* L.). *Front. Plant Sci.* **2016**, *7*, 574. [CrossRef] [PubMed]
17. Gupta, S.; Malviya, N.; Kushwaha, H.; Nasim, J.; Bisht, N.C.; Singh, V.K.; Yadav, D. Insights into structural and functional diversity of Dof (DNA binding with one finger) transcription factor. *Planta* **2015**, *241*, 549–562. [CrossRef]
18. Li, S.; Zhang, W.; Si, C.; Chen, J.; Huang, Y.; Li, M.; Liang, H.; Duan, J.; He, C. Genome-Wide identification and functional characterization of the Dof family in *Dendrobium officinale*. *Int. J. Mol. Sci.* **2025**, *26*, 2671. [CrossRef]
19. Wang, Y.; Wang, H.; Li, W.; Dai, G.; Chen, J. Genome-wide identification and expression analysis of the LbDof transcription factor family genes in *Lycium barbarum*. *Plants* **2025**, *14*, 1567. [CrossRef]
20. Wang, P.; Wang, D.; Li, Y.; Li, J.; Liu, B.; Wang, Y.; Gao, C. The transcription factor ThDOF8 binds to a novel *cis*-element and mediates molecular responses to salt stress in *Tamarix hispida*. *J. Exp. Bot.* **2024**, *75*, 3171–3187. [CrossRef]
21. Zhao, C.; Bai, H.; Li, C.; Pang, Z.; Xuan, L.; Lv, D.; Niu, S. Genome-wide identification of the *Dof* gene family in Kiwifruit (*Actinidia chinensis*) and functional validation of AcDOF22 in response to drought stress. *Int. J. Mol. Sci.* **2024**, *25*, 9103. [CrossRef]
22. Dai, J.; Wu, Y.; Liu, J.; Wei, L.; Zeng, Y.; Liu, S.; Zhang, J.; Liu, G.; Huang, G. Genome-wide identification and expression analysis of *Dof* gene family members in mulberry trees (*Morus notabilis* L.) under drought stress. *BMC Genomics* **2025**, *26*, 744. [CrossRef]
23. Liu, Y.; Liu, N.; Deng, X.; Liu, D.; Li, M.; Cui, D.; Hu, Y.; Yan, Y. Genome-wide analysis of wheat DNA-binding with one finger (*Dof*) transcription factor genes: Evolutionary characteristics and diverse abiotic stress responses. *BMC Genom.* **2020**, *21*, 276. [CrossRef] [PubMed]
24. Ramirez-Parra, E.; Perianez-Rodriguez, J.; Navarro-Neila, S.; Gude, I.; Moreno-Risueno, M.A.; del Pozo, J.C. The transcription factor OBP4 controls root growth and promotes callus formation. *New Phytol.* **2017**, *213*, 1787–1801. [CrossRef]
25. Li, T.; Wang, X.; Elango, D.; Zhang, W.; Li, M.; Zhang, F.; Pan, Q.; Wu, Y. Genome-wide identification, phylogenetic and expression pattern analysis of Dof transcription factors in blueberry (*Vaccinium corymbosum* L.). *PeerJ* **2022**, *10*, e14087. [CrossRef]
26. Su, Y.; Liang, W.; Liu, Z.; Wang, Y.; Zhao, Y.; Ijaz, B.; Hua, J. Overexpression of *GhDof1* improved salt and cold tolerance and seed oil content in *Gossypium hirsutum*. *J. Plant Physiol.* **2017**, *218*, 222–234. [CrossRef] [PubMed]
27. Fornara, F.; Panigrahi, K.C.; Gissot, L.; Sauerbrunn, N.; Rühl, M.; Jarillo, J.A.; Coupland, G. Arabidopsis Dof transcription factors act redundantly to reduce CONSTANS expression and are essential for a photoperiodic flowering response. *Dev. Cell* **2009**, *17*, 75–86. [CrossRef] [PubMed]
28. Zhang, W.J.; Ma, C.N.; Du, L.D.; Xiang, Y.; Xiao, F.; Liu, Y.T.; Wang, C.K.; Li, W.K.; Zhao, T.T.; Hu, D.G. Two DNA-binding one zinc finger transcription factors, MdCDOF3 and MdDOF3.6, accelerate leaf senescence by activating cytokinin oxidase *MdCKX7* in response to sorbitol signaling in apple. *Hortic. Res.* **2025**, *12*, uhaf120. [CrossRef]
29. Ding, R.; Xiao, T.; Li, S.; Qiang, J.; Zhang, H.; Chang, H.; Yan, Y.; Li, X. Wheat endosperm-specific transcription factor TaDOF6 enhances grain development by regulating *TaSWEET13h* expression and facilitating sugar and gibberellin transport. *Front. Plant Sci.* **2025**, *16*, 1608090. [CrossRef]
30. Cai, X.; Zhang, C.; Shu, W.; Ye, Z.; Li, H.; Zhang, Y. The transcription factor SlDof22 involved in ascorbate accumulation and salinity stress in tomato. *Biochem. Biophys. Res. Commun.* **2016**, *474*, 736–741. [CrossRef]
31. Wen, Y.; Tan, C.; Zhang, Y.; Wu, H.; Chen, D.; Yue, H.; Ding, Z.; Cao, S.; Zheng, K. Genome-wide characterization and functional analysis of CsDOF transcription factors in *Camellia sinensis* cv. Tieguanyin under combined heat-drought stress. *Plants* **2025**, *14*, 1829. [CrossRef]
32. Song, F.; Goodman, R.M. Cloning and identification of the promoter of the tobacco *Sar8.2b* gene, a gene involved in systemic acquired resistance. *Gene* **2002**, *290*, 115–124. [CrossRef]
33. Qiu, T.; Wei, S.; Fang, K.; Zhang, M.; Li, Y.; Feng, Y.; Cheng, Y.; Zhang, S.; Tian, J.; Gao, A.; et al. The atypical Dof transcriptional factor OsDes1 contributes to stay-green, grain yield, and disease resistance in rice. *Sci. Adv.* **2024**, *10*, eadp0345. [CrossRef] [PubMed]

34. Trusov, Y.; Sewelam, N.; Rookes, J.E.; Kunkel, M.; Nowak, E.; Schenk, P.M.; Botella, J.R. Heterotrimeric G proteins-mediated resistance to necrotrophic pathogens includes mechanisms independent of salicylic acid-, jasmonic acid/ethylene- and abscisic acid-mediated defense signaling. *Plant J.* **2009**, *58*, 69–81. [CrossRef] [PubMed]
35. Campos, M.L.; Kang, J.H.; Howe, G.A. Jasmonate-triggered plant immunity. *J. Chem. Ecol.* **2014**, *40*, 657–675. [CrossRef]
36. Mersmann, S.; Bourdais, G.; Rietz, S.; Robatzek, S. Ethylene signaling regulates accumulation of the FLS2 receptor and is required for the oxidative burst contributing to plant immunity. *Plant Physiol.* **2010**, *154*, 391–400. [CrossRef] [PubMed]
37. Charitha, P.A.J.; Emilee, R.M.S.; Jocelyn, A.O.; Stephen, E.S. The complex roles of plant hormones during clubroot disease development in the Brassicaceae. *J. Plant Growth Regul.* **2025**, *44*, 5692–5712. [CrossRef]
38. Cai, M.; Lin, J.; Li, Z.; Lin, Z.; Ma, Y.; Wang, Y.; Ming, R. Allele specific expression of *Dof* genes responding to hormones and abiotic stresses in sugarcane. *PLoS ONE* **2020**, *15*, e0227716. [CrossRef]
39. Virág, E.; Nagy, Á.; Tóth, B.B.; Kutasy, B.; Pallos, J.P.; Szigeti, Z.M.; Máthé, C.; Kardos, G.; Hegedűs, G. Master regulatory transcription factors in β-aminobutyric acid-induced resistance (BABA-IR): A perspective on phytohormone biosynthesis and signaling in *Arabidopsis thaliana* and *Hordeum vulgare*. *Int. J. Mol. Sci.* **2024**, *25*, 9179. [CrossRef]
40. Li, J.; Zhang, Y.; Xu, L.; Wang, C.; Luo, Y.; Feng, S.; Yuan, Y.; Yang, Q.; Feng, B. Genome-wide identification of DNA binding with one finger (*dof*) gene family in tartary buckwheat (*Fagopyrum tataricum*) and analysis of its expression pattern after exogenous hormone stimulation. *Biology* **2022**, *11*, 173. [CrossRef]
41. Yu, Y.H.; Bian, L.; Wan, Y.T.; Jiao, Z.L.; Yu, K.K.; Zhang, G.H.; Guo, D.L. Grape (*Vitis vinifera*) VvDOF3 functions as a transcription activator and enhances powdery mildew resistance. *Plant Physiol. Biochem.* **2019**, *143*, 183–189. [CrossRef]
42. Paz, M.M.; Shou, H.; Guo, Z.; Zhang, Z.; Banerjee, A.K.; Wang, K. Assessment of conditions affecting *Agrobacterium*-mediated soybean transformation using the cotyledonary node explants. *Euphytica* **2004**, *136*, 167–179. [CrossRef]
43. Li, S.; Cong, Y.; Liu, Y.; Wang, T.; Shuai, Q.; Chen, N.; Gai, J.; Li, Y. Optimization of *Agrobacterium*-mediated transformation in soybean. *Front. Plant Sci.* **2017**, *8*, 246. [CrossRef]
44. Shrestha, S.D.; Chapman, P.; Zhang, Y.; Gijzen, M. Strain specific factors control effector gene silencing in *Phytophthora sojae*. *PLoS ONE* **2016**, *11*, e0150530. [CrossRef]
45. Yang, X.; Jiang, X.; Yan, W.; Huang, Q.; Sun, H.; Zhang, X.; Zhang, Z.; Ye, W.; Wu, Y.; Govers, F.; et al. The mevalonate pathway is important for growth, spore production, and the virulence of *Phytophthora sojae*. *Front. Microbiol.* **2021**, *12*, 772994. [CrossRef]
46. Alexander, D.; Goodman, R.M.; Gut-Rella, M.; Glascock, C.; Weymann, K.; Friedrich, L.; Maddox, D.; Ahl-Goy, P.; Luntz, T.; Ward, E. Increased tolerance to two oomycete pathogens in transgenic tobacco expressing pathogenesis-related protein 1a. *Proc. Natl. Acad. Sci. USA* **1993**, *90*, 7327–7331. [CrossRef]
47. Sessa, G.; Yang, X.Q.; Raz, V.; Eyal, Y.; Fluhr, R. Dark induction and subcellular localization of the pathogenesis-related PRB-1b protein. *Plant Mol. Biol.* **1995**, *28*, 537–547. [CrossRef] [PubMed]
48. Xu, P.F.; Jiang, L.Y.; Wu, J.J.; Li, W.B.; Fan, S.J.; Zhang, S.Z. Isolation and characterization of a pathogenesis-related protein 10 gene (*GmPR10*) with induced expression in soybean (*Glycine max*) during infection with *Phytophthora sojae*. *Mol. Biol. Rep.* **2014**, *41*, 4899–4909. [CrossRef] [PubMed]
49. Breen, S.; Williams, S.J.; Outram, M.; Kobe, B.; Solomon, P.S. Emerging insights into the functions of pathogenesis-related protein 1. *Trends Plant Sci.* **2017**, *22*, 871–879. [CrossRef]
50. Umemura, Y.; Ishiduka, T.; Yamamoto, R.; Esaka, M. The Dof domain, a zinc finger DNA-binding domain conserved only in higher plants, truly functions as a Cys2/Cys2 Zn finger domain. *Plant J.* **2004**, *37*, 741–749. [CrossRef] [PubMed]
51. Yanagisawa, S. The Dof family of plant transcription factors. *Trends Plant Sci.* **2002**, *7*, 555–560. [CrossRef]
52. Chen, P.; Yan, M.; Li, L.; He, J.; Zhou, S.; Li, Z.; Niu, C.; Bao, C.; Zhi, F.; Ma, F.; et al. The apple DNA-binding one zinc-finger protein MdDof54 promotes drought resistance. *Hortic. Res.* **2020**, *7*, 195. [CrossRef]
53. Khan, I.; Khan, S.; Zhang, Y.; Zhou, J.P. Genome-wide analysis and functional characterization of the Dof transcription factor family in rice (*Oryza sativa* L.). *Planta* **2021**, *253*, 101. [CrossRef]
54. Yang, C.; Lai, Y.M.; Yao, N. Plant sphingolipids: Subcellular distributions and functions. *Curr. Opin. Plant Biol.* **2025**, *85*, 102704. [CrossRef]
55. Marques, A.C.; Vinckenbosch, N.; Brawand, D.; Kaessmann, H. Functional diversification of duplicate genes through subcellular adaptation of encoded proteins. *Genome Biol.* **2008**, *9*, R54. [CrossRef]
56. Yanagisawa, S.; Schmidt, R.J. Diversity and similarity among recognition sequences of Dof transcription factors. *Plant J.* **1999**, *17*, 209–214. [CrossRef] [PubMed]
57. Wu, J.; Chen, L.; Chen, M.; Zhou, W.; Dong, Q.; Jiang, H.; Cheng, B. The Dof-domain transcription factor ZmDOF36 positively regulates starch synthesis in transgenic maize. *Front. Plant Sci.* **2019**, *10*, 465. [CrossRef]
58. Luo, T.; Song, Y.; Gao, H.; Wang, M.; Cui, H.; Ji, C.; Wang, J.; Yuan, L.; Li, R. Genome-wide identification and functional analysis of Dof transcription factor family in *Camelina sativa*. *BMC Genom.* **2022**, *23*, 812. [CrossRef]
59. Magadum, S.; Banerjee, U.; Murugan, P.; Gangapur, D.; Ravikesavan, R. Gene duplication as a major force in evolution. *J. Genet.* **2013**, *92*, 155–161. [CrossRef] [PubMed]

60. Panchy, N.; Lehti-Shiu, M.; Shiu, S.H. Evolution of gene duplication in plants. *Plant Physiol.* **2016**, *171*, 2294–2316. [CrossRef] [PubMed]
61. Qiao, X.; Li, Q.; Yin, H.; Qi, K.; Li, L.; Wang, R.; Zhang, S.; Paterson, A.H. Gene duplication and evolution in recurring polyploidization-diploidization cycles in plants. *Genome Biol.* **2019**, *20*, 38. [CrossRef]
62. Kondrashov, F.A. Gene duplication as a mechanism of genomic adaptation to a changing environment. *Proc. Biol. Sci.* **2012**, *279*, 5048–5057. [CrossRef]
63. Wu, Q.; Liu, X.; Yin, D.D.; Yuan, H.; Xie, Q.; Zhao, X.F.; Li, X.B.; Zhu, L.H.; Li, S.G.; Li, D.Y. Constitutive expression of *OsDof4*, encoding a C_2-C_2 zinc finger transcription factor, confesses its distinct flowering effects under long- and short-day photoperiods in rice (*Oryza sativa* L.). *BMC Plant Biol.* **2017**, *17*, 166. [CrossRef] [PubMed]
64. Wu, Y.F.; Lee, S.K.; Yoo, Y.; Wei, J.; Kwon, S.Y.; Lee, S.W.; Jeon, J.S.; An, G. Rice transcription factor OsDOF11 modulates sugar transport by promoting expression of sucrose transporter and *SWEET* genes. *Mol. Plant* **2018**, *11*, 833–845. [CrossRef] [PubMed]
65. Qin, H.; Wang, J.; Chen, X.B.; Wang, F.F.; Peng, P.; Zhou, Y.; Miao, Y.C.; Zhang, Y.O.; Gao, Y.D.; Qi, Y.D.; et al. Rice OsDOF15 contributes to ethylene-inhibited primary root elongation under salt stress. *New Phytol.* **2019**, *223*, 798–813. [CrossRef] [PubMed]
66. Shim, Y.; Kang, K.; An, G.; Paek, N.C. Rice DNA-binding one zinc finger 24 (OsDOF24) delays leaf senescence in a jasmonate-mediated pathway. *Plant Cell Physiol.* **2019**, *60*, 2065–2076. [CrossRef]
67. Zhang, Y.; Verhoeff, N.I.; Chen, Z.; Chen, S.; Wang, M.; Zhu, Z.; Ouwerkerk, P.B.F. Functions of OsDof25 in regulation of *OsC4PPDK*. *Plant Mol. Biol.* **2015**, *89*, 229–242. [CrossRef]
68. Zuo, Z.F.; Kang, H.G.; Park, M.Y.; Jeong, H.; Sun, H.J.; Song, P.S.; Lee, H.Y. *Zoysia japonica* MYC type transcription factor ZjICE1 regulates cold tolerance in transgenic Arabidopsis. *Plant Sci.* **2019**, *289*, 110254. [CrossRef]
69. Mayordomo, I.; Estruch, F.; Sanz, P. Convergence of the target of rapamycin and the Snf1 protein kinase pathways in the regulation of the subcellular localization of Msn2, a transcriptional activator of STRE (Stress Response Element)-regulated genes. *J. Biol. Chem.* **2002**, *277*, 35650–35656. [CrossRef]
70. Lohani, N.; Babaei, S.; Singh, M.B.; Bhalla, P.L. Genome-wide in silico identification and comparative analysis of *Dof* gene family in *Brassica napus*. *Plants* **2021**, *10*, 709. [CrossRef]
71. Liu, J.; Meng, Q.L.; Xiang, H.T.; Shi, F.M.; Ma, L.G.; Li, Y.C.; Liu, C.L.; Liu, Y.; Su, B.H. Genome-wide analysis of Dof transcription factors and their response to cold stress in rice (*Oryza sativa* L.). *BMC Genom.* **2021**, *22*, 800. [CrossRef]
72. Wong, J.; Gao, L.; Yang, Y.; Zhai, J.X.; Arikit, S.; Yu, Y.; Duan, S.Y.; Chan, V.; Xiong, Q.; Yan, J.; et al. Roles of small RNAs in soybean defense against *Phytophthora sojae* infection. *Plant J.* **2014**, *79*, 928–940. [CrossRef]
73. Cheng, Q.; Dong, L.D.; Gao, T.J.; Liu, T.F.; Li, N.H.; Wang, L.; Chang, X.; Wu, J.J.; Xu, P.F.; Zhang, S.Z. The bHLH transcription factor GmPIB1 facilitates resistance to *Phytophthora sojae* in *Glycine max*. *J. Exp. Bot.* **2018**, *69*, 2527–2541. [CrossRef]
74. Li, W.; Zheng, X.; Cheng, R.; Zhong, C.; Zhao, J.; Liu, T.H.; Yi, T.; Zhu, Z.; Xu, J.; Meksem, K.; et al. Soybean ZINC FINGER PROTEIN03 targets two SUPEROXIDE DISMUTASE1s and confers resistance to *Phytophthora sojae*. *Plant Physiol.* **2023**, *69*, 2527–2541. [CrossRef]
75. Zhu, X.; Guo, L.; Zhu, R.; Zhou, X.; Zhang, J.; Li, D.; He, S.; Qiao, Y. *Phytophthora sojae* effector PsAvh113 associates with the soybean transcription factor GmDPB to inhibit catalase-mediated immunity. *Plant Biotechnol. J.* **2023**, *21*, 1393–1407. [CrossRef] [PubMed]
76. Kang, H.G.; Singh, K.B. Characterization of salicylic acid-responsive, Arabidopsis Dof domain proteins: Overexpression of *OBP3* leads to growth defects. *Plant J.* **2000**, *21*, 329–339. [CrossRef]
77. van Verk, M.C.; Pappaioannou, D.; Neeleman, L.; Bol, J.F.; Linthorst, H.J.M. A novel WRKY transcription factor is required for induction of *PR-1a* gene expression by salicylic acid and bacterial elicitors. *Plant Physiol.* **2008**, *146*, 1983–1995. [CrossRef] [PubMed]
78. Zhang, Y.; Fan, W.; Kinkema, M.; Li, X.; Dong, X. Interaction of NPR1 with basic leucine zipper protein transcription factors that bind sequences required for salicylic acid induction of the *PR-1* gene. *Proc. Natl. Acad. Sci. USA* **1999**, *96*, 6523–6528. [CrossRef] [PubMed]
79. He, K.; Gou, X.P.; Yuan, T.; Lin, H.H.; Asami, T.; Yoshida, S.; Russell, S.D.; Li, J. BAK1 and BKK1 regulate Brassinosteroid-dependent growth and Brassinosteroidindependent cell-death pathways. *Curr. Biol.* **2007**, *17*, 1109–1115. [CrossRef]
80. Ward, E.R.; Uknes, S.J.; Williams, S.C.; Dincher, S.S.; Wiederhold, D.L.; Alexander, D.C.; Ahl-Goy, P.; Metraux, J.P.; Ryals, J.A. Coordinate gene activity in response to agents that induce systemic acquired resistance. *Plant Cell* **1991**, *3*, 1085–1094. [CrossRef]

plants

MDPI

Article

Transcriptomics Reveals Cold Tolerance Maize Lines Involved in the Phenylpropanoid and Flavonoid Pathways

Shuna Zhou, Xinling Yu, Jian Tan, Haixiao Sun, Wei Yang, Liangyu Jiang, Zhenyuan Zang, Jiabin Ci * and Xuejiao Ren *

College of Agriculture, Jilin Agricultural University, Changchun 130118, China; zsn16655805901@163.com (S.Z.); yxl18654060901@163.com (X.Y.); 18097479424@163.com (J.T.); 17767764577@163.com (H.S.); davidyoung588@126.com (W.Y.); liangyu0113@163.com (L.J.); zhenyuanzang1989@163.com (Z.Z.)
* Correspondence: cjb6666@163.com (J.C.); rxj0342@163.com (X.R.)

Abstract

Low temperature during early spring severely impairs maize germination, leading to significant yield losses. To elucidate the mechanisms underlying cold tolerance at the germination stage, we compared two cold-tolerant maize inbred lines (AM and CM) with a cold-sensitive line (BM) under control (25 °C) and chilling (6 °C) conditions. Phenotypic observations showed that AM and CM maintained high germination rates and exhibited enhanced coleoptile elongation under cold stress, whereas BM displayed substantial growth inhibition. Cold-tolerant lines accumulated less malondialdehyde and showed markedly higher SOD and POD activities, indicating a stronger antioxidant defense. Transcriptome profiling revealed that cold tolerance is associated with a more robust transcriptional response in AM and CM, characterized by significant activation of the phenylpropanoid and flavonoid biosynthesis pathways. Among the differentially expressed genes, the class III peroxidase gene *ZmPER5* was strongly upregulated in AM and CM but only weakly induced in BM, suggesting its central role in reinforcing the cell wall structure and enhancing ROS-scavenging capacity under chilling conditions. Other lignin- and flavonoid-related genes, including *ZmHCT4* and *ZmCYP75*, also exhibited genotype-specific induction patterns consistent with cold tolerance. qRT-PCR validation confirmed the RNA-seq expression trends. These results demonstrate that maize cold tolerance during germination relies on the coordinated enhancement of antioxidant enzyme activity, activation of phenylpropanoid-derived lignin biosynthesis, and accumulation of protective flavonoids. The identified candidate genes, especially *ZmPER5*, provide valuable targets for improving cold tolerance in maize breeding.

Keywords: maize germination; low-temperature stress; phenylpropanoid biosynthesis; flavonoid biosynthesis; transcriptomics; ROS scavenging; lignin biosynthesis

1. Introduction

Maize (*Zea mays* L.) is the world's third most widely grown cereal crop and a major source of food, feed, and bioenergy, contributing substantially to global food security and agricultural sustainability [1,2]. However, in temperate and cool regions, early spring low-temperature stress is a major constraint to maize establishment. Chilling conditions during germination significantly delay seedling emergence, impair metabolic activity, and ultimately reduce yield, causing estimated annual global losses of 12–15% [3,4].

Low temperature disrupts key physiological processes, including energy metabolism, antioxidant activity, and membrane stability. It reduces membrane fluidity, triggers excessive reactive oxygen species (ROS) accumulation, and induces lipid peroxidation, collectively leading to inhibited radicle and coleoptile elongation and high seedling mortality [5,6]. Coleoptile growth is particularly sensitive to chilling stress, and its elongation ability has been widely recognized as a rapid and reliable phenotypic indicator of low-temperature tolerance in maize and other cereals [7–9].

Cold tolerance during germination is controlled by complex genetic and metabolic networks. Several studies have identified cold-responsive loci through genome-wide association studies (GWASs) in rice and maize [10,11]. In maize, cold-induced alterations in coleoptile and mesocotyl growth have also been linked to light quality, hormonal balance, and transcriptional regulation [12]. At the molecular level, cold stress activates signaling pathways involving calcium-dependent protein kinases (CDPKs) and mitogen-activated protein kinases (MAPKs), which modulate downstream transcription factors and stress-responsive genes [13–15]. Furthermore, antioxidant enzymes such as SOD, POD, and APX play essential roles in ROS detoxification, and their activities are closely associated with chilling tolerance in maize and other crops [16–18].

Recent studies highlight the importance of secondary metabolism, particularly the phenylpropanoid pathway, in plant cold responses. This pathway produces lignin, flavonoids, and related metabolites that participate in cell wall reinforcement and non-enzymatic antioxidant defense [19]. In maize, cold stress has been shown to modulate phenylpropanoid and flavonoid accumulation in radicles and seedlings, suggesting a key role in cold tolerance [20,21]. However, most studies to date have focused on individual pathways, specific developmental stages, or isolated genotypes, and the integrated molecular mechanisms linking phenylpropanoid activation, antioxidant capacity, and coleoptile elongation during germination remain insufficiently understood.

To address these gaps, we investigated two cold-tolerant maize inbred lines (AM, CM) and one cold-sensitive line (BM) subjected to control and chilling conditions. By integrating phenotypic, physiological, and transcriptomic analyses, we aimed to (i) characterize genotype-specific responses to cold stress during germination, (ii) identify key pathways and genes associated with cold tolerance, and (iii) determine how phenylpropanoid and flavonoid biosynthesis contribute to the enhanced coleoptile growth observed in tolerant lines. Our findings provide new mechanistic insights and potential molecular targets for improving cold resilience in maize breeding.

2. Results

2.1. Low Temperature Differentially Affects Germination and Coleoptile Growth in Three Maize Inbred Lines

Cold stress induced clear and genotype-dependent variations in early seedling performance (Figure 1a,b). Under control conditions (25 °C), the three inbred lines exhibited high germination rates (91–100%). However, exposure to 6 °C significantly reduced germination in the cold-sensitive line BM ($p < 0.05$), whereas AM and CM maintained high germination (>95%) without significant decline (Figure 1a). Coleoptile elongation displayed even stronger genotype differentiation (Figure 1b). BM showed a 50% reduction in coleoptile length at 6 °C (3.60 → 1.80 cm), confirming its chilling sensitivity. In contrast, AM and CM exhibited increased coleoptile elongation under cold stress, with CM showing the largest response (2.70 → 4.05 cm), indicating enhanced early growth vigor. Representative seedling images visually confirm these phenotypic differences.

https://doi.org/10.3390/plants15010161

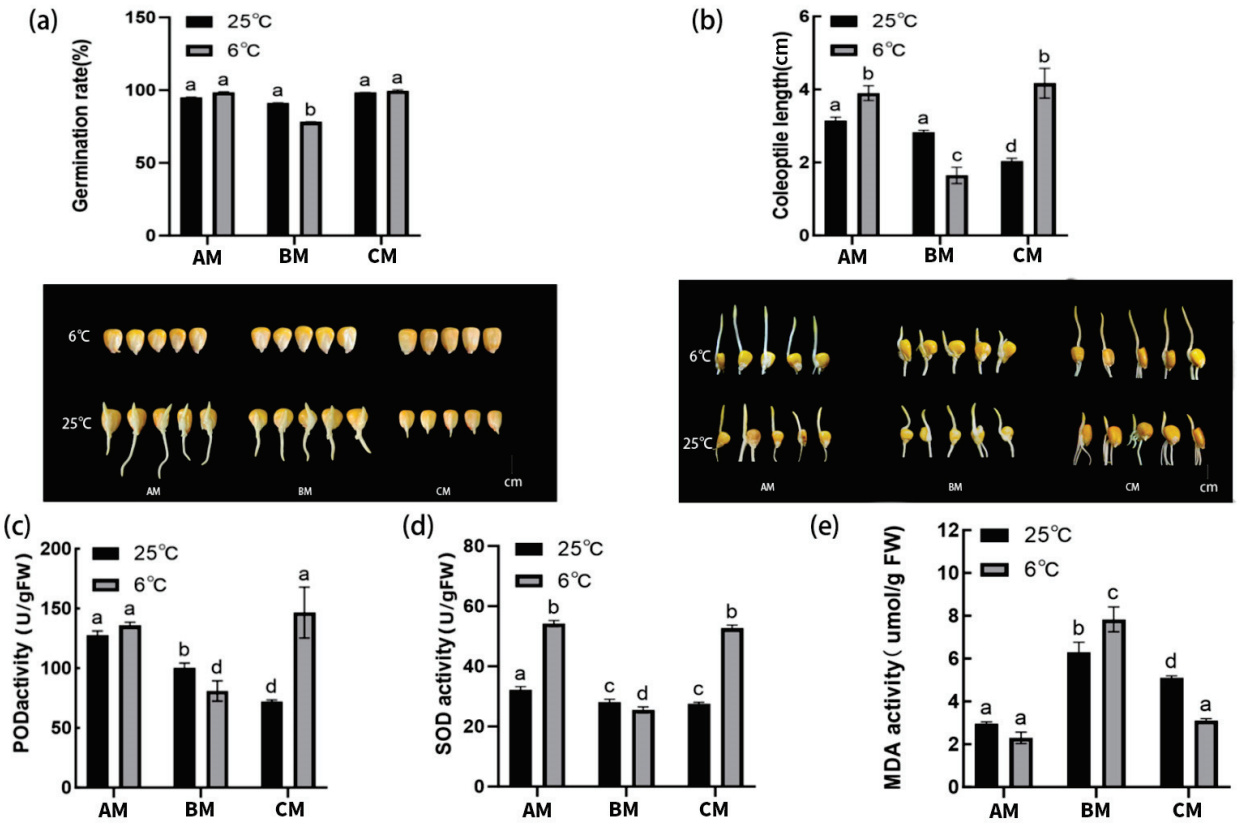

Figure 1. Phenotypic performance and oxidative stress-related physiological responses of three maize inbred lines (AM, BM, and CM) under control (25 °C) and low-temperature (6 °C) conditions during germination. (**a**) Germination rate (%) after 3 days of incubation at 25 °C or 6 °C, showing genotype-dependent sensitivity to low temperature. (**b**) Coleoptile length of germinated seedlings under control and cold stress; representative images of seedlings are shown below the bar chart to illustrate visual differences in early growth vigor. (**c**) Peroxidase (POD) activity. (**d**) Superoxide dismutase (SOD) activity. (**e**) Malondialdehyde (MDA) content. Values are presented as mean ± SD (n = 3 biological replicates). Different lowercase letters indicate statistically significant differences among genotypes and temperature treatments ($p < 0.05$).

2.2. Low Temperature Induces Genotype-Dependent Changes in Oxidative Stress-Related Physiological Parameters

Low temperature substantially affected membrane integrity and redox homeostasis (Figure 1c–e). MDA content increased sharply in BM (4.92 → 7.85 μmol g^{-1} FW), indicating enhanced lipid peroxidation, whereas AM and CM maintained significantly lower MDA levels ($p < 0.05$), reflecting better membrane stability (Figure 1e). Antioxidant enzyme activities showed contrasting trends among the genotypes. SOD and POD activities increased significantly in AM and CM under cold stress, with CM exhibiting the highest enzyme induction (Figure 1c,d). In contrast, BM showed no significant increase in SOD activity and even reduced POD activity. These results indicate that tolerant lines possess stronger ROS-scavenging capacity, consistent with their phenotypic resilience.

2.3. Transcriptome Profiling Reveals Strong Genotype- and Temperature-Dependent Transcriptional Reprogramming

To investigate the molecular basis underlying cold responses, transcriptomic analyses were performed (Figure 2a–d). PCA clearly separated samples by temperature and genotype (Figure 2a), with strong intra-group correlation (Figure 2b). Cold stress triggered extensive transcriptional activation in the tolerant lines. CM exhibited the largest number of upregulated DEGs (1388), followed by AM (690), whereas BM showed significantly

fewer DEGs (90), indicating a weaker transcriptional response (Figure 2c). Venn diagrams revealed 320 co-upregulated genes shared between AM and CM but largely absent in BM, suggesting a core cold-tolerance module (Figure 2d).

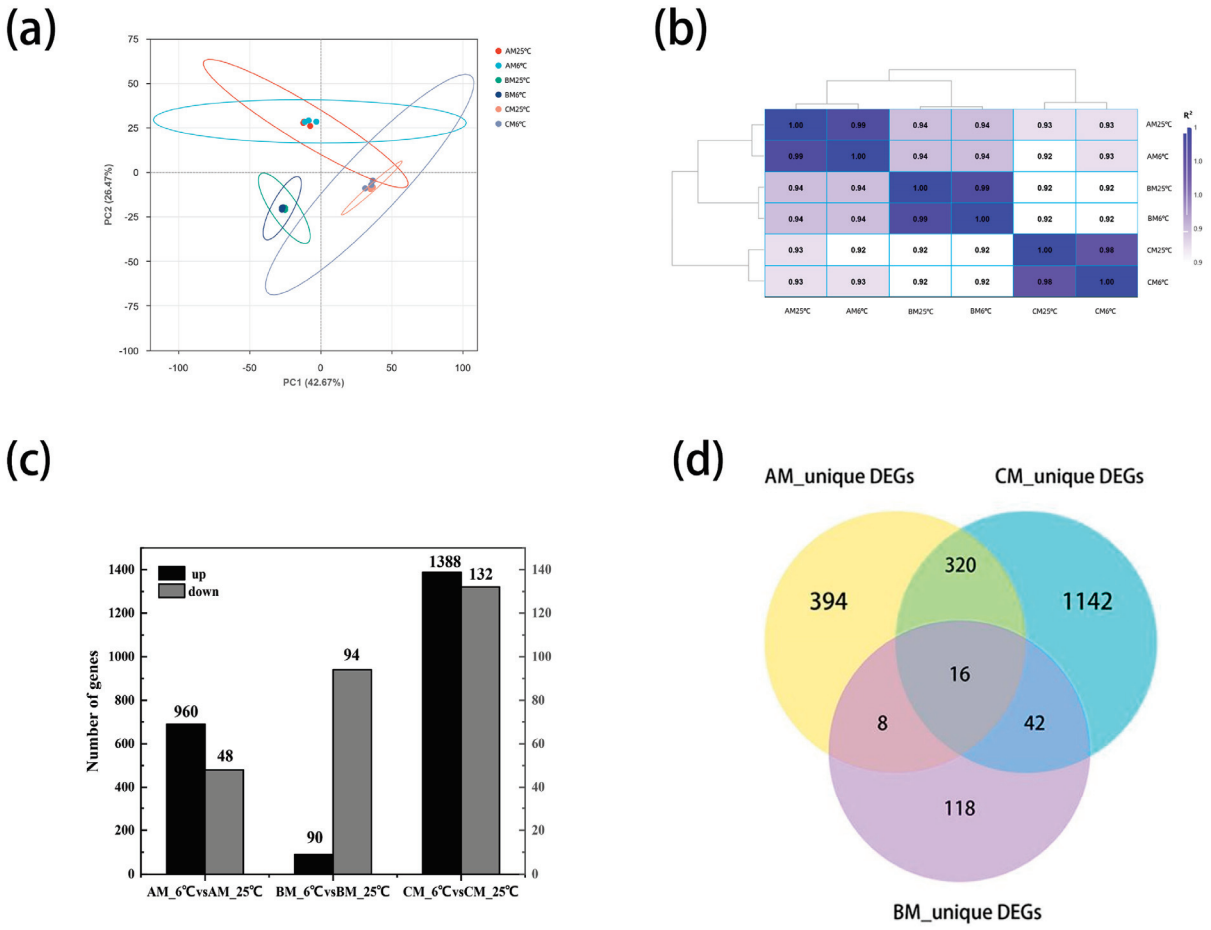

Figure 2. Global transcriptomic responses of maize coleoptiles to low-temperature stress in AM, BM, and CM lines. (**a**) Principal component analysis (PCA) of all transcriptome samples based on normalized gene expression levels. Each point represents one biological replicate, and the separation among samples reflects differences in overall transcriptional profiles driven by genotype and temperature treatment. (**b**) Pearson correlation heatmap showing the similarity of transcript expression patterns among all samples, demonstrating high reproducibility between biological replicates. (**c**) Number of upregulated and downregulated differentially expressed genes (DEGs) identified in each inbred line under low-temperature treatment (6 °C) compared with the corresponding control (25 °C). (**d**) Venn diagram showing the overlap and uniqueness of upregulated DEGs among AM, BM, and CM under cold stress. Shared DEGs represent common cold-responsive genes, whereas unique DEGs indicate genotype-specific transcriptional responses.

2.4. GO Enrichment Analysis Identifies Cold-Induced Activation of Oxidative Stress- and Ion Transport-Related Processes in Tolerant Lines

GO enrichment of the 320 shared DEGs revealed significant enrichment in oxidative stress response, oxidoreductase activity, peroxidase activity, and cation/metal ion transport (Figure 3a,b). These enriched functions are consistent with the increased SOD/POD activities observed physiologically. Notably, peroxidase-related terms were strongly represented, consistent with the upregulation of class III peroxidases such as ZmPER5. Ion transport–related terms suggest strengthened metal homeostasis, potentially supporting antioxidant enzyme cofactor requirement (e.g., Cu/Zn-SOD).

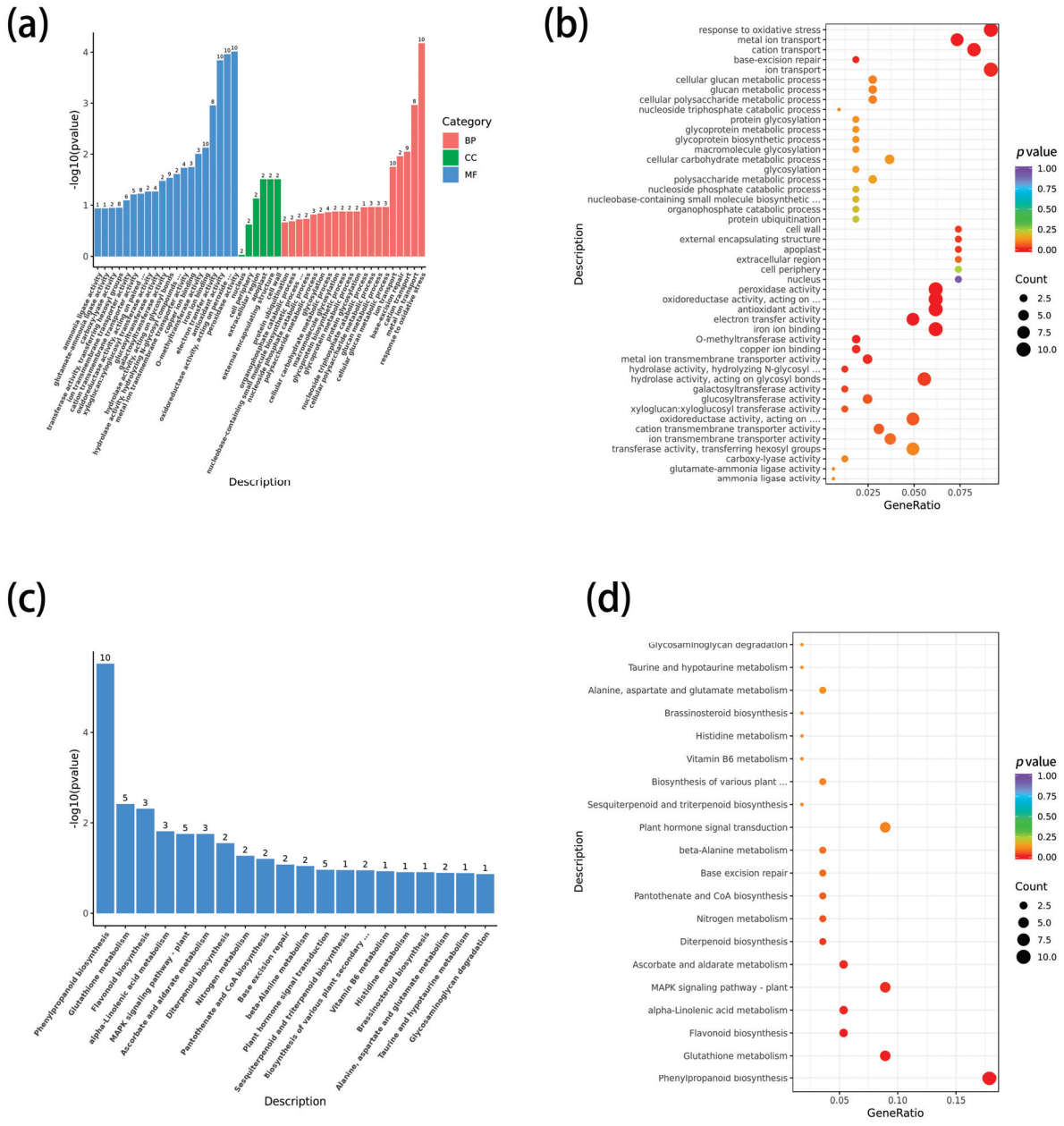

Figure 3. Functional characterization of cold-responsive genes shared by cold-tolerant maize lines. (**a**) Gene Ontology (GO) enrichment analysis of differentially expressed genes commonly induced by low-temperature stress in the cold-tolerant lines AM and CM, categorized into biological process, molecular function, and cellular component. (**b**) Bubble plot of significantly enriched GO terms, where bubble size indicates the number of genes and color represents the level of statistical significance. (**c**) Kyoto Encyclopedia of Genes and Genomes (KEGG) pathway enrichment analysis of shared DEGs, highlighting pathways significantly associated with cold stress response. (**d**) Bubble plot showing the top enriched KEGG pathways, illustrating the relative contribution and significance of each pathway in cold-tolerant genotypes.

2.5. KEGG Pathway Enrichment Shows Specific Activation of Phenylpropanoid and Flavonoid Biosynthesis in Cold-Tolerant Lines

We performed functional annotation and expression analysis of 320 differentially expressed genes (DEGs), with detailed annotations and FPKM expression values provided in Supplementary Tables S1–S3. Heatmap analysis revealed that these DEGs were generally highly expressed in the AC inbred line, suggesting that AC may enhance cold response through these genes (Figure 4c). KEGG enrichment analysis showed that phenylpropanoid

biosynthesis and flavonoid biosynthesis were significantly enriched in the AM and CM inbred lines (Figure 3c,d). The specific pathways and genes that were significantly enriched are listed in Supplementary Table S4. In the pathway visualization (Figure 4a,b), we marked the positions of these DEGs to show their enrichment at specific nodes within the pathways, particularly in the key nodes related to lignin monomer synthesis and flavonoid metabolism. However, this enrichment does not imply that the entire pathway was globally activated, but rather that these specific nodes were enriched with differentially expressed genes. The heatmap also revealed that cold-tolerant AM and CM lines exhibited notable differential expression of key genes, including lignin-related genes (ZmHCT4), peroxidase genes (ZmPER5), and flavonoid biosynthesis genes. Notably, ZmPER5 was significantly enriched in both phenylpropanoid and flavonoid biosynthesis pathways, suggesting a central role in the cold response. In contrast, the BM inbred line showed minimal differences in these key genes, consistent with its lower cold tolerance. Overall, cold-tolerant inbred lines may enhance low-temperature adaptation through differential expression of key genes at specific nodes in lignin and flavonoid metabolic pathways, with ZmPER5 potentially serving as a key regulatory node in this network.

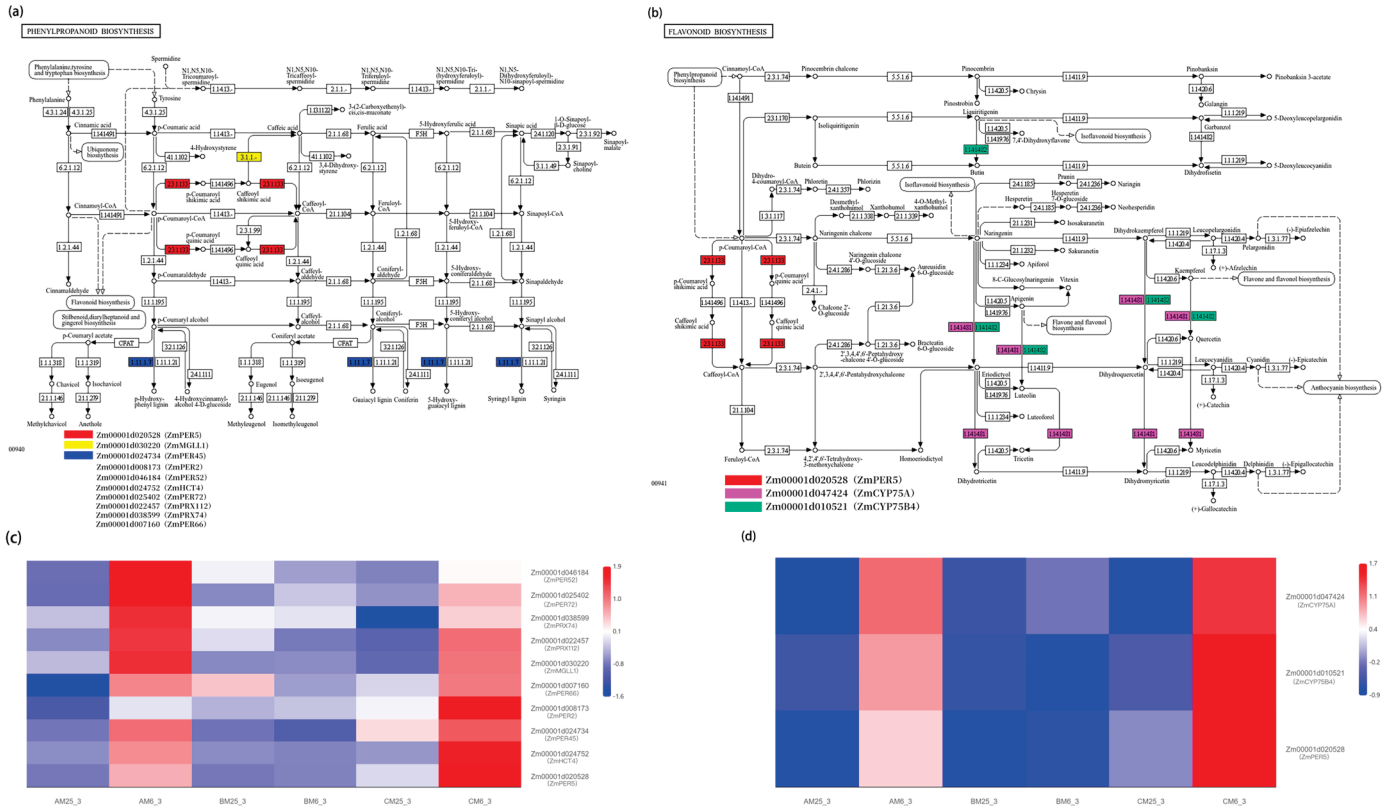

Figure 4. KEGG pathway enrichment and expression profiles of genes associated with phenylpropanoid and flavonoid biosynthesis under low-temperature stress. (**a**) KEGG phenylpropanoid biosynthesis pathway showing differentially expressed genes (DEGs) enriched in this pathway under low-temperature treatment. Colored boxes indicate DEGs identified by KEGG enrichment analysis, corresponding to the gene list shown in the legend. (**b**) KEGG flavonoid biosynthesis pathway showing DEGs enriched in the flavonoid biosynthesis pathway under low-temperature treatment. Colored boxes correspond to genes listed in the legend. (**c**) Heatmap of expression profiles of phenylpropanoid pathway–related genes across different sample groups defined by genotype (AM, BM, and CM) and temperature treatments (25 °C and 6 °C). Color intensity represents relative gene expression levels (blue, low expression; red, high expression). Sample labels indicate different genotype × temperature combinations. (**d**) Heatmap of expression profiles of flavonoid biosynthesis-related genes across the same sample groups. Color scale and sample definitions are the same as in panel (**c**).

https://doi.org/10.3390/plants15010161

2.6. Validation of RNA-Seq Data by qRT-PCR

The reliability of the transcriptome data was confirmed by quantitative real-time PCR (qRT-PCR). A subset of genes from the 320 differentially expressed genes (DEGs), including Zm00001d047441, Zm00001d029558, Zm00001d005570, Zm00001d005251, Zm00001d019734, Zm00001d011425, Zm00001d047424, Zm00001d024752, Zm00001d020528, were selected for validation across all sample groups. The expression trends (log2 fold change) detected by qRT-PCR were highly consistent with the RNA-Seq data (Figure 5), validating the identified DEGs.

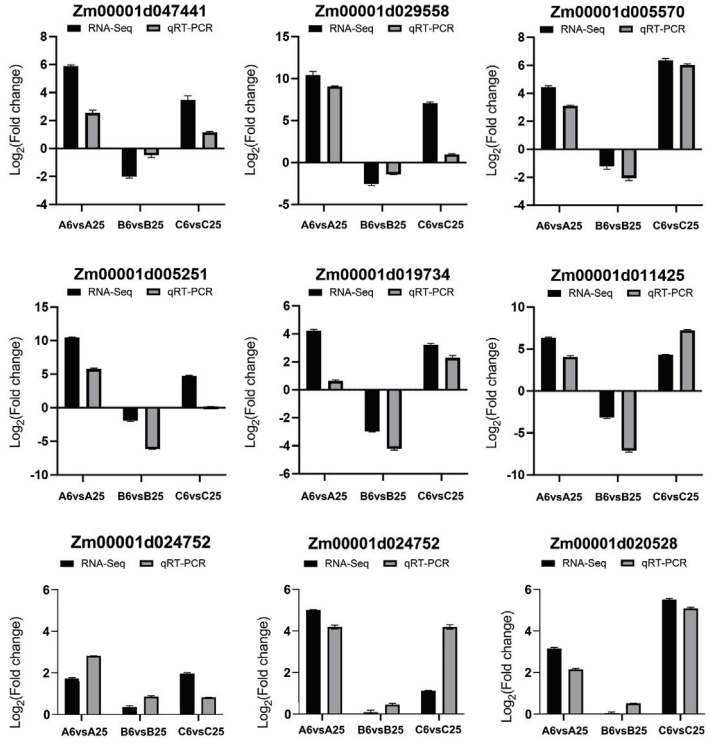

Figure 5. qRT-PCR validation of RNA-seq results. Comparison of $\log_2$ fold-change values obtained by RNA-seq and qRT-PCR for six representative genes across all genotype temperature comparisons.

3. Discussion

This study delineates the molecular mechanisms of low-temperature tolerance during maize germination by integrating phenotypic, physiological, and transcriptomic analyses of cold-tolerant (AM, CM) and cold-sensitive (BM) inbred lines.

3.1. Phenotypic and Physiological Distinctions Define Cold Tolerance

Under 6 °C stress, the cold-tolerant lines (AM and CM) exhibited markedly greater resilience than the sensitive BM line. The BM line displayed reduced germination (78.3%) and 31% coleoptile shortening. In contrast, the AM and CM lines maintained germination rates above 98%, with the CM line showing notable coleoptile elongation (a 50% increase). This phenotypic advantage was underpinned by a 20–50% decrease in malondialdehyde (MDA) content and significantly elevated activities of superoxide dismutase (SOD) and peroxidase (POD) in the tolerant lines, contrasting with the opposite trends in BM.

The capacity of our tolerant lines to maintain >95% germination at 6 °C aligns with the performance of cold-tolerant rice genotypes at 8 °C [22] and contrasts with the 10–25% germination loss reported for many maize varieties below 10 °C [23]. Furthermore, the paradoxical coleoptile elongation under cold stress mirrors the enhanced growth phenotype

https://doi.org/10.3390/plants15010161

of Arabidopsis eskimo1 mutants at 4 °C [24]. This response represents a distinct adaptive strategy compared to the growth suppression typical in wheat under similar conditions.

3.2. Specific Activation of Phenylpropanoid and Flavonoid Biosynthesis Pathways Drives Adaptive Responses

Transcriptome analysis revealed the cold-specific activation of the phenylpropanoid (map00940) and flavonoid biosynthesis (map00941) pathways in the tolerant lines. This finding aligns with the reported upregulation of flavonoid-related metabolism under cold stress in maize [25]. However, our study extends this knowledge by directly linking the co-activation of these two pathways to the distinctive phenotypic trait of coleoptile elongation and by elucidating a key downstream structural adaptation. Key genes ZmPER5 and *ZmHCT4* were upregulated by 5-fold and 4-fold, respectively. *ZmPER5* exhibits dual functionality in antioxidant activity and phenylpropanoid metabolism regulation [26], consistent with research on cold-induced phenylpropanoid accumulation in winter cereals. This activation synergizes with the flavonoid-mediated antioxidant mechanism, analogous to the anthocyanin ROS scavenging pathway in Arabidopsis [27].

Beyond antioxidant roles, these pathways crucially contribute to structural adaptation. The concerted upregulation of phenylpropanoid biosynthesis genes, particularly those involved in lignin monomer synthesis (e.g., *ZmHCT4*) and polymerization (e.g., *ZmPER5*), indicates a reprogramming of cell wall metabolism. In maize, abiotic stresses such as salinity induce a coordinated "cell wall remodeling" response, where targeted deposition of lignin and other components reinforces structural integrity to mitigate stress damage while supporting continued growth [28]. Such spatially regulated lignification can fortify specific tissues (e.g., vascular bundles) without globally arresting organ elongation [29]. Therefore, we propose that in our cold-tolerant lines, the induced lignin biosynthesis is a component of adaptive cell wall fortification. This remodeling likely enhances the mechanical strength and integrity of the coleoptile under cold stress, protecting against cellular damage and sustaining turgor-driven cell expansion, thereby facilitating the observed organ elongation.

3.3. Coordinated Enhancement of the Integrated Antioxidant System

Redox homeostasis under cold was maintained by the coordinated enrichment of genes involved in oxidative stress response (GO:0006979), antioxidant activity (GO:0016209), and metal ion transport (GO:0030001). The upregulation of peroxidase genes showed a positive correlation with SOD/POD activities ($r = 0.92$). This finding corroborates studies linking robust antioxidant systems to cold tolerance in barley [30] and provides a transcriptional explanation for the physiological reduction in MDA. Concurrently, the induction of metal ion transporter genes (e.g., Zn^{2+}/Cu^{2+} transporters) offers new evidence in maize for mechanisms ensuring SOD cofactor homeostasis under cold stress, a supporting mechanism also noted in rice [31].

3.4. Genotypic Variation in the Transcriptional Response and Implications

The scale of the transcriptional response to cold stress varied significantly between the tolerant genotypes. The CM line exhibited a far greater number of cold-responsive and uniquely expressed genes than AM, indicating that superior tolerance may be associated with a more expansive and potentially specialized gene regulatory network. This variation in the breadth and intensity of gene expression changes aligns with findings in other plants, where differences in cold signaling and regulation lead to distinct adaptive outcomes [32]. While our study confirms the involvement of conserved stress-response pathways, it also highlights that the degree and coordination of their transcriptional activation are key determinants of phenotypic resilience.

https://doi.org/10.3390/plants15010161

3.5. Synthesis and Mechanistic Model

This study elucidates the molecular mechanisms of low-temperature tolerance during maize germination by integrating phenotypic, physiological, and transcriptomic analyses and proposes a synergistic model (Figure 6). The cold-tolerant inbred lines, especially CM, respond to low-temperature stress by activating a dual adaptive strategy: first, the phenylpropanoid pathway is specifically activated, driving the biosynthesis and accumulation of lignin and related metabolites; second, the flavonoid pathway enhances non-enzymatic antioxidant capacity, which works in concert with a strengthened enzymatic antioxidant system (SOD/POD) to effectively scavenge reactive oxygen species and maintain redox homeostasis. The superior cold tolerance of the CM line is attributed to its stronger and more coordinated activation of these key pathways, along with more extensive and systematic transcriptional reprogramming. These findings establish a mechanistic framework linking specific metabolic pathways to the crucial early-vigor trait of coleoptile elongation, providing valuable targets for molecular breeding of cold-resilient maize.

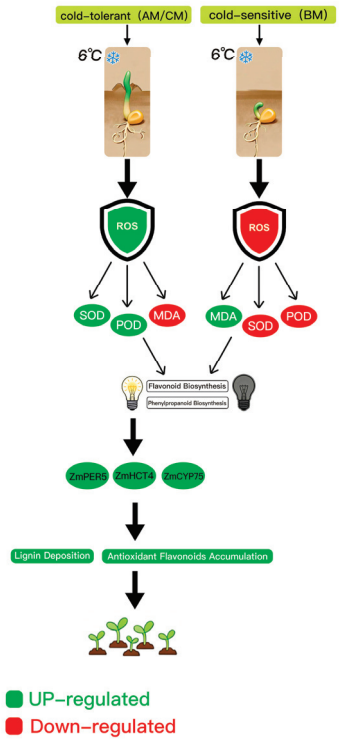

Figure 6. A proposed mechanistic model of cold tolerance in maize germination under 6 °C stress.

4. Materials and Methods

4.1. Plant Materials

Three maize (*Zea mays* L.) inbred lines with previously characterized contrasting cold tolerance were used: J1898 (cold-tolerant, designated AM in this study), J1218 (cold-tolerant, designated CM), and PH4CV (cold-sensitive, designated BM). Seeds were provided by the Maize Breeding Innovation Team, College of Agriculture, Jilin Agricultural University, Changchun, China.

4.2. Seed Germination Assay

Seed germination was evaluated using the rolled paper method [32] in a completely randomized block design. For each inbred line and temperature treatment (25 °C or 6 °C), three biological replicates were performed, each consisting of 100 surface-sterilized seeds on 40 × 50 cm germination paper. Seeds were placed with ventral grooves downward and

embryos upward, and the papers were rolled and incubated vertically at the corresponding temperature. Germination was recorded daily, and a seed was considered germinated when the radicle protruded ≥2 mm beyond the seed coat, totaling 300 seeds per line per treatment [33].

4.3. Germination Rate and Coleoptile Length Measurement

During the germination period, seeds were observed daily. On day 3, germination status was recorded using the criterion of radicle protrusion ≥2 mm beyond the seed coat. The number of germinated seeds was counted, and coleoptile length was measured using a ruler [34].

4.4. Physiological Index Determination

4.4.1. SOD Activity Assay

SOD activity was determined using the nitroblue tetrazolium (NBT) photochemical reduction method [35]. The reaction mixture contained:1.5 mL of 0.05 M phosphate buffer (pH 7.8); 0.3 mL of 180 μM methionine; 0.3 mL of 750 μM NBT; 0.3 mL of 100 μM EDTA-Na_2; 0.3 mL distilled water; 0.05 mL enzyme extract. After thorough mixing, reactions were illuminated at 4000 lux for 10 min. Absorbance was immediately measured at 560 nm using a spectrophotometer. Blank controls contained phosphate buffer instead of enzyme extract. Three biological replicates were performed.

4.4.2. POD Activity Assay

POD activity was measured using the guaiacol method [36]. The reaction was initiated by adding 1 mL of crude POD extract to 3 mL of reaction mixture (containing 25 mM guaiacol and 10 mM H_2O_2 in 50 mM phosphate buffer, pH 6.0). Absorbance changes at 470 nm were recorded at 1-min intervals for 3 min using a spectrophotometer. Blank controls lacked enzyme extract. Three biological replicates were performed.

4.4.3. Malondialdehyde (MDA) Content Determination

MDA content was quantified via the thiobarbituric acid (TBA) reaction [37]. MDA reacts with TBA to form a red adduct with maximum absorbance at 532 nm. Absorbance at 532 nm was measured spectrophotometrically and MDA concentration calculated using an extinction coefficient of 155 $mM^{-1}cm^{-1}$. Three technical replicates were performed per sample.

4.5. Transcriptome Sequencing

4.5.1. RNA Sequencing and Data Processing

Coleoptile tissues from three inbred lines under 6 °C and 25 °C treatments were harvested from rolled paper germination assays for RNA extraction [38]. Samples were collected from 3-day-old coleoptiles, immediately flash-frozen in liquid nitrogen, and stored at −80 °C. Total RNA was isolated from coleoptiles using TRIzol reagent (Invitrogen, Carlsbad, CA, USA, cat. no. GT0240) with three biological replicates per treatment group. RNA integrity was verified using an Agilent 2100 Bioanalyzer (Agilent Technologies, Santa Clara, CA, USA), and only samples with an RNA Integrity Number (RIN) ≥ 8.0 were selected for subsequent experiments. Strand-specific cDNA libraries were prepared using the NEBNext Ultra II RNA Library Prep Kit (New England Biolabs, Ipswich, MA, USA, cat. no. E7775L) [39]. Libraries were quantified with Qubit 3.0 and sequenced on the Illumina NovaSeq 6000 platform (150-bp paired-end reads; ≥20 million reads per sample).

Raw data were processed using Trimmomatic v0.39 to remove adapter sequences and low-quality bases (Phred score < 20). High-quality filtered reads were aligned to the maize B73 reference genome (version 4) using HISAT2 v2.2.1 with default parameters [40].

4.5.2. Differential Gene Expression Analysis

Differentially expressed genes (DEGs) were identified using DESeq2 (v1.20.0) with thresholds of $|\log_2(\text{fold change})| > 1$ and a false discovery rate (FDR) < 0.05 [41]. Comparisons were performed for each inbred line (AM, BM, CM) between cold-treated (6 °C) and control (25 °C) groups. Additional comparisons examined differences between cold-tolerant (AM/CM) and cold-sensitive (BM) germplasms under cold stress. Gene Ontology (GO) enrichment analysis was conducted using clusterProfiler with significance threshold of $p < 0.05$. Gene Set Enrichment Analysis (GSEA) was performed using the local GSEA tool (http://www.broadinstitute.org/gsea/index.jsp) against maize-specific GO and KEGG datasets.

4.5.3. Quantitative Real-Time PCR (qRT-PCR) Validation

Key differentially expressed genes were validated using SYBR Green-based quantitative PCR [42]. Total RNA was extracted from plant tissues using TRIzol reagent (Invitrogen, cat. no. GT0240) [43]. First-strand cDNA synthesis was performed with 1 μg RNA using the ReverTra Ace qPCR RT Kit (TOYOBO, Shanghai, China; Code No. FSQ-101). qPCR reactions were conducted using 2× RealStar Universal SYBR qPCR Mix (Kangyuan Xingye Biotechnology, Beijing, China; Code No. A308-10) on a Bio-Rad CFX96 Real-Time PCR Detection System (USA). Fluorescence signals were monitored in real-time during amplification. Post-amplification, melting curve analysis was performed to verify reaction specificity. ZmActin5 was used as the internal control gene for normalization due to its stable expression across samples. The primers used for ZmActin5 were qActin5-F (GCCGAGCGAGAAATTGTAAG) and qActin5-R (TGGTGATTACTTGGCCATCA) [44]. Relative gene expression was calculated using the $2^{(-\Delta\Delta Ct)}$ method [45]. Three biological replicates with three technical replicates each were included in the experiment.

Supplementary Materials: The following supporting information can be downloaded at https://www.mdpi.com/article/10.3390/plants15010161/s1.

Author Contributions: Conceptualization, J.T. and X.R.; Methodology, X.Y.; Software, Z.Z.; Formal analysis, H.S., W.Y. and J.C.; Investigation, L.J.; Writing—original draft, S.Z. All authors have read and agreed to the published version of the manuscript.

Funding: This research was funded by the Jilin Province Focused Tackling Project grant number 2025JLGJ0004NC.

Data Availability Statement: The original sequencing data generated in this study have been deposited in the Sequence Read Archive (SRA) database under the accession number PRJNA1378803.

Conflicts of Interest: The authors declare no conflict of interest.

References

1. Erenstein, O.; Jaleta, M.; Sonder, K.; Mottaleb, K.; Prasanna, B.M. Global maize production, consumption and trade: Trends and R&D implications. *Food Secur.* **2022**, *14*, 1295–1319. [CrossRef]
2. Choudhary, M.; Singh, A.; Gupta, M.; Rakshit, S. Enabling technologies for utilization of maize as a bioenergy feedstock. *Biofuels Bioprod. Biorefining* **2020**, *14*, 402–416. [CrossRef]
3. Yang, S.; Li, Y.; Wang, Y.; Zhang, X.; Liu, X. A natural variant of COOL1 enhances cold tolerance for high-latitude adaptation in maize. *Cell* **2025**, *188*, 1024–1039.
4. FAO. *Agricultural Production Statistics 2000–2020. FAOSTAT Analytical Brief 41*; FAO: Rome, Italy, 2022.
5. Li, X.; Sun, Y.; Liu, J.; Wang, Y. Chilling stress disrupts starch metabolism and redox homeostasis during maize seed germination. *Plant Physiol. Biochem.* **2023**, *189*, 432–443.
6. Zhang, J.; Huang, B. Chilling-induced oxidative stress and antioxidant responses in maize seedlings. *J. Integr. Plant Biol.* **2012**, *54*, 968–980.

7. Hou, P.; Li, X.; Liu, Y.; Zhang, S. GWAS identifies loci for low-temperature germination ability in maize. *Front. Plant Sci.* **2021**, *12*, 689345.
8. Fuentes, M.; Alvarado, D.; Pinto, M. Cold tolerance evaluation in Chilean rice genotypes at the germination stage. *J. Agron. Crop Sci.* **2020**, *206*, 215–224.
9. Zhao, X.; Niu, Y.; Hossain, Z.; Bai, X.; Mao, T. Light-quality–regulated plasticity of maize coleoptile and mesocotyl elongation during germination. *Front. Plant Sci.* **2023**, *14*, 1152399.
10. Liu, X.; Wang, Y.; Zhang, X.; Li, J.; Zhao, H.; Chen, L.; Yang, M.; Zhou, Q.; Wu, S.; Sun, T.; et al. Identification of cold-tolerant genes in rice via GWAS. *Rice Sci.* **2020**, *27*, 203–212.
11. Shakiba, E.; Eizenga, G.C.; McCouch, S.R. SNPs Associated with rice seedling cold tolerance identified by GWAS. In Proceedings of the Rice Technical Workshop Group, Hangzhou, China, 12–15 October 2014.
12. Zhao, X.; Wang, P.; Si, T.; Hsu, C.-C.; Wang, L.; Zayed, O.; Yu, Z.; Zhu, Y.; Dong, J.; Tao, W.A.; et al. MAP kinase cascades regulate the cold response by modulating ICE1 stability. *Dev. Cell* **2017**, *42*, 637–651. [CrossRef]
13. Saijo, Y.; Hata, S.; Kyozuka, J.; Shimamoto, K.; Izui, K. Overexpression of a Ca^{2+}-dependent protein kinase confers cold tolerance in rice. *Plant J.* **2000**, *23*, 319–332. [CrossRef]
14. Wang, Y.; Zhang, L.; Li, J.; Zhao, H.; Chen, F. Wheat TaSOD1.2 maintains redox homeostasis under cold stress. *Plant Physiol.* **2020**, *184*, 1325–1340.
15. Lee, G.H.; Kim, J.; Lee, S.C. Cytosolic ascorbate peroxidase contributes to cold tolerance in rice. *Plant Cell Environ.* **2013**, *36*, 1881–1895.
16. Tavu, L.E.J.; Redillas, M.C.F.R. Oxidative Stress in Rice (*Oryza sativa*): Mechanisms, Impact, and Adaptive Strategies. *Plants* **2025**, *14*, 1463. [CrossRef] [PubMed]
17. Gulzar, F.; Yang, H.; Chen, J.; Hassan, B.; Huang, X.; Qiong, F. 6-BA Reduced Yield Loss under Waterlogging Stress by Regulating the Phenylpropanoid Pathway in Wheat. *Plants* **2024**, *13*, 1991. [CrossRef]
18. Wang, C.; Hao, N.; Li, Y.; Sun, N.; Wang, L.; Ye, Y. Cold-tolerance candidate gene identification during maize germination via multi-omics. *Agronomy* **2025**, *15*, 1067. [CrossRef]
19. Zhang, J.; Liu, J.P.; Yang, R.J.; Yuan, Y.Y.; Li, D.Y.; Zhang, Z.H. Melatonin differentially regulates the activities of antioxidant enzymes in roots and coleoptiles of etiolated maize seedlings. *J. Plant Growth Regul.* **2019**, *38*, 1438–1449.
20. Dou, Y.; Luo, W.; Zhang, Y.; Li, W.; Zhang, C.; Lv, Y.; Liu, X.; Yu, S. Integrated transcriptome–metabolome analysis reveals the flavonoids metabolism mechanism of maize radicle in response to low temperature. *Plants* **2025**, *14*, 2988. [CrossRef]
21. Kusvuran, S.; Kiran, S.; Ellialtioglu, S.S. Antioxidant enzyme activities and abiotic stress tolerance relationship in vegetable crops. In *Abiotic and Biotic Stress in Plants—Recent Advances and Future Perspectives*; InTech: London, UK, 2016; pp. 481–506.
22. Vogt, T. Phenylpropanoid biosynthesis. *Mol. Plant* **2010**, *3*, 221–237. [CrossRef]
23. Zhang, Y.; Li, Y.; Zhao, X.; Wang, H.; Chen, J.; Liu, S.; Zhou, Q.; Wu, L.; Sun, M.; Han, Z.; et al. Effects of low-temperature stress on seed germination and seedling growth of different maize varieties. *J. Northeast Agric. Univ. Engl. Ed.* **2018**, *25*, 79–86.
24. Li, Y.; Zhang, H.; Wang, X. Effects of low temperature on coleoptile growth and cell elongation in wheat. *J. Cereal Sci.* **2015**, *62*, 210–216.
25. Bindschedler, L.V.; Feussner, I.; Kwon, S.J.; Lee, J.; Choi, Y.; Apel, K.; Durner, J.; Klessig, D.F.; Park, C.M.; Kang, B.G.; et al. The role of class III peroxidases in plant defence. *Trends Plant Sci.* **2006**, *11*, 533–540.
26. Agati, G.; Tattini, M. Flavonoids as antioxidants in plants: Location and functional significance. *Plant Sci.* **2010**, *179*, 673–681. [CrossRef]
27. Sato, Y.; Tanaka, Y.; Nakano, Y.; Asada, K. Ascorbate peroxidase 2 is a key enzyme for hydrogen peroxide scavenging during photooxidative stress in rice leaves. *Plant Cell Physiol.* **2011**, *52*, 1780–1792.
28. Qin, Y.; Li, J.; Zhang, S. Transcriptome profiling reveals key genes involved in cold stress response in maize seedlings. *BMC Genom.* **2020**, *21*, 648.
29. Mao, Y.; Zhang, L.; Li, J.; Wang, H.; Chen, S.; Liu, Q.; Zhao, Y.; Huang, J.; Zhou, X.; Sun, W.; et al. Genome-wide association study reveals divergent genetic architectures for cold tolerance at germination and seedling stages in rice. *New Phytol.* **2021**, *231*, 1166–1181.
30. Li, J.; Zhang, Y.; Dong, C.; Yang, S.; Wang, H.; Chen, L.; Liu, Q.; Zhao, X.; Huang, M.; Zhou, T.; et al. Heat shock transcription factor HSF21 enhances cold tolerance in maize by activating the CBF pathway and antioxidant system. *Mol. Plant* **2023**, *16*, 823–838.
31. He, R.Y.; Zheng, J.J.; Chen, Y.; Pan, Z.Y.; Yang, T.; Zhou, Y.; Li, X.-F.; Nan, X.; Li, Y.-Z.; Cheng, M.-J.; et al. QTL-seq and Transcriptomic Integrative Analyses Reveal Two Positively Regulated Genes That Control the Low-Temperature Germination Ability of MTP–Maize Introgression Lines. *Theor. Appl. Genet.* **2023**, *136*, 116. [CrossRef]
32. Draves, M.A.; Banerjee, A.; Eckardt, N.A. Maize seedling growth and hormone response assays using the rolled towel method. *Curr. Protoc.* **2022**, *2*, e562. [CrossRef] [PubMed]

33. Tandon, J.P.; Grover, S.K.; Chaturvedi, S.K. *Guidelines for Testing Crop Varieties Under the All-India Coordinated Crop Improvement Projects*; Indian Council of Agricultural Research: New Delhi, India, 2015.
34. Hakizimana, F.; Haley, S.D.; Turnipseed, E.B. Repeatability and genotype × environment interaction of coleoptile length measurements in winter wheat. *Crop Sci.* **2000**, *40*, 1233–1237. [CrossRef]
35. Yan, N.; Cao, J.; Wang, J.; Zou, X.; Yu, X.; Zhang, X.; Si, T. Seed priming with graphene oxide improves salinity tolerance and increases productivity of peanut through modulating multiple physiological processes. *J. Nanobiotechnol.* **2024**, *22*, 565. [CrossRef] [PubMed]
36. Pruitt, K.M.; Reiter, B. Biochemistry of peroxidase system: Antimicrobial effects. In *The Lactoperoxidase System: Chemistry and Biological Significance*; Reiter, B., Hjorth, S., Tenovuo, J., Eds.; Marcel Dekker: Washington, DC, USA, 1985; pp. 143–178.
37. Senthilkumar, M.; Prasad, M.N.V. Estimation of malondialdehyde (MDA) by thiobarbituric acid (TBA) assay. In *Handbook of Stress Tolerance in Plants: Volume 2: Assessment of Plant Stress Tolerance*; Sahu, P.K., Mandal, S.C., Mishra, S., Eds.; Springer: Singapore, 2021; pp. 325–333.
38. Hadi, M.; Stacy, E.A. An optimized RNA extraction method for diverse leaves of Hawaiian Metrosideros, a hypervariable tree species complex. *Appl. Plant Sci.* **2023**, *11*, e11518. [CrossRef]
39. Anders, S.; Huber, W. Differential expression analysis for sequence count data. *Genome Biol.* **2010**, *11*, R106. [CrossRef]
40. Garber, M.; Grabherr, M.G.; Guttman, M.; Trapnell, C. Computational methods for transcriptome annotation and quantification using RNA-seq. *Nat. Methods* **2011**, *8*, 469–477. [CrossRef]
41. Goldstein, L.D.; Cao, Y.; Pau, G.; Lawrence, M.; Wu, T.D.; Seshagiri, S.; Gentleman, R. Prediction and quantification of splice events from RNA-Seq data. *PLoS ONE* **2016**, *11*, e0156132. [CrossRef]
42. Huang, J.; Wu, J.; Li, C.; Xiao, C.; Wang, G. Specific and sensitive detection of Ralstonia solanacearum in soil with quantitative, real-time PCR assays. *J. Appl. Microbiol.* **2009**, *107*, 1729–1739. [CrossRef]
43. Litholdo, C.G., Jr.; da Fonseca, G.C. Circular RNAs and plant stress responses. In *Circular RNAs: Biogenesis and Functions*; Springer: Berlin/Heidelberg, Germany, 2018; pp. 345–353.
44. Jia, X.; Wang, F.; Sun, B.; Zhang, X. Selection of reliable reference genes for quantitative real-time PCR studies in maize grains. *Plant Mol. Biol. Report.* **2012**, *30*, 254–263.
45. Livak, K.J.; Schmittgen, T.D. Analysis of relative gene expression data using real-time quantitative PCR and the $2^{-\Delta\Delta Ct}$ method. *Methods* **2001**, *25*, 402–408. [CrossRef] [PubMed]

plants

MDPI

Article

BnaMYB73, a *Brassica napus* L. R2R3-MYB Transcription Factor, Enhances Plant Salt and Osmotic Stress Tolerance

Limin Wang [1,2,†], Yuzhe Zhang [1,2,†], Xiaoyan Zhou [1,2,†], Xin Xu [1,2], Hongxia Zhang [1,2,3], Nan Sun [1,2,*], Dong Li [1,2,*] and Yanfeng Liu [1,2,*]

[1] Yantai Technology Center of Characteristic Plant Gene Editing and Germplasm Innovation, Engineering Research Institute of Agriculture and Forestry, Ludong University, Yantai 264025, China; wanglimin9696@163.com (L.W.); yzzhang_0818@126.com (Y.Z.); zhouxiaoy1999@163.com (X.Z.); xx2332736082@163.com (X.X.); hxzhang@sibs.ac.cn (H.Z.)
[2] Yantai Key Laboratory of Crop Molecular Breeding for High-Yield and Stress-Resistant Crops and Efficient Cultivation, College of Horticulture, Ludong University, Yantai 264025, China
[3] School of Biological Science and Technology, University of Jinan, 336 Nanxinzhuangxi Road, Jinan 250024, China
* Correspondence: sunn9021@163.com (N.S.); ld@nwafu.edu.cn (D.L.); liuyf3097@126.com (Y.L.)
† These authors contributed equally to this work.

Abstract

MYB transcription factors (TFs) are crucial for plant growth, development, and response to abiotic stress. However, their exact functions in abiotic stress responses in rapeseed remain largely unexplored. In this study, we identified and characterized *BnaMYB73*, a member of the R2R3-MYB subfamily, and investigated its role in abiotic stress tolerance. The transcription level of *BnaMYB73* was significantly upregulated in response to salt and osmotic stress. Transgenic *Arabidopsis thaliana* lines expressing *BnaMYB73* displayed significantly enhanced tolerance to salt and osmotic stress, while showing no phenotypic differences in growth compared with wild-type (WT) plants under normal conditions. Physiological analyses revealed that the *BnaMYB73*-expressing plants accumulated higher proline levels, exhibited elevated superoxide dismutase (SOD) and peroxidase (POD) activities, and reduced malondialdehyde (MDA) content under stress conditions. Moreover, the *BnaMYB73*-expressing plants significantly upregulated key stress-responsive genes, including *AtRD29B*, *AtDREB2A*, *AtRAB18*, *AtP5CS1*, *AtSOS1* and *AtCAT1*. Collectively, these findings establish BnaMYB73 functions as a stress-responsive transcription factor that enhances abiotic stress tolerance and provide a promising target for breeding stress-resilient rapeseed cultivars.

Keywords: *Brassica napus* L.; BnaMYB73 transcription factors; salt and osmotic stress; transgenic plants

1. Introduction

Adverse external environments, such as salt and drought, severely inhibit plant growth and development, leading to lower yields [1]. To cope, plants have evolved efficient regulatory mechanisms [2]. Proline accumulation during stress helps regulate osmotic balance and reduces reactive oxygen species (ROS)-induced oxidative damage [3,4]. Additionally, stress-responsive genes, including *SOS1*, *P5CS1* and *CAT1*, are activated to improve stress tolerance [5–7]. Key transcription factors (TFs) like MYB, WRKY, NAC and AP2/ERF mediate these responses through binding to these gene promoter *cis*-elements [8–11].

MYB TFs are prevalent and essential, controlling growth, development, and stress responses via interaction with *Myb cis*-acting elements of target gene promoters [10]. Their conserved DNA-binding domain contains one to four repeats (each ~52 amino acids), folding into three α-helices, with the second and third helices forming a helix-turn-helix structure [12]. Repeats are designated R1, R2, and R3 based on their homology with the c-Myb protein [12]. According to the repeats, MYB are classified as MYB-related, R2R3, R1R2R3, and 4R, with R2R3 MYBs being the most abundant [12].

It is well documented that R2R3 MYB members have essential functions in plant growth, development, and abiotic stress responses. In Arabidopsis, *AtMYB20* is upregulated by salt and drought, and its overexpression enhances salt tolerance through suppression of *PP2Cs* expression [13]. Similarly, *AtMYB21* overexpression increases salt tolerance during both germination and vegetative growth in Arabidopsis [14]. *AtMYB49* improves salt tolerance in an ABA-dependent manner by regulating cuticle biosynthesis and antioxidant defense [15]. *AtMYB68* enhances drought resistance and ABA sensitivity during germination and seedling growth. Correspondingly, transgenic canola plants expressing *AtMYB68* display superior tolerance to diverse abiotic stresses, accompanied by higher yield performance [16]. *AtMYB93* negatively regulates lateral root formation through interacting with ARABIDILLO and promoting its degradation [17]. In rice, *OsMYB2* is induced with salinity, drought, and low temperature, and transgenic lines exhibit enhanced tolerance and increased ABA sensitivity due to increased osmolyte accumulation, antioxidant activity, and reduced oxidative damage [18]. In tomato, *SlMYB49* enhances resistance to *Phytophthora infestans*, leading to reduced necrosis, smaller lesion size, lower pathogen load, and decreased disease severity [19]. In alfalfa, *MsMYB4* expressed in Arabidopsis markedly improves salt tolerance in an ABA-dependent manner, as evidenced by higher germination rates and increased root elongation [20].

Different from the one described above, *MYB73* exhibits dual regulatory behavior, acting positively or negatively depending on plant species. In Arabidopsis, *AtMYB73* acts as a negative regulator, as evidenced by the greater salt tolerance of *atmyb73* mutants relative to WT plants [21]. Similarly, *GmMyb73*, mainly expressed in the root, suppresses tolerance to low-phosphorus stress in soybean [22]. Contrary to its negative regulatory activity, MYB73 acts as a positive regulator in wheat and cotton. In wheat, *TaMYB73* expression is induced by various abiotic stresses, including salinity, drought, and hormonal signals. Arabidopsis lines overexpressing *TaMYB73* display greater tolerance to NaCl, LiCl, and KCl, as well as enhanced germination under salt and ABA stress [23]. In cotton, *GhMYB73*, induced by salt and ABA, improves salt resistance, while its silencing increases NaCl sensitivity [24].

Rapeseed (*Brassica napus* L.) is a widely cultivated oil crop. However, its growth and yield are frequently constrained by adverse environmental factors, particularly salinity and drought [25,26]. Despite extensive research on MYB73 in various plants, its biological functions in stress regulation in oilseed crops remain largely uncharacterized. In this work, we cloned the rapeseed *BnaMYB73* and elucidated its role in salt and drought stress responses. *BnaMYB73* expression was upregulated by salt and osmotic stress, and heterologous expression of *BnaMYB73* in Arabidopsis conferred elevated salt and drought resilience, identifying it as a positive modulator in abiotic stress responses.

2. Materials and Methods

2.1. Multiple Sequence Alignment, Phylogenetic Analysis and Three-Dimensional Structure Prediction

MYB protein sequences from *Brassica napus*, *Arabidopsis thaliana*, *Gossypium hirsutum*, and *Glycine max* were aligned using the ClustalW program v2.0.11. A Neighbor-Joining

https://doi.org/10.3390/plants15050694

phylogenetic tree was generated to elucidate the evolutionary relationships among these sequences, with 1000 bootstrap replications performed in MEGA 11.0. The three-dimensional structure of BnaMYB73 was predicted using the SWISS-MODEL server and visualized with Pymol software v3.1.

2.2. Rapeseed Growth Environments and Stress Treatments

The *Brassica napus* cultivar 'Zhongshuang 11' and *Arabidopsis thaliana* ecotype Col-0 were used in this study. Plant growth conditions followed previously reported protocols [27]. Seeds were surface-sterilized with 75% (*v*/*v*) ethanol and rinsed five times with sterile ddH_2O. Sterilized seeds were germinated on half-strength Murashige and Skoog (1/2 MS) medium and grown under controlled conditions (24 °C/22 °C, 50–60% relative humidity, 16 h light/8 h dark photoperiod). After one week, seedlings were transplanted to a 1:1 (*v*/*v*) mixture of vermiculite and nutrient soil and cultivated in a greenhouse. For tissue-specific expression analysis, roots, stems, leaves, flowers, and siliques were collected from six-month-old rapeseed plants. For stress treatments, five-week-old rapeseed plants were treated with either 150 mM NaCl or 20% (*w*/*v*) PEG6000 for 0 h, 1 h, 3 h, 6 h, 9 h, 12 h and 24 h, after which leaf and root samples were harvested for further experiments. Two-week-old Arabidopsis seedlings, including wild-type and transgenic lines, were exposed to 200 mM NaCl or 300 mM mannitol for 9 h, followed by leaf sampling for RNA extraction and physiological measurements.

2.3. Transactivation Analysis of BnaMYB73 in Yeast Cells

The full-length coding sequence of *BnaMYB73* was amplified using gene-specific primers listed in Table S1 and cloned into the pGBKT7 vector to generate the recombinant plasmid pGBKT7-*BnaMYB73*. This resulting plasmid was then introduced into the yeast strain AH109. Yeast cells transformed with the empty pGBKT7 vector and pGBKT7-VP16 served as negative and positive controls, respectively. Yeast transformants were first selected on SD/-Trp medium and subsequently replicated onto SD/-Trp/-His medium supplemented with 4 mg/mL X-α-gal (SD/-Trp/-His/X). After incubation for three days, the transactivation activity of BnaMYB73 was assessed based on yeast phenotypes.

2.4. Subcellular Localization of BnaMYB73

To determine the subcellular localization, the coding sequence of *BnaMYB73* was fused to the pGreen-35S-GFP vector (35S-GFP), resulting in the 35S:*BnaMYB73*-GFP construct. This recombinant plasmid was introduced into *Agrobacterium tumefaciens* GV3101 and transiently expressed in *Nicotiana benthamiana* leaves as previously described [28]. For co-localization analysis, transgenic tobacco plants expressing a nuclear-localized red fluorescent protein (NLS-mCherry) were used as a nuclear marker [29]. Forty-eight hours post-injection, fluorescence signals were observed using laser scanning confocal microscopy (Zeiss LSM710, Jena, Germany). GFP was excited at 488 nm with emission collected between 500 and 540 nm, while mCherry was excited at 559 nm with emission collected between 600 and 680 nm.

2.5. Quantitative Real-Time PCR Experiment

The collected samples were homogenized for RNA extraction and subsequent RT-qPCR analysis. Total RNA was isolated and reverse-transcribed into cDNA using the Vazyme R423-01 kit (Vazyme Biotech Co., Ltd., Nanjing, China) according to the manufacturer's instructions. *BnaActin* from rapeseed and *AtActin* from Arabidopsis were used as the reference genes. Primers used to perform RT-qPCR are listed in Table S1. The $2^{-\Delta\Delta Ct}$ method established by Livak and Schmittgen [30] was used to quantify relative gene expression.

2.6. Stress Tolerance Experiments of the Transgenic Yeast

The coding sequence of rapeseed *BnaMYB73* was inserted into the yeast expression vector pYES2 (Coolaber (Beijing, China), PL001) and transformed into yeast strain INVSc1 (Coolaber, CC303). Yeast carrying either pYES2-*BnaMYB73* or the empty vector was initially cultured in SC-ura liquid medium supplemented with 2% glucose at 30 °C for 24 h. Subsequently, cultures were then diluted to an OD_{600} of 0.4 in induction medium (SC-ura liquid medium with 2% galactose) and incubated for 36 h, after which cell densities were adjusted to OD_{600} = 1.8. For assessing salt and osmotic stress tolerance, the transformed yeasts were cultured in 4 M NaCl or 1 M mannitol for 48 h in an incubator, with sterile ddH_2O as a control.

2.7. Plant Genetic Generation

To create *BnaMYB73*-expressing Arabidopsis, the coding sequence was amplified and inserted into the binary vector pCAMBIA2301 under the CaMV35S promoter using Vazyme ClonExpress II One Step Cloning Kit. The resulting construct was introduced into GV3101 for subsequent Arabidopsis transformation according to the established protocol [31]. After transformation, the harvested seeds were germinated on 1/2 MS medium with 50 μg/mL kanamycin [32]. Kanamycin-resistant seedlings were transplanted to soil and cultivated to maturity. Homozygous lines were confirmed through antibiotic resistance segregation analysis in the subsequent generations. Expression verification of *BnaMYB73* was performed using RT-qPCR on eight independently derived overexpression lines.

2.8. Germination Assay

For germination assays, fifty surface-sterilized seeds from each genotype were sown on 1/2 MS medium supplemented with either 100 mM NaCl, 250 mM mannitol, or without additives as the control. Plates were incubated under controlled growth conditions. Seed germination was monitored daily for 7 days and was defined by radicle emergence through the seed coat. Additionally, cotyledon greening rate, defined as the percentage of seedlings with fully expanded green cotyledons, was also assessed. All experiments were performed with three biological replicates.

2.9. Stress Tolerance Assays

To assess stress tolerance at the seedling stage, three-day-old *Arabidopsis thaliana* seedlings were transplanted to 1/2 MS medium supplemented with either 100 mM NaCl, 300 mM mannitol, or without additives as the control. Seedling growth was monitored daily, and after seven days of treatment, growth performance was recorded. Growth parameters included fresh biomass and primary root length, and the root length inhibition rate was calculated to quantify the effects of salt and osmotic stress. For stress tolerance assays at the adult plant stage, ten-day-old seedlings were transplanted into pots containing a 1:1 (v/v) mixture of vermiculite and nutrient soil and grown under controlled environmental conditions for three weeks. Thereafter, salt stress was imposed by irrigating with 300 mM NaCl for seven days, while drought stress was induced by withholding irrigation for three weeks. During the stress treatments, plant growth parameters and phenotypic responses were systematically recorded to assess stress tolerance.

2.10. Physiological and Gene Expression Analysis

Fourteen-day-old WT and *BnaMYB73*-expressing lines were exposed to 200 mM NaCl or 300 mM mannitol for nine hours under controlled growth conditions. Following stress exposure, leaves were harvested to evaluate a range of physiological parameters, including superoxide dismutase (SOD) and peroxidase (POD) activities, malondialde-

hyde (MDA) and proline contents. All measurements were conducted using standardized assay kits (Solarbio, Beijing, China; BC5165 for SOD activity; BC0090 for POD activity; BC0025 for MDA content; BC0290 for proline content). Concurrently, total RNA was extracted from treated leaves for RT-qPCR to determine the transcript levels of stress-responsive genes: *RD29B*, *DREB2A*, *RAB18*, *P5CS1*, *SOS1*, and *CAT1*. Gene expression was normalized to internal reference genes *AtActin* (AT2G37620) and *BnaActin* (FJ529167.1) using the $2^{-\Delta\Delta Ct}$ method. The corresponding accession numbers for the analyzed genes and proteins are as follows: BnaMYB73 (XP_013686616.1), AtMYB73 (AT4G37260; NP_195443.1), GhMYB73 (XP_016709948.2), GmMYB73 (Glyma.01G190100.1), *RD29B* (AT5G52300), *DREB2A* (AT5G05410), *RAB18* (AT5G66400), *P5CS1* (AT2G39800), *SOS1* (AT2G01980), *CAT1* (AT1G20630), *AtActin* (AT2G37620), and *BnaActin* (FJ529167.1).

2.11. Statistical Analysis

All data, expressed as means ± SD, are from three independent biological replicates, each consisting of at least 10 plants to ensure accuracy and reproducibility. Statistical significance was established using Student's *t*-test, with *p*-value less than 0.05 (*) and 0.01 (**).

3. Results

3.1. BnaMYB73 Encodes an R2R3 MYB Transcription Factor in Rapeseed

To characterize the functional role of *BnaMYB73* in rapeseed, the gene was cloned and analyzed using multiple sequence alignment, phylogenetic relationship, and 3D structure analysis. The *BnaMYB73* coding sequence spans 915 bp and encodes 304 amino acids. Sequence analysis revealed two highly conserved R2 and R3 repeats at the N-terminal region, classifying it within the R2R3-MYB subfamily (Figure 1A). Further phylogenetic analysis revealed that BnaMYB73 exhibited the highest sequence similarity with the *Arabidopsis thaliana* AtMYB73, sharing 79.63% amino acid identity (Figure 1B). Moreover, the 3D structure model indicated that the R2 and R3 repeats domain contains three α-helices, where the second and third helices form a characteristic helix-turn-helix structure (Figure 1C).

3.2. BnaMYB73 Is a Nuclear-Localized Transcriptional Activator

To investigate the subcellular localization of BnaMYB73, 35S:*BnaMYB73*-GFP or 35S:GFP constructs were transiently expressed in *Nicotiana benthamiana* leaves, together with the nuclear marker NLS-mCherry. Overlapping GFP and mCherry signals revealed that rapeseed BnaMYB73 is predominantly localized in the nucleus (Figure 2A). To assess its transcriptional activation, pGBKT7-*BnaMYB73*, pGBKT7-*VP16*, or the empty pGBKT7 vector was transformed into the yeast strain AH109. All transformants grew on SD/-Trp medium, confirming successful transformation. Notably, yeast cells carrying pGBKT7-*BnaMYB73* and pGBKT7-*VP16* turned blue on SD/-Trp/-His/X medium, suggesting that BnaMYB73 can activate the *MEL1* reporter gene and functions as a transcriptional activator (Figure 2B).

3.3. BnaMYB73 Expression Is Upregulated in Response to Salt and Osmotic Stress in Rapeseed

To investigate the tissue-specific expression, *BnaMYB73* transcript levels were quantified in various tissues and organs, including silique, root, stem, leaf, and flower, from six-month-old rapeseed plants. The results indicated rapeseed *BnaMYB73* is widely expressed across all examined tissues, with the highest abundance detected in roots (Figure 2C). We further investigated the *BnaMYB73* expression in five-week-old rapeseed plants treated with 150 mM NaCl or 20% PEG6000. Under both salt and osmotic stress, *BnaMYB73* expression was upregulated in leaves and roots, suggesting a potential role in mediating responses to abiotic stress (Figure 2D,E).

https://doi.org/10.3390/plants15050694

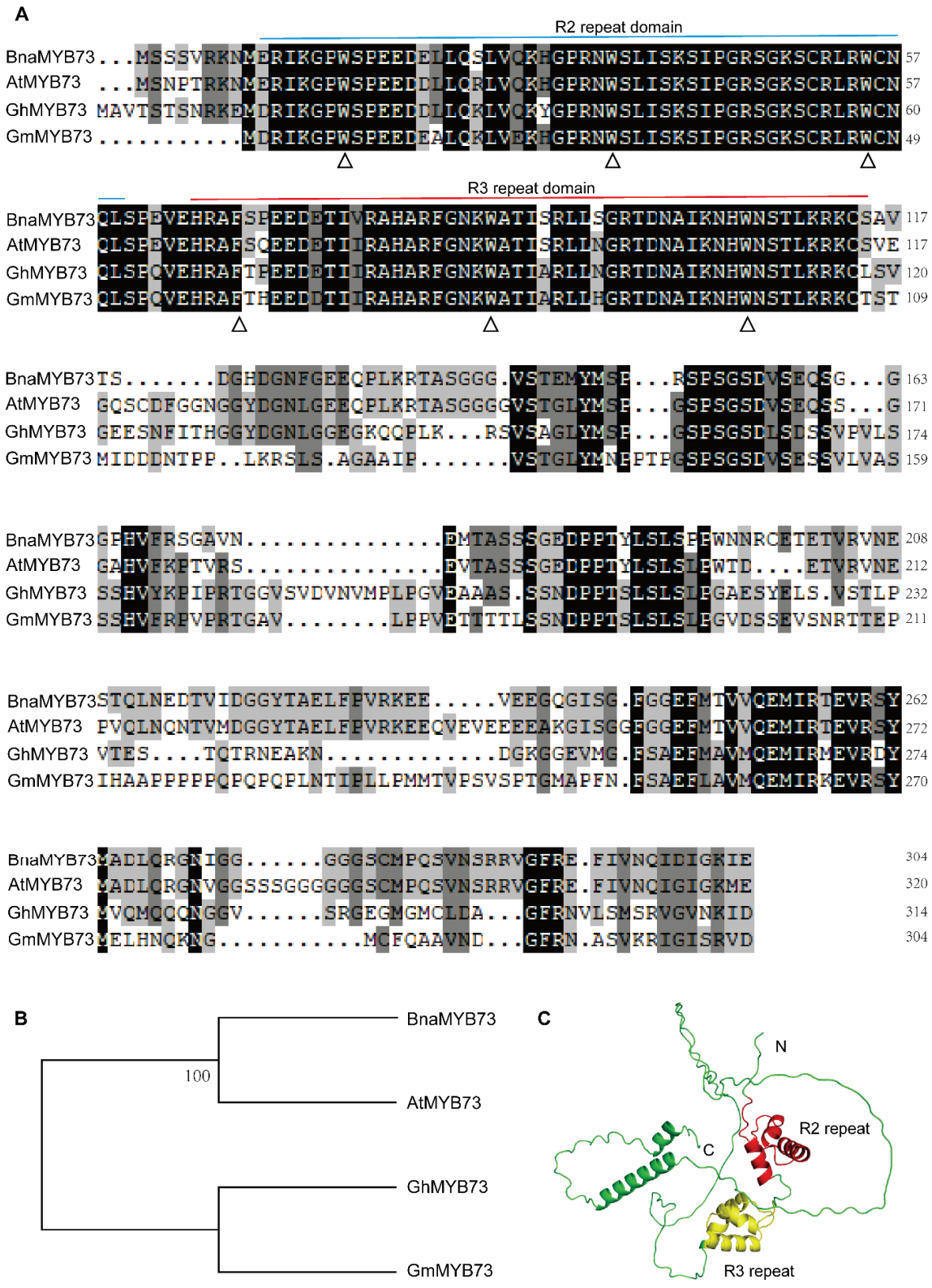

Figure 1. Phylogenetic and structural characterization of BnaMYB73. (**A**) Multiple sequence alignment of BnaMYB73 and its orthologs from various species. The highly conserved amino acids, Phenylalanine (F) and Tryptophan (W), were marked by triangles. The R2 and R3 domains were labeled by blue and red lines, respectively. Bna, *Brassica napus*; At, *Arabidopsis thaliana*; Gh, *Gossypium hirsutum*; Gm, *Glycine max*. Residues were labeled in black, dark gray and light gray to denote their conservation levels of 100%, 75% and 50%. (**B**) Phylogenetic tree of BnaMYB73, AtMYB73, GhMYB73, and GmMYB73. (**C**) The 3D structure of BnaMYB73. The R2 and R3 repeats were labeled in red and yellow, respectively. C: the C- terminal of BnaMYB73. N: the N- terminal of BnaMYB73.

https://doi.org/10.3390/plants15050694

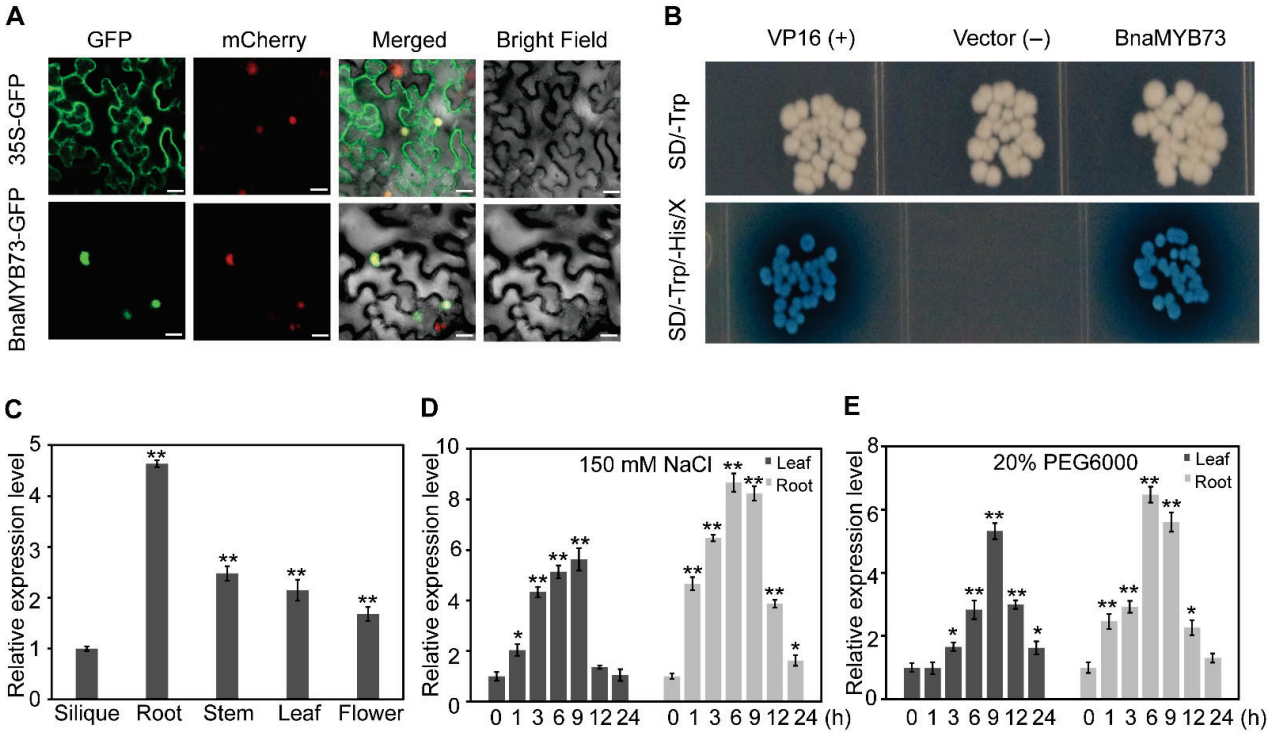

Figure 2. Subcellular localization of BnaMYB73 and expression profiles of *BnaMYB73*. (**A**) Subcellular localization of BnaMYB73 in tobacco leaves. mCherry: red fluorescent protein fused with a nuclear-localized protein. Merge: overlay of bright field, GFP and mCherry. Bars = 25 μm. (**B**) Transactivation activity assay of BnaMYB73. (**C**) The expression level of *BnaMYB73* in silique, root, stem, leaf, and flower from six-month-old rapeseed. (**D**,**E**) The expression patterns of *BnaMYB73* in leaf and root in five-week-old rapeseed treated by 150 mM NaCl or 20% PEG6000, respectively. The housekeeping gene *BnaActin* served as the internal reference gene. Each data was presented as means ± SD. * and ** represented $p < 0.05$, and $p < 0.01$, respectively.

3.4. BnaMYB73 Enhances Salt and Osmotic Tolerance in Yeast

To preliminarily investigate the functional roles of *BnaMYB73* in eukaryotic systems, the gene was inserted into the yeast expression vectors pYES2 and transformed into the yeast strain INVSc1. Transformed yeast harboring either pYES2-*BnaMYB73* or the empty vector was exposed to ddH_2O, 4 M NaCl, or 1 M mannitol for 48 h. However, under normal conditions, all yeast strains displayed similar growth phenotypes. However, under salt and osmotic stress, yeast cells carrying pYES2-*BnaMYB73* exhibited significantly enhanced growth compared to those carrying the empty vector, suggesting increased tolerance to both salt and osmotic stress (Figure S1).

3.5. BnaMYB73 Expression Enhances Seed Germination in Response to Salt and Osmotic Stress

To investigate the biological role of *BnaMYB73* in response to salt and osmotic stress, eight homozygous Arabidopsis lines expressing *BnaMYB73* were generated and their expression levels were confirmed via RT-qPCR. Three independent transgenic lines (OE#3, OE#4, and OE#7), representing high, medium, and low expression levels, were selected for further analysis (Figure S2). Seed germination and cotyledon greening rates were evaluated through sowing WT and *BnaMYB73*-expressing seeds on 1/2 MS medium supplemented with 0, 100 mM NaCl, or 250 mM mannitol for 7 days (Figure 3A). Under normal growth conditions, germination and cotyledon greening rates were comparable between WT and transgenic seeds (Figure 3B,E). In contrast, under salt and osmotic stress conditions, both germination rate and cotyledon greening rate were significantly reduced. Notably, OE#3 and OE#4 seeds showed significantly higher germination and cotyledon greening rates

compared to WT and OE#7 seeds, although their germination rate became comparable after 7 days (Figure 3C–E). In conclusion, *BnaMYB73*-expression Arabidopsis lines led to enhanced seed germination and cotyledon development under NaCl and osmotic stress, indicating improved salt and osmotic stress tolerance during early seedling development.

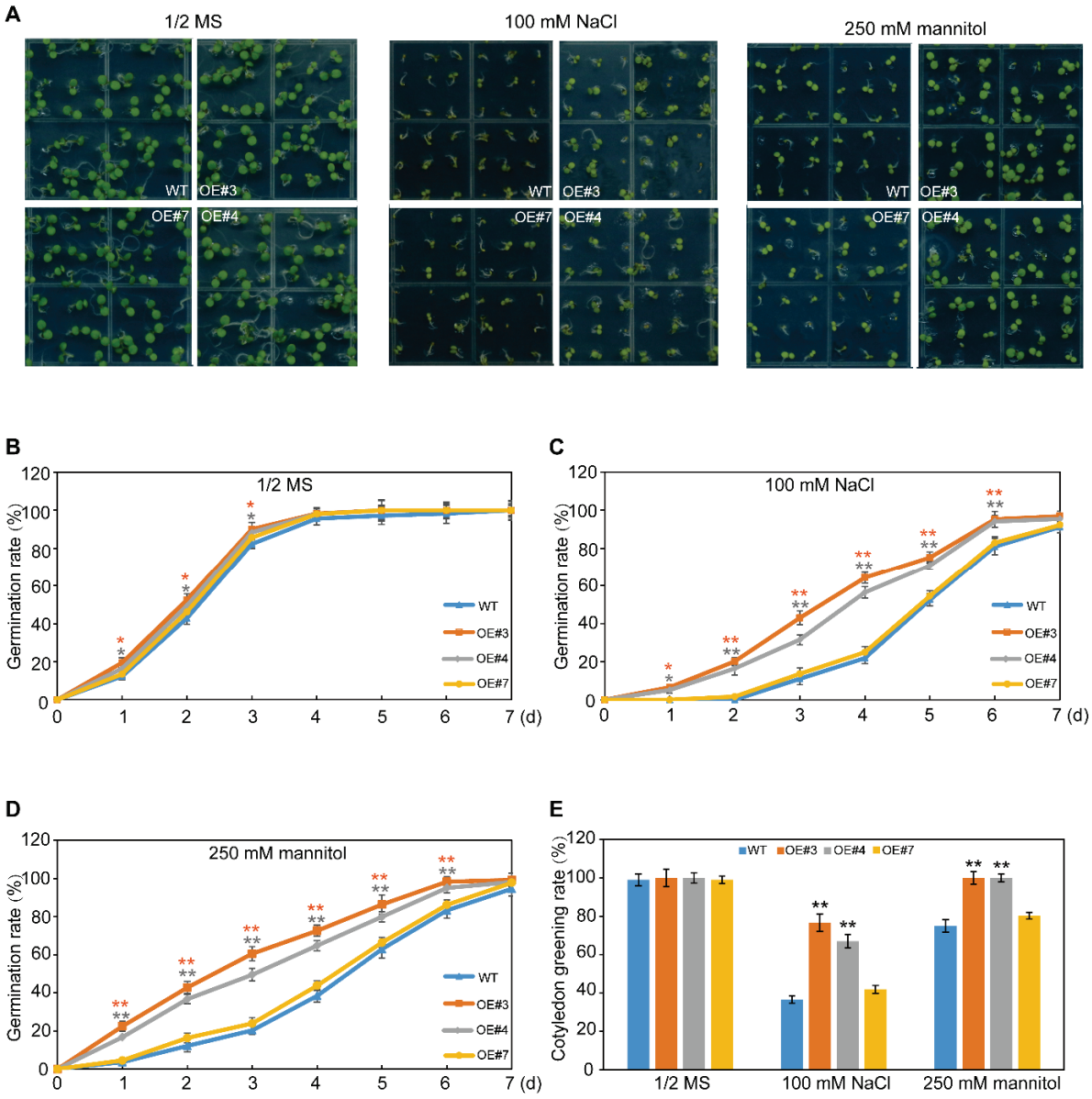

Figure 3. Germination rate assay of seeds of WT and *BnaMYB73*-expressing lines on 1/2 MS with 0, 100 mM NaCl or 250 mM mannitol for 7 days. (**A**) Representative germinations of WT and transgenic seeds. (**B**–**D**) Germination rate statistics of seeds of WT and transgenic lines. (**E**) Cotyledon greening rates of WT and transgenic seedlings after 7 days of treatment. Data are expressed as means ± SD from three independent biological replicates. Asterisks denote significant differences relative to WT (* $p < 0.05$, ** $p < 0.01$).

3.6. BnaMYB73 Expression Improves Salt and Drought Tolerance in Arabidopsis Seedlings and Adult Plants

We then examined the effects of salt and osmotic stress on the growth of transgenic Arabidopsis at the seedling stage. Under control conditions, all lines displayed comparable growth and morphology (Figure 4A,D,E). Upon exposure to 100 mM NaCl or 300 mM mannitol conditions, growth was suppressed in every line, with the transgenic seedlings

exhibiting significantly greater root length, biomass, and reduced root length inhibition relative to WT (Figure 4B–F). These results indicate that *BnaMYB73* expression in Arabidopsis enhances salt and osmotic tolerance at the seedling stage.

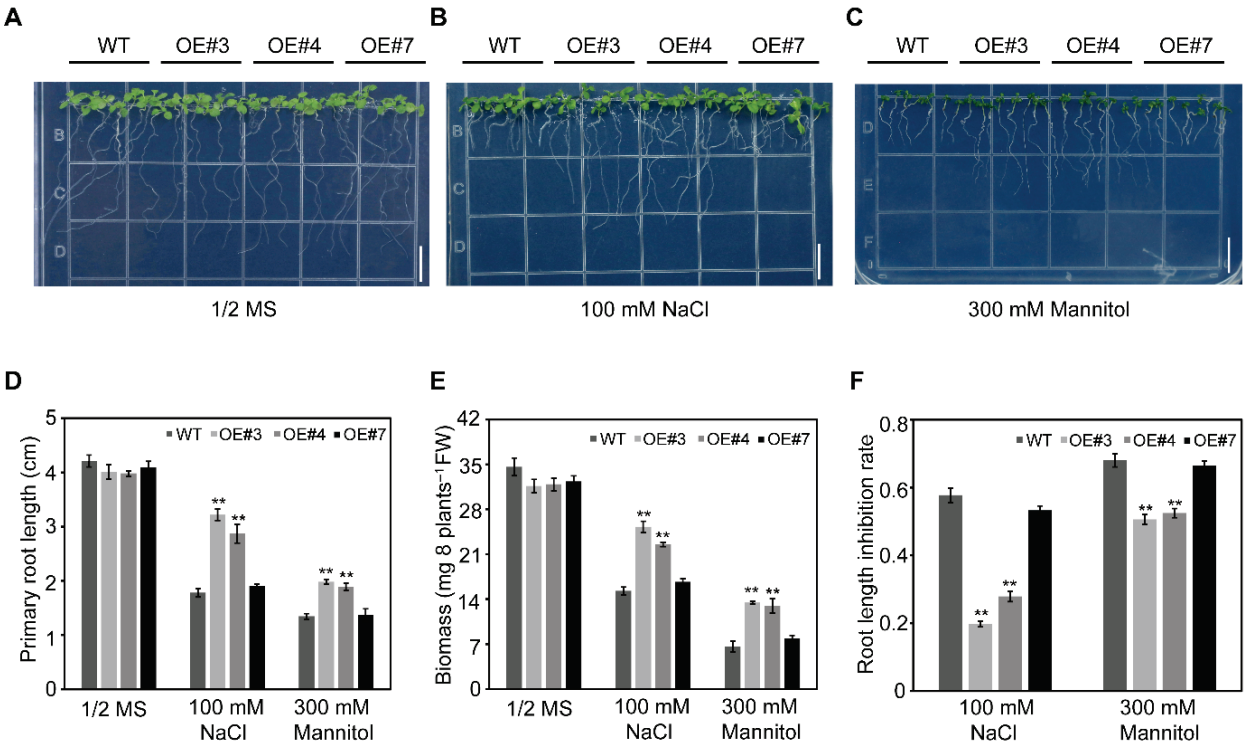

Figure 4. Phenotypic characterization of WT and *BnaMYB73*-expressing seedlings on 1/2 MS containing 0, 100 mM NaCl or 300 mM mannitol. (**A**–**C**) Representative growth phenotypes of seedlings. Bars = 1 cm. (**D**–**F**) Statistical assessment of primary root length (**D**), fresh biomass (**E**), and root length inhibition rate (**F**) corresponding to panels (**A**–**C**). The data represented means ± SD. Asterisks indicate statistically significant differences between transgenic and WT plants (** $p < 0.01$).

To further evaluate the effect of abiotic stress on the growth of mature plants, seedlings were transplanted into greenhouse soil and subjected to 300 mM NaCl for one week or drought stress via withholding water for three weeks. Under normal conditions, both WT and transgenic lines exhibited similar survival rates, plant heights, and overall growth (Figure 5A,D,F). Following stress treatments, transgenic plants outperformed WT plants, exhibiting higher survival, greater plant height, lower growth inhibition and water loss rate (Figure 5B–G). Collectively, these findings suggest that expression of *BnaMYB73* enhances salt and drought tolerance in adult plants.

3.7. BnaMYB73 Expression Increases Antioxidant Capacity and Reduces Lipid Peroxidation in Transgenic Arabidopsis

Given that salt and drought can induce osmotic stress in plants, we further investigated whether *BnaMYB73* expression could enhance oxidative stress resistance in transgenic plants. To assess this, key physiological parameters, such as SOD activity, POD activity, proline content, and MDA content, were quantified in both WT and *BnaMYB73*-expressing lines. Under normal conditions, no significant differences were observed between WT and transgenic lines. However, under salt or osmotic stress, all lines showed elevated SOD and POD activities, as well as increased proline and MDA levels. Notably, compared to WT, transgenic Arabidopsis exhibited significantly higher SOD and POD activities, greater proline accumulation, and notably lower MDA levels than WT (Figure 6). These

https://doi.org/10.3390/plants15050694

findings imply that *BnaMYB73* promotes ROS scavenging and alleviates membrane lipid peroxidation, thereby strengthening the plants' tolerance to abiotic stress.

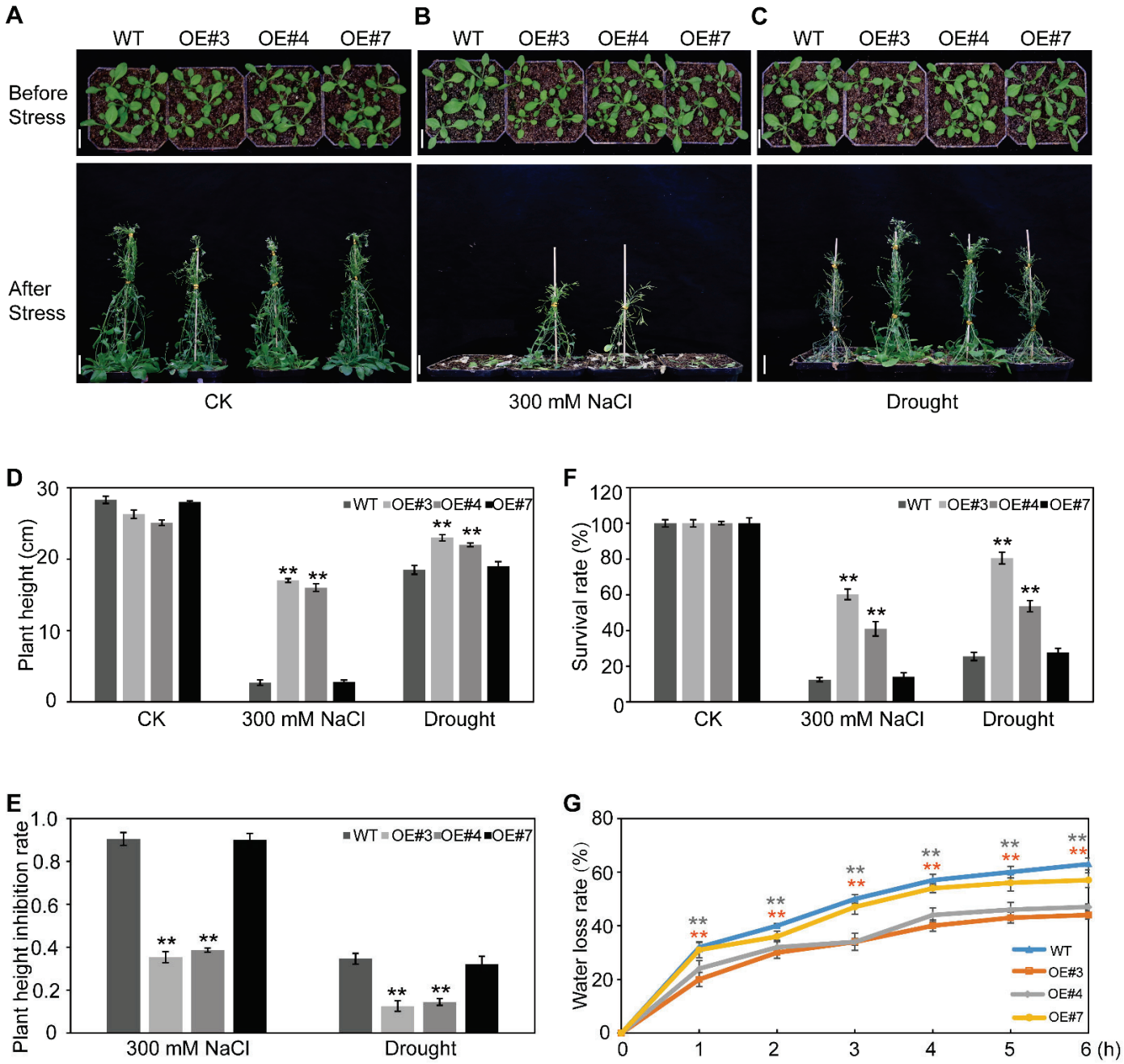

Figure 5. Growth performance of WT and *BnaMYB73*-expressing Arabidopsis plants under soil-grown salt and drought stress conditions. (**A**–**C**) Morphological phenotypes of 3-week-old WT, OE#3, OE#4 and OE#7 subjected to 300 mM NaCl or drought. Bars = 4 cm. Quantitative analysis of plant height (**D**), height inhibition rate (**E**), and survival rate (**F**) under the indicated treatments. (**G**) Water loss rates of detached leaves from 4-week-old WT and transgenic plants subjected to natural dehydration for 6 h. The data represented means ± SD. Significant differences compared with WT are marked as ** $p < 0.01$.

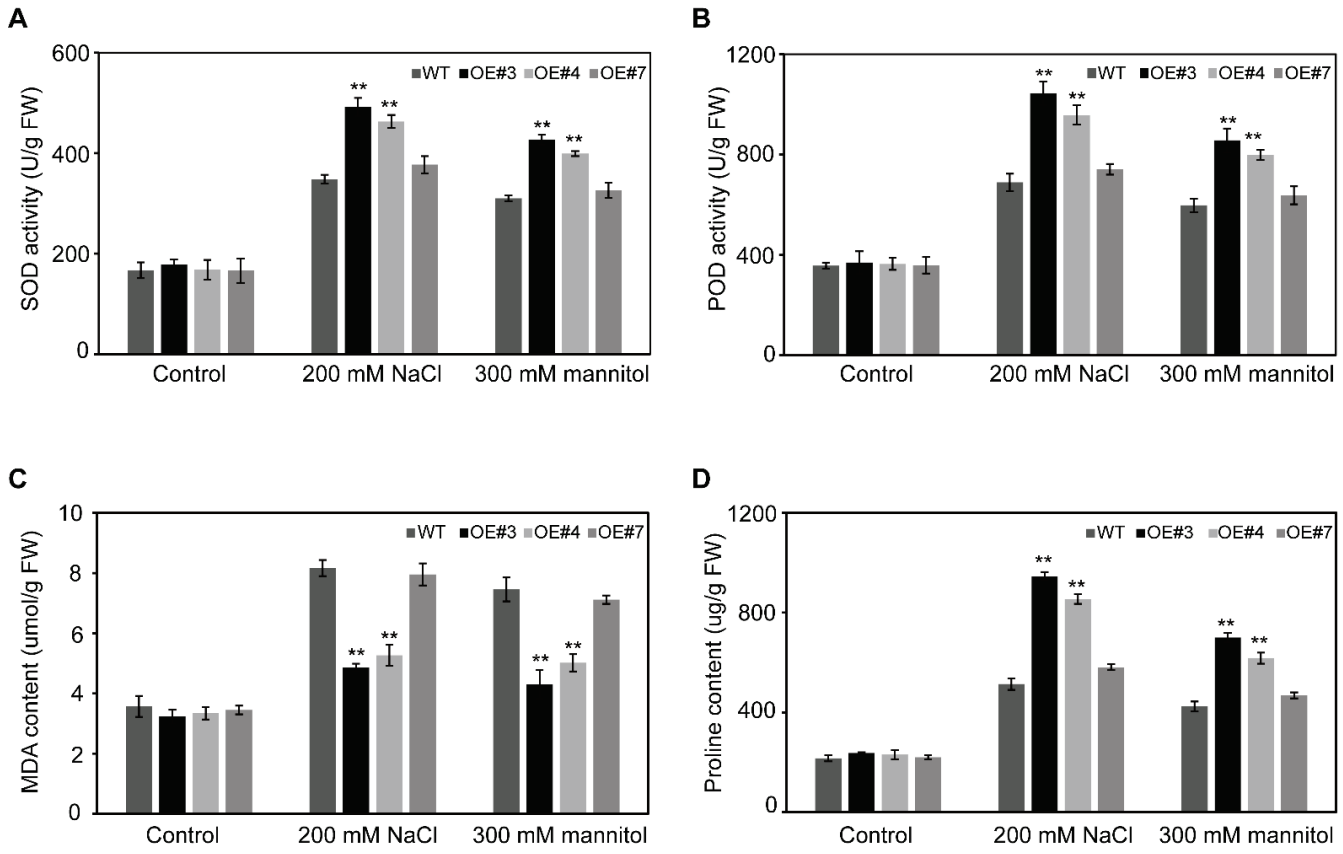

Figure 6. Physiological responses of WT and *BnaMYB73*-expressing *Arabidopsis thaliana* under normal and abiotic stress treatments. Treated leaves were sampled to determine various physiological parameters, including (**A**) SOD activity, (**B**) POD activity, (**C**) MDA content, (**D**) proline accumulation. The data represented means ± SD. Asterisks indicate statistically significant differences between transgenic and WT plants (** $p < 0.01$).

3.8. Expression of BnaMYB73 Upregulates Stress-Responsive Genes in Transgenic Arabidopsis

To elucidate how *BnaMYB73* enhances abiotic stress tolerance, we detected the expression levels of six well-characterized stress-responsive genes (*RD29B*, *DREB2A*, *RAB18*, *P5CS1*, *SOS1*, and *CAT1*) in both WT and *BnaMYB73*-expressing Arabidopsis under normal and stress conditions using RT-qPCR. Under normal conditions, the transcript levels of all six genes were relatively low, with no significant differences between WT and transgenic lines (Figure 7). However, upon exposure to salt or osmotic stress, the expression of *RD29B*, *DREB2A*, *RAB18*, *P5CS1*, *SOS1*, and *CAT1* was significantly upregulated in all Arabidopsis lines. Specifically, transgenic lines exhibited substantially higher expression accumulation of all six genes compared to WT. This pronounced upregulation correlates with the enhanced tolerance to abiotic stress observed in *BnaMYB73*-expressing plants (Figure 7). These findings strongly indicate that *BnaMYB73* enhances salt and osmotic stress tolerance via activating a network of stress-responsive genes involved in osmotic regulation, antioxidant defense, and ion homeostasis.

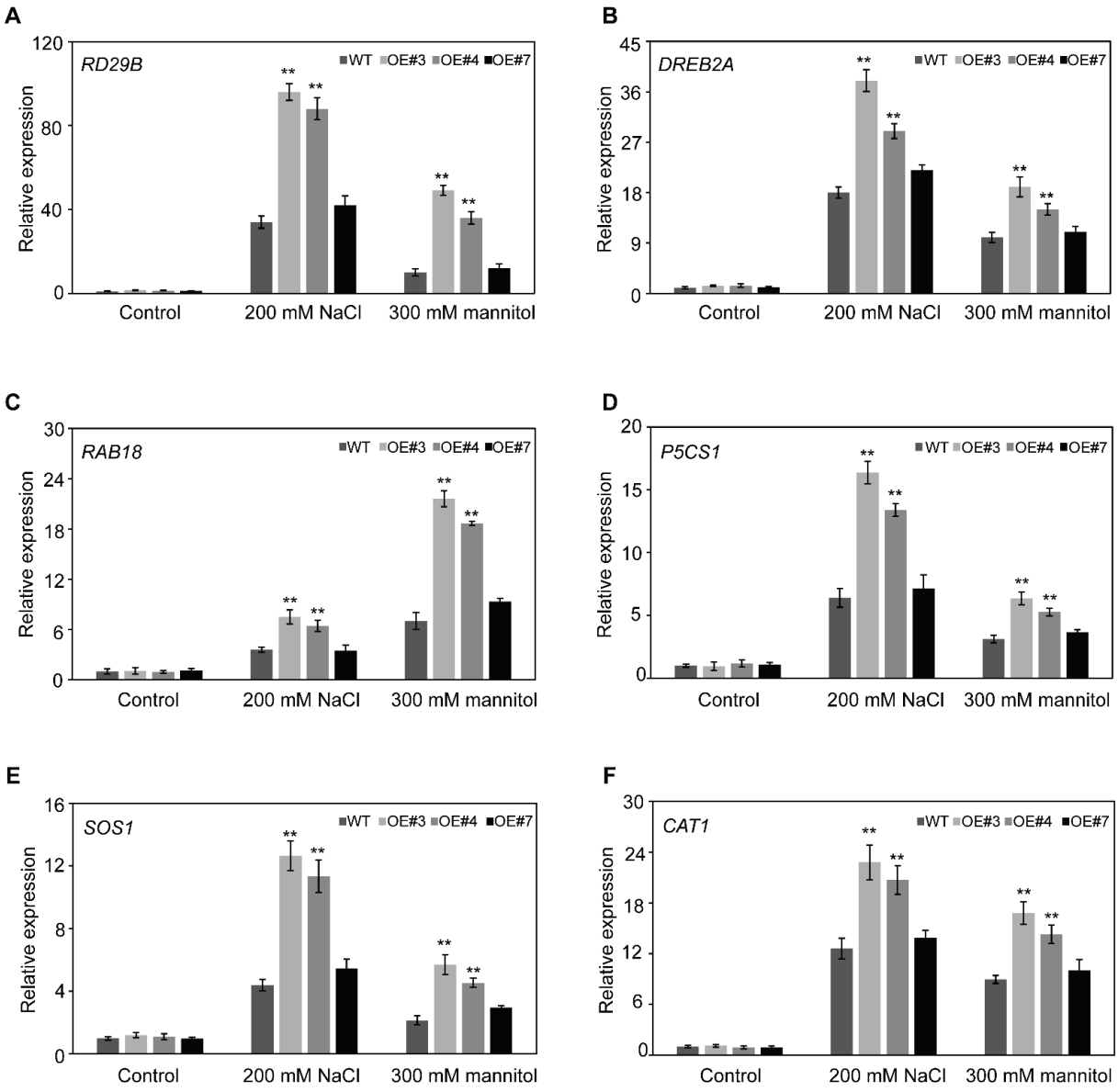

Figure 7. Relative expression of *RD29B* (**A**), *DREB2A* (**B**), *RAB18* (**C**), *P5CS1* (**D**), *SOS1* (**E**), and *CAT1* (**F**) in WT and *BnaMYB73*-expressing Arabidopsis plants grown under normal conditions, 200 mM NaCl, or 300 mM mannitol treatments. Data are presented as means ± SD from three independent biological replicates. Asterisks (**) denote statistically significant differences compared with WT at $p < 0.01$, respectively.

4. Discussion

Adverse environments impose serious constraints on crop growth, development and yield. Numerous studies have emphasized the pivotal functions of TFs in regulating downstream stress-responsive gene expression to mitigate abiotic stress effects. Among them, R2R3 MYB TFs, the most abundant MYB family members in plants, are key regulators in governing plant growth, developmental processes, and adaptation to abiotic stress [12]. Rapeseed, an important oil crop widely used for consumption and oil extraction, has substantial economic value and ecological benefits. However, it is highly susceptible to environmental stressors, leading to poor quality and decreased production [25,26]. Previous analysis has revealed that there are 249 R2R3 MYB TFs in the *B. napus* genome, yet their roles in abiotic stress responses remain largely unexplored [33]. In this work, we isolated and characterized an R2R3 *MYB* gene, *BnaMYB73*. Previous research has shown that MYB

proteins with sequence similarity typically share similar functions [34]. The investigation into *BnaMYB73* not only helps to elucidate its role in the abiotic stress response of rapeseed but also contributes to a broader comprehension of MYB TFs in other plants. Despite the divergence in full-length sequences, the MYB domains exhibited remarkable conservation among these homologs (Figure 1). The differences in the full-length sequences, coupled with the conserved MYB domain, suggested that MYB proteins retained core functions across plant species, while acquiring specific functions during evolution.

Numerous studies have revealed that the majority of transcription factor-encoding genes are induced by abiotic stresses, and their overexpression in plants has emerged as a useful approach to enhance crop tolerance to such stressors [35–39]. In this study, RT-qPCR indicated a significant upregulation of *BnaMYB73* expression in rapeseed under various stress conditions (Figure 2). Furthermore, we generated transgenic Arabidopsis overexpressing the *BnaMYB73* gene to assess its role in the abiotic stress response. Under stress conditions (salt and osmotic stress), these transgenic plants exhibited faster germination and improved growth compared to WT, consistent with the functions reported for other *MYB* genes, such as *AtMYB49* [15], *GhMYB73* [24], *OsMYB2* [18], and *TaMYB19* [40] (Figures 3–5). These results suggested that overexpression of *BnaMYB73* in Arabidopsis enhanced plant growth under salt and drought, confirming that *BnaMYB73* elevated stress tolerance at different developmental stages. In summary, our findings implied a positive role of *BnaMYB73* in regulating salt and drought tolerance.

To adapt to unfavorable conditions, plants undergo rapid physiological alterations [41,42]. Hence, measuring physiological indicators related to plant stress response can evaluate plant stress resistance. In this study, we assessed four physiological parameters, SOD activity, POD activity, proline content and MDA content (Figure 6). Our study revealed a significant increase in proline content in *BnaMYB73*-expressing plants compared to WT under all stress conditions, suggesting that the accumulated proline contributed to the enhanced stress tolerance in the transgenic lines. The reduced MDA content in *BnaMYB73*-expressing plants compared to WT suggested that *BnaMYB73* could improve stress tolerance by alleviating lipid peroxidation and maintaining osmotic homeostasis. While changes in physiological indicators alone may not fully alleviate the damages caused by abiotic stress, they are undoubtedly key factors in plant resistance to adverse conditions. Collectively, the physiological changes in *BnaMYB73*-expressing plants promoted their adaptation to an adverse environment.

The overexpression of *BnaMYB73* led to the upregulation of six genes, *RD29B*, *DREB2A*, *RAB18*, *P5CS1*, *SOS1* and *CAT1* under abiotic stresses, thereby enhancing the stress tolerance of *BnaMYB73*-expressing Arabidopsis lines (Figure 7). In transgenic lines, the increased expression of *P5CS1* resulted in proline accumulation, which helped regulate osmotic pressure. Additionally, relative to WT, the elevated expression level of *SOS1* in *BnaMYB73*-overexpressing lines under salt and osmotic stress alleviated the cellular toxicity induced by Na^+. The upregulation of *CAT1* in these plants facilitated the removal of excess ROS, further enhancing abiotic stress resilience. While the heterologous overexpression in Arabidopsis provides robust initial evidence for *BnaMYB73*'s positive regulatory role in abiotic stress tolerance, we acknowledge that a significant amount of work remains to be done to fully understand the regulatory mechanisms by which *BnaMYB73* elevates abiotic stress resilience. First, the functional validation relies heavily on a heterologous system in this study, and the physiological relevance within the rapeseed remains to be fully established. Second, the proposed regulatory mechanism, while supported by correlative expression data, lacks direct molecular evidence for BnaMYB73 binding to the promoters of downstream stress-responsive genes. To build upon these findings and address these gaps, our future work will focus on the following: (1) generating and characterizing both

BnaMYB73-overexpressing and CRISPR/Cas9-mediated knockout lines in rapeseed to confirm its function in the native genetic background and assess its potential for crop improvement; and (2) employing chromatin immunoprecipitation sequencing (ChIP-seq) in conjunction with Dual-LUC to identify its direct target genes, thereby elucidating the precise transcriptional network it governs under stress conditions.

5. Conclusions

In conclusion, we cloned an R2R3 MYB gene, *BnaMYB73*, from rapeseed and identified its role in the abiotic stress response. To extensively characterize *BnaMYB73*, we examined its expression patterns, phenotypic analysis of transgenic plants, and its mechanistic study. Expression examinations disclosed that *BnaMYB73* was responsive to salt and osmotic stress. The differences in germination and growth between WT and *BnaMYB73*-expressing plants indicated that *BnaMYB73* expression enhanced tolerance to abiotic stress. Additionally, constitutive expression of *BnaMYB73* also improved antioxidant defense to confront abiotic stress. The above findings elucidate the role of *BnaMYB73* in stress adaptation and position it as a promising candidate for advancing stress-tolerant rapeseed breeding.

Supplementary Materials: The following supporting information can be downloaded at: https://www.mdpi.com/article/10.3390/plants15050694/s1, Figure S1: Growth phenotypes of yeast cells harboring pYES2-BnaMYB73 and pYES2 empty vector under control, salt and mannitol treatments. Figure S2: The construction of the BnaMYB73-expressing vector. Table S1: Primer sequences.

Author Contributions: Conceptualization, N.S. and L.W.; methodology, Y.Z., X.Z. and X.X.; software, Y.Z., X.Z. and X.X.; validation, D.L.; formal analysis, H.Z. and Y.L.; investigation, N.S., L.W., D.L. and Y.L.; resources, L.W.; data curation, H.Z., N.S., L.W., D.L. and Y.L.; writing—original draft preparation, L.W.; writing—review and editing, N.S., D.L. and Y.L.; visualization, Y.Z., X.Z. and X.X.; supervision, N.S., D.L. and Y.L.; project administration, H.Z.; funding acquisition, H.Z., N.S. and L.W. All authors have read and agreed to the published version of the manuscript.

Funding: This work was funded by the National Natural Science Foundation of China (31901572, 32071733, 32371915), the Natural Science Foundation of Shandong Province, China (ZR2020QC115, ZR2019PC015), and the Double-Hundred Talents Project of Yantai City.

Data Availability Statement: All data used in this study are included in this published article and its Supplementary Information files.

Conflicts of Interest: The authors declare no conflicts of interest.

References

1. Markham, K.K.; Greenham, K. Abiotic stress through time. *New Phytol.* **2021**, *231*, 40–46. [CrossRef] [PubMed]
2. Kopecká, R.; Kameniarová, M.; Černý, M.; Brzobohatý, B.; Novák, J. Abiotic Stress in Crop Production. *Int. J. Mol. Sci.* **2023**, *24*, 6603. [CrossRef] [PubMed]
3. Xin, Z.; Browse, J. Eskimo1 mutants of Arabidopsis are constitutively freezing-tolerant. *Proc. Natl. Acad. Sci. USA* **1998**, *95*, 7799–7804. [CrossRef] [PubMed]
4. Suzuki, N.; Mittler, R. Reactive oxygen species and temperature stresses: A delicate balance between signaling and destruction. *Physiol. Plant.* **2006**, *126*, 45–51. [CrossRef]
5. Kishor, P.; Hong, Z.; Miao, G.H.; Hu, C.; Verma, D. Overexpression of [delta]- Pyrroline-5-carboxylate synthetase increases proline production and confers Osmotolerance in transgenic plants. *Plant Physiol.* **1995**, *108*, 1387. [CrossRef]
6. Guan, L.M.; Zhao, J.; Scandalios, J.G. Cis-elements and trans-factors that regulate expression of the maize *Cat1* antioxidant gene in response to ABA and osmotic stress: H_2O_2 is the likely intermediary signaling molecule for the response. *Plant J. Cell Mol. Biol.* **2000**, *22*, 87–95. [CrossRef]
7. Qiu, Q.S.; Guo, Y.; Dietrich, M.A.; Schumaker, K.S.; Zhu, J.K. Regulation of SOS1, a plasma membrane Na^+/H^+ Exchanger in *Arabidopsis thaliana*, by SOS2 and SOS3. *Proc. Natl. Acad. Sci. USA* **2002**, *99*, 8436–8441. [CrossRef]
8. Xie, Z.; Nolan, T.M.; Jiang, H.; Yin, Y. AP2/ERF Transcription Factor Regulatory Networks in Hormone and Abiotic Stress Responses in Arabidopsis. *Front. Plant Sci.* **2019**, *10*, 228. [CrossRef]

9. Diao, P.; Chen, C.; Zhang, Y.; Meng, Q.; Lv, W.; Ma, N. The role of NAC transcription factor in plant cold response. *Plant Signal. Behav.* **2020**, *15*, 1785668. [CrossRef]
10. Wang, X.; Niu, Y.; Zheng, Y. Multiple Functions of MYB Transcription Factors in Abiotic Stress Responses. *Int. J. Mol. Sci.* **2021**, *22*, 6125. [CrossRef]
11. Ma, Z.; Hu, L. WRKY Transcription Factor Responses and Tolerance to Abiotic Stresses in Plants. *Int. J. Mol. Sci.* **2024**, *25*, 6845. [CrossRef] [PubMed]
12. Dubos, C.; Stracke, R.; Grotewold, E.; Weisshaar, B.; Martin, C.; Lepiniec, L. MYB transcription factors in Arabidopsis. *Trends Plant Sci.* **2010**, *15*, 573–581. [CrossRef] [PubMed]
13. Cui, M.H.; Yoo, K.S.; Hyoung, S.; Nguyen, H.T.; Kim, Y.Y.; Kim, H.J.; Ok, S.H.; Yoo, S.D.; Shin, J.S. An Arabidopsis R2R3-MYB transcription factor, AtMYB20, negatively regulates type 2C serine/threonine protein phosphatases to enhance salt tolerance. *FEBS Lett.* **2013**, *587*, 1773–1778. [CrossRef] [PubMed]
14. Zhang, X.; Wu, S.; Liu, S.; Takano, T. The Arabidopsis sucrose non-fermenting-1-related protein kinase AtSnRK2.4 interacts with a transcription factor, AtMYB21, that is involved in salt tolerance. *Plant Sci. Int. J. Exp. Plant Biol.* **2021**, *303*, 110685. [CrossRef]
15. Zhang, P.; Wang, R.; Yang, X.; Ju, Q.; Li, W.; Lü, S.; Tran, L.P.; Xu, J. The R2R3-MYB transcription factor AtMYB49 modulates salt tolerance in Arabidopsis by modulating the cuticle formation and antioxidant defence. *Plant Cell Environ.* **2020**, *43*, 1925–1943. [CrossRef]
16. Deng, M.; Wang, Y.; Kuzma, M.; Chalifoux, M.; Tremblay, L.; Yang, S.; Ying, J.; Sample, A.; Wang, H.M.; Griffiths, R.; et al. Activation tagging identifies Arabidopsis transcription factor AtMYB68 for heat and drought tolerance at yield determining reproductive stages. *Plant J. Cell Mol. Biol.* **2020**, *104*, 1535–1550. [CrossRef]
17. Gibbs, D.J.; Voss, U.; Harding, S.A.; Fannon, J.; Moody, L.A.; Yamada, E.; Swarup, K.; Nibau, C.; Bassel, G.W.; Choudhary, A.; et al. AtMYB93 is a novel negative regulator of lateral root development in Arabidopsis. *New Phytol.* **2014**, *203*, 1194–1207. [CrossRef]
18. Yang, A.; Dai, X.; Zhang, W.H. A R2R3-type MYB gene, *OsMYB2*, is involved in salt, cold, and dehydration tolerance in rice. *J. Exp. Bot.* **2012**, *63*, 2541–2556. [CrossRef]
19. Cui, J.; Jiang, N.; Zhou, X.; Hou, X.; Yang, G.; Meng, J.; Luan, Y. Tomato MYB49 enhances resistance to Phytophthora infestans and tolerance to water deficit and salt stress. *Planta* **2018**, *248*, 1487–1503. [CrossRef]
20. Dong, W.; Liu, X.; Li, D.; Gao, T.; Song, Y. Transcriptional profiling reveals that a MYB transcription factor MsMYB4 contributes to the salinity stress response of alfalfa. *PLoS ONE* **2018**, *13*, e0204033. [CrossRef]
21. Kim, J.H.; Nguyen, N.H.; Jeong, C.Y.; Nguyen, N.T.; Hong, S.W.; Lee, H. Loss of the R2R3 MYB, *AtMyb73*, causes hyper-induction of the *SOS1* and *SOS3* genes in response to high salinity in Arabidopsis. *J. Plant Physiol.* **2013**, *170*, 1461–1465. [CrossRef]
22. Hu, D.; Cui, R.; Wang, K.; Yang, Y.; Wang, R.; Zhu, H.; He, M.; Fan, Y.; Wang, L.; Wang, L.; et al. The Myb73-GDPD2-GA2ox1 transcriptional regulatory module confers phosphate deficiency tolerance in soybean. *Plant Cell* **2024**, *36*, 2176–2200. [CrossRef] [PubMed]
23. He, Y.; Li, W.; Lv, J.; Jia, Y.; Wang, M.; Xia, G. Ectopic expression of a wheat MYB transcription factor gene, *TaMYB73*, improves salinity stress tolerance in *Arabidopsis thaliana*. *J. Exp. Bot.* **2012**, *63*, 1511–1522. [CrossRef] [PubMed]
24. Zhao, Y.; Yang, Z.; Ding, Y.; Liu, L.; Han, X.; Zhan, J.; Wei, X.; Diao, Y.; Qin, W.; Wang, P.; et al. Over-expression of an R2R3 MYB Gene, *GhMYB73*, increases tolerance to salt stress in transgenic Arabidopsis. *Plant Sci. Int. J. Exp. Plant Biol.* **2019**, *286*, 28–36. [CrossRef] [PubMed]
25. Zhang, X.; Lu, G.Y.; Long, W.H.; Zou, X.L.; Li, F.; Nishio, T. Recent progress in drought and salt tolerance studies in *Brassica* crops. *Breed. Sci.* **2014**, *64*, 60–73. [CrossRef]
26. Wang, L.M.; Jin, X.; Li, Q.B.; Wang, X.C.; Li, Z.Y.; Wu, X.M. Comparative proteomics reveals that phosphorylation of β carbonic anhydrase 1 might be important for adaptation to drought stress in *Brassica napus*. *Sci Rep* **2016**, *6*, 39024. [CrossRef]
27. Sun, N.; Zhou, J.; Liu, Y.; Li, D.; Xu, X.; Zhu, Z.; Xu, X.; Zhan, R.; Zhang, H.; Wang, L. Genome-wide characterization of *Remorin* gene family and their responsive expression to abiotic stresses and plant hormone in *Brassica napus*. *Plant Cell Rep.* **2024**, *43*, 155. [CrossRef]
28. Sparkes, I.; Runions, J.; Kearns, A.; Hawes, C. Rapid, transient expression of fluorescent fusion proteins in tobacco plants and generation of stably transformed plants. *Nat. Protoc.* **2006**, *1*, 2019–2025. [CrossRef]
29. Liu, T.; Li, Y.; Wang, C.; Zhang, D.; Liu, J.; He, M.; Chen, M.; Guo, Y. *Brassica napus* Transcription Factor *Bna.A07.WRKY70* Negatively Regulates Leaf Senescence in *Arabidopsis thaliana*. *Plants* **2023**, *12*, 347. [CrossRef]
30. Livak, K.J.; Schmittgen, T.D. Analysis of relative gene expression data using real-time quantitative PCR and the $2^{-\Delta\Delta Ct}$ method. *Methods* **2001**, *25*, 402–408. [CrossRef]
31. Clough, S.J.; Bent, A.F. Floral dip: A simplified method for Agrobacterium-mediated transformation of Arabidopsis thaliana. *Plant J. Cell Mol. Biol.* **1998**, *16*, 735–743. [CrossRef]
32. Murashige, T.; Skoog, F. A revised medium for rapid growth and bioassays with tobacco tissue cultures. *Physiol. Plant* **1962**, *15*, 473–495. [CrossRef]

33. Hajiebrahimi, A.; Owji, H.; Hemmati, S. Genome-wide identification, functional prediction, and evolutionary analysis of the R2R3-MYB superfamily in *Brassica napus*. *Genome* **2017**, *60*, 797–814. [CrossRef] [PubMed]
34. Matus, J.T.; Aquea, F.; Arce-Johnson, P. Analysis of the grape MYB R2R3 subfamily reveals expanded wine quality-related clades and conserved gene structure organization across Vitis and Arabidopsis genomes. *BMC Plant Biol.* **2008**, *8*, 83. [CrossRef] [PubMed]
35. Chen, W.; Provart, N.J.; Glazebrook, J.; Katagiri, F.; Chang, H.S.; Eulgem, T.; Mauch, F.; Luan, S.; Zou, G.; Whitham, S.A.; et al. Expression profile matrix of Arabidopsis transcription factor genes suggests their putative functions in response to environmental stresses. *Plant Cell* **2002**, *14*, 559–574. [CrossRef] [PubMed]
36. Bhatnagar-Mathur, P.; Vadez, V.; Sharma, K.K. Transgenic approaches for abiotic stress tolerance in plants: Retrospect and prospects. *Plant Cell Rep.* **2008**, *27*, 411–424. [CrossRef]
37. Hussain, S.S.; Kayani, M.A.; Amjad, M. Transcription factors as tools to engineer enhanced drought stress tolerance in plants. *Biotechnol. Prog.* **2011**, *27*, 297–306. [CrossRef]
38. Song, L.; Huang, S.C.; Wise, A.; Castanon, R.; Nery, J.R.; Chen, H.; Watanabe, M.; Thomas, J.; Bar-Joseph, Z.; Ecker, J.R. A transcription factor hierarchy defines an environmental stress response network. *Science* **2016**, *354*, aag1550. [CrossRef]
39. Li, J.; Han, G.; Sun, C.; Sui, N. Research advances of MYB transcription factors in plant stress resistance and breeding. *Plant Signal. Behav.* **2019**, *14*, 1613131. [CrossRef]
40. Zhang, L.; Liu, G.; Zhao, G.; Xia, C.; Jia, J.; Liu, X.; Kong, X. Characterization of a wheat R2R3-MYB transcription factor gene, *TaMYB19*, involved in enhanced abiotic stresses in Arabidopsis. *Plant Cell Physiol.* **2014**, *55*, 1802–1812. [CrossRef]
41. Sahi, C.; Singh, A.; Blumwald, E.; Grover, A. Beyond osmolytes and transporters: Novel plant salt-stress tolerance-related genes from transcriptional profiling data. *Physiol. Plant.* **2006**, *127*, 1–9. [CrossRef]
42. Nadarajah, K.K. ROS Homeostasis in Abiotic Stress Tolerance in Plants. *Int. J. Mol. Sci.* **2020**, *21*, 5208. [CrossRef]

plants

MDPI

Article

Integrated Metabolomic and Transcriptomic Analyses Reveal the Coumarin Biosynthesis Pathway and Key Regulatory Genes in the Pericarp of *Zanthoxylum*

Shengqun Chen [1,2,3,†], Lianwen Shen [1,2,†], Yajun Zeng [1,2,3], Shijing Feng [4], Hong Luo [1,*] and Gang Wang [1,*]

[1] Guizhou Academy of Forestry, Guiyang 550005, China; squnchen@163.com (S.C.)
[2] Key Laboratory of National Forestry and Grassland Administration on Biodiversity Conservation in Karst Mountainous Areas of Southwestern China, Guiyang 550005, China
[3] Guizhou Walnut Research Institute, Guiyang 550025, China
[4] College of Forestry, Guizhou University, Guiyang 550005, China
* Correspondence: luohong841014@sina.com (H.L.); wang3540307@163.com (G.W.)
† These authors contributed equally to this work.

Abstract

Coumarins in the pericarp of *Zanthoxylum* contribute to the characteristic numbing–aromatic flavor and are associated with diverse bioactivities. To characterize coumarin divergence between two *Zanthoxylum* materials, mature pericarps of Dahongpao *Z. bungeanum* (red Sichuan pepper) and *Z. planispinum* var. *dingtanensis* (green Sichuan pepper) were analyzed by widely targeted UPLC–ESI–MS/MS metabolomics integrated with transcriptome sequencing. This approach enabled joint profiling of metabolites and transcripts to identify genes associated with material-specific coumarin accumulation. Across the two materials, 583 metabolites were detected, with flavonoids, phenolic acids, and alkaloids as the predominant classes. Among these, 24 coumarins were identified, and most showed significantly higher abundance in green Sichuan pepper than in red Sichuan pepper. Pathway enrichment analysis indicated that differentially accumulated coumarins were mainly associated with the phenylpropanoid biosynthesis pathway, consistent with coordinated metabolic and transcriptional regulation. The integration of metabolite abundance with gene expression patterns identified 56 candidate genes strongly correlated with scopoletin and scopolin accumulation. To evaluate functional relevance, *CCoAOMT*, *COMT*, and *F6H* were cloned and transiently overexpressed in *Nicotiana benthamiana*. Transient expression assays showed that overexpression of each gene increased scopoletin and scopolin, supporting their involvement in coumarin biosynthesis. Collectively, these results clarify molecular determinants of coumarin variation between the two materials and highlight candidate genes for quality improvement and metabolic engineering.

Keywords: *Zanthoxylum*; coumarins; metabolomics; transcriptomics; functional genes

1. Introduction

Sichuan pepper broadly refers to several economically important *Zanthoxylum* species and varieties used in China as spices and medicinal resources, including *Zanthoxylum bungeanum*, *Zanthoxylum schinifolium*, and *Zanthoxylum planispinum* var. *dingtanensis*, which belongs to the genus *Zanthoxylum* in the family Rutaceae. These species are widely used as both flavoring agents and traditional medicinal materials. Previous phytochemical investigations have shown that the pericarp of Sichuan pepper contains a wide array

of secondary metabolites, including essential oils, amides, alkaloids, flavonoids, lignans and coumarins [1–4]. Multiple simple coumarins and furanocoumarins, including 7-oxo-7H-furo [3,2-g]chromen-9-dimethyl carbamate, have been isolated from the pericarp of red-fruited Sichuan pepper [5]. More than 70 coumarins, predominantly simple coumarins with a smaller proportion of furanocoumarins, have been identified in green Sichuan pepper (*Z. schinifolium*), including 7-methoxycoumarin, isoscopoletin and fraxinol [3]. Coumarins concentrated in the pericarp of Sichuan pepper are thought to contribute to its aromatic profile and may contribute to its pharmacological effects [2]. In particular, simple coumarins such as scopoletin and its glucoside scopolin are frequently detected in *Zanthoxylum* pericarps and are considered representative metabolites that connect the phenylpropanoid metabolism to pericarp aroma and bioactivity. In addition to simple coumarins, furanocoumarins (e.g., bergapten- and xanthotoxin-type compounds) have also been reported in some *Zanthoxylum* materials, highlighting the chemical diversity of coumarins in Sichuan pepper pericarp [3,5]. Simple coumarins refer to compounds characterized by the 1,2-benzopyran-2-one core scaffold, which are further substituted on the benzene ring with groups such as hydroxyl, methoxy, methylenedioxy, or prenyl. Importantly, these compounds do not contain any additional fused heterocyclic systems, meaning they lack fused furan or pyran rings. In contrast, coumarins that have a fused furan ring on the coumarin scaffold are designated as 'furanocoumarins', while those with a fused pyran ring are referred to as 'pyranocoumarins'. This structure-based classification is extensively utilized in the study and review of plant coumarins, providing a clear framework for distinguishing between coumarin subclasses in Sichuan pepper and elucidating their potential biosynthetic origins [3,5].

Coumarins extracted from Sichuan pepper exhibit a broad spectrum of pharmacological activities, including anti-inflammatory, antioxidant, analgesic, anticancer, antithrombotic, cardioprotective and neuroregulatory effects. They constitute a major chemical basis for the pharmacological actions of Sichuan pepper [3]. In addition to cytotoxic and apoptosis-inducing effects in tumor cells, coumarin and its derivatives show antimicrobial, antispasmodic, and anti-platelet (antiaggregation) activities. They have also been reported to exert anti-rheumatic effects in arthritis models [6,7]. Beyond the volatile oils and amide compounds that dictate the characteristic numbing and aromatic flavor of Sichuan pepper, coumarins also contribute to its distinctive taste profile. Furthermore, increasing attention has been paid to the potential of coumarin and related phenylpropanoid derivatives from Sichuan pepper in the management of immunological, digestive, and cardiovascular problems [1,6].

Plant coumarins are generally derived from the phenylpropanoid pathway. In the early steps of this pathway, key enzymes such as phenylalanine ammonia-lyase (*PAL*), cinnamate 4-hydroxylase (*C4H*), and 4-coumarate: CoA ligase (*4CL*) convert phenylalanine into hydroxycinnamoyl-CoA derivatives. Subsequently, ortho-hydroxylation, cis-trans isomerization, and lactonization generate the characteristic 2H-1-benzopyran-2-one skeleton [8,9]. Among these, the primary rate-limiting enzyme in simple coumarin biosynthesis is feruloyl-CoA 6′-hydroxylase (*F6′H*), a dioxygenase that is dependent on ferredoxin. Its structure and function have been confirmed in species such as Clematis, *Manihot esculenta*, and *Arabidopsis thaliana*. Coumarin accumulation is often positively associated with *F6′H* expression levels [2,9–11]. Nevertheless, compared with these model plants, research on the coumarin biosynthesis and its key structural and regulatory genes in Sichuan pepper pericarp remains limited. Existing work has largely focused on isolation/identification of individual coumarins and bioactivity evaluation, whereas systematic analyses of coumarin metabolic networks across different Sichuan pepper pericarps are still scarce [4,12].

https://doi.org/10.3390/plants15050769

Zanthoxylum planispinum var. *dingtanensis* is a green Sichuan pepper variety widely distributed in the karst plateau canyon regions of Guizhou Province and is characterized by rapid growth and strong stress tolerance. Dahongpao, an important red Sichuan pepper cultivar of *Z. bungeanum*, is widely cultivated in China. These two cultivars show significant differences in pericarp aroma and numbing intensity. To elucidate coumarin-related biosynthetic pathways in Sichuan pepper pericarp and to prioritize key candidate genes, we performed integrated transcriptomic and metabolomic analyses of mature pericarp (fresh weight) from *Z. planispinum* var. *dingtanensis* and Dahongpao *Z. bungeanum*. Heterologous overexpression was employed to validate the functions of selected candidate genes. This study aims to provide a theoretical basis for targeted genetic improvement of Sichuan pepper and to elucidate the molecular mechanisms underlying its aromatic and therapeutic properties.

2. Materials and Methods

2.1. Plant Materials

Dahongpao *Zanthoxylum bungeanum* (red Sichuan pepper) and *Zanthoxylum planispinum* var. *dingtanensis* (green Sichuan pepper) were used as experimental materials (Figure 1A). One-year-old seedlings of *Z. bungeanum* were sourced from Hanyuan County, Sichuan Province, China, whereas one-year-old seedlings of *Z. planispinum* var. *dingtanensis* were obtained from Zhenfeng County, Qianxinan Buyi and Miao nationality Autonomous Prefecture. Both *Zanthoxylum* species were planted in 2019 at the same cultivation base in Zhenfeng County, Guizhou Province, China (105°38′36″ E, 25°24′10″ N). In 2023, five-year-old plants with vigorous growth and comparable field conditions (management practices, light exposure, and soil moisture) were selected from this site for subsequent analyses. Nine plants per species were sampled; three plants were pooled as one biological replicate, yielding three biological replicates in total. During sampling, fruits with uniform ripeness, similar color and shape, and no mechanical damage were collected from four directions of each plant (40 fruits per plant; 120 fruits per replicate). After rinsing with sterile water and air-drying, the fruits were promptly dehusked. The pericarps were immediately transferred into prechilled 50 mL centrifuge tubes, snap-frozen in liquid nitrogen, transported to the laboratory on dry ice, and stored at −80 °C until further analysis. Tissue-cultured tobacco seedlings were provided by the Mianyang Academy of Agricultural Sciences (Mianyang, China).

2.2. Reagents

Scopolin (CAS No. 531-44-2, purity ≥ 98%) and scopoletin (CAS No. 92-61-5, purity > 98%) standards were purchased from Shanghai Yuanye Biotechnology Co., Ltd. (Shanghai, China). These standards were used for metabolite identification and quantification, including the preparation of calibration curves, as described in the corresponding analytical procedures. In addition, the pB1121 vector, *Escherichia coli* strain DH5α, and *Agrobacterium tumefaciens* strain GV3101 were obtained from BioMADE (St. Paul, MN, USA)

2.3. Metabolite Extraction and UPLC–MS/MS Analysis

Pericarp samples were removed from −80 °C storage and kept on ice prior to extraction. The biological samples were freeze-dried using a vacuum freeze-dryer (SCIENTZ-100F (Ningbo Scientz Biotechnology Co., Ltd., Ningbo, China)) and then ground to a fine powder with a mixer mill (MM400, Retsch (Haan, Germany) at 30 Hz for 1.5 min under liquid nitrogen. Approximately 100 mg of powder was transferred to a 2 mL microcentrifuge tube and extracted with 1.2 mL of pre-chilled 70% (*v*/*v*) methanol. The mixture was vor-

https://doi.org/10.3390/plants15050769

texed thoroughly and extracted by shaking at 4 °C. After incubation, the samples were centrifuged at 12,000 rpm for 10 min, and the supernatant was filtered through a 0.22 μm organic membrane filter prior to UPLC–MS/MS analysis. Scopolin standard (CAS No. 531-44-2, purity ≥ 98%; Shanghai Yuanye Bio (Shanghai, China)) was used for instrument calibration and metabolite quantification/verification, as appropriate. Metabolite profiling of the two Sichuan pepper pericarp samples was performed using UPLC–MS/MS as described previously [13,14]. Metabolite detection and date acquisition were conducted by Maiwei Metabolic Biotechnology Co., Ltd. (Wuhan, China).

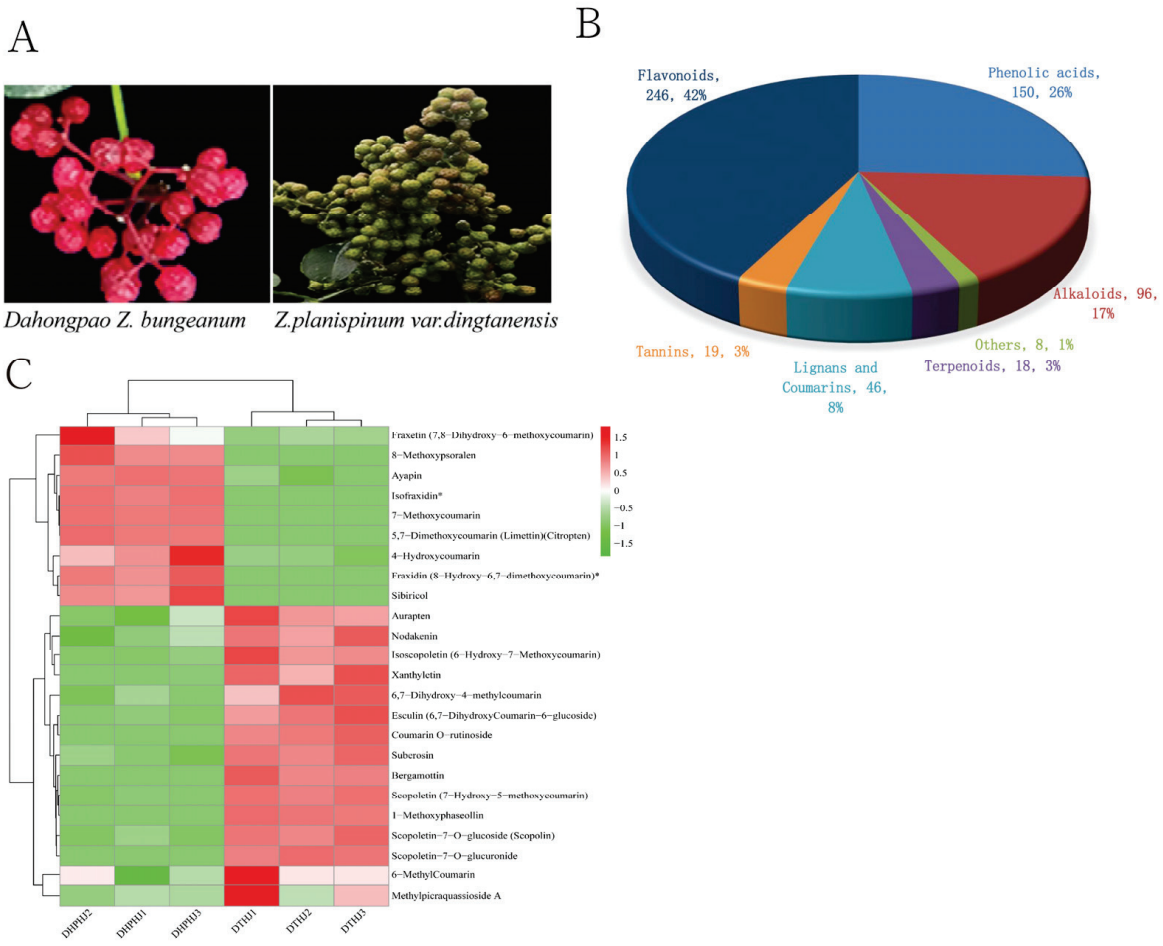

Figure 1. (**A**) Sichuan pepper materials. (**B**) Classification diagram of 583 secondary metabolites in Sichuan pepper pericarpium. (**C**) Cluster analysis of coumarin compounds: The heatmap displays the relative abundance patterns of 24 coumarin-related metabolites detected in pericarp samples of green Sichuan pepper (DTHJ1–DTHJ3) and red Sichuan pepper (DHPHJ1–DHPHJ3). The *X*-axis indicates sample names, and the *Y*-axis lists secondary metabolite information; red represents higher abundance, whereas green indicates lower abundance.

2.4. Metabolome Data Analysis

Following identification, peak alignment, and normalization of the raw mass spectrometry data, principal component analysis (PCA) and orthogonal partial least squares discriminant analysis (OPLS-DA) were used to assess metabolic differences and samples clustering. Differential metabolites (DMs) were identified using both of the following criteria: fold change (FC) ≥ 2.0 or $|\log2FC| \leq 1$ and a false discovery rate (FDR)-adjusted p value (q value) < 0.05 [15]. The KEGG database was utilized to annotate DMs. Metabolite set enrichment analysis was performed using MetaboAnalyst (MSEA module), and pathways with FDR-adjusted p values < 0.05 were considered significantly enriched [15].

2.5. RNA Extraction and Transcriptome Sequencing

Total RNA was extracted from Sichuan pepper pericarp tissues using standard plant RNA isolation procedures. The integrity of the RNA and potential genomic DNA contamination were assessed by agarose gel electrophoresis. RNA purity was evaluated using a NanoPhotometer spectrophotometer (OD260/280 and OD260/230) (Implen, Munich, Germany), and RNA concentration was quantified using a Qubit 2.0 fluorometer (Thermo Fisher Scientific, Waltham, MA, USA). RNA integrity was further evaluated using an Agilent 2100 Bioanalyzer (Agilent Technologies, Santa Clara, CA, USA). mRNA was enriched based on the poly(A) tail using Oligo(dT) beads, then fragmented with fragmentation buffer, and reverse-transcribed into first-strand cDNA using random hexamer primers, followed by second-strand cDNA synthesis [15]. Purified double-stranded cDNA underwent end repair, A-tailing, and adapters ligation, followed by purification and size selection using AMPure XP (Beckman Coulter, Brea, CA, USA) beads and PCR enrichment to generate the final cDNA libraries. Prior to sequencing, library quality was assessed by Qubit 2.0 quantification, insert-size evaluation using an Agilent 2100 Bioanalyzer, and qPCR based quantification (effective library concentration > 2 nM) [15]. Qualified libraries were pooled and sequenced on an Illumina HiSeq platform (Illumina, Inc., San Diego, CA, USA) using sequencing-by-synthesis (SBS). Raw image data were base-called and converted to FASTQ format using CASAVA (Illumina, Inc., San Diego, CA, USA) to generate raw reads. These raw reads were stringently filtered to obtain clean reads by (i) removing adapter-containing reads; (ii) discarding read pairs in which either read contained >10% 'N' bases; and (iii) discarding read pairs in which low-quality bases ($Q \leq 20$) accounted for >50% of the read length [15]. Sequencing was performed by Maiwei Metabolic Biotechnology Co., Ltd.

2.6. Transcriptome Data Analysis

Clean reads were de novo assembled using Trinity (v2.6.6) [16], and the resulting transcripts were hierarchically clustered with Corset (v1.07) [16]. The longest sequence in each cluster was retained to generate the unigene set for downstream analyses. Clean reads from each sample were subsequently mapped to the unigene reference, and transcript abundance was estimated using RSEM with Bowtie2 [16–18]. Expression levels were normalized to FPKM (Fragments Per Kilobase of transcript per Million fragments mapped). For functional annotation, unigene sequences were searched against the KEGG, NR, Swiss-Prot, GO, COG/KOG, and TrEMBL databases using BLAST (2.16.0), and Pfam annotation was performed using HMMER; annotation statistics were summarized accordingly. Differential expression analysis was conducted using DESeq2 (v1.22.2) based on raw read counts generated by featureCounts. Genes with $|\log2FC| \geq 1$ and FDR < 0.05 were considered differentially expressed [16–18].

2.7. Integrated Metabolome and Transcriptome Analysis

Differentially accumulated metabolites (DAMs) and differentially expressed genes (DEGs) were independently mapped to the KEGG database. Pathways that were significantly enriched in both datasets were extracted to delineate coumarin-related functional modules. Candidate genes were subsequently screened based on their pathway annotations and differential expression patterns between 'green Sichuan pepper' and 'red Sichuan pepper'. To quantitatively assess gene–metabolite relationships, the relative abundances of representative coumarins (scopoletin and scopolin) were paired with unigene expression levels (FPKM) across biological replicates, followed by Pearson correlation analysis. Statistically significant associations ($p < 0.05$) were retained and assembled into a correlation network to identify genes showing significant associations with scopoletin and/or scopolin.

https://doi.org/10.3390/plants15050769

2.8. Validation of Gene Expression by qRT-PCR

Quantitative reverse transcription polymerase chain reaction (qRT-PCR) was performed using the SYBR® Premix Ex Taq™ II Reagent Kit (Takara Bio Inc., Kusatsu, Shiga, Japan). The internal reference gene was the *Zanthoxylum* polyubiquitinase gene (UBQ), as reported by Ruijie et al. [19]. Primers were designed using Primer 5.0 (Table S1) with the following conditions: annealing temperature 58–65 °C, primer length 18–24 bp, and amplicom length of 80–150 bp. Relative gene expression was quantified using the $2^{-}\Delta\Delta Ct$ method, with reverse-transcribed cDNA as the template [20]. The total reaction volume was 20 μL (Table S3). Cycling conditions were as follows: 95 °C for 2 min; 95 °C for 15 s, 60 °C for 30 s, and 60 °C for 30 s. Melting curve analysis was performed at 95 °C for 15 s, 60 °C for 1 min, 95 °C for 15 s, and 60 °C for 15 s. The cycling program was repeated for 36 cycles, and the reactions were held at 4 °C.

2.9. Candidate Gene Cloning and Overexpression in Tobacco

The three candidate genes, *CCoAOMT (Cluster-21146.94405)*, *COMT (Cluster-21146.25660)*, and *F6H (Cluster-21146.64498)*, were significantly associated with scopoletin and scopolin levels. The complete primer sequences for these three genes are provided in Table S2. The CaMV 35S promoter was used to drive expression of the cloned CDS in a plant overexpression vector. After sequence verification, the recombinant vector was introduced into *Agrobacterium tumefaciens* strain GV3101. The *Agrobacterial* suspension carrying the recombinant vector was infiltrated into *Nicotiana benthamiana* leaves (See Supplementary Materials for details). After infiltration, the plants were maintained under standard growth conditions for 48–72 h, after which the infiltrated leaves were harvested for RNA extraction and qRT-PCR to confirm transgene expression. Metabolite were then extraction as described previously [20,21]. Changes in coumarin content in tobacco leaves, including scopoletin and its glycoside scopolin, were determined using UPLC-MS/MS.

3. Results

3.1. Metabolomics Data Analysis

3.1.1. Sample Stability Assessment and Quantitative Analysis

In both positive and negative ion modes, the total ion chromatograms (TIC) of quality control (QC) samples exhibited a high degree of overlap (Figure S1), indicating stable instrument performance. In negative ion mode, the response peaks of each QC sample showed consistent retention times and peak shapes, with sharp, non-tailing peaks. This observation indicates that neither ionization efficiency nor chromatographic separation performance drifted during the run. In positive ion mode, early-eluting peaks exhibited considerable overlap; moreover, the locations and intensities of the most abundant peaks remained consistent across QC samples. Later-eluting signals were stable, showing no significant signal attenuation or retention-time shift. These results demonstrate good repeatability and stability of the ion source and chromatographic system, supporting their suitability for subsequent metabolite measurements. Using UPLC-ESI-MS/MS, six pericarp samples of green Sichuan pepper and red Sichuan pepper were analyzed, and 583 metabolites were identified and grouped into seven classes (Figure 1B). The classes comprised 246 flavonoids, 150 phenolic acids, 96 alkaloids, 46 lignans and coumarins, 19 tannins, 18 terpenoids, and 8 other compounds. A total of 24 coumarin derivatives were detected, including scopoletin, scopoletin-7-O-glucoside, 6-methylcoumarin, and suberosin (Figure 1C).

https://doi.org/10.3390/plants15050769

3.1.2. PCA and PLS-DA Analysis

The OPLS-DA model showed clear separation structure between the two groups in the predictive component(p1), with $R^2X = 0.855$, $R^2Y = 1.000$, and $Q^2 = 0.997$ (Figure 2A). The model captured differences in metabolite accumulation in Sichuan pepper pericarp and exhibited strong predictive performance. Principal Component Analysis (PCA) revealed intrinsic compositional differences between the two pericarp types across major metabolic classes (Figure 2B). PC1 and PC2 together exceeded >84% of the total variance, indicating that these components captured the major sources of metabolic variation. Green Sichuan pepper and red Sichuan pepper samples were distinctly separated along PC1 axis, while samples within each group clustering tightly, suggesting high within-group consistency of metabolite profiles. The hierarchical clustering heatmap showed marked differences in metabolite distributions between the two pericarp types, indicating systematic shifts in accumulation across multiple metabolite categories. Green Sichuan pepper and red Sichuan pepper formed two distinct clusters in the standardized expression of most metabolites, with particularly pronounced differences observed in flavonoids, phenolic acids, and lignan-coumarin compounds (Figure 2C).

3.1.3. Identification and Analysis of Differential Metabolites

Significant differences were observed in secondary metabolites of the pericarps of two Zanthoxylum species. Differential metabolites were mainly flavonoids (103 upregulated and 58 downregulated metabolites), phenolic acids (39 upregulated and 51 downregulated metabolites), alkaloids (35 upregulated and 21 downregulated metabolites), and lignans and coumarins (14 upregulated and 18 downregulated metabolites) (Figure 3A).

To further investigate differences in coumarin constituents between the pericarps of the two *Zanthoxylum* samples, we conducted a volcano plot analysis of coumarin-derived secondary metabolites (Figure 3B). The results showed that among the 24 coumarin-related metabolites, 16 differed significant between DHPHJ and DTHJ, comprising eight upregulated and eight downregulated compounds, whereas the remaining eight metabolites showed no significant changes. Comparison with green Sichuan pepper, red Sichuan pepper showed a bidirectional shift in its coumarin profile: several methoxylated and furanocoumarin-related metabolites accumulated significantly, whereas certain coumarins and their conjugated derivatives decreased markedly. These findings suggest a clear redistribution of metabolic flux within the coumarin network between the two sample groups. Hierarchical clustering was performed for the 24 coumarin compounds across both samples (Figure 1C). The clustering results indicated that the concentrations of nine compounds, including 4-Hydroxycoumarin, 7-Methoxycoumarin, Ayapin, and 5,7-Dimethoxycoumarin, were significantly higher in DHPHJ. In contrast, the remaining 15 compounds, such as Aurapten, Nodakenin, Esculin, and Scopoletin-7-O-glucoside (Scopolin), formed a major cluster and showed higher concentrations in green Sichuan pepper. This pattern indicates that most coumarin compounds were present at relatively higher concentrations in green Sichuan pepper.

3.1.4. KEGG Enrichment Analysis

In the comparison between green Sichuan pepper and red Sichuan pepper, 363 differential metabolites were identified and mapped to the KEGG database, and 32 metabolic pathways were enriched. The top 20 enriched KEGG pathways are shown in Figure 3C, indicating that the most significantly overrepresented pathways are closely related to secondary metabolism. Notably, biosynthesis of secondary metabolites and flavonoid biosynthesis exhibited the strongest enrichment signals. In contrast, enrichment in phenylpropanoid biosynthesis and related upstream amino acid pathways, such as phenylalanine

metabolism and biosynthesis, was comparatively weaker. Importantly, the 363 differential metabolites were predominantly enriched in the phenylpropanoid biosynthesis pathway (ko00940), the biosynthesis of secondary metabolites (ko01110), and flavonoid biosynthesis (ko00941). Specifically, the coumarin compounds scopoletin and scopolin showed significant enrichment within phenylpropanoid biosynthesis.

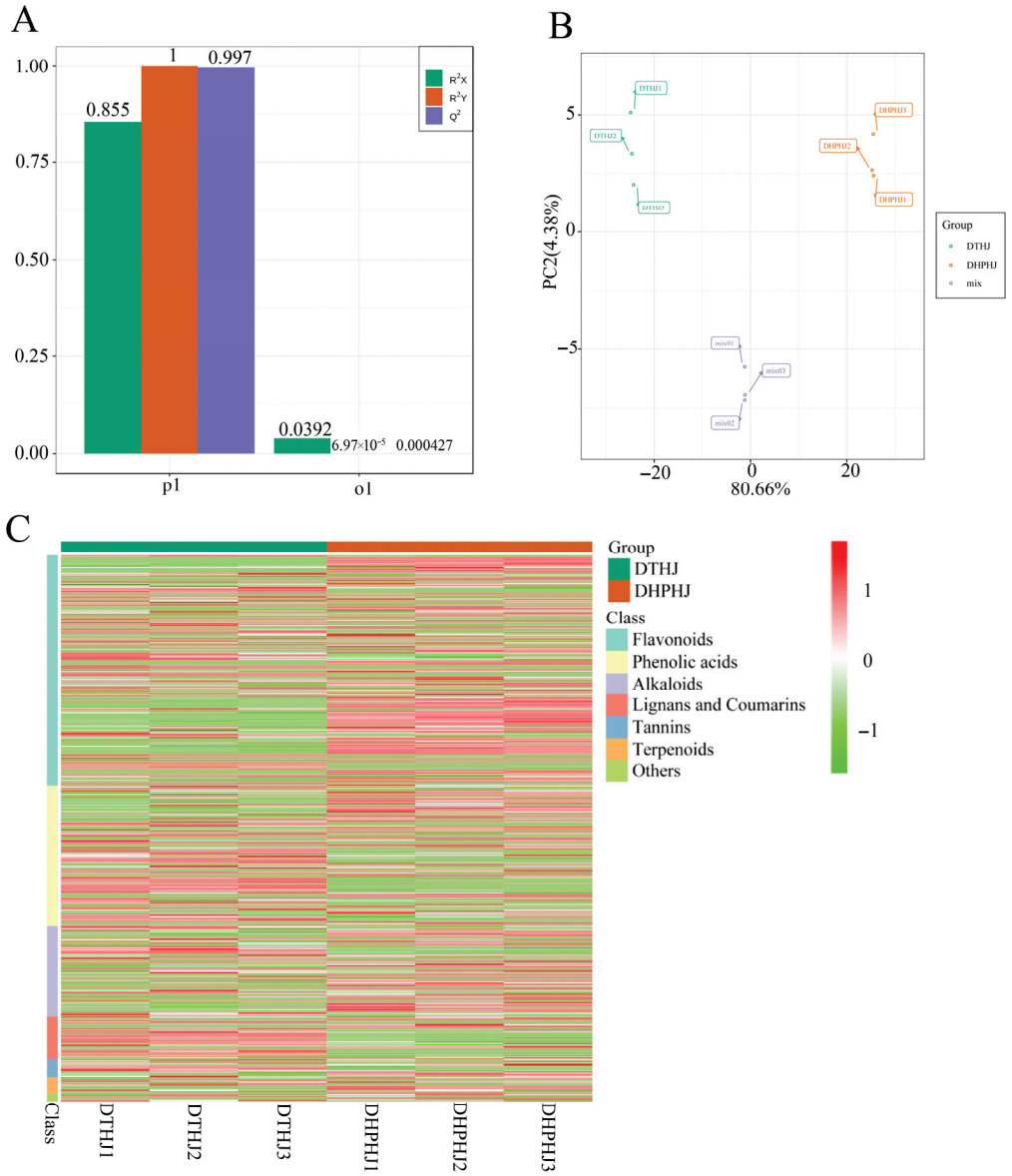

Figure 2. (**A**) Scatterplot of the Orthogonal Partial Least Squares Discriminant Analysis (OPLS-DA) model. The diagram shows R^2X, R^2Y, and Q^2 for the predictive and orthogonal components within the OPLS-DA model. On the *x*-axis, P1 represents the predictive component and O1 represents the orthogonal component; the *y*-axis shows the corresponding R^2X, R^2Y, and Q^2 values. (**B**) Principal Component Analysis (PCA). (**C**) Hierarchical heatmap clustering analysis of samples. Green indicates low abundance, and red indicates high abundance. In this figure, DTHJ denotes green Sichuan pepper, and DHPHJ denotes red Sichuan pepper.

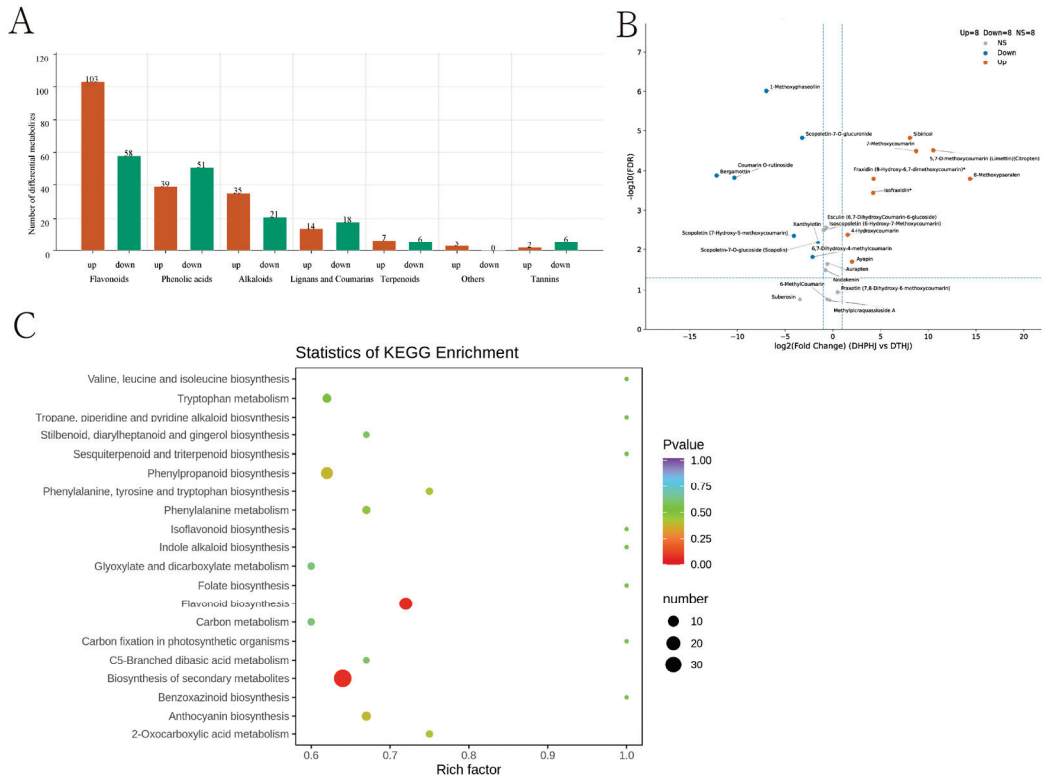

Figure 3. Differential metabolite analysis. (**A**) Bar plot of differentially accumulated metabolites; (**B**) the volcano plot specifically for coumarin compounds indicates that the double dashed line represents no significant difference, with the left side denoting downregulated and the right side indicating upregulated metabolites; (**C**) The KEGG enrichment analysis of differential metabolites, The *x*-axis represents the enrichment factor (Rich factor), which is defined as the proportion of differential metabolites mapped to a specific pathway relative to the total number of metabolites annotated in that pathway. The *y*-axis lists the enriched KEGG pathway names. The size of the bubbles indicates the number of differential metabolites annotated in each pathway, while the color of the bubbles denotes the significance of the enrichment (*p*-value). Larger bubbles with a redder color indicate a higher number of differential metabolites associated with the pathway and a greater significance of enrichment. In this figure, DTHJ denotes green Sichuan pepper, and DHPHJ denotes red Sichuan pepper.

3.2. Transcriptomic Analysis

3.2.1. Quality Assessment of Sequencing

DataHigh-throughput sequencing was performed on six pericarp samples of *Z. bungeanum* using the Illumina HiSeq platform, with three biological replicates for each of green Sichuan pepper and red Sichuan pepper. Separate cDNA libraries were constructed for each sample. The number of clean reads ranged from 4.26×10^7 to 5.28×10^7, per sample, and sample yielding over 6 Gb of clean data. The average GC content exceeded 43%, with Q20 values surpassing 97% and Q30 values exceeding 93%, while the sequencing error rate was maintained at 0.03% (Table 1). These quality metrics indicated that the data were suitable for downstream transcriptome analysis. Using Trinity, a total of 191,959 unigenes were assembled and annotated against seven major databases: KEGG, NR, SwissProt, Trembl, GO, KOG, and Pfam. The annotation counts were as follows: 96,043 (50.03%); 136,059 (70.88%); 93,201 (48.55%); 134,046 (69.83%); 82,909 (43.19%); 108,677 (56.61%); and 86,321 (44.97%).

https://doi.org/10.3390/plants15050769

Table 1. Quality control analysis data statistics.

Sample	Raw Reads	Clean Reads	Error Rate (%)	Q20 (%)	Q30 (%)	GC Content (%)
DHPHJ1	54,883,362	52,755,620	0.03	97.84	93.78	43.89
DHPHJ2	45,909,914	44,014,810	0.03	97.85	93.74	44.06
DHPHJ3	46,306,260	44,432,196	0.03	97.67	93.38	44.12
DTHJ1	47,677,896	45,711,152	0.03	97.76	93.55	43.71
DTHJ2	44,608,926	42,561,718	0.03	97.53	93.02	43.59
DTHJ3	46,886,006	45,111,670	0.03	97.73	93.49	43.53

Notes: Q20 and Q30 indicate the proportion of bases with Qphred scores of 20 or higher and 30 or higher, respectively, in relation to the total number of bases. GC content: Represents the percentage of G + C bases relative to the overall number of bases. In this table, DTHJ denotes green Sichuan pepper, and DHPHJ denotes red Sichuan pepper.

Following PCA (Figure 4A), the green Sichuan pepper and red Sichuan pepper groups separated clearly along PC1, with PC1 and PC2 explaining 85.54% and 4.35% of the total variation, respectively. Both groups showed tight within-group clustering, indicating high reproducibility among biological replicates. The sample correlation heatmap (Figure 4B) showed within-group correlation coefficients of approximately 0.99 for red Sichuan pepper and 0.98 for green Sichuan pepper, whereas between -group correlations were significantly lower (0.63–0.67), suggesting substantial transcriptional differences between the two materials. Furthermore, box plots of FPKM expression distributions (Figure 4C) reinforce the consistency of expression across samples, indicating an adequate sequencing depth that is suitable for differential expression analysis.

3.2.2. Expression Characteristics of DEGs

A total of 68,619 differentially expressed genes (DEGs) were identified between green Sichuan pepper and red Sichuan pepper, with 37,721 upregulated and 30,898 downregulated (Figure 5A). By mapping these DEGs to the KEGG database, we characterized metabolic pathways represented in Sichuan pepper pericarp and identified DEGs associated with coumarin-related biosynthesis. The DEGs were significantly enriched in pathways related to metabolism, biosynthesis of secondary metabolites, and phenylpropanoid biosynthesis (Figure 5B).

Thirteen genes were selected for qRT-PCR validation. The RNA-seq heatmap results indicated that key genes involved in the phenylpropanoid and coumarin-related pathways exhibited distinct group-specific expression patterns (Figure 5C). Multiple transcripts showed higher expression in green Sichuan pepper, whereas another subset was preferentially expressed in red Sichuan pepper, highlighting substantial transcriptional divergence between the two pericarp materials. These findings further suggest that both the upstream steps of the phenylpropanoid pathway and the downstream modification processes of coumarin biosynthesis may be differentially regulated. To further validate the transcriptomic data, qRT-PCR analysis was conducted using *SUBA* as the reference gene (Figure 5D). The qRT-PCR results corroborated the expression trends observed in the RNA-seq data, and the relative expression changes between red Sichuan pepper and green Sichuan pepper showed high concordance with the transcriptomic results for each gene. This concordance between qRT-PCR and RNA-seq supports the reliability of the expression patterns of these candidate genes.

https://doi.org/10.3390/plants15050769

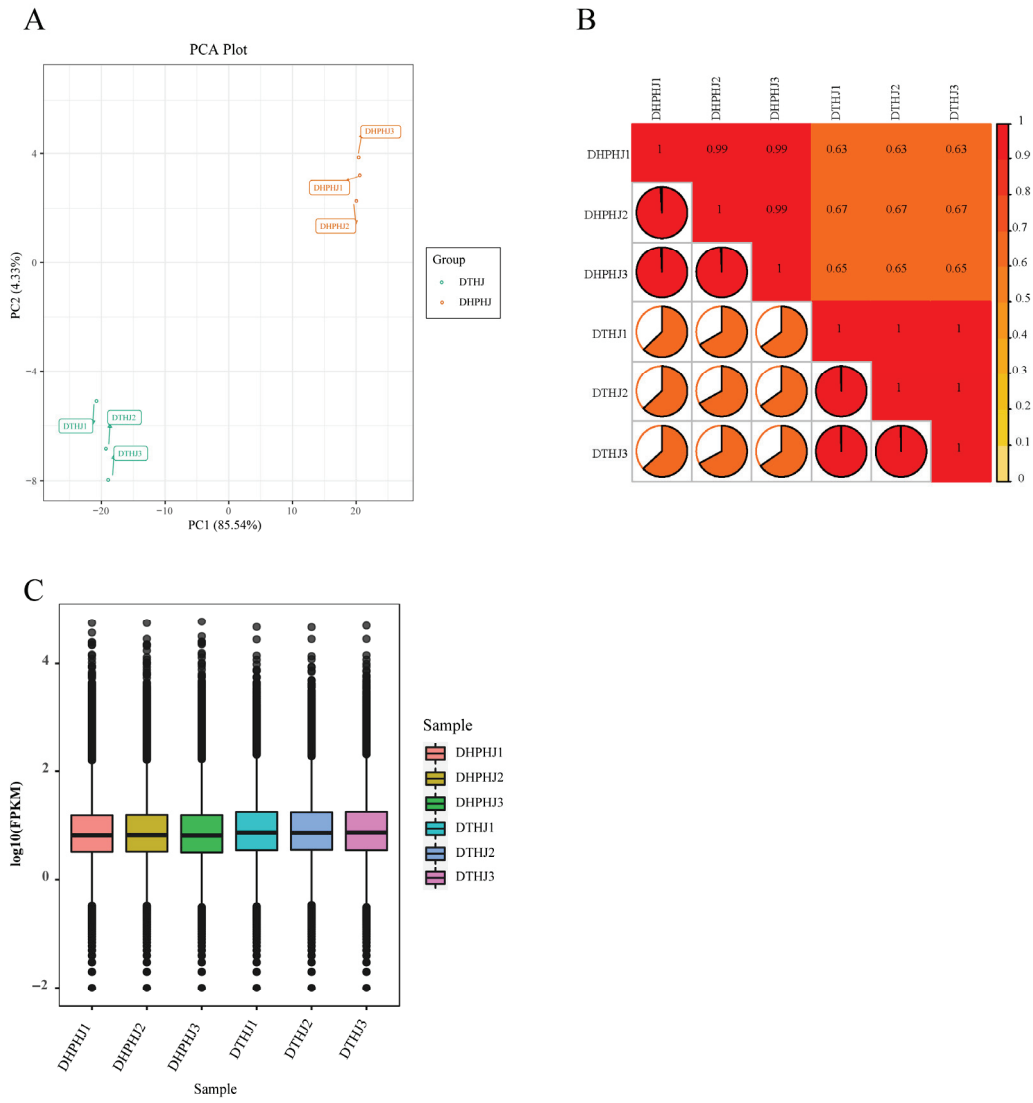

Figure 4. Gene expression and correlation analysis in the sample. (**A**) Principal component analysis (PCA); (**B**) Gene correlation coefficient analysis diagram; (**C**) Box plots of expression levels. In this figure, DTHJ denotes green Sichuan pepper, and DHPHJ denotes red Sichuan pepper.

3.3. Reconstruction of the Coumarin Biosynthetic Pathway in Zanthoxylum Pericarp and Screening of Candidate Genes

By integrating KEGG enrichment results from metabolomics and transcriptomics, we constructed a biosynthetic pathway framework for the simple coumarins scopoletin and scopolin in the pericarp of *Z. bungeanum* (Figure 6A). The upstream pathway initiates with the PAL-catalyzed deamination of phenylalanine, resulting in the formation of cinnamic acid, which is subsequently converted to p-coumaroyl-CoA through the action of *Cinnamate-4-hydroxylase (C4H)* and *4-coumarate-CoA ligase (4CL)*. Enzymatic processes involving *hydroxycinnamate O-methyltransferase (HCT)*, *Cinnamate-3-hydroxylase (C3′H)*, *Caffeoyl shikimate esterase (CSE)*, *Caffeoyl-CoA O-methyltransferase (CCoAOMT)*, and *caffeic acid O-methyltransferase (COMT)* yield various hydroxycinnamic acid derivatives. The key ortho-hydroxylation step is mediated by cytochrome P450 enzymes (*CYP73A*) and 2-oxoglutarate-dependent dioxygenases (*F6H*), resulting in intermediates that readily undergo lactonization. Subsequently, enzymes such as *TOGT1* and *BGLU* facilitate the glycosylation–deglycosylation cycle, culminating in the formation of scopoletin and scopolin.

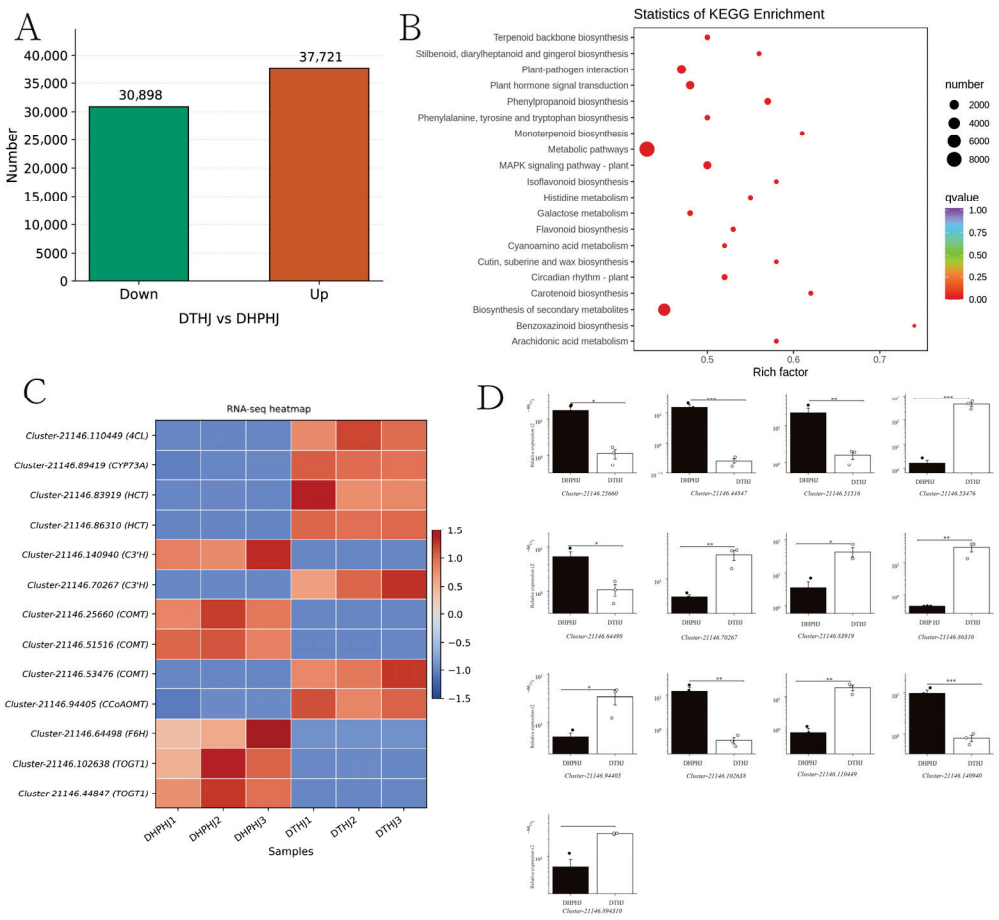

Figure 5. (**A**) Histogram of differentially expressed genes; (**B**) KEGG enrichment analysis diagram for DEGs; (**C**) Transcriptome expression heatmap. Red indicates high expression; purple indicates low expression; (**D**) qRT-PCR validation of candidate genes associated with coumarin biosynthesis in Sichuan pepper pericarp. The expression levels of selected candidate genes in red Sichuan pepper and green Sichuan pepper pericarps were determined by qRT-PCR. *X*-axis: sample groups (DHPHJ and DTHJ). *Y*-axis: relative gene expression level, presented as $2^{-}\Delta\Delta$Ct (logarithmic scale). Bars represent the mean values, error bars indicate standard deviation (SD), and dots indicate biological replicates. Asterisks above brackets indicate significant differences between the two groups (* $p < 0.05$, ** $p < 0.01$, *** $p < 0.001$). Gene IDs are shown below each panel. In this figure, DTHJ denotes green Sichuan pepper, and DHPHJ denotes red Sichuan pepper.

Based on pathway localization and differential expression analysis, a total of 102 coding genes potentially involved in the coumarin biosynthesis of *Zanthoxylum* were identified. This includes 9 *PAL*, 7 *4CL*, 4 *C3′H*, 9 *CCoAOMT*, 17 *COMT*, 8 *CYP73A*, 6 *F6H*, 19 *HCT*, 11 *TOGT1*, 13 *BGLU*, and 3 *CSE* genes (Figure 6B). Most of these genes showed significantly higher expression in DTHJ than in DHPHJ, consistent with the higher overall coumarin content in DTHJ. Further correlation analysis between the contents of scopoletin and scopolin and the expression levels of these genes identified 56 candidate genes that were highly correlated with the contents of these two coumarins, including *PAL*, *4CL*, *CCoAOMT*, and *COMT*. The correlation network indicated that some midstream enzymes (*CCoAOMT*, *COMT*, and *F6H*) exhibited high correlation coefficients with both coumarins, thus displaying 'hub' node characteristics within the network (Figure 6C).

https://doi.org/10.3390/plants15050769

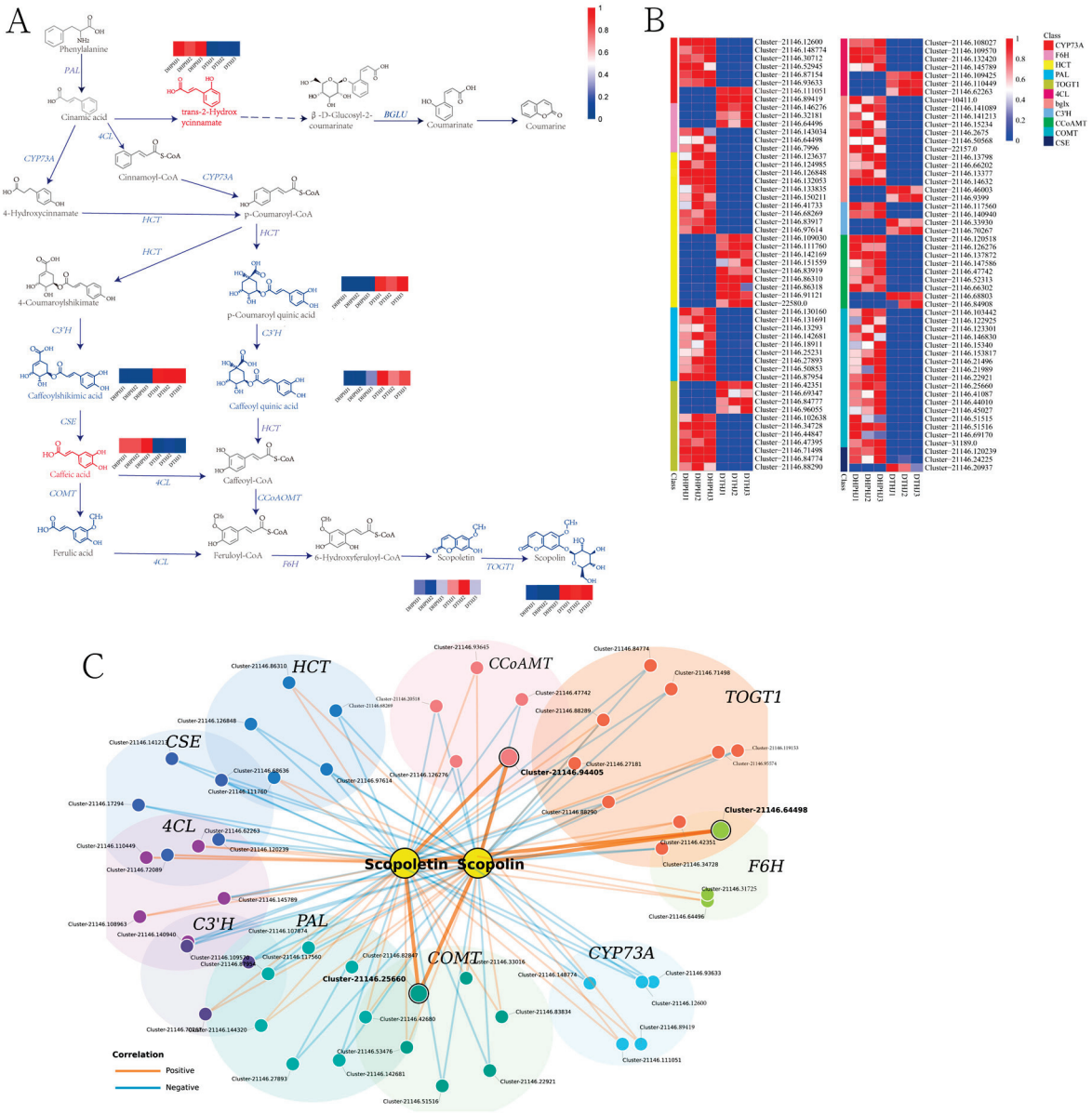

Figure 6. Analysis of metabolites and genes related to the coumarin biosynthesis pathway in *Zanthoxylum* pericarp. (**A**) The coumarin biosynthesis pathway; (**B**) Heatmap of structural genes involved in coumarin biosynthesis. The color gradient from blue to red indicates gene expression levels from low to high, with deeper red representing higher gene expression levels. (**C**) Correlation network between candidate genes and scopoletin and scopolin. Blue lines indicate negative correlations, while red lines indicate positive correlations. In this figure, DTHJ denotes green Sichuan pepper, and DHPHJ denotes red Sichuan pepper.

3.4. Functional Validation of CCoAOMT, COMT, and F6H

Based on the correlation network and expression patterns, three candidate genes—*CCoAOMT (Cluster-21146.94405)*, *COMT (Cluster-21146.25660)*, and *F6H (Cluster-21146.64498)*—were selected for gene cloning and heterologous expression analyses. The constructed overexpression vectors were introduced into tobacco leaves via Agrobacterium-mediated transient infiltration (Figure S2). PCR verification confirmed that constructs carrying the three target genes were detectable in tobacco leaves after transient infiltration (Figure S3), and transient overexpression was achieved (Figure S4). UPLC-based quantitative analysis demonstrated that, compared with the control, the contents of scopoletin and scopolin significantly increased in tobacco leaves overexpressing each of the three genes, with more

pronounced increases observed in the COMT- and F6H-overexpression lines (Figure 7). Coupled with their expression profiles in *Zanthoxylum* pericarp and the metabolite-gene correlation analysis, these results indicate that the three genes play crucial catalytic roles in the biosynthesis of coumarins in *Zanthoxylum*, particularly in the formation of scopoletin and its glycoside.

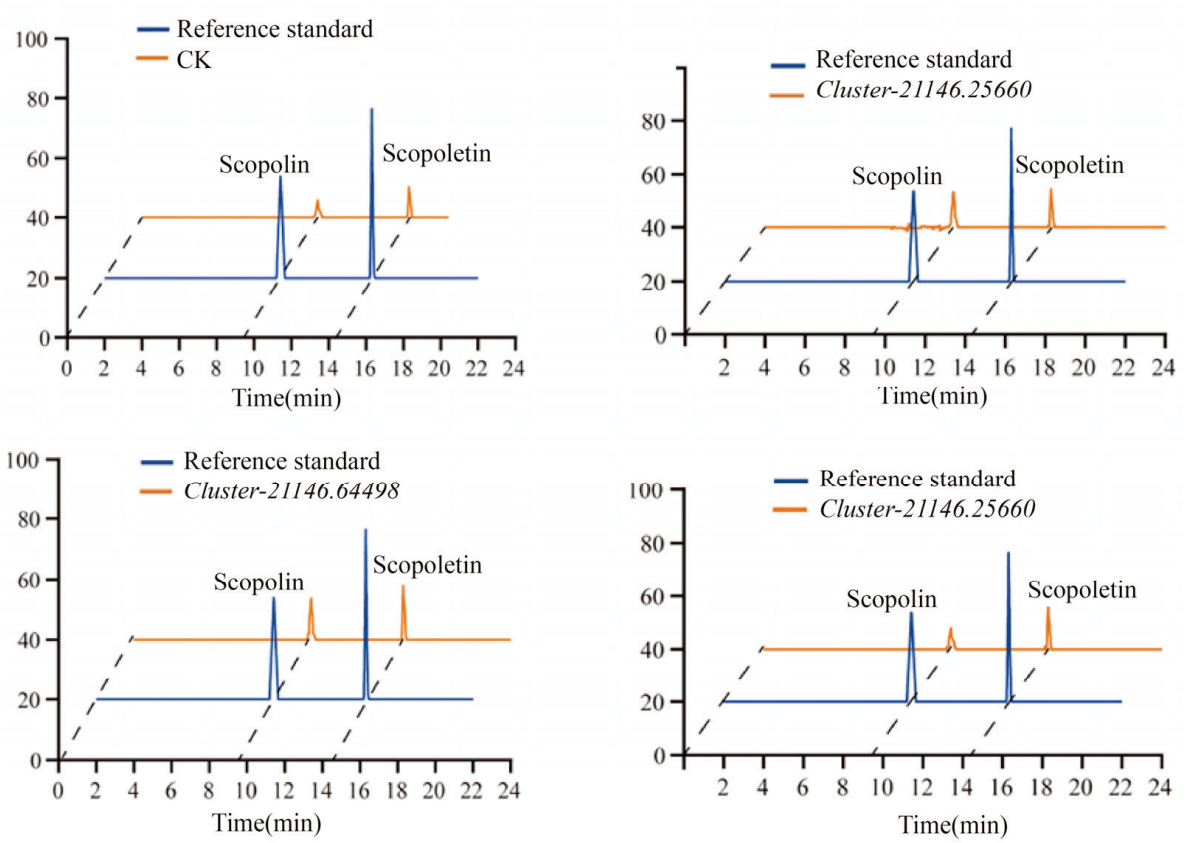

Figure 7. Ultra-Performance Liquid Chromatography (UPLC) analysis of scopoletin and scopolin.

4. Discussion

This study analyzed coumarin metabolites and their synthesis-related genes in the mature pericarp of two Sichuan pepper cultivars. Significant variations were identified in the overall secondary metabolite composition between green Sichuan pepper and red Sichuan pepper, with green Sichuan pepper pericarp demonstrating higher overall abundance of simple coumarins. This conclusion is consistent with previous reports of differences in volatile oils, flavonoids, and amides among Sichuan pepper cultivars, and further supports the observation that green Sichuan pepper contains higher coumarin levels than red Sichuan pepper [22–25].

The coumarin biosynthesis framework proposed in this study is fundamentally consistent with the phenylpropanoid branch pathways previously discovered in plants of the Apiaceae, Rutaceae, and Brassicaceae families. This process originates with *PAL-C4H-4CL*, catalysed by enzymes including *HCT*, *C3′H*, and *CCoAOMT/COMT* to create various hydroxycinnamic acid derivatives. Subsequently, crucial ortho-hydroxylation reactions are catalysed by 2-oxoglutarate-dependent dioxygenases such as *F6′H*, leading to intermediates that undergo lactonisation and glycosylation [22–25]. Multiple gene family members including *PAL, 4CL, HCT, C3′H, CCoAOMT, COMT, F6H, TOGT1* and *BGLU* were similarly discovered in Sichuan pepper, demonstrating that coumarin production in this plant follows the normal phenylpropanoid metabolic pathway. The diversity and abundance of coumarins in Sichuan pepper pericarp differ markedly from those reported in species such

as *Arabidopsis thaliana* and Angelica sinensis, in which roots are the principal medicinal tissues [25–27]. For example, in *A. sinensis*, simple coumarins are primarily concentrated in roots, whereas Sichuan pepper pericarp exhibits a distinct coumarin profile consistent with its use as a seasoning [28]. Variations in the division of labour across various plants or tissues in defensive functions, signal transduction, and interactions with microbes could be the cause of this specificity discrepancy. This pattern may also be influenced by synergistic defense networks involving other secondary metabolites, including volatile oils and amides [29].

Although green Sichuan pepper DTHJ and red Sichuan pepper differ in coumarin content, the expression patterns of major enzyme-encoding genes within the *CCoAOMT*, *COMT*, and *F6H* families also show substantial divergence. Research reveals that these enzymes hold critical locations within the phenylpropanoid metabolic pathway, where even modest alterations in their expression can drastically alter the distribution of carbon flux among diverse products such as flavonoids, coumarins, and lignin [30]. In this study, most structural genes associated with coumarin synthesis exhibited higher expression in green Sichuan pepper, while several genes involved in lignin biosynthesis showed relatively higher expression in red Sichuan pepper. This pattern suggests that carbon flux allocation may differ between the two materials, potentially favouring coumarin and flavonoid biosynthesis in green Sichuan pepper; however, this interpretation remains hypothetical and requires further experimental validation, such as lignin quantification, total phenolic measurements, or metabolic flux analysis. *CCoAOMT*, *COMT*, and *F6H* exhibited strong positive correlations with scopoletin and scopoletin glycoside within the network and demonstrated the capacity to enhance coumarin content in heterologous systems. This observation is consistent with reports in other species identifying F6′H and related methyltransferases as key enzymes in coumarin biosynthesis [24]. However, the presence of numerous members within the *TOGT1* and *BGLU* gene families in Sichuan pepper, coupled with the significant correlation of multiple members with coumarin content, suggests that glycosylation-deglycosylation cycles may play a more pivotal role in regulating the dynamic equilibrium of coumarin in pericarp. Although such cycles have been reported less frequently in species in which roots are the primary site of coumarin accumulation, further functional evidence is required to substantiate this regulatory role.

5. Conclusions

Metabolomic analysis of mature pericarps from green Sichuan pepper and red Sichuan pepper identified a total of 583 metabolites, including 24 coumarins that differed significant between the two *Zanthoxylum* materials. The pericarp of DTHJ showed a higher overall abundance of simple coumarins. Integrating metabolomic and transcriptomic datasets identified 102 structural genes potentially involved in coumarin metabolism; among these, 56 candidates showed significant correlations with scopoletin glycoside accumulation. Transient overexpression assays conducted in Nicotiana benthamiana revealed that *CCoAOMT (Cluster-21146.94405)*, *COMT (Cluster-21146.25660)*, and *F6H (Cluster-21146.64498)* significantly enhanced the accumulation of scopoletin and scopolin, thereby supporting their roles in coumarin biosynthesis. These functional data were obtained from heterologous transient expression, and genetic validation in *Zanthoxylum* remains to be established. Future studies employing gene knockdown or knockout techniques (e.g., RNAi or CRISPR/Cas9), in vitro enzymatic assays, and absolute metabolite quantification using internal standards will be essential to further validate gene functions and refine the regulatory framework of coumarin biosynthesis.

https://doi.org/10.3390/plants15050769

Supplementary Materials: The following supporting information can be downloaded at: https://www.mdpi.com/article/10.3390/plants15050769/s1, Figure S1: Overlay of TIC from mass spectrometry analysis of QC samples. Note: N, negative ion mode; P, positive ion mode; Figure S2: A. E. coli culture of cloned strains B. Agrobacterium sensory state preparation; Figure S3: PCR assay of bacterial fluid; Figure S4: PCR amplification results of the target gene; Table S1: qRT-PCR primers; Table S2: Full length primers of 3 candidate genes; Table S3: qRT-PCR reaction components; Table S4: Statistical table of differential coumarins of DTHJ vs. DHPHJ.

Author Contributions: H.L. and G.W. planned and supervised the project, conceived and designed the experiments, and were involved in funding acquisition. S.C. and L.S. analyzed the data and wrote the manuscript. Y.Z. contributed to manuscript writing. S.F. performed data curation and formal analysis. All authors have read and agreed to the published version of the manuscript.

Funding: This work was supported by the National Natural Science Foundation of China (Grant No. 32260410), Guizhou Provincial Basic Research Program (Natural Science) (No. ZK [2023] general121), Guizhou Provincial Key Technology R&D Program (Qian Ke He [2021] No. 222 and [2022] No. 118), Guizhou forestry industry project (Research 2020-18) and Guizhou Provincial Key Laboratory for Cultivation of Forest Trees in Plateau and Mountainous Areas (Qiaikehe Platform ZSYS [2025]025).

Institutional Review Board Statement: The pericarps of *Zanthoxylum planispinum var. dingtanensis* and *Dahongpao Zanthoxylum bungeanum* were collected from cultivated orchards in Guizhou Province, Southwest China. All plant materials were obtained from managed agricultural plantations rather than wild populations; therefore, no special permission was required for sample collection. Species identification was performed by Prof. Wang Gang and Prof. Hou Na from Guizhou Academy of Forestry, based on morphological characteristics and taxonomic descriptions. Voucher specimens (Z. planispinum var. dingtanensis, no. WG-2019–GZ-ZF-018; Dahongpao *Z. bungeanum*, no. HN-2019-SC-HY-001) were deposited at Guizhou Academy of Forestry Herbarium. All experimental procedures complied with institutional, national, and regional guidelines for plant research in China.

Data Availability Statement: The datasets generated and/or analysed during the current study are available in the Supplementary Information Files repository. The RNA-seq data generated in this study have been deposited in the China National Center for Bioinformation (CNCB) (https://ngdc.cncb.ac.cn/) under BioProject accession number PRJCA055049.

Acknowledgments: We thank the Mianyang Academy of Agricultural Sciences, Sichuan Province, for providing tissue-cultured tobacco seedlings.

Conflicts of Interest: The authors declare no conflicts of interest.

Abbreviations

DTHJ: *Zanthoxylum planispinum* var. *dingtanensis*, DHPHJ: Dahongpao *Zanthoxylum bungeanum*.

References

1. Wen, J.; Xiang, Q.; Guo, J.; Zhang, J.; Yang, N.; Huang, Y.; Chen, Y.; Hu, T.; Rao, C. Pharmacological activities of *Zanthoxylum* L. plants and its exploitation and utilization. *Heliyon* **2024**, *10*, e33207. [CrossRef]
2. Okagu, I.U.; Ndefo, J.C.; Aham, E.C.; Udenigwe, C.C. *Zanthoxylum* species: A review of traditional uses, phytochemistry and pharmacology in relation to cancer, infectious diseases and sickle cell anemia. *Front. Pharmacol.* **2021**, *12*, 713090. [CrossRef] [PubMed]
3. Yan, H.; Zhou, F.; Liu, Y.; Zhang, Y.; Xu, H.; Zhang, J.; Wang, J.; Jiang, S.; Qin, D.; Wang, T. *Zanthoxylum bungeanum* Maxim: A review of its phytochemistry, pharmacology, and pharmacokinetics. *Nat. Prod. Commun.* **2023**, *18*, 1–7. [CrossRef]
4. Wang, K.; Meng, X.-H.; Chai, T.; Wang, C.-B.; Sang, C.-Y.; Wang, W.-F.; Shang, X.-Y.; Yang, J.-L. Chemical constituents from the fruits of *Zanthoxylum bungeanum* and their chemotaxonomic significance. *Biochem. Syst. Ecol.* **2021**, *99*, 104356. [CrossRef]
5. Zhang, M.; Wang, J.; Zhu, L.; Li, T.; Jiang, W.; Zhou, J.; Peng, W.; Wu, C. *Zanthoxylum bungeanum* Maxim. (Rutaceae): A systematic review of its traditional uses, botany, phytochemistry, pharmacology, pharmacokinetics, and toxicology. *Int. J. Mol. Sci.* **2017**, *18*, 2172. [CrossRef] [PubMed]
6. Du, C.; Li, X.; Chen, J.; Luo, L.; Yuan, C.; Yang, J.; Hao, X.; Gu, W. Discovery of coumarins from *Zanthoxylum dimorphophyllum* var. spinifolium and their potential against rheumatoid arthritis. *Molecules* **2024**, *29*, 4395. [CrossRef] [PubMed]

7. Shi, Y.; Zhang, S.; Peng, D.; Shan, C.; Zhao, L.; Wang, B.; Wu, J. De novo transcriptome analysis of *Cnidium monnieri* (L.) Cuss and detection of genes related to coumarin biosynthesis. *PeerJ* **2020**, *8*, e10157. [CrossRef]
8. Wang, Y.; Guan, T.; Yue, X.; Yang, J.; Zhao, X.; Chang, A.; Yang, C.; Fan, Z.; Liu, K.; Li, Y. The biosynthetic pathway of coumarin and its genetic regulation in response to biotic and abiotic stresses. *Front. Plant Sci.* **2025**, *16*, 1599591. [CrossRef]
9. He, B.-T.; Liu, Z.-H.; Li, B.-Z.; Yuan, Y.-J. Advances in biosynthesis of scopoletin. *Microb. Cell Factories* **2022**, *21*, 152. [CrossRef]
10. Liu, S.; Zainuddin, I.M.; Vanderschuren, H.; Doughty, J.; Beeching, J.R. RNAi inhibition of feruloyl CoA 6′-hydroxylase reduces scopoletin biosynthesis and post-harvest physiological deterioration in cassava (*Manihot esculenta* Crantz) storage roots. *Plant Mol. Biol.* **2017**, *94*, 185–195. [CrossRef] [PubMed]
11. Kai, K.; Mizutani, M.; Kawamura, N.; Yamamoto, R.; Tamai, M.; Yamaguchi, H.; Sakata, K.; Shimizu, B. Scopoletin is biosynthesized via ortho-hydroxylation of feruloyl CoA by a 2-oxoglutarate-dependent dioxygenase in *Arabidopsis thaliana*. *Plant J.* **2008**, *55*, 989–999. [CrossRef] [PubMed]
12. Wang, C.; Han, F.; Chen, X.; Zhao, A.; Wang, D. Time-series based metabolomics reveals the characteristics of the color-related metabolites during the different coloration stages of *Zanthoxylum bungeanum* peel. *Food Res. Int.* **2022**, *155*, 111077. [CrossRef]
13. Gao, J.; Ren, R.; Wei, Y.; Jin, J.; Ahmad, S.; Lu, C.; Wu, J.; Zheng, C.; Yang, F.; Zhu, G. Comparative metabolomic analysis reveals distinct flavonoid biosynthesis regulation for leaf color development of *Cymbidium sinense* 'Red Sun'. *Int. J. Mol. Sci.* **2020**, *21*, 1869. [CrossRef]
14. Yuan, H.; Zeng, X.; Shi, J.; Xu, Q.; Wang, Y.; Jabu, D.; Sang, Z.; Nyima, T. Time-course comparative metabolite profiling under osmotic stress in tolerant and sensitive Tibetan hulless barley. *BioMed Res. Int.* **2018**, *2018*, 9415409. [CrossRef]
15. Anders, S.; Huber, W. Differential expression analysis for sequence count data. *Genome Biol.* **2010**, *11*, R106. [CrossRef]
16. Lou, H.; Yang, Y.; Zheng, S.; Ma, Z.; Chen, W.; Yu, C.; Song, L.; Wu, J. Identification of key genes contributing to amino acid biosynthesis in *Torreya grandis* using transcriptome and metabolome analysis. *Food Chem.* **2022**, *379*, 132078. [CrossRef]
17. Conesa, A.; Madrigal, P.; Tarazona, S.; Gomez-Cabrero, D.; Cervera, A.; McPherson, A.; Szcześniak, M.W.; Gaffney, D.J.; Elo, L.L.; Zhang, X.; et al. A survey of best practices for RNA-seq data analysis. *Genome Biol.* **2016**, *17*, 13. [CrossRef] [PubMed]
18. Ruijie, N.; Haiyan, Y.; Honglei, T.; Ping, Z.; Yuyu, Z. Characterization of key odorants in fried red and green huajiao (*Zanthoxylum bungeanum* Maxim. and *Zanthoxylum schinifolium* Sieb. et Zucc.) oils. *Food Chem.* **2022**, *377*, 131984. [CrossRef] [PubMed]
19. Liu, Z. Evaluation of Melilotus Germplasm Resources and Mapping of Key Enzyme Genes in Coumarin Biosynthesis. Master's Thesis, Lanzhou University, Lanzhou, China, 2019.
20. Zhao, Y.; Liu, T.; Luo, J.; Zhang, Q.; Xu, S.; Han, C.; Xu, J.; Chen, M.; Chen, Y.; Kong, L. Integration of a decrescent transcriptome and metabolomics dataset of *Peucedanum praeruptorum* to investigate the CYP450 and MDR genes involved in coumarins biosynthesis and transport. *Front. Plant Sci.* **2015**, *6*, 996. [CrossRef]
21. Vogt, T. Phenylpropanoid biosynthesis. *Mol. Plant* **2010**, *3*, 2–20. [CrossRef]
22. Ihnatowicz, A.; Siwinska, J.; Perkowska, I.; Grosjean, J.; Hehn, A.; Bourgaud, F.; Lojkowska, E.; Olry, A. Genes to specialized metabolites: Accumulation of scopoletin, umbelliferone and their glycosides in natural populations of *Arabidopsis thaliana*. *BMC Plant Biol.* **2024**, *24*, 806. [CrossRef]
23. Liu, H.; Wang, Y.; Chang, Q.; Li, Q.; Fang, J.; Cao, N.; Tong, X.; Jiang, X.; Yu, X.; Cheng, Y. Combined metabolome and transcriptome reveal HmF6′H1 regulating simple coumarin accumulation against powdery mildew infection in *Heracleum moellendorffii* Hance. *BMC Plant Biol.* **2024**, *24*, 507. [CrossRef] [PubMed]
24. Ji, J.; Han, X.; Zang, L.; Li, Y.; Lin, L.; Hu, D.; Sun, S.; Ren, Y.; Maker, G.; Lu, Z.; et al. Integrative multi-omics data provide insights into the biosynthesis of furanocoumarins and mechanisms regulating their accumulation in *Angelica dahurica*. *Commun. Biol.* **2025**, *8*, 649. [CrossRef] [PubMed]
25. Yang, B.; Liu, S.-H.; He, Y.; Li, Y.; Feng, L.; Zhang, M.; Zhao, J.; Zhang, Y.; Yu, X.; Chen, H. Integration of transcriptomics and metabolomics to identify key coumarin biosynthetic genes in *Bupleurum chinense*. *Biotechnol. Biotechnol. Equip.* **2021**, *35*, 1858–1868. [CrossRef]
26. Tine, Y.; Renucci, F.; Costa, J.; Wélé, A.; Paolini, J. A method for LC-MS/MS profiling of coumarins in *Zanthoxylum zanthoxyloides* (Lam.) B. Zepernich and Timler extracts and essential oils. *Molecules* **2017**, *22*, 174. [CrossRef]
27. Guo, J.; He, C.-X.; Zhang, Q.; Li, R.-L.; Qian, D.; Wu, C.-J.; Chen, W.-W.; Hou, S.-G.; Peng, W. The pericarp of *Zanthoxylum bungeanum* Maxim.: An excellent source for the development of alternative drugs for improving glucose and lipid metabolism disorder related diseases. *Arab. J. Chem.* **2024**, *17*, 105594. [CrossRef]
28. Righetti, L.; Gottwald, S.; Tortorella, S.; Spengler, B.; Bhandari, D.R. Mass spectrometry imaging disclosed spatial distribution of defense-related metabolites in *Triticum* spp. *Metabolites* **2022**, *12*, 48. [CrossRef]

29. Ninkuu, V.; Aluko, O.O.; Yan, J.; Zeng, H.; Liu, G.; Zhao, J.; Li, H.; Chen, S.; Dakora, F.D. Phenylpropanoids metabolism: Recent insight into stress tolerance and plant development cues. *Front. Plant Sci.* **2025**, *16*, 1571825. [CrossRef]
30. Vismans, G.; van Bentum, S.; Spooren, J.; Song, Y.; Goossens, P.; Valls, J.; Snoek, B.L.; Thiombiano, B.; Schilder, M.; Dong, L.; et al. Coumarin biosynthesis genes are required after foliar pathogen infection for the creation of a microbial soil-borne legacy that primes plants for SA-dependent defenses. *Sci. Rep.* **2022**, *12*, 22473. [CrossRef]

plants

MDPI

Article

A Genome-Wide Pseudogene Map Reveals the Asymmetric Evolution of the A, B, and D Subgenomes in Common Wheat

Haifeng Zhu [1,2,3], Hao Tang [1,2,3], Yang Li [1,2,3], Ning Yang [1,2,3], Qin Wang [1,2,3], Fan Yang [4], Hongshen Wan [1,2,3], Wuyun Yang [1,2,3], Jun Li [1,2,3,*] and Zehou Liu [1,2,3,*]

[1] Crop Research Institute, Sichuan Academy of Agricultural Sciences, Chengdu 610066, China
[2] Crop Germplasm Innovation and Genetic Improvement Key Laboratory of Sichuan Province, Chengdu 610066, China
[3] Key Laboratory of Wheat Biology and Genetic Improvement on Southwestern China, Ministry of Agriculture and Rural Affairs, Chengdu 610066, China
[4] Biotechnology and Nuclear Technology Research Institute, Sichuan Academy of Agricultural Sciences, Chengdu 610066, China
* Correspondence: lijunchd@126.com (J.L.); zehouliu@163.com (Z.L.)

Abstract

Formerly considered nonfunctional "junk DNA," pseudogenes have been re-evaluated in light of technological advances in bioinformatics and high-throughput sequencing. The limited research to date on pseudogenes in hexaploid common wheat (*Triticum aestivum* L.) is largely confined to individual gene families, thus hindering our understanding of the long-term evolutionary dynamics among the A, B, and D subgenomes. Using the IWGSC RefSeq v2.1 genome assembly, we performed genome-wide identification, classification, and analysis of pseudogenes in wheat, including their distribution, evolutionary history, and parental gene functions. Marked asymmetries in pseudogene abundance, distribution, evolutionary dynamics, and constraints were detected among the subgenomes. The B subgenome harbored significantly more pseudogenes and showed distinct evolutionary patterns compared with the A and D subgenomes. Pseudogenes were strongly associated with transposable elements and peaks in their formation were incongruent with ancient genomic upheavals of wheat ancestral lineages. The parent genes were predominantly enriched in non-core functions and showed tissue-specific expression. The findings provide direct evidence for long-term asymmetric, post-polyploidization evolution in wheat, enhance our understanding of polyploid genome evolution, and offer a methodological framework for research on other genetically complex polyploid crops.

Keywords: *Triticum aestivum*; pseudogenization; parent gene; functional divergence; evolutionary dynamics

1. Introduction

Common wheat (*Triticum aestivum* L.) is a hexaploid species with a genome composition of AABBDD ($2n = 6x = 42$). As a crop of global importance for food security, wheat production occupies more than 220 million ha of farmland, with an annual production of almost 750 million tonnes, supplying approximately 15% of the global daily calorie intake. Following the transition from a hunter–gatherer lifestyle to sedentary agrarian societies, common wheat has been pivotal in the rise of civilizations, and through selection, it has been continuously improved to better meet human needs and for adaptation to diverse

environments [1]. Its exceptional ecological adaptability and agricultural productivity are largely attributable to the genetic diversity arising from polyploidization events [2].

The evolutionary history of common wheat involves the early divergence of three diploid ancestral lineages (A, B, and D) and two subsequent allopolyploidization events [3]. One polyploidization event approximately 0.8–1.5 million years ago (MYA) involved hybridization between the A subgenome donor *Triticum urartu* (AA) and a close relative of *Aegilops speltoides* (the B subgenome donor, BB), followed by chromosome doubling, which gave rise to a tetraploid ancestor (AABB). The second polyploidization event occurred approximately 8000–10,000 years ago in the Fertile Crescent, where a cultivated tetraploid wheat hybridized with *Aegilops tauschii* (DD) to form modern hexaploid common wheat [1]. The combination of three differentiated subgenomes within a single nucleus creates a dynamic genomic architecture, making wheat an ideal model system for comparative studies of subgenome evolution following polyploidization [4].

Subgenome differentiation and coevolution are integral to understanding the environmental adaptability of common wheat [5]. Polyploidization is the process whereby an organism undergoes whole-genome duplication (WGD), resulting in an increase in the number of chromosome sets. Polyploidization is a widespread evolutionary mechanism and has been a major driver of diversification in the plant kingdom [6]. Following polyploidization, plant subgenomes often exhibit asymmetric functional and evolutionary differentiation; the synergistic coexistence of the A, B, and D subgenomes in wheat is dynamic and leads to functional partitioning and differential evolutionary rates. Coding gene expression bias [7], differential transposon activity [8], epigenetic differences [9], and structural variation [10] provide evidence for asymmetry among the wheat subgenomes. This asymmetry reflects the functional differentiation of subgenomes following polyploidization and endows wheat with remarkable regulatory plasticity, thereby enabling adaptation to diverse environments and selection developmental stages [8]. Pseudogenes, which are gene copies that have lost their original protein-coding function as a result of inactivating mutations, may provide a unique and stable genetic record for tracing long-term evolutionary dynamics [11].

Pseudogenes arise primarily by three core mechanisms [12]: (1) DNA-mediated duplication, encompassing processes such as unequal crossing over and polyploidization, which generates functionally redundant paralogs that subsequently accumulate degenerative mutations; (2) RNA-mediated retrotransposition, by which reverse-transcribed mRNAs are integrated randomly into the genome, often lacking regulatory elements and hence cannot be expressed, and ultimately result in degeneration; and (3) direct degeneration of functional genes following the relaxation of selective pressure triggered by changes in the genetic background or environmental conditions. The prevalence of pseudogene types generated by these distinct pathways varies among species. For instance, processed pseudogenes—derived from retrotransposition—are abundant in mammalian genomes, but are substantially less prevalent than unprocessed (duplicated) pseudogenes in plants [13–16]. Owing to the loss of their ancestral protein-coding function, pseudogenes are frequently overlooked in conventional plant genome annotation and subsequent functional studies [17].

The conventional perspective that pseudogenes are nonfunctional has been revised in light of evidence that some pseudogenes remain functional and participate in gene expression regulatory networks [18]. Pseudogenes whose biological functions are poorly characterized may contain information on various aspects of genomic evolution differing from that derived from functional loci [14,19]. This dual characteristic, combining the properties of neutral markers with potential regulatory functions, means that pseudogenes serve as "testing grounds" for genomic innovation: they can accumulate mutations without compromising biological fitness, while their quasi-gene architecture facilitates

functional reactivation and the acquisition of novel functions [17,20]. Although the value of pseudogenes in evolutionary research has been directly or indirectly validated in diverse plants, including Arabidopsis and rice [13,16,21–24], information on pseudogenes at the whole-genome level in common wheat remains limited.

Unlike previous studies of wheat pseudogenes that focused on individual or several specific genes [25–27], this study performed a genome-wide identification of pseudogenes using the IWGSC RefSeq v2.1 reference genome. We analyzed the pseudogenes for their distribution, evolutionary dynamics, and divergence from parent genes, and examined the functional differentiation and biases of the parent genes across distinct pseudogene types. This study aimed to elucidate the genome-wide evolutionary dynamics of pseudogenes and the asymmetric evolution of the three subgenomes. Our findings offer a technical framework for further pseudogene research in wheat and serve as a reference for similar genome-wide studies in other plant species.

2. Results

2.1. Genome-Wide Identification and Classification of Pseudogenes

We identified 79,285 pseudogenes in the wheat genome. The number of different pseudogene types varied substantially. Unitary pseudogenes (Unitary, UNI) and fragmented pseudogenes (FRAG) were the predominant types, comprising 29,237 and 23,394 members, respectively, and accounting for 36.88% and 29.51% of the total pseudogenes, respectively. This result suggests that pseudogene formation in wheat has been primarily driven by gene degeneration and fragmentation. Based on alignment with the parent genes, the number of truncated pseudogenes was significantly lower than that of full-length (FULL) pseudogenes (Supplementary Table S1).

Localized duplication was the primary mechanism of origin detected for duplication-derived pseudogenes (DUP). A total of 7883 DUP pseudogenes (including DUP-full and DUP-truncated) were identified, representing 9.94% of the total number. Chromosomal location association analysis showed that 1598 pseudogenes (2.02%) were located on the same chromosome as their parent genes. A total of 13,985 processed pseudogenes (Retropseudogenes, RET), including RET-full and RET-truncated, were identified, accounting for 17.64% of the total pseudogenes. This result suggests that pseudogene formation in wheat has been primarily driven by gene degeneration and fragmentation, a pattern consistently observed across all three subgenomes.

2.2. Genome-Wide Distribution Characteristics of Pseudogenes

The genomic distribution of pseudogenes differed at the subgenome, genomic region, and chromosome levels.

At the subgenome level, the total number of pseudogenes in the B subgenome (27,187) exceeded that in the A (24,794) and D (24,078) subgenomes. Nevertheless, the proportion of each pseudogene type was relatively consistent across the subgenomes (Figure 1A). Notably, significant differences in physical length were observed among the A, B, and D subgenomes of common wheat. We therefore calculated the subgenome length-corrected pseudogene density, defined as the number of pseudogenes per megabase (Mb) of genomic sequence. The results showed that the pseudogene densities of the A, B, and D subgenomes were 4.98, 5.18, and 6.02 per Mb, respectively.

https://doi.org/10.3390/plants15050818

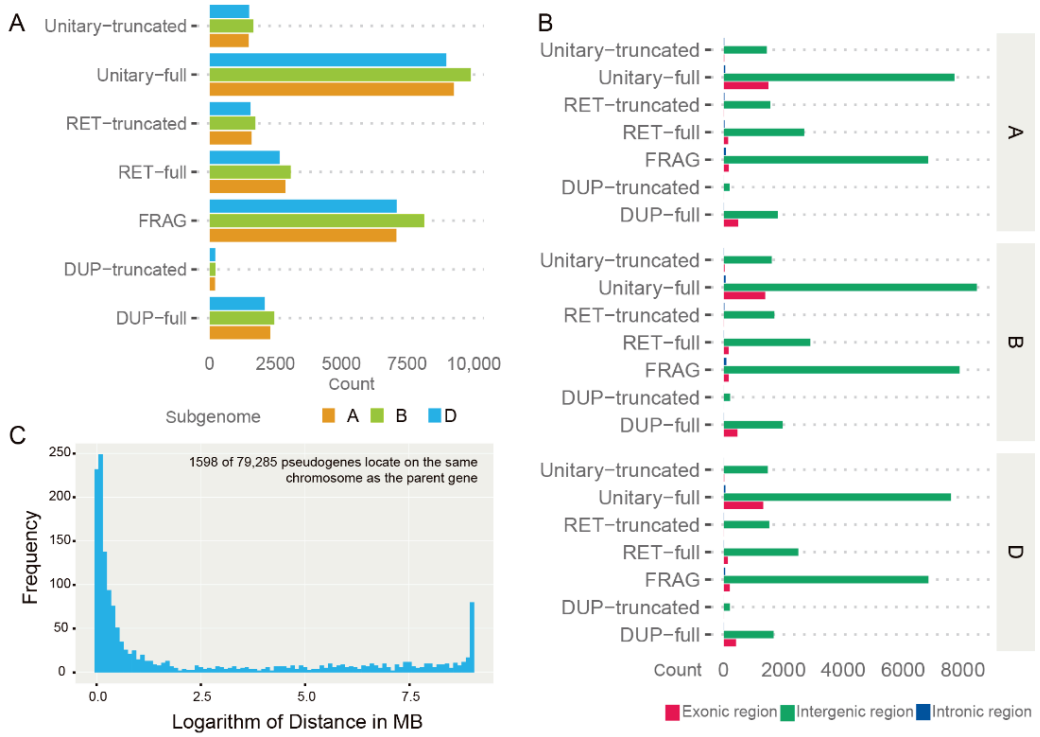

Figure 1. Genome-level Characteristics of Pseudogene Distribution in Common Wheat. (**A**) Total numbers of each pseudogene type in the A, B, and D subgenomes. (**B**) Proportion of pseudogenes located in intergenic regions, introns, and exons. (**C**) Distribution of physical distances between pseudogenes and their parent genes located on the same chromosome. The *x*-axis represents physical distance values transformed by $\log_2$(Mb + 1); the *y*-axis represents the number of pseudogenes in the corresponding distance intervals.

Regarding genomic region distribution, pseudogenes were strongly concentrated in intergenic regions, accounting for as much as 90.7% of the total, whereas those located in intronic regions and exonic regions each accounted for less than 1% of the total number (Figure 1B). This distribution pattern directly reflected the strength of functional constraints in the different genomic regions. Pseudogene insertion into introns may disrupt splicing signals or the regulation of gene expression, and may lead to their rapid elimination by natural selection; thus, pseudogenes may be highly unstable in intronic regions [28].

The pseudogene distribution at the chromosomal level showed complementarity to and association with the distribution of functional genes and transposable elements (TEs). The density of functional genes was significantly higher in terminal/subtelomeric regions than in pericentromeric regions. In contrast, TEs were concentrated in pericentromeric regions, showing distinct complementarity with the distribution of functional genes, which is consistent with the general structural characteristics of wheat chromosomes [26]. The majority of pseudogenes (especially the DUP and FRAG types) were distributed consistently with functional genes, i.e., concentrated in the gene-dense terminal regions, reflecting their derivation by duplication or mutation of functional genes. Notably, the distribution of processed pseudogenes (RET) strongly overlapped with TE-rich regions, reflecting the influence of retrotransposition on the formation of this pseudogene type (Figure 2).

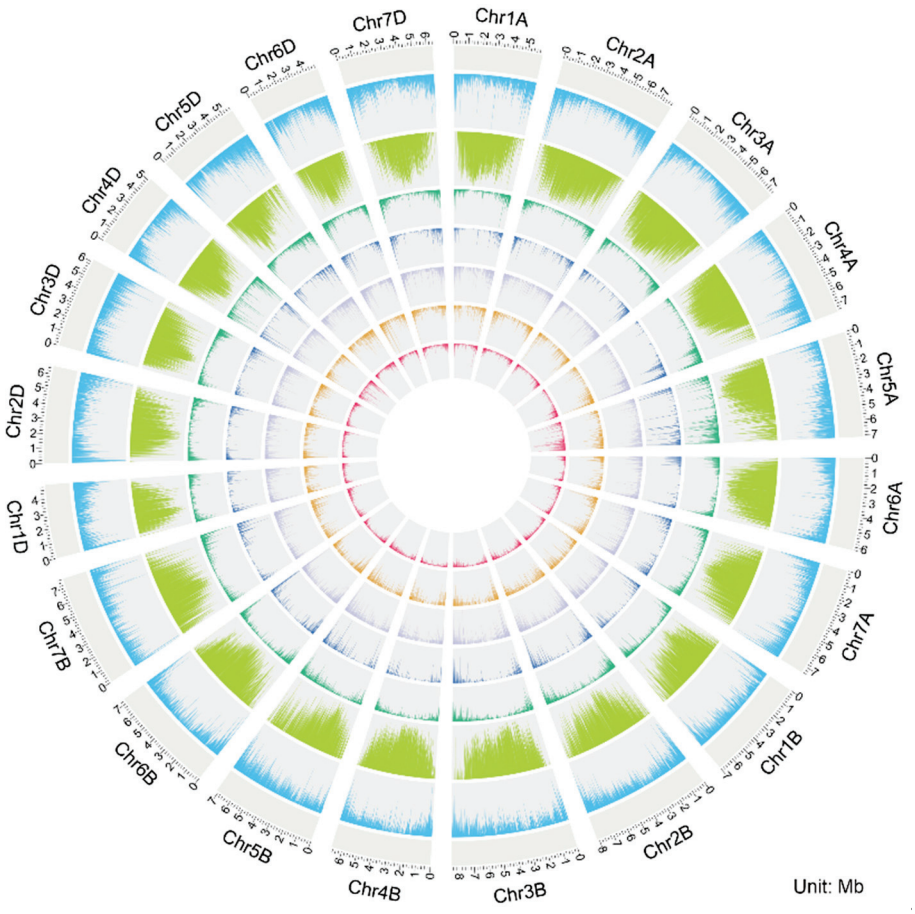

Figure 2. Genome-wide Distribution of Pseudogenes in Common Wheat. Chromosomes are arranged by subgenome (Chr1A to Chr7D). From the outermost to the innermost, the rings represent functional gene density (sky blue), transposable element density (light green), total pseudogene density (green), and the density distribution of four pseudogene types: duplication-derived (DUP, blue), fragmented (FRAG, light purple), processed (RET, orange), and unitary (UNITARY, red). All density values were calculated based on a 1 Mb sliding window and are expressed as the percentage of covered base pairs.

2.3. Evolutionary Dynamics of Pseudogenes

To investigate subgenomic differentiation in wheat following polyploidization, we performed a one-to-one single-copy syntenic orthologous element analysis. The majority of these orthologous elements (17,720, 61.66%) remained functional in all three subgenomes, suggesting that strong purifying selection is an evolutionary constraint on the wheat genome as a whole. Nevertheless, a substantial number of elements (11,018, 38.34%) showed gene absence (null) or pseudogenization (pseudo) in at least one subgenome. These characteristics exhibited significant evolutionary asymmetry among the three subgenomes. Gene absence or pseudogenization events in the B subgenome totaled 5390, accounting for 36.1% of all variation events (14,945). This proportion was higher than those for the A subgenome (5747, 35.3%) and the D subgenome (4610, 26.6%). The frequency of gene absence and pseudogenization events in the B subgenome was significantly higher than that in the D subgenome ($p < 0.001$), but not significantly different from that in the A subgenome ($p = 0.36$). Collectively, these results indicate that the B subgenome shows relatively high genetic instability, although not statistically significantly higher than that of the A subgenome (Supplementary Table S2).

The K_a values for the three subgenomes were consistently low with minimal variation, although the values differed significantly between subgenomes A and B ($p = 0.015$), and were marginally significantly different between subgenomes A and D ($p = 0.071$). Similarly,

the K_s values were low with limited variation among the subgenomes, although the differences between subgenomes A and B (p = 0.005) and between subgenomes A and D ($p = 6.4 \times 10^5$) were highly significant. The K_a/K_s ratios for pseudogenes across the three subgenomes were all less than 0.5 (Figure 3A). Comparisons between subgenomes revealed significant differences between subgenomes A and B (p = 0.032) and between subgenomes A and D (p = 0.046), whereas the difference between subgenomes B and D was non-significant (p = 0.88).

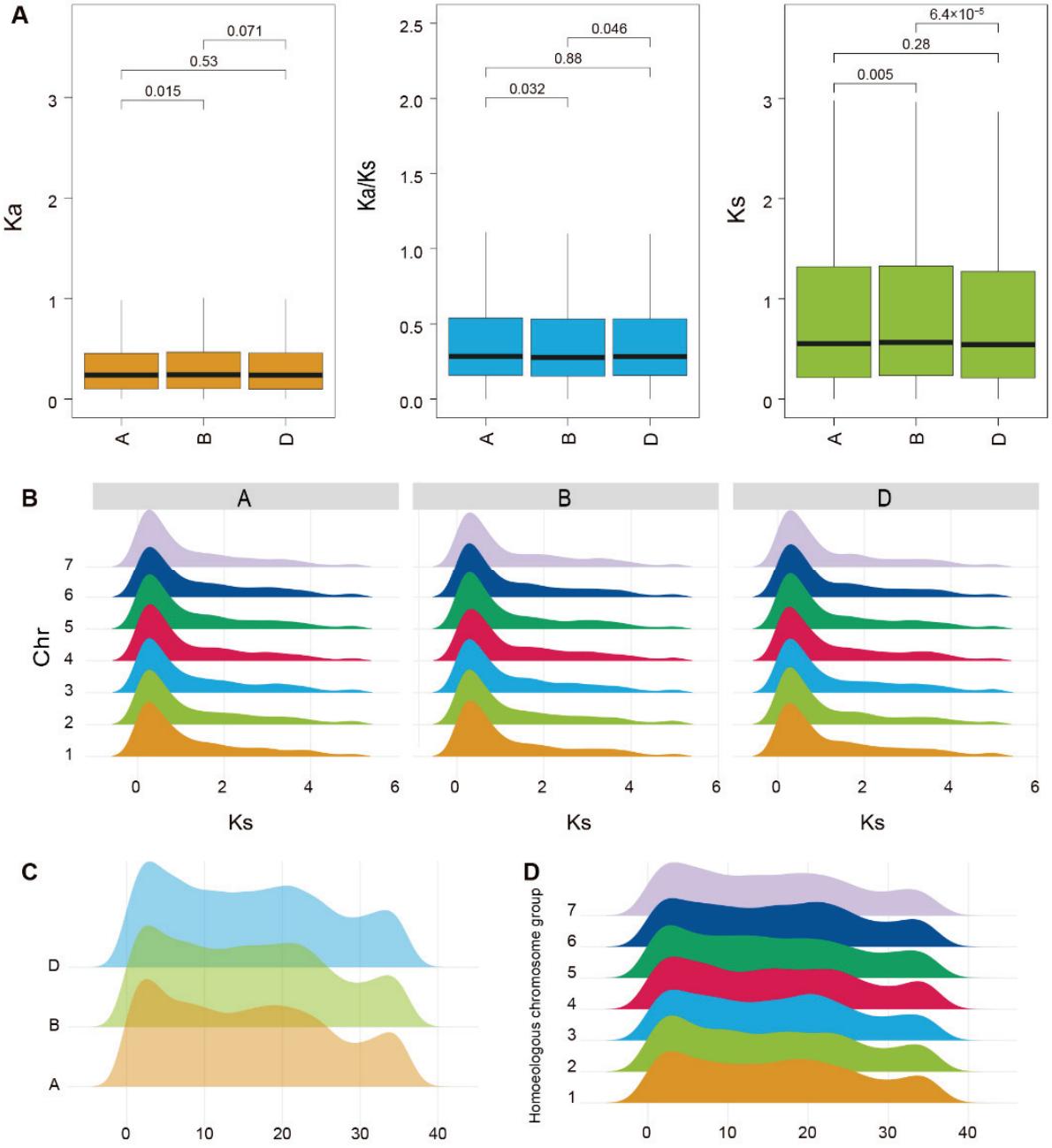

Figure 3. Core Evolutionary Indices Analysis of Wheat Pseudogenes. (**A**) Selection pressure-related indices for pseudogenes across the three subgenomes, comprising the nonsynonymous substitution rate (K_a), synonymous substitution rate (K_s), and their ratio (K_a/K_s). (**B**) K_s values for pseudogenes for each chromosome across all subgenomes. (**C**) Temporal distribution of pseudogene formation in individual subgenomes (Unit: MYA). (**D**) Temporal distribution of pseudogene formation across individual chromosomes (Unit: MYA).

The K_s distribution patterns across chromosomes were highly consistent in subgenomes A, B, and D, suggesting that pseudogenization events occurred synergistically across the three subgenomes. The K_s values were predominantly in the range of 0–1, with a median of 0.69, which was lower than the mean (2.71), thus representing a right-skewed distribution (Figure 3B).

Temporal distribution curves for pseudogene formation exhibited a distinct three-peak pattern for each subgenome, with strong consistency in the timing of the peaks among the subgenomes (Figure 3C,D). The first peak, which showed the smallest inter-subgenome variation, was concentrated at 3.24–3.68 MYA. The first peak for subgenome A (3.24 MYA) was slightly earlier than those for subgenomes B (3.64 MYA) and D (3.68 MYA). The second peak spanned 18.78–20.18 MYA, which represented the greatest inter-subgenome variation among the three peaks. The third peak displayed strong overlap at 32.31–32.91 MYA. Thus, the timing of pseudogene formation showed considerable evolutionary conservation.

The temporal distribution curves showed a broadly consistent trend at the chromosome level. Pseudogene formation was primarily concentrated in the 0–40 MYA interval. This conserved temporal pattern across chromosomes suggests that pseudogene generation underwent synchronous changes during wheat evolution (Figure 3D).

2.4. Comparative Features of Pseudogenes and Their Parent Genes

The number of pseudogenes and the size of the corresponding parent gene families showed a highly significant, weakly positive correlation (Spearman's rank correlation analysis; $\rho = 0.1901$, $p < 0.001$). This indicates that the larger gene families in wheat tended to accumulate greater numbers of pseudogenes. The weak correlation suggests that specific gene families may have distinct pseudogenization propensities, and that pseudogene formation is also regulated by other biological processes (Figure 4A).

The sequence identity between pseudogenes and their parent genes reflects the degree of evolutionary divergence. Significant differences in sequence identity were detected among different pseudogene types. Note that Unitary pseudogenes were excluded from this analysis because they originate from mutations in single-copy genes with the loss of the parent gene copy, thus precluding sequence alignment. This finding suggests that different pseudogene types have undergone distinct evolutionary trajectories. The majority of pseudogenes exhibited > 0.25 sequence identity with their parent genes, with the peak sequence identity concentrated in the 0.3–0.6 range. Among the pseudogene types, DUP-FULL pseudogenes were over-represented in high-identity intervals, whereas FRAG pseudogenes showed notable enrichment in the 0.7–0.8 sequence identity range (Figure 4B).

Significant differences in sequence coverage were observed among the pseudogene types (Figure 4C). Full-length types (DUP-FULL and RET-FULL) showed the highest coverage, truncated types (DUP-truncated and RET-truncated) had lower coverage, and fragmented pseudogenes (FRAG) showed the lowest coverage. Most pseudogenes showed 0–50% coverage and 40–80% identity, consistent with the pattern exhibited by the FRAG pseudogenes (Figure 4C(f)). The DUP-derived pseudogenes exhibited higher coverage and higher sequence identity than processed pseudogenes (RET; Figure 4C(b,d)). This finding is consistent with the "dead-on-arrival" hypothesis, which proposes that processed pseudogenes rapidly accumulate mutations after their origin, leading to faster divergence from their parent genes compared with DUP pseudogenes [29].

https://doi.org/10.3390/plants15050818

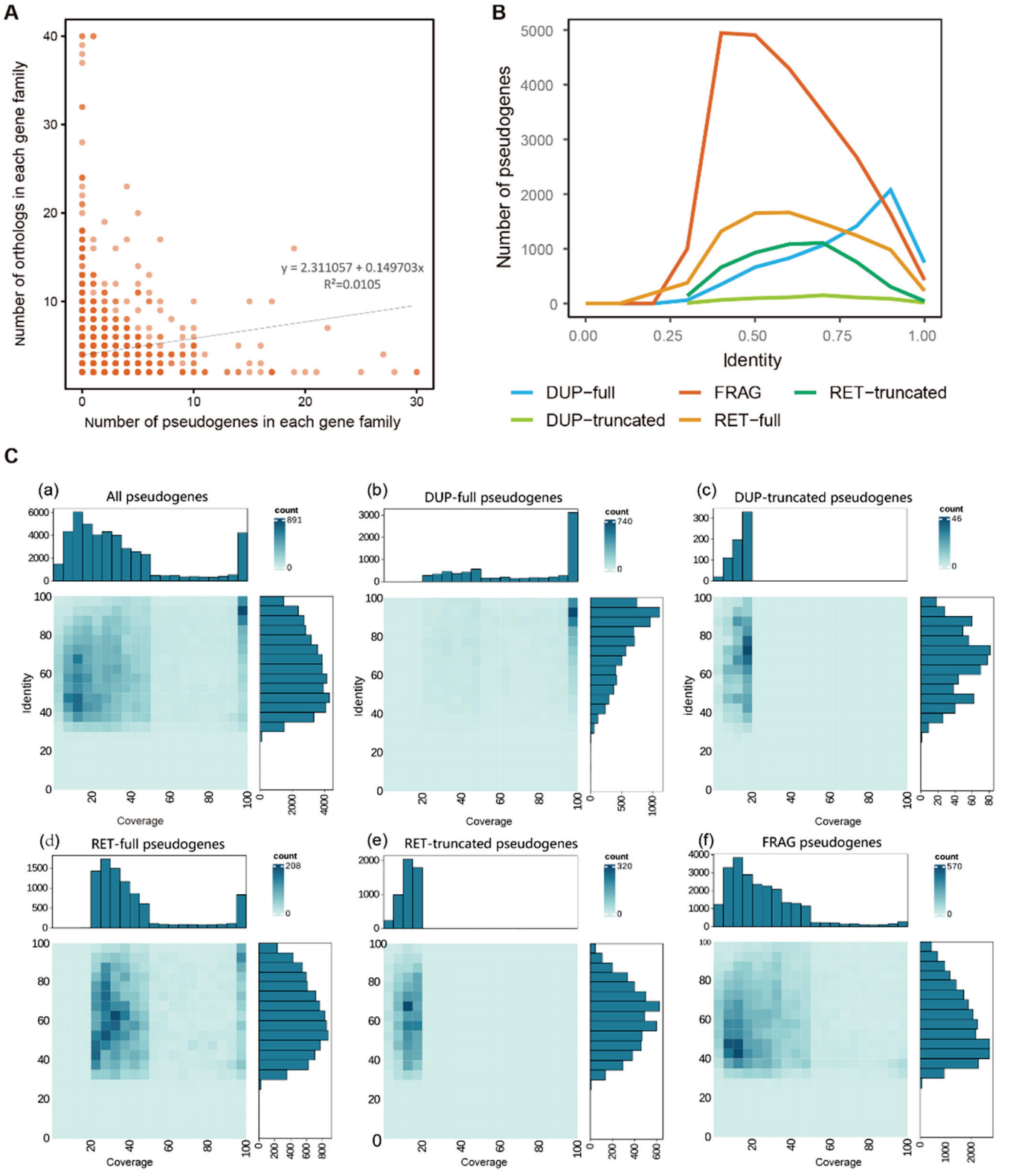

Figure 4. Comparative Analysis of Pseudogenes and Their Parent Genes. (**A**) Distribution of number of pseudogenes versus corresponding number of parent genes in each gene family. (**B**) Distribution of sequence identity for each pseudogene type and their parent genes. (**C**) Comparison of sequence coverage and sequence identity among the pseudogene types and their parent genes: (**a**) all pseudogenes, (**b**) full-length duplicated (DUP-full) pseudogenes, (**c**) truncated duplicated (DUP-truncated) pseudogenes, (**d**) full-length processed (RET-full) pseudogenes, (**e**) truncated processed (RET-truncated) pseudogenes, and (**f**) fragmented (FRAG) pseudogenes.

2.5. Functional Divergence of Parent Genes Among Pseudogene Types

Gene ontology (GO) and Kyoto Encyclopedia of Genes and Genomes (KEGG) enrichment analyses revealed the potential biological functions of the parent genes corresponding to each pseudogenes type. For example, the parent genes of DUP pseudogenes were significantly enriched in molecular functions related to basic biological interactions and energy-associated binding in GO enrichment analysis, such as ADP binding (GO:0043531) and protein binding (GO:0005515) (Supplementary Table S3). The corresponding KEGG pathway enrichment analysis showed that these parent genes were significantly enriched in the plant–plant pathogen interaction pathway (map04626) (Figure 5A), indicating that the parent genes are involved in biological stress defense responses.

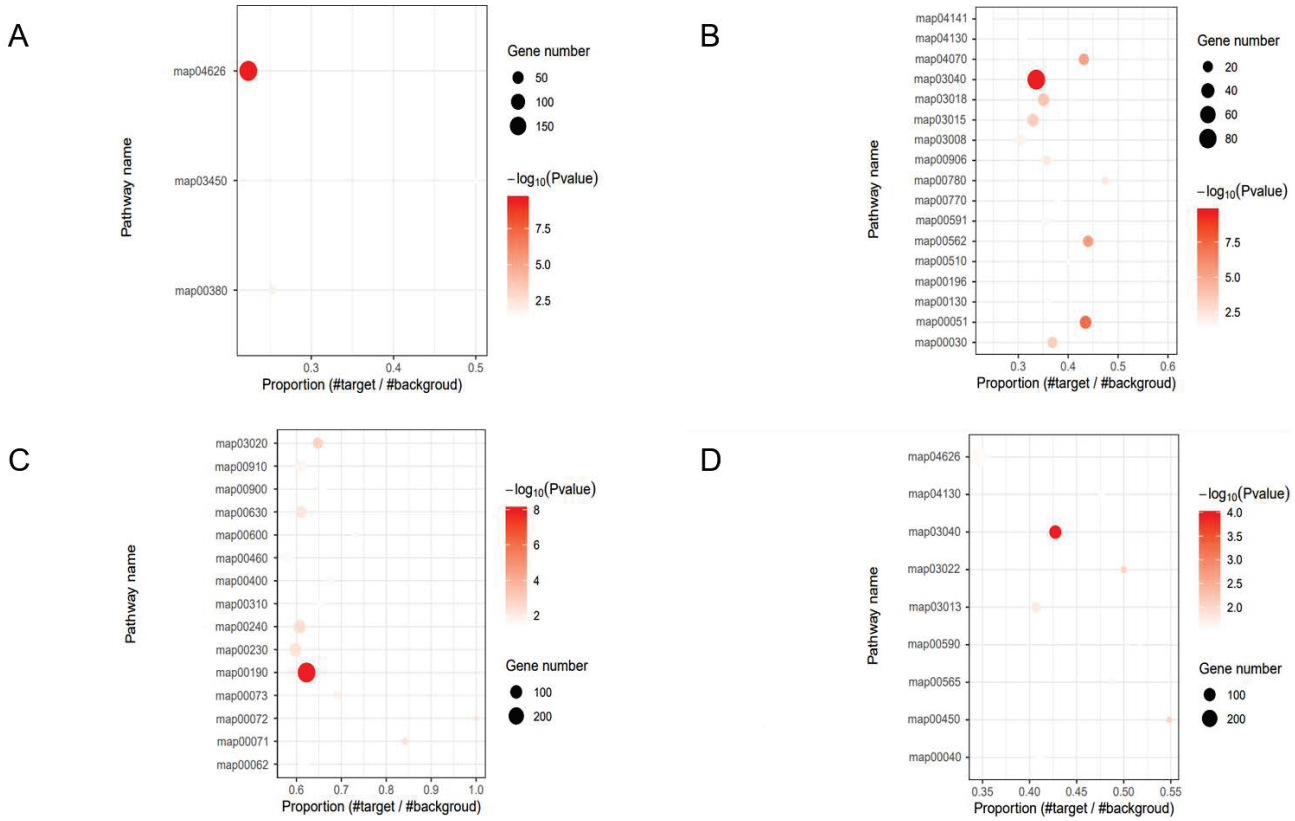

Figure 5. KEGG Pathway Enrichment Analysis of Parent Genes for Each Pseudogene Type in Common Wheat. (**A**) Duplicated pseudogenes, (**B**) processed pseudogenes, (**C**) unitary pseudogenes, and (**D**) fragmented pseudogenes.

In contrast, the KEGG pathway enrichment analysis of the parent genes for RET pseudogenes revealed that the spliceosome pathway (map03040), fructose and mannose metabolism (map00051), and inositol phosphate metabolism (map00562) were the most significantly enriched. Notably, the parent genes of FRAG pseudogenes shared similar functional characteristics with those of RET pseudogenes and were significantly enriched in the spliceosome pathway (map03040). This finding indicates that RET and FRAG pseudogenes originated from parent genes involved in post-transcriptional regulatory processes (Figure 5B,D).

The parent genes of Unitary pseudogenes were significantly enriched in the oxidative phosphorylation pathway (map00190) (Figure 5C), which is critical for cellular energy production.

These results demonstrated distinct functional divergence among the parent genes of each pseudogene type, each corresponding to distinct core biological processes.

2.6. Characteristics of Conserved Domains in Pseudogenes and the Functional Bias of the Parent Genes

The conserved domains retained by the pseudogenes, which are important molecular imprints of the functions of their parent genes, can further corroborate and improve understanding of the origin and functional preferences of wheat pseudogenes from a sequence structure perspective [30]. Proteins deduced from the pseudogene sequences were annotated based on 1783 Pfam conserved domains (Supplementary Table S4). High-frequency domains (those with occurrence counts $\geq$500) were mainly associated with three major functional categories. First, a large proportion corresponded to proteins related to mobile genetic elements, such as reverse transcriptases (e.g., PF13456; 3792), integrases/transposases (e.g., PF00665; 1162), and Gag proteins (e.g., PF03732; 649). Domains directly linked to transposition activity accounted for approximately 62% of all annotations. Second, many domains were associated with disease resistance and immune signaling, including NB-ARC (PF00931; 1893), protein kinase (PF00069; 1907), and leucine-rich repeat (PF13855; 1498) domains, which are primarily associated with plant-specific pathogen recognition and defense pathways. Finally, an important category included transcriptional and developmental regulatory proteins, such as those containing FAR1 (PF03101; 1035), PPR (PF01535; 857), and BTB/POZ (PF00651; 716) domains, which mediate the precise regulation of gene expression.

Notably, the intra-species parent genes of these pseudogenes generally exhibited significant tissue-specific expression patterns (Supplementary Figure S1). This expression characteristic reflects the functional attributes of the aforementioned domains, collectively suggesting that the pseudogenization process in common wheat mainly affected "non-core" functional genes that function under specific spatiotemporal conditions.

3. Discussion

3.1. Dominant Pseudogene Types and Transposition-Driven Mechanism of Origin

This study represents the first genome-wide systematic analysis and classification of pseudogenes in common wheat. Specifically, we identified 24,794, 27,187, and 24,078 pseudogenes in the A, B, and D subgenomes, respectively (Table S1, Figure 1A). Unitary and FRAG pseudogenes are the dominant types in wheat, which is consistent with reports of abundant short gene fragments in closely related species, such as barley [17]. Although Unitary and FRAG pseudogenes predominate in the extant genome, conserved domain analysis revealed that approximately 62% of pseudogene sequences contained transposition-related domains (e.g., reverse transcriptases and integrases) (Supplementary Table S4). However, the mechanisms of pseudogene origins were inferred by retrospective inference based on the sequence characteristics, from which the pseudogenes were classified, rather than classifying the pseudogenes directly based on their mechanism of origin. Transposable element insertions are prevalent in the promoters, UTRs, introns, and exons of wheat genes, with 95.0% of the genes co-localizing with transposons, which are core drivers of pseudogenization [31,32]. Transposon activity provides abundant materials for pseudogene formation by generating incomplete gene copies or disrupting functional genes via insertions [33]. Notably, some gene fragments captured by TEs may be misclassified as FRAG pseudogenes owing to their short length or continuous sequence deletions; in contrast, some genes impacted by TE insertions may be misclassified as Unitary pseudogenes because loss of function occurs through point mutations without large-scale sequence deletions. During the degeneration of pseudogene sequences, non-conserved regions (e.g., functional domains) are prone to mutation or deletion, whereas TE-related domains are more likely to be conserved owing to methylation-mediated protection and sequence con-

https://doi.org/10.3390/plants15050818

servation [34,35]. This explains why transposition-related domains can still be detected even when the main functional sequences of pseudogenes are completely degenerated.

This transposition-dominated mechanism of origin directly explains the genomic distribution characteristics of pseudogenes. In the present study, *cis*-localized pseudogenes (i.e., those located on the same chromosome as their parental genes) account for only 2.02% of the total number. Pseudogene formation in wheat relies on the reverse transcription function of TEs (e.g., LINE-1), leading to the random insertion of newly generated pseudogenes into non-ancestral loci. In addition, extensive genomic rearrangements that have occurred during wheat polyploidization have further exacerbated the physical separation between pseudogenes and their parental genes [25,33,36].

3.2. Evolutionary Asymmetry of Subgenomic Pseudogenes

Compared with its diploid and tetraploid progenitors, common wheat exhibits greater genomic plasticity and broader adaptability, which is partially attributable to the generation of novel genetic diversity following allopolyploidization [37]. The present results showed that the proportions of pseudogene types were relatively consistent among the A, B, and D subgenomes, whereas significant differences were observed in pseudogene abundance and the evolutionary dynamics revealed by synteny analysis. Specifically, the B subgenome harbors the highest number of pseudogenes (27,187), with higher frequencies of gene loss (12.35%) and pseudogenization events (12.53%) compared to the other two subgenomes—significantly so relative to the D subgenome, though with no statistical difference from the A subgenome (Figure 1A, Supplementary Table S2). Notably, the normalized pseudogene density per megabase of genomic sequence was highest in the D subgenome, reflecting a more compact distribution of pseudogenes in this shorter subgenome.

Analysis of evolutionary selective pressure revealed that the K_a/K_s ratio for the B subgenome was slightly lower than those of the A and D subgenomes (Figure 3A). This unique evolutionary pattern may reflect the earlier divergence of its donor species (≈7 MYA) and potential outcrossing background [38]. These historical factors have promoted the incidence of gene duplication events in the B subgenome, increased its sequence diversity, and a larger number of functionally redundant genes have accumulated. These redundant gene copies provided "raw materials" for pseudogenization, thus explaining why the B subgenome retains the largest number of pseudogenes.

Although pseudogenes are generally considered to evolve neutrally [12], the present findings showed that the K_a/K_s ratios of pseudogenes across all subgenomes were much lower than 1, consistent with reports for rice and barley [13,17,39]. This phenomenon may be explained by two scenarios: first, except for a few cases of annotation bias (potentially functional genes misannotated as pseudogenes), the integrity of the open reading frame is critical for potential "non-coding functions" of pseudogenes, which are thus subject to moderate purifying selection [30,40]; and second, these pseudogenes may have been subject to strong purifying selection as functional genes for a prolonged evolutionary period before recently undergoing pseudogenization [21,41].

3.3. Temporal Dynamics of Pseudogene Formation and Association with Ancient Genomic Events

To clarify the evolutionary origin and temporal dynamics of pseudogenes in wheat, we estimated their formation times, which showed three temporal peaks in pseudogenization (3.24–3.68, 18.78–20.18, and 32.31–32.91 MYA). These peaks are inconsistent with the two known allopolyploidization events in common wheat (0.8–1.5 MYA and 8000–10,000 years ago) (Figure 3C,D). Thus, massive pseudogene accumulation is not a direct consequence of recent polyploidization but is a delayed, selective long-term process; polyploidization pri-

marily releases purifying selection on redundant genes, laying the evolutionary foundation for subsequent pseudogenization [42].

The three ancient peaks may record genomic upheavals experienced by ancestral lineages during geological periods. The earliest peak (≈32–33 MYA) may be associated with the ancient polyploidization event (rho WGD, 98.2 MYA) during the early evolution of the Poaceae lineage and its prolonged diploidization process [43]. the middle peak (≈18–20 MYA) may result from gene duplication cluster events within the Pooideae subfamily (≈33 MYA) [44]; the most recent peak (≈3–4 MYA) may coincide with the key hybridization stage after the divergence of the A and B subgenomes from their common ancestor (6.5 MYA) and before the formation of modern common wheat [45]. These associations suggest that pseudogenes in the current wheat genome are "genomic fossils" of its long evolutionary history, with their formation more closely linked to ancient genome duplication and differentiation events.

Notably, the low median Ks value (0.69) of pseudogene-parent orthologous pairs (Figure 3A,B) seems contradictory to the ancient formation times. Two plausible explanations exist for this. First, the molecular clock evolutionary rate used in the present study may be higher than the actual evolutionary rate for these pseudogenes, leading to systematic overestimation of the absolute formation times. Second, as discussed earlier in this article, pseudogenization is not an absolute functional endpoint—the pseudogene sequences may not evolve entirely neutrally and purifying selection may partially constrain the accumulation of synonymous substitutions (K_s) [30,40]. Thus, calibration of the mutation rate (μ) using species-specific divergence events and other approaches is required in future studies.

3.4. Which Genes Are More Susceptible to Pseudogenization?

Functional selectivity is a core characteristic of pseudogenization. The parent genes of pseudogenes are significantly enriched in functional categories related to environmental adaptation, including defense responses, cell wall modification, secondary metabolism, and protein degradation (Supplementary Figure S1; Supplementary Table S1 for GO/KEGG enrichment results). These parent genes are predominantly derived from highly redundant gene families and exhibit distinct tissue-specific expression patterns.

This functional selectivity is consistent with findings reported for Arabidopsis, rice, and other plant species [21], and reflects a conserved rule throughout the plant kingdom: core housekeeping genes (e.g., those involved in DNA replication and energy metabolism) are constrained by strong purifying selection, thus maintaining high sequence conservation and a low likelihood of pseudogenization. In contrast, environment-related genes evolve more rapidly, undergo more frequent variation in copy numbers, and exhibit greater tolerance to functional loss, and thus are primary targets for pseudogenization. This selective pattern alleviates the genomic functional burden and preserves the evolutionary flexibility among functional genes, providing a foundation for genomic plasticity that confers adaptability to complex environmental and artificial selection pressures.

4. Materials and Methods

4.1. Genomic and Transcriptomic Dataset Collection

All genomic sequences and annotations were downloaded from public databases.

This study utilized common wheat Chinese Spring (CS) as the reference genome, owing to its well-annotated genome and abundant genetic and molecular resources [46]. The core dataset was the IWGSC RefSeq v2.1 reference genome sequence [47] (https://www.wheatgenome.org, accessed on 4 March 2026), supplemented with data from four public databases: (1) SWISS-PROT [48] (https://www.sib.swiss/swiss-prot, accessed on 4 March

2026) for protein sequence data; (2) Repbase, a database of genomic repetitive sequences [49] (https://www.girinst.org/repbase, accessed on 4 March 2026) for retrieving transposable element (TE) sequences; (3) the Pfam database [50] (https://pfam.xfam.org, accessed on 4 March 2026) for annotating conserved protein domains; and (4) TriticeaeExpDB (https://triticeaeexpdb.cn, accessed on 4 March 2026), which provides expression levels of parent genes of pseudogenes across different tissues and developmental stages.

4.2. Construction of the Reference Protein Sequence Set

To ensure the accuracy of pseudogene identification, we integrated two protein datasets to construct a reference sequence set in this study: (1) Dataset 1 comprised proteins from the target species and its closely related homologs including *Triticum urartu*, *Triticum turgidum*, *Aegilops tauschii*, *Aegilops speltoides*, *Thinopyrum elongatum*, Secale cereale and Hordeum vulgare, with the following selection criteria: intact start and stop codons, functionally validated via alignment against SWISS-PROT, and exclusion of transposon-associated proteins following alignment with the RepBase database; (2) Dataset 2 was retrieved directly from the SWISS-PROT database, excluding fragmented sequences annotated as "fragment" in RepBase and transposon-related proteins. After merging these two datasets, CD-HIT [51] was employed for sequence deduplication, and non-redundant reference protein sequences were ultimately obtained.

4.3. Pseudogene Identification and Classification

Pseudogene identification was performed via a three-step strategy. First, high-quality Coding Sequence (CDS) sequences—extracted from the reference genome after hard-masking repetitive regions—were aligned against the reference protein set using the BLASTX algorithm implemented in DIAMOND v0.9.24.125 [52]. Second, candidate pseudogene loci were extracted: Genomic regions aligned to the same protein were merged, with 2-kbp extensions upstream and downstream to define candidate loci. For overlapping genomic regions aligned to distinct reference proteins, the optimal alignment was retained according to bit scores. Third, Genewise (wise2-4-1) [53] was employed to perform precise alignment between each candidate locus and its corresponding reference protein, enabling the detection of characteristic features of pseudogenes, including frameshift mutations, premature stop codons, abnormal introns, incomplete coding regions, and absence of promoters/regulatory regions. This step ultimately yielded the final set of identified pseudogenes.

Pseudogenes were classified into four categories based on sequence characteristics and alignment results: Duplicate Pseudogenes (DUP), Unitary Pseudogenes (Unitary, UNI), Processed Pseudogenes (retropseudogenes, RET), and Fragmented Pseudogenes (FRAG). First only sequences with an identity greater than 30% can be identified as pseudogenes, as this threshold is the established standard for reliable homology inference, effectively eliminating false-positive random matches while retaining bona fide pseudogene loci of homologous origin [54]. Among these, FRAG pseudogenes were defined as those that align exclusively to a single CDS region of a multi-exon parent gene and do not span exon-intron boundaries, with zero introns. RET were identified by the criteria of zero introns and an intron-spanning alignment value equal to 1, DUP were defined as duplicated copies originating from their own parental loci, and Unitary pseudogenes were defined as those with a parental source from other gene loci. DUP, Unitary, and RET pseudogenes were further subcategorized into two classes—FULL (alignment coverage $\geq$ 20%) and TRUNCATED (coverage < 20%)—based on their alignment coverage relative to their respective parental genes.

4.4. Multidimensional Analysis of Pseudogene Distribution

We performed a multidimensional analysis of the genomic distribution of pseudogenes across four aspects as follows. For distribution across genomic features, pseudogenes were assigned based on their overlap with exonic, intronic, or intergenic regions using positional annotation, and the results were visualized. Regarding distribution along chromosomes, each chromosome was partitioned into consecutive, non-overlapping 1 Mb windows, with the base-pair coverage of functional genes, transposable elements (TEs), and each pseudogene type calculated per window; these distributions were visualized using Circos (v0.69-8) [55] to generate a circular ideogram, where concentric rings from outer to inner represent the density of functional genes, TEs, all pseudogenes, and the four individual pseudogene types (DUP, FRAG, RET, UNI). For distribution among subgenomes, pseudogenes and their parent genes were assigned to the A, B, or D subgenome based on chromosomal location, and the counts of each pseudogene type across the subgenomes were tallied. Additionally, the distance to parent genes was analyzed: for pseudogene-parent gene pairs located on the same chromosome, the intrachromosomal physical distance between them was calculated, and the distribution of these distances was plotted on a $\log_2(\text{Mb} + 1)$ scale.

4.5. Enrichment Analysis of Different Types of Pseudogenes

To infer pseudogene functions based on their parent genes, functional annotations of GO and KEGG were performed for all parent genes of wheat pseudogenes using InterProScan (GO) and KoFamScan (KEGG) [56], respectively, and this set of genes served as the background gene set. Subsequently, functional enrichment analysis was conducted on the parental genes of distinct pseudogene types (DUP, RET, UNI). For this analysis, the parental gene sets corresponding to DUP, RET and UNI pseudogenes were treated analogously to differentially expressed gene sets in transcriptome analysis. GO terms and KEGG pathways with a corrected $p < 0.05$ were considered statistically significant.

4.6. Association Analysis Between Pseudogenes and Parent Genes

We analyzed pseudogene–parent gene associations from two key dimensions: First, to characterize quantitative relationship within gene families, wheat genes were clustered into gene families using OrthoFinder2 v2.2.6 [57], we then counted the number of functional genes and pseudogenes in each family and visualized their quantitative associations via graphical plotting. Second, for the distribution of sequence similarity, Unitary Pseudogenes (UNI) were excluded, and sequence similarity between the remaining pseudogene types and their parent genes was analyzed using two key metrics—percentage identity and alignment coverage—both extracted from the pseudogene annotation files.

4.7. Phylogenetic Analysis of Pseudogene Evolution Dynamics

We conducted three interrelated analyses to characterize the evolutionary dynamics of pseudogenes, including collinearity verification, estimation of formation time, and selection pressure analysis.

First, to construct a set of high-confidence orthologous gene pairs for evolutionary comparison, we performed collinearity analysis. Annotations of protein-coding genes and pseudogenes were merged and partitioned according to the A, B, and D subgenomes. For Unitary and duplicate (DUP) pseudogenes, an all-against-all BLASTP v2.7.1 [58–60] search was performed to identify reciprocal best hits (RBHs). Collinear relationships were then identified from these RBH pairs using MCScanX v20200820 [61], with only 1:1 single-copy collinear relationships retained. These filtered orthologous pairs served as the basis for subsequent molecular clock and selection pressure analyses.

https://doi.org/10.3390/plants15050818

Subsequently, it was assumed that sequences of pseudogenes following mutation were not subject to selection pressure. The formation time of these pseudogenes (containing premature termination codons or frameshift mutations) was estimated based on their sequence divergence from parent genes. For each such pseudogene, the genomic sequence downstream of the inactivating mutation was extracted. Sequences shorter than 50 bp or representing less than 50% of the total alignment length were filtered out. Pairwise nucleotide distances (d) between the retained pseudogene sequences and their parent gene CDSs were calculated using the distmat tool from the EMBOSS suite [62]. Divergence time (T) was estimated using the formula $T = d/(2\mu)$, with a mutation rate (μ) of 1.3×10^{-8} substitutions per site per year [63]. All pseudogene formation time data were performed using custom scripts written in Python v3.7.9 with pandas [64], numpy [65], and scipy packages [66] for data processing, numerical calculation, and kernel density estimation, respectively. Visualization was implemented via matplotlib v3.7.1 [67].

Finally, selection pressure acting on these orthologous pairs was assessed by calculating the ratio of non-synonymous to synonymous substitution rates (Ka/Ks). The coding sequences (CDSs) of each pseudogene–parent gene pair were aligned with MUSCLE. Ka and Ks values were then calculated using the yn00 program in the PAML package. The distribution of Ka/Ks ratios across different subgenomes and chromosomes was statistically analyzed to infer patterns of selective constraint. Generally, a $Ka/Ks < 1$, =1, or >1 indicates purifying selection, neutral selection, and positive selection, respectively.

4.8. Functional Annotation of Pseudogenes and Expression Analysis of Their Parent Genes

For protein domain annotation: The predicted protein sequences of wheat pseudogenes were searched against the Pfam database (https://pfam.xfam.org, accessed on 4 March 2026) using InterProScan v5.59-91.0 [68] to systematically identify conserved domains. The frequency of each domain type was quantified to evaluate functional modules that may have been retained or lost during pseudogenization across the subgenomes.

For tissue-specific expression analysis of parent genes: Based on transcriptomic data from the TriticeaeExpDB database (https://www.triticeaeexpdb.cn, accessed on 4 March 2026), we screened parent genes derived from common wheat with reliable expression (transcripts per kilobase of exon model per million mapped reads [TPM] > 0.5 in at least three samples). The average expression levels of these parent genes across different wheat tissues and developmental stages were calculated, and the values were transformed to $\log_{10}(\text{TPM} + 1)$. Heatmaps were generated to visualize the tissue-specific expression patterns of the parent genes.

5. Conclusions

In conclusion, this study presents the first systematic, genome-wide identification and classification of pseudogenes in the A, B, and D subgenomes of common wheat. Our genome-wide analysis reveals that unitary and fragmented pseudogenes are the dominant types in wheat. Transposable elements serve as the core driver of pseudogenization, and our data explain the extremely low proportion of cis-localized pseudogenes in the genome through their mediated mechanisms. The evolution of pseudogenes displays significant asymmetry among the three subgenomes: the B subgenome exhibits higher frequencies of gene loss and pseudogenization events compared to the D subgenome, and a numerically higher (though statistically non-significant) frequency than the A subgenome. This characteristic is associated with the early divergence of its donor species and the consequent accumulation of numerous functionally redundant genes. Meanwhile, wheat pseudogenes do not evolve in a strictly neutral manner but are instead subject to the constraints of purifying selection. The formation of pseudogenes shows three ancient peaks,

which may be linked to genomic upheavals experienced by ancestral lineages during different geological periods, rather than being a direct consequence of recent polyploidization. Furthermore, pseudogenization demonstrates clear functional selectivity, with parent genes significantly enriched in functional pathways related to environmental adaptation. This research provides important empirical evidence for deciphering the evolutionary mechanisms of polyploid genomes in wheat and offers a methodological framework and theoretical reference for related studies in other complex polyploid crops.

Supplementary Materials: The following supporting information can be downloaded at https://www.mdpi.com/article/10.3390/plants15050818/s1, Table S1: Master list of genome-wide identified pseudogenes in common wheat; Table S2: Statistical results of pseudogene collinearity types; Table S3: GO enrichment of the parent gene of DUP-type pseudogenes; Table S4: Frequency and annotation of conserved protein domains (Pfam) identified in wheat pseudogenes; Figure S1: Heatmap depicting tissue-specific expression patterns of pseudogene parent genes.

Author Contributions: Z.L. and J.L. designed the study and provided the funding; H.Z. and Z.L. drafted the manuscript; H.Z., H.T., Y.L., N.Y. and Q.W. data analyses; F.Y., H.W. and W.Y. revised the manuscript. All authors have read and agreed to the published version of the manuscript.

Funding: This study was supported by the Sichuan Natural Science Foundation Project of China (2025ZNSFSC0175) and the Sichuan Provincial Finance Department Project of China (1+3 ZYGG01).

Data Availability Statement: The original contributions presented in this study are included in the article/Supplementary Material. Further inquiries can be directed to the corresponding author.

Conflicts of Interest: The authors declare no conflict of interest.

Abbreviations

The following abbreviations are used in this manuscript:

TE	Transposable Element
MYA	Million Years Ago
WGD	Whole-Genome Duplication
DUP	Duplicate Pseudogenes
UNI	Unitary Pseudogenes
RET	Processed Pseudogenes (Retropseudogenes)
FRAG	Fragmented Pseudogenes
GO	Gene Ontology
KEGG	Kyoto Encyclopedia of Genes and Genomes
Ka	Non-synonymous substitution rate
Ks	Synonymous substitution rate
Ka/*Ks*	Ratio of Non-synonymous to Synonymous Substitution Rate
CDS	Coding Sequence
RBH	Reciprocal Best Hits
TPM	Transcripts Per Kilobase of exon model per Million mapped reads

References

1. Balfourier, F.; Bouchet, S.; Robert, S.; De Oliveira, R.; Rimbert, H.; Kitt, J.; Choulet, F.; Paux, E. Worldwide Phylogeography and History of Wheat Genetic Diversity. *Sci. Adv.* **2019**, *5*, eaav0536. [CrossRef]
2. Sertse, D.; You, F.M.; Klymiuk, V.; Haile, J.K.; N'Diaye, A.; Pozniak, C.J.; Cloutier, S.; Kagale, S. Historical Selection, Adaptation Signatures, and Ambiguity of Introgressions in Wheat. *Int. J. Mol. Sci.* **2023**, *24*, 8390. [CrossRef]
3. Yue, H.; Shu, D.; Wang, M.; Xing, G.; Zhan, H.; Du, X.; Song, W.; Nie, X. Genome-Wide Identification and Expression Analysis of the HD-Zip Gene Family in Wheat (*Triticum aestivum* L.). *Genes* **2018**, *9*, 70. [CrossRef]
4. Salamini, F.; Özkan, H.; Brandolini, A.; Schäfer-Pregl, R.; Martin, W. Genetics and Geography of Wild Cereal Domestication in the near East. *Nat. Rev. Genet.* **2002**, *3*, 429–441. [CrossRef]

5. Wang, X.; Chen, S.; Shi, X.; Liu, D.; Zhao, P.; Lu, Y.; Cheng, Y.; Liu, Z.; Nie, X.; Song, W.; et al. Hybrid Sequencing Reveals Insight into Heat Sensing and Signaling of Bread Wheat. *Plant J.* **2019**, *98*, 1015–1032. [CrossRef]
6. Zhang, K.; Wang, X.; Cheng, F. Plant Polyploidy: Origin, Evolution, and Its Influence on Crop Domestication. *Hortic. Plant J.* **2019**, *5*, 231–239. [CrossRef]
7. Pingault, L.; Choulet, F.; Alberti, A.; Glover, N.; Wincker, P.; Feuillet, C.; Paux, E. Deep Transcriptome Sequencing Provides New Insights into the Structural and Functional Organization of the Wheat Genome. *Genome Biol.* **2015**, *16*, 29. [CrossRef] [PubMed]
8. Xie, Y.; Ying, S.; Li, Z.; Zhang, Y.; Zhu, J.; Zhang, J.; Wang, M.; Diao, H.; Wang, H.; Zhang, Y.; et al. Transposable Element-Initiated Enhancer-like Elements Generate the Subgenome-Biased Spike Specificity of Polyploid Wheat. *Nat. Commun.* **2023**, *14*, 7465. [CrossRef] [PubMed]
9. Feldman, M.; Levy, A.A. Allopolyploidy—A Shaping Force in the Evolution of Wheat Genomes. *Cytogenet. Genome Res.* **2005**, *109*, 250–258. [CrossRef] [PubMed]
10. Huang, Y.; Liu, Y.; Liu, C.; Yi, C.; Lai, J.; Ling, H.; Su, H.; Han, F. Distinct Evolutionary Trajectories of Subgenomic Centromeres in Polyploid Wheat. *Genome Biol.* **2025**, *26*, 271. [CrossRef]
11. Mighell, A.J.; Smith, N.R.; Robinson, P.A.; Markham, A.F. Vertebrate Pseudogenes. *FEBS Lett.* **2000**, *468*, 109–114. [CrossRef]
12. Podlaha, O.; Zhang, J. Pseudogenes and Their Evolution. In *Encyclopedia of Life Sciences*; Wiley: Hoboken, NJ, USA, 2010; ISBN 978-0-470-01617-6.
13. Mascagni, F.; Usai, G.; Cavallini, A.; Porceddu, A. Structural Characterization and Duplication Modes of Pseudogenes in Plants. *Sci. Rep.* **2021**, *11*, 5292. [CrossRef]
14. Sisu, C.; Pei, B.; Leng, J.; Frankish, A.; Zhang, Y.; Balasubramanian, S.; Harte, R.; Wang, D.; Rutenberg-Schoenberg, M.; Clark, W.; et al. Comparative Analysis of Pseudogenes Across Three Phyla. *Proc. Natl. Acad. Sci. USA* **2014**, *111*, 13361–13366. [CrossRef]
15. Liu, Y.-J.; Zheng, D.; Balasubramanian, S.; Carriero, N.; Khurana, E.; Robilotto, R.; Gerstein, M.B. Comprehensive Analysis of the Pseudogenes of Glycolytic Enzymes in Vertebrates: The Anomalously High Number of GAPDH Pseudogenes Highlights a Recent Burst of Retrotrans-Positional Activity. *BMC Genom.* **2009**, *10*, 480. [CrossRef] [PubMed]
16. Xie, J.; Chen, S.; Xu, W.; Zhao, Y.; Zhang, D. Origination and Function of Plant Pseudogenes. *Plant Signal. Behav.* **2019**, *14*, 1625698. [CrossRef]
17. Prade, V.M.; Gundlach, H.; Twardziok, S.; Chapman, B.; Tan, C.; Langridge, P.; Schulman, A.H.; Stein, N.; Waugh, R.; Zhang, G.; et al. The Pseudogenes of Barley. *Plant J.* **2018**, *93*, 502–514. [CrossRef] [PubMed]
18. Poliseno, L.; Salmena, L.; Zhang, J.; Carver, B.; Haveman, W.J.; Pandolfi, P.P. A Coding-Independent Function of Gene and Pseudogene mRNAs Regulates Tumour Biology. *Nature* **2010**, *465*, 1033–1038. [CrossRef] [PubMed]
19. Cheetham, S.W.; Faulkner, G.J.; Dinger, M.E. Overcoming Challenges and Dogmas to Understand the Functions of Pseudogenes. *Nat. Rev. Genet.* **2020**, *21*, 191–201. [CrossRef]
20. Sen, K.; Ghosh, T.C. Pseudogenes and Their Composers: Delving in the "debris" of Human Genome. *Brief. Funct. Genom.* **2013**, *12*, 536–547. [CrossRef]
21. Zou, C.; Lehti-Shiu, M.D.; Thibaud-Nissen, F.; Prakash, T.; Buell, C.R.; Shiu, S.-H. Evolutionary and Expression Signatures of Pseudogenes in Arabidopsis and Rice. *Plant Physiol.* **2009**, *151*, 3–15. [CrossRef]
22. Xu, Y.-C.; Niu, X.-M.; Li, X.-X.; He, W.; Chen, J.-F.; Zou, Y.-P.; Wu, Q.; Zhang, Y.E.; Busch, W.; Guo, Y.-L. Adaptation and Phenotypic Diversification in Arabidopsis Through Loss-of-Function Mutations in Protein-Coding Genes. *Plant Cell* **2019**, *31*, 1012–1025. [CrossRef]
23. Wang, L.; Si, W.; Yao, Y.; Tian, D.; Araki, H.; Yang, S. Genome-Wide Survey of Pseudogenes in 80 Fully Re-Sequenced Arabidopsis Thaliana Accessions. *PLoS ONE* **2012**, *7*, e51769. [CrossRef] [PubMed]
24. Zhou, L.; Chen, T.; Qiu, X.; Liu, J.; Guo, S. Evolutionary Differences in Gene Loss and Pseudogenization among Mycoheterotrophic Orchids in the Tribe Vanilleae (*Subfamily vanilloideae*). *Front. Plant Sci.* **2023**, *14*, 1160446. [CrossRef]
25. Wicker, T.; Mayer, K.F.X.; Gundlach, H.; Martis, M.; Steuernagel, B.; Scholz, U.; Šimková, H.; Kubaláková, M.; Choulet, F.; Taudien, S.; et al. Frequent Gene Movement and Pseudogene Evolution Is Common to the Large and Complex Genomes of Wheat, Barley, and Their Relatives. *Plant Cell* **2011**, *23*, 1706–1718. [CrossRef]
26. Choulet, F.; Alberti, A.; Theil, S.; Glover, N.; Barbe, V.; Daron, J.; Pingault, L.; Sourdille, P.; Couloux, A.; Paux, E.; et al. Structural and Functional Partitioning of Bread Wheat Chromosome 3B. *Science* **2014**, *345*, 1249721. [CrossRef]
27. Xia, C.; Zhang, L.; Zou, C.; Gu, Y.; Duan, J.; Zhao, G.; Wu, J.; Liu, Y.; Fang, X.; Gao, L.; et al. A TRIM Insertion in the Promoter of Ms2 Causes Male Sterility in Wheat. *Nat. Commun.* **2017**, *8*, 15407. [CrossRef]
28. Prade, V.M. Pseudogene Dynamics in Plants. Doctoral Dissertation, Technical University of Munich, Munich, Germany, 2018.
29. Zheng, D.; Frankish, A.; Baertsch, R.; Kapranov, P.; Reymond, A.; Choo, S.W.; Lu, Y.; Denoeud, F.; Antonarakis, S.E.; Snyder, M.; et al. Pseudogenes in the ENCODE Regions: Consensus Annotation, Analysis of Transcription, and Evolution. *Genome Res.* **2007**, *17*, 839–851. [CrossRef]
30. Balakirev, E.S.; Ayala, F.J. Pseudogenes: Are They "Junk" or Functional DNA? *Annu. Rev. Genet.* **2003**, *37*, 123–151. [CrossRef] [PubMed]

31. Jia, J.; Deng, P.; Li, T.; Wang, K.; Gao, L.; Zhao, G.; Cui, D.; Dong, Z.; Li, C.; Zhan, K.; et al. Transposable Elements Drive the Subgenomic Divergence of Homoeologous Genes to Shape Wheat Domestication and Improvement. *Plant Commun.* **2025**, *6*, 101341. [CrossRef] [PubMed]
32. Charles, M.; Belcram, H.; Just, J.; Huneau, C.; Viollet, A.; Couloux, A.; Segurens, B.; Carter, M.; Huteau, V.; Coriton, O.; et al. Dynamics and Differential Proliferation of Transposable Elements during the Evolution of the B and a Genomes of Wheat. *Genetics* **2008**, *180*, 1071–1086. [CrossRef]
33. Brenchley, R.; Spannagl, M.; Pfeifer, M.; Barker, G.L.A.; D'Amore, R.; Allen, A.M.; McKenzie, N.; Kramer, M.; Kerhornou, A.; Bolser, D.; et al. Analysis of the Bread Wheat Genome Using Whole-Genome Shotgun Sequencing. *Nature* **2012**, *491*, 705–710. [CrossRef]
34. Slotkin, R.K.; Martienssen, R. Transposable Elements and the Epigenetic Regulation of the Genome. *Nat. Rev. Genet.* **2007**, *8*, 272–285. [CrossRef]
35. Kim, M.Y.; Zilberman, D. DNA Methylation as a System of Plant Genomic Immunity. *Trends Plant Sci.* **2014**, *19*, 320–326. [CrossRef]
36. Kazazian, H.H. Mobile Elements: Drivers of Genome Evolution. *Science* **2004**, *303*, 1626–1632. [CrossRef] [PubMed]
37. Kenchanmane Raju, S.K. Epigenomic Atlas in Wheat Reveals Regulatory Elements Specifying Subgenome Divergence. *Plant Cell* **2021**, *33*, 783–785. [CrossRef] [PubMed]
38. Akhunov, E.D.; Akhunova, A.R.; Linkiewicz, A.M.; Dubcovsky, J.; Hummel, D.; Lazo, G.; Chao, S.; Anderson, O.D.; David, J.; Qi, L.; et al. Synteny Perturbations between Wheat Homoeologous Chromosomes Caused by Locus Duplications and Deletions Correlate with Recombination Rates. *Proc. Natl. Acad. Sci. USA* **2003**, *100*, 10836–10841. [CrossRef] [PubMed]
39. Thibaud-Nissen, F.; Ouyang, S.; Buell, C.R. Identification and Characterization of Pseudogenes in the Rice Gene Complement. *BMC Genom.* **2009**, *10*, 317. [CrossRef]
40. Pink, R.C.; Wicks, K.; Caley, D.P.; Punch, E.K.; Jacobs, L.; Francisco Carter, D.R. Pseudogenes: Pseudo-Functional or Key Regulators in Health and Disease? *RNA* **2011**, *17*, 792–798. [CrossRef]
41. Yadav, S.; Kalwan, G.; Meena, S.; Gill, S.S.; Yadava, Y.K.; Gaikwad, K.; Jain, P.K. Unravelling the Due Importance of Pseudogenes and Their Resurrection in Plants. *Plant Physiol. Biochem.* **2023**, *203*, 108062. [CrossRef]
42. Proost, S.; Pattyn, P.; Gerats, T.; Van De Peer, Y. Journey Through the Past: 150 Million Years of Plant Genome Evolution. *Plant J.* **2011**, *66*, 58–65. [CrossRef]
43. Ma, P.-F.; Liu, Y.-L.; Jin, G.-H.; Liu, J.-X.; Wu, H.; He, J.; Guo, Z.-H.; Li, D.-Z. The *Pharus latifolius* Genome Bridges the Gap of Early Grass Evolution. *Plant Cell* **2021**, *33*, 846–864. [CrossRef]
44. Zhang, L.; Zhu, X.; Zhao, Y.; Guo, J.; Zhang, T.; Huang, W.; Huang, J.; Hu, Y.; Huang, C.-H.; Ma, H. Phylotranscriptomics Resolves the Phylogeny of Pooideae and Uncovers Factors for Their Adaptive Evolution. *Mol. Biol. Evol.* **2022**, *39*, msac026. [CrossRef]
45. Marcussen, T.; Sandve, S.R.; Heier, L.; Spannagl, M.; Pfeifer, M.; The International Wheat Genome Sequencing Consortium; Jakobsen, K.S.; Wulff, B.B.H.; Steuernagel, B.; Mayer, K.F.X.; et al. Ancient Hybridizations Among the Ancestral Genomes of Bread Wheat. *Science* **2014**, *345*, 1250092. [CrossRef]
46. Gill, B.S.; Appels, R.; Botha-Oberholster, A.-M.; Buell, C.R.; Bennetzen, J.L.; Chalhoub, B.; Chumley, F.; Dvořák, J.; Iwanaga, M.; Keller, B.; et al. A Workshop Report on Wheat Genome Sequencing. *Genetics* **2004**, *168*, 1087–1096. [CrossRef]
47. Zhu, T.; Wang, L.; Rimbert, H.; Rodriguez, J.C.; Deal, K.R.; De Oliveira, R.; Choulet, F.; Keeble-Gagnère, G.; Tibbits, J.; Rogers, J.; et al. Optical Maps Refine the Bread Wheat *Triticum aestivum* Cv. Chinese Spring Genome Assembly. *Plant J.* **2021**, *107*, 303–314. [CrossRef]
48. Bairoch, A. The SWISS-PROT Protein Sequence Data Bank and Its New Supplement TREMBL. *Nucleic Acids Res.* **1996**, *24*, 21–25. [CrossRef]
49. Bao, W.; Kojima, K.K.; Kohany, O. Repbase Update, a Database of Repetitive Elements in Eukaryotic Genomes. *Mob. DNA* **2015**, *6*, 11. [CrossRef] [PubMed]
50. Mistry, J.; Chuguransky, S.; Williams, L.; Qureshi, M.; Salazar, G.A.; Sonnhammer, E.L.L.; Tosatto, S.C.E.; Paladin, L.; Raj, S.; Richardson, L.J.; et al. Pfam: The Protein Families Database in 2021. *Nucleic Acids Res.* **2021**, *49*, D412–D419. [CrossRef] [PubMed]
51. Li, W.; Godzik, A. Cd-Hit: A Fast Program for Clustering and Comparing Large Sets of Protein or Nucleotide Sequences. *Bioinformatics* **2006**, *22*, 1658–1659. [CrossRef] [PubMed]
52. Buchfink, B.; Xie, C.; Huson, D.H. Fast and Sensitive Protein Alignment Using DIAMOND. *Nat. Methods* **2015**, *12*, 59–60. [CrossRef]
53. Birney, E.; Clamp, M.; Durbin, R. GeneWise and Genomewise. *Genome Res.* **2004**, *14*, 988–995. [CrossRef]
54. Pearson, W.R. An Introduction to Sequence Similarity ("Homology") Searching. *Curr. Protoc. Bioinform.* **2013**, *42*, 3.1.1–3.1.8. [CrossRef]
55. Krzywinski, M.; Schein, J.; Birol, I.; Connors, J.; Gascoyne, R.; Horsman, D.; Jones, S.J.; Marra, M.A. Circos: An Information Aesthetic for Comparative Genomics. *Genome Res.* **2009**, *19*, 1639–1645. [CrossRef]

56. Aramaki, T.; Blanc-Mathieu, R.; Endo, H.; Ohkubo, K.; Kanehisa, M.; Goto, S.; Ogata, H. KofamKOALA: KEGG Ortholog Assignment Based on Profile HMM and Adaptive Score Threshold. *Bioinformatics* **2020**, *36*, 2251–2252. [CrossRef] [PubMed]
57. Emms, D.M.; Kelly, S. OrthoFinder: Phylogenetic Orthology Inference for Comparative Genomics. *Genome Biol.* **2019**, *20*, 238. [CrossRef] [PubMed]
58. Altschul, S.F.; Gish, W.; Miller, W.; Myers, E.W.; Lipman, D.J. Basic Local Alignment Search Tool. *J. Mol. Biol.* **1990**, *215*, 403–410. [CrossRef]
59. Altschul, S. Gapped BLAST and PSI-BLAST: A New Generation of Protein Database Search Programs. *Nucleic Acids Res.* **1997**, *25*, 3389–3402. [CrossRef]
60. Camacho, C.; Coulouris, G.; Avagyan, V.; Ma, N.; Papadopoulos, J.; Bealer, K.; Madden, T.L. BLAST+: Architecture and Applications. *BMC Bioinf.* **2009**, *10*, 421. [CrossRef]
61. Wang, Y.; Tang, H.; DeBarry, J.D.; Tan, X.; Li, J.; Wang, X.; Lee, T.; Jin, H.; Marler, B.; Guo, H.; et al. MCScanX: A Toolkit for Detection and Evolutionary Analysis of Gene Synteny and Collinearity. *Nucleic Acids Res.* **2012**, *40*, e49. [CrossRef]
62. Rice, P.; Longden, I.; Bleasby, A. EMBOSS: The European Molecular Biology Open Software Suite. *Trends Genet.* **2000**, *16*, 276–277. [CrossRef] [PubMed]
63. SanMiguel, P.; Gaut, B.S.; Tikhonov, A.; Nakajima, Y.; Bennetzen, J.L. The Paleontology of Intergene Retrotransposons of Maize. *Nat. Genet.* **1998**, *20*, 43–45. [CrossRef]
64. McKinney, W. Data Structures for Statistical Computing in Python. In Proceedings of the 9th Python in Science Conference, Austin, TX, USA, 28 June–3 July 2010; pp. 56–61.
65. Harris, C.R.; Millman, K.J.; Van Der Walt, S.J.; Gommers, R.; Virtanen, P.; Cournapeau, D.; Wieser, E.; Taylor, J.; Berg, S.; Smith, N.J.; et al. Array Programming with NumPy. *Nature* **2020**, *585*, 357–362. [CrossRef] [PubMed]
66. Virtanen, P.; Gommers, R.; Oliphant, T.E.; Haberland, M.; Reddy, T.; Cournapeau, D.; Burovski, E.; Peterson, P.; Weckesser, W.; Bright, J.; et al. SciPy 1.0: Fundamental Algorithms for Scientific Computing in Python. *Nat. Methods* **2020**, *17*, 261–272. [CrossRef] [PubMed]
67. Hunter, J.D. Matplotlib: A 2D Graphics Environment. *Comput. Sci. Eng.* **2007**, *9*, 90–95. [CrossRef]
68. Jones, P.; Binns, D.; Chang, H.-Y.; Fraser, M.; Li, W.; McAnulla, C.; McWilliam, H.; Maslen, J.; Mitchell, A.; Nuka, G.; et al. InterProScan 5: Genome-Scale Protein Function Classification. *Bioinformatics* **2014**, *30*, 1236–1240. [CrossRef]

MDPI AG
Grosspeteranlage 5
4052 Basel
Switzerland
Tel.: +41 61 683 77 34

Plants Editorial Office
E-mail: plants@mdpi.com
www.mdpi.com/journal/plants

Academic Open
Access Publishing

mdpi.com

ISBN 978-3-7258-7686-0